

# Determining the Zone of Influence for High Energy Arcing Faults Using Fire Dynamics Simulator

**U.S. Nuclear Regulatory Commission  
Office of Nuclear Regulatory Research  
Washington DC 20555-0001**

**Electric Power Research Institute  
3420 Hillview Avenue  
Palo Alto, CA 94304**



**Disclaimer**

Legally binding regulatory requirements are stated only in laws, NRC regulations, licenses, including technical specifications, or orders; not in Research Information Letters (RILs). A RIL is not regulatory guidance, although NRC's regulatory offices may consider the information in a RIL to determine whether any regulatory actions are warranted.

# Determining the Zone of Influence for High Energy Arcing Faults Using Fire Dynamics Simulator

RIL 2022-09

EPRI 3002025123

Final Report, November 2022  
NRC Research Information Letter

U.S. Nuclear Regulatory Commission (NRC)  
Office of Nuclear Regulatory Research (RES)  
Washington, D.C. 20555-0001

Electric Power Research Institute (EPRI)  
3420 Hillview Avenue  
Palo Alto, CA 94304-1338

U.S. NRC-RES Project Manager  
M. H. Salley

EPRI Project Manager  
M. Randelovic

All or a portion of the requirements of the EPRI Nuclear  
Quality Assurance Program apply to this product.

YES



EPRI

3420 Hillview Avenue, Palo Alto, California 94304-1338 • USA  
800.313.3774 • 650.855.2121 • [askepri@epri.com](mailto:askepri@epri.com) • [www.epri.com](http://www.epri.com)

## **DISCLAIMER OF WARRANTIES AND LIMITATION OF LIABILITIES**

THIS DOCUMENT WAS PREPARED BY THE ORGANIZATIONS NAMED BELOW AS AN ACCOUNT OF WORK SPONSORED OR COSPONSORED BY THE ELECTRIC POWER RESEARCH INSTITUTE, INC. (EPRI). NEITHER EPRI, ANY MEMBER OF EPRI, ANY COSPONSOR, THE ORGANIZATIONS BELOW, NOR ANY PERSON ACTING ON BEHALF OF ANY OF THEM:

(A) MAKES ANY WARRANTY OR REPRESENTATION WHATSOEVER, EXPRESS OR IMPLIED, (I) WITH RESPECT TO THE USE OF ANY INFORMATION, APPARATUS, METHOD, PROCESS, OR SIMILAR ITEM DISCLOSED IN THIS DOCUMENT, INCLUDING MERCHANTABILITY AND FITNESS FOR A PARTICULAR PURPOSE, OR (II) THAT SUCH USE DOES NOT INFRINGE ON OR INTERFERE WITH PRIVATELY OWNED RIGHTS, INCLUDING ANY PARTY'S INTELLECTUAL PROPERTY, OR (III) THAT THIS DOCUMENT IS SUITABLE TO ANY PARTICULAR USER'S CIRCUMSTANCE; OR

(B) ASSUMES RESPONSIBILITY FOR ANY DAMAGES OR OTHER LIABILITY WHATSOEVER (INCLUDING ANY CONSEQUENTIAL DAMAGES, EVEN IF EPRI OR ANY EPRI REPRESENTATIVE HAS BEEN ADVISED OF THE POSSIBILITY OF SUCH DAMAGES) RESULTING FROM YOUR SELECTION OR USE OF THIS DOCUMENT OR ANY INFORMATION, APPARATUS, METHOD, PROCESS, OR SIMILAR ITEM DISCLOSED IN THIS DOCUMENT.

REFERENCE HEREIN TO ANY SPECIFIC COMMERCIAL PRODUCT, PROCESS, OR SERVICE BY ITS TRADE NAME, TRADEMARK, MANUFACTURER, OR OTHERWISE, DOES NOT NECESSARILY CONSTITUTE OR IMPLY ITS ENDORSEMENT, RECOMMENDATION, OR FAVORING BY EPRI.

THE FOLLOWING ORGANIZATIONS PREPARED THIS REPORT:

### **EPRI**

**U.S. Nuclear Regulatory Commission, Office of Nuclear Regulatory Research**

**Fleischer Consultants, LLC**

**Jensen Hughes**

**National Institute of Standards and Technology**

**Sandia National Laboratories**

THE TECHNICAL CONTENTS OF THIS PRODUCT WERE **NOT** PREPARED IN ACCORDANCE WITH THE EPRI QUALITY PROGRAM MANUAL THAT FULFILLS THE REQUIREMENTS OF 10 CFR 50, APPENDIX B. THIS PRODUCT IS **NOT** SUBJECT TO THE REQUIREMENTS OF 10 CFR PART 21.

## **NOTE**

For further information about EPRI, call the EPRI Customer Assistance Center at 800.313.3774 or e-mail [askepri@epri.com](mailto:askepri@epri.com).

Together...Shaping the Future of Energy®

# ABSTRACT

---

This report documents the development of zones of influence (ZOIs) using Fire Dynamics Simulator (FDS) for equipment subject to the effects of a high energy arcing fault (HEAF). This multi-part effort consisted of:

- Building FDS input files to calculate thermal exposure at specific locations for targets exposed to a HEAF,
- Validation and benchmarking of the FDS models against available data,
- Development of a simulation matrix of relevant HEAF FDS scenarios, and
- Documentation of results.

FDS simulations of HEAFs are performed for three classes of equipment: low-voltage switchgear, medium-voltage switchgear, and non-segregated bus ducts. Simulation variables include the fault current magnitude and duration, location, electrode composition, and type of equipment. The end result is a detailed tabulation of the energetic ZOIs for each simulated HEAF scenario. In addition to developing energetic HEAF ZOIs, the research objectives also investigated the various parameters that could affect the ZOIs, including the arc energy and location, the equipment orientation, the electrode composition, and the housing composition (bus ducts). The evaluation and analysis of the energetic phase HEAF ZOIs are based on the current state-of-knowledge, which has been significantly advanced through collaborative research efforts between the NRC-RES and EPRI, which this report is a product of.

## **Keywords**

Arcing fault  
Electrical explosion hazard  
Fire Dynamics Simulator (FDS)  
Fire probabilistic risk assessment  
High energy arcing fault (HEAF)  
Zone of influence (ZOI)



# CONTENTS

---

<b>ABSTRACT .....</b>	<b>III</b>
<b>LIST OF FIGURES .....</b>	<b>XIII</b>
<b>LIST OF TABLES .....</b>	<b>XXIX</b>
<b>EXECUTIVE SUMMARY .....</b>	<b>XXXI</b>
<b>CITATIONS.....</b>	<b>XXXV</b>
<b>ACKNOWLEDGEMENTS .....</b>	<b>XXXVII</b>
<b>ACRONYMS .....</b>	<b>XXXIX</b>
<b>1 INTRODUCTION .....</b>	<b>1-1</b>
1.1 Background.....	1-1
1.2 Overview of the Energetic Phase of the HEAF Zone of Influence .....	1-2
1.3 Objectives .....	1-2
1.4 Scope.....	1-2
<b>2 HEAF DESCRIPTION AND FDS CAPABILITIES.....</b>	<b>2-1</b>
2.1 HEAF Description .....	2-1
2.2 HEAF ZOI Components .....	2-2
2.2.1 MV SWGR and LV SWGR ZOIs .....	2-2
2.2.2 NSBD ZOIs .....	2-3
2.3 Fire Dynamics Simulator Capabilities Applicable to HEAF Phenomena.....	2-4
2.3.1 Primary FDS Model Assumptions .....	2-4
2.3.2 FDS Sub-Models Applicable to Modeling HEAF Effects .....	2-5
2.3.2.1 Combustion.....	2-5
2.3.2.2 Radiation.....	2-6
2.3.2.3 Solid-Phase .....	2-6

---

2.3.3	HEAF Phenomena Not Modeled by FDS.....	2-7
<b>3</b>	<b>FDS SIMULATIONS TO DETERMINE THE ENERGETIC ZOI.....</b>	<b>3-1</b>
3.1	Model Simulation Time .....	3-1
3.2	Gas Properties .....	3-3
3.3	Radiation.....	3-3
3.4	Computational Grid .....	3-4
3.5	Combustion.....	3-5
3.6	Enclosure Breach .....	3-5
3.7	Electrode Mass Loss.....	3-5
3.7.1	Electrode Mass Loss Rate .....	3-6
3.7.2	Electrode Mass Loss Particle Size Distribution.....	3-9
3.7.2.1	Electrode Mass Loss Particle Size Distribution.....	3-9
3.7.2.2	Electrode Oxidation.....	3-9
3.7.2.3	Treatment of Electrode Particles in FDS.....	3-10
3.8	Arc Power Input .....	3-11
3.8.1	Arc Power Profiles.....	3-11
3.8.2	Power Input for FDS Simulations .....	3-13
3.9	Input File Generation .....	3-14
3.10	Outputs and Output Processing .....	3-15
<b>4</b>	<b>VALIDATION AND BENCHMARKING OF FDS FOR HEAF.....</b>	<b>4-1</b>
4.1	2018 Medium Voltage Switchgear Experiments .....	4-1
4.1.1	Summary of Experiments.....	4-1
4.1.2	Discussion of FDS Inputs.....	4-4
4.1.3	Results of FDS Simulations .....	4-5
4.1.4	Model Uncertainty Statistics.....	4-8
4.2	Benchmarking Against FEDB 50935 .....	4-12
4.2.1	Summary of Event.....	4-12
4.2.2	Discussion of FDS Inputs.....	4-13
4.2.3	Results of FDS Simulation .....	4-13
4.3	Benchmarking against the Full-Scale Test of FEDB 51764.....	4-14
4.3.1	Summary of Event.....	4-14
4.3.2	Discussion of FDS Inputs.....	4-15
4.3.3	FDS Simulation Results .....	4-16

---

4.4	Benchmarking against the Bus Duct Event in an Elbow (FEDB 51765)	4-16
4.4.1	Summary of Event	4-16
4.4.2	Discussion of FDS Inputs	4-17
4.4.3	FDS Simulation Results	4-18
4.5	Summary of FDS Validation for Modeling HEAFs	4-19
<b>5</b>	<b>DEVELOPMENT OF THE HEAF SIMULATION MATRIX</b>	<b>5-1</b>
5.1	Development of HEAF Model Simulations	5-1
5.1.1	Medium Voltage Switchgear	5-2
5.1.1.1	Bus Bar Material	5-2
5.1.1.2	Switchgear Type and Circuit Breaker Orientation	5-3
5.1.1.3	Fault Location and Power Flow	5-6
5.1.1.4	Arc Current and Arc Voltage	5-9
5.1.1.5	Arcing Fault Duration	5-9
5.1.1.6	Arc Energies	5-10
5.1.1.7	Medium Voltage Switchgear FDS Simulation Matrix	5-10
5.1.2	Low Voltage Switchgear	5-15
5.1.2.1	LV SWGR Type and Arc Initiation Location	5-15
5.1.2.2	Bus Bar Material	5-16
5.1.2.3	Arc Current, Arc Voltage, and Duration	5-17
5.1.2.4	Low Voltage Switchgear FDS Simulation Matrix	5-17
5.1.3	Non-Segregated Bus Ducts	5-20
5.1.3.1	Orientation	5-21
5.1.3.2	NSBD Type	5-21
5.1.3.3	Arc Current, Arc Voltage, and Duration	5-21
5.1.3.4	Bus Bar and Bus Duct Enclosure Material	5-22
5.1.3.5	Non-Segregated Bus Duct FDS Simulation Matrix	5-23
5.2	Geometry and Domain Details for the HEAF FDS Simulations	5-27
5.2.1	Medium Voltage Switchgear HEAFs	5-27
5.2.1.1	GE Vertical-Lift Circuit Breaker	5-27
5.2.1.2	ABB Horizontal Draw-Out Circuit Breaker	5-29
5.2.2	Low Voltage Switchgear HEAFs	5-31
5.2.3	Non-Segregated Bus Duct HEAFs	5-33

---

<b>6 FDS SIMULATION RESULTS</b> .....	<b>6-1</b>
6.1 Medium Voltage Switchgear HEAF Simulations .....	6-1
6.1.1 Selected GE Vertical-Lift Circuit Breaker MV SWGR HEAF Simulations .....	6-1
6.1.1.1 GE Vertical-Lift Circuit Breaker MV SWGR Design with a HEAF at the Main Bus Bar .....	6-2
6.1.1.2 GE Vertical-Lift Circuit Breaker MV SWGR Design with a HEAF at the Circuit Breaker Stabs .....	6-6
6.1.1.3 GE Vertical-Lift Circuit Breaker MV SWGR Design with a HEAF at the Primary Cable Compartment Bus Bars in the Load Configuration.....	6-11
6.1.1.4 GE Vertical-Lift Circuit Breaker MV SWGR Design with a HEAF at the Primary Cable Compartment Bus Bars in the Supply Configuration.....	6-15
6.1.1.5 Summary of GE Vertical-Lift Circuit Breaker MV SWGR Design Results.....	6-20
6.1.2 ABB Horizontal Draw-Out Style Circuit Breaker MV SWGR with a HEAF at the Circuit Breaker Stabs.....	6-20
6.1.3 Summary of MV SWGR Results .....	6-25
6.1.3.1 Energetic ZOI Symmetry.....	6-25
6.1.3.2 MV SWGR Energetic ZOI Dependencies .....	6-26
6.1.3.3 FDS Modeling Insights for MV SWGR.....	6-32
6.1.3.4 Tabulated MV SWGR Energetic ZOIs .....	6-33
6.2 Low Voltage Switchgear HEAF Simulations .....	6-37
6.2.1 Selected Low Voltage Switchgear HEAF Simulations .....	6-37
6.2.1.1 Middle-Height Elevation HEAF .....	6-37
6.2.1.2 Top Height Elevation HEAF.....	6-42
6.2.1.3 Summary of LV SWGR Results .....	6-46
6.2.2 Summary of LV SWGR Results.....	6-46
6.2.2.1 LV SWGR Energetic ZOI Dependencies .....	6-46
6.2.2.2 Modeling Insights .....	6-49
6.2.2.3 Tabulated LV SWGR Energetic ZOIs .....	6-50
6.3 Non-Segregated Bus Duct HEAFs.....	6-53
6.3.1 Selected Non-Segregated Bus Duct HEAF Simulations .....	6-54
6.3.1.1 Non-Segregated Bus Duct Straight Section.....	6-54
6.3.1.2 Non-Segregated Bus Duct Elbow .....	6-58
6.3.1.3 Non-Segregated Bus Duct Tee.....	6-62

6.3.2	Summary of Results.....	6-66
6.3.2.1	Energetic ZOI Dependencies.....	6-66
6.3.2.2	FDS Model Insights.....	6-72
6.3.2.3	Tabulated NSBD Energetic ZOIs.....	6-73
<b>7</b>	<b>SUMMARY AND CONCLUSIONS .....</b>	<b>7-1</b>
7.1	FDS Input Summary .....	7-1
7.2	FDS HEAF Validation Summary .....	7-2
7.3	FDS Results.....	7-3
7.4	Significant HEAF Modeling Insights.....	7-4
<b>8</b>	<b>REFERENCES .....</b>	<b>8-1</b>
<b>A</b>	<b>ARC POWER AND PROFILE.....</b>	<b>A-1</b>
A.1	Arc Voltage .....	A-1
A.2	Medium Voltage Arc Energy Profiles .....	A-1
A.2.1	Medium Voltage Constant-Current Arc Profile .....	A-3
A.2.2	Arc Energy Profile of the Generator-fed Fault.....	A-4
A.3	Arc Power Profiles for Low Voltage Switchgear.....	A-7
A.4	Implementation of the Arc Power Profiles in the FDS Model .....	A-11
<b>B</b>	<b>DETAILED FDS RESULTS .....</b>	<b>B-1</b>
B.1	Medium Voltage Switchgear .....	B-1
B.1.1	Vertical-Lift Circuit Breaker Design .....	B-1
B.1.1.1	Main Bus Bar Compartment .....	B-1
B.1.1.2	Circuit Breaker Stabs.....	B-7
B.1.1.3	Primary Compartment Bus Bar (PCCBB) Load Configuration .....	B-10
B.1.1.4	Primary Cable Compartment Bus Bar Supply Configuration.....	B-16
B.1.2	Horizontal Draw-Out Circuit Breaker Stabs.....	B-22
B.2	Low Voltage Switchgear .....	B-25
B.2.1	Circuit Breaker Compartment Middle-Height Elevation.....	B-25
B.2.2	Circuit Breaker Compartment Top Elevation.....	B-26
B.2.3	Bus Bar Compartment Middle-Height Elevation.....	B-27
B.2.4	Bus Bar Compartment Top Elevation.....	B-28
B.2.5	Circuit Breaker to Bus Bar Compartment.....	B-29

B.3	Non-Segregated Bus Ducts .....	B-30
B.3.1	Bus Duct Straight Segment.....	B-30
B.3.2	Bus Duct Elbow.....	B-44
B.3.3	Bus Duct Tee .....	B-47
<b>C</b>	<b>FDS INPUT FILE TEMPLATES .....</b>	<b>C-1</b>
C.1	FDS Input File Simulation Matrix .....	C-1
C.2	FDS Input File Templates for Medium Voltage Switchgear .....	C-5
C.2.1	Vertical-Lift Circuit Breaker Style .....	C-5
C.2.2	Horizontal Draw-Out Style Circuit Breaker.....	C-18
C.3	FDS Input File Template for Low Voltage Switchgear .....	C-46
C.4	FDS Input File Template for Non-Segregated Bus Ducts .....	C-52
<b>D</b>	<b>SANDIA PARTICLE TESTING .....</b>	<b>D-1</b>
D.1	Summary of Testing Approach and Parameters.....	D-1
D.1.1	Experimental Aims for Scaled Arc Testing and Outputs .....	D-1
D.1.2	Scaled Arc Fault Experimental Approach .....	D-2
D.1.3	Particle Capture and Analysis Method .....	D-6
D.2	Scaled Three-Phase Arc Fault Experimental Results.....	D-7
D.2.1	Aluminum and Copper 1 to 2 s Arcs: 600 V <sub>AC</sub> , 3 Phase, 100 A/mm <sup>2</sup> .....	D-7
D.2.2	Heat Rise Versus Arc Duration for Aluminum and Copper .....	D-8
D.2.3	Heat Rise Versus Arc Duration for Aluminum and Copper .....	D-9
D.2.4	Analysis of Mass Percent Melted Versus Potential Vaporized.....	D-10
D.2.5	Differences Between Aluminum and Copper Melt Rates .....	D-11
D.3	Evolved Particle Oxidation Analysis.....	D-11
D.3.1	Electron Microscope Analysis of Evolved Aluminum Particles.....	D-11
D.3.2	Electron Microscope Analysis of Evolved Copper Particles.....	D-14
D.3.3	Summary of Particle Collection Data for FDS Modeling Input .....	D-16
<b>E</b>	<b>HEAF PRESSURE WAVE EFFECTS .....</b>	<b>E-1</b>
E.1	Background.....	E-1
E.2	NUREG/CR-6850 Guidance .....	E-2
E.3	Operating Experience .....	E-2
E.3.1	Turkey Point (FEDB 51634).....	E-2
E.3.2	GER022-19890909 .....	E-3

---

E.4	Test Data .....	E-3
E.4.1	2014-2016 OECD HEAF Testing Program .....	E-3
E.4.2	2018 Medium-Voltage Switchgear Experiments .....	E-3
E.4.3	2019 Low-Voltage Switchgear Experiments .....	E-3
E.4.4	JNRA Box Tests.....	E-4
E.5	Analysis .....	E-4
E.6	Conclusion .....	E-5



# LIST OF FIGURES

---

Figure 2-1 Energetic phase of the HEAF ZOI: left representative of shorter fault clearing times, right representative of longer fault clearing times (figures not to scale, ZOI subject to the target fragilities and fault characteristics) .....	2-2
Figure 2-2 Post-HEAF ensuing fire ZOI (figure not to scale, ZOI subject to the size of fire calculated by analyst and consideration of secondary combustibles).....	2-3
Figure 2-3 NSBD ZOI showing energetic (red shaded) and waterfall (yellow box) components.....	2-3
Figure 3-1 Incident energy for a typical plate thermometer (PTC-18) measured during MV SWGR Test 2-21 [6] .....	3-2
Figure 3-2 FDS-predicted heat flux at PTC-18 for MV SWGR Test 2-21 [6].....	3-2
Figure 3-3 Arc power versus radiant fraction data of Cressault [26].....	3-4
Figure 3-4 Predicted versus measured electrode mass loss for the open-box [4] and MV SWGR [6] tests. Symbol shape indicates test series (OB is open-box, OBMV is medium-voltage open-box, and MV SWGR is full-scale medium-voltage switchgear with aluminum electrodes), and shading indicates aluminum (hollow) or copper (filled) .....	3-7
Figure 3-5 Results of fitting Equation 3-3 using different exponents to the MV SWGR mass loss data. The empirical constant $a$ is the constant in the equation for the blue dashed line shown in each graph .....	3-8
Figure 3-6 Power curve for a 0 s stiff and 15 s decay HEAF .....	3-12
Figure 3-7 Power curve for a 3 s stiff and 15 s decay HEAF .....	3-12
Figure 3-8 Power curve for a 5 s stiff and 15 s decay HEAF .....	3-13
Figure 3-9 Low voltage HEAF power profile .....	3-13
Figure 3-10 FDS output devices (green dots) for the GE Magne-Blast geometry with the arc in the main bus bar compartment.....	3-16
Figure 3-11 Depiction of the adjusted FDS results for the bias and error (Section 4.1.4). Dotted lines are 95% confidence interval and dot-dot-dash lines are 15 MJ/m <sup>2</sup> and 30 MJ/m <sup>2</sup> target fragility criteria .....	3-17
Figure 4-1 GE Type M-36 switchgear enclosure .....	4-1
Figure 4-2 MV SWGR instrumentation racks (top left – racks 1,2, and 4; top right – rack 3; bottom – rack 5) [6]. Device symbols are: ASTM (ASTM copper slug calorimeter), P <sub>TC</sub> (plate thermometer), T (tungsten slug calorimeter), and CC <sub>n</sub> (cable coupon) .....	4-3
Figure 4-3 FDS geometry showing particles used for instrumentation (magenta is a tungsten slug calorimeter, yellow is a plate thermometer, and teal is an ASTM copper slug calorimeter).....	4-4
Figure 4-4 Enclosure condition post-HEAF for experiment 2-19 .....	4-6

Figure 4-5 Enclosure condition post-HEAF for experiment 2-21 .....	4-6
Figure 4-6 Enclosure condition post-HEAF for experiment 2-22 .....	4-7
Figure 4-7 Enclosure condition post-HEAF for experiment 2-24 .....	4-7
Figure 4-8 Scatterplot of measured versus FDS-predicted temperature rise for the 2018 MV SWGR experiments. Top left – Racks 1 and 4 (enclosure side), top right – Racks 2 and 3 (enclosure back), bottom – Rack 5 (enclosure top). Symbol type indicates gauge type .....	4-8
Figure 4-9 Scatterplot of measured versus FDS-predicted temperature rise for the 2018 MV SWGR experiments with model uncertainty statistics. Top left – Racks 2 and 3 (rear) for 4 s arc duration experiments, top right – All racks, 4 s arc exposure duration experiments, bottom – all racks, 2 s arc exposure experiments. Solid lines are the average measured or predicted values and the dashed lines are the 95 <sup>th</sup> percentile confidence intervals for measured and predicted values.....	4-11
Figure 4-10 Back side of initiating circuit breaker (left) showing damaged bus bars and back side of low-voltage switchgear (right) showing smoke stains and discolored paint behind the arc location (brown stain at the mid-height of the middle section) [33] .....	4-13
Figure 4-11 FDS-predicted damage for FEDB 50935. Left image clips the back of the enclosure to show the panel separating the circuit breaker cubicles from the middle main bus bar compartment. Right image clips the back face of the enclosure to show the partition between the main bus bar compartment and rear cable compartment.....	4-14
Figure 4-12 FDS-predicted holing in the bottom of the top duct (left) and no observable damage to the top of the bottom duct (right) .....	4-15
Figure 4-13 Repaired NSBD from the HEAF event showing cable tray location (left), aluminum metal and charred cables in cable tray (right) .....	4-17
Figure 4-14 FDS model of NSBD vertical elbow. Incident energy measurement devices shown as green dots .....	4-17
Figure 4-15 Contour plot of the FDS simulation results for a 0 s stiff, 15 s decay arc at a NSBD elbow. The approximate location of the cable tray for this event shown below bus duct elbow as indicated. Magenta contours are the 15 MJ/m <sup>2</sup> and 30 MJ/m <sup>2</sup> target fragility thresholds applicable to thermoplastic (TP) and thermoset (TS) cables.....	4-19
Figure 5-1 MV SWGR designs with aluminum.....	5-3
Figure 5-2 Circuit breaker orientation for MV SWGR designs with aluminum .....	5-3
Figure 5-3 GE Magne-Blast vertical-lift style circuit breaker switchgear. Red arrows indicate current flow direction in supply configuration; current flow is reversed for load configuration. Blue shaded area is approximate location of the circuit breaker .....	5-5
Figure 5-4 ABB/ITE HK horizontal draw-out style circuit breaker switchgear. Red arrows indicate current flow direction in supply configuration; current flow is reversed for load configuration. Blue shaded area is approximate location of the circuit breaker .....	5-5
Figure 5-5 Westinghouse DH-P horizontal draw-out style circuit breaker switchgear. Red arrows indicate current flow direction in supply configuration; current flow is reversed for load configuration. Blue shaded area is approximate location of the	

circuit breaker. Due to similarities between this switchgear design and the ABB/ITE HK switchgear design, the Westinghouse DH-P design is not specifically modeled .....	5-6
Figure 5-6 GE Magne-Blast vertical-lift circuit breaker SWGR showing location of circuit breaker stabs, primary cable compartment bus bars, and the main bus bars.....	5-7
Figure 5-7 Vertical-lift style circuit breaker switchgear with consolidated fault locations. Red arrows indicate current flow direction in supply configuration; current flow is reversed for load configuration. Blue shaded area is approximate location of the circuit breaker.....	5-8
Figure 5-8 Horizontal draw-out style circuit breaker switchgear with consolidated fault location. Red arrows indicate current flow direction in supply configuration; current flow is reversed for load configuration. Blue shaded area is approximate location of the circuit breaker .....	5-8
Figure 5-9 Westinghouse DS electrical cabinet and arc test location [5] .....	5-16
Figure 5-10 Example of a non-segregated bus duct configuration .....	5-21
Figure 5-11 Bus bar and enclosure material type distribution. N/A indicates the plant uses cables rather than NSBDs [3] .....	5-22
Figure 5-12 FDS model for the GE MV SWGR. Top left – view of enclosure with side clipped showing the internal layout. Top right – view of enclosure front with open door. Bottom – Rear isometric view showing the entire FDS domain .....	5-28
Figure 5-13 GE MV SWGR exposure measurement locations (green dots) Top left – circuit breaker stabs. Top right – main bus bar compartment. Bottom left – primary cable compartment (load). Bottom right – primary cable compartment (supply) .....	5-29
Figure 5-14 FDS model for the ABB MV SWGR. Top left – view of enclosure with side clipped showing internal layout. Top right – view of enclosure front with open door. Bottom – Rear isometric view showing the entire FDS domain .....	5-30
Figure 5-15 ABB MV SWGR exposure measurement locations (green dots).....	5-31
Figure 5-16 FDS model for the LV SWGR. Top left – view of enclosure with side clipped showing the internal layout. Top right – view of enclosure front with open door. Bottom – Rear isometric view showing the entire FDS domain .....	5-32
Figure 5-17 LV SWGR exposure measurement locations (green dots) Left – View of side with the arc. Right – View of non-arc side of the enclosure .....	5-33
Figure 5-18 NSBD geometry and exposure measurement locations (green dots) Top left – straight segment. Top right – elbow. Bottom – Tee .....	5-34
Figure 6-1 Particle distribution at various times for a 233 MJ HEAF located at the main bus bars of a vertical-lift circuit breaker MV SWGR design.....	6-3
Figure 6-2 Luminous portion of the thermal plume at various times for a 233 MJ HEAF located at the main bus bars of a vertical-lift circuit breaker MV SWGR design .....	6-4
Figure 6-3 Heat release rate per unit volume at 4 s for a 233 MJ HEAF located at the main bus bars of a vertical-lift circuit breaker MV SWGR design. The heat release rate per unit volume for the electrode is shown as a rectangular orange region within the switchgear.....	6-5
Figure 6-4 Wall temperature at 15 s for a 233 MJ HEAF located at the main bus bars of a vertical-lift circuit breaker MV SWGR design .....	6-5

---

Figure 6-5 Total energy exposure as a function of distance from each face for a 233 MJ HEAF located at the main bus bars of a vertical-lift circuit breaker MV SWGR design (HEAF simulation ID MV-GE-36). Note the results for the left- and right-sides are nearly coincident. Dashed horizontal lines correspond to the 15 MJ/m <sup>2</sup> and 30 MJ/m <sup>2</sup> target fragility thresholds .....	6-6
Figure 6-6 Particle distribution at various times for a 233 MJ HEAF located at the circuit breaker stabs of a vertical-lift circuit breaker MV SWGR design.....	6-8
Figure 6-7 Luminous portion of the thermal plume at various times for a 233 MJ HEAF located at the circuit breaker stabs of a vertical-lift circuit breaker MV SWGR design.....	6-9
Figure 6-8 Heat release rate per unit volume at 4 s for a 233 MJ HEAF located at the circuit breaker stabs of a vertical-lift circuit breaker MV SWGR design. The heat release rate per unit volume for the electrode is shown as a rectangular orange region within the switchgear. ....	6-9
Figure 6-9 Wall temperature at 15 s for a 233 MJ HEAF located at the circuit breaker stabs of a vertical-lift circuit breaker MV SWGR design.....	6-10
Figure 6-10 Total energy exposure as a function of distance from each face for a 233 MJ HEAF located at the circuit breaker stabs of a vertical-lift circuit breaker MV SWGR design (HEAF simulation ID MV-GE-35). Note the results for the left- and right-sides are nearly coincident. Dashed horizontal lines correspond to the 15 MJ/m <sup>2</sup> and 30 MJ/m <sup>2</sup> target fragility threshold .....	6-10
Figure 6-11 Particle distribution at various times for a 233 MJ HEAF located at the primary cable compartment bus bars in the load configuration of a vertical-lift circuit breaker MV SWGR design .....	6-12
Figure 6-12 Luminous portion of the thermal plume at various times for a 233 MJ HEAF located at the primary cable compartment bus bars in the load configuration of a vertical-lift circuit breaker MV SWGR design .....	6-13
Figure 6-13 Heat release rate per unit volume at 4 s for a 233 MJ HEAF located at the primary cable compartment bus bars in the load configuration of a vertical-lift circuit breaker MV SWGR design. The heat release rate per unit volume for the electrode is shown as a rectangular orange region within the switchgear .....	6-14
Figure 6-14 Wall temperature at 15 s for a 233 MJ HEAF located at the primary cable compartment bus bars in the load configuration of a vertical-lift circuit breaker MV SWGR design .....	6-14
Figure 6-15 Total energy exposure as a function of distance from each face for a 233 MJ HEAF located at the primary cable compartment bus bars in the load configuration of a vertical-lift circuit breaker MV SWGR design (HEAF simulation ID MV-GE-37). Note the results for the left- and right-sides are nearly coincident. Dashed horizontal lines correspond to the 15 MJ/m <sup>2</sup> and 30 MJ/m <sup>2</sup> target fragility threshold .....	6-15
Figure 6-16 Particle distribution at various times for a 233 MJ HEAF located at the primary cable compartment bus bars in the supply configuration of a vertical-lift circuit breaker MV SWGR design .....	6-17
Figure 6-17 Luminous portion of the thermal plume at various times for a 233 MJ HEAF located at the primary cable compartment bus bars in the supply configuration of a vertical-lift circuit breaker MV SWGR design .....	6-18

Figure 6-18 Heat release rate per unit volume at 12.5 s for a 233 MJ HEAF located at the primary cable compartment bus bars in the supply configuration of a vertical-lift circuit breaker MV SWGR design. The heat release rate per unit volume for the electrode is shown as a squared orange region within the switchgear .....	6-18
Figure 6-19 Wall temperature at 15 s for a 233 MJ HEAF located at the primary cable compartment bus bars in the supply configuration of a vertical-lift circuit breaker MV SWGR design .....	6-19
Figure 6-20 Total energy exposure as a function of distance from each face for a 233 MJ HEAF located at the primary cable compartment bus bars in the supply configuration of a vertical-lift circuit breaker MV SWGR design (HEAF simulation ID MV-GE-38). Note the results for the left- and right-sides are nearly coincident. Dashed horizontal lines correspond to the 15 MJ/m <sup>2</sup> and 30 MJ/m <sup>2</sup> target fragility threshold .....	6-19
Figure 6-21 Particle distribution at various times for a 233 MJ HEAF located at the circuit breaker stabs of the horizontal draw-out style circuit breaker MV SWGR .....	6-22
Figure 6-22 Luminous portion of the thermal plume at various times for a 233 MJ HEAF located at the circuit breaker stabs of the horizontal draw-out style circuit breaker MV SWGR.....	6-23
Figure 6-23 Heat release rate per unit volume at 11.5 s for a 233 MJ HEAF located at the circuit breaker stabs of the horizontal draw-out style circuit breaker MV SWGR (viewed from below for clarity). The heat release rate per unit volume for the electrode is shown as a rectangular orange region within the switchgear. ....	6-24
Figure 6-24 Wall temperature at 11 s for a 233 MJ HEAF located at the circuit breaker stabs of the horizontal draw-out style circuit breaker MV SWGR.....	6-24
Figure 6-25 Total energy exposure as a function of distance from each face for a 233 MJ HEAF located at the circuit breaker stabs of the horizontal draw-out style circuit breaker MV SWGR (HEAF simulation ID MV-ABB-5). Note the results for the left and right-sides are nearly coincident. Dashed horizontal lines correspond to the 15 MJ/m <sup>2</sup> and 30 MJ/m <sup>2</sup> target fragility threshold.....	6-25
Figure 6-26 Left versus right energetic ZOIs for all MV SWGR HEAF simulations.....	6-26
Figure 6-27 Energetic ZOIs as a function of arc energy for all MV SWGR HEAF simulations. Top (solid symbols) – 15 MJ/m <sup>2</sup> fragility target, bottom (open symbols) – 30 MJ/m <sup>2</sup> fragility target. Symbol shape and color indicates the enclosure face.....	6-27
Figure 6-28 Energetic ZOIs as a function of arc energy for MV SWGR HEAF simulations with the arc initiated at the circuit breaker stabs. Top (solid symbols) – 15 MJ/m <sup>2</sup> fragility target, bottom (open symbols) – 30 MJ/m <sup>2</sup> fragility target. Symbol shape and color indicates the enclosure face.....	6-28
Figure 6-29 Energetic ZOIs as a function of arc energy for MV SWGR HEAF simulations with the arc initiated at the main bus bars. Top (solid symbols) – 15 MJ/m <sup>2</sup> fragility target, bottom (open symbols) – 30 MJ/m <sup>2</sup> fragility target. Symbol shape and color indicates the enclosure face.....	6-29
Figure 6-30 Energetic ZOIs as a function of arc energy for MV SWGR HEAF simulations with arc initiated at the primary cable compartment bus bars (PCCBB) in the load configuration. Top (solid symbols) – 15 MJ/m <sup>2</sup> fragility target, bottom (open symbols) – 30 MJ/m <sup>2</sup> fragility target. Symbol shape and color indicates the enclosure face.....	6-30

Figure 6-31 Energetic ZOIs as a function of arc energy for MV SWGR HEAFs with arc initiated at the PCCBB in the supply configuration. Top (solid symbols) – 15 MJ/m <sup>2</sup> fragility target, bottom (open symbols) – 30 MJ/m <sup>2</sup> fragility target. Symbol shape and color indicates the enclosure face .....	6-31
Figure 6-32 Aluminum versus copper bus bar energetic ZOIs for all MV SWGR HEAF simulations (except for the circuit breaker stab HEAFs which only used copper).....	6-32
Figure 6-33 Particle distribution at various times for a LV SWGR HEAF at the cabinet middle-height elevation with an arc energy profile based on FEDB 50935.....	6-39
Figure 6-34 Luminous portion of the thermal plume at various times for a LV SWGR HEAF at the cabinet middle-height elevation with an arc energy profile based on FEDB 50935.....	6-40
Figure 6-35 Heat release rate per unit volume at 30.2 s for a LV SWGR HEAF at the cabinet middle- height elevation with an arc energy profile based on FEDB 50935 (viewed from below to show the arc).....	6-41
Figure 6-36 Wall temperature at 33.7 s for a LV SWGR HEAF with an arc energy profile based on FEDB 50935.....	6-41
Figure 6-37 Total energy exposure as a function of distance from each face for a LV SWGR HEAF at the cabinet middle-height elevation with an arc power profile based on FEDB 50935 (HEAF simulation LV-BASE-5). Dashed horizontal lines correspond to the 15 MJ/m <sup>2</sup> and 30 MJ/m <sup>2</sup> target fragility threshold .....	6-42
Figure 6-38 Particle distribution at various times for a LV SWGR HEAF at the cabinet top having an arc energy profile based on FEDB 50935 .....	6-43
Figure 6-39 Luminous portion of the thermal plume at various times for a LV SWGR HEAF at the cabinet top with an arc energy profile based on FEDB 50935.....	6-44
Figure 6-40 Heat release rate per unit volume at 32.4 s for a LV SWGR HEAF at the cabinet top with an arc energy profile based on FEDB 50935 (viewed from top) .....	6-45
Figure 6-41 Wall temperature at 34.3 s for a LV SWGR HEAF at the cabinet top with an arc power profile based on FEDB 50935 .....	6-45
Figure 6-42 Total energy exposure as a function of distance from each face for a LV SWGR HEAF at the cabinet top with an arc power profile based on FEDB 50935 (HEAF simulation LV-BASE-6). Dashed horizontal lines correspond to the 15 MJ/m <sup>2</sup> and 30 MJ/m <sup>2</sup> target fragility threshold .....	6-46
Figure 6-43 Energetic ZOIs as a function of arc energy for the LV SWGR HEAF simulations. Top (solid symbols) – 15 MJ/m <sup>2</sup> fragility target, bottom (open symbols) – 30 MJ/m <sup>2</sup> fragility target. Symbol shape and color indicates the enclosure face .....	6-48
Figure 6-44 Aluminum versus copper bus bar energetic ZOIs for all LV SWGR HEAF simulations. Solid symbols are 15 MJ/m <sup>2</sup> fragility targets and open symbols are 30 MJ/m <sup>2</sup> fragility targets.....	6-49
Figure 6-45 Energetic ZOI orientations for the NSBD arc locations. Straight NSBD arc location (top left), elbow arc location (top right), and tee arc location (bottom).....	6-53
Figure 6-46 Copper particle distribution at various times for a 233 MJ NSBD HEAF in a straight duct segment with copper bus bars and steel duct housing.....	6-55
Figure 6-47 Luminous portion of the thermal plume at various times for a 233 MJ NSBD HEAF in a straight duct segment with copper bus bars and steel duct housing .....	6-56

---

Figure 6-48 Heat release rate per unit volume at 18 s for a 233 MJ NSBD HEAF in a straight duct segment with copper bus bars and steel duct housing.....	6-57
Figure 6-49 Wall temperature of the duct housing at 3.9 s for a 233 MJ NSBD HEAF in a straight duct segment with copper bus bars and steel duct housing.....	6-57
Figure 6-50 Total energy exposure as a function of distance from each face for a 233 MJ NSBD HEAF in a straight duct segment with copper bus bars and steel duct housing (HEAF simulation NSBD-19). Dashed horizontal lines correspond to the 15 MJ/m <sup>2</sup> and 30 MJ/m <sup>2</sup> target fragility threshold.....	6-58
Figure 6-51 Aluminum particle distribution at various times for a 233 MJ NSBD HEAF in a vertical elbow duct segment with aluminum bus bars and aluminum duct housing.....	6-59
Figure 6-52 Luminous portion of the thermal plume at various times for a 233 MJ NSBD HEAF in a vertical elbow duct segment with aluminum bus bars and aluminum duct housing.....	6-60
Figure 6-53 Heat release rate per unit volume at 15.5 s for a 233 MJ NSBD HEAF in a vertical elbow duct segment with aluminum bus bars and aluminum duct housing.....	6-61
Figure 6-54 Wall temperature of the duct housing at 5.2 s for a 233 MJ NSBD HEAF in a vertical elbow duct segment with aluminum bus bars and aluminum duct housing.....	6-61
Figure 6-55 Total energy exposure as a function of distance from each face for a 233 MJ NSBD HEAF in a vertical elbow duct segment with aluminum bus bars and aluminum duct housing (HEAF simulation NSBD-56). Dashed horizontal lines correspond to the 15 MJ/m <sup>2</sup> and 30 MJ/m <sup>2</sup> target fragility threshold.....	6-62
Figure 6-56 Aluminum particle distribution at various times for a 233 MJ NSBD HEAF in a vertical tee duct segment with aluminum bus bars and steel duct housing.....	6-63
Figure 6-57 Luminous portion of the thermal plume at various times for a 233 MJ NSBD HEAF in a vertical tee duct segment with aluminum bus bars and steel duct housing.....	6-64
Figure 6-58 Heat release rate per unit volume at 18.1 s for a 233 MJ NSBD HEAF in a vertical tee duct segment with aluminum bus bars and steel duct housing.....	6-65
Figure 6-59 Wall temperature of the duct housing at 7.8 s for a 233 MJ NSBD HEAF in a vertical tee duct segment with aluminum bus bars and steel duct housing.....	6-65
Figure 6-60 Total energy exposure as a function of distance from each face for a 233 MJ NSBD HEAF in a vertical tee duct segment with aluminum bus bars and steel duct housing (HEAF simulation NSBD-32). Dashed horizontal lines correspond to the 15 MJ/m <sup>2</sup> and 30 MJ/m <sup>2</sup> target fragility threshold. Note there is no bottom exposure for this duct configuration.....	6-66
Figure 6-61 Energetic ZOIs as a function of arc energy for the NSBD HEAF simulations. Top (solid symbols) – 15 MJ/m <sup>2</sup> fragility target, bottom (open symbols) – 30 MJ/m <sup>2</sup> fragility target. Symbol shape and color indicates the enclosure face. Sides without an energetic ZOI component are shown with 0 m ZOI dimensions. Note that there is no left ZOI shown as two geometries (straight and elbow) do not have a left direction and the left direction for the tee is inside the initiating bus duct (see Figure 6-45).....	6-67
Figure 6-62 Energetic ZOIs as a function of arc energy for the NSBD straight segment HEAF simulations. Top – 15 MJ/m <sup>2</sup> fragility target, bottom – 30 MJ/m <sup>2</sup> fragility target. Symbol shape and color indicates the enclosure face.....	6-68

Figure 6-63 Energetic ZOIs as a function of arc energy for the NSBD tee HEAF simulations. Top – 15 MJ/m <sup>2</sup> fragility target, bottom – 30 MJ/m <sup>2</sup> fragility target. Symbol shape and color indicates the enclosure face .....	6-69
Figure 6-64 Energetic ZOIs as a function of arc energy for the NSBD elbow HEAF simulations. Top – 15 MJ/m <sup>2</sup> fragility target, bottom – 30 MJ/m <sup>2</sup> fragility target. Symbol shape and color indicates the enclosure face .....	6-70
Figure 6-65 Aluminum versus copper bus bar energetic ZOIs for all NSBD HEAF simulations .....	6-71
Figure 6-66 Steel duct versus aluminum duct energetic ZOIs for all NSBD HEAF simulations .....	6-72
Figure A-1 Plot of the arc current for a generator-fed HEAF event (December 2020).....	A-5
Figure A-2 Plot of the arc power for a generator-fed HEAF event (December 2020) .....	A-5
Figure A-3 Power curve for a 0 s stiff and 15 s decay HEAF .....	A-6
Figure A-4 Power curve for a 3 s stiff and 15 s decay HEAF .....	A-6
Figure A-5 Power curve for a 5 s stiff and 15 s decay HEAF .....	A-7
Figure A-6 FEDB 50935 arc power profile .....	A-8
Figure A-7 Low voltage HEAF current profile .....	A-8
Figure A-8 Low voltage HEAF power profile .....	A-11
Figure B-1 Results for a vertical-lift circuit breaker MV SWGR with an aluminum bus bar – 68 MJ HEAF located at the main bus bar (FDS simulation MV-GE-1).....	B-1
Figure B-2 Results for a vertical-lift circuit breaker MV SWGR with an aluminum bus bar – 135 MJ HEAF located at the main bus bar (FDS simulation MV-GE-4).....	B-2
Figure B-3 Results for a vertical-lift circuit breaker MV SWGR with an aluminum bus bar – 169 MJ HEAF located at the main bus bar (FDS simulation MV-GE-7).....	B-2
Figure B-4 Results for a vertical-lift circuit breaker MV SWGR with an aluminum bus bar – 132 MJ HEAF located at the main bus bar (FDS simulation MV-GE-10).....	B-3
Figure B-5 Results for a vertical-lift circuit breaker MV SWGR with an aluminum bus bar – 233 MJ HEAF located at the main bus bar (FDS simulation MV-GE-13).....	B-3
Figure B-6 Results for a vertical-lift circuit breaker MV SWGR with an aluminum bus bar – 300 MJ HEAF located at the main bus bar (FDS simulation MV-GE-16).....	B-4
Figure B-7 Results for a vertical-lift circuit breaker MV SWGR with a copper bus bar – 68 MJ HEAF located at the main bus bar (FDS simulation MV-GE-20).....	B-4
Figure B-8 Results for a vertical-lift circuit breaker MV SWGR with a copper bus bar – 135 MJ HEAF located at the main bus bar (FDS simulation MV-GE-24).....	B-5
Figure B-9 Results for a vertical-lift circuit breaker MV SWGR with a copper bus bar – 169 MJ HEAF located at the main bus bar (FDS simulation MV-GE-28).....	B-5
Figure B-10 Results for a vertical-lift circuit breaker MV SWGR with a copper bus bar – 132 MJ HEAF located at the main bus bar (FDS simulation MV-GE-32).....	B-6
Figure B-11 Results for a vertical-lift circuit breaker MV SWGR with a copper bus bar – 233 MJ HEAF located at the main bus bar (FDS simulation MV-GE-36).....	B-6
Figure B-12 Results for a vertical-lift circuit breaker MV SWGR with a copper bus bar – 300 MJ HEAF located at the main bus bar (FDS simulation MV-GE-40).....	B-7

---

Figure B-13 Results for a vertical-lift circuit breaker MV SWGR with copper electrodes – 68 MJ HEAF located at the circuit breaker stabs (FDS simulation MV-GE-19) .....	B-7
Figure B-14 Results for a vertical-lift circuit breaker MV SWGR with copper electrodes – 135 MJ HEAF located at the circuit breaker stabs (FDS simulation MV-GE-23) .....	B-8
Figure B-15 Results for a vertical-lift circuit breaker MV SWGR with copper electrodes – 169 MJ HEAF located at the circuit breaker stabs (FDS simulation MV-GE-27) .....	B-8
Figure B-16 Results for a vertical-lift circuit breaker MV SWGR with copper electrodes – 132 MJ HEAF located at the circuit breaker stabs (FDS simulation MV-GE-31) .....	B-9
Figure B-17 Results for a vertical-lift circuit breaker MV SWGR with copper electrodes – 233 MJ HEAF located at the circuit breaker stabs (FDS simulation MV-GE-35) .....	B-9
Figure B-18 Results for a vertical-lift circuit breaker MV SWGR with copper electrodes – 300 MJ HEAF located at the circuit breaker stabs (FDS simulation MV-GE-39) .....	B-10
Figure B-19 Results for a vertical-lift circuit breaker MV SWGR with an aluminum bar – 68 MJ HEAF located at the PCCBB (load configuration) (FDS simulation MV-GE-2) .....	B-10
Figure B-20 Results for a vertical-lift circuit breaker MV SWGR with an aluminum bar – 135 MJ HEAF located at the PCCBB (load configuration) (FDS simulation MV-GE-5) .....	B-11
Figure B-21 Results for a vertical-lift circuit breaker MV SWGR with an aluminum bar – 169 MJ HEAF located at the PCCBB (load configuration) (FDS simulation MV-GE-8) .....	B-11
Figure B-22 Results for a vertical-lift circuit breaker MV SWGR with an aluminum bar – 132 MJ HEAF located at the PCCBB (load configuration) (FDS simulation MV-GE-11).....	B-12
Figure B-23 Results for a vertical-lift circuit breaker MV SWGR with an aluminum bar – 233 MJ HEAF located at the PCCBB (load configuration) (FDS simulation MV-GE-14) .....	B-12
Figure B-24 Results for a vertical-lift circuit breaker MV SWGR with an aluminum bar – 300 MJ HEAF located at the PCCBB (load configuration) (FDS simulation MV-GE-17) .....	B-13
Figure B-25 Results for a vertical-lift circuit breaker MV SWGR with a copper bar – 68 MJ HEAF located at the PCCBB (load configuration) (FDS simulation MV-GE-21) ...	B-13
Figure B-26 Results for a vertical-lift circuit breaker MV SWGR with a copper bar – 135 MJ HEAF located at the PCCBB (load configuration) (FDS simulation MV-GE-25) ...	B-14
Figure B-27 Results for a vertical-lift circuit breaker MV SWGR with a copper bar – 169 MJ HEAF located at the PCCBB (load configuration) (FDS simulation MV-GE-29) ...	B-14
Figure B-28 Results for a vertical-lift circuit breaker MV SWGR with a copper bar – 132 MJ HEAF located at the PCCBB (load configuration) (FDS simulation MV-GE-33) ...	B-15
Figure B-29 Results for a vertical-lift circuit breaker MV SWGR with a copper bar – 233 MJ HEAF located at the PCCBB (load configuration) (FDS simulation MV-GE-37) ...	B-15
Figure B-30 Results for a vertical-lift circuit breaker MV SWGR with a copper bar – 300 MJ HEAF located at the PCCBB (load configuration) (FDS simulation MV-GE-41) ...	B-16
Figure B-31 Results for a vertical-lift circuit breaker MV SWGR with an aluminum bar – 68 MJ HEAF located at the PCCBB (supply configuration) (FDS simulation MV-GE-3) .....	B-16

---

Figure B-32 Results for a vertical-lift circuit breaker MV SWGR with an aluminum bar – 135 MJ HEAF located at the PCCBB (supply configuration) (FDS simulation MV-GE-6) .....	B-17
Figure B-33 Results for a vertical-lift circuit breaker MV SWGR with an aluminum bar – 169 MJ HEAF located at the PCCBB (supply configuration) (FDS simulation MV-GE-9) .....	B-17
Figure B-34 Results for a vertical-lift circuit breaker MV SWGR with an aluminum bar – 132 MJ HEAF located at the PCCBB (supply configuration) (FDS simulation MV-GE-12) .....	B-18
Figure B-35 Results for a vertical-lift circuit breaker MV SWGR with an aluminum bar – 233 MJ HEAF located at the PCCBB (supply configuration) (FDS simulation MV-GE-15) .....	B-18
Figure B-36 Results for a vertical-lift circuit breaker MV SWGR with an aluminum bar – 300 MJ HEAF located at the PCCBB (supply configuration) (FDS simulation MV-GE-18) .....	B-19
Figure B-37 Results for a vertical-lift circuit breaker MV SWGR with a copper bar – 68 MJ HEAF located at the PCCBB (supply configuration) (FDS simulation MV-GE-22) .....	B-19
Figure B-38 Results for a vertical-lift circuit breaker MV SWGR with a copper bar – 135 MJ HEAF located at the PCCBB (supply configuration) (FDS simulation MV-GE-26) .....	B-20
Figure B-39 Results for a vertical-lift circuit breaker MV SWGR with a copper bar – 169 MJ HEAF located at the PCCBB (supply configuration) (FDS simulation MV-GE-30) .....	B-20
Figure B-40 Results for a vertical-lift circuit breaker MV SWGR with a copper bar – 132 MJ HEAF located at the PCCBB (supply configuration) (FDS simulation MV-GE-34) .....	B-21
Figure B-41 Results for a vertical-lift circuit breaker MV SWGR with a copper bar – 233 MJ HEAF located at the PCCBB (supply configuration) (FDS simulation MV-GE-38) .....	B-21
Figure B-42 Results for a vertical-lift circuit breaker MV SWGR with a copper bar – 300 MJ HEAF located at the PCCBB (supply configuration) (FDS simulation MV-GE-42) .....	B-22
Figure B-43 Results for a horizontal draw-out circuit breaker MV SWGR with copper electrodes – 68 MJ HEAF located at the circuit breaker stabs (FDS simulation MV-ABB-1) .....	B-22
Figure B-44 Results for a horizontal draw-out circuit breaker MV SWGR with copper electrodes – 135 MJ HEAF located at the circuit breaker stabs (FDS simulation MV-ABB-2) .....	B-23
Figure B-45 Results for a horizontal draw-out circuit breaker MV SWGR with copper electrodes – 169 MJ HEAF located at the circuit breaker stabs (FDS simulation MV-ABB-3) .....	B-23
Figure B-46 Results for a horizontal draw-out circuit breaker MV SWGR with copper electrodes – 132 MJ HEAF located at the circuit breaker stabs (FDS simulation MV-ABB-4) .....	B-24

---

Figure B-47 Results for a horizontal draw-out circuit breaker MV SWGR with copper electrodes – 233 MJ HEAF located at the circuit breaker stabs (FDS simulation MV-ABB-5) .....	B-24
Figure B-48 Results for a horizontal draw-out circuit breaker MV SWGR with copper electrodes – 300 MJ HEAF located at the circuit breaker stabs (FDS simulation MV-ABB-6) .....	B-25
Figure B-49 Results for a LV SWGR with an aluminum bus bar with a HEAF based on FEDB 50935 – HEAF located in a middle-height circuit breaker compartment (FDS simulation LV-BASE-1) .....	B-25
Figure B-50 Results for a LV SWGR with a copper bus bar with a HEAF based on FEDB 50935 – HEAF located in a middle-height circuit breaker compartment (FDS simulation LV-BASE-7) .....	B-26
Figure B-51 Results for a LV SWGR with an aluminum bus bar with a HEAF based on FEDB 50935 – HEAF located in a circuit breaker compartment at the top of the switchgear (FDS simulation LV-BASE-2) .....	B-26
Figure B-52 Results for a LV SWGR with a copper bus bar with a HEAF based on FEDB 50935 – HEAF located in a circuit breaker compartment at the top of the switchgear (FDS simulation LV-BASE-8) .....	B-27
Figure B-53 Results for a LV SWGR with an aluminum bus bar with a HEAF based on FEDB 50935 – HEAF located in a middle-height bus bar compartment (FDS simulation LV-BASE-3) .....	B-27
Figure B-54 Results for a LV SWGR with a copper bus bar with a HEAF based on FEDB 50935 – HEAF located in a middle-height bus bar compartment (FDS simulation LV-BASE-9) .....	B-28
Figure B-55 Results for a LV SWGR with an aluminum bus bar with a HEAF based on FEDB 50935 – HEAF located in a bus bar compartment at the top of the switchgear (FDS simulation LV-BASE-4) .....	B-28
Figure B-56 Results for a LV SWGR with a copper bus bar with a HEAF based on FEDB 50935 – HEAF located in a bus bar compartment at the top of the switchgear (FDS simulation LV-BASE-10) .....	B-29
Figure B-57 Results for a LV SWGR with an aluminum bus bar with a HEAF based on FEDB 50935 – HEAF initially located in a middle-height circuit breaker compartment and moves to the bus bar compartment at the same height (FDS simulation LV-BASE-5) .....	B-29
Figure B-58 Results for a LV SWGR with an aluminum bus bar with a HEAF based on FEDB 50935 – HEAF initially located in a circuit breaker compartment at the top of the switchgear and moves to the bus bar compartment at the same height (FDS simulation LV-BASE-6) .....	B-30
Figure B-59 Results for a straight run, steel duct NSBD with aluminum bus bars – 34 MJ HEAF (FDS simulation NSBD-1) .....	B-30
Figure B-60 Results for a straight run, steel duct NSBD with aluminum bus bars – 68 MJ HEAF (FDS simulation NSBD-2) .....	B-31
Figure B-61 Results for a straight run, steel duct NSBD with aluminum bus bars – 135 MJ HEAF (FDS simulation NSBD-3) .....	B-31
Figure B-62 Results for a straight run, steel duct NSBD with aluminum bus bars – 169 MJ HEAF (FDS simulation NSBD-4) .....	B-32

---

Figure B-63 Results for a straight run, steel duct NSBD with aluminum bus bars – 132 MJ HEAF (FDS simulation NSBD-5).....	B-32
Figure B-64 Results for a straight run, steel duct NSBD with aluminum bus bars – 233 MJ HEAF (FDS simulation NSBD-6).....	B-33
Figure B-65 Results for a straight run, steel duct NSBD with aluminum bus bars – 300 MJ HEAF (FDS simulation NSBD-7).....	B-33
Figure B-66 Results for a straight run, aluminum duct NSBD with aluminum bus bars – 34 MJ HEAF (FDS simulation NSBD-8).....	B-34
Figure B-67 Results for a straight run, aluminum duct NSBD with aluminum bus bars – 68 MJ HEAF (FDS simulation NSBD-9).....	B-34
Figure B-68 Results for a straight run, aluminum duct NSBD with aluminum bus bars – 135 MJ HEAF (FDS simulation NSBD-10).....	B-35
Figure B-69 Results for a straight run, aluminum duct NSBD with aluminum bus bars – 169 MJ HEAF (FDS simulation NSBD-11).....	B-35
Figure B-70 Results for a straight run, aluminum duct NSBD with aluminum bus bars – 233 MJ HEAF (FDS simulation NSBD-12).....	B-36
Figure B-71 Results for a straight run, aluminum duct NSBD with aluminum bus bars – 300 MJ HEAF (FDS simulation NSBD-13).....	B-36
Figure B-72 Results for a straight run, steel duct NSBD with copper bus bars – 34 MJ HEAF (FDS simulation NSBD-14).....	B-37
Figure B-73 Results for a straight run, steel duct NSBD with copper bus bars – 68 MJ HEAF (FDS simulation NSBD-15).....	B-37
Figure B-74 Results for a straight run, steel duct NSBD with copper bus bars – 135 MJ HEAF (FDS simulation NSBD-16).....	B-38
Figure B-75 Results for a straight run, steel duct NSBD with copper bus bars – 169 MJ HEAF (FDS simulation NSBD-17).....	B-38
Figure B-76 Results for a straight run, steel duct NSBD with copper bus bars – 132 MJ HEAF (FDS simulation NSBD-18).....	B-39
Figure B-77 Results for a straight run, steel duct NSBD with copper bus bars – 233 MJ HEAF (FDS simulation NSBD-19).....	B-39
Figure B-78 Results for a straight run, steel duct NSBD with copper bus bars – 300 MJ HEAF (FDS simulation NSBD-20).....	B-40
Figure B-79 Results for a straight run, aluminum duct NSBD with copper bus bars – 34 MJ HEAF (FDS simulation NSBD-21).....	B-40
Figure B-80 Results for a straight run, aluminum duct NSBD with copper bus bars – 68 MJ HEAF (FDS simulation NSBD-22).....	B-41
Figure B-81 Results for a straight run, aluminum duct NSBD with copper bus bars – 135 MJ HEAF (FDS simulation NSBD-23).....	B-41
Figure B-82 Results for a straight run, aluminum duct NSBD with copper bus bars – 169 MJ HEAF (FDS simulation NSBD-24).....	B-42
Figure B-83 Results for a straight run, aluminum duct NSBD with copper bus bars – 132 MJ HEAF (FDS simulation NSBD-25).....	B-42
Figure B-84 Results for a straight run, aluminum duct NSBD with copper bus bars – 233 MJ HEAF (FDS simulation NSBD-26).....	B-43

---

Figure B-85 Results for a straight run, aluminum duct NSBD with copper bus bars – 300 MJ HEAF (FDS simulation NSBD-27).....	B-43
Figure B-86 Results for an aluminum duct NSBD elbow with aluminum bus bars – 68 MJ HEAF (FDS simulation NSBD-52).....	B-44
Figure B-87 Results for an aluminum duct NSBD elbow with aluminum bus bars – 135 MJ HEAF (FDS simulation NSBD-53).....	B-44
Figure B-88 Results for an aluminum duct NSBD elbow with aluminum bus bars – 169 MJ HEAF (FDS simulation NSBD-54).....	B-45
Figure B-89 Results for an aluminum duct NSBD elbow with aluminum bus bars – 132 MJ HEAF (FDS simulation NSBD-55).....	B-45
Figure B-90 Results for an aluminum duct NSBD elbow with aluminum bus bars – 233 MJ HEAF (FDS simulation NSBD-56).....	B-46
Figure B-91 Results for an aluminum duct NSBD elbow with aluminum bus bars – 300 MJ HEAF (FDS simulation NSBD-57).....	B-46
Figure B-92 Results for a steel duct NSBD tee with aluminum bus bars – 68 MJ HEAF (FDS simulation NSBD-28) .....	B-47
Figure B-93 Results for a steel duct NSBD tee with aluminum bus bars – 135 MJ HEAF (FDS simulation NSBD-29) .....	B-47
Figure B-94 Results for a steel duct NSBD tee with aluminum bus bars – 169 MJ HEAF (FDS simulation NSBD-30) .....	B-48
Figure B-95 Results for a steel duct NSBD tee with aluminum bus bars – 132 MJ HEAF (FDS simulation NSBD-31) .....	B-48
Figure B-96 Results for a steel duct NSBD tee with aluminum bus bars – 233 MJ HEAF (FDS simulation NSBD-32) .....	B-49
Figure B-97 Results for a steel duct NSBD tee with aluminum bus bars – 300 MJ HEAF (FDS simulation NSBD-33) .....	B-49
Figure B-98 Results for an aluminum duct NSBD tee with aluminum bus bars – 68 MJ HEAF (FDS simulation NSBD-34).....	B-50
Figure B-99 Results for an aluminum duct NSBD tee with aluminum bus bars – 135 MJ HEAF (FDS simulation NSBD-35).....	B-50
Figure B-100 Results for an aluminum duct NSBD tee with aluminum bus bars – 169 MJ HEAF (FDS simulation NSBD-36).....	B-51
Figure B-101 Results for an aluminum duct NSBD tee with aluminum bus bars – 132 MJ HEAF (FDS simulation NSBD-37).....	B-51
Figure B-102 Results for an aluminum duct NSBD tee with aluminum bus bars – 233 MJ HEAF (FDS simulation NSBD-38).....	B-52
Figure B-103 Results for an aluminum duct NSBD tee with aluminum bus bars – 300 MJ HEAF (FDS simulation NSBD-39).....	B-52
Figure B-104 Results for a steel duct NSBD tee with copper bus bars – 68 MJ HEAF (FDS simulation NSBD-40) .....	B-53
Figure B-105 Results for a steel duct NSBD tee with copper bus bars – 135 MJ HEAF (FDS simulation NSBD-41) .....	B-53
Figure B-106 Results for a steel duct NSBD tee with copper bus bars – 169 MJ HEAF (FDS simulation NSBD-42) .....	B-54

---

Figure B-107 Results for a steel duct NSBD tee with copper bus bars – 132 MJ HEAF (FDS simulation NSBD-43) .....	B-54
Figure B-108 Results for a steel duct NSBD tee with copper bus bars – 233 MJ HEAF (FDS simulation NSBD-44) .....	B-55
Figure B-109 Results for a steel duct NSBD tee with copper bus bars – 300 MJ HEAF (FDS simulation NSBD-45) .....	B-55
Figure B-110 Results for an aluminum duct NSBD tee with copper bus bars – 68 MJ HEAF (FDS simulation NSBD-46).....	B-56
Figure B-111 Results for an aluminum duct NSBD tee with copper bus bars – 135 MJ HEAF (FDS simulation NSBD-47).....	B-56
Figure B-112 Results for an aluminum duct NSBD tee with copper bus bars – 169 MJ HEAF (FDS simulation NSBD-48).....	B-57
Figure B-113 Results for an aluminum duct NSBD tee with copper bus bars – 132 MJ HEAF (FDS simulation NSBD-49).....	B-57
Figure B-114 Results for an aluminum duct NSBD tee with copper bus bars – 233 MJ HEAF (FDS simulation NSBD-50).....	B-58
Figure B-115 Results for an aluminum duct NSBD tee with copper bus bars – 300 MJ HEAF (FDS simulation NSBD-51).....	B-58
Figure D-1 Summary of open-box calorimeter energy vs. electrical energy for 1-30 kA, 0.5 inch and 1 inch diameter copper and aluminum bus bars.....	D-2
Figure D-2 Pacific Power 3-phase continuous AC power source for scaled arc testing .....	D-3
Figure D-3 Schematic of scaled test method .....	D-4
Figure D-4 Images of copper calorimeter enclosure and scaled three-phase bus bars .....	D-5
Figure D-5 Oscilloscope collection of three-phase voltage and current (left), internal view of scaled three-phase copper and aluminum bus bars within copper calorimeter (upper right) and schematic of commercial three-phase switchgear bus bar configuration (lower right).....	D-6
Figure D-6 A three-phase, 544 V <sub>AC</sub> , 858 ms duration arc shown on oscilloscope produced a sustained 108 A arc current on all phases (left), image of three-phase electrical connections (center) and measured heat rise versus time for calorimeter thermocouples (blue and orange traces) and at end cap (gray). The temperature rise $\Delta T$ is taken as the average of the blue and orange temperatures .....	D-7
Figure D-7 Images of scaled aluminum bus bar before and after sustained three-phase arc, including collected molten particles (top); copper bus bar samples before (bottom left) and after a sustained arc, including collected droplets (bottom right).....	D-8
Figure D-8 Summary of measured temperature rise $\Delta T$ versus arc duration for all aluminum and copper arc experiments .....	D-9
Figure D-9 Calculated calorimeter heat rise plotted vs. electrical energy input .....	D-9
Figure D-10 Image of pre-arc copper bus bar and shorting wire (left), representative collection of post-arc bus bars and collected spherical particles (center) and tabulation of % metal melted and maximum percent vaporized particles (right).....	D-10
Figure D-11 Plot of percent melted and maximum percent metal vaporized versus arc duration .....	D-11

---

Figure D-12 Histogram of size in $\mu\text{m}$ of 50 aluminum bus bar-evolved particles; the average particle size of these evolved aluminum particles was $8.96 \mu\text{m}$ .....	D-12
Figure D-13 Histogram of volume in cubic $\mu\text{m}$ of 50 aluminum bus bar-evolved particles; the average particle volume calculated for evolved aluminum particles was $880 \text{ cubic } \mu\text{m}$ .....	D-12
Figure D-14 Representative SEM image and size measurements of aluminum bus bar-evolved particles; the average particle size for these evolved aluminum particles was $8.96 \mu\text{m}$ .....	D-13
Figure D-15 Representative EDS analysis of a three-phase arc-evolved aluminum particle; from the peak ratios of aluminum, magnesium, and oxygen, an estimated degree of oxidation of 73% was calculated .....	D-13
Figure D-16 SEM of $600 V_{AC}$ arc-evolved, $0.02 - 1.2 \mu\text{m}$ copper particles.....	D-14
Figure D-17 Histogram of particle sizes of 50 particles evolved from $600 V_{AC}$ arcs, displaying a median particle size of $0.225 \mu\text{m}$ and median particle volume of $0.056 \text{ mm}^3$ .....	D-15
Figure D-18 EDS spectrum of $600 V_{AC}$ arc-evolved, $0.02-2 \mu\text{m}$ copper particles, displaying oxygen and copper peaks, with an oxygen to copper ratio of 0.28 .....	D-15
Figure D-19 EDS spectrum of $600 V_{AC}$ arc-evolved, $0.02 - 2 \mu\text{m}$ copper particles, displaying oxygen and copper peaks, with an oxygen to copper ratio of 0.51 .....	D-16



# LIST OF TABLES

---

Table ES-1-1 Summary of medium-voltage switchgear energetic ZOI ranges .....	xxxii
Table ES-1-2 Summary of low-voltage switchgear energetic ZOI ranges .....	xxxii
Table ES-1-3 Summary of non-segregated bus duct energetic ZOI ranges .....	xxxii
Table 3-1 Summary of 2019 open-box tests [4] and the 2018 full-scale medium-voltage switchgear tests used to assess electrode mass loss [6].....	3-6
Table 3-2 Particle size distribution for mass lost from different electrodes (see Appendix D) .....	3-9
Table 4-1 Summary of 2018 medium-voltage switchgear experiments [6] .....	4-2
Table 4-2 FDS versus observed electrical enclosure breach times for the 2018 MV SWGR experiments [6] .....	4-5
Table 4-3 Model bias and normalized standard deviation for different temperature data point groupings [6].....	4-10
Table 5-1 Matrix of MV SWGR HEAF FDS simulations.....	5-11
Table 5-2 Matrix of LV SWGR HEAF FDS simulations.....	5-18
Table 5-3 Matrix of NSBD HEAF FDS simulations .....	5-24
Table 6-1 Summary of MV SWGR energetic ZOIs .....	6-34
Table 6-2 Summary of LV SWGR energetic ZOIs .....	6-51
Table 6-3 Summary of NSBD energetic ZOIs.....	6-74
Table 7-1 Summary of MV SWGR energetic ZOI ranges .....	7-3
Table 7-2 Summary of LV SWGR energetic ZOI ranges .....	7-3
Table 7-3 Summary of NSBD energetic ZOI ranges.....	7-3
Table A-1 Medium voltage HEAF events with fault currents.....	A-2
Table A-2 Fault currents at various times for a generator-fed HEAF event (December 2020) .....	A-4
Table A-3 Low voltage HEAF events with fault currents.....	A-7
Table A-4 Sampling of low-voltage fault clearing times and fault energies.....	A-9
Table A-5 Arc power profile total energy.....	A-12
Table C-1 FDS input file simulation matrix.....	C-1



# EXECUTIVE SUMMARY

---

**PRIMARY AUDIENCE:** Fire protection, electrical, and probabilistic risk assessment (PRA) engineers conducting or reviewing fire risk assessments related to high energy arcing faults (HEAFs).

**SECONDARY AUDIENCE:** Engineers, reviewers, utility managers, and other stakeholders who conduct, review, or manage fire protection programs and need to understand the underlying technical basis for the hazards associated with HEAFs.

## KEY RESEARCH QUESTION

At what distance from a HEAF (in an electrical enclosure or non-segregated bus duct) will targets be exposed to conditions that exceed their failure threshold criteria?

## RESEARCH OVERVIEW

The U.S. Nuclear Regulatory Commission (NRC) Office of Nuclear Regulatory Research and the Electric Power Research Institute (EPRI) HEAF working group (WG) is tasked with improving the methodology for assessing HEAF hazards at nuclear power plants. A major part of this effort includes updating the energetic zone of influence (ZOI). Hazard modeling with Fire Dynamics Simulator (FDS) is used in conjunction with target fragility limits to determine the energetic ZOIs associated with HEAFs. There are three parts to this research effort:

- The development of the geometric computational fluid dynamic (CFD) models, key assumptions, and input data used in FDS to predict the thermal exposure of targets in the vicinity of a HEAF.
- The benchmarking and validation of FDS using data from full-scale testing and operational experience (OE).
- The development of a simulation matrix of runs that encompasses a broad range of fault current magnitude and duration, electrode composition, and fault locations within each class of equipment.

FDS simulations of HEAFs are performed for three classes of equipment: low-voltage switchgear, medium-voltage switchgear, and medium-voltage non-segregated bus ducts. Simulation variables included the fault current magnitude and duration, arc location, electrode composition, and type of equipment. The result is a detailed tabulation of the energetic ZOIs predicted by FDS for each HEAF simulation. These ZOIs are used as input for future PRA method development. The resulting energetic ZOI ranges are summarized in Table ES-1 for medium-voltage switchgear, Table ES-2 for low-voltage switchgear, and Table ES-3 for non-segregated bus ducts.

**Table ES-1-1**  
**Summary of medium-voltage switchgear energetic ZOI ranges**

Switchgear enclosure face	Energetic ZOI (m) for a 15 MJ/m <sup>2</sup> target fragility	Energetic ZOI (m) for a 30 MJ/m <sup>2</sup> target fragility
Back	0 – 1.13	0 – 0.76
Left	0 – 1.24	0 – 0.92
Right	0 – 1.24	0 – 0.92
Top	0 – 1.01	0 – 0.58
Front	0 – 1.31	0 – 0.97

**Table ES-1-2**  
**Summary of low-voltage switchgear energetic ZOI ranges**

Switchgear enclosure face	Energetic ZOI (m) for a 15 MJ/m <sup>2</sup> target fragility	Energetic ZOI (m) for a 30 MJ/m <sup>2</sup> target fragility
Back	0 – 0.17	0
Left	0	0
Right	0 – 0.9	0 – 0.59
Top	0 – 0.84	0 – 0.53
Front	0	0

**Table ES-1-3**  
**Summary of non-segregated bus duct energetic ZOI ranges**

Non-segregated bus duct enclosure face	Energetic ZOI (m) for a 15 MJ/m <sup>2</sup> target fragility	Energetic ZOI (m) for a 30 MJ/m <sup>2</sup> target fragility
Back	0 – 1.32	0 – 0.86
Front	0 – 1.32	0 – 0.86
Right	0.41 – 1.31	0.21 – 0.84
Above	0 – 1.39	0 – 0.93
Below	0 – 1.37	0 – 0.92

## KEY FINDINGS

This research resulted in a number of insights related to the HEAF hazard phenomena. These are summarized as follows:

- The difference between the energetic ZOIs from HEAFs with aluminum electrodes and HEAFs with copper electrodes is insignificant for all equipment classes (Sections 6.1.3.3, 6.2.2.2, and 6.3.2.2).
- The dominant parameter affecting the energetic ZOIs in medium-voltage switchgear is the total arc energy.

- 
- A secondary parameter for medium-voltage switchgear is the circuit breaker orientation (vertical-lift style circuit breaker or horizontal draw-out style circuit breaker) (Section 6.1.3.3).
    - The side energetic ZOIs are smaller for vertical-lift circuit breaker style medium-voltage switchgear as compared to horizontal draw-out circuit breaker style medium-voltage switchgear.
    - In addition, for vertical-lift circuit breaker style switchgear in the supply configuration, there is no vertical (top) energetic ZOI component. The load configuration vertical-lift circuit breaker style switchgear and the horizontal draw-out style circuit breaker switchgear have comparable top energetic ZOIs (Section 6.1.3.3).
  - The energetic ZOIs for low-voltage switchgear are smaller than Appendix M of NUREG/CR-6850. The energetic ZOIs for low-voltage switchgear are documented in Table 6-2 for 15 MJ/m<sup>2</sup> and 30 MJ/m<sup>2</sup> target fragilities (Section 6.2.2.3).
  - The energetic ZOIs for medium-voltage switchgear and bus ducts are smaller than the existing guidance for some configurations and directions, but larger for others. The energetic ZOIs for medium-voltage switchgear are documented in Table 6-1 for 15 MJ/m<sup>2</sup> and 30 MJ/m<sup>2</sup> target fragilities (Section 6.1.3.4). Similarly, the energetic ZOIs for non-segregated bus ducts are documented in Table 6-3 for 15 MJ/m<sup>2</sup> and 30 MJ/m<sup>2</sup> target fragilities (Section 6.3.2.3).
  - The composition of bus duct housing (steel versus aluminum) has a significant impact on the energetic ZOIs. HEAFs in aluminum bus ducts have energetic ZOIs that are, on average, 0.15 m larger than those in steel bus ducts (Section 6.3.2.2).
  - The energetic ZOIs for low- and medium-voltage switchgear are sensitive to the equipment geometry and circuit breaker orientation. Bus ducts, with comparatively simple geometries, do not display this sensitivity (Sections 6.1.3.3, 6.2.2.2, and 6.3.2.2).

## WHY THIS MATTERS

This report provides energetic ZOI dimensions to assist researchers, analysts, and stakeholders in evaluating the HEAF hazard. The conclusions provided will support future advances in the methods, tools, and data to assess the HEAF hazard in nuclear facilities.

## HOW TO APPLY RESULTS

Engineers and scientists should focus on the tabulated summaries of the energetic ZOIs in sections 6.1.3.4, 6.2.2.3, and 6.3.2.3.

## LEARNING AND ENGAGEMENT OPPORTUNITIES

Users of this report may be interested in periodic stakeholder engagement opportunities with EPRI and/or NRC on this topic.

**EPRI CONTACT:** Marko Randelovic, Principal Technical Leader, [mrandelovic@epri.com](mailto:mrandelovic@epri.com)

**NRC CONTACT:** Kenneth Hamburger, Fire Protection Engineer, [Kenneth.Hamburger@nrc.gov](mailto:Kenneth.Hamburger@nrc.gov)

**PROGRAMS:** Nuclear Power, P41; and Risk and Safety Management, P41.07.01

**IMPLEMENTATION CATEGORY:** Reference – Technical Basis



# CITATIONS

---

This report was prepared by the following:

Electric Power Research Institute  
3420 Hillview Avenue  
Palo Alto, CA 94304

Principal Investigators  
M. Randelovic  
T. Short  
A. Lindeman

Under contract to EPRI:

Jensen Hughes  
3610 Commerce Drive, Suite 817  
Baltimore, MD 21227

Principal Investigators  
J. Floyd  
D. Lovelace  
S. Hunt

Fleischer Consultants, LLC  
Lansdale, PA 19446

Principal Investigator  
K. Fleischer

U.S. Nuclear Regulatory Commission  
Washington, D.C. 20555-0001

Principal Investigator  
K. Hamburger

Under contract to NRC:

Sandia National Laboratories  
1515 Eubank SE  
Albuquerque, NM 87123

Principal Investigators  
C. LaFleur  
A. Glover  
P. Clem

National Institute of Standards and Technology  
100 Bureau Dr.  
Gaithersburg, MD 20899

Principal Investigator  
K. McGrattan

This report describes research sponsored jointly by the U.S. Nuclear Regulatory Commission's (NRC's) Office of Nuclear Regulatory Research (RES) and the Electric Power Research Institute (EPRI) performed under a formal Memorandum of Understanding (MOU).

---

This publication is a corporate document that should be cited in the literature in the following manner:

*Determining the Zone of Influence for High Energy Arcing Faults Using Fire Dynamics Simulator*. U.S. Nuclear Regulatory Commission, Office of Nuclear Regulatory Research (RES), Washington, DC, and EPRI, Palo Alto, CA: 2022. RIL 2022-09 and EPRI 3002025123.

The report should be cited internally in NRC documents in this way:

Determining the Zone of Influence for High Energy Arcing Faults Using Fire Dynamics Simulator, RIL 2022-09, ([EPRI] 3002025123), November 2022.



## **ACKNOWLEDGMENTS**

---

The authors would like to thank Engineering Planning and Management (EPM) and the Nuclear Energy institute (NEI) for providing valuable feedback on the draft report. A record of the draft report, Federal Register notice, and the comments received can be found in the NRC's Agencywide Documents Access and Management System (ADAMS) under accession number ML22259A188.



# ACRONYMS

---

ASTM	ASTM International, formerly American Society for Testing and Materials
CFD	computational fluid dynamics
CT	current transformer
CVT	current voltage transformer
DNS	direct numerical simulation
EDS	electrical distribution system
EMI	electromagnetic interference
EPRI	Electric Power Research Institute
FCT	fault clearing time
FEDB	Fire Events Database
FDS	Fire Dynamics Simulator
GE	General Electric
GSU	generator step-up
HEAF	high energy arcing fault
IEEE	Institute of Electrical and Electronics Engineers
KEMA	Keiring van Ekektrotechnische Materialen te Arnhem
LES	large eddy simulation
LV	low-voltage
MOU	memorandum of understanding
MV	medium-voltage
NASA	National Aeronautics and Space Administration
NEA	Nuclear Energy Agency
NIST	National Institute of Standards and Technology
NPP	nuclear power plant
NRC	Nuclear Regulatory Commission
NSBD	non-segregated bus duct
OB	open box (low-voltage)

---

OBMV	open box (medium-voltage)
OE	operational experience
OECD	Organisation for Economic Cooperation and Development
PCCBB	primary cable compartment bus bar
PIRT	phenomena identification and ranking table
PRA	probabilistic risk assessment
PTC	plate thermometer
RES	NRC's Office of Nuclear Regulatory Research
RIL	Research Information Letter
RMS	root mean square
SEM	scanning electron microscopy
SNL	Sandia National Laboratories
SWGR	switchgear
TCC	time current characteristic
TP	thermoplastic
TS	thermoset
UAT	unit auxiliary transformer
VLES	very large eddy simulation
WG	working group
ZOI	zone of influence

# 1

## INTRODUCTION

---

### 1.1 Background

High energy arcing faults (HEAFs) are hazardous events where an electrical arc leads to the rapid release of energy in the form of heat, vaporized metal, and mechanical force. The existing methodology for modeling switchgear and load center HEAFs in fire probabilistic risk assessment (PRA) is documented in Appendix M of NUREG/CR-6850 [1]. The methodology for HEAFs in bus ducts and iso-phase bus ducts is contained in Section 7 of NUREG/CR-6850 Supplement 1, *Fire Probabilistic Risk Assessment Methods Enhancements* [2]. Both reports provide energetic zone of influence (ZOI) estimates based on well-documented United States nuclear power plant (NPP) operational experience (OE).

Under a memorandum of understand (MOU), the Nuclear Regulatory Commission Office of Research (NRC-RES) and the Electric Power Research Institute (EPRI) formed a joint HEAF working group (WG) to advance the state of practice. The HEAF WG is chartered to update the methods, tools, and data to support realistic estimates of HEAF risk in industry fire PRAs based on experimental data, operating experience, and engineering judgment.

To develop an updated PRA methodology, several intermediate steps were necessary, including:

- Survey the United States nuclear fleet to determine presence of aluminum and transformer backup fault clearing times. Insights from this effort are documented in EPRI 3002020692, *Survey and Analysis of U.S. Nuclear Industry Relative to High Energy Arcing Faults in the Presence of Aluminum* [3].
- Perform small, medium, and full-scale physical tests. Small-scale testing characterized the morphology and oxidation states of aluminum particles (see Appendix D). Medium-scale “open-box” experiments characterized the spectral emission of the arc and conductivity of the arc ejecta [4]. Full-scale experiments [5-9] provided data on the enclosure breach time and the pressure effects on the enclosure and serve as a benchmark for the predictions of National Institute of Standards and Technology (NIST’s) Fire Dynamics Simulator (FDS), a computational fluid dynamics (CFD) model.
- Evaluate target fragility. This two-part effort involved physical testing and analysis to determine the conditions when targets external to the HEAF are likely to be damaged [10].
- Construct and validate the FDS models for simulating HEAF effects (the subject of this report). The purpose of this model is to calculate the incident energy at target locations with respect to a HEAF across a wide variety of configurations (e.g., fault duration, arc voltage, arcing fault current, equipment geometry, and electrode composition).

- Develop PRA methodology. This step combines the insights concluded in preceding efforts and provides a methodology to model HEAFs in fire PRA. This task includes an evaluation of United States NPP operating experience, updated fire ignition frequencies and manual non-suppression probabilities, and provides the structure to model the potential outcomes of a HEAF given the ignition source and location within the electrical distribution system (EDS).

## 1.2 Overview of the Energetic Phase of the HEAF Zone of Influence

The energetic phase of the HEAF ZOIs provided in NUREG/CR-6850 [1] and NUREG/CR-6850 Supplement 1 [2] include one ZOI for switchgear and load centers, one ZOI for non-segregated bus ducts, and one ZOI for isophase bus ducts. The energetic phase of the ZOIs are estimated based on a review of damage from previous HEAF events (neither testing nor specific HEAF fragility criteria existed when References 1 and 2 were published). This set of one-size-fits all ZOIs does not account for arc duration, arc power, or the impact of arc location and enclosure configuration.

During HEAF target fragilities development [10] additional characterization of HEAF elements were performed include a detailed review of EPRI's survey of industry transformer backup fault clearing times [3], a review of more recent HEAF events [11, 12], and analysis of data from testing [4-9]. From these reviews, the working group concluded that the exposure to a target is dependent on the duration, power, and location of an arc. It was not clear, however, whether the electrode composition (i.e., copper or aluminum) was a significant factor.

While the various full-scale testing efforts provided a wealth of data for generating insights, the limited number of tested configurations (geometries, initial conditions, material type) and the limited instrumentation per test (for the objective of determining the energetic phase of the ZOI), required CFD modeling to provide quantitative outputs to capture configurations that were not tested but present in the majority of NPPs in the United States [3].

## 1.3 Objectives

The objectives of this report are to document the development of FDS input files [13-17] to calculate the thermal exposure at specific locations for targets exposed to a HEAF, validate and benchmark the FDS models against data from experiments, and document the results. A matrix of configurations varying the arc duration, arc power, arc location, electrode composition, and type of equipment (geometry and construction) are simulated. The end result is a detailed tabulation of the energetic ZOIs for each simulation in the matrix.

## 1.4 Scope

The scope of the modeling task is to develop a dataset of energetic ZOIs that encompasses a broad range of potential HEAFs. These ZOIs are used as input to develop consensus ZOIs for the PRA methodology documented in a subsequent report.

# 2

## HEAF DESCRIPTION AND FDS CAPABILITIES

---

The section provides a description of a HEAF and an overview of FDS and its capabilities to model the effects of a HEAF. The review of HEAF events is performed for the identification of the major phenomena and initial/boundary conditions impacting the modeling of HEAF phenomena. The FDS overview reviews the basic capabilities and assumptions in FDS for the simulation development.

### 2.1 HEAF Description

A HEAF begins with a weakness in the electrical distribution system components that results in a fault that persists until it is cleared by the removal of the power source. The HEAF will persist until either the current feeding the fault is terminated by tripping the overcurrent protection (circuit breakers, fuses, etc.) or the arc self-extinguishes which can result from a decay in current and/or voltage feeding the fault or an inability to sustain an arc given the geometric and material configuration present in the faulted equipment. The HEAF location and the arc power profile are not phenomena that FDS can predict.

When the arc first initiates, there is a pressure wave that results from the sudden release of energy from the arc. In OE and in testing, this pressure wave has opened enclosure access doors and fire compartment doors [18, 19]. As discussed in Section 2.3.1, this pressure wave cannot be modeled by FDS and is not in scope of this report. The impacts of the pressure wave on the fire risk are assumed by the HEAF WG as having negligible impact on PRA targets; therefore, the lack of FDS capability to model the pressure wave is considered acceptable by the HEAF WG (see Appendix E).

The electromagnetic fields present in the faulted equipment and associated bus bars may result in the arc moving from its initial location. This is not a phenomenon that FDS can predict. The location of the arcs (replicated from the OE) in the FDS model has been selected to provide representative incident energies at target locations and includes several scenarios in which the arc is modeled in two locations (i.e., relocated); therefore, the lack of FDS capability to model the relocation of the arcs is considered acceptable by the HEAF WG (see Section 2.3.3).

The main hazards of a HEAF are the energy released by the arc, which is dominated by thermal radiation and, to a lesser extent, the oxidation of vaporized bus bar metal material. There are two primary effects associated with these hazards that impact the exposure to targets outside the enclosure. First, at the location where the arc attaches to the electrodes inside the enclosure, temperatures can exceed the boiling point of the electrode metal. This will lead to electrode mass loss in the form of metal vapor and droplets of molten metal. The high temperatures that develop inside the enclosure and the resistive heating from the current flow will act to further increase the electrode temperature and mass loss rate during the arcing period. Prior to a HEAF, the electrodes are normally coated with a thin layer of metal oxide. The release of metal vapor and

liquid metal droplets will expose unoxidized metal in a configuration with a high surface area. When exposed to oxygen, the metal will undergo exothermic oxidation reactions which add to the overall energy released during the HEAF. The fraction of metal that oxidizes is a function of the droplet size and the fraction of metal that transitions to vapor.

The second effect impacting the target exposure is the rapid increase in the internal temperature of the enclosure. The resulting thermal expansion will result in outflow from any available vent path, including fixed vent openings present for normal heat dissipation as well as leakage through gaps in the enclosure's external bolted covers. High internal gas temperature and direct radiation from the arc will also heat the external walls of the enclosure. If the arcing fault duration is long enough, portions of the external walls may develop openings or fail (i.e., breach) due to melting and/or tearing from loss of yield strength. Once there is a breach in the enclosure walls, a high-temperature outflow will occur through the opening. Targets near the opening may be enveloped by the outflow and targets with a direct line of site through the opening to the arc will be directly exposed to thermal radiation from the arc.

The HEAF hazard does not terminate immediately after the arc is extinguished. Outflow leaving the enclosure will take time to dissipate. Additionally, the remaining enclosure surfaces near the arc location will be very hot and serve as a source of radiant heat that will continue to expose targets. Both of these will rapidly decay following arc extinguishment. In addition, an ensuing fire can develop within the switchgear or load centers. The analysis of the ensuing fire is outside the capabilities of FDS and is out of scope for this report.

## 2.2 HEAF ZOI Components

### 2.2.1 MV SWGR and LV SWGR ZOIs

Medium-voltage (MV) switchgear (SWGR) and low-voltage (LV) SWGR HEAFs are modeled with two distinct phases: 1) the energetic phase and 2) the ensuing fire. Figure 2-1 depicts the energetic ZOI typical of short and long fault clearing times. The ensuing fire is modeled with a 98th percentile peak heat release rate (with its own defined ZOI associated with the thermal radiation from the flame and the fire plume). Figure 2-2 depicts a typical ensuing fire ZOI.

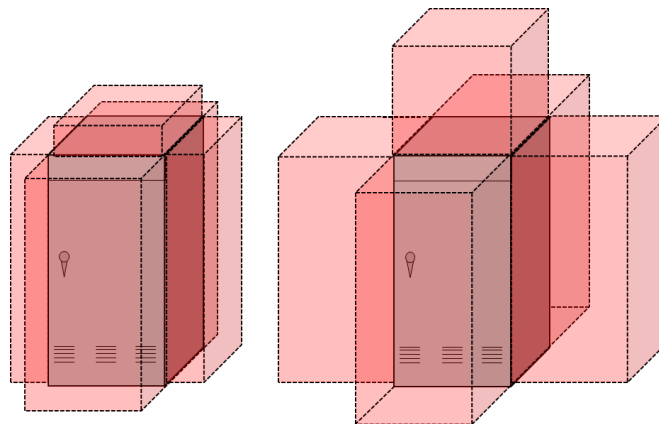


**Figure 2-1**  
Energetic phase of the HEAF ZOI: left representative of shorter fault clearing times, right representative of longer fault clearing times (figures not to scale, ZOI subject to the target fragilities and fault characteristics)

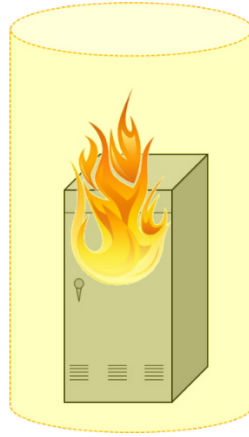


**Figure 2-2**  
**Post-HEAF ensuing fire ZOI (figure not to scale, ZOI subject to the size of fire calculated by analyst and consideration of secondary combustibles)**

The energetic phase and the ensuing fire ZOIs are not necessarily equal. For short fault clearing times, the ensuing fire ZOI may be larger than the energetic ZOI. For longer fault clearing times, some or all components of the energetic ZOI may be larger than the ensuing fire ZOI. The ZOIs calculated in this report correspond to the energetic phase of the HEAF.

### 2.2.2 NSBD ZOIs

HEAFs in NSBDs are also treated with two distinct components: 1) the energetic phase and 2) the waterfall. The energetic ZOI is determined using FDS results (e.g., using the same process as MV SWGR and LV SWGR). This energetic NSBD ZOI is applied along the bus duct at the location where the fault is postulated as depicted in Figure 2-3. The waterfall component addresses the exposure to vulnerable equipment located below the bus duct faulted location (see Figure 2-3). The waterfall component accounts for heated portions of the bus duct, slag, and heated particles dropping onto equipment under the bus duct. The waterfall is not evaluated further in this report.

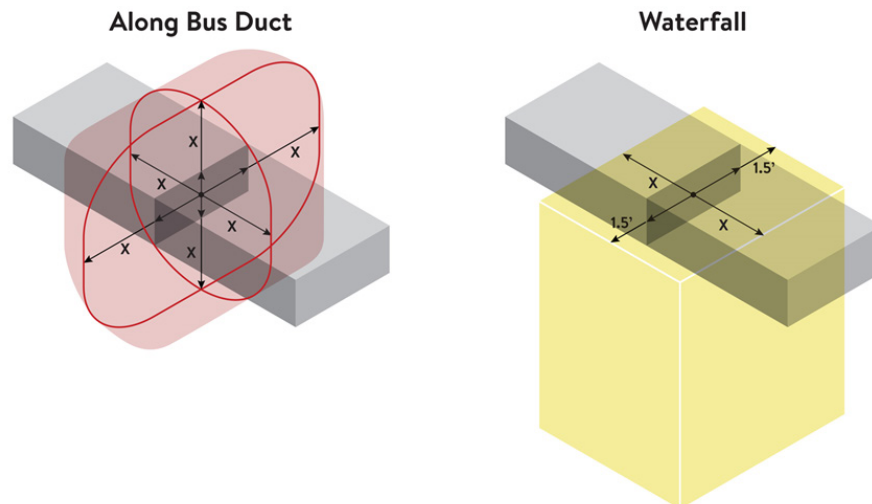


**Figure 2-3**  
**NSBD ZOI showing energetic (red shaded) and waterfall (yellow box) components**

## 2.3 Fire Dynamics Simulator Capabilities Applicable to HEAF Phenomena

FDS is a computational fluid dynamics (CFD) model that has been under development for approximately 30 years by a multinational team led by the National Institute of Standards and Technology (NIST) [13-17]. The physical sub-models within FDS and the overall solution calculated by FDS is primarily developed to support modeling fires within compartments. However, FDS is a general purpose CFD model, and its use is not restricted to modeling enclosure fires or fires in general. FDS has undergone extensive verification and validation [15, 16, 20] for a wide range of fire-related applications, though these applications do not include modeling the effects of HEAFs.

A CFD model numerically solves the Navier-Stokes equations. The Navier-Stokes equations are a set of coupled, partial differential equations that describe the three-dimensional mass, momentum, and energy conservation of fluids over time. Except for some simple cases, the Navier-Stokes equations do not have an analytical solution and CFD models often make some simplifying assumptions to reduce the computational expense of solving the equations. Since the Navier-Stokes equations only describe fluid motion, CFD fire models need other physical sub-models for combustion, radiation, surface heat transfer, and other fire-related phenomena.

### 2.3.1 Primary FDS Model Assumptions

FDS has two primary assumptions that underlie all uses of FDS. The first assumption is that the equation of state (relationship between temperature, pressure, and density) is the ideal gas law. This means that FDS cannot model the flow of fluids in the liquid state, only the gaseous state.

The second is the assumption of low-speed flow. A key component of numerically solving the Navier-Stokes equations is determining the pressure field, as pressure gradients drive fluid flow. High-speed flows (i.e., flows having a Mach number over 0.3) introduce compressibility effects such as shock waves. This assumption means that FDS cannot model explosions or other events where pressure waves must be resolved, as the low-speed assumption means that pressure waves are filtered out of the equations solved by FDS. Although fire-driven flows are normally considered low-speed flow in terms of compressibility effects, flows associated with HEAFs may have velocities that are comparable to the FDS low-speed limit. However, pressure waves (shocks) and compressibility effects are expected to be minor given that target exposure is dominated by thermal radiation and, to a lesser extent, the surrounding gas temperatures, which justifies the use of the low-speed flow assumption. Appendix E describes the WG assessment of pressure effects on targets, which supports the use of a low-speed flow modeling approach.

Another major assumption in FDS is the mode of operation. FDS can run in two primary modes: direct numerical simulation (DNS) and large eddy simulation (LES).

- For DNS, the grid size needs to be small enough to directly resolve turbulence and the diffusion of gas species into and out of combusting regions. This requires grid sizes of a millimeter or less and is not practical for engineering scale calculations.

- For LES, larger grid cells can be used and the effects of turbulence occurring at smaller length scales are determined using a turbulence model. FDS has three types of LES methods which are applicable to different grid scales. Although the use of the LES method may introduce uncertainty with regard to the turbulence structure and momentum transport as compared to a DNS method, this uncertainty is expected to be minor given the target exposure is dominated by thermal radiation and, to a lesser extent, the surrounding gas temperatures.

### **2.3.2 FDS Sub-Models Applicable to Modeling HEAF Effects**

FDS contains a number of sub-models that enable FDS to predict fire-specific behavior. Key sub-models relevant to HEAFs are discussed in Section 2.3.2.1 through 2.3.2.3. A brief description is provided as context for the Section 3 (using FDS to model the effects of a HEAF). Full details on the sub-models can be found in Volume 1 of the FDS Technical Reference Guide [14].

#### **2.3.2.1 Combustion**

FDS uses a turbulent batch reactor model to predict the energy release and production/destruction of species due to combustion. For this model, each grid cell is treated as if it were a combustion chamber where fuel and air are introduced and react. The heat release rate is determined by two factors: how quickly the fuel and air can mix inside the chamber (i.e., the grid cell) and how quickly chemical reactions take place once mixing occurs.

The rate at which mixing occurs in the model is a function of the grid size. At very small length scales where species gradients in the flame are being resolved, mixing is simply given by diffusion times. For very coarse grid cells, mixing is driven by buoyant acceleration or, for extremely large cells, the minimum quantity of fuel that must burn within a single grid cell to support a specified burning rate. At intermediate scales, like those expected for the inside of the electrical enclosure containing the HEAF as well as the high temperature outflow regions from the electrical enclosure, the mixing is driven by the modeled sub-grid turbulence.

Combustion reactions are complex. Something as simple as the combustion of methane to water vapor and carbon dioxide involves dozens of intermediate reactions and chemical species. The rate at which each of these reactions occurs is a function of temperature and the concentrations of species present. Modeling at this level of detail is only possible if the temperature and species concentrations are being resolved at flame thickness (~1 mm) length scales. For practical engineering applications, FDS considers just the single total reaction of fuel plus air producing products plus heat. As long as a reaction is taking place, temperatures should be high enough that the reaction rates are faster than the hydrodynamic timestep. Under these conditions, the assumption of fast chemistry can be used where the heat release rate is determined by how quickly fuel and air mix and by the consumption of the limiting species that mix (i.e., if there is more fuel than air, only that fuel that has enough air is allowed to burn).

FDS also contains an extinction model. This model looks at the conditions in a grid cell and determines if the mixed fuel and air is allowed to burn. For a flame to sustain itself, the flame must produce enough heat such that, after convective and radiative losses from the flame, there is still enough heat present to maintain a high reaction rate. If this is not the case, the heat losses drop the flame temperature, which drops the reaction rate and quickly leads to extinction of the

flame. If temperature-dependent reaction rates are being used, this sub-model is not necessary; however, with fast chemistry, fuel and air will always burn unless an extinction model prevents it. For typical fuels in pre-flashover compartments, extinction will occur once oxygen levels drop below 12 to 15%. At higher temperatures, extinction will occur at lower oxygen concentrations.

### 2.3.2.2 Radiation

FDS has a sub-model for the transport of thermal radiation from a fire. FDS uses a finite volume calculation method where radiation is transported along a finite number of angular directions. In the radiation transport model, each grid cell emits and absorbs radiation as a function of the cell temperature and the gas species present in the cell. The gas-phase radiative properties used in FDS are based on a small number of fuel types: water vapor, soot, carbon dioxide, and carbon monoxide for temperatures in the approximate range of 300 to 2,500 K and for pressures near atmospheric pressure. However, the properties for carbonaceous soot can be replaced with properties of other species, including aluminum oxide. For radiating species that are not defined within FDS, one can select among existing species as a surrogate.

Radiative emissions are proportional to the temperature of the emitting item to the fourth power. For hot surfaces and hot gas layers, the surface or gas temperature is appropriate to use directly. In cells with combustion, unless the grid is very refined, the grid cell temperature will represent some average of the temperature of the flame in the grid cell and the temperature of the remaining volume of the grid cell. To avoid underpredicting radiative emission from a fire, FDS allows the user to specify a radiant fraction and, in cells with combustion, FDS ensures that at least the radiant fraction is emitted.

### 2.3.2.3 Solid-Phase

The solid-phase sub-model provides a treatment of solids and solid surfaces within an FDS simulation, such as the walls of an electrical enclosure. As discussed in Section 2.1, a key phenomenon during a HEAF is the breaching of an electrical enclosure. The breach time and the size of the resulting opening have a significant impact on heat flux exposure to targets outside of the enclosure. Predicting this phenomenon requires predicting the temperature of the solid and predicting failure of the material.

In most cases, solid-phase temperatures in FDS are predicted using a one-dimensional heat transfer model; that is, every wall cell in an FDS model has its own heat transfer solution that treats that wall cell as a one-dimensional surface. This means that FDS is not modeling conduction between grid cells. FDS does have some three-dimensional heat transfer capabilities, but this currently only operates on the same numerical mesh as the hydrodynamic solver, which limits its application. In the case of a HEAF, centimeter-scale grid cells are used to cover the domain, which means the three-dimensional model would not be suitable for the bus bars (with centimeter-scale cross-sections) or the electrical enclosure housing (with millimeter-scale thicknesses). For a surface like a bus duct or switchgear enclosure, the one-dimensional heat transfer approximation is sufficient when the area being exposed is significantly larger than the material thickness. Since the total electrode width (which defines the area being exposed) is tens of centimeters, and the enclosure wall thickness is a few millimeters, the one-dimensional approximation is sufficient.

### **2.3.3 HEAF Phenomena Not Modeled by FDS**

As a fire model, FDS lacks physical sub-models for some HEAF-related phenomena:

- FDS does not model the dissociation of molecules at high temperatures or the formation of plasma. At very high temperatures, there will be some errors in the FDS temperature prediction due to unaccounted enthalpy changes associated with dissociation and ionization. The impact of this is primarily inside the enclosure in the arc volume where the highest temperatures are seen. There is likely a minor impact on target exposures since the overall energy is still conserved and since the source term for the arc used a predefined radiant fraction.
- FDS does not have equations for the electric and magnetic field. The impacts of voltage fields on ionized gas cannot be accounted for. This means that FDS cannot predict movement of the arc due to voltage fields. Movement of the arc, however, can be scripted in FDS inputs should subject matter experts assess it is important for a specific HEAF. The effects of the electric and magnetic fields on the arc location are addressed through the selection of the arc location and arc volume.
- An alternating current, 3-phase arc is very dynamic with the arc jumping from phase to phase as the current in each phase crosses zero and reverses polarity. These rapid changes in local power introduce rapidly cycling and large local changes in the pressure or flow divergence. This is not compatible with the low-speed flow assumption and a fully dynamic arc cannot be specified. The effects of the cycling arc are expected to be localized near the arc volume over the first few cycles and will tend to average out over the distances and timescales of interest.



# 3

## FDS SIMULATIONS TO DETERMINE THE ENERGETIC ZOI

---

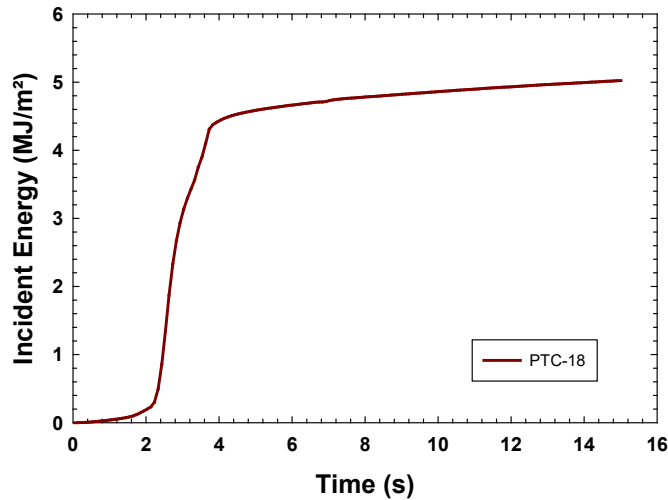
This section describes the approach for applying FDS to model the exposure from the HEAF energetic phase to define the dimensional components for the energetic phase. Initial development began with feasibility calculations to assess the merit of applying FDS to HEAFs. Subsequent efforts increased the level of detail and complexity along with some minor enhancements to FDS. The initial development began in December 2019 and continued through November 2021.

Validation and benchmarking are presented in Section 4. The results from the FDS simulations (Section 6) are subsequently used by the HEAF WG to determine the HEAF energetic ZOIs.

### 3.1 Model Simulation Time

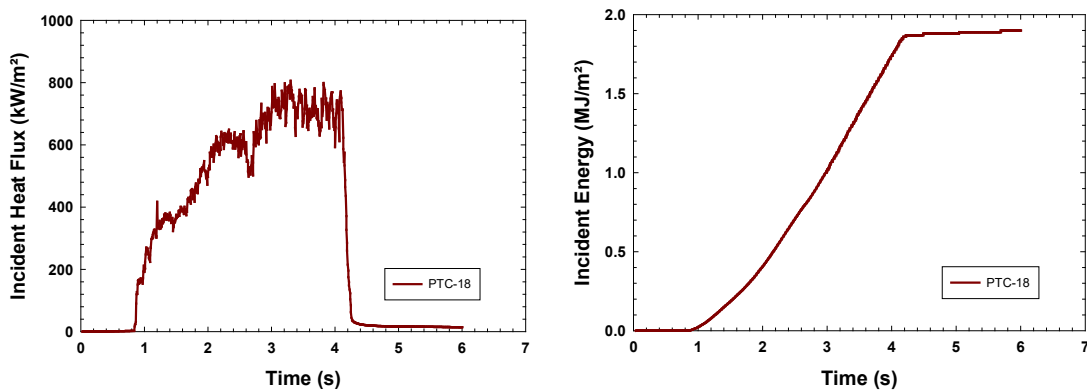
The model simulation time is the duration the HEAF effects are evaluated in FDS. This time needs to be long enough to capture the key target impacts from the HEAF modeled. Because targets will still be exposed to convective and radiative heat flux after extinguishment of the arc, the simulation time needs to extend for a period after the fault is cleared. This time may be estimated through consideration of the rate at which the temperatures and heat fluxes decay as well as observations from test data of the total incident energy at target locations. However, given the computational cost of running the model, the simulation time also should not be extended excessively beyond the period over which the HEAF can affect a target.

Figure 3-1 plots the incident energy over time for a typical plate thermometer (PTC) used in a medium-voltage (MV) switchgear (SWGR) large-scale test [6]. This test involved a 4 s arc, which is expected to have a longer post-arc exposure relative to a shorter arc since there is a larger amount of arc energy to dissipate. The PTC shows a rapid increase in temperature during the 4 s arc due to a high incident heat flux. Within a couple of seconds of the end of the arc, the temperature rise has slowed significantly. From 8 s post-arc to 12 s post arc, 4% or less additional energy deposition is recorded.



**Figure 3-1**  
**Incident energy for a typical plate thermometer (PTC-18) measured during MV SWGR Test 2-21 [6]**

Figure 3-2 shows the FDS-predicted heat flux and incident energy for the plate thermometer shown in Figure 3-1. The FDS simulation for this test was run about 2 s beyond the time at which the arc cleared (see Section 4.1). Within a couple of seconds after the arc ends, the heat flux to the plate thermometer predicted by FDS has dropped by at least a factor of 15 from the peak value. The flux continues to decay with the highest locations dropping about 15% from 5 s to 6 s. Extrapolating that decay rate out 8 s after the arc would add approximately 2% incident energy. For 12 s after the arc, the value would be about 4% additional incident energy relative to the incident energy at 6 s, or an increase of 2% relative to the incident energy at 8 s. This is in line with the measured data shown in Figure 3-1.



**Figure 3-2**  
**FDS-predicted heat flux at PTC-18 for MV SWGR Test 2-21 [6]**

Both the data and the FDS validation simulation show that by 8 s following the end of the arc, a target in a high heat flux zone (where it could reach the fragility criteria) will accumulate little additional incident energy. Based upon these observations, FDS simulations are run for the fault duration plus an additional 8 s.

## 3.2 Gas Properties

FDS requires a number of gas-phase thermophysical properties. These consist of the molecular weight, specific heat, viscosity, and diffusivity. Given the computational grids selected (Section 3.4), the default very large eddy simulation (VLES) mode of operation for FDS was used. As a large eddy simulation (LES) approach, a turbulence model is employed, which means that the tabulated molecular viscosity and diffusivity properties of the gases involved are not directly used in the transport equations. Instead, values derived from the sub-grid turbulence model are used with the molecular values setting a lower bound. This approach is appropriate for simulations where the resolvable length scales are at least an order of magnitude greater than those appropriate for direct numerical simulation (DNS) calculation methods, which is the case for the HEAF models. The specific heat is used at all length scales since this is needed to determine the enthalpy present at a given temperature.

FDS had been developed to support thermophysical data up to 5,000 K. This was a programming decision for setting array sizes for temperature-based thermophysical data. To support high-temperature HEAF applications, FDS was modified to allow a user-definable upper limit for the temperature arrays. This enabled defining extended specific heat values for nitrogen, carbon dioxide, and oxygen (up to 20,000 K, the maximum values in the National Aeronautics and Space Administration (NASA) polynomials used in FDS [21]). Specific heat data for copper vapor, aluminum vapor, and  $\text{Al}_2\text{O}_3$  were taken from NIST-JANAF tables [22] for each of those species. Detailed specific heat data were not located for  $\text{Cu}_2\text{O}$ ; as such, a constant specific heat of  $0.7 \text{ kJ}/(\text{kg}\cdot\text{K})$  was assumed, which is comparable to the specific heat for various metallic and non-metallic materials. Lennard-Jones data used to determine viscosity, diffusivity, and conductivity for gas-phase metallic species were taken from Cressault et al. [23, 24].

## 3.3 Radiation

FDS uses a finite volume calculation method for solving the radiation transport equation. This approach subdivides a unit sphere into a series of solid angles, which define the directions used for radiation transport. The default number of angles is 100, which is generally adequate for typical FDS applications. For HEAFs, the arc occupies a much smaller volume than the flame volume of a typical design fire. This condition requires additional resolution. Scoping calculations indicated that 500 angles provided a reasonable balance between realism and computational resources. Given this, the number of angles was set to 500.

The radiation solver uses the NIST RADCAL program [25] to define the absorptivity of a grid cell based on the species present in the grid cell. There is an option to replace the radiative properties of soot aerosols with the radiative properties of  $\text{Al}_2\text{O}_3$  aerosols. This option is selected. It is assumed that the  $\text{Al}_2\text{O}_3$  properties are more applicable for  $\text{Cu}_2\text{O}$  than those for soot and this option also applied to  $\text{Cu}_2\text{O}$  aerosols. Although this reflects an inherent limitation of the state of knowledge for the copper oxide radiant properties, the FDS results indicated the dominant factor affecting the target exposure prediction was the distance between the target and the arc (the radiant heat flux directly from the arc). Uncertainty in the radiant heat flux from the heated gases due to this assumption is expected to be a secondary effect that is addressed through bias adjustments for the model predictions.

As discussed in Section 2.3.2.2, at typical engineering length scales the flame temperature and flame species are not resolved well enough to use those values directly for the radiation source term. Instead, a radiative fraction is used to define a minimum amount of radiation from the flame volume of a fire. A similar approach is taken for the HEAF simulations. As discussed in Section 3.8, the arc input power is applied as a volumetric heat source. A radiative fraction is then applied to this source with a value based on research by Cressault et al. [26]. This research measured the radiant fraction from vertically oriented, cylindrical electrodes, and testing varied the electrode metal and the arc power. Figure 3-3 shows the measured data from Cressault et al. [26] as well as a power law fit to the data. This power law fit is used to define the radiant fraction input for each HEAF simulation.

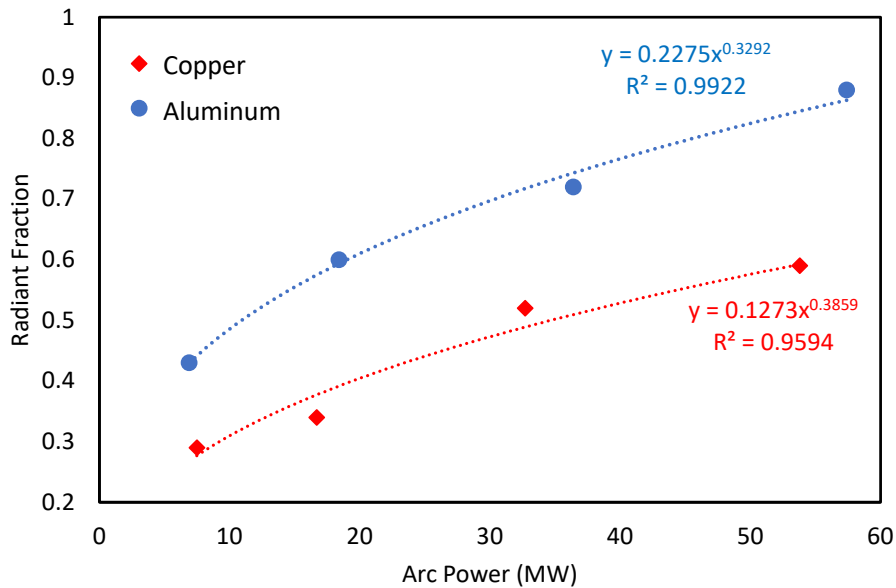


**Figure 3-3**  
Arc power versus radiant fraction data of Cressault [26]

### 3.4 Computational Grid

For the MV SWGR and LV SWGR cases, a grid resolution of 0.0762 m is used. This puts at least a dozen grid cells between the face of the enclosure and the energetic ZOIs from NUREG/CR-6850 [1] and allows for some resolution of the flow dynamics at closer distances to the enclosure. Given the physical size of these enclosures, smaller grid resolutions would significantly add to the expense of the simulations given the number of simulations being performed.

For the non-segregated bus duct (NSBD) cases, a grid resolution of 0.02 m is used. The NSBD configurations modeled are significantly smaller in cross-section than the two SWGR enclosures, and a finer grid is necessary to avoid only having a few grid cells across the span of the NSBD.

For all geometries, the grid is extended 1.5 to 2 m from the face of the enclosure. Based on the data from testing and from scoping calculations, this distance is expected to fully contain the energetic ZOI.

### 3.5 Combustion

Combustion is modeled for the oxidation of metal vapor (see Section 3.7 for discussion of vapor addition). This is either aluminum to aluminum oxide ( $\text{Al}_2\text{O}_3$ ), releasing 31,100 kJ/kg of aluminum or copper to copper (II) oxide ( $\text{Cu}_2\text{O}$ ), releasing 1,340 kJ/kg of copper. Although oxidation of copper may also produce copper (I) oxide ( $\text{CuO}$ ), data suggest  $\text{Cu}_2\text{O}$  forms at higher temperatures [23, 27]. In addition, the heat of formation for copper (II) oxide is lower than copper (I) oxide, which maximizes the differences between copper and aluminum electrodes. Regardless, the energy involved for the formation of either copper oxide is small compared to the aluminum oxide and a small fraction of the arc energy. As such, the results are not expected to be sensitive to this assumption.

The heats of combustion for the oxidation reactions are from NIST-JANAF data [22]. Given the multiple centimeter grid cell size, fast chemistry is used. Because of the very high temperatures seen in HEAFs, Arrhenius-based rates are expected to be essentially instantaneous compared to timestep sizes. Additionally, the FDS extinction mode is disabled. This extinction model prevents combustion based on the local cell temperature and oxygen concentration. The inputs for this model are only well known for typical organic materials and not for metal oxidation. The very high temperatures associated with the HEAF would likely allow for near complete consumption of oxygen in grid cells with metal vapor.

### 3.6 Enclosure Breach

In the large-scale testing, metal enclosures containing a HEAF were observed to breach within 1 s [4, 6]. Typical enclosure wall thicknesses are a couple of millimeters and will quickly heat to the melting point of the metal given the intense heat fluxes from a HEAF. To incorporate this phenomenon in the FDS model, the metal enclosure walls are defined using a phase change material. This is a material with a single-step reaction that occurs at a threshold temperature (i.e., the melting point). For steel, a melting point of 1,300°C and a heat of fusion of 250 kJ/kg of steel are used. For aluminum, a melting point of 650°C and a heat of fusion of 320 kJ/kg of aluminum are used. The melting points for both steel and aluminum are set slightly below (about 10 – 70°C) the actual melting point temperatures for these materials to account for enclosure failure due to dynamic forces tearing the metal before it actually melts.

### 3.7 Electrode Mass Loss

During a HEAF the electrodes lose mass due to melting and vaporization of the electrode material. The rate at which mass loss occurs and the resulting amount of metal oxidation both have an impact on the energetic ZOI. FDS inputs are required for both of these phenomena. The FDS simulations use a single electrode material; the feasibility of using two electrode materials (e.g., an arc starting in one material and migrating to an electrode composed of a different material) are not assessed in this effort and is not expected to be a significant factor in the exposure conditions at a target.

### 3.7.1 Electrode Mass Loss Rate

The total mass lost from the electrodes was measured in the open-box tests [4] and the MV SWGR tests [6] as summarized in Table 3-1. Measurements of the time dependence of the mass loss are not available. Prior research by Stanback [28] established a functional relationship for the electrode mass loss rate,  $\dot{m}_{\text{electrode}}(t)$  in kg/s, as a function of the arc current,  $I(t)$  in amps for single phase-to-ground arc fault tests. To use these results for the FDS modeling, the Stanback [28] equations are converted to a mass loss rate using the metal density and multiplied by 3 to account for a three-phase arc fault. This is shown in equations 3-1 and 3-2 for copper and aluminum, respectively.

Copper, with a density of 8,960 kg/m<sup>3</sup>:

$$\dot{m}_{\text{electrode}}(t) = 3.19 \times 10^{-7} I(t)^{1.5} \quad (3-1)$$

Aluminum, with a density of 2,700 kg/m<sup>3</sup>:

$$\dot{m}_{\text{electrode}}(t) = 2.02 \times 10^{-7} I(t)^{1.5} \quad (3-2)$$

These equations are used to predict the total mass loss from the open-box tests. The results compared with the measured mass loss are shown in Figure 3-4. While data for the low-voltage open box (OB) and medium-voltage open-box (OBMV) tests are reasonably predicted by the Stanback equations, the full-scale MV SWGR tests performed with aluminum electrodes are not. Based on these results, the HEAF WG consensus was to use the Stanback equations for determining the mass loss rate for low-voltage HEAFs (due to the low-voltage open-box data) and bus duct events (where a breached bus duct is more geometrically similar to the open-box configuration than the full-scale MV SWGR configuration) and develop an alternative treatment for MV SWGR.

**Table 3-1**  
**Summary of 2019 open-box tests [4] and the 2018 full-scale medium-voltage switchgear tests used to assess electrode mass loss [6]**

Test	Electrode	System voltage (kV)	Current (kA)	Arcing fault duration (s)	Arc energy (MJ)	Test type	Electrode mass loss (kg)
OB01(a)	Copper	1.03	1.05	2.01	0.2	Open Box	0.0245
OB01(b)	Copper	1.03	1.03	2.02	0.7	Open Box	
OB02	Copper	1.01	14.0	2.02	12.0	Open Box	0.762
OB03	Copper	1.01	13.8	3.03	20.0	Open Box	1.33
OB04	Copper	1.06	27.8	1.03	12.4	Open Box	0.789
OB05	Aluminum	1.03	1.02	2.01	0.8	Open Box	Not measured
OB06	Aluminum	1.01	12.0	2.02	12.7	Open Box	0.74
OB07	Aluminum	1.01	13.0	1.52	10.3	Open Box	0.552
OB08	Aluminum	1.06	24.9	1.02	20.1	Open Box	0.597
OB09	Copper	1.03	4.79	2.01	2.2	Open Box	0.213

**Table 3-1 (continued)**  
**Summary of 2019 open-box tests [4] and the 2018 full-scale medium-voltage switchgear tests used to assess electrode mass loss [6]**

Test	Electrode	System voltage (kV)	Current (kA)	Arcing fault duration (s)	Arc energy (MJ)	Test type	Electrode mass loss (kg)
OB10	Aluminum	1.03	4.87	2.01	4.1	Open Box	0.175
OBMV1	Aluminum	6.9	14.3	3.18	37.5	Open Box	1.32
OBMV2	Aluminum	6.9	29.1	1.12	21.4	Open Box	0.945
OBMV3	Aluminum	6.9	14.4	5.05	55.7	Open Box	2.30
OBMV4	Copper	6.9	14.3	5.08	51.8	Open Box	3.25
OBMV5	Copper	7.0	28.6	2.32	43.5	Open Box	3.22
OBMV6	Aluminum	7.0	14.6	2.05	22.7	Open Box	0.727
2-19	Aluminum	6.9	25.8	2.05	39.3	Full-Scale	0.458
2-21	Aluminum	6.9	26.6	4.11	101	Full-Scale	1.97
2-22	Aluminum	6.9	32.0	2.07	51.3	Full-Scale	0.894
2-24	Aluminum	6.9	29.8	4.15	122	Full-Scale	2.57

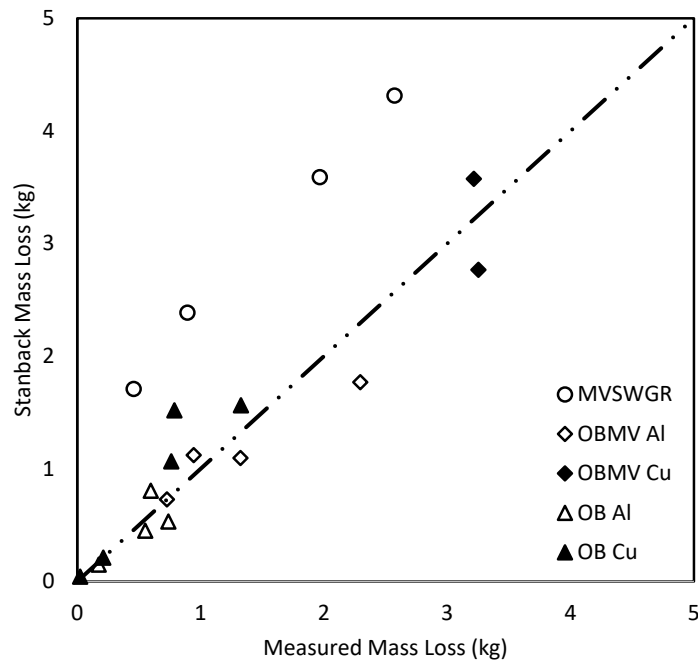


**Figure 3-4**  
**Predicted versus measured electrode mass loss for the open-box [4] and MV SWGR [6] tests. Symbol shape indicates test series (OB is open-box, OBMV is medium-voltage open-box, and MV SWGR is full-scale medium-voltage switchgear with aluminum electrodes), and shading indicates aluminum (hollow) or copper (filled)**

For the full-scale MV SWGR tests, an alternative approach for specifying the electrode mass loss rate is developed. The total measured mass loss ( $m_{\text{electrode}}$ ) is plotted as the function shown in Equation 3-3:

$$m_{\text{electrode}} = a E^b \quad (3-3)$$

where  $E$  is the total energy (MJ) dissipated over the test and  $a$  and  $b$  are empirical constants. Three values for the exponent  $b$  are assessed with the correlation (1, 1.5, and 2). The results are shown in Figure 3-5.

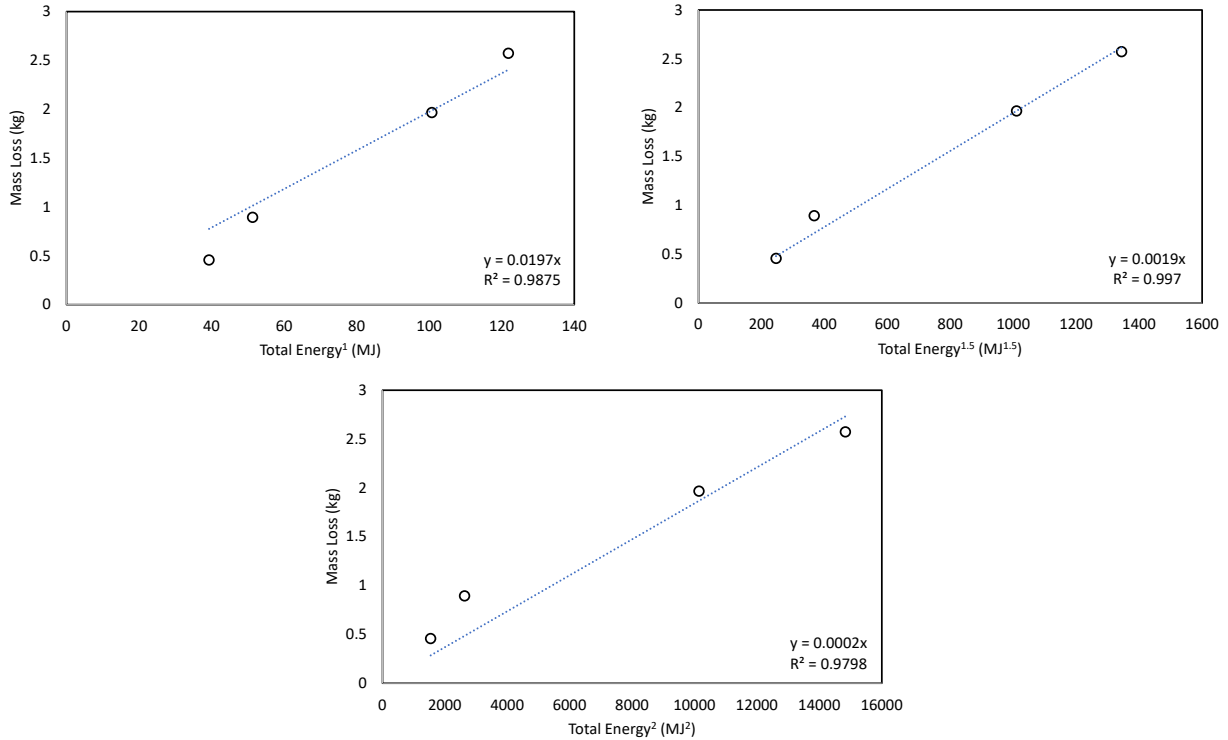


**Figure 3-5**  
**Results of fitting Equation 3-3 using different exponents to the MV SWGR mass loss data. The empirical constant  $a$  is the constant in the equation for the blue dashed line shown in each graph**

The best fit is obtained with an exponent of 1.5 (the HEAF WG uses this exponent for determining the mass loss rate). All of the MV SWGR tests [6] used aluminum electrodes. The HEAF WG consensus assumes the same ratio of copper to aluminum mass loss in the Stanback equations (1.58) applied to the MV SWGR tests. The end results are equations 3-4 and 3-5 for the mass loss for copper and aluminum electrodes, respectively. The mass loss rate in the FDS model is obtained by taking the time derivative of equations 3-4 and 3-5.

Copper:

$$m_{\text{electrode}}(t) = 1.58 \times 0.019 E(t)^{1.5} = 0.030 E(t)^{1.5} \quad (3-4)$$

Aluminum:

$$m_{\text{electrode}}(t) = 0.019 E(t)^{1.5} \quad (3-5)$$

### 3.7.2 Electrode Mass Loss Particle Size Distribution and Oxidation

The mass loss from the electrodes during a HEAF consists of vaporized metal and various sized metal droplets, all of which may oxidize to some extent during or after the arc fault clears. Because oxidation will potentially add to the incident energy seen by targets, the treatment of the electrode mass loss in the FDS model includes this process.

#### 3.7.2.1 Electrode Mass Loss Particle Size Distribution

A review of particle data collected during the 2018 MV SWGR tests [6] shows both nanoscale particles (which were likely condensed metal vapor) and small metal droplets. Relative masses of the particles collected were not provided, and particles were only collected at locations far from the enclosure where large droplets would not be expected.

To improve knowledge of particle size distributions, Sandia National Laboratories (SNL) performed small-scale testing of HEAF-type events. Sandia replicated the conditions of the 2018 MV SWGR tests at a reduced scale where the voltage and current density was preserved in the electrodes. The particles collected included nanoscale material, likely condensed metal vapor, small droplets, and large droplets. This effort is documented in Appendix D. Table 3-2 summarizes the particle size distribution for aluminum and copper electrode tests.

Table 3-2 shows that nanoscale particles, which represent the vaporized metal, have a negligible mass fraction. Large droplets, characterized as those with diameters over 15  $\mu\text{m}$ , represent the majority of the electrode mass lost.

**Table 3-2**  
**Particle size distribution for mass lost from different electrodes (see Appendix D)**

Electrode	Mass fraction		
	Nanoscale particles (condensed metal vapor)	Small droplets (~ 2 – 15 $\mu\text{m}$ )	Large droplets (over 15 $\mu\text{m}$ )
Aluminum	~ 0.0	0.10	0.90
Copper	~ 0.0	0.08	0.92

#### 3.7.2.2 Electrode Oxidation

Metal vapor and metal droplets generated by a HEAF around 10  $\mu\text{m}$  or smaller in diameter will eventually see complete or near complete oxidation and will be transported within the outflow from an enclosure. Larger droplets (around 100  $\mu\text{m}$  or more) will only see limited oxidation over the arc fault timescales. The thickness of the oxide layer that can develop during and shortly after an arc fault is on the order of several  $\mu\text{m}$  since the test data show 10  $\mu\text{m}$  drops are nearly completely oxidized. If the oxide layer is 3  $\mu\text{m}$ , then about 94% of the mass of a 10  $\mu\text{m}$  diameter drop mass would be oxidized, whereas only about 17% of a 100  $\mu\text{m}$  diameter drop would be oxidized. Additionally, larger droplets will more quickly fall out of outflow. As a result, the electrode mass lost to larger droplets will not significantly contribute to the energetic ZOI as they will have significantly less oxidation and that oxidation will occur at locations that do not influence the energetic ZOI.

The 2018 full-scale MV SWGR tests [6] noted that between 30 – 75% of aluminum droplets oxidized [6], which provides some confirmation of the estimated oxidation levels. The small-scale testing performed by Sandia considered the oxidation levels for specific particle size ranges. The results of these tests are as summarized below (see Appendix D).

- Aluminum electrode: 75% oxidation for micron sized particles (small droplets)
- Copper electrode: 25% oxidation for micron sized particles (small droplets)

### 3.7.2.3 Treatment of Electrode Particles in FDS

Particles are included in the FDS model primarily to account for the oxidation process. The incorporation of the energy associated with melting and vaporizing the electrode metal in the FDS model is described in Section 3.8.1.

Based on the observations of the particle size mass distribution and oxidation fraction, the following approach is adopted:

1. Nanoscale particles, representing the portion of the electrode converted to metal vapor, are ignored. They represent a near zero mass fraction and the energy associated with vaporization and transport of these particles is negligible relative to the arc energy.
2. Small diameter particles, with characteristic diameters between 2 – 15  $\mu\text{m}$  represent a non-negligible mass fraction of the electrode mass and will have high levels of oxidation; therefore, the particles are included in the FDS model.
3. Large diameter particles, with characteristic diameters greater than 15  $\mu\text{m}$ , are ignored. These particles do not significantly oxidize or absorb a significant amount of energy in the areas of interest. They also tend to fall out of the outflow and do not influence the energetic ZOI.

The particles included in the FDS model are introduced using a uniform diameter that is representative of the small diameter droplets with diameters between 2 – 15  $\mu\text{m}$ . Oxidation of these particles is incorporated through a pyrolysis model where the oxidation process occurs in the vapor phase but represents surface oxidation. Thus, the energy required to vaporize the metal is not included in the model.

This approach was implemented in the FDS model as described in the following bullets:

- 10  $\mu\text{m}$  particles are injected into the FDS domain from the arc volume. This particle diameter is within the small droplet range observed in the Sandia tests and represents all particles in this range. The particles are injected into the domain using three spray nozzles, with one nozzle at each bus bar location. A 120° cone with a particle velocity of 10 m/s [29] is used. The cone is oriented to face the largest expected breach. The mass flow rate is set using Equations 3-4 and 3-5.
- The particles are defined with a simple pyrolysis model involving a constant reaction rate. That rate was set such that the particles emitted 75% or 25% for aluminum or copper, respectively, of their mass as metal vapor over 0.3 s. This represents surface oxidation; therefore, the energy associated with the vaporization process is not included in the model. The metal vapors that are pyrolyzed combust as soon as they mix with oxygen in the FDS model, guaranteeing the correct amount of oxidative heat release. The pyrolysis (oxidation) time of 0.3 s is the approximate time needed for particles to move past the instrument racks and past the energetic ZOI based on simulations of the 2018 MV SWGR tests [6] and forces

oxidation in the areas of interest. This is expected to result in a slight overestimate of the energy released between the arc and the target as it is likely some surface oxidation occurs after particles move past the instrumentation racks.

- The particles are defined with a surface temperature of the respective melting point of metal. The energy needed to melt the metal and form the particles is described in Section 3.8.2 and is not directly associated with the modeling of the particles. In addition, the heat transfer coefficient and emissivity are set to zero for the particles. This means the vapor from the particle oxidation model is injected at high temperature, but the particles themselves are neutral in terms of gas-phase heat exchange. In the volume of space defining the energetic ZOI, gas temperatures are generally much higher than the melting point and the droplets or solid particles should act as heat sinks within that volume. Therefore, not including heat transfer between the particles and the surroundings results in an overestimate of the gas temperatures.

## 3.8 Arc Power Input

### 3.8.1 Arc Power Profiles

The arc power profiles are used to define the energy released from the arc in the FDS model domain. Three generic arc power profiles are used: two applied to MV SWGR and NSBD HEAFs and one applied to LV SWGR HEAFs. These arc power profiles are selected after a review of HEAF operational experience in Section 5.1 and Appendix A. Appendix A provides a detailed review and summary of the arc power profiles and the corresponding HEAF simulations developed using these arc power profiles. The generic profiles are briefly summarized as:

- A constant-current arcing fault (stiff-source). The stiff current selected is 30 kA and the arc line-to-line voltage ( $V_{L-L}$ ) is 650  $V_{L-L}$  resulting in a maximum three-phase arc power of 33.8 MW. This is implemented in the FDS model with a 0.1 s ramp up and down at the start and end of the arc to avoid numerical instabilities that could arise when a large energy source is imposed instantaneously. This arc power profile is used to model the exposure from MV SWGR and NSBD HEAFs.
- Generator-fed faults (constant-current arc followed by 15 s of decaying arc current). The constant-current arc portion of this arc power profile is characterized the same way as the constant-current arc fault power profile using a 30 kA stiff current. The decay portion is characterized with a 20 kA starting current, 650  $V_{L-L}$  arc voltage, and an exponential decay profile estimated from operational experience (see Appendix A). A 1 s ramp from the stiff current to the decaying current is used to provide consistency with the exponential decay profile used on the generator-fed fault portion. This arc power profile is used to model the exposure from MV SWGR and NSBD HEAFs (see Figure 3-6, Figure 3-7, and Figure 3-8).
- A two-stage, constant-current arc. This arc power profile is based on EPRI's fire events database (FEDB) 50935 [12] and is implemented by a 20 s constant initial arc current followed by a 21 s constant reduced arc current, both at 375  $V_{L-L}$  as described in Appendix A. This arc power profile is used to model the exposure from LV SWGR HEAFs (Figure 3-9).

The generic profiles are used to construct different HEAF model simulations primarily by changing the constant-current arcing fault duration.

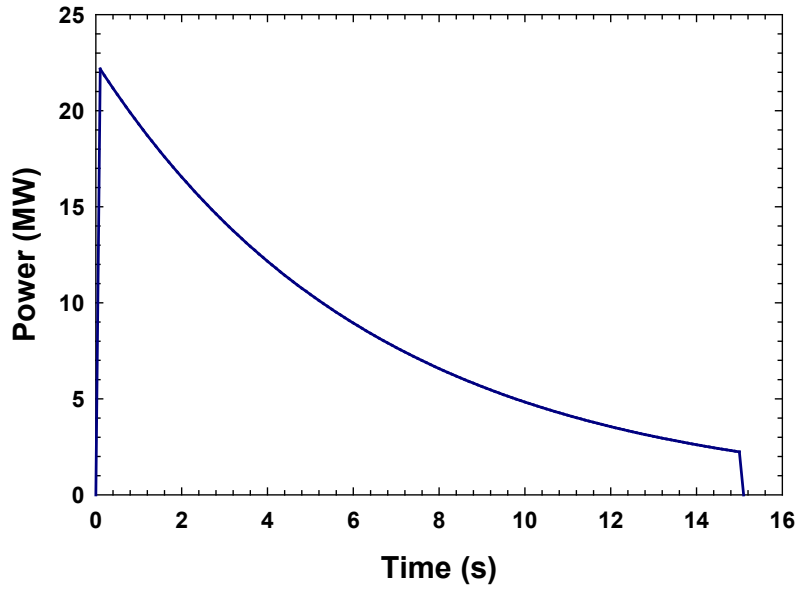


Figure 3-6  
Power curve for a 0 s stiff and 15 s decay HEAF

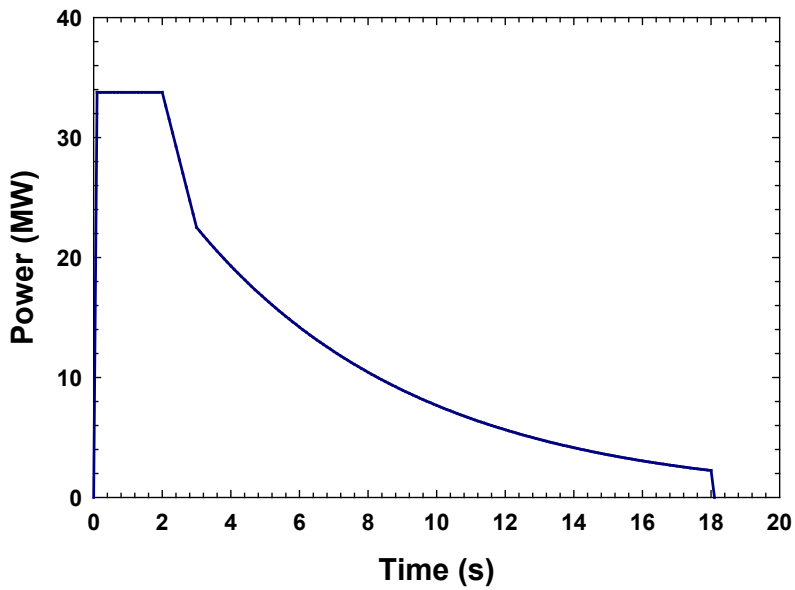
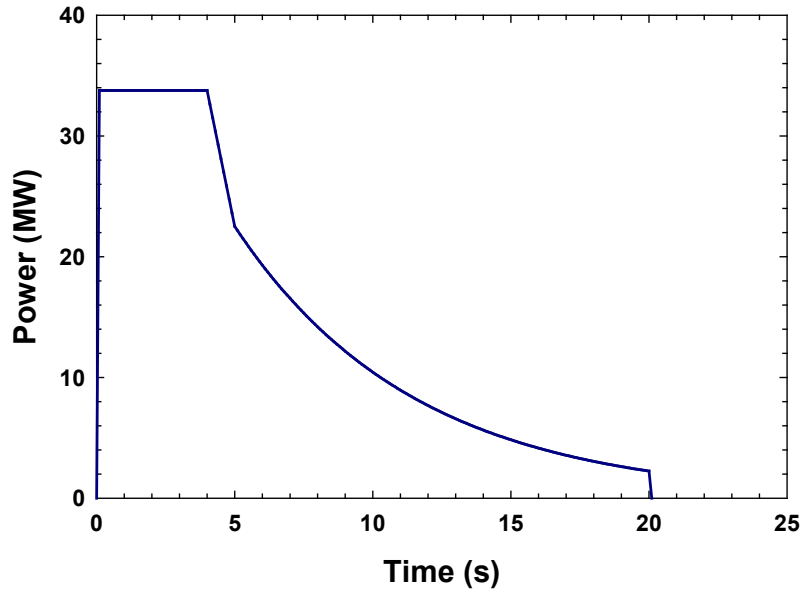
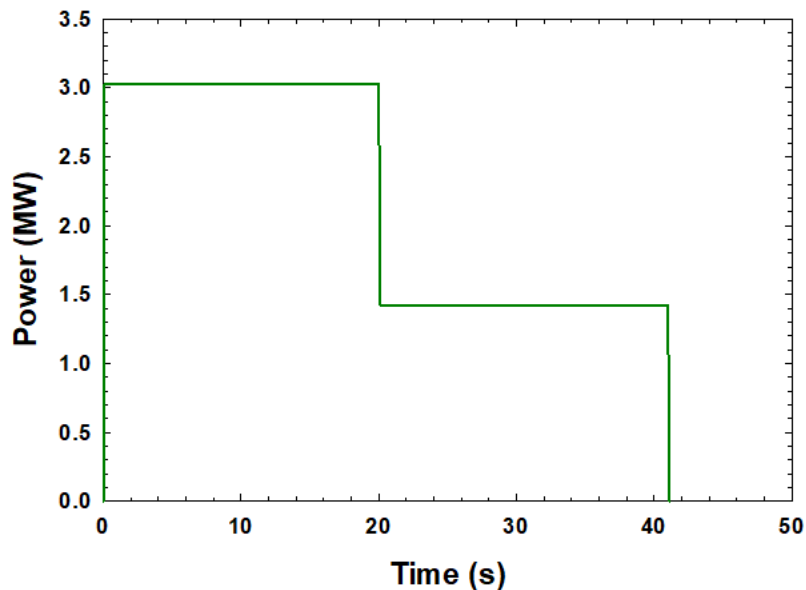


Figure 3-7  
Power curve for a 3 s stiff and 15 s decay HEAF



**Figure 3-8**  
Power curve for a 5 s stiff and 15 s decay HEAF



**Figure 3-9**  
Low voltage HEAF power profile

### 3.8.2 Power Input for FDS Simulations

For the FDS simulations, the electrical power dissipated inside the enclosure is used as an input. The actual power dissipation for a HEAF is the heating, melting, and vaporization of the bus bars and the convective and radiative energy released by the arc (some of which goes into the electrodes). Within FDS, the heating, melting, and vaporization of the electrode metal is not modeled directly; therefore, the energy needed to accomplish this is not present in the FDS model as an energy sink. Based on the discussion in Section 3.7.2.3, the mass fraction of vaporized metal is negligible and is not considered when determining the power dissipation.

In addition, the energy associated with heating melted droplets is conservatively ignored (also discussed in Section 3.7.2.3). The FDS model only considers the energy required to melt the electrodes. This is the energy it takes to heat the metal up to its melting point and the energy needed to change the phase from solid to liquid. Using the NIST-JANAF data [22], this energy ( $\Delta E_{\text{melt}}$ ) is 1.063 MJ/kg for aluminum and 0.695 MJ/kg for copper assuming an initial temperature of 25°C. The time dependent arc power input used for FDS ( $\dot{E}_{\text{FDS}}(t)$ ) is shown in Equation 3-6:

$$\dot{E}_{\text{FDS}}(t) = \dot{E}(t) - \Delta E_{\text{melt}} \dot{m}_{\text{electrode}}(t) \quad (3-6)$$

where  $\dot{E}(t)$  in MJ/s is the HEAF-dependent power and  $\dot{m}_{\text{electrode}}$  is the mass loss rate of the electrodes (Section 3.7.1). This adjustment is applied only to the MV SWGR and MV NSBD arc power profiles.

The FDS input power is defined in a fixed volume where the arc fault is located within the electrical enclosure. The fixed volume covered the width occupied by the electrodes plus a small number of grid cells perpendicular to the plane of the electrodes and along the electrodes. The volumetric heat release was assigned a fixed radiant fraction in Section 3.3. To avoid numerical instabilities by instantaneously introducing an extreme volumetric energy source, the arc power is increased from zero to its initial value over 0.1 s using a linear ramp.

### 3.9 Input File Generation

Over 100 FDS simulations are performed to determine the dimensions of the HEAF energetic phase (see Sections 5.1.1.7, 5.1.2.4, and 5.1.3.5). The large number of simulations posed some challenges. First, multiple sets of simulations where each set involved a series of inputs with minor input-to-input changes introduced a significant likelihood of user error if input files were edited manually. Second, after running through the entire HEAF simulation matrix, there could be an issue with one or more of the input assumptions/approaches not revealed in the smaller set of HEAF simulations used for validation. Having to manually re-edit a large number of inputs would also introduce a significant likelihood of user error. Third, the long-term maintenance of the input files introduces its own risk error. Over time, institutional knowledge of what changes were made to which files can be lost if not documented in an appropriate fashion. Also, as FDS continues to evolve, there may be a desire to update the input files to reflect new FDS capabilities which would again raise the risk of user error if edited by hand.

To reduce the risk of user error and support the long-term maintenance of the inputs, an algorithmic approach is used to develop the input files. The FDS repository contains a Python utility called `swaps.py`. This utility reads a comma-delimited file called `paramfile.csv`. This file has the format:

```
template, param1, param2, ..., paramn
file01.fds, val1,01, val2,01, ... valn,01
file02.fds, val1,02, val2,02, ... valn,02
...
filem.fds, val1,m, val2,m, ... valn,m
```

On the first line, `template` is the name of a template FDS file that serves as the baseline input file, each `param` is a unique text string that corresponds to an input parameter, and each `val` is a text string that sets the parameter value (the text string can be a number). For each of the following lines, FDS creates the input file `filem.fds` and in that file it replaces each `param` with its corresponding `val`. For example, if a template file called `template.fds` has the contents:

```
&MESH ID='meshname',XB=x1,x2,0,1,0,1,IJK=ival,jval,kval/
```

and the `paramfile.csv` contained:

```
template.fds, meshname, x1, x2, ival, jval, kval
scenario1.fds, Mesh1, -1, 2, 20, 10, 10
```

then `swaps.py` would create the file `scenario1.fds` with the contents:

```
&MESH ID='Mesh1',XB=-1,2,0,1,0,1,IJK=20,10,10/
```

With this approach, all of the FDS input file editing is done by the Python script. There is a single file to review that contains a tabulation of all the scenarios and the input changes needed. If future change to FDS meant that some input needed to be changed, only the template file with the scenario file parameters would need to be updated, and then the input files could be regenerated by the Python script.

For this effort, a template file and a parameter file are created and reviewed for each geometry type. The parameter files are created using Excel. One sheet of the Excel file contained a series of columns containing the variables being permuted (electrode composition, arc location, fault current magnitude, duration, etc.) and all of the parameters in the parameter files. Other sheets contained lookup tables for items like arc location. Logical formulas are defined for each parameter to autogenerate its value based on the specific permutation for the HEAF simulation. File names are also autogenerated based on the specific variable permutation. This approach meant adding or removing a HEAF simulation is a simple process of adding or removing rows and ensuring the correct permutations are defined.

### 3.10 Outputs and Output Processing

Data from testing, observations of test videos, and the results of FDS simulations indicate that the highest exposures occur where targets are immersed in high-temperature outflow from the electrical enclosure or where targets have a direct line of site to the arc. FDS simulations are instrumented with planes of devices measuring the FDS output quantity of `GAUGE HEAT FLUX GAS` in units of  $\text{kW/m}^2$  integrated over time, resulting in a total exposure energy output quantity in units of  $\text{MJ/m}^2$ . The planes are located where outflow is expected to occur either due to a fixed vent opening in the enclosure or where openings are expected to develop as a result of enclosure breach. Figure 3-10 shows an example of the FDS instrumentation for a General Electric (GE) Magne-Blast series of circuit breakers with an arc in the main bus bar compartment (see Section 4.1 and Section 5.2.1 for more details).

The planes are implemented as line devices in FDS, where a starting point and end point are given along with a number of devices to place between the two points including the start and end. In this case, devices are defined as a line normal to the enclosure face starting at the first grid cell with devices in every grid cell moving outward along the normal. The inputs are grouped in the FDS input file such that all line devices for a particular enclosure face are together.

The GAUGE HEAT FLUX GAS output quantity inserts a massless particle at the device location (i.e., each green dot in Figure 3-10) and the particle is treated as a virtual water-cooled heat flux gauge. The particle is given an ORIENTATION input which defines the normal vector to the particle used to determine the radiative flux. The orientation for the device particles is directed toward the electrical enclosure face. The local gas velocity and temperature are used to predict the convective flux component. This approach of measuring the target exposure as the exposure to a cold wall is consistent with how target fragilities have been defined for both fire exposures [1] and HEAF exposures [10]. The device outputs are further defined to integrate the heat flux over the simulation time to obtain the total exposure energy.

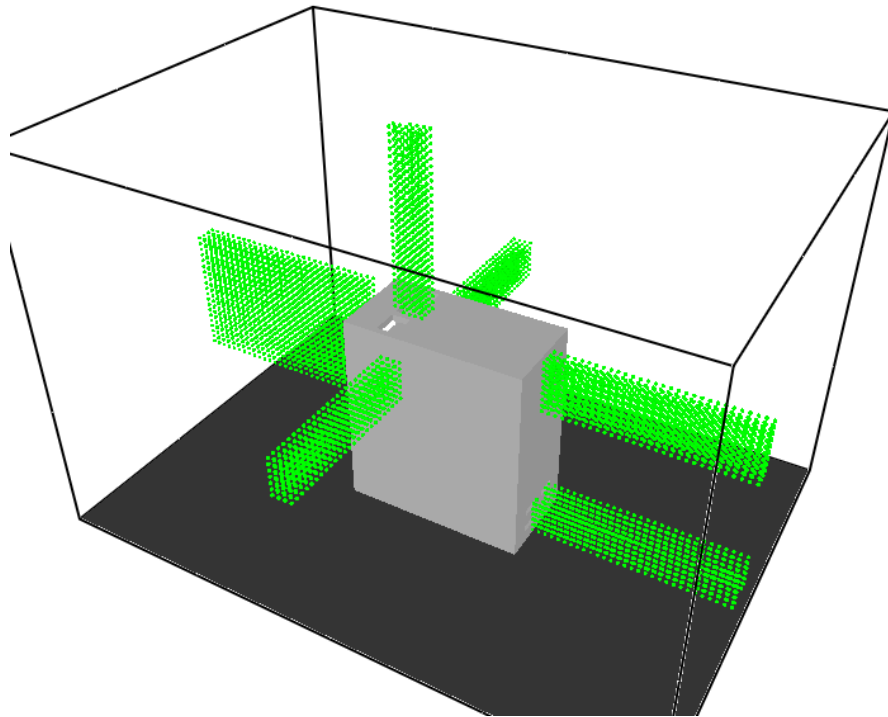


**Figure 3-10**  
**FDS output devices (green dots) for the GE Magne-Blast geometry with the arc in the main bus bar compartment**

At the end of an FDS simulation, there is a comma separate variable (csv) file containing a column for each line device where the first row is the identity of the device, and the remaining rows are the output for each point along the line. Since points are defined in each grid cell normal to the enclosure, each row is simply one more grid cell away from the enclosure. This makes it simple to query the output file and determine for each face of the enclosure what the maximum exposure is as a function of distance.

For determining the energetic ZOI for each face for each HEAF simulation, the FDS-predicted exposures are adjusted to account for the FDS bias as discussed in Section 4.1.4. This process is depicted in Figure 3-11, which shows the back face exposure for a GE Magne-Blast enclosure with aluminum bus bars, power flow in the load configuration, and a 4 s stiff (constant power) arc located in the primary cable compartment. The plot shows the predicted FDS exposure (black solid line), the bias adjusted exposure (red solid line), the 5<sup>th</sup> and 95<sup>th</sup> percentile confidence intervals (red dashed lines), and the 15 MJ/m<sup>2</sup> and 30 MJ/m<sup>2</sup> target fragility criteria (horizontal dash-dot-dot lines). The bias-adjusted exposure is used to determine the energetic ZOI through linear interpolation of the FDS results data and the target fragility criteria. In this specific case (Figure 3-11), this results in a 15 MJ/m<sup>2</sup> target fragility energetic ZOI of 0.97 m with a 0.76 to 1.20 m 95% confidence interval and a 30 MJ/m<sup>2</sup> target fragility energetic ZOI of 0.63 m with a 0.46 to 0.82 m 95% confidence interval.

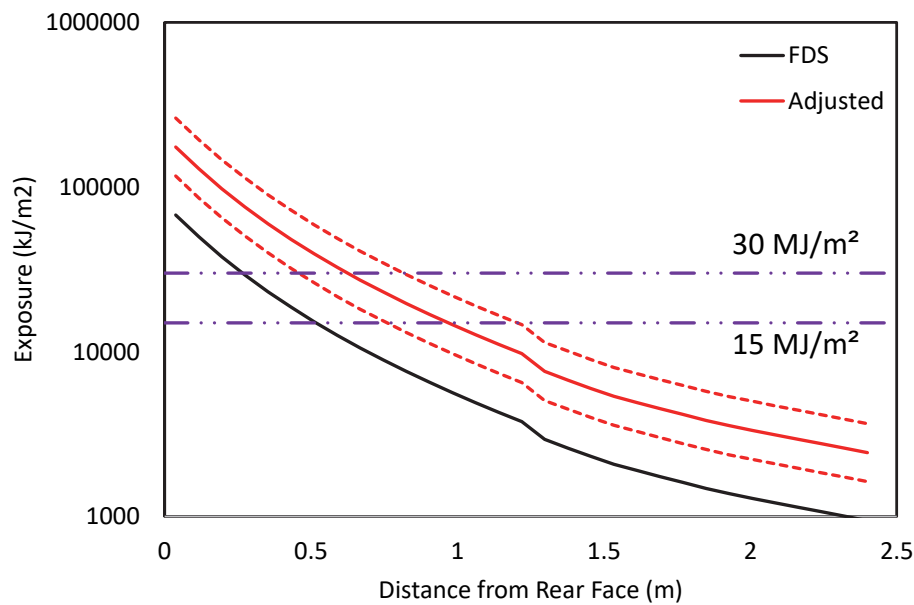


**Figure 3-11**  
 Depiction of the adjusted FDS results for the bias and error (Section 4.1.4). Dotted lines are 95% confidence interval and dot-dot-dash lines are 15 MJ/m<sup>2</sup> and 30 MJ/m<sup>2</sup> target fragility criteria



# 4

## VALIDATION AND BENCHMARKING OF FDS FOR HEAF

This section documents the validation of FDS for HEAF. Validation consists of evaluating the FDS results against data from the 2018 MV SWGR tests [6], a LV SWGR event, a NSBD event in an elbow, and a full-scale test replicating a NSBD event in a straight segment of bus duct.

### 4.1 2018 Medium Voltage Switchgear Experiments

#### 4.1.1 Summary of Experiments

The MV SWGR experiments used General Electric Type M-36 switchgear enclosures with Magne-Blast circuit breakers (see Figure 4-1). The enclosures were previously used and refurbished for the experiments. The four enclosures used in the testing were identical except for the components attached to the front door. However, those components did not play a significant role in the thermal environment generated by the HEAFs induced on the bus bars in the rear primary cable compartment. The enclosures were 202 cm (79 in.) long, 91 cm (36 in.) wide, and 229 cm (90 in.) tall. The bus bars in all experiments were aluminum. Further details of the enclosure construction are provided in the test report [6].

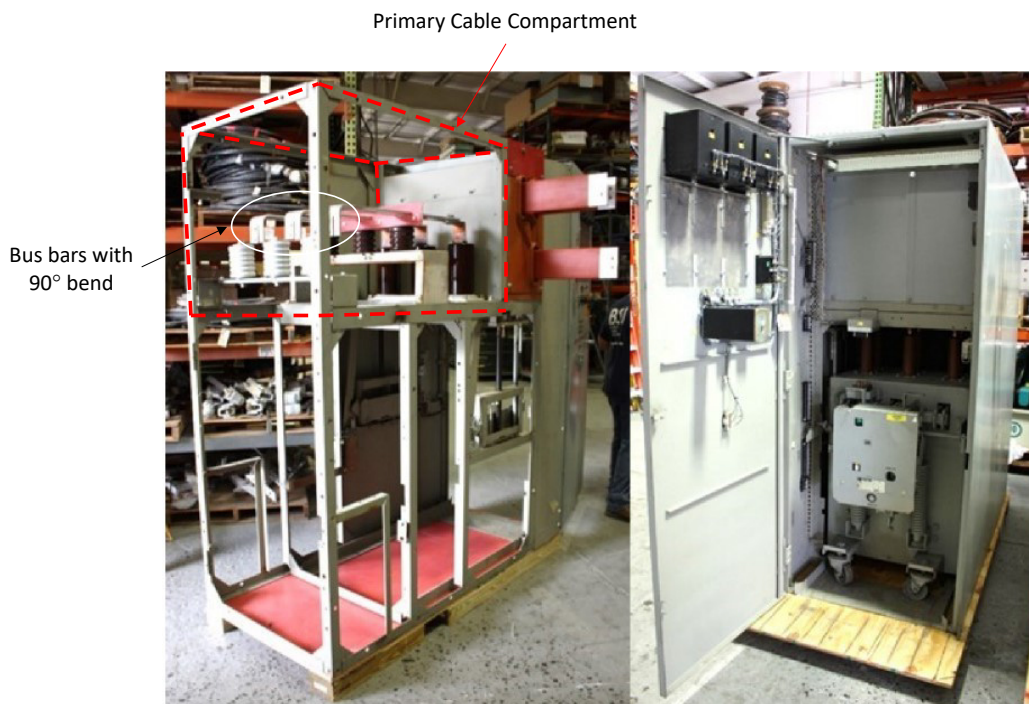


**Figure 4-1**  
**GE Type M-36 switchgear enclosure**

There were five racks of instrumentation. Two racks (Rack 1 and Rack 4) were placed 0.91 m from the enclosure sides adjacent to the bus bar location, two racks were placed at 0.91 m (Rack 2) and 1.82 m (Rack 3) from the back face of the cabinet where the bus bars were located, and a fifth rack (Rack 5) was placed 0.91 m above the top of the cabinet. Each rack contained a number of measurement devices including ASTM copper slug calorimeters, plate thermometers, tungsten slug calorimeters, as well as cut segments of electrical cables or cable coupons. Device construction is described in the test report [6]. Instrumentation layouts are shown in Figure 4-2.

All four experiments used aluminum bus bars and initiated the arc inside the primary cable compartment (at the upper left where the bus bars bend 90° in the left image in Figure 4-1). Table 4-1 [6] summarizes the test conditions.

**Table 4-1**  
**Summary of 2018 medium-voltage switchgear experiments [6]**

Experiment	Electrode	System voltage (kV)	Current (kA)	Arcing fault duration (s)	Arc energy <sup>1</sup> (MJ)	Arc power <sup>2</sup> (MW)	Electrode mass loss (kg)
2-19	Aluminum	6.9	25.8	2.05	39.3	19.2	0.458
2-21	Aluminum	6.9	26.6	4.11	101	24.5	1.97
2-22	Aluminum	7.0	32.0	2.07	51.3	24.8	0.894
2-24	Aluminum	7.0	29.8	4.15	122	29.3	2.57

<sup>1</sup>Arc energy estimated from energy at generator.

<sup>2</sup>Average, determined by dividing arc energy by the arc duration.

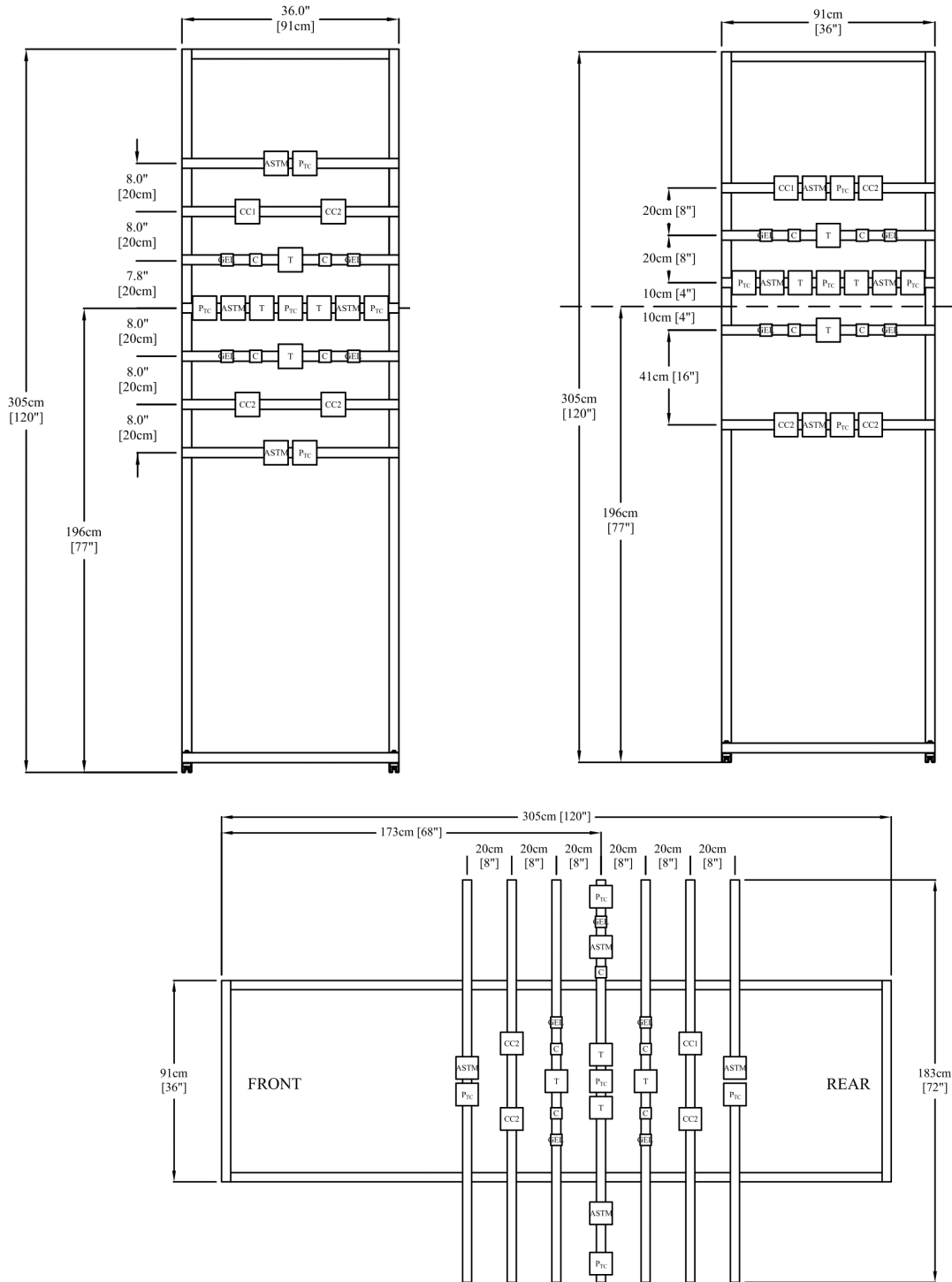


**Figure 4-2**  
 MV SWGR instrumentation racks (top left – racks 1,2, and 4; top right – rack 3; bottom – rack 5) [6]. Device symbols are: ASTM (ASTM copper slug calorimeter), P<sub>TC</sub> (plate thermometer), T (tungsten slug calorimeter), and CCn (cable coupon)

#### 4.1.2 Discussion of FDS Inputs

The FDS input geometry and other simulation parameters are identical to those described in Section 5.2.1. The exceptions are the definition of outputs, arc power, and simulation duration.

Devices are placed in FDS to provide output that corresponds to the actual devices used to measure the heat flux and incident energy during the tests. The output devices in the FDS model use static particles, which are a model feature that can respond to the exposure conditions but not affect the flow. A particle class is defined within the FDS model as a set of particle response parameters associated with each test measurement device as described below. The thermal response of the particles is evaluated by FDS by solving the one-dimensional heat condition equation at the appropriate device locations and orientations (see Figure 4-2). Figure 4-3 shows the FDS geometry with the device locations modeled. These particle classes are defined to model the specific construction of each instrument. The particle classes are defined as follows:

- The plate thermometer is a cartesian surface with a 0.79 mm plate of Inconel backed by a 2.54 cm layer of ceramic fiber.
- The ASTM slug calorimeter is a cartesian surface with a 1.6 mm copper plate, a 9.7 mm air-gap, a 3.4 mm red board plate backed by a 2.54 cm layer of marinite board.
- The tungsten slug calorimeter is a cartesian surface with a 1.5 cm tungsten plate backed by a 1.7 cm layer of marinite board.

For validation purposes, it is better to replicate the physical measurement being made rather than quantities derived from the physical measurement (i.e., heat flux).

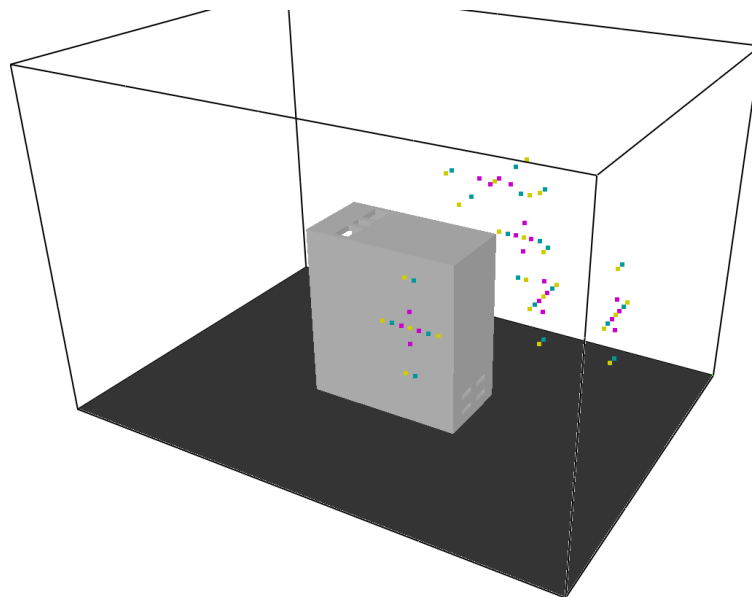


**Figure 4-3**  
FDS geometry showing particles used for instrumentation (magenta is a tungsten slug calorimeter, yellow is a plate thermometer, and teal is an ASTM copper slug calorimeter)

The arc power is defined using the power indicated in Table 4-1 with adjustments to account for the electrode mass loss per the discussion in Sections 3.7 and 3.8. Equations 3-4 and 4-5 are used instead of the measured mass loss for validation.

The four FDS simulations run for 6 s. For each experiment, this was sufficient time to capture the peak temperatures seen in the various gauges. The temperature rise of each gauge (which is proportional to the total exposure) is used to assess the performance of FDS.

### 4.1.3 Results of FDS Simulations

There are three experimental outputs considered for FDS validation. The first is the enclosure breach time. PRA targets outside of an enclosure do not see significant exposures from a HEAF unless they have a direct line of sight to the arc or can be engulfed in the high-temperature outflow from the electrical enclosure. For a given HEAF duration, the breach time determines how long targets are exposed to the high-temperature outflow. The second is the amount of damage to the enclosure. The size of holes in the enclosure defines the view factor that a target has of the volume inside the HEAF enclosure (arc location). The third is the maximum temperature achieved by the plate or slug calorimeter during the experiment. This represents the actual target exposure and is the primary quantity of interest for defining the energetic ZOIs.

Table 4-2 shows the breach time estimated from videos of the experiment and the breach time predicted by FDS. Also shown is the highest exposure measured during the experiment. Breach times are overestimated for all experiments with larger errors for shorter experiments (tests 2-19 and 2-22). For the 2 s experiment, while the breach times result in 0.21 – 0.57 second over-predictions in the breach time, these experiments had exposures of 1.4 MJ/m<sup>2</sup> and 2.1 MJ/m<sup>2</sup> or less compared to the 15 MJ/m<sup>2</sup> target fragility criteria which corresponds to thermoplastic (TP) jacketed cables or aluminum bus ducts [10]. The energetic ZOIs for these experiments are small and predictive errors for small energetic ZOIs are unlikely to have a large risk significance given that there is generally clearance around MV SWGR to support operation and maintenance activities. For the 4 s experiments, the difference in the predicted and observed breach time is less than 0.2 s for both cases. Note that part of the differences between measured and predicted breach times is due to the 0.1 s time FDS uses to increase the arc energy from zero to its full value.

**Table 4-2**  
**FDS versus observed electrical enclosure breach times for the 2018 MV SWGR experiments [6]**

Experiment	Experiment duration (s)	Breach time (s)		Post-breach time difference <sup>1</sup> (s)	Highest exposure at 0.9 m (MJ/m <sup>2</sup> )
		Experiment video	FDS		
2-19	2.05	0.53	1.1	– 0.57	1.4
2-21	4.11	0.65	0.82	– 0.17	7.0
2-22	2.07	0.60	0.81	– 0.21	2.1
2-24	4.15	0.61	0.73	– 0.12	15 <sup>2</sup>

<sup>1</sup>Experimental result relative to the predicted value.

<sup>2</sup>Fragility report estimate using test 2-24 Rack 3 data at 1.8 m and relative ratio of Rack 2 and Rack 3 for other tests [10].

Figure 4-4 through Figure 4-7 show the post-test enclosure condition at the end of the FDS simulations for the four experiments. For experiment 2-19, FDS predicts small holes on the sides and a larger hole on the back enclosure face. During the experiment, only a back breach occurred; the hole size is similar. For experiment 2-21, holes are seen on both sides and the back face with FDS predicting similar hole sizes. FDS also predicts a hole on the top. The post-test photos for this experiment show that the top face is not breached in this experiment [6]. For experiment 2-22 (Figure 4-6) and experiment 2-24 (Figure 4-7) FDS predicts hole sizes and locations similar to those observed in the experiments.



**Figure 4-4**  
**Enclosure condition post-HEAF for experiment 2-19**

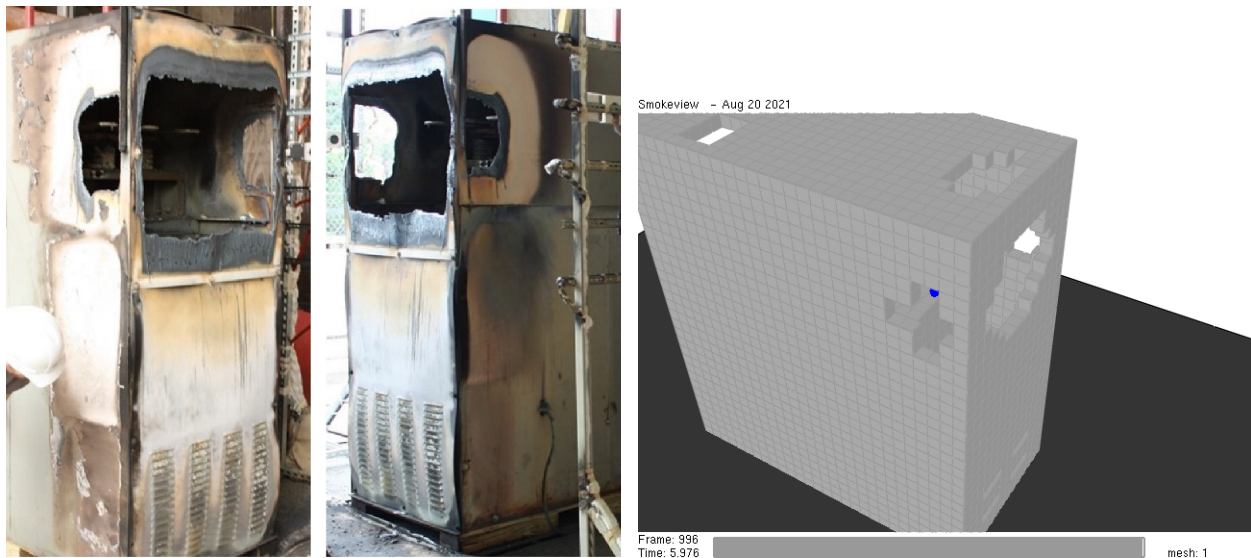


**Figure 4-5**  
**Enclosure condition post-HEAF for experiment 2-21**

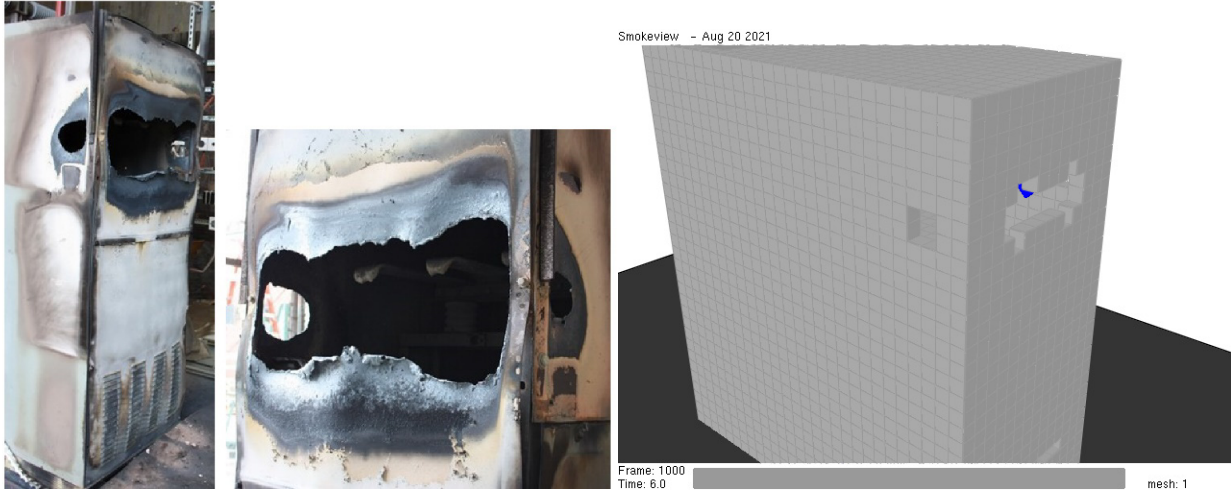


**Figure 4-6**  
**Enclosure condition post-HEAF for experiment 2-22**

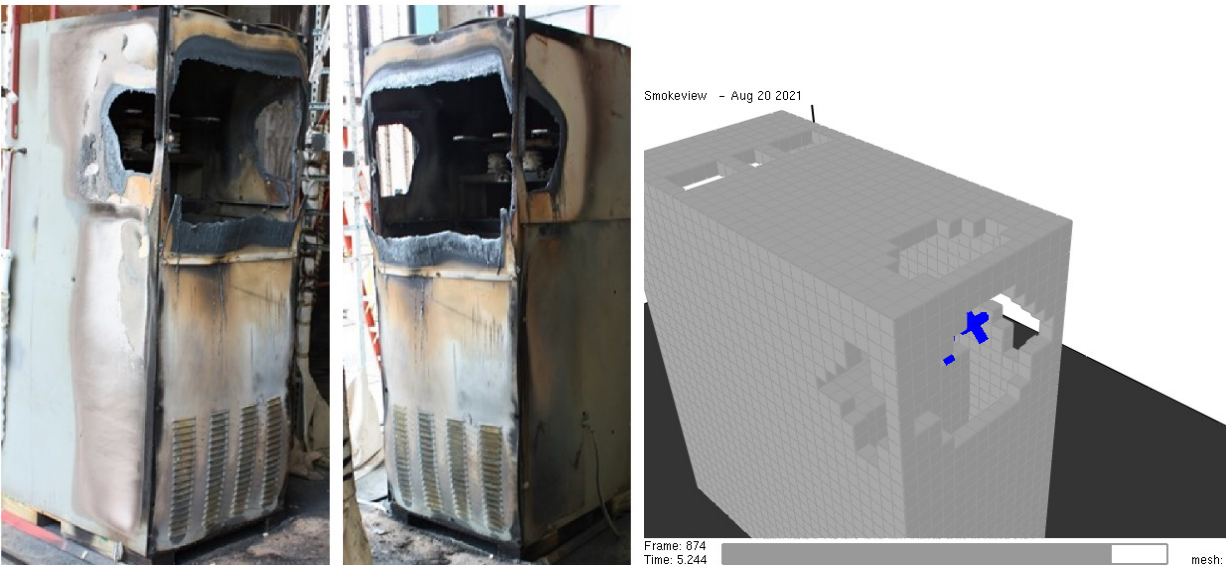


**Figure 4-7**  
**Enclosure condition post-HEAF for experiment 2-24**

Figure 4-8 shows the measured and predicted temperature rise for each instrument gauge for the four MV SWGR experiments. There is a tendency for FDS to underpredict the values for Racks 1 and 4 (combined) and for Rack 5. During the experiments, the internal pressure of the enclosure increased and caused the enclosure exterior panels to bulge outward slightly. This opened small gaps along the edges of the panels where high-temperature outflow occurred. These gaps are not included in the FDS model. This is likely a significant factor in the differences between FDS predictions and the test results for these cases. The locations with the largest under predictions are also locations with the lower temperature rises. It is the highest temperature location at a given distance from the enclosure that determines the energetic ZOI, and data corresponding to those locations are better predicted than the lower temperature points for Racks 1 and 4 (combined) and for Rack 5. Racks 2 and 3, oriented facing the large hole in the back of the enclosure, are much better predicted by FDS.

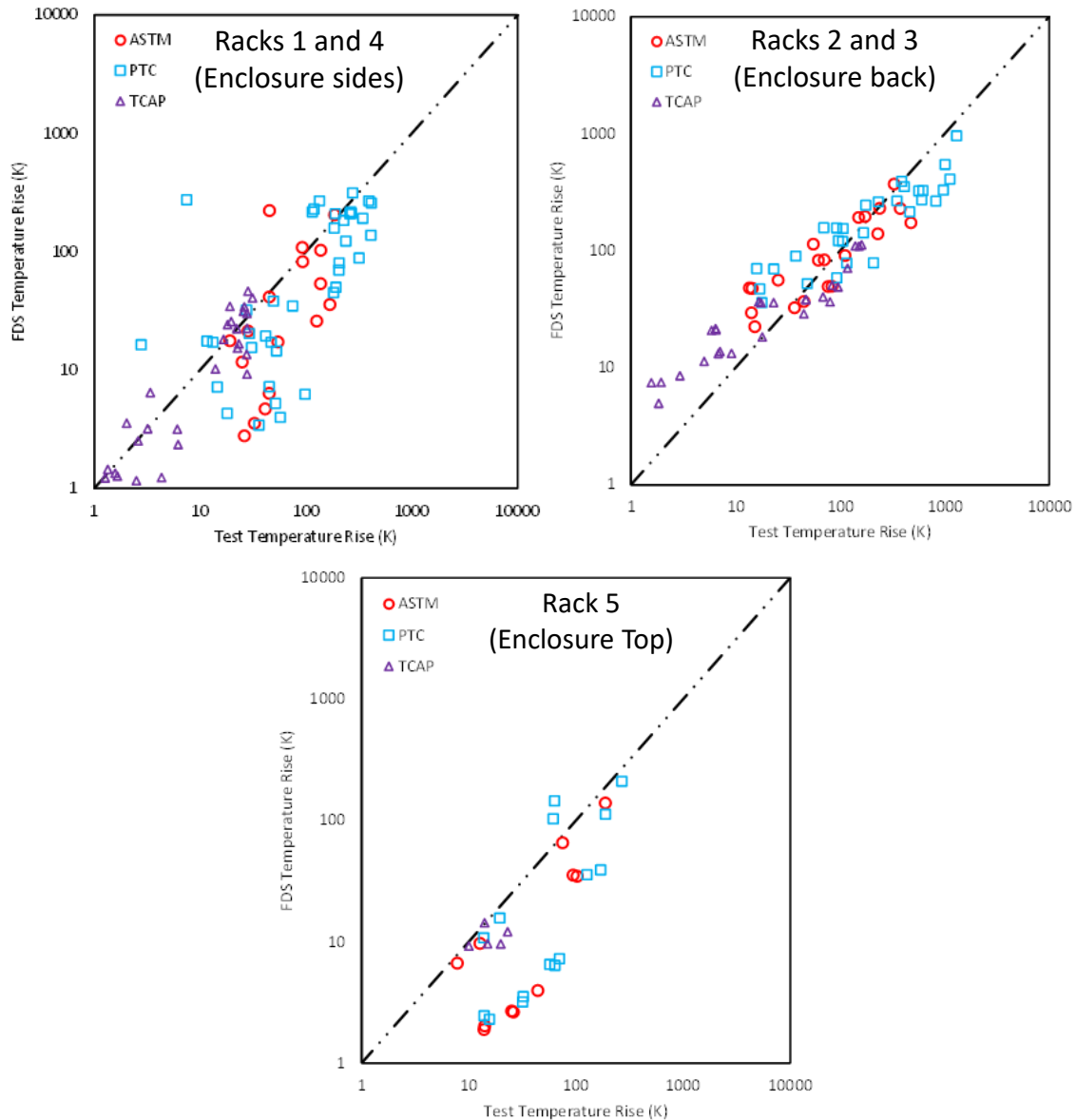


**Figure 4-8**  
**Scatterplot of measured versus FDS-predicted temperature rise for the 2018 MV SWGR experiments. Top left – Racks 1 and 4 (enclosure side), top right – Racks 2 and 3 (enclosure back), bottom – Rack 5 (enclosure top). Symbol type indicates gauge type**

#### 4.1.4 Model Uncertainty Statistics

The process outlined in the FDS Validation Guide [16] is used to estimate the FDS bias and relative standard deviation (uncertainty) for modeling the exposure from a HEAF. The relative standard deviation represents the degree of scatter, and the bias represents the tendency to over- or under-predict the data. In statistical terms, if the expected (true) measured value is  $\mu$ , then the expected FDS value,  $M$ , would be  $M = \mu \times \delta$  where  $\delta$  is the bias. The expected FDS value has a normal distribution with a relative deviation of  $\sigma$ .

The calculation process is applied to a set of measured values ( $M$ ) and predicted values ( $E$ ) as shown in Equation 4-1 [16]:

$$\overline{\ln(M/E)} = \frac{1}{n} \sum_{i=1}^n \ln(M_i/E_i) \quad (4-1)$$

where  $M_i$  is the  $i^{\text{th}}$  model prediction corresponding to the  $i^{\text{th}}$  measured value  $M_i$  and  $n$  is the total number of pairs of measured and predicted data. The normalized standard deviation of the model error can be computed using Equation 4-2 [16]:

$$\sqrt{\tilde{\sigma}_M^2 + \tilde{\sigma}_E^2} \cong \sqrt{\frac{1}{n-1} \sum_{i=1}^n [\ln(M_i/E_i) - \overline{\ln(M/E)}]^2} \quad (4-2)$$

where  $\tilde{\sigma}_M$  is the normalized standard deviation of the model error and  $\tilde{\sigma}_E$  is the normalized standard deviation of the experimental error. The model bias is calculated using Equation 4-3 [16]:

$$\delta = \exp\left(\overline{\ln(M/E)} + \frac{\tilde{\sigma}_M^2 - \tilde{\sigma}_E^2}{2}\right) \quad (4-3)$$

where  $\delta$  is the model bias. A bias greater than one indicates that on average, the model tends to overpredict the parameter and vice versa for a bias less than one.

The normalized standard deviation of the experimental error is unknown; however, estimates are provided by McGrattan et al. [30] based on work described in NUREG-1824, Volume 1 [31]. For heat flux and temperature measurements, a conservative estimate of the normalized standard deviation of the experimental error is 0.2 [30, 31].

The relative standard deviation and model bias vary with the set of data points considered. Table 4-3 summarizes these parameters based on temperature measurements for different rack groupings for the 2 s and 4 s tests. Although the temperature is not directly used to estimate the energetic ZOIs, the temperature is directly measured rather than integrated. Since the devices used to measure temperature are close to room temperature, the incident heat flux and the integrated energy are assumed to scale linearly with the temperature and have the same error statistics.

The rack groupings shown in Table 4-3 correspond to the measurement locations at the MV SWGR rear (Racks 2 and 3), sides (Racks 1 and 4), and top (Rack 5). The highest exposures generally occur in the rear, and this is where the greatest model error (lowest model bias) occurs, except for the top of the 2 s tests where FDS underpredicts the exposure. Since the arc location varies within the equipment, the use of location specific model statistics may not be appropriate for configurations that are different from the 2018 MV SWGR experiments.

**Table 4-3**  
**Model bias and normalized standard deviation for different temperature data point groupings [6]**

Arc Duration	Datapoint Set	Model Bias, $\delta$	Normalized Standard Deviation of Model Error, $\tilde{\sigma}_M$
2 s	Racks 2 and 3	1.25	0.89
	Racks 1 and 4	0.727	0.99
	Rack 5	0.202	0.80
	All racks	1.56 <sup>1</sup>	1.33
4 s	Racks 2 and 3	0.596	0.25
	Racks 1 and 4	1.21	0.87
	Rack 5	0.765	0.58
	All racks	0.908	0.71

<sup>1</sup>The standard deviation is large compared to  $\overline{\ln(M/E)}$  in Equation 4-1, resulting in a bias that is greater than the component data sets. The large standard deviation results from a mix of moderately high and moderately low predictions and very low predictions in the selected dataset.

The FDS-predicted temperature rise is sensitive to enclosure breach times. The various gauges see a rapid increase in the heat flux exposure once a breach occurs. Since FDS is slightly delayed in predicting breach time, this effect is much more significant for the 2 s experiments than the 4 s experiments. As an example, if the breach time was 0.5 s, and FDS predicted 0.8 s, then for a 2 s experiment, that would be a change from 1.5 s to 1.2 s of post-breach exposure, which is a 20% reduction. For the 4 s experiments, it is 9%. Data from the 2 s MV SWGR experiments indicate the energetic ZOI on all faces is relatively close to the enclosure and within the ZOI in NUREG/CR-6850 [1]. Data from the 4 s experiments indicate the energetic ZOI is comparable to the ZOI recommended in NUREG/CR-6850 [1]. As discussed in Section 5.1.1.5, there are potential HEAFs with longer durations and higher total energies than the 2018 experiments. HEAFs with the largest energetic ZOIs have more opportunity to damage nearby cable trays and conduits and can be more consequential in certain circumstances. To ensure the energetic ZOIs for those events are well characterized, the WG selected the most conservative model bias among the 4 s dataset groupings listed in Table 4-3, which corresponds to Racks 2 and 3, to represent the model uncertainty for all locations and arc durations. As seen in Figure 4-8, the FDS performance for the 4 s experiments is significantly better than the 2 s experiments. In large part, this is due to the 4 s experiments failing both the top and sides of the enclosure making leakage around gaps less important to the total exposure. The normalized standard deviation of the model error is conservatively selected using the dataset for all racks to provide a more representative estimate of the data scatter among all datasets. The results are as listed as follows:

- Model bias,  $\delta$ : 0.596
- Normalized standard deviation of the model error,  $\tilde{\sigma}_M$ : 0.71

The model uncertainty statistics are shown in Figure 4-9 in combination with the predicted and measured data for the 4 s combined Rack 2 and 3 dataset. Figure 4-9 also shows the model uncertainty statistics with the complete 2 s and 4 s datasets. The 2 s dataset plot shows that the FDS underpredictions are dominated by low temperature points (under 100 K) and overall, the 2 s is reasonably well characterized using the 4 s results at higher temperatures.

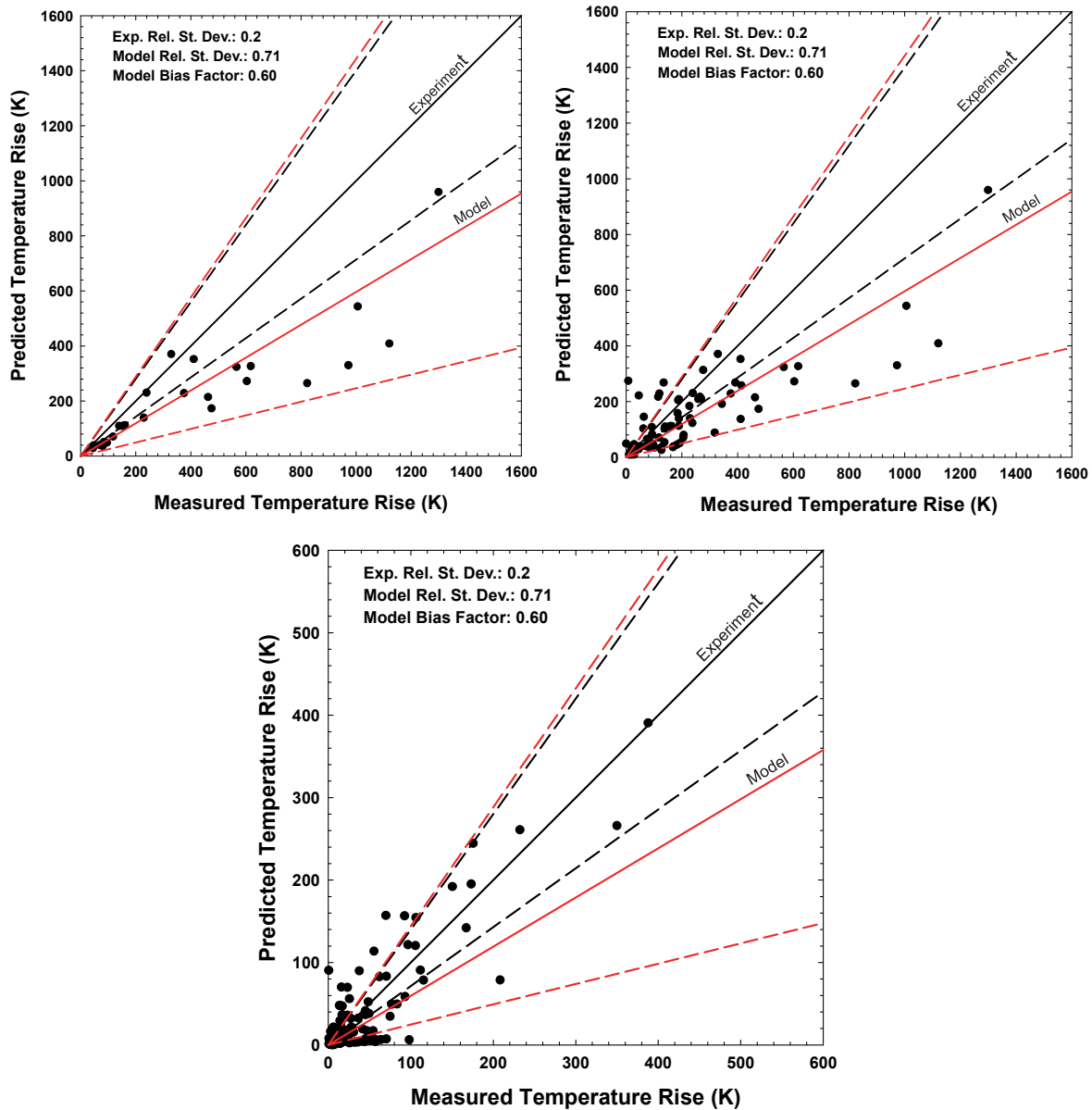


**Figure 4-9**

Scatterplot of measured versus FDS-predicted temperature rise for the 2018 MV SWGR experiments with model uncertainty statistics. Top left – Racks 2 and 3 (rear) for 4 s arc duration experiments, top right – All racks, 4 s arc exposure duration experiments, bottom – all racks, 2 s arc exposure experiments. Solid lines are the average measured or predicted values and the dashed lines are the 95<sup>th</sup> percentile confidence intervals for measured and predicted values

Figure 4-9 depicts the average experimental value (solid black line) and average model prediction (solid red line) for a given measured value, both with 95% confidence intervals. FDS on average underpredicts the experimental measurement by the bias factor. Dividing the FDS prediction by the bias factor brings the average experimental prediction and average FDS predictions into alignment as shown in Equation 4-4 [32]:

$$\bar{M} = \frac{M}{\delta} \quad (4-4)$$

where  $\bar{M}$  is the updated FDS model prediction (aligned with experimental measurement average),  $M$  is the model prediction, and  $\delta$  is the model bias factor. The 95<sup>th</sup> percentile confidence interval (two standard deviations above from the mean) is then defined as Equation 4-5:

$$M_{95} = \left(\frac{M}{\delta}\right) \cdot (1 + 2\tilde{\sigma}_M) \quad (4-5)$$

where  $M_{95}$  is the 95<sup>th</sup> percentile confidence interval and all other terms have been defined. The 5<sup>th</sup> percentile confidence interval (two standard deviations below the mean) is then defined as Equation 4-6:

$$M_5 = \left(\frac{M}{\delta}\right) \cdot \left(\frac{1}{(1+2\tilde{\sigma}_M)}\right) \quad (4-6)$$

where  $M_5$  is the 5<sup>th</sup> percentile confidence interval and all other terms have been defined. The model bias is used to bring the FDS output values into alignment with experimental values to determine the energetic ZOIs.

## 4.2 Benchmarking Against FEDB 50935

### 4.2.1 Summary of Event

In 2011, a HEAF occurred in the circuit breaker cubicle of a low-voltage switchgear (FEDB 50935 [12]). The arc started at the circuit breaker stabs and then moved into the bus bar compartment. No damage occurred to cables or equipment outside the switchgear. The cubicle containing the circuit breaker stabs (where the HEAF initiated) and one other circuit breaker were damaged in the event. The event reports and supporting information do not describe the damage to the enclosure or its contents other than the circuit breaker and bus bars. Figure 4-10 shows the cabinet where the HEAF initiated (right-side of the figure) and the back side where the bus bars were located (left side of the figure). The left photo in Figure 4-10 shows that the arc failed the partition between the circuit breakers and the middle main bus bar compartment. The photo of the rear cable compartment shows a region of discolored paint opposite the circuit breaker location on the front. There may have been some damage to the partition between the main bus bar and rear cable compartments.



**Figure 4-10**  
**Back side of initiating circuit breaker (left) showing damaged bus bars and back side of low-voltage switchgear (right) showing smoke stains and discolored paint behind the arc location (brown stain at the mid-height of the middle section) [33]**

This event is the basis for the FDS LV SWGR simulations described in Section 5. The event lasted 41 s and had two distinct periods: a 20 s period of fluctuating current at a higher average value followed by a 21 s period at a lower average value, as recorded in the current profile in Appendix A.

#### **4.2.2 Discussion of FDS Inputs**

The FDS model geometry for the LV SWGR event is based on the Westinghouse DS metal-clad switchgear (Section 5.2.2). For validation purposes, the FDS simulation placed the arc at the circuit breaker at the mid-height of the enclosure. The arc is simulated with using two constant-current segments as described in Section A.3 of Appendix A (see Figure A-7).

#### **4.2.3 Results of FDS Simulation**

Results of the FDS simulations are shown in Figure 4-11. The FDS geometry consisted of a Westinghouse DS enclosure with two columns of circuit breakers. The FDS simulation predicts more extensive damage to the partition between the circuit breakers and bus bar compartment than observed in post-event photos. The FDS model predicts small holes in the sides of the bus bar and circuit breaker compartments which were not reported in the event documentation; however, the FDS model did not include the mounting rails for the circuit breaker or the enclosure panels. The FDS model shows a small hole between the middle main bus bar compartment and the rear cable compartment. This was not mentioned in the event report, but it appears to be consistent with the discolored paint on the rear compartment panel.

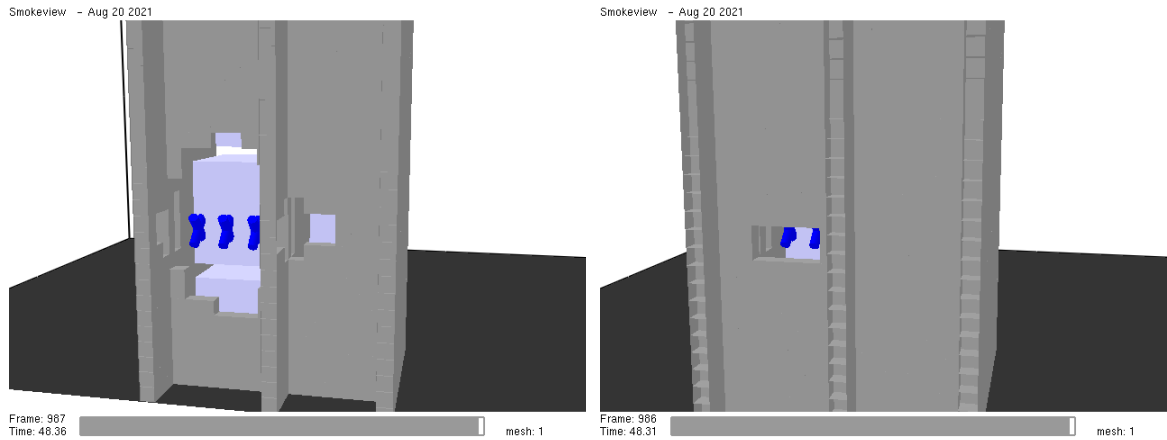


**Figure 4-11**  
FDS-predicted damage for FEDB 50935. Left image clips the back of the enclosure to show the panel separating the circuit breaker cubicles from the middle main bus bar compartment. Right image clips the back face of the enclosure to show the partition between the main bus bar compartment and rear cable compartment

### 4.3 Benchmarking against the Full-Scale Test of FEDB 51764

The NRC did not conduct any usable laboratory testing of bus duct HEAFs and there is little data against which to compare the FDS modeling results. The EPRI/NRC working group identified two events that could be modeled to support benchmarking: the first was a NSBD HEAF that occurred in a U.S. nuclear power plant and was later replicated in full-scale testing at Keiring van Ekektrotechnische Materialen te Arnhem (KEMA) laboratories. The second was a generator-fed NSBD HEAF that occurred at a different U.S. nuclear power plant. This section presents the benchmarking using the full-scale testing at KEMA and Section 4.4 provides the benchmarking using the generator-fed, NSBD HEAF.

#### 4.3.1 Summary of Event

On January 17<sup>th</sup>, 2017, a HEAF occurred in a NSBD (FEDB 51764). The event was replicated in a full-scale test on October 3, 2017. The test apparatus consisted of two parallel bus ducts, one located 0.3 m above the other, supported by a frame. The upper duct housing was constructed of 3.2 mm thick steel on the top and sides and the bottom was a removable cover constructed of aluminum. The upper duct was 0.64 m wide and 0.42 m high. The lower duct housing was constructed of aluminum. Both ducts contained insulated aluminum bus bars with Glastic bus bar supports every 0.91 m. The upper duct bus bars measures 0.015 m wide and 0.15 m high, spaced 0.17 m apart on center. The ends of the upper duct were 86% covered, leaving an opening of 14%, or approximately 0.038 m<sup>2</sup>.

The arcing fault was initiated at the bottom of the bus bars in the upper duct. A small area of insulation was removed adjacent to the center bus bar support, and a 3.2 mm hole was drilled near the bottom of each bus bar. A 24-gauge bare tinned copper wire was strung across all three phases to initiate the fault.

The electrical energy delivered to the upper duct had the following properties:

- 4,500 V (line-to-line voltage of 650 volts)
- 14,700 A
- 1.02 s

### 4.3.2 Discussion of FDS Inputs

A simplified model of the test apparatus was constructed in FDS (Figure 4-12). The model included the upper bus duct housing, the upper bus duct bus bars, and the lower bus duct housing. The model did not include the frame where the ducts were resting, the bus bars of the lower duct, or the Glastic bus bar supports, as they are assumed to have no impact on the simulated quantities of interest.

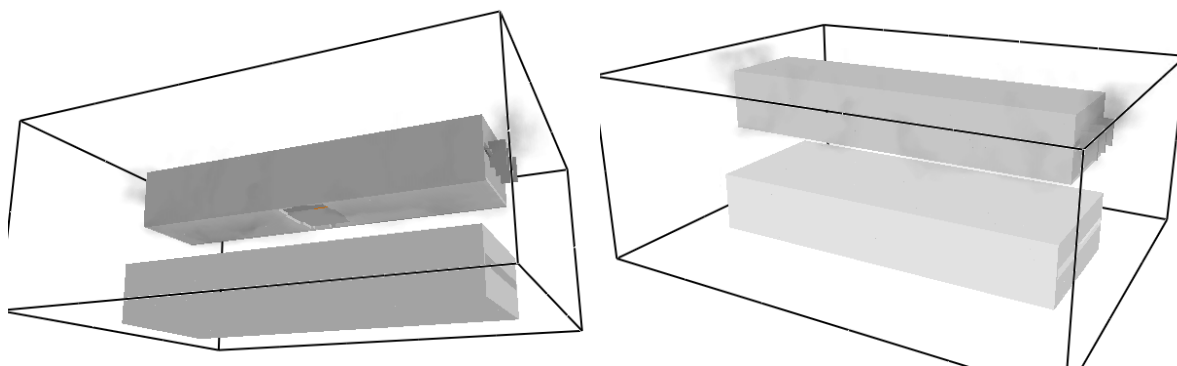


**Figure 4-12**  
FDS-predicted holing in the bottom of the top duct (left) and no observable damage to the top of the bottom duct (right)

The FDS model of the bus ducts relied on several additional assumptions, including:

- Liquid droplets from molten metal are not assumed to affect the results and are neglected. Gaseous particles that oxidize and release energy are included in the model.
- The duct housing, while melted, does not participate in any oxidation process nor contribute to any heat release. This is because the FDS model is developed to simulate a multi-phase bus bar fault rather than a ground-fault to the aluminum duct housing. For this bus bar fault model, the underlying assumption is the housing would tend to melt in large sections rather than generate significant amounts of oxidizing particles, and this source of energy is not included.
- The fraction of the mass of aluminum bus bar lost that is converted to vapor is 0.075.
- The bus bar vaporization begins 0.2 s after arc initiation and ends 0.2 s after arc extinguishment.

The test report states that 0.3 kg of aluminum bus bar material was lost across all three phases. Using the assumed 0.075 vapor fraction, a total of 0.0225 kg of aluminum vapor is injected into the computational domain using three nozzles located at the arc initiation point on each bus bar to simulate the contribution of oxidizing aluminum.

The total electrical energy delivered to the fault is calculated as:

$$E = \sqrt{3} \times V_{\text{arc,L-L}} \times I \times t = \sqrt{3} \cdot 650 \cdot 14700 \cdot 1.02 = 16.9 \text{ MJ}$$

The radiative fraction of the arc energy for an aluminum bus bar is estimated from the data provided by Cressault [26] as 0.573 (see Figure 3-3 in Section 3.3). The 16.9 MJ of energy is introduced into the computational domain by specifying a volumetric heat release rate in a volume comparable to that of the arc volume. To avoid numerical instabilities, the heat release rate is ramped up and down over 0.1 s as previously described. The heat release rate volume is biased slightly downward from the center of the duct to replicate the arc initiation location at the bottom of the bus bars.

### **4.3.3 FDS Simulation Results**

The laboratory testing did not include instrumentation to measure temperature, heat flux, or incident energy. The goal of the testing was to investigate whether a fault in the upper duct would affect the lower duct. Accordingly, the FDS validation relied on qualitative comparisons between the test observations and the model predictions. Two points of comparison are used: the time from arc initiation to breach of the duct housings and the size of the duct housing breach.

The bottom aluminum panel of the upper duct was first observed to breach 0.28 s after the initiation of the arc in the laboratory experiment. FDS predicts an initial breach of the same panel at 0.39 s, which includes a 0.1 s arc power ramp as previously described. This 40% overprediction of time-to-breach is consistent with the results of the MV SWGR modeling.

The size of the breach in the bottom panel is described in the test report as 0.28 m long and 0.58 m wide (0.16 m<sup>2</sup>). FDS predicts a final breach size of 0.18 m<sup>2</sup>, representing a 12.5% overprediction.

Although there are no measurements of temperature, heat flux, or incident energy taken around the duct in the experiment, there was no observable damage to the steel sides and top of the upper duct, nor the aluminum housing of the lower duct, which provides some indication of the maximum thermal conditions outside the duct. Consistent with these experimental observations, FDS predicted no damage to any of the panels on either of the ducts with the exception of the bottom aluminum panel of the upper duct.

## **4.4 Benchmarking against the Bus Duct Event in an Elbow (FEDB 51765)**

### **4.4.1 Summary of Event**

A generator-fed HEAF occurred at a vertical elbow in a NSBD with aluminum bus bars and an aluminum duct housing (FEDB 51765) [34]. The HEAF lasted for 15 s, the time it took for the generator energy decay to result in arc extinguishment. A solid-bottom cable tray was located approximately 25 cm (10 in.) below the bottom of the elbow, with 13 cm (5 in.) of overhang in the horizontal plane. Post-event photos show charred cables and molten aluminum slag from the bus bars and duct housing on the cables and in the tray (Figure 4-13). The plant reported that the cables experienced jacket damage and exposed insulation but remained functional. The cables in this tray were Kerite, which is expected to have a fragility threshold between the thermoplastic and thermoset limits, but this depends on the specific formulation [35].

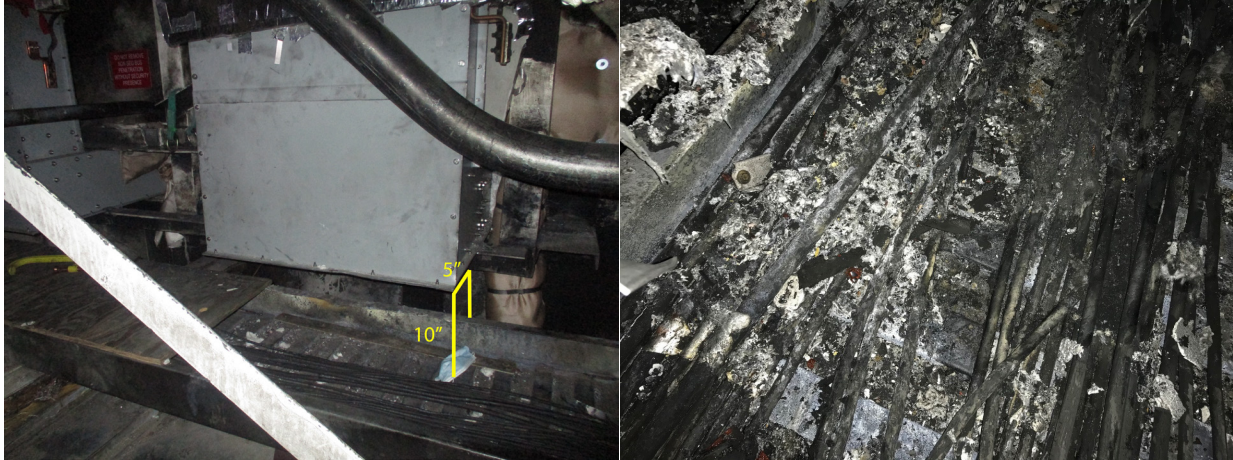


**Figure 4-13**  
 Repaired NSBD from the HEAF event showing cable tray location (left), aluminum metal and charred cables in cable tray (right)

#### 4.4.2 Discussion of FDS Inputs

A simplified model of the vertical elbow is constructed in FDS (Figure 4-14). In addition to the arrays of incident energy measurement devices located orthogonally to the faces of the duct near the elbow, an extended array of measurement devices is placed in the region of the cable tray.

Because of the high degree of similarity between this event and the comparably configured geometry for the bus duct simulations from the matrix (elbow geometry, aluminum bus bars, aluminum duct housing, 0 s stiff-source duration, 15 s generator decay duration), the working group elected to use the nominal duct dimensions from the FDS simulation matrix for bus ducts: 0.4 m tall, 0.56 m wide and with a duct housing thickness of 3.2 mm, corresponding to 11-gauge sheet metal.

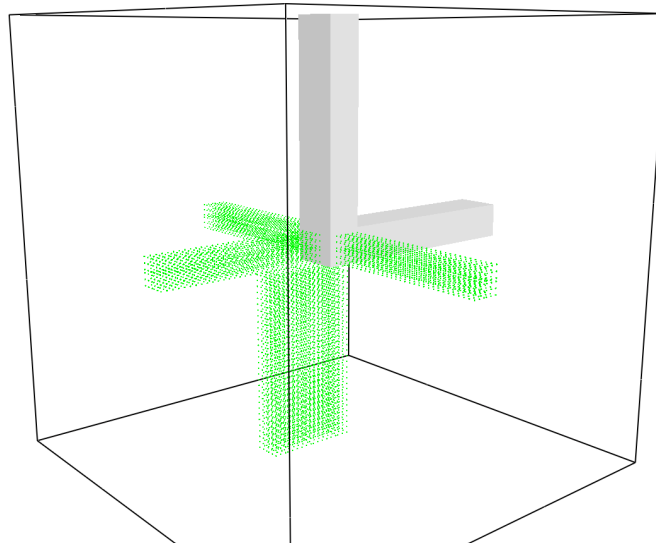


**Figure 4-14**  
 FDS model of NSBD vertical elbow. Incident energy measurement devices shown as green dots

The FDS model relied on several assumptions, including:

- The arc is modeled as stationary, despite evidence that during the actual event, the arc initiated several inches away from the elbow in the horizontal portion of the duct and moved towards the elbow. Modeling the Lorentz forces that push the arc along the bus bars is beyond the scope of this effort. Accordingly, the model results are expected to overpredict the incident energies in the cable tray region.
- Though the radiative fraction of the arc given by Cressault [26] is dependent upon arc power, a single, static radiative fraction corresponding to the initial arc power is assumed for generator-fed faults.
- Liquid droplets from molten metal are not assumed to affect the results and are neglected. Gaseous particles that oxidize and release energy are included.
- The duct housing, while melted, does not participate in any oxidation process nor contribute to any heat release.
- The ends of the duct are open to the computational boundary, i.e., the hot gases that pass through the ends of the duct are no longer accounted for. This computational boundary is sufficiently far from the location of the fault and targets and is not expected to affect the results.

#### **4.4.3 FDS Simulation Results**

A contour plot of the total incident energy in the central plane of the bus duct predicted by FDS is shown in Figure 4-15. The FDS results in Figure 4-15 are adjusted using the model bias determined in Section 4.1.4. The 15 MJ/m<sup>2</sup> and 30 MJ/m<sup>2</sup> target fragility thresholds are outlined in magenta and are applicable to the cable targets in the cable tray. The cables in the cable tray are predicted to experience incident energies ranging from 20 MJ/m<sup>2</sup> to 50 MJ/m<sup>2</sup> depending on their location within the tray.

Given that the fragility for the Kerite cables should lie between 15 MJ/m<sup>2</sup> and 30 MJ/m<sup>2</sup>, depending on the formulation [35], one would expect to see loss of cable functionality across most, if not all, of the cables in the cable tray. However, in the actual event, the arc did not start at the elbow; it initiated several inches away in the horizontal segment of the duct and moved towards the elbow. Because the FDS model places the arc at the elbow for the entire duration of the HEAF, some overprediction of incident energy is expected, given 30% of the arc energy of a generator-fed fault is released in the first 2 s. Considering this overprediction and the near-failure state (damaged jacket, exposed insulation) of the cables in the tray, the results of the simulation are a reasonable approximation of the actual event.

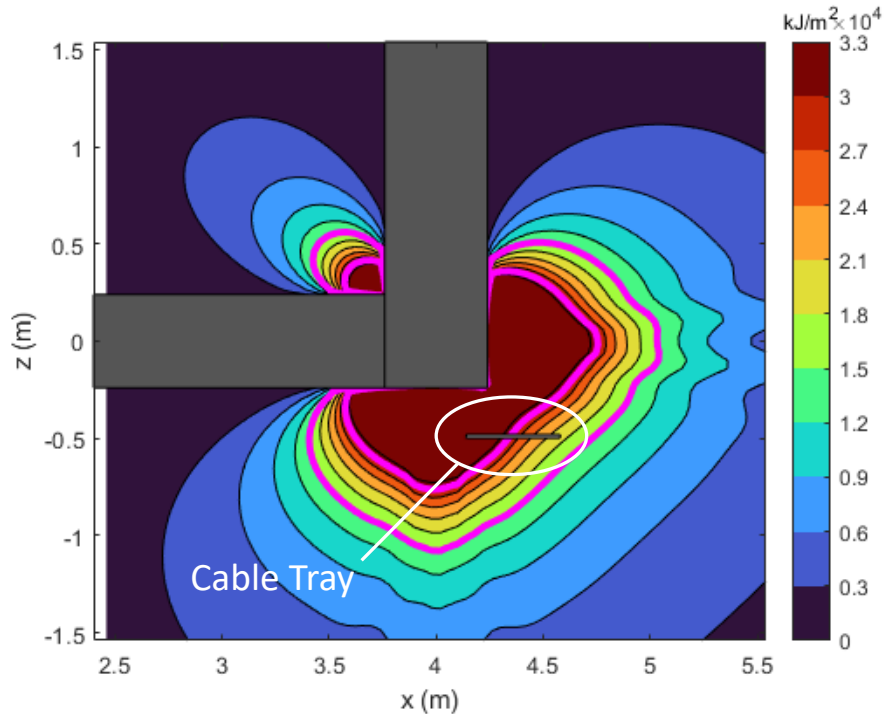


**Figure 4-15**  
**Contour plot of the FDS simulation results for a 0 s stiff, 15 s decay arc at a NSBD elbow. The approximate location of the cable tray for this event shown below bus duct elbow as indicated. Magenta contours are the 15 MJ/m<sup>2</sup> and 30 MJ/m<sup>2</sup> target fragility thresholds applicable to thermoplastic (TP) and thermoset (TS) cables**

#### 4.5 Summary of FDS Validation for Modeling HEAFs

The following experiments and events are used to validate FDS for modeling HEAFs:

- The 2018 MV SWGR experiments [6]
- A LV SWGR event (FEDB 50935)
- A full-scale experiment replicating a NSBD event (FEDB 51764)
- A HEAF event at a NSBD elbow (FEDB 51765) [34]

The 2018 MV SWGR experiments are used to assess FDS capability to predict enclosure breach time, the extent of the enclosure damage, and the gauge temperature at a fixed location (i.e., target exposure). Overall, the predicted breach times are reasonably well predicted, though there are significant differences in some situations with a small predicted external energetic ZOI.

Generally, the extent of damage predicted by FDS is comparable to the observed damage extent for the tests considered. Finally, FDS is shown to underpredict the gauge temperature, likely due to differences in the actual versus predicted breach time.

The 2018 MV SWGR 4 s experiments are considered in the validation effort and are used to develop the overall relative standard deviation ( $\sigma$ ) and bias ( $\delta$ ) applied to the predicted exposure (see Section 4.1.4). The relative standard deviation and bias are calculated using the two 4 s switchgear tests since these experiments resulted in breaches of the top and sides of the electrical enclosures, making leakage around the gaps less important to the total exposure. The resulting

relative standard deviation and bias as determined from these FDS predictions and experimental results are 0.71 ( $\sigma$ ) and 0.596 ( $\delta$ ), respectively. These parameters are consistent for various device combinations for the 4 s MV SWGR tests and are applicable and adapted to all FDS simulations performed (including LV switchgear, MV switchgear, and NSBDs). The bias is used to adjust the predicted output quantity by  $M/\delta$  and the confidence interval was determined using Equations 4-5 and 4-6 in Section 4.1.4.

The LV SWGR event (FEDB 50935) [12, 33] is used to assess the overall ability of FDS to predict the damage extent in LV SWGR. The FDS geometry for the LV SWGR event included a Westinghouse DS type enclosure with two columns of circuit breakers. The FDS simulation showed more extensive damage to the partition between the circuit breaker and the middle main bus bar compartment than observed in post-event photos. The damage extent in other portions of the switchgear is comparable to the event observations.

The NSBD full-scale test is used to assess the capability of FDS to predict the breach time and damage extent in NSBDs. FDS predicted a longer breach time and comparable damage extent on all sides for this configuration. The HEAF that occurred at a NSBD elbow (FEDB 51765) [34] is used to assess the exposure predictions of FDS. In this case, FDS overpredicted the exposure and the damage potential to the target cables when characterized using the 15 MJ/m<sup>2</sup> target fragility criterion. However, the target cables were Kerite, which could have an intermediate damage threshold between TP and TS cables, depending on the Kerite formulation [35], and some overprediction is expected due to the stationary placement of the arc. The WG concluded that the FDS results for this model are reasonable.

From the metrics analyzed for the NSBD benchmarks, the predictive capabilities of FDS are comparable for NSBDs and switchgear enclosures. Because high-quality heat flux data only exists for switchgear enclosures, the HEAF WG chose to use the same bias factor when evaluating the results of the NSBD simulations.

The use of FDS for HEAF incorporates a larger number of assumptions with respect to the arcing phenomena and the response of the enclosure containing the arc than the types of applications considered in NUREG-1824 Supplement 1 [20]. These assumptions tend to result in greater uncertainty in the results, with FDS tending to underpredict the exposure resulting in a bias factor less than 1.0. In addition, the timescales are short and comparable to the breach times for metal enclosures. As noted in Section 4.1.4, FDS predictions are more accurate for 4 s arc durations than for 2 s arc durations due to small differences in the predicted breach time having less of an effect. The FDS results are adjusted by dividing the output by the bias factor, which increases the predicted exposure conditions since the bias factor is less than 1.0. This process aligns the predictions with the test observations used to calculate the bias factor. When these effects are incorporated into the model results with the model bias, the overall predictions are reasonable and useful for developing insights for different enclosure configurations and arc power.

# 5

## DEVELOPMENT OF THE HEAF SIMULATION MATRIX

---

This section discusses the approach for defining HEAFs evaluated in FDS and subsequently used to determine the energetic ZOIs for the LV SWGR, MV SWGR, and NSBDs. Insights into the energetic phase are obtained from full-scale testing, including the OECD and KEMA tests [5-7]. Due to the cost of testing, only a few HEAF experiments have been performed [5-9]. With limited full-scale testing, only a small number of possible configurations and boundary conditions associated with HEAFs have been tested. These testing programs have yielded insights on important variables that impact the size of the energetic ZOIs; however, the U.S. OE [11, 12] and the EPRI survey [3] indicated that the U.S. industry has significant variations of important parameters that must be accounted for to derive the most realistic energetic ZOIs. The following sections include detailed discussions on the derivation of important parameters and provides a set of HEAF simulations using these parameters to account for different physical, equipment, and electrical configurations.

### 5.1 Development of HEAF Model Simulations

The review of the limited full-scale test results [5-9], the open-box tests [4], and the relevant U.S. operating experience clearly underline the importance of variables such as 1) the arc energy, 2) the geometry and the physical configuration of the faulted equipment, 3) the location of the arcing fault in relation to the electrical distribution system (which affects the fault duration), and 4) fault origination location inside the faulted equipment in determining the level of damage of the faulted equipment and the energetic ZOIs. The EPRI survey [3] and operating experience [11, 12] are used to determine the most predominant equipment designs, equipment materials (conductor and enclosure), expected fault durations, arcing fault currents, and fault locations.

Given the different equipment designs and electrical configurations across the NPP fleet, the WG's main objective is to develop energetic ZOIs that could be used for general NPP electrical distribution system design, equipment type and orientation, and electrical protection scheme characteristics. A large number of plant-specific variables resulted in a significant number of parameter combinations for FDS modeling. Since the effort would not be economically or computationally viable, the HEAF WG defined a minimum number of HEAF simulations encompassing the predominant configurations and characteristics. The HEAF WG acknowledges that differences exist; however, the minimum number of simulations provides sufficient data to determine the energetic ZOIs for relevant characteristics such as equipment type, equipment orientation, and electrical distribution alignment.

The following sections provide the rationale for the selection of important parameters to develop representative FDS simulations for MV SWGR HEAFs (Section 5.1.1), LV SWGR HEAFs (Section 5.1.2), and NSBD HEAFs (Section 5.1.3).

### 5.1.1 Medium Voltage Switchgear

Based on OE events [11, 12], full-scale tests [6], and survey results [3], the parameters identified as the most impactful on the energetic ZOI are listed as:

- Bus bar material: copper or aluminum
- Switchgear manufacturer/models typically found in the NPPs, and used during the full-scale testing/FDS validation:<sup>1</sup>
  - GE Magne-Blast (vertical-lift circuit breaker)
  - ABB HK (horizontal draw-out circuit breaker)
- Fault initiation location:
  - Circuit breaker
    - Stab connection to the primary cable compartment bus bars or risers
    - Stab connection to main bus bars
    - Circuit breaker internal poles
  - Primary cable compartment bus bars (PCCBBs) or risers (also referred to as a riser compartment)
  - Main bus bars
- Power flow (bus supply or load circuit breaker)
- Energy level (fault current, fault duration, and arc voltage):
  - Best estimate fault current of 30 kA
  - Arc fault durations
    - Arcing fault duration of 2 to 5 s for faults with a constant current. The expected range of 2 to 5 s is obtained from transformer backup fault clearing time provided in the EPRI survey [3]
    - Generator-fed faults of up to 15 s in duration, with generator fault current decay during the coast-down immediately after a unit trip, either without a constant-current arc or with a constant-current arc duration of 3 s or 5 s
  - Arc voltage set to 650 V<sub>L-L</sub>, derived from full-scale testing (see Appendix A)

#### 5.1.1.1 Bus Bar Material

The EPRI survey [3] found that almost half of the US NPP fleet has some MV SWGR bus bar material made from aluminum. From the HEAF testing program, it was not clear if the electrode composition (e.g., copper versus aluminum) was a significant factor in determining target exposure and the associated energetic ZOI. Therefore, both materials are considered in the FDS

---

<sup>1</sup>There are other types and designs of the MV SWGR in the U.S. fleet. Subsection 5.1.1.2 explains the difference between the designs and justifies modeling only two types and designs is adequate for defining the ZOIs for similar types/designs.

modeling of bus bar faults (main bus bars or the riser/primary compartment bus bars). Only copper is used to simulate faults occurring at the circuit breaker connections, since aluminum is not used for the construction of the current carrying portions of circuit breakers in U.S. NPP switchgear.

### 5.1.1.2 Switchgear Type and Circuit Breaker Orientation

The EPRI survey collected MV SWGR manufacturer/model designs determined that 89% of the switchgear that contain aluminum in the U.S. fleet are either GE Magne-Blast, ABB/ITE HK, or Westinghouse DHP switchgear. The remaining 11% consists of Gould, Siemens Type 3AH, and Allis Chalmers switchgear (see Figure 5-1).

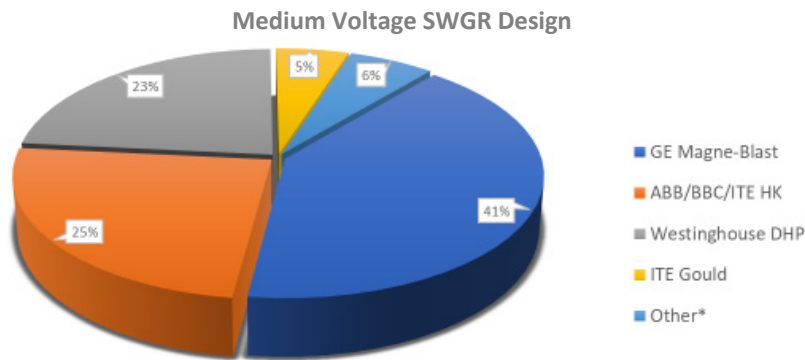


**Figure 5-1**  
MV SWGR designs with aluminum

The EPRI survey indicates that there are two circuit breaker/switchgear orientation styles of MV SWGR: horizontal draw-out circuit breaker and a vertical-lift circuit breaker. Identifying the configuration style of MV SWGR is important in understanding how that particular configuration can influence the high-temperature outflow from the MV SWGR and the time to cabinet breach. Per the EPRI survey results, 55% of the GE Magne-Blast MV SWGR are horizontal draw-out style circuit breaker and 45% are vertical-lift circuit breaker style. Since all other MV SWGR manufacturers used in U.S. NPPs produce only horizontal draw-out style circuit breakers, the GE Magne-Blast vertical-lift circuit breaker switchgear represents 18% of the population of MV SWGR containing aluminum (see Figure 5-2).

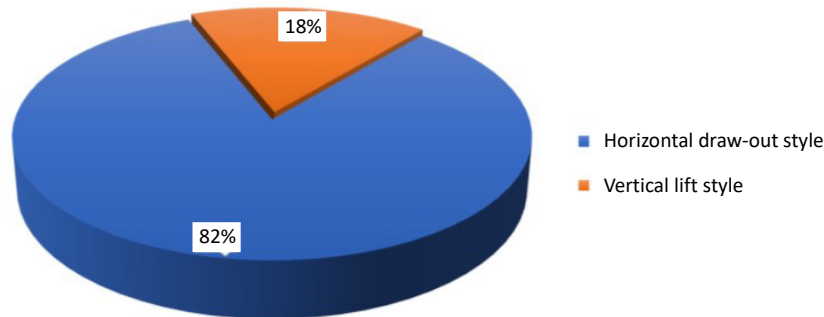


**Figure 5-2**  
Circuit breaker orientation for MV SWGR designs with aluminum

The three common switchgear manufacturer/models and orientations (vertical-lift and horizontal draw out styles) are further reviewed to compare similarities between the internal compartment design and location of various current carrying subcomponents. Simplified cross sections of the switchgear are in Figure 5-3 through Figure 5-5.

Figure 5-3 through Figure 5-5 show that the configurations of the internal compartments are relatively similar, particularly when comparing the horizontal style circuit breaker switchgear (Westinghouse DHP, GE Magne-Blast AMH and ABB HK). The internal compartments have similar physical dimensions and the number of barriers between the arc location and the external surface of the cabinet are also similar.

The vertical-lift circuit breaker style or horizontal draw-out style circuit breaker is identified as the most likely to have an effect on the size of the energetic phase ZOI. The two different switchgear styles have similar potential fault locations for horizontal distances from the cabinet sides and rear compartments. For faults occurring in the circuit breaker or at the circuit breaker stab connections, the configuration of the horizontal style switchgear has the mass of the circuit breaker between the potential fault locations and the front of the switchgear cabinet. The circuit breaker will provide a barrier at the front of the switchgear that will block a large portion of the HEAF energy, limiting the exposure to targets outside of the cabinet. The vertical-lift circuit breaker style switchgear does not have the circuit breaker between the front of the cabinet and circuit breaker stab connections where arcing can occur. This shielding effect necessitates the modeling of the circuit breaker mass in evaluating the differences between the two switchgear styles.

The GE Magne-Blast AMH (vertical-lift circuit breaker style) and ABB HK (horizontal draw-out circuit breaker style) are selected to represent the population of MV SWGR and their enclosure geometries are modeled in FDS. The full-scale MV SWGR experiments used for validation also used the GE Magne-Blast (vertical-lift circuit breaker style) enclosures. Small variations in equipment geometry do not significantly impact the energetic ZOIs.

For plants that have horizontal draw-out circuit breaker switchgear other than ABB HK (such as GE Magne-Blast AMH, Westinghouse DHP, Gould, Siemens Type 3AH, and Allis Chalmers), the horizontal draw-out circuit breaker designs are similar enough with respect to the FDS model geometry for the most relevant features (e.g., similar location for the circuit breaker in relation to circuit breaker stabs) that it is not expected to impact the energetic ZOI. Among the horizontal draw-out circuit breaker styles the layout is similar and the energetic ZOIs are not expected to differ across manufacturers.

Observed and potential fault locations on the selected MV SWGR designs (GE Magne-Blast (vertical) and ABB HK (horizontal)) are shown as red circles on Figure 5-3, Figure 5-4, and Figure 5-5 based on U.S. HEAF OE and the HEAF WG investigations. To reduce the number of FDS simulations (while preserving the overall fault locations), additional insights from early sensitivity analyses and WG expertise are considered. In particular, due to similarities between the ABB HK and the Westinghouse DH-P designs, only the ABB HK design, which has somewhat less shielding between the arc locations and the top, is specifically modeled.

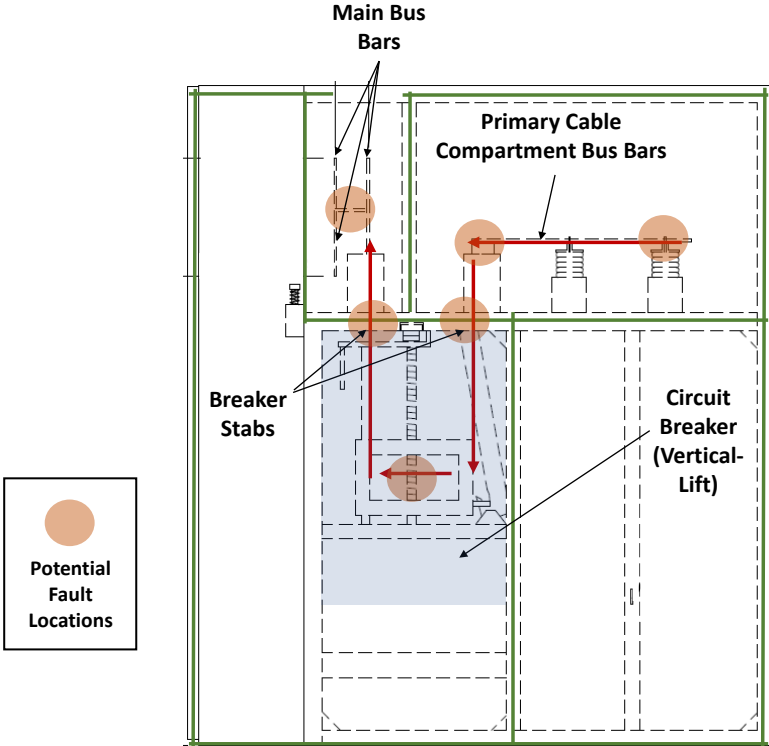


**Figure 5-3**  
GE Magne-Blast vertical-lift style circuit breaker switchgear. Red arrows indicate current flow direction in supply configuration; current flow is reversed for load configuration. Blue shaded area is approximate location of the circuit breaker

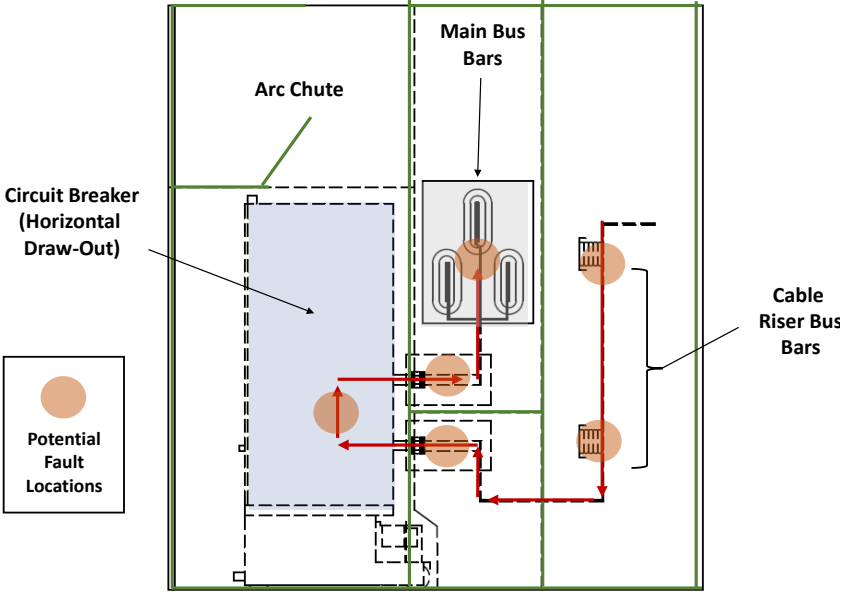


**Figure 5-4**  
ABB/ITE HK horizontal draw-out style circuit breaker switchgear. Red arrows indicate current flow direction in supply configuration; current flow is reversed for load configuration. Blue shaded area is approximate location of the circuit breaker

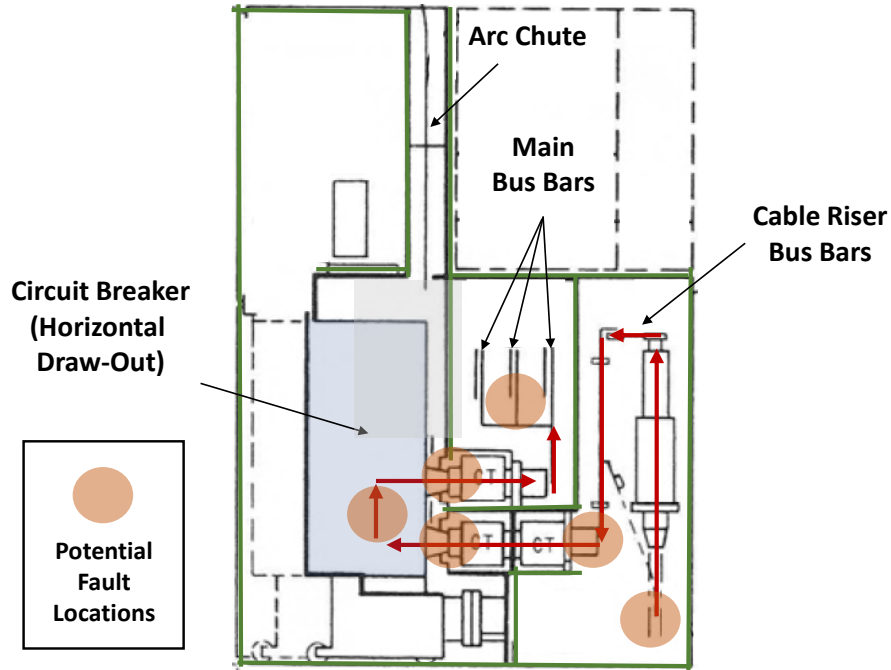


**Figure 5-5**  
**Westinghouse DH-P horizontal draw-out style circuit breaker switchgear. Red arrows indicate current flow direction in supply configuration; current flow is reversed for load configuration. Blue shaded area is approximate location of the circuit breaker. Due to similarities between this switchgear design and the ABB/ITE HK switchgear design, the Westinghouse DH-P design is not specifically modeled**

### 5.1.1.3 Fault Location and Power Flow

The fault locations are determined using representative U.S. HEAF operating experience [11, 12]. Of the seven MV SWGR HEAF events, four originated at the circuit breakers for the switchgear bus supply due to either high resistance connections at the circuit breaker cubicle stabs or as a result of internal circuit breaker failures. Three of the four events occurred during or immediately following a switching demand associated with a bus transfer. Each event resulted in a generator-fed HEAF due to the failure of the single circuit breaker to isolate the residual rotating energy from the tripped generator. The remaining three events occurred outside the switchgear circuit breaker cubicle, including:

- One HEAF occurred where the incoming power supply cable faulted at the switchgear enclosure entry
- One HEAF was a result of the main bus bar failure
- One HEAF was a result of insulation failure on the switchgear primary cable compartment bus

Figure 5-6 illustrates the location of the circuit breaker stabs, primary cable compartment bus bars and main bus bars from the GE Magne-Blast vertical-lift circuit breaker SWGR design where faults are postulated.

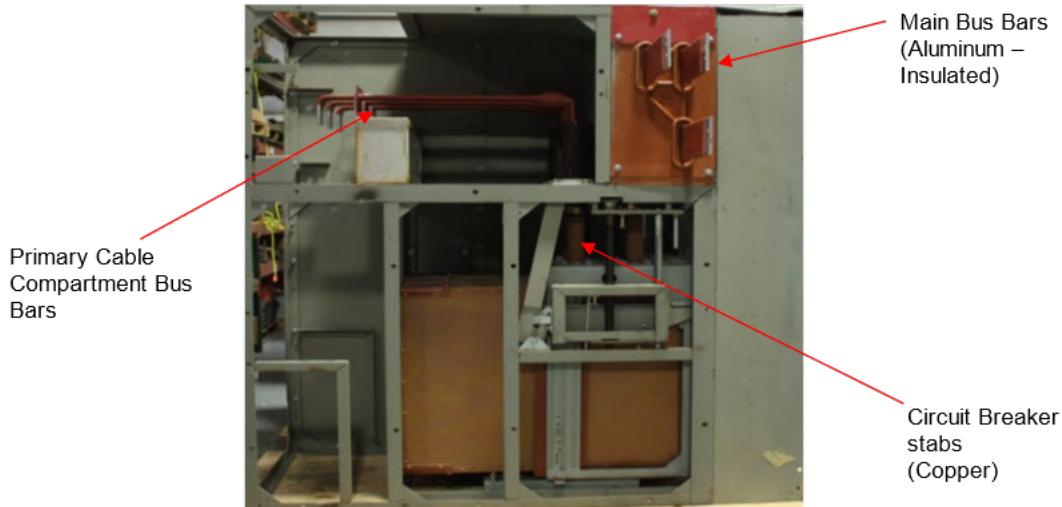


**Figure 5-6**  
**GE Magne-Blast vertical-lift circuit breaker SWGR showing location of circuit breaker stabs, primary cable compartment bus bars, and the main bus bars**

FDS models the energy from the arc in a volumetric space. For small volumes, such as the circuit breaker or at the circuit breaker stab connections, the energetic ZOIs predicted by FDS are expected to be similar, provided these locations are in the same general area. Therefore, the fault locations of the load and line side circuit breaker stab connections are consolidated with the circuit breaker fault location.

The load and supply circuit breaker power flow are not a direct input variable considered in FDS; however, it is a variable in the expected directionality of the arc since magnetic forces will push the arc along the conductor until impeded. In reviewing the horizontal draw-out style circuit breaker switchgear (Figure 5-4 and Figure 5-5), the configuration of the switchgear vertical riser bus section in the supply (current flow from the riser/primary cable compartment bus to the circuit breaker) or load (current flows from the main bus to the circuit breaker) does not affect the distance between the fault and the back face of the switchgear, so the energetic ZOIs will be the same. For the vertical-lift circuit breaker switchgear, the primary cable compartment bus (upper right compartment shown in Figure 5-3 and Figure 5-7) utilizes a horizontal run bus bar. For faults in the supply configuration, the arc will be pushed to the left end of the bus bar. For the load configurations the arc will be pushed to the closet point on the bus bar towards the rear cabinet wall.

Based on the previous discussion and justifications:

- The fault locations chosen for vertical-lift style circuit breakers are shown in Figure 5-7.
- A single fault location in the horizontal draw-out style circuit breaker is modeled due to similarities between the ABB HK and the Westinghouse DH-P designs, only the ABB HK design, which has somewhat less shielding between the arc locations and the top. The arc location for the horizontal draw-out style circuit breaker is shown in Figure 5-8.

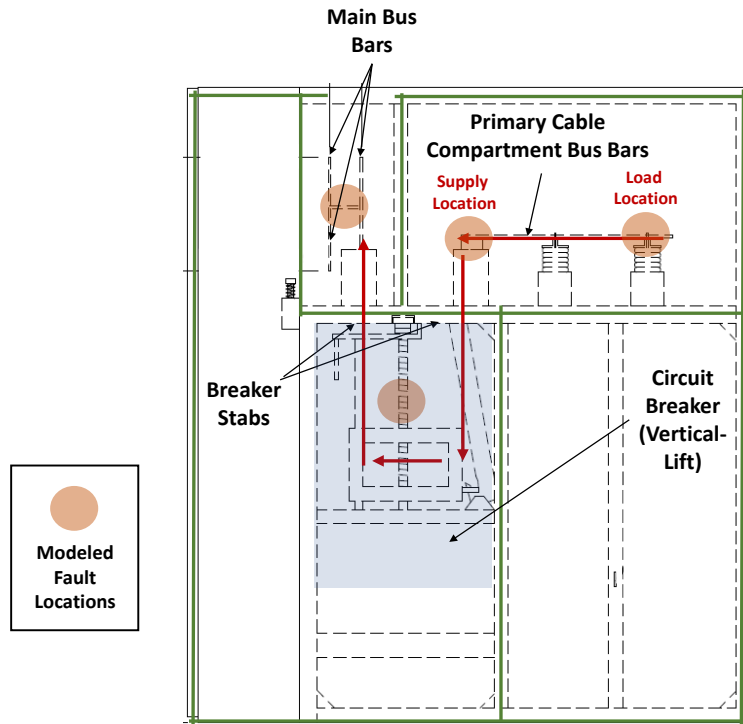


**Figure 5-7**  
Vertical-lift style circuit breaker switchgear with consolidated fault locations. Red arrows indicate current flow direction in supply configuration; current flow is reversed for load configuration. Blue shaded area is approximate location of the circuit breaker

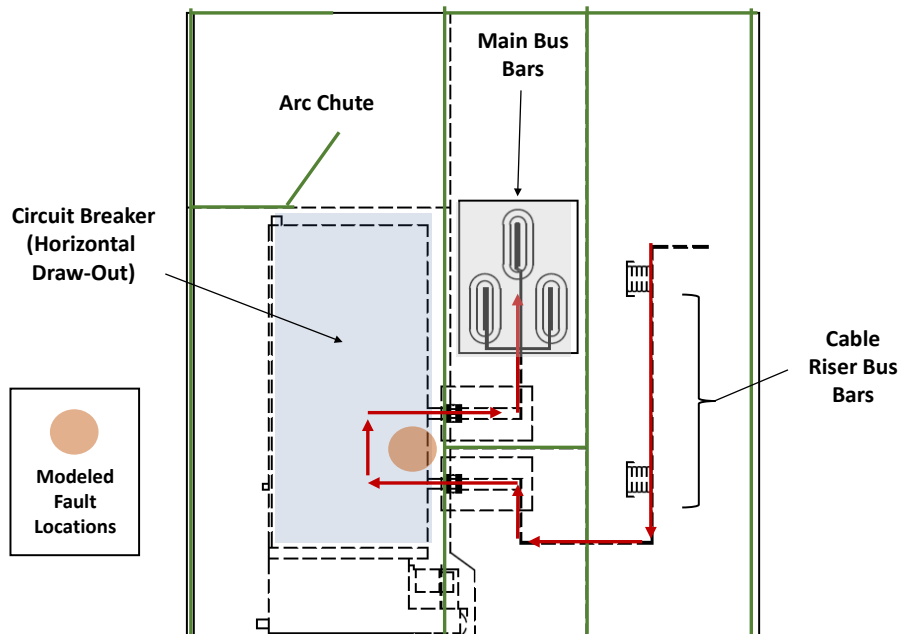


**Figure 5-8**  
Horizontal draw-out style circuit breaker switchgear with consolidated fault location. Red arrows indicate current flow direction in supply configuration; current flow is reversed for load configuration. Blue shaded area is approximate location of the circuit breaker

#### 5.1.1.4 Arc Current and Arc Voltage

A constant arc voltage of 650 V<sub>L-L</sub> is used for the for the MV SWGR HEAFs regardless of the system voltage. This value is derived from the available HEAF testing data as explained in Appendix A. This voltage is used to calculate the arc power and arc energy of the HEAF.

For arcing faults with a stiff source (constant current and voltage) and representing a three-phase, low impedance fault, the arcing current is constant until the overcurrent protective device trips and isolates the faulted equipment. The arcing current in this case depends on multiple parameters such as available fault current, system voltage, grounding type, enclosure type, and other variables that are not always readily available or known. For this analysis, the fault current is selected based on observed values from U.S. MV SWGR operating experience [11, 12]. The range of fault currents varied from 28 kA to 32 kA. The middle of the range, 30 kA, is used for the arc energy calculation. See Appendix A for a list of HEAF events with known fault currents.

The arc voltage for the generator-fed fault arc energy calculation is the same as above with the exception that the arc current is no longer constant but rather decayed with time. The arcing current decayed exponentially over the time needed for the generator to coast down to a voltage level at which the arc fault can no longer be sustained. The current decay profile of a generator-fed HEAF event is discussed in Appendix A. This decaying current profile is used in FDS models of the generator-fed HEAFs.

#### 5.1.1.5 Arcing Fault Duration

The arcing fault duration is a significant factor in determining the total arc energy during a HEAF. The fault durations are determined by the overcurrent protective element settings in the NPP's electrical distribution system. It has been observed in U.S. HEAF OE [11, 12] that HEAF events usually involve the failure of a circuit breaker or primary overcurrent protection and relied on the upstream circuit breaker or back-up time overcurrent protection to clear the fault. In cases of generator-fed faults, there is no circuit breaker to clear the fault.

EPRI conducted a survey [3] in which U.S. NPPs provided the fault clearing time (FCT) of the backup time overcurrent protection for the auxiliary transformers. This data set along with a review of coordination calculations for a sampling of plants, indicated that the expected duration of the FCT is typically 2 s, but can last up to 5 s. This FCT is applicable for the constant-current faults (stiff source). The arcing fault duration for the constant-current faults evaluated in FDS use a low (2 s), a mid (4 s), and a high (5 s) FCT. The selection of these values allowed a curve fit against a power trendline.

Generator-fed faults in historical U.S. HEAF OE [11, 12] have little data available as to the actual duration of the arcing fault. Data from a recent HEAF event (FEDB 51765) summarized in Section 4.4.1 is used to characterize the generator-fed fault energy and duration. In this event, the generator tripped within several cycles of the phase-to-phase fault; however, the residual energy of the generator continued to feed the fault for an additional 15 s. The current decay profile over the 15 s duration is shown in Figure A-2. There is a potential for generator-fed arc faults to occur outside the instantaneous differential fault protection zone (87) in which a time overcurrent (51) device is relied upon to trip the generator. This delay causes the energy profile to be that of a constant-current fault followed by the generator decay profile after the generator is tripped (via

generator protection). The delay times selected include 0 s, 3 s, and 5 s, all with a subsequent generator decay profile. These profiles are described and shown in Figure A-3 through Figure A-5.

#### 5.1.1.6 Arc Energies

The arc energies considered for the MV switchgear constant-current arc faults are calculated as:

$$\text{Arc Energy} = \text{Arc Current} \cdot \text{Line-to-Line Arc Voltage} \cdot \text{Arcing fault Duration} \cdot \sqrt{3}$$

For an arc current of 30 kA and a line-to-line voltage of 650 V, this equates to an arc energy of 68 MJ for a 2 s constant arc fault, 135 MJ for a 4 s constant arc fault, and 169 MJ for a 5 s constant arc fault as calculated in Table 5-1. Although not evaluated as a separate constant-current case, a 3 s constant arc fault has an energy of 101 MJ.

The generator-fed faults are defined as a constant-current arc followed by an exponentially decaying arc current. The arc energy for these faults is the sum of the two current stages. The constant-current arc energy is determined as previously described. The arc energy for the decaying arc current is determined by integrating the decay function over time and is equal to 132 MJ for a 15 s decay (see Appendix A). This equates to an arc energy of 132 MJ for a generator-fed fault without a constant-current arc (0 s), 233 MJ for a 3 s constant arc fault followed by a 15 s generator-fed fault, and 300 MJ for a 5 s constant arc fault followed by a 15 s generator-fed fault as calculated in Table 5-1.

#### 5.1.1.7 Medium Voltage Switchgear FDS Simulation Matrix

Sections 5.1.1.1 through 5.1.1.6 provide details on the important parameters for the MV SWGR energetic ZOIs. The matrix of 48 FDS HEAF simulations developed from these parameters are summarized in Table 5-1. These simulations and their output are used as input for the HEAF WG to derive the energetic ZOIs for MV SWGR configurations.

**Table 5-1**  
**Matrix of MV SWGR HEAF FDS simulations**

HEAF ID	Enclosure material	Bus bar material	SWGR type	Circuit breaker orientation	Fault location	Power configuration	Arc voltage (V <sub>L-L</sub> )	Arc current (kA)	Power (MW)	Stiff (s)	Decay (s)	Arc energy (MJ)
MV-GE-1	Steel	Aluminum	GE Magne-Blast	Vertical	Main Bus Bars	Supply and Load	650	30	33.8	2	0	68
MV-GE-2	Steel	Aluminum	GE Magne-Blast	Vertical	Riser/Primary Compartment Bus Bars	Load	650	30	33.8	2	0	68
MV-GE-3	Steel	Aluminum	GE Magne-Blast	Vertical	Riser/Primary Compartment Bus Bar	Supply	650	30	33.8	2	0	68
MV-GE-4	Steel	Aluminum	GE Magne-Blast	Vertical	Main Bus Bars	Supply and Load	650	30	33.8	4	0	135
MV-GE-5	Steel	Aluminum	GE Magne-Blast	Vertical	Riser/Primary Compartment Bus Bar	Load	650	30	33.8	4	0	135
MV-GE-6	Steel	Aluminum	GE Magne-Blast	Vertical	Riser/Primary Compartment Bus Bar	Supply	650	30	33.8	4	0	135
MV-GE-7	Steel	Aluminum	GE Magne-Blast	Vertical	Main Bus Bars	Supply and Load	650	30	33.8	5	0	169
MV-GE-8	Steel	Aluminum	GE Magne-Blast	Vertical	Riser/Primary Compartment Bus Bar	Load	650	30	33.8	5	0	169
MV-GE-9	Steel	Aluminum	GE Magne-Blast	Vertical	Riser/Primary Compartment Bus Bar	Supply	650	30	33.8	5	0	300
MV-GE-10	Steel	Aluminum	GE Magne-Blast	Vertical	Main Bus Bars	Supply and Load	650	30	23	0	15	132
MV-GE-11	Steel	Aluminum	GE Magne-Blast	Vertical	Riser/Primary Compartment Bus Bars	Load	650	30	23	0	15	132
MV-GE-12	Steel	Aluminum	GE Magne-Blast	Vertical	Riser/Primary Compartment Bus Bar	Supply	650	30	23	0	15	132
MV-GE-13	Steel	Aluminum	GE Magne-Blast	Vertical	Main Bus Bars	Supply and Load	650	30	33.8	3	15	233

Development of the HEAF Simulation Matrix

HEAF ID	Enclosure material	Bus bar material	SWGR type	Circuit breaker orientation	Fault location	Power configuration	Arc voltage (V <sub>L-L</sub> )	Arc current (kA)	Power (MW)	Stiff (s)	Decay (s)	Arc energy (MJ)
MV-GE-14	Steel	Aluminum	GE Magne-Blast	Vertical	Riser/Primary Compartment Bus Bar	Load	650	30	33.8	3	15	233
MV-GE-15	Steel	Aluminum	GE Magne-Blast	Vertical	Riser/Primary Compartment Bus Bar	Supply	650	30	33.8	3	15	233
MV-GE-16	Steel	Aluminum	GE Magne-Blast	Vertical	Main Bus Bars	Supply and Load	650	30	33.8	5	15	300
MV-GE-17	Steel	Aluminum	GE Magne-Blast	Vertical	Riser/Primary Compartment Bus Bar	Load	650	30	33.8	5	15	300
MV-GE-18	Steel	Aluminum	GE Magne-Blast	Vertical	Riser/Primary Compartment Bus Bar	Supply	650	30	33.8	5	15	300
MV-GE-19	Steel	Copper	GE Magne-Blast	Vertical	Circuit Breaker	Supply and Load	650	30	33.8	2	0	68
MV-GE-20	Steel	Copper	GE Magne-Blast	Vertical	Main Bus Bars	Supply and Load	650	30	33.8	2	0	68
MV-GE-21	Steel	Copper	GE Magne-Blast	Vertical	Riser/Primary Compartment Bus Bars	Load	650	30	33.8	2	0	68
MV-GE-22	Steel	Copper	GE Magne-Blast	Vertical	Riser/Primary Compartment Bus Bar	Supply	650	30	33.8	2	0	68
MV-GE-23	Steel	Copper	GE Magne-Blast	Vertical	Circuit Breaker	Supply and Load	650	30	33.8	4	0	135
MV-GE-24	Steel	Copper	GE Magne-Blast	Vertical	Main Bus Bars	Supply and Load	650	30	33.8	4	0	135
MV-GE-25	Steel	Copper	GE Magne-Blast	Vertical	Riser/Primary Compartment Bus Bar	Load	650	30	33.8	4	0	135
MV-GE-26	Steel	Copper	GE Magne-Blast	Vertical	Riser/Primary Compartment Bus Bar	Supply	650	30	33.8	4	0	135
MV-GE-27	Steel	Copper	GE Magne-Blast	Vertical	Circuit Breaker	Supply and Load	650	30	33.8	5	0	169

HEAF ID	Enclosure material	Bus bar material	SWGR type	Circuit breaker orientation	Fault location	Power configuration	Arc voltage (V <sub>L-L</sub> )	Arc current (kA)	Power (MW)	Stiff (s)	Decay (s)	Arc energy (MJ)
MV-GE-28	Steel	Copper	GE Magne-Blast	Vertical	Main Bus Bars	Supply and Load	650	30	33.8	5	0	169
MV-GE-29	Steel	Copper	GE Magne-Blast	Vertical	Riser/Primary Compartment Bus Bar	Load	650	30	33.8	5	0	169
MV-GE-30	Steel	Copper	GE Magne-Blast	Vertical	Riser/Primary Compartment Bus Bar	Supply	650	30	33.8	5	0	169
MV-GE-31	Steel	Copper	GE Magne-Blast	Vertical	Circuit Breaker	Supply and Load	650	30	23	0	15	132
MV-GE-32	Steel	Copper	GE Magne-Blast	Vertical	Main Bus Bars	Supply and Load	650	30	23	0	15	132
MV-GE-33	Steel	Copper	GE Magne-Blast	Vertical	Riser/Primary Compartment Bus Bars	Load	650	30	23	0	15	132
MV-GE-34	Steel	Copper	GE Magne-Blast	Vertical	Riser/Primary Compartment Bus Bar	Supply	650	30	23	0	15	132
MV-GE-35	Steel	Copper	GE Magne-Blast	Vertical	Circuit Breaker	Supply and Load	650	30	33.8	3	15	233
MV-GE-36	Steel	Copper	GE Magne-Blast	Vertical	Main Bus Bars	Supply and Load	650	30	33.8	3	15	233
MV-GE-37	Steel	Copper	GE Magne-Blast	Vertical	Riser/Primary Compartment Bus Bar	Load	650	30	33.8	3	15	233
MV-GE-38	Steel	Copper	GE Magne-Blast	Vertical	Riser/Primary Compartment Bus Bar	Supply	650	30	33.8	3	15	233
MV-GE-39	Steel	Copper	GE Magne-Blast	Vertical	Circuit Breaker	Supply and Load	650	30	33.8	5	15	300
MV-GE-40	Steel	Copper	GE Magne-Blast	Vertical	Main Bus Bars	Supply and Load	650	30	33.8	5	15	300
MV-GE-41	Steel	Copper	GE Magne-Blast	Vertical	Riser/Primary Compartment Bus Bar	Load	650	30	33.8	5	15	300

*Development of the HEAF Simulation Matrix*

HEAF ID	Enclosure material	Bus bar material	SWGR type	Circuit breaker orientation	Fault location	Power configuration	Arc voltage (V <sub>L-L</sub> )	Arc current (kA)	Power (MW)	Stiff (s)	Decay (s)	Arc energy (MJ)
MV-GE-42	Steel	Copper	GE Magne-Blast	Vertical	Riser/Primary Compartment Bus Bar	Supply	650	30	33.8	5	15	300
MV-ABB-1	Steel	Copper	ABB/ITE HK	Horizontal	Circuit Breaker	Supply and Load	650	30	33.8	2	0	68
MV-ABB-2	Steel	Copper	ABB/ITE HK	Horizontal	Circuit Breaker	Supply and Load	650	30	33.8	4	0	135
MV-ABB-3	Steel	Copper	ABB/ITE HK	Horizontal	Circuit Breaker	Supply and Load	650	30	33.8	5	0	169
MV-ABB-4	Steel	Copper	ABB/ITE HK	Horizontal	Circuit Breaker	Supply and Load	650	30	23	0	15	132
MV-ABB-5	Steel	Copper	ABB/ITE HK	Horizontal	Circuit Breaker	Supply and Load	650	30	33.8	3	15	233
MV-ABB-6	Steel	Copper	ABB/ITE HK	Horizontal	Circuit Breaker	Supply and Load	650	30	33.8	5	15	300

### 5.1.2 Low Voltage Switchgear

Based on OE events [11, 12], survey results [3], and the insights from the full-scale testing [5], the most impactful parameters on the energetic ZOI are listed as:

- Bus bar material: copper or aluminum
- Switchgear manufacturer/models/geometry typically found in the NPPs, and used during the full-scale testing/FDS validation
- Fault initiation location: circuit breaker connection to cubicle switchgear bus stabs
- Energy level (fault current, fault duration, and arc voltage)

Per the HEAF OE [11, 12], only two LV SWGR HEAF events have occurred in the United States. FEDB 50935 [12] reported information with respect to the arc fault current and duration. These values are used to determine the arc energy profile for all LV SWGR HEAF simulations. Section A.3 provides a discussion and justification for this arc energy profile. The characteristics of the LV SWGR HEAF parameters are listed below. Additional details are provided in Section 5.1.2.3.

- The arcing current profile for the baseline simulations is 4.67 kA for 20 s and 2.20 kA for 21 s
- The arcing current profiles for the sensitivity simulations use 21.5 kA for arc durations ranging from 2-6 s
- The arc voltage is 375 V<sub>L-L</sub>, derived from full-scale testing as described in Section A.1

#### 5.1.2.1 LV SWGR Type and Arc Initiation Location

The EPRI survey results [3] determined that 86% of the LV switchgear designs that contain aluminum in the U.S. nuclear fleet are either ABB/ITE K Line, GE AKD, or Westinghouse Type DS. The remaining 14% are Westinghouse DB, Allis Chalmers, Powell Nelson, LVME, Sorgel, ABB RLN, or LMAZ-LK-32 C-IC designs.

The three most common types of LV SWGR that contain aluminum are compared to highlight any major difference in design (geometry, free volume, barrier usage). The main bus compartment arrangements of these LV SWGRs are similar across the manufacturers (i.e., vertically stacked circuit breakers connected to a vertical bus for each load center tower, with each adjacent load center tower connected by horizontal main bus bars). For the supply circuit breaker, the incoming bus is typically horizontal and is powered by the LV SWGR transformer. Short sections of bus connecting the line side of the circuit breaker to the vertical main bus bars are commonly referred to as the jumper bus. Although some bus bar spacing and dimensional differences exist between manufacturers, the overall geometry, free volume, bus bar arrangements, and lack of arc trapping barriers of the three major U.S. types of LV SWGR are similar. Similarity between the major LV SWGR designs reduces the number of simulations in FDS since the energetic ZOIs are expected to be similar among the major LV switchgear designs.

The majority of the LV HEAF testing was performed using the Westinghouse Type DS cabinet design (Figure 5-9). For most tests, the fault was initiated at the bus bars in the main bus bar middle compartment where the aluminum bus is located. For most tests performed with the Westinghouse Type DS with the fault location at the bus bars, the arc self-extinguished before reaching the intended test duration. Although many tests were performed with the arc initiated at the main compartment bus bars, very little data from the LV SWGR testing is used for FDS benchmarking and validation due to the lack of arc sustainability. In these cases, there was no cabinet breaching and, therefore, no energetic ZOIs.

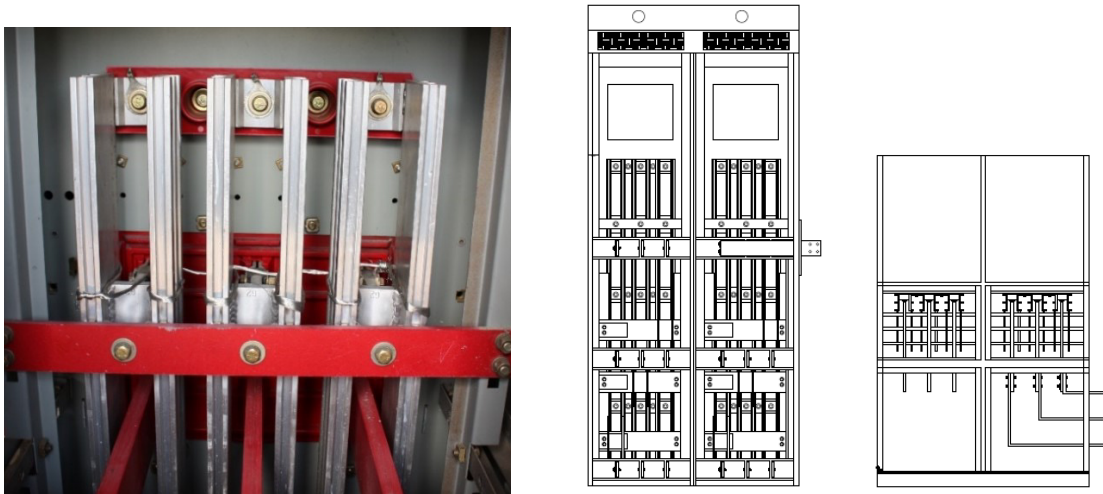


**Figure 5-9**  
**Westinghouse DS electrical cabinet and arc test location [5]**

Due to the small number of LV HEAF events in OE [11, 12] and the lack of directly applicable test data from the HEAF testing program, several fault locations are evaluated in FDS to determine the impact on the energetic ZOIs. The LV HEAF testing highlighted the lack of sustainability at the bus bars located on the back of the cabinet, and this location is not included in the FDS simulation matrix. Based on this, arcs are evaluated at the circuit breaker and the mid compartment (jumper bus). Arc relocation between the circuit breaker and the aluminum bus bars (circuit breaker to mid), as observed in FEDB 50935, is also evaluated.

#### 5.1.2.2 Bus Bar Material

The EPRI survey results [3] show that almost 60% of US NPPs have some LV SWGR with aluminum bus bars while the other 40% have only copper bus bars. The HEAF testing program did not provide conclusive evidence as to whether electrode composition (i.e., copper versus aluminum) was a significant factor in determining target exposure and the associated energetic ZOI. Both aluminum and copper bus bar materials are considered in the FDS simulation matrix for fault locations that initiate in the mid-main bus bar compartment or are expected to experience arc migration from the circuit breaker to the mid compartment.

Arcs that initiate at the circuit breaker stabs involve copper electrode materials since the circuit breaker stabs use copper. Although there are no actual configurations with aluminum, arcs that initiate in the circuit breaker stabs are evaluated with both copper and aluminum to further assess the differences in the energetic ZOIs. In addition, FDS simulations aimed at reproducing FEDB 50935, where the arc begins at the circuit breaker stabs and migrates to the bus bar compartment, use aluminum rather than copper electrode material. At the beginning of this effort, it was postulated that the aluminum electrodes release more energy due to particle oxidation and heat of reaction as compared to copper. Therefore, this was considered as a conservative modeling choice for the electrode material where a single material is modeled.

#### 5.1.2.3 Arc Current, Arc Voltage, and Duration

The arcing current profile of 4.67 kA for 20 s and 2.20 kA for 21 s is selected to reproduce FEDB 50935. An arc voltage of 375 V<sub>L-L</sub> is selected. The profiles for arc current and arc power are documented in Section A.3. Sensitivity studies are performed to compare a larger fault current of 21.5 kA on a low-voltage switchgear with arc durations of 2 s, 4 s, and 6 s.

#### 5.1.2.4 Low Voltage Switchgear FDS Simulation Matrix

Section 5.1.2.1 through 5.1.2.3 provide details on the important parameters for the LV SWGR simulations. The matrix of 34 FDS HEAF simulations developed from these parameters are summarized in Table 5-2. These simulations and their output are used as input for the HEAF WG to derive the energetic ZOIs for LV SWGR configurations.

**Table 5-2**  
**Matrix of LV SWGR HEAF FDS simulations**

HEAF ID	Enclosure material	Bus Bar material	Fault location	Elevation	Arc voltage (V <sub>L-L</sub> )	Arc current (kA)	Power (MW)	Duration (s)	Arc energy (MJ)
LV-BASE-1	Steel	Aluminum	Circuit Breaker	Mid	375	4.67/2.20	3.0/1.4	41	90
LV-BASE-2	Steel	Aluminum	Circuit Breaker	Top	375	4.67/2.20	3.0/1.4	41	90
LV-BASE-3	Steel	Aluminum	Mid	Mid	375	4.67/2.20	3.0/1.4	41	90
LV-BASE-4	Steel	Aluminum	Mid	Top	375	4.67/2.20	3.0/1.4	41	90
LV-BASE-5	Steel	Aluminum	Circuit Breaker to Mid	Mid	375	4.67/2.20	3.0/1.4	41	90
LV-BASE-6	Steel	Aluminum	Circuit Breaker to Mid	Top	375	4.67/2.20	3.0/1.4	41	90
LV-BASE-7	Steel	Copper	Circuit Breaker	Mid	375	4.67/2.20	3.0/1.4	41	90
LV-BASE-8	Steel	Copper	Circuit Breaker	Top	375	4.67/2.20	3.0/1.4	41	90
LV-BASE-9	Steel	Copper	Mid	Mid	375	4.67/2.20	3.0/1.4	41	90
LV-BASE-10	Steel	Copper	Mid	Top	375	4.67/2.20	3.0/1.4	41	90
LV-SENS-1	Steel	Aluminum	Circuit Breaker	Mid	375	21.5	14	2	28
LV-SENS-2	Steel	Aluminum	Circuit Breaker	Top	375	21.5	14	2	28
LV-SENS-3	Steel	Aluminum	Mid	Mid	375	21.5	14	2	28
LV-SENS-4	Steel	Aluminum	Mid	Top	375	21.5	14	2	28
LV-SENS-5	Steel	Copper	Circuit Breaker	Mid	375	21.5	14	2	28
LV-SENS-6	Steel	Copper	Circuit Breaker	Top	375	21.5	14	2	28
LV-SENS-7	Steel	Copper	Mid	Mid	375	21.5	14	2	28
LV-SENS-8	Steel	Copper	Mid	Top	375	21.5	14	2	28
LV-SENS-9	Steel	Aluminum	Circuit Breaker	Mid	375	21.5	14	4	56

HEAF ID	Enclosure material	Bus Bar material	Fault location	Elevation	Arc voltage (V <sub>L-L</sub> )	Arc current (kA)	Power (MW)	Duration (s)	Arc energy (MJ)
LV-SENS-10	Steel	Aluminum	Circuit Breaker	Top	375	21.5	14	4	56
LV-SENS-11	Steel	Aluminum	Mid	Mid	375	21.5	14	4	56
LV-SENS-12	Steel	Aluminum	Mid	Top	375	21.5	14	4	56
LV-SENS-13	Steel	Copper	Circuit Breaker	Mid	375	21.5	14	4	56
LV-SENS-14	Steel	Copper	Circuit Breaker	Top	375	21.5	14	4	56
LV-SENS-15	Steel	Copper	Mid	Mid	375	21.5	14	4	56
LV-SENS-16	Steel	Copper	Mid	Top	375	21.5	14	4	56
LV-SENS-17	Steel	Aluminum	Circuit Breaker	Mid	375	21.5	14	6	84
LV-SENS-18	Steel	Aluminum	Circuit Breaker	Top	375	21.5	14	6	84
LV-SENS-19	Steel	Aluminum	Mid	Mid	375	21.5	14	6	84
LV-SENS-20	Steel	Aluminum	Mid	Top	375	21.5	14	6	84
LV-SENS-21	Steel	Copper	Circuit Breaker	Mid	375	21.5	14	6	84
LV-SENS-22	Steel	Copper	Circuit Breaker	Top	375	21.5	14	6	84
LV-SENS-23	Steel	Copper	Mid	Mid	375	21.5	14	6	84
LV-SENS-24	Steel	Copper	Mid	Top	375	21.5	14	6	84

### **5.1.3 Non-Segregated Bus Ducts**

Based on OE events [11, 12] and survey results [3], the parameters most impactful on the energetic ZOI are identified as:

- Orientation of the bus duct
  - Straight run
    - Horizontal
    - Vertical
  - Elbow
  - Tee
- NSBD construction type based on voltage class type:
  - Bus duct (insulated or non-insulated bus bars with air-gap spacing)
  - Armor clad busway (insulated bus bars with no air-gap spacing – low voltage only)
- Bus bar material: copper or aluminum
- Bus enclosure material: steel or aluminum
- Energy level (arc current, duration, and voltage)

The arc current and arc voltage for MV bus ducts are assumed the same as MV SWGR (Section 5.1.1.4). HEAF durations smaller than those considered for the MV SWGR are investigated (in addition to the durations used for MV SWGR). The bus duct breach time can be shorter than MV SWGR, which necessitated the development of energetic ZOIs at times less than 2 s. A summary of the energy variables considered for NSBD are listed below. Additional details are provided in Section 5.1.3.3.

- Fault current
  - The best estimate of 30 kA as described in Section A.2.1
- Arc fault durations
  - Constant-current arcing fault durations between 1 to 5 s are considered. The expected range of 1 to 5 s is documented in the EPRI survey results [3] and OE.
  - Generator-fed faults of 15 s duration, with generator voltage/current decay during the coast-down immediately after a unit trip, either without a constant-current arc or with a constant-current arc duration of 3 s or 5 s.
- Arc voltage
  - Set to 650 VL-L, derived from full-scale testing (see Section A.1 and Section A.2.2 [36, 37])

### 5.1.3.1 Orientation

From a review of typical bus duct configurations and bus duct HEAF operating experience [11, 12], it is determined that the arcing fault can breach the end of a bus duct when the fault occurs near the edge of a segmented transition. This applies to bus duct configurations such as tees and elbows. Arcing faults in straight runs tend to breach perpendicular to the bus duct. Due to the small number of NSBD HEAF tests, the impact of the bus duct orientation on the energetic ZOIs remains unknown; therefore, all three orientations (straight runs, elbows, and tees) are modeled in FDS.

### 5.1.3.2 NSBD Type

Bus ducts in HEAF OE [11, 12] have either flat-facing or edge-facing bus bars (single set of bars or multiple sets in parallel). An example of edge-facing bus bars is shown in Figure 5-10. Although other bus bar configurations exist, such as square tubes, the configuration in Figure 5-10 is used the FDS simulations.

HEAF OE [11, 12] documents the arc fault potential for low-voltage armor-clad busways. This configuration consists of bus bars with smaller gap spacing, due to an insulating material used instead of an air gap. This smaller gap spacing lowers the expected arc voltage. This specific low-voltage NSBD type is not modeled in FDS; instead, the MV bus duct configuration shown in Figure 5-10 and its associated energies yielded energetic ZOIs that bound the expected ZOIs from the low-voltage busway with smaller arc energies.

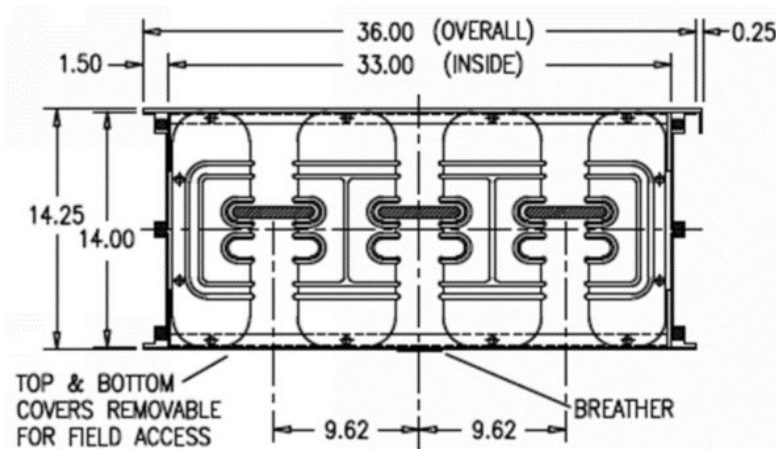


**Figure 5-10**  
Example of a non-segregated bus duct configuration

### 5.1.3.3 Arc Current, Arc Voltage, and Duration

Medium voltage NSBDs rely on similar overcurrent protective schemes as MV switchgear and are subject to approximately the same available fault current. An arcing current of 30 kA is also selected for bus ducts. A predominant factor in determining arc voltage is the gap spacing between conductors. Minor differences are expected between the gap spacing of bus bars in switchgear and bus ducts; however, the difference is not large enough to have a significant impact on the resulting energetic ZOIs. Therefore, the same arc voltage of 650 V<sub>L-L</sub> is used for NSBDs.

Similarly, the same arcing fault durations with an additional duration of 1 s are considered for the constant-current faults as previously described. Arc durations of 1 s, 2 s, 4 s, and 5 s are modeled in FDS.

For generator-fed faults on NSBDs, the same are power profile and durations as MV SWGR are used.

#### 5.1.3.4 Bus Bar and Bus Duct Enclosure Material

The material used for the construction of NSBDs in U.S. NPPs was surveyed by EPRI [3]. The survey results identified four main material types of medium-voltage NSBDs in the U.S. fleet:

1. Aluminum bus bars with aluminum enclosure
2. Aluminum bus bars with steel enclosure
3. Copper bus bars with aluminum enclosure, and
4. Copper bus bars with steel enclosure

Figure 5-11 provides the material type breakdown for bus bars and the bus duct enclosure.

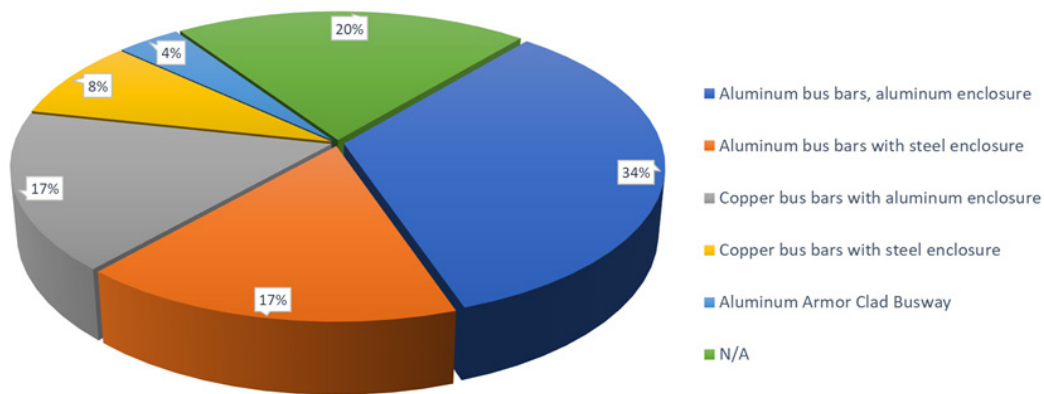


**Figure 5-11**  
**Bus bar and enclosure material type distribution. N/A indicates the plant uses cables rather than NSBDs [3]**

Twenty percent of U.S. NPPs do not use NSBDs and instead use cables. Four percent of U.S. NPPs reported use of armor-clad busways for some low-voltage NSBDs.

For FDS simulations, both copper and aluminum electrodes (bus bars) are evaluated. Simulations with aluminum bus bars are compared to a set of simulations using copper bus bars while keeping other variables the same for a direct comparison of the electrode composition effects.

For bus duct enclosures, the time to breach aluminum versus steel enclosures is expected to differ. Assuming the same enclosure thickness and arc energies, it will take more time to breach a steel enclosure than an aluminum enclosure. Lower or higher breaching times directly impact the target exposure and the associated energetic ZOIs. Based on this, simulations are run with different bus bar and enclosure materials to allow for direct comparison of the duct housing effects.

#### 5.1.3.5 Non-Segregated Bus Duct FDS Simulation Matrix

Section 5.1.3.1 through 5.1.3.4 provide details on the important parameters for the NSBD energetic ZOIs. The matrix of 58 FDS HEAF simulations developed from these parameters are summarized in **Table 5-3**. These simulations and their output are used as input for the HEAF WG to derive the energetic ZOIs for NSBD configurations.

**Table 5-3**  
**Matrix of NSBD HEAF FDS simulations**

HEAF ID	Enclosure material	Bus bar material	NSBD type	Orientation	Fault location	Arc voltage (V <sub>L-L</sub> )	Arc current (kA)	Power (MW)	Stiff (s)	Decay (s)	Arc energy (MJ)
NSBD-1	Steel	Aluminum	Typical	Straight-Horizontal	Bus Bar	650	30	33.8	1	0	34
NSBD-2	Steel	Aluminum	Typical	Straight-Horizontal	Bus Bar	650	30	33.8	2	0	68
NSBD-3	Steel	Aluminum	Typical	Straight-Horizontal	Bus Bar	650	30	33.8	4	0	135
NSBD-4	Steel	Aluminum	Typical	Straight-Horizontal	Bus Bar	650	30	33.8	5	0	169
NSBD-5	Steel	Aluminum	Typical	Straight-Horizontal	Bus Bar	650	30	23	0	15	132
NSBD-6	Steel	Aluminum	Typical	Straight-Horizontal	Bus Bar	650	30	33.8	3	15	233
NSBD-7	Steel	Aluminum	Typical	Straight-Horizontal	Bus Bar	650	30	33.8	5	15	300
NSBD-8	Aluminum	Aluminum	Typical	Straight-Horizontal	Bus Bar	650	30	33.8	1	0	34
NSBD-9	Aluminum	Aluminum	Typical	Straight-Horizontal	Bus Bar	650	30	33.8	2	0	68
NSBD-10	Aluminum	Aluminum	Typical	Straight-Horizontal	Bus Bar	650	30	33.8	4	0	135
NSBD-11	Aluminum	Aluminum	Typical	Straight-Horizontal	Bus Bar	650	30	33.8	5	0	169
NSBD-12	Aluminum	Aluminum	Typical	Straight-Horizontal	Bus Bar	650	30	33.8	3	15	233
NSBD-13	Aluminum	Aluminum	Typical	Straight-Horizontal	Bus Bar	650	30	33.8	5	15	300
NSBD-14	Steel	Copper	Typical	Straight-Horizontal	Bus Bar	650	30	33.8	1	0	34
NSBD-15	Steel	Copper	Typical	Straight-Horizontal	Bus Bar	650	30	33.8	2	0	68
NSBD-16	Steel	Copper	Typical	Straight-Horizontal	Bus Bar	650	30	33.8	4	0	135
NSBD-17	Steel	Copper	Typical	Straight-Horizontal	Bus Bar	650	30	33.8	5	0	169
NSBD-18	Steel	Copper	Typical	Straight-Horizontal	Bus Bar	650	30	23	0	15	132
NSBD-19	Steel	Copper	Typical	Straight-Horizontal	Bus Bar	650	30	33.8	3	15	233

NSBD-20	Steel	Copper	Typical	Straight-Horizontal	Bus Bar	650	30	33.8	5	15	300
NSBD-21	Aluminum	Copper	Typical	Straight-Horizontal	Bus Bar	650	30	33.8	1	0	34
NSBD-22	Aluminum	Copper	Typical	Straight-Horizontal	Bus Bar	650	30	33.8	2	0	68
NSBD-23	Aluminum	Copper	Typical	Straight-Horizontal	Bus Bar	650	30	33.8	4	0	135
NSBD-24	Aluminum	Copper	Typical	Straight-Horizontal	Bus Bar	650	30	33.8	5	0	169
NSBD-25	Aluminum	Copper	Typical	Straight-Horizontal	Bus Bar	650	30	23	0	15	132
NSBD-26	Aluminum	Copper	Typical	Straight-Horizontal	Bus Bar	650	30	33.8	3	15	233
NSBD-27	Aluminum	Copper	Typical	Straight-Horizontal	Bus Bar	650	30	33.8	5	15	300
NSBD-28	Steel	Aluminum	Typical	Tee	Bus Bar	650	30	33.8	2	0	68
NSBD-29	Steel	Aluminum	Typical	Tee	Bus Bar	650	30	33.8	4	0	135
NSBD-30	Steel	Aluminum	Typical	Tee	Bus Bar	650	30	33.8	5	0	169
NSBD-31	Steel	Aluminum	Typical	Tee	Bus Bar	650	30	23	0	15	132
NSBD-32	Steel	Aluminum	Typical	Tee	Bus Bar	650	30	33.8	3	15	233
NSBD-33	Steel	Aluminum	Typical	Tee	Bus Bar	650	30	33.8	5	15	300
NSBD-34	Aluminum	Aluminum	Typical	Tee	Bus Bar	650	30	33.8	2	0	68
NSBD-35	Aluminum	Aluminum	Typical	Tee	Bus Bar	650	30	33.8	4	0	135
NSBD-36	Aluminum	Aluminum	Typical	Tee	Bus Bar	650	30	33.8	5	0	169
NSBD-37	Aluminum	Aluminum	Typical	Tee	Bus Bar	650	30	23	0	15	132
NSBD-38	Aluminum	Aluminum	Typical	Tee	Bus Bar	650	30	33.8	3	15	233
NSBD-39	Aluminum	Aluminum	Typical	Tee	Bus Bar	650	30	33.8	5	15	300
NSBD-40	Steel	Copper	Typical	Tee	Bus Bar	650	30	33.8	2	0	68
NSBD-41	Steel	Copper	Typical	Tee	Bus Bar	650	30	33.8	4	0	135
NSBD-42	Steel	Copper	Typical	Tee	Bus Bar	650	30	33.8	5	0	169

*Development of the HEAF Simulation Matrix*

NSBD-43	Steel	Copper	Typical	Tee	Bus Bar	650	30	23	0	15	132
NSBD-44	Steel	Copper	Typical	Tee	Bus Bar	650	30	33.8	3	15	233
NSBD-45	Steel	Copper	Typical	Tee	Bus Bar	650	30	33.8	5	15	300
NSBD-46	Aluminum	Copper	Typical	Tee	Bus Bar	650	30	33.8	2	0	68
NSBD-47	Aluminum	Copper	Typical	Tee	Bus Bar	650	30	33.8	4	0	135
NSBD-48	Aluminum	Copper	Typical	Tee	Bus Bar	650	30	33.8	5	0	169
NSBD-49	Aluminum	Copper	Typical	Tee	Bus Bar	650	30	23	0	15	132
NSBD-50	Aluminum	Copper	Typical	Tee	Bus Bar	650	30	33.8	3	15	233
NSBD-51	Aluminum	Copper	Typical	Tee	Bus Bar	650	30	33.8	5	15	300
NSBD-52	Aluminum	Aluminum	Typical	Elbow	Bus Bar	650	30	33.8	2	0	68
NSBD-53	Aluminum	Aluminum	Typical	Elbow	Bus Bar	650	30	33.8	4	0	135
NSBD-54	Aluminum	Aluminum	Typical	Elbow	Bus Bar	650	30	33.8	5	0	169
NSBD-55	Aluminum	Aluminum	Typical	Elbow	Bus Bar	650	30	23	0	15	132
NSBD-56	Aluminum	Aluminum	Typical	Elbow	Bus Bar	650	30	33.8	3	15	233
NSBD-57	Aluminum	Aluminum	Typical	Elbow	Bus Bar	650	30	33.8	5	15	300
NSBD-58	Aluminum	Aluminum	Typical	Straight-Horizontal	Bus Bar	650	30	23	0	15	132

## **5.2 Geometry and Domain Details for the HEAF FDS Simulations**

### **5.2.1 Medium Voltage Switchgear HEAFs**

#### **5.2.1.1 GE Vertical-Lift Circuit Breaker**

The FDS geometry for the GE MV SWGR is shown in Figure 5-12. The light-colored object near the base of the structure represents the circuit breaker, and the gray surfaces represent the enclosure structure. The walls and internal partitions are modeled as 2.38 mm thick steel with the phase change model. The circuit breaker is modeled as 0.02 m thick steel without the phase change model, which accounts for the circuit breaker mass and its internal construction.

The domain uses 0.076 m grid cells. The as-modeled external dimensions of the enclosure are 2.13 m × 1.07 m × 2.36 m. The enclosure walls are one cell thick resulting in internal dimensions of 1.98 m × 0.91 m × 2.21 m. Although the enclosure boundaries are modeled as one cell thick to assist the FDS pressure solver, the thermal behavior of the enclosure is governed by the specified surface thickness. The switchgear enclosure is centered at the base of the model domain that measures 7.01 m × 5.03 m × 4.57 m and is divided into 36 meshes. This provides 2.44 m to the front and rear of the enclosure, 1.98 m to the sides of the enclosure, and 2.21 m above the top of the enclosure. As seen in Figure 5-12, the enclosure is modeled with the front door opened to account for the initial pressure pulse from the arc. Four arc locations are modeled in this enclosure: one at the circuit breaker stab connections, one in the middle main bus bar compartment, and in the primary cable compartment for both supply and load configurations. Figure 5-13 shows the instrumentation layouts for the four configurations, which are placed at the locations where the exposure is expected to be the greatest. The arc at the circuit breaker stab connection is located just above the top of the circuit breaker centered below the partition for the main and primary cable compartments. The arc dimensions for each simulation are 0.15 m front to back and top to bottom and 0.46 m side to side.

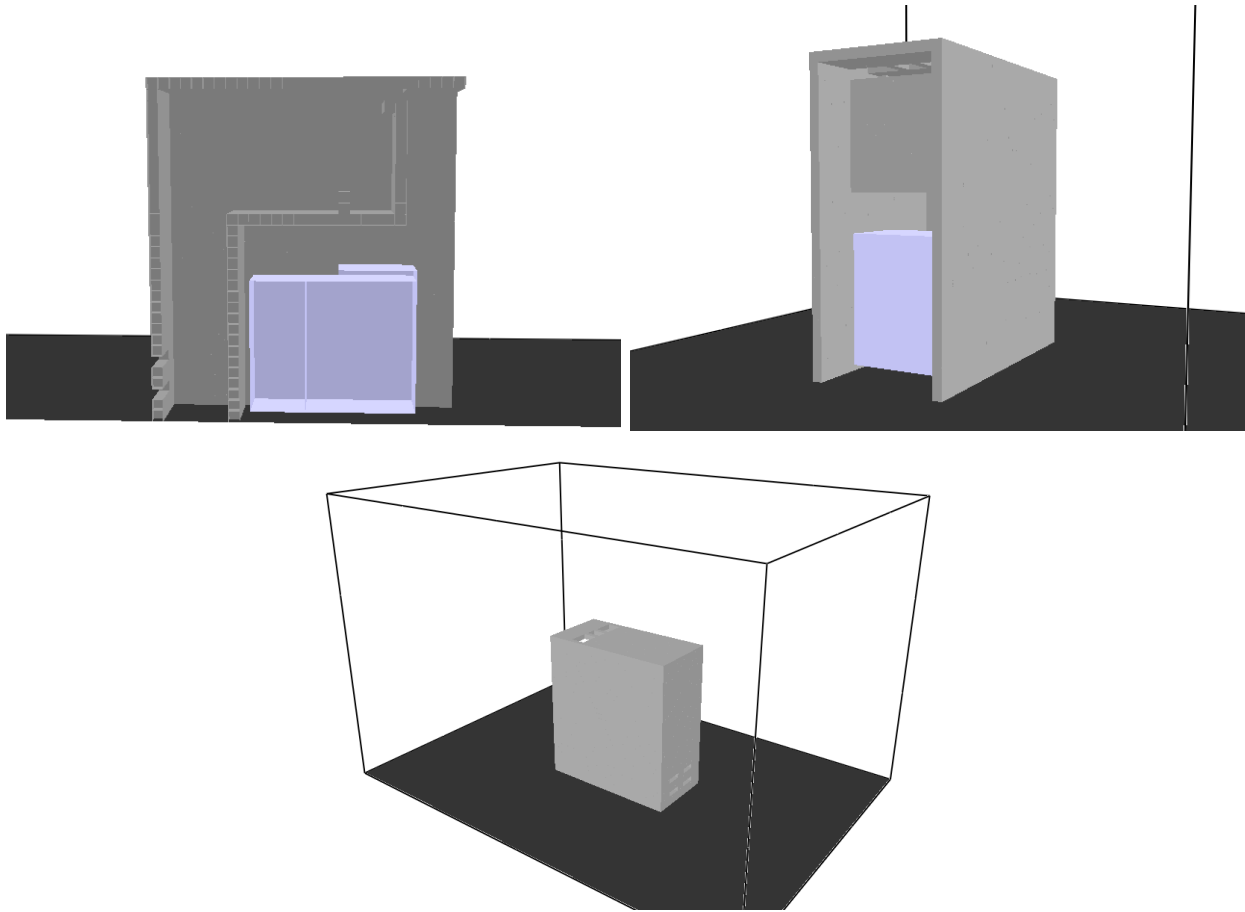


**Figure 5-12**  
FDS model for the GE MV SWGR. Top left – view of enclosure with side clipped showing the internal layout. Top right – view of enclosure front with open door. Bottom – Rear isometric view showing the entire FDS domain

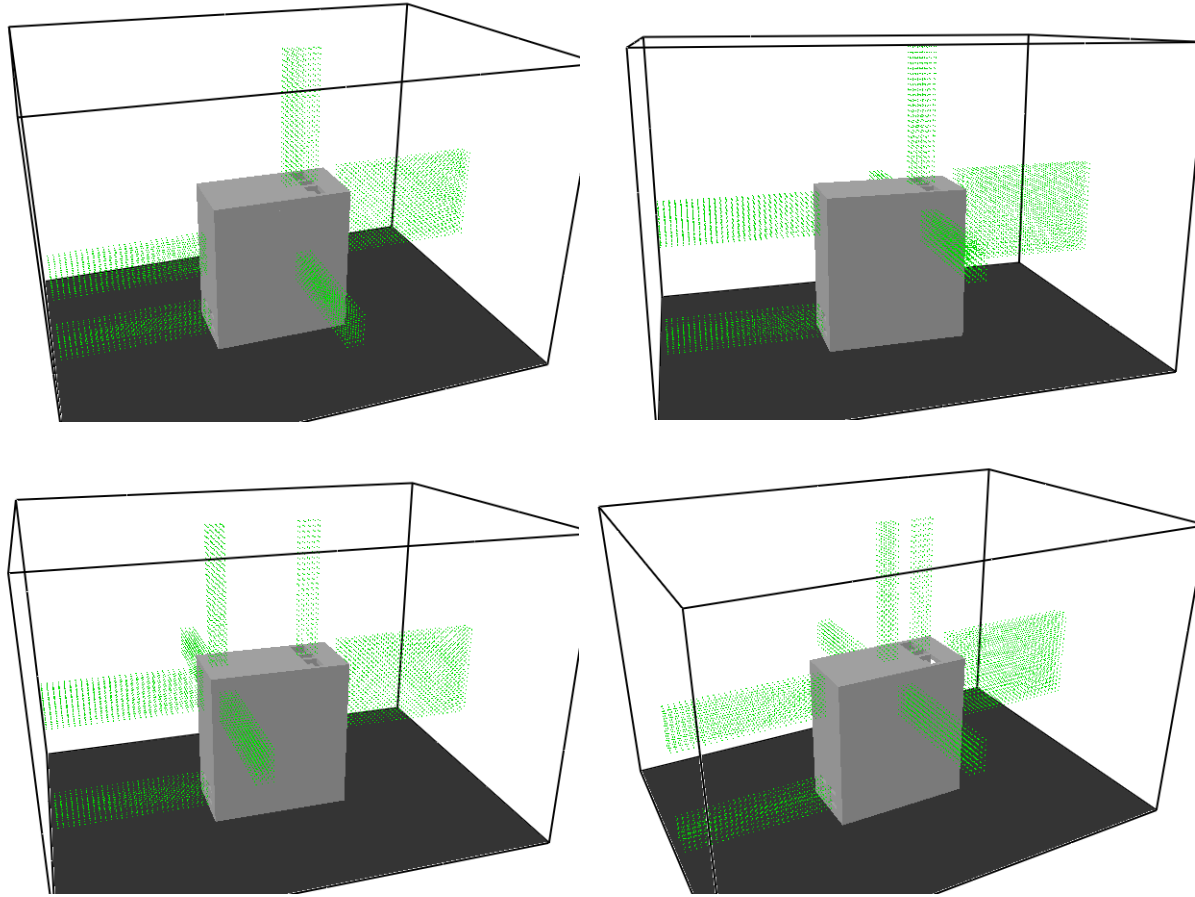


**Figure 5-13**  
**GE MV SWGR exposure measurement locations (green dots) Top left – circuit breaker stabs. Top right – main bus bar compartment. Bottom left – primary cable compartment (load). Bottom right – primary cable compartment (supply)**

#### 5.2.1.2 ABB Horizontal Draw-Out Circuit Breaker

The FDS geometry for the ABB MV SWGR is shown in Figure 5-14. The light-colored object near the base of the structure represents the circuit breaker, and the gray surfaces represent the enclosure structure. The walls and internal partitions are modeled as 2.38 mm thick steel with the phase change model. The circuit breaker is modeled as 0.02 m thick steel without the phase change model, which accounts for the circuit breaker mass and its internal construction.

The domain uses 0.076 m grid cells. The as-modeled external dimensions of the enclosure are 2.06 m × 0.914 m × 2.29 m. The enclosure walls are one cell thick, resulting in internal dimensions of 1.91 m × 0.76 m × 2.21 m. Although the enclosure boundaries are modeled as one cell thick to assist the FDS pressure solver, the thermal behavior of the enclosure is governed by the specified thickness of surface. The switchgear enclosure is centered at the base of a model domain that measures 7.32 m × 5.03 m × 4.57 m and is divided into 36 meshes. This provides 2.63 m to the front and rear of the enclosure, 2.06 m to the sides of the enclosure, and 2.29 m above the top of the enclosure. As seen in Figure 5-14, the enclosure is modeled assuming the front door is opened by the initial pressure pulse from the arc. The arc location in Figure 5-14 is modeled at the circuit breaker stabs. Figure 5-15 shows the instrumentation layouts, placed at the

locations where the exposure is expected to be the greatest. The arc at the circuit breaker stab connection is located in the front center of the switchgear. The arc for each simulation is 0.15 m front to back and top to bottom and 0.46 m side to side.

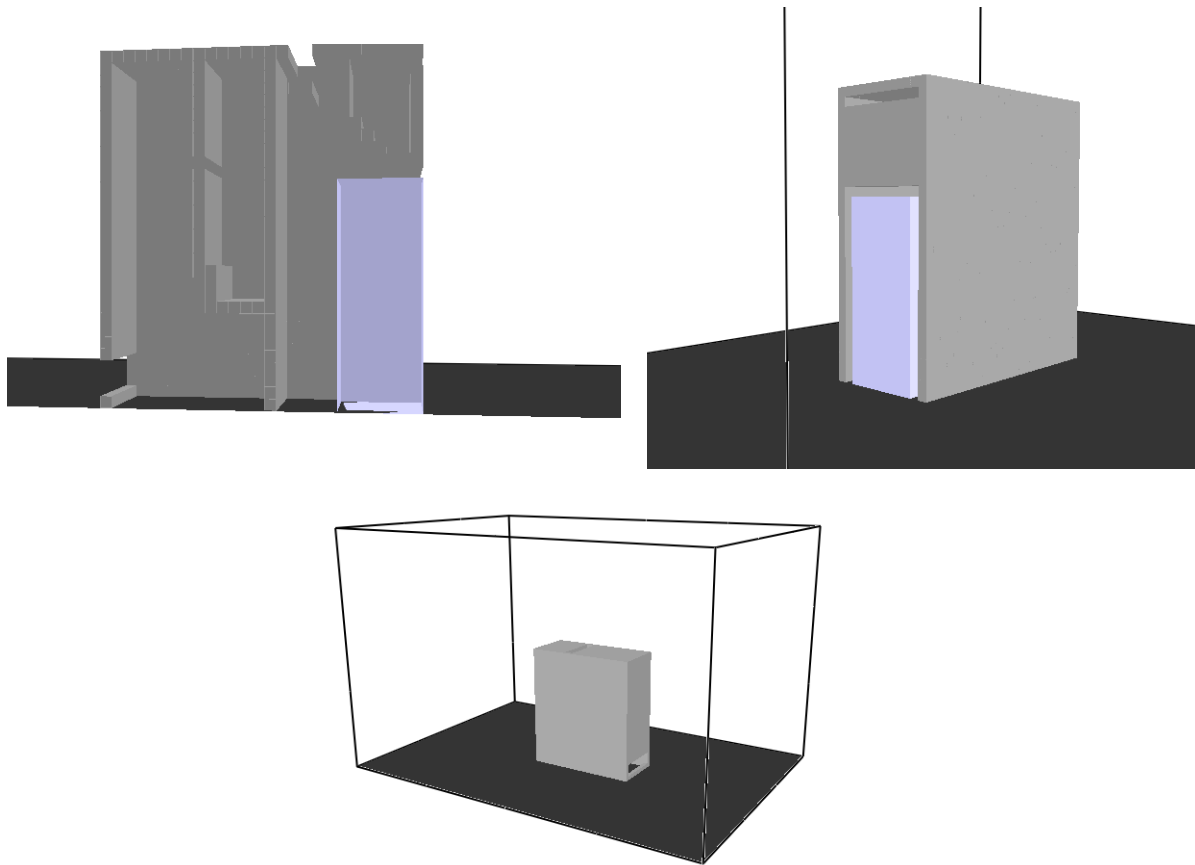


**Figure 5-14**  
FDS model for the ABB MV SWGR. Top left – view of enclosure with side clipped showing internal layout. Top right – view of enclosure front with open door. Bottom – Rear isometric view showing the entire FDS domain

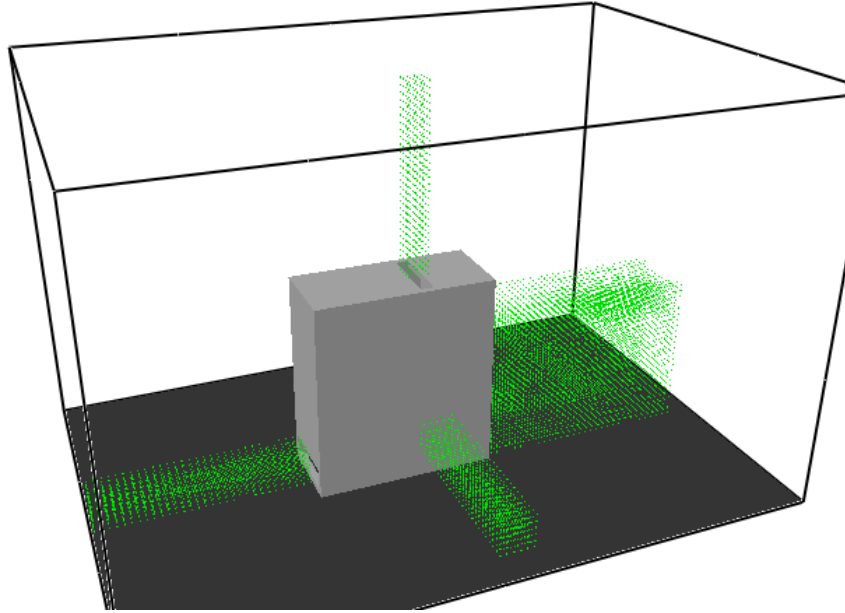


**Figure 5-15**  
**ABB MV SWGR exposure measurement locations (green dots)**

### 5.2.2 Low Voltage Switchgear HEAFs

The FDS geometry for the LV SWGR is shown in Figure 5-16. The four light-colored objects represent the circuit breakers, and the gray surfaces represent the enclosure structure. The walls and internal partitions are modeled as 2.38 mm thick steel with the phase change model. The circuit breaker is modeled as 0.02 m thick steel without the phase change model, which accounts for the circuit breaker mass and its internal construction.

The domain uses 0.076 m grid cells. The as-modeled external dimensions of the enclosure are 1.83 m × 1.22 m × 2.44 m. The enclosure walls are one cell thick resulting in internal dimensions of 1.68 m × 1.07 m × 2.29 m. Although the enclosure boundaries are modeled as one cell thick to assist the FDS pressure solver, the thermal behavior of the enclosure is governed by the specified thickness of surface. The model domain measures 5.26 m × 5.03 m × 4.57 m and is divided into 27 meshes. This provides 1.72 m to the front and rear of the enclosure, 1.91 m to the sides of the enclosure, and 2.14 m above the top of the enclosure. As seen in Figure 5-16, the enclosure is modeled assuming the circuit breaker cubicle door is open due to the initial pressure pulse from the arc.

Six arc locations are modeled in this enclosure:

- Circuit breaker connection stabs, mid-height location
- Circuit breaker connection stabs, top location
- Middle main bus bar, mid-height location
- Middle main bus bar, top location
- Circuit breaker connection stabs, migrating to the middle compartment (mid-height location)
- Circuit breaker connection stabs, migrating to the middle compartment (top location)

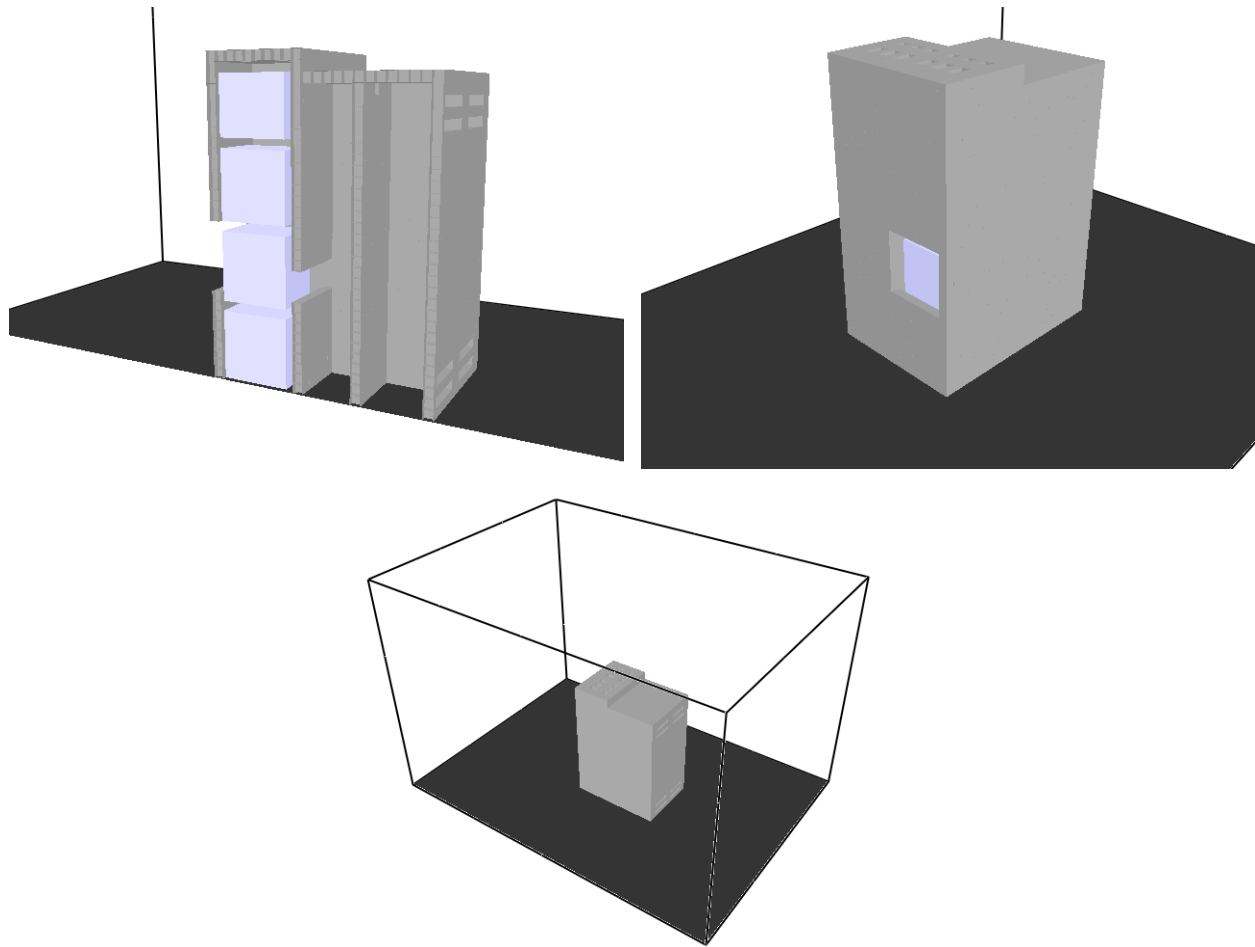


**Figure 5-16**  
**FDS model for the LV SWGR. Top left – view of enclosure with side clipped showing the internal layout. Top right – view of enclosure front with open door. Bottom – Rear isometric view showing the entire FDS domain**

The top right of Figure 5-16 shows the mid-height circuit breaker connection stab location. The barrier between the circuit breaker compartment and the middle main bus bar compartment starts with a hole in it to accommodate the arc volume. Given the arc's proximity to that barrier, this is a reasonable approach since the breach time should be short. Figure 5-16 also shows a small hole at the top of the barrier between the bus bar compartment and the back compartment. This is added to prevent large pressure rises inside a sealed space. Figure 5-17 shows the measurement locations for the LV SWGR HEAFs. One set of measurements is used for all HEAF simulations. On the arc side of the enclosure, groups of measurement devices are located to the side at the top and mid arc locations. On the non-arc side of the enclosure, a single plane of devices are located immediately adjacent to the face. While the HEAF is capable of breaching the partition between the two columns of the circuit breaker cubicles, it is not capable of breaching the next barrier. It is too far away from the arc to receive enough exposure to breach; therefore, only a single plane of devices is needed to capture the maximum exposure. The arc dimensions for each simulation are 0.076 m front to back, 0.15 m top to bottom, and 0.38 m side to side. For simulations where the arc moves from the circuit breaker stab connection to the mid compartment, two arc volumes of the aforementioned size are defined, with only one volume active at a time.

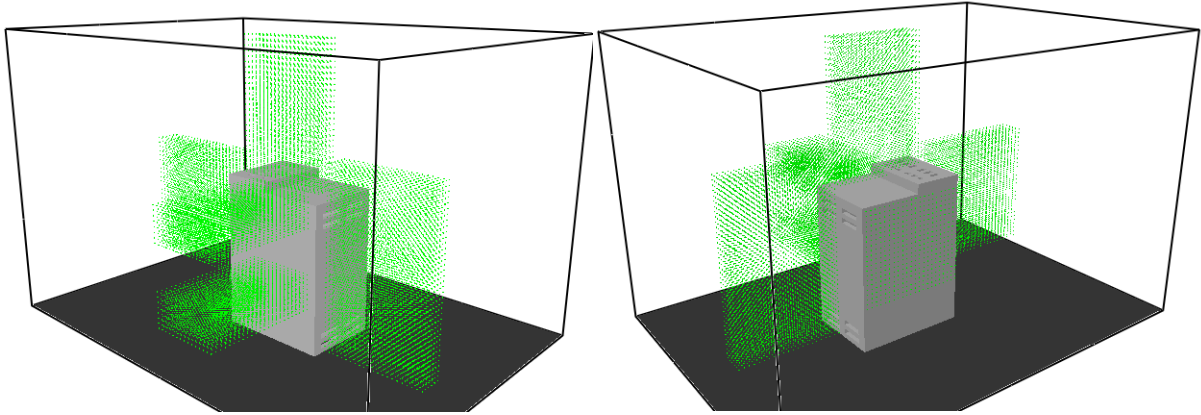


**Figure 5-17**  
**LV SWGR exposure measurement locations (green dots) Left – View of side with the arc.**  
**Right – View of non-arc side of the enclosure**

### 5.2.3 Non-Segregated Bus Duct HEAFs

The FDS geometry and the measurement locations for the NSBD HEAF simulations are shown in Figure 5-18. The duct walls are modeled as 3.18 mm steel or aluminum with the phase change model. No internal partitions are modeled in the bus ducts, and the FDS boundary at the edge of the domain is an open-pressure boundary condition at the inside of the duct.

The domain mesh uses 0.04 m grid cells. The as-modeled cross-section of the ducts is 0.56 m × 0.48 m. The duct walls are one cell thick, resulting in internal dimensions of 0.48 m × 0.40 m. Although the enclosure boundaries are modeled as one cell thick to assist the FDS pressure solver, the thermal behavior of the enclosure is governed by the specified thickness of surface. The model domain for each duct measures 6 m × 6 m × 6 m and is divided into 27 meshes. This provides 2.7 m model domain around the duct arc volume. The arc dimensions for each simulation are 0.24 m along the duct length, 0.16 m top to bottom, and 0.4 m across the duct width. The arcs are centered in the straight segment and elbow. For the tee, the arcs are centered in the upper branch of the tee.

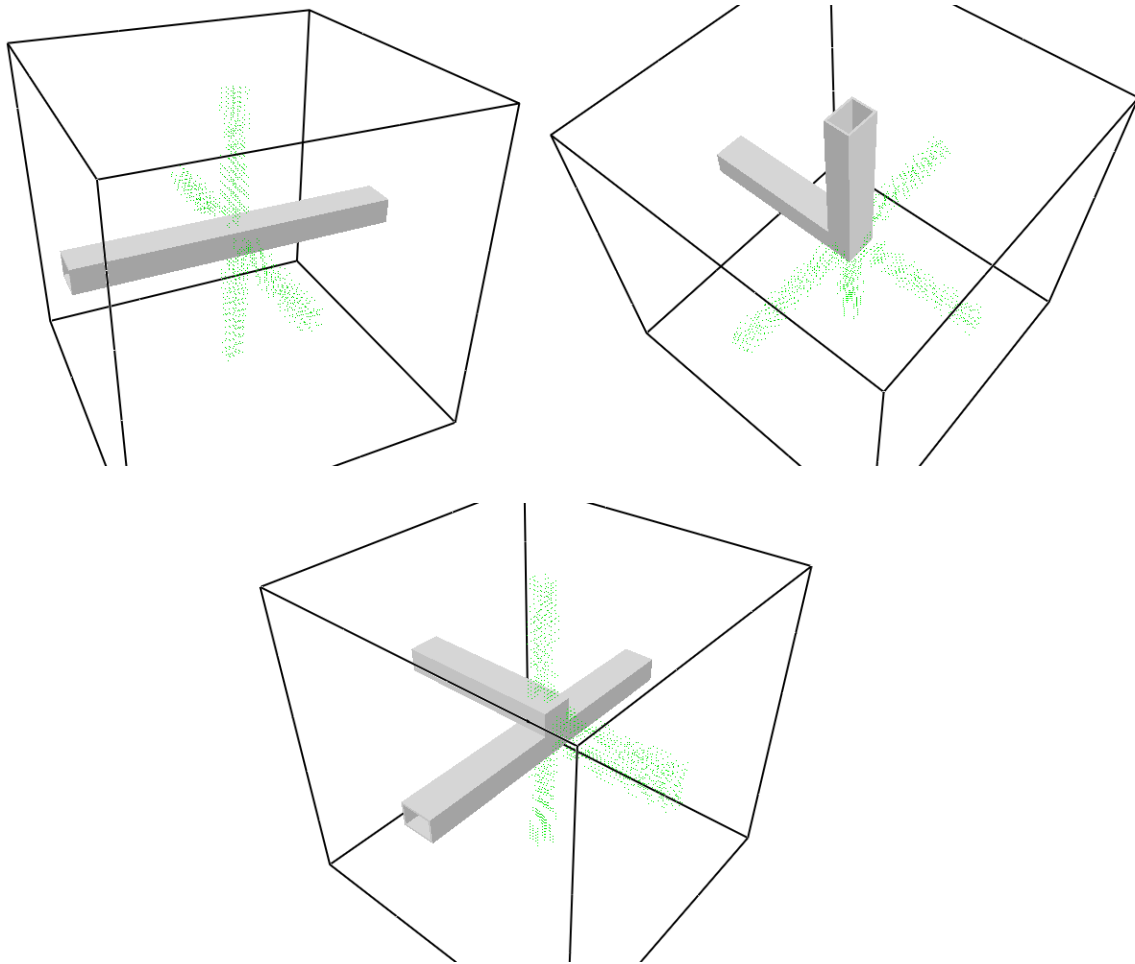


**Figure 5-18**  
NSBD geometry and exposure measurement locations (green dots) Top left – straight segment. Top right – elbow. Bottom – Tee

# 6

## FDS SIMULATION RESULTS

---

This section provides the energetic ZOI results from the FDS HEAF simulations. One FDS simulation for each geometry and arc location is presented in detail, including selected temperature contours and incident energy plots. The graphical results for all simulations are provided in Appendix B.

### 6.1 Medium Voltage Switchgear HEAF Simulations

This section provides a summary of the FDS results for the GE vertical-lift circuit breaker and the ABB horizontal draw-out circuit breaker MV SWGR HEAF simulations. The detailed FDS results presented are typical of the HEAF simulations and highlight the key predictive features of FDS. Graphical results showing the exposure as a function of distance from each face of the enclosure are provided in Appendix B.1. A general discussion of the MV SWGR results, observations from these results, and the tabulated energetic ZOIs are presented in Section 6.1.3.

#### 6.1.1 Selected GE Vertical-Lift Circuit Breaker MV SWGR HEAF Simulations

The FDS results for four GE Magne-Blast vertical-lift circuit breaker simulations are reviewed in detail:

- A HEAF at the main bus bar (Section 6.1.1.1)
- A HEAF at the circuit breaker stab (Section 6.1.1.2)
- A HEAF at the primary cable compartment bus bar load configuration (Section 6.1.1.3)
- A HEAF at the primary cable compartment bus bar supply configuration (Section 6.1.1.4)

These are the four basic locations where a HEAF could occur in the GE MV SWGR geometry. The detailed FDS results for these four locations use the same HEAF arc power profile to highlight the effect of the HEAF initiation location:

- 3 s of stiff current
- 15 s of decaying current (generator-fed)
- Copper electrode
- 233 MJ arc energy

The arc energy power profile for this HEAF is in Figure A-4. The detailed results presented in this section include depictions of the switchgear enclosure breach, the particle dispersion around the enclosure, the luminous thermal plume, the heat release rate per unit volume (arc), the enclosure wall temperatures, and the target exposure profiles as a function of distance.

### 6.1.1.1 GE Vertical-Lift Circuit Breaker MV SWGR Design with a HEAF at the Main Bus Bar

Figure 6-1 depicts the metal particle distribution around the upper portion of the GE vertical-lift circuit breaker switchgear at various times for a HEAF located at the main bus bar. At 0 s, there are no particles and the switchgear enclosure is intact. The openings at 0 s are the top surface vents and the upper front below the top vents. At 0.3 s, the switchgear enclosure is still intact, but there are metal particles ejected from the top vents. The switchgear enclosure is breached at about 0.6 s (not shown in Figure 6-1), with particles ejected from the front face through portions of the switchgear enclosure that have disintegrated. At about 1.3 s, the left and right sides are breached, with particles ejected from the openings in the switchgear enclosure wall (only the right side is shown in Figure 6-1). The front face openings continue to expand between 0.6 and 1.3 s. At about 3.5 s, a small portion of the switchgear enclosure at the top near the vent is breached. Between 1.3 s and 3.5 s, the front and right sides as well as the front openings continue to grow larger as more portions of the switchgear enclosure are breached. The left and right side openings are the same size, and the front opening is symmetric about the vertical centerline. The breach openings continue to expand during the decay stage, up to about 15 s. At 20 s, after the fault has cleared, nearly all particles have dispersed. The final state of the switchgear enclosure boundary is depicted at 20 s, with significant openings on the left, right, front, and top surfaces visible. There are no openings on the rear of the switchgear enclosure.

Figure 6-2 depicts the luminous portion of the thermal plume at 0.3 s, 1.3 s, 3.5 s, and 15 s, corresponding to the times at which the particle distributions are shown. The luminous thermal plume reaches a peak near the start of the decay phase where significant portions of the switchgear enclosure are breached.

Figure 6-3 depicts the heat release rate per unit volume at 4 s, which corresponds to the arc energy location in the FDS model. The size of the holes at this time are large enough to view the arc clearly. The intent of this figure is to show the approximate location where holes develop relative to the location where the arc energy is modeled in FDS.

Figure 6-4 depicts the wall temperature at 15 s, the time at which the greatest extent of the switchgear enclosure boundary is heated. Although the heated wall temperature contributes to the heat flux at a fixed location, the temperatures are relatively low, suggesting this component is small compared to the energy flux directly from the arc fault and gases.

The total exposure energy as a function of distance is shown in Figure 6-5, which shows the energetic ZOI for this simulation is less than 1 m from the sides (left/right), top, and front, and zero from the rear of the switchgear enclosure. This is consistent with the particle distribution in Figure 6-1 and the luminous plume progression depicted in Figure 6-2.

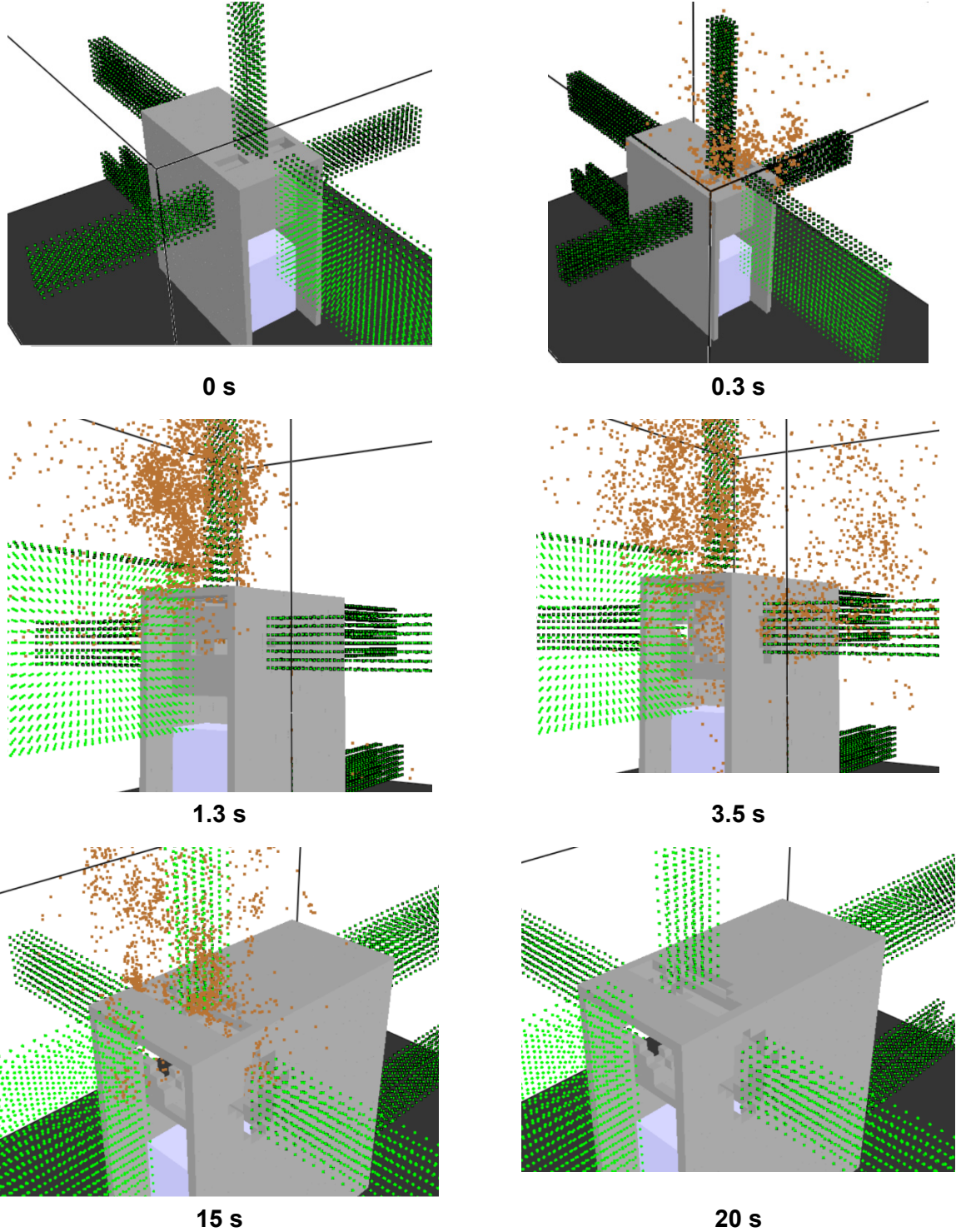
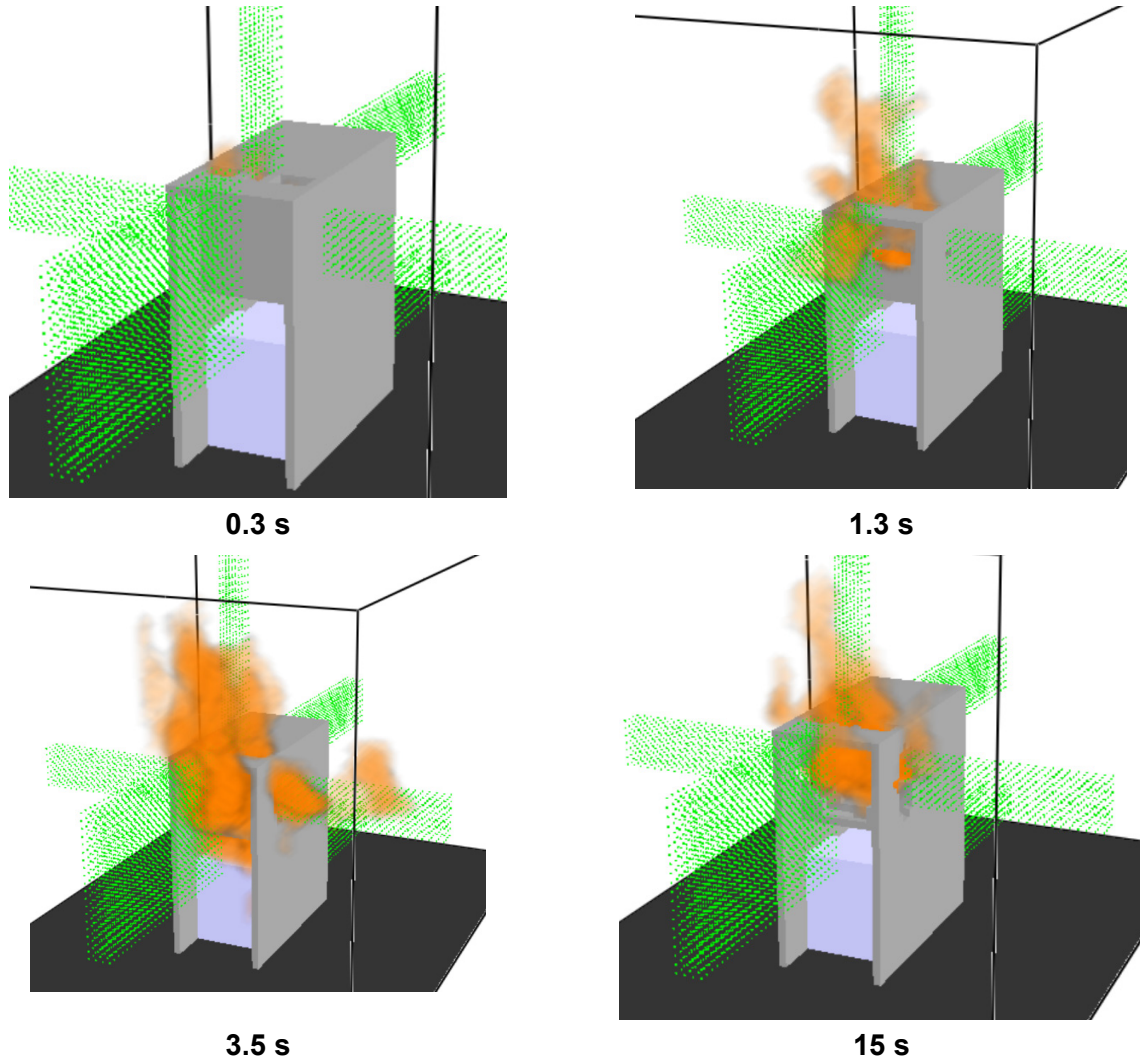
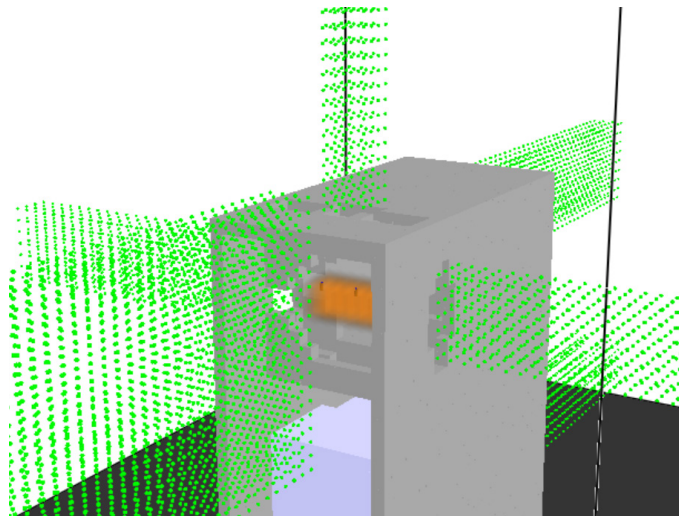


Figure 6-1  
Particle distribution at various times for a 233 MJ HEAF located at the main bus bars of a vertical-lift circuit breaker MV SWGR design



**Figure 6-2**  
Luminous portion of the thermal plume at various times for a 233 MJ HEAF located at the main bus bars of a vertical-lift circuit breaker MV SWGR design



**Figure 6-3**  
Heat release rate per unit volume at 4 s for a 233 MJ HEAF located at the main bus bars of a vertical-lift circuit breaker MV SWGR design. The heat release rate per unit volume for the electrode is shown as a rectangular orange region within the switchgear.

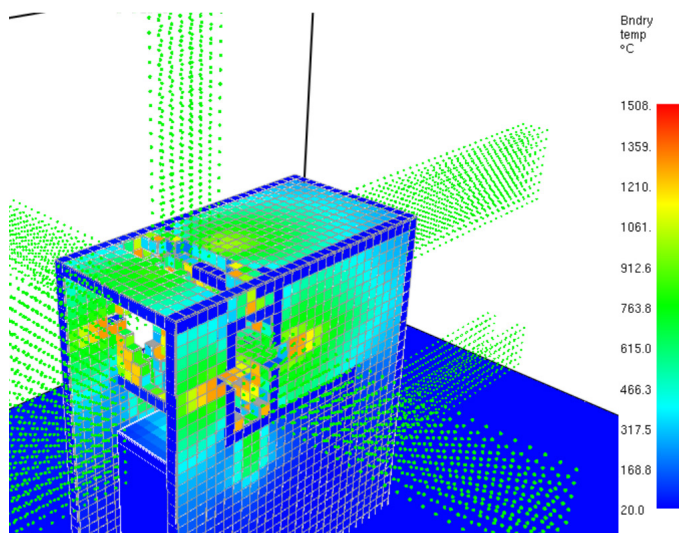


**Figure 6-4**  
Wall temperature at 15 s for a 233 MJ HEAF located at the main bus bars of a vertical-lift circuit breaker MV SWGR design

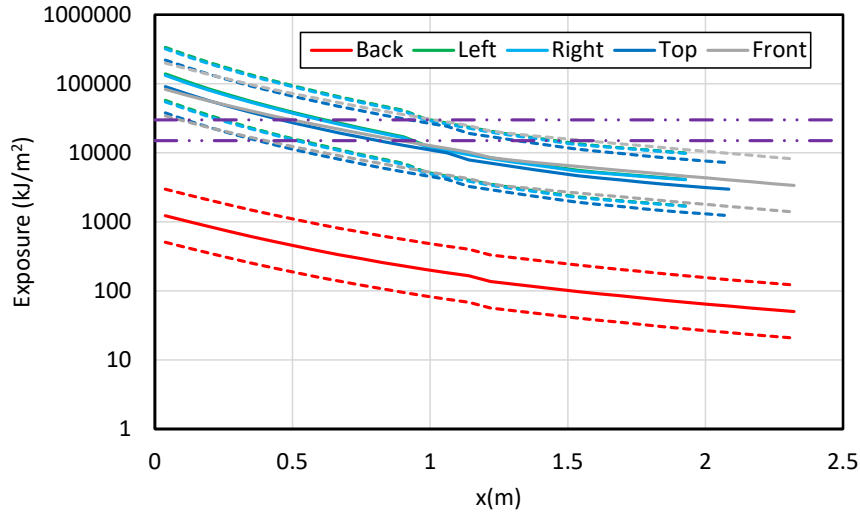


**Figure 6-5**  
**Total energy exposure as a function of distance from each face for a 233 MJ HEAF located at the main bus bars of a vertical-lift circuit breaker MV SWGR design (HEAF simulation ID MV-GE-36). Note the results for the left- and right-sides are nearly coincident. Dashed horizontal lines correspond to the 15 MJ/m<sup>2</sup> and 30 MJ/m<sup>2</sup> target fragility thresholds**

#### 6.1.1.2 GE Vertical-Lift Circuit Breaker MV SWGR Design with a HEAF at the Circuit Breaker Stabs

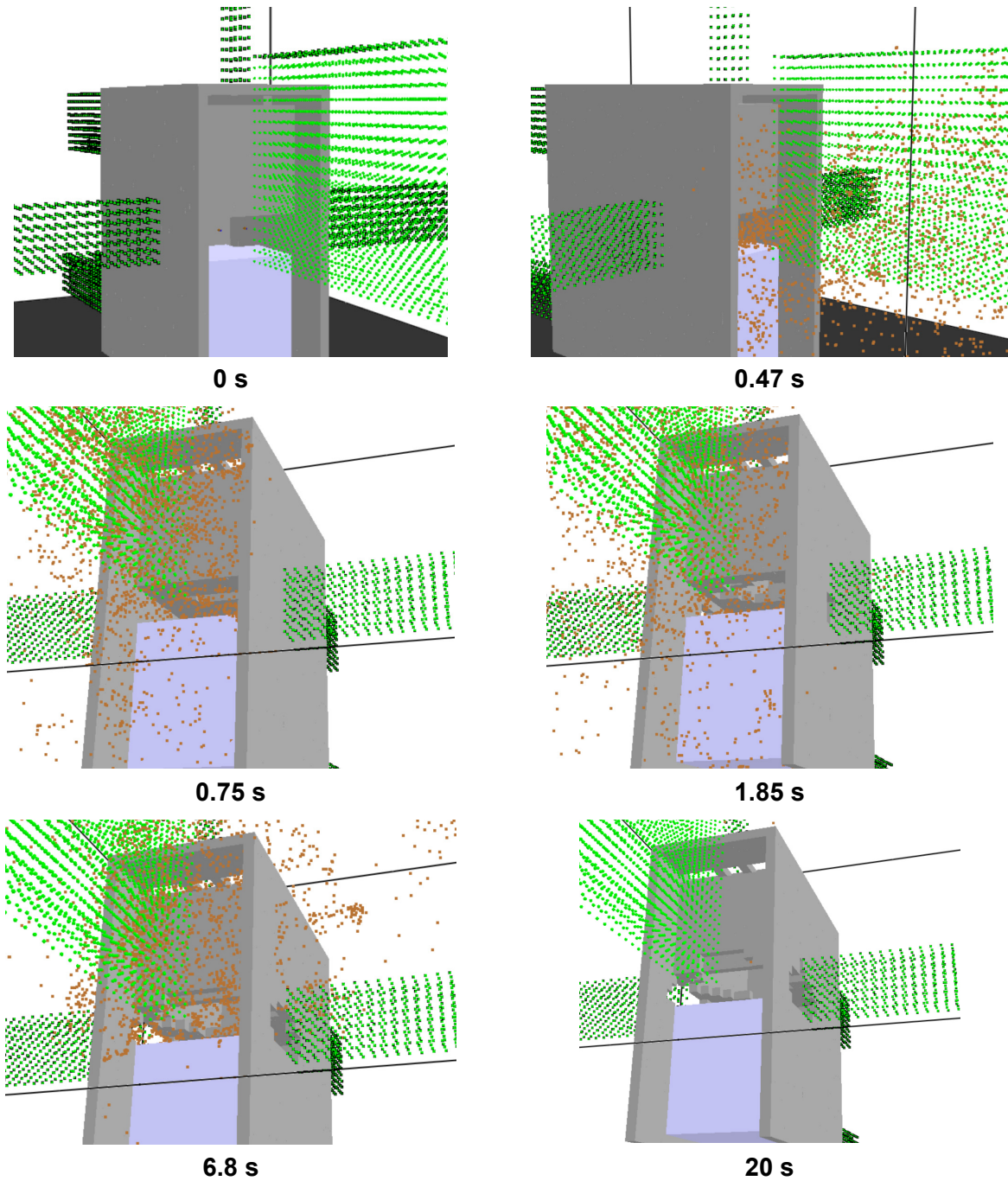
Figure 6-6 depicts the metal particle distribution around the upper portion of the GE vertical-lift circuit breaker style switchgear at various times for a HEAF at the circuit breaker stabs. At 0 s, there are no particles and the switchgear enclosure is intact. The openings at 0 s are in the front face of the switchgear enclosure. At 0.47 s, the switchgear enclosure is still intact, but there are metal particles ejected from the front opening. The switchgear enclosure is breached at about 0.75 s, with the switchgear enclosure breach on the upper surface. At about 1.85 s, the left and right switchgear enclosure faces are breached, with particles ejected from these openings (only the right side is shown in Figure 6-6). The side and top switchgear enclosure breach openings continue to expand between 1.85 and 6.8 s, where the maximum damage to the switchgear enclosure is reached. The left and right side openings are the same size, and the rear opening is symmetric about the vertical centerline. After 20 s, the fault is cleared and nearly all particles have dispersed. The final state of the switchgear enclosure is depicted at 20 s, after the fault has cleared and the particles have dispersed showing significant openings on the left, top, and right enclosure faces.

Figure 6-7 depicts the luminous portion of the thermal plume at 0.47 s, 0.75 s, 1.85 s, and 6.8 s, corresponding to the times at which the particle distributions are shown. The luminous thermal plume reaches a peak near the start of the decay phase between 1.85 s and 6.8 s where significant portions of the switchgear enclosure are breached.

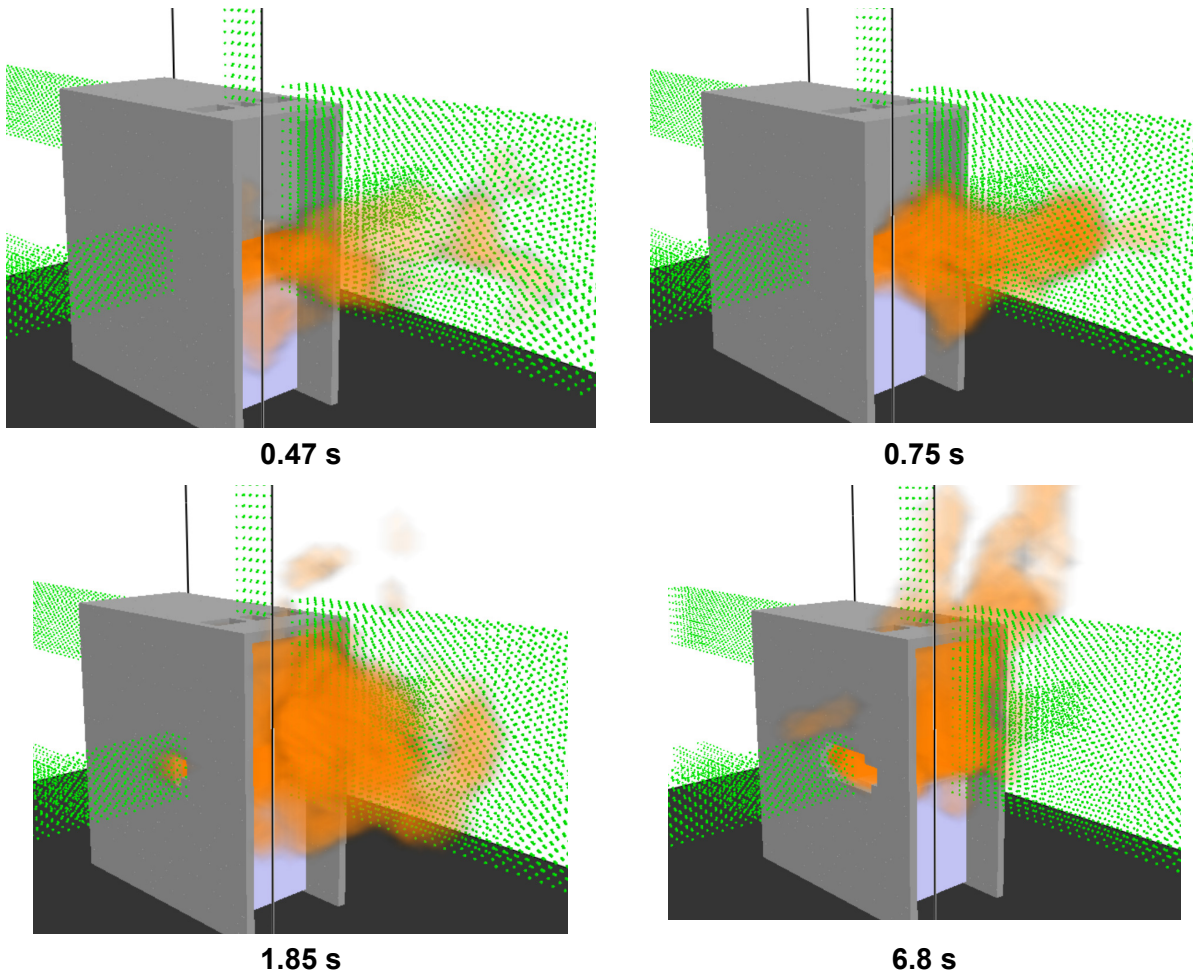
Figure 6-8 depicts the heat release rate per unit volume at 4 s, which corresponds to the arc energy location in the FDS model. The size of the holes at this time are large enough to view the arc clearly. The intent of this figure is to show the approximate location where holes develop relative to the location where the arc energy is modeled in FDS.

Figure 6-9 depicts the wall temperature at 15 s, the time at which the greatest extent of the switchgear enclosure boundary is heated. Although the heated wall temperature contributes to the heat flux at a fixed location, the temperatures are relatively low, suggesting this component is small compared to the energy flux directly from the arc fault and gases.

The total exposure energy as a function of distance is shown in Figure 6-10, which indicates the energetic ZOI for this simulation is less than 1 m from the sides and top and nearly zero from the front and rear of the switchgear enclosure. The energetic ZOIs for the front are slightly smaller than the sides even though the particle distribution and luminous plume (Figure 6-6 and Figure 6-7) suggest a more severe exposure. In this case, the energetic ZOI is primarily dependent on the distance from the arc emitter, which is toward the rear of the switchgear enclosure and further from the front face.



**Figure 6-6**  
Particle distribution at various times for a 233 MJ HEAF located at the circuit breaker stabs of a vertical-lift circuit breaker MV SWGR design



**Figure 6-7**  
Luminous portion of the thermal plume at various times for a 233 MJ HEAF located at the circuit breaker stabs of a vertical-lift circuit breaker MV SWGR design

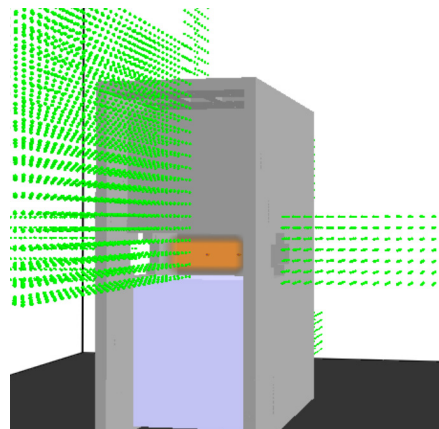


**Figure 6-8**  
Heat release rate per unit volume at 4 s for a 233 MJ HEAF located at the circuit breaker stabs of a vertical-lift circuit breaker MV SWGR design. The heat release rate per unit volume for the electrode is shown as a rectangular orange region within the switchgear.

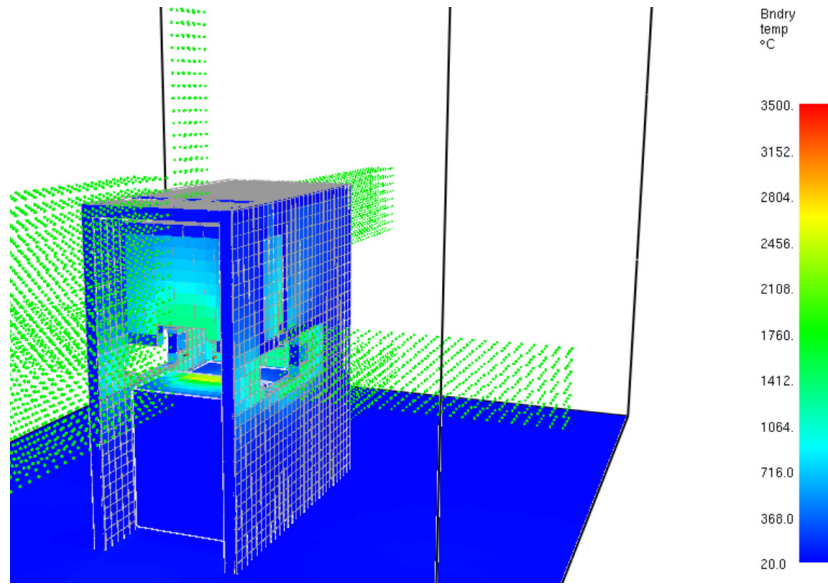


**Figure 6-9**  
**Wall temperature at 15 s for a 233 MJ HEAF located at the circuit breaker stabs of a vertical-lift circuit breaker MV SWGR design**

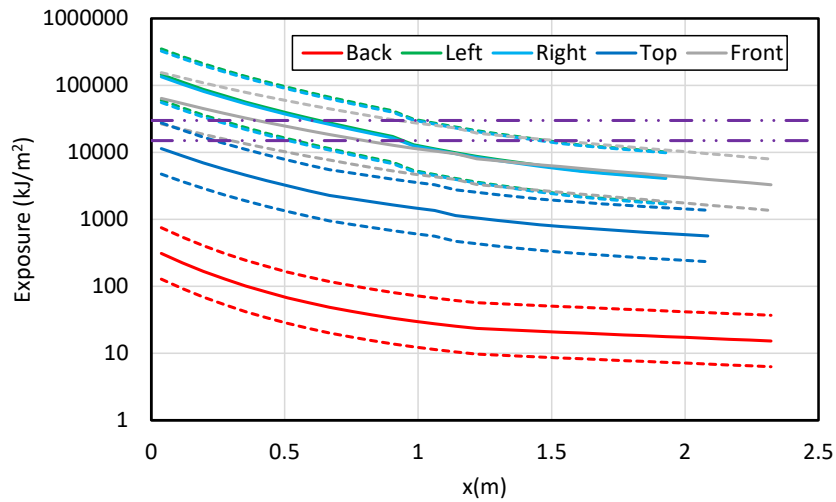


**Figure 6-10**  
**Total energy exposure as a function of distance from each face for a 233 MJ HEAF located at the circuit breaker stabs of a vertical-lift circuit breaker MV SWGR design (HEAF simulation ID MV-GE-35). Note the results for the left- and right-sides are nearly coincident. Dashed horizontal lines correspond to the 15 MJ/m<sup>2</sup> and 30 MJ/m<sup>2</sup> target fragility threshold**

### 6.1.1.3 GE Vertical-Lift Circuit Breaker MV SWGR Design with a HEAF at the Primary Cable Compartment Bus Bars in the Load Configuration

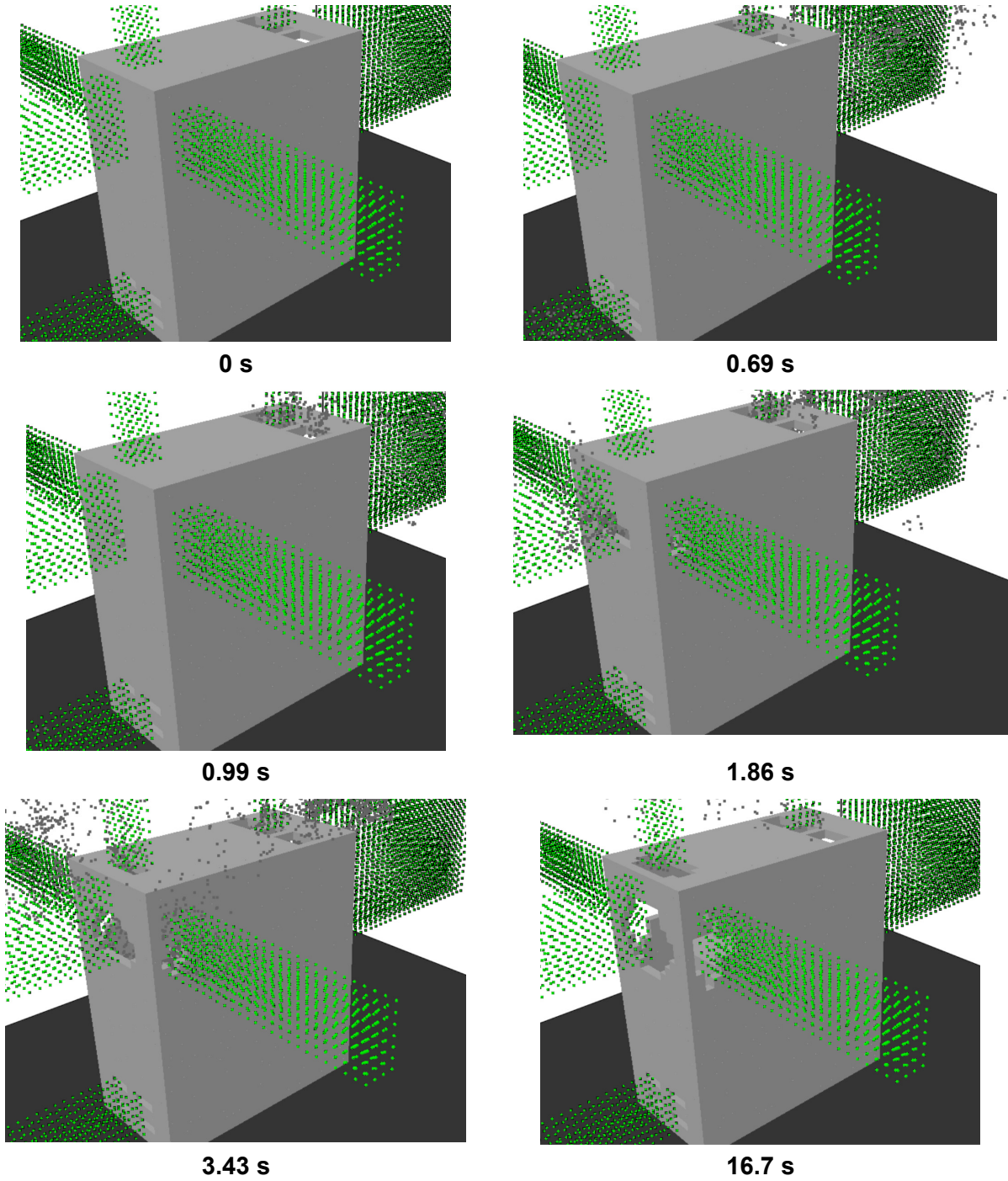
Figure 6-11 depicts the metal particle distribution around the rear, side, and upper portion of the GE vertical-lift circuit breaker switchgear at various times for a HEAF located at the primary cable compartment bus bars in the load configuration. At 0 s, there are no particles and the switchgear enclosure is intact. The openings at 0 s are the front top vents, the rear top vents, and the rear bottom vents. At 0.69 s, the switchgear enclosure is still intact, but there are metal particles ejected from the three vent openings. The switchgear enclosure is breached at 0.99 s, with the initial switchgear enclosure breach on the upper rear surface near the electrode. At 1.86 s, the left and right switchgear enclosure faces are breached, with particles ejected from these openings (only the left side is shown in Figure 6-11). The side and rear switchgear enclosure breach openings continue to expand between 1.86 and 3.43 s, when the top rear of the switchgear enclosure is breached. The switchgear enclosure openings continue to grow during the decay stage and reach a maximum at about 16.7 s (near the end of the decay stage). At 20 s (not shown in Figure 6-11), after the fault has cleared, nearly all particles have dispersed. Although particles are ejected from the lower rear vents, the majority of the particles are ejected through the upper vents and later through the damaged switchgear enclosure.

Figure 6-12 depicts the luminous portion of the thermal plume at 0.69 s, 0.99 s, 1.86 s, and 3.43 s, corresponding to the times at which the particle distributions are shown. The luminous thermal plume is primarily confined to the switchgear enclosure prior to the breach as shown at 0.69 s and 0.99 s. After 0.99 s, the luminous thermal plume expands outside the switchgear and reaches a peak near the start of the decay phase between 1.86 s and 3.43 s where significant portions of the switchgear enclosure are breached.

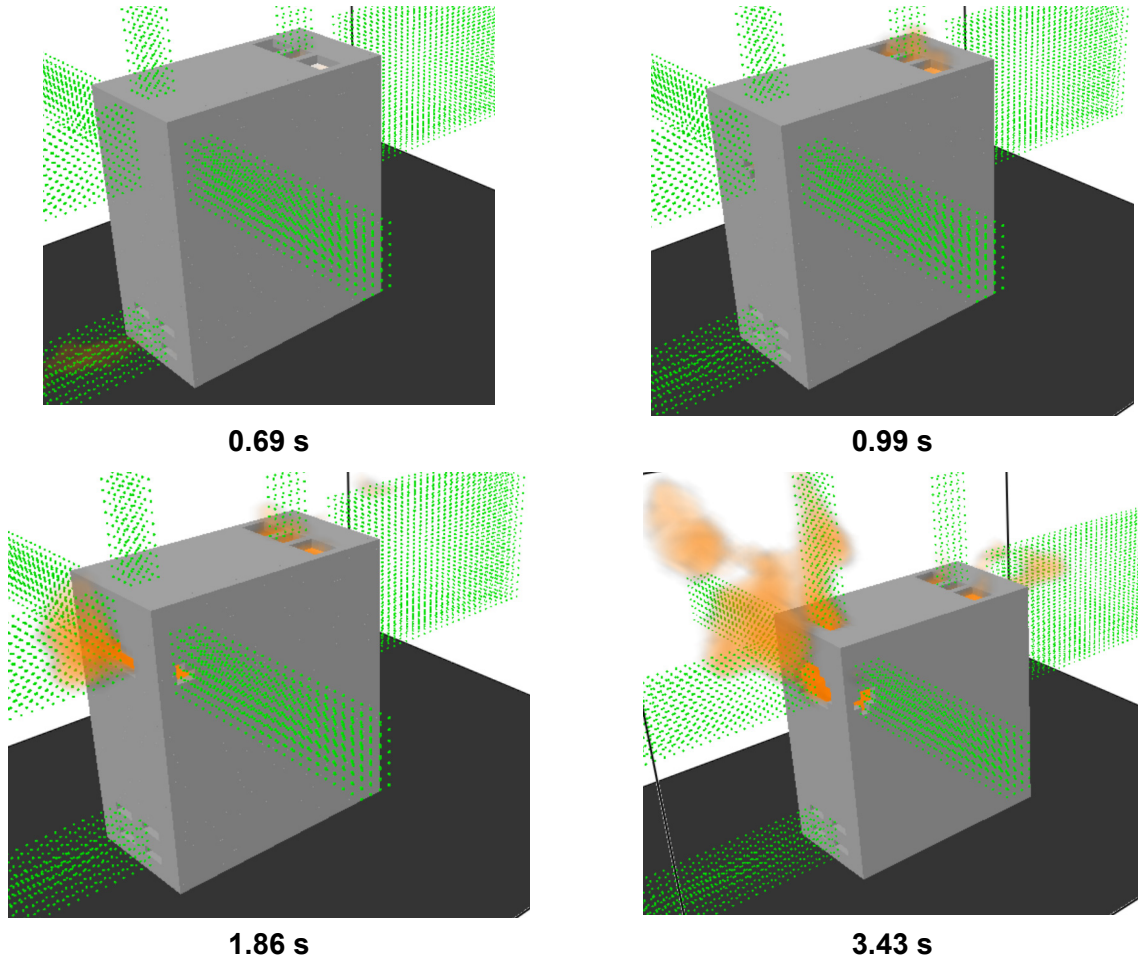
Figure 6-13 depicts the heat release rate per unit volume corresponding at 4 s, which corresponds to the arc energy location in the FDS model. The size of the holes at this time are large enough to view the arc clearly. The intent of this figure is to show the approximate location where holes develop relative to the location where the arc energy is modeled in FDS. The location of openings and the view are different from Figure 6-8 so that the arc for this scenario may be seen more clearly.

Figure 6-14 depicts the wall temperature at 15 s, the time at which the greatest extent of the switchgear enclosure boundary is heated. Although the heated wall temperature contributes to the heat flux at a fixed location, the temperatures are relatively low, suggesting this component is small compared to the energy flux directly from the arc fault and gases.

The total exposure energy as a function of distance is shown in Figure 6-15, which shows the energetic ZOI for this simulation is between 0.5 – 1.2 m for the rear, side (left/right), and top faces and zero from the front face, consistent with the particle distribution and luminous plume location.



**Figure 6-11**  
Particle distribution at various times for a 233 MJ HEAF located at the primary cable compartment bus bars in the load configuration of a vertical-lift circuit breaker MV SWGR design



**Figure 6-12**  
Luminous portion of the thermal plume at various times for a 233 MJ HEAF located at the primary cable compartment bus bars in the load configuration of a vertical-lift circuit breaker MV SWGR design

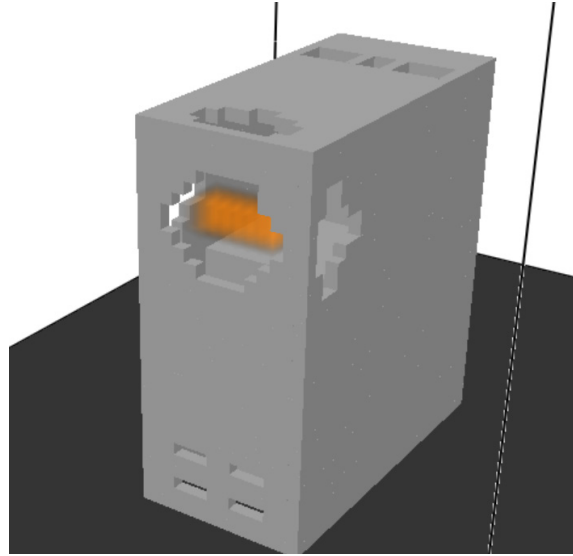


**Figure 6-13**  
Heat release rate per unit volume at 4 s for a 233 MJ HEAF located at the primary cable compartment bus bars in the load configuration of a vertical-lift circuit breaker MV SWGR design. The heat release rate per unit volume for the electrode is shown as a rectangular orange region within the switchgear

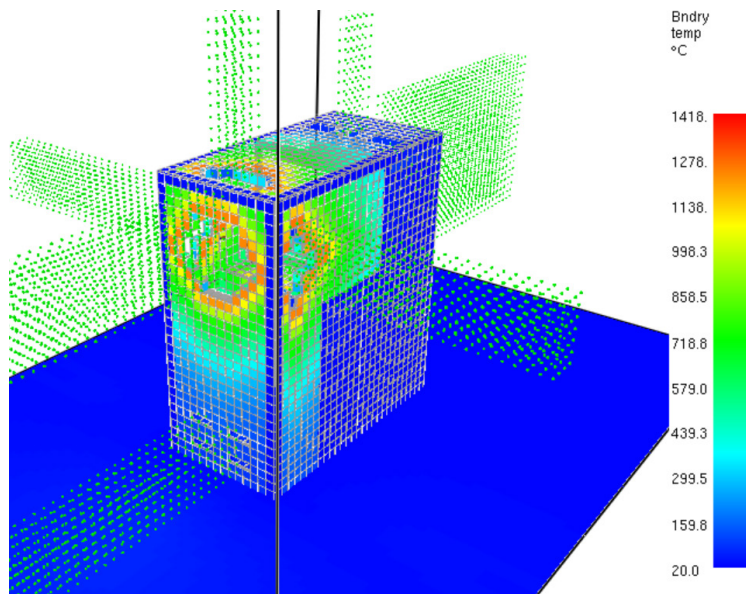


**Figure 6-14**  
Wall temperature at 15 s for a 233 MJ HEAF located at the primary cable compartment bus bars in the load configuration of a vertical-lift circuit breaker MV SWGR design

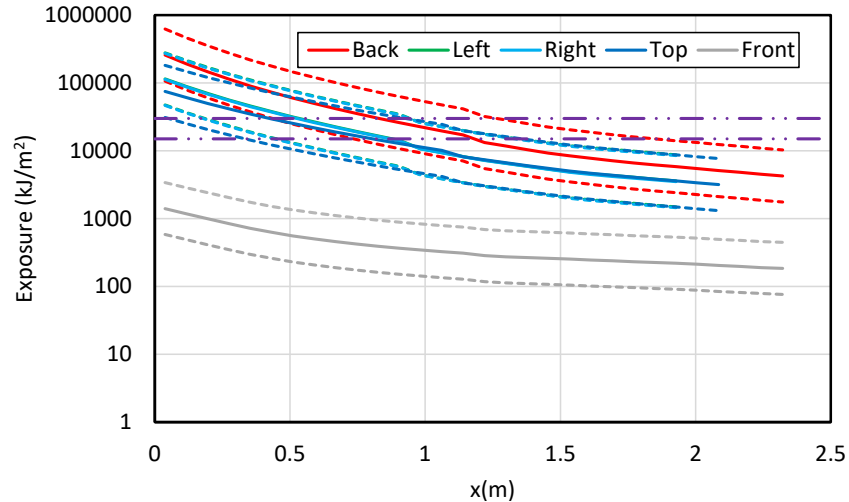


**Figure 6-15**

**Total energy exposure as a function of distance from each face for a 233 MJ HEAF located at the primary cable compartment bus bars in the load configuration of a vertical-lift circuit breaker MV SWGR design (HEAF simulation ID MV-GE-37). Note the results for the left- and right-sides are nearly coincident. Dashed horizontal lines correspond to the 15 MJ/m<sup>2</sup> and 30 MJ/m<sup>2</sup> target fragility threshold**

#### 6.1.1.4 GE Vertical-Lift Circuit Breaker MV SWGR Design with a HEAF at the Primary Cable Compartment Bus Bars in the Supply Configuration

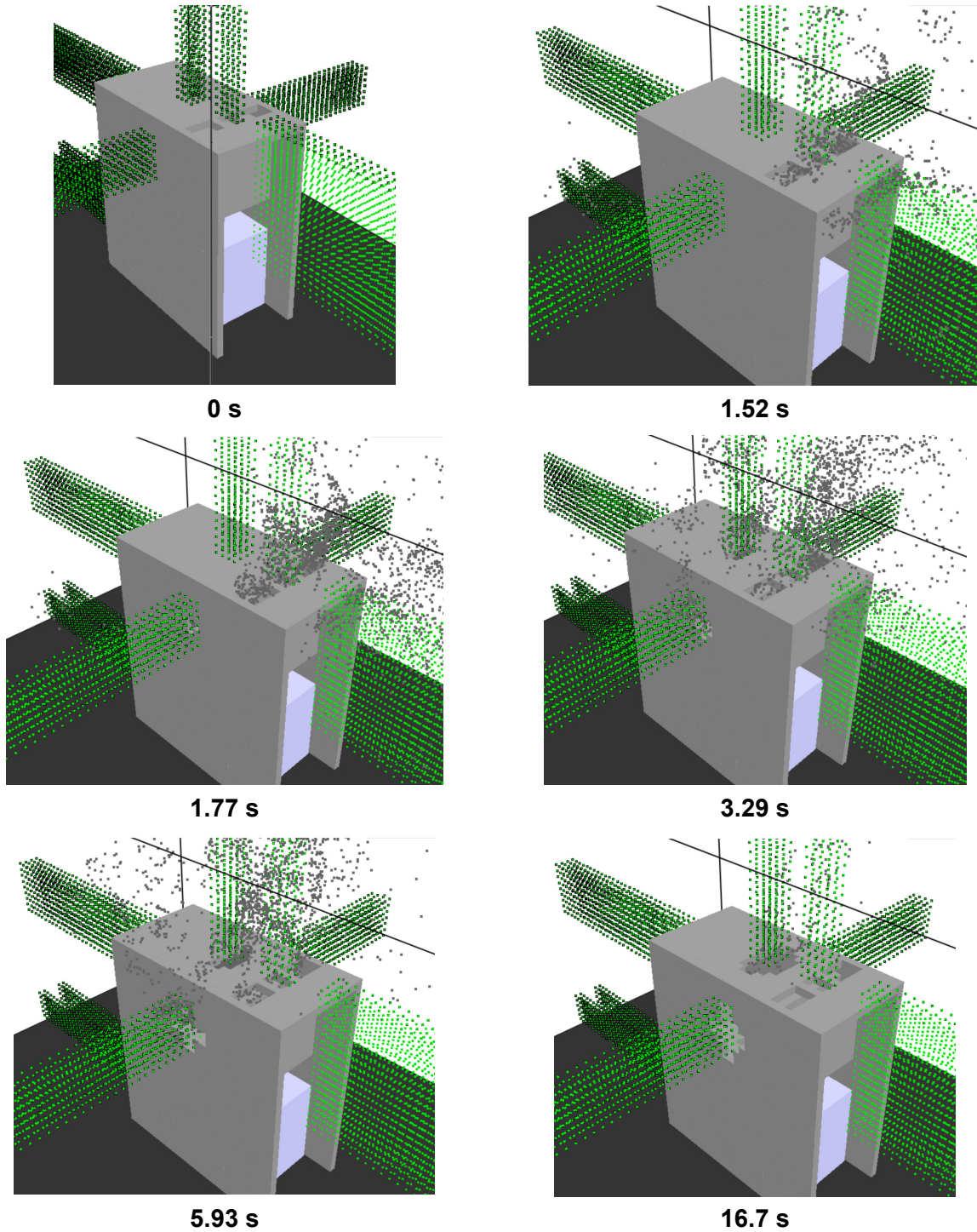
Figure 6-16 depicts the metal particle distribution around the rear, side, and upper portion of the GE vertical-lift circuit breaker switchgear at various times for a HEAF located at the primary cable compartment bus bars in the supply configuration. At 0 s, there are no particles and the switchgear enclosure is intact. The openings at 0 s are the front top vents, the upper front (not shown in Figure 6-16), the rear top vent, and the rear bottom vent (also not shown in Figure 6-16). At 1.52 s, the switchgear enclosure is still intact, but there are metal particles ejected from the top and, to a lesser extent, the rear vent openings. The switchgear enclosure is breached at 1.77 s on the upper side surfaces near the electrode. At 3.29 s, the top of the switchgear enclosure is breached, with particles ejected from the sides and top openings (only the left side is shown in Figure 6-16). The side and top switchgear enclosure openings continue to expand between 3.29 and 5.93 s, about the time the opening size growth begins to slow. The breach openings continue to grow slowly during the remainder of the decay stage and reach a maximum at 16.7 s. At 20 s (not shown in Figure 6-16), after the fault has cleared, nearly all particles have dispersed. Although particles are ejected from the lower rear vent, the majority of the particles are ejected through the upper vents, and later, through the damaged switchgear enclosure.

Figure 6-17 depicts the luminous portion of the thermal plume at 1.52 s, 1.77 s, 3.29 s, and 5.93 s, corresponding to the times at which the particle distributions are shown. The luminous thermal plume is primarily confined to the switchgear enclosure prior to the breach as shown at 1.52 s and 1.77 s. After 1.77 s, the luminous thermal plume expands outside the switchgear enclosure and reaches a peak near the start of the decay phase between 3.29 s and 5.93 s where significant portions of the switchgear enclosure are breached.

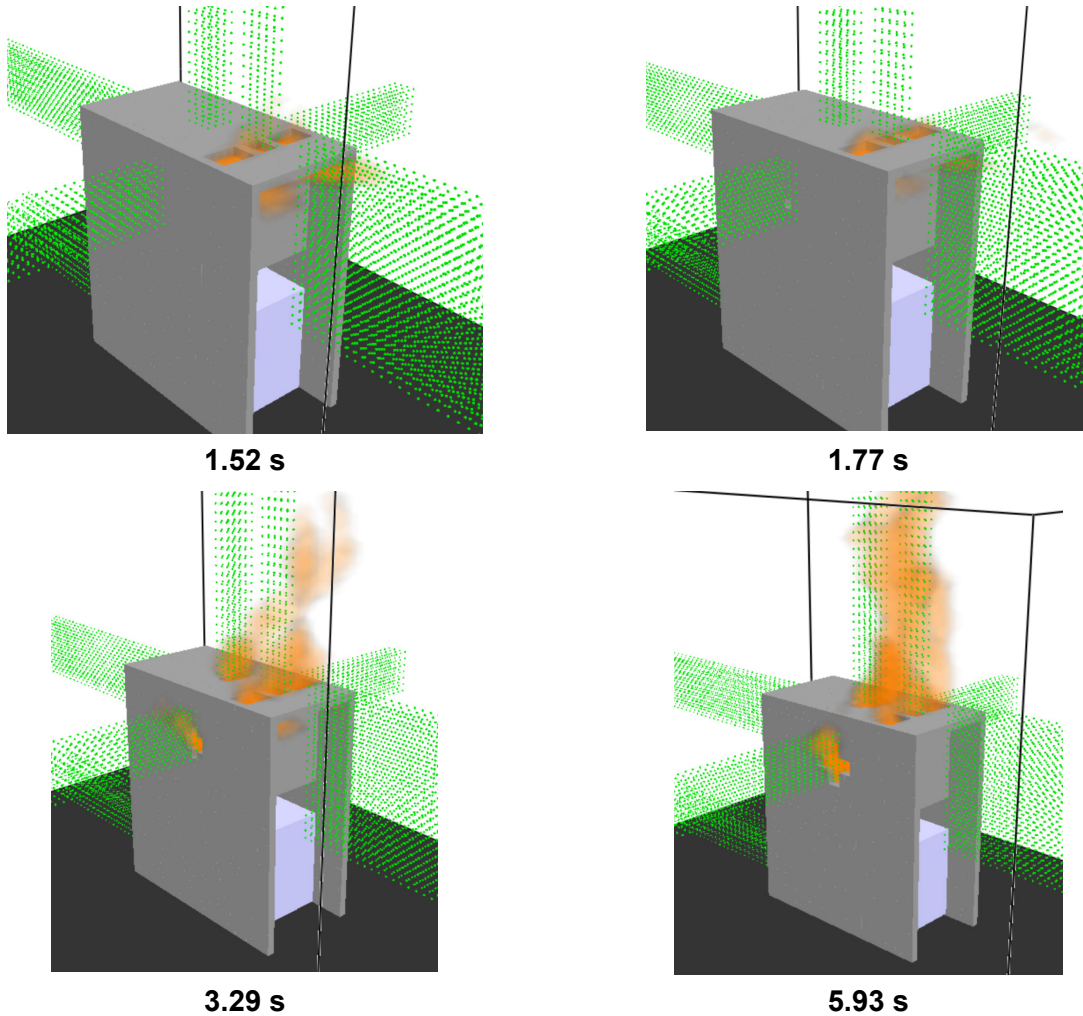
Figure 6-18 depicts the heat release rate per unit volume at 12.5 s, which corresponds to the arc energy location in the FDS model. The time selected for this view is greater than the time selected for arcs located at the main bus bar, the circuit breaker stabs, and the PCCBB (load configuration) because it is near the middle of the enclosure and not easily viewed with the hole size at 4 s. At 12.5 s, the holes are larger and allow for an improved view of the arc energy. The intent of this figure is to show the approximate location where holes develop relative to the location where the arc energy is modeled in FDS.

Figure 6-19 depicts the wall temperature at 15 s, the time at which the greatest extent of the switchgear enclosure boundary is heated. Although the heated wall temperature contributes to the heat flux at a fixed location, the temperatures are relatively low, suggesting this component is small compared to the energy flux directly from the arc fault and gases.

The total exposure energy as a function of distance is shown in Figure 6-20, which shows the energetic ZOI for this HEAF is between 0.5 – 1.0 m for the sides (left/right) and top faces and zero from the front and rear faces, consistent with the particle distribution and luminous plume location.



**Figure 6-16**  
Particle distribution at various times for a 233 MJ HEAF located at the primary cable compartment bus bars in the supply configuration of a vertical-lift circuit breaker MV SWGR design



**Figure 6-17**  
Luminous portion of the thermal plume at various times for a 233 MJ HEAF located at the primary cable compartment bus bars in the supply configuration of a vertical-lift circuit breaker MV SWGR design

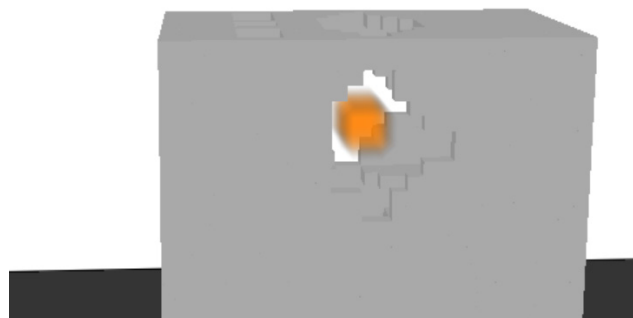


**Figure 6-18**  
Heat release rate per unit volume at 12.5 s for a 233 MJ HEAF located at the primary cable compartment bus bars in the supply configuration of a vertical-lift circuit breaker MV SWGR design. The heat release rate per unit volume for the electrode is shown as a squared orange region within the switchgear

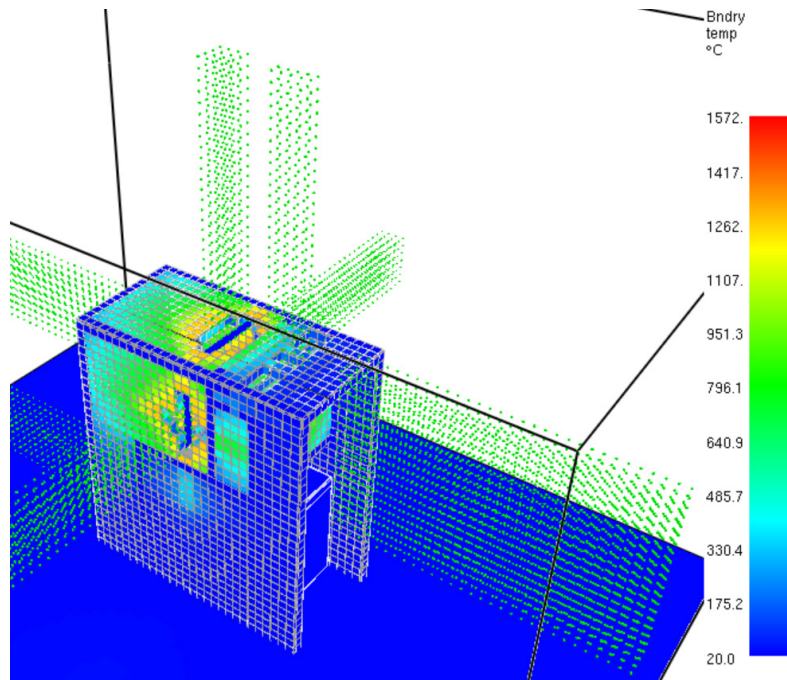


**Figure 6-19**  
**Wall temperature at 15 s for a 233 MJ HEAF located at the primary cable compartment bus bars in the supply configuration of a vertical-lift circuit breaker MV SWGR design**

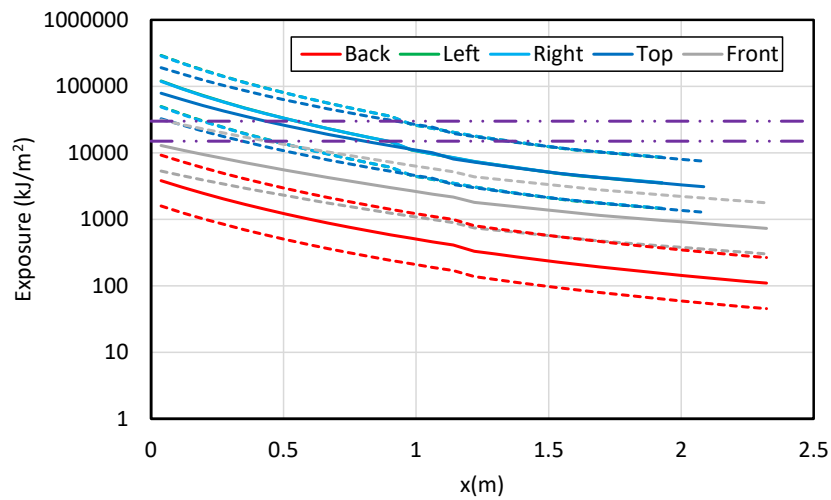


**Figure 6-20**  
**Total energy exposure as a function of distance from each face for a 233 MJ HEAF located at the primary cable compartment bus bars in the supply configuration of a vertical-lift circuit breaker MV SWGR design (HEAF simulation ID MV-GE-38). Note the results for the left- and right-sides are nearly coincident. Dashed horizontal lines correspond to the 15 MJ/m<sup>2</sup> and 30 MJ/m<sup>2</sup> target fragility threshold**

### 6.1.1.5 Summary of GE Vertical-Lift Circuit Breaker MV SWGR Design Results

Sections 6.1.1.1 through 6.1.1.4 present detailed FDS results for the 233 MJ HEAF in the four basic locations an arc fault is expected to occur in the GE vertical-lift circuit breaker MV SWGR design. The FDS results are presented to show the exposure severity around the switchgear enclosure, including the metal particle distribution, the luminous plume, the arc energy volume, and the switchgear enclosure boundary temperature. The exposure profiles for each switchgear enclosure face are also presented, which are used to determine the energetic ZOIs. These profiles are generally consistent with the HEAF simulation results as visualized using the particle distributions and luminous plume. The exposure severity is primarily dependent on the location of the HEAF within the switchgear. For example, HEAFs located toward the middle and front of the switchgear enclosure (i.e., the circuit breaker stabs, the main bus bar, and the primary cable compartment main bus bar in the supply configuration) have no energetic ZOI predicted for the rear face. Conversely, a HEAF located at the rear of the switchgear enclosure (primary cable compartment main bus bar in the load configuration) has no energetic ZOI predicted for the front face. In all cases, the side face energetic ZOIs are comparable. These results show the general consistency of the energetic ZOIs and FDS model predictions are as expected.

### **6.1.2 ABB Horizontal Draw-Out Style Circuit Breaker MV SWGR with a HEAF at the Circuit Breaker Stabs**

The FDS results for an ABB horizontal draw-out style circuit breaker MV SWGR with a HEAF at the circuit breaker stabs is reviewed in detail. This HEAF is representative of HEAFs initiated in the horizontal draw-out circuit breaker designs. The 233 MJ energy HEAF is selected, which is the same energy as the GE vertical-lift style circuit breaker:

- 3 s of stiff current
- 15 s of decaying current
- Copper electrode
- 233 MJ arc energy

The arc energy power profile for this HEAF is provided in Figure A-4. Similar to the HEAFs postulated on the GE vertical-lift circuit breaker MV SWGR, the detailed results include depictions of the switchgear enclosure breach, the particle dispersion around the enclosure, the luminous thermal plume, the heat release rate per unit volume (arc), the enclosure wall temperatures, and the target exposure profiles as a function of distance.

Figure 6-21 depicts the metal particle distribution around the rear, side, and upper portion of the ABB horizontal draw-out style circuit breaker stabs at various times during the simulation. At 0 s, there are no particles and the switchgear enclosure is intact. The openings at 0 s are the front top vents, the top vents, and the lower rear vent (not shown in Figure 6-21). At 0.57 s, the switchgear enclosure is still intact, but there are metal particles ejected from the top and front vent openings. The switchgear enclosure is breached at 0.94 s, with boundary penetration on the left and right sides adjacent to the electrode. The side openings continue to grow rapidly through 3.35 s. Between 3.35 s and 7.31 s, the breach openings continue to grow, but less rapidly and reach their maximum extent at 10 s (not shown in Figure 6-21). At 19.6 s (not shown in Figure 6-21), after the fault has cleared, nearly all particles have dispersed. A small number of

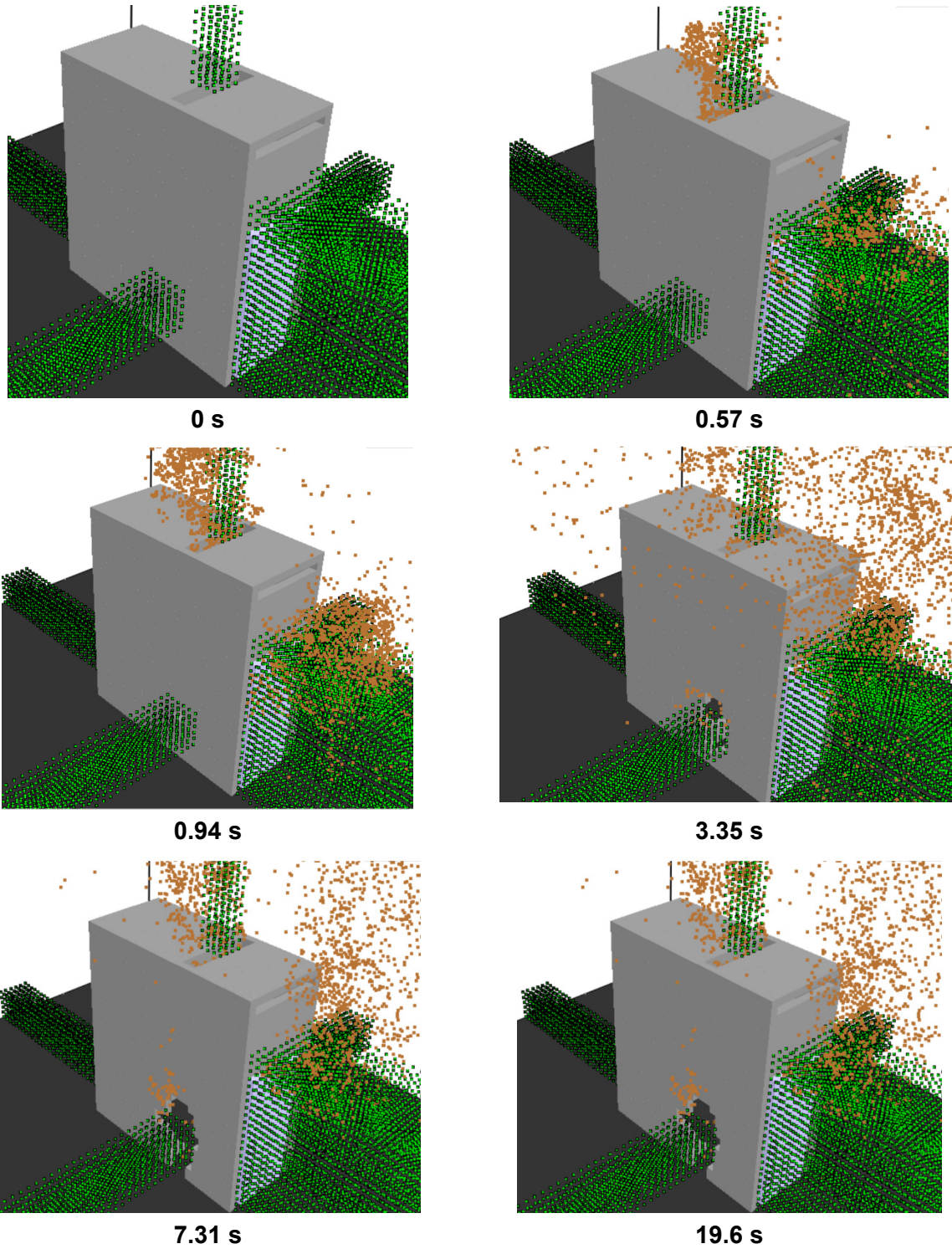
particles are ejected from the lower rear vent before the switchgear enclosure is breached; however, the majority of the particles are ejected through the upper and front vents, and later, through the damaged switchgear enclosure walls.

Figure 6-22 depicts the luminous portion of the thermal plume at 0.57 s, 0.94 s, 3.35 s, and 7.31 s, corresponding to the times at which the particle distributions exit the enclosure. The luminous thermal plume extends out the top and front vents before the switchgear enclosure wall is breached at 0.57 s and 0.94 s. After 0.94 s, the luminous thermal plume expands outside the cubicle sides as well as the top and front vents and reaches a peak near the start of the decay phase between 3.35 s and 7.31 s, at which time significant portions of the switchgear enclosure are breached.

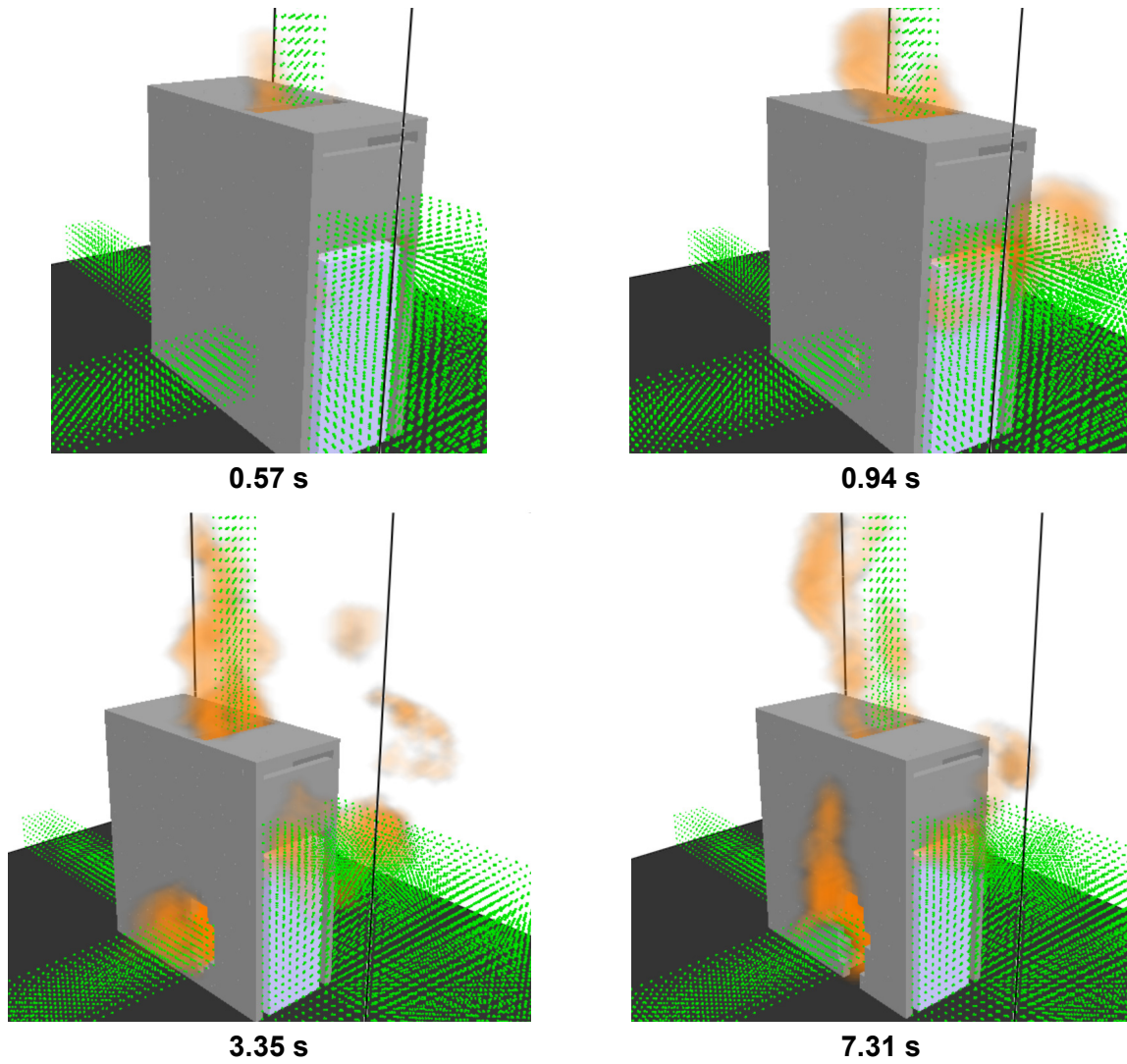
Figure 6-23 depicts the heat release rate per unit volume at 11.5 s, which corresponds to the arc energy location in the FDS model. The time selected for this view is greater than the time selected for arcs located at the main bus bar, the circuit breaker stabs, and the PCCBB (load configuration) in the GE SWGR because it is near the middle of the enclosure and not easily viewed with the hole size at 4 s. At 11.5 s, the holes are larger and allow for an improved view of the arc energy. The intent of this figure is to show the approximate location where holes develop relative to the location where the arc energy is modeled in FDS.

Figure 6-24 depicts the wall temperature at 11 s, the time at which the greatest extent of the switchgear enclosure boundary is heated. Although the heated wall temperature contributes to the heat flux at a fixed location, the temperatures are relatively low, suggesting this component is small compared to the energy flux directly from the arc fault and gases.

The total exposure energy as a function of distance is shown in Figure 6-25. Figure 6-25 shows the energetic ZOI for this simulation is 0.75 – 1.1 m for the sides (left/right) and zero from the front, top, and back faces, consistent with the particle distribution and luminous plume location. This energetic ZOI is comparable to the energetic ZOIs for the vertical-lift circuit breaker style switchgear summarized in sections 6.1.1.1 through 6.1.1.4. One key difference is that the left and right energetic ZOIs for the horizontal draw-out style circuit breaker are about 0.1 – 0.2 m greater than the vertical lift style switchgear.



**Figure 6-21**  
Particle distribution at various times for a 233 MJ HEAF located at the circuit breaker stabs of the horizontal draw-out style circuit breaker MV SWGR



**Figure 6-22**  
Luminous portion of the thermal plume at various times for a 233 MJ HEAF located at the circuit breaker stabs of the horizontal draw-out style circuit breaker MV SWGR

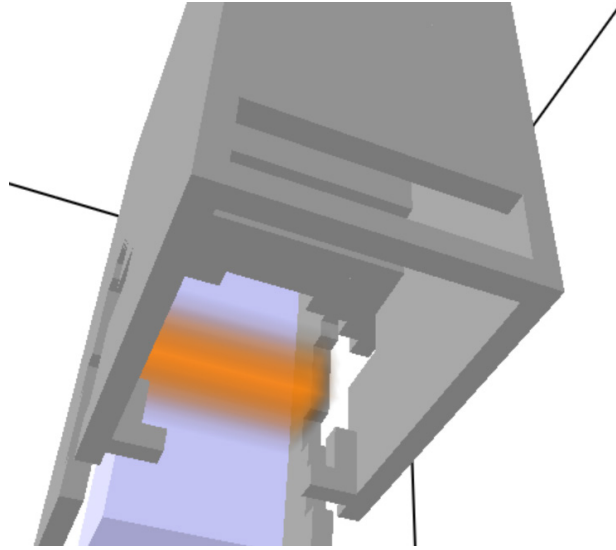


**Figure 6-23**  
Heat release rate per unit volume at 11.5 s for a 233 MJ HEAF located at the circuit breaker stabs of the horizontal draw-out style circuit breaker MV SWGR (viewed from below for clarity). The heat release rate per unit volume for the electrode is shown as a rectangular orange region within the switchgear.

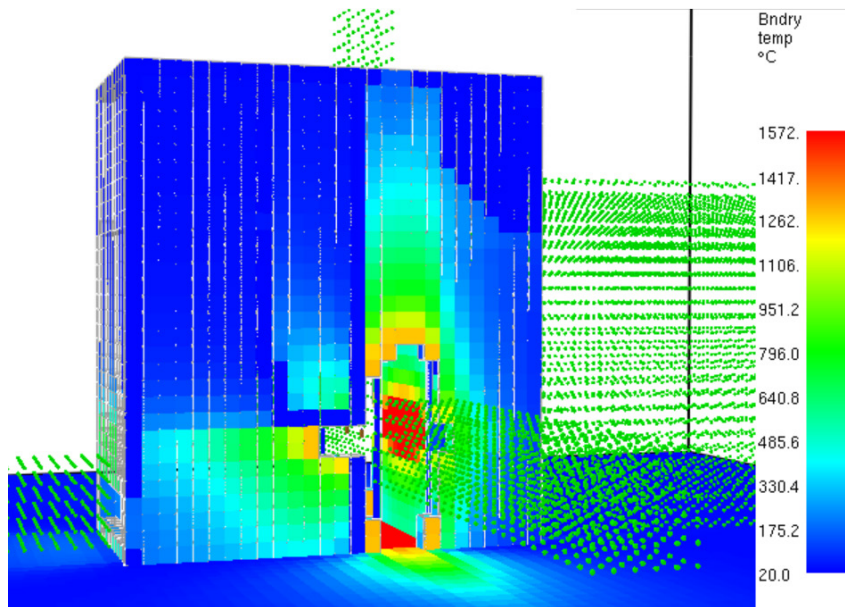


**Figure 6-24**  
Wall temperature at 11 s for a 233 MJ HEAF located at the circuit breaker stabs of the horizontal draw-out style circuit breaker MV SWGR

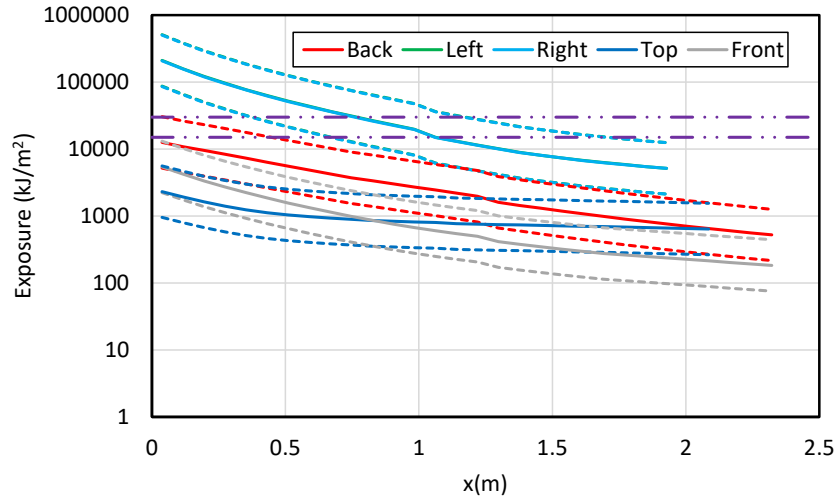


**Figure 6-25**  
**Total energy exposure as a function of distance from each face for a 233 MJ HEAF located at the circuit breaker stabs of the horizontal draw-out style circuit breaker MV SWGR (HEAF simulation ID MV-ABB-5). Note the results for the left and right-sides are nearly coincident. Dashed horizontal lines correspond to the 15 MJ/m<sup>2</sup> and 30 MJ/m<sup>2</sup> target fragility threshold**

### 6.1.3 Summary of MV SWGR Results

#### 6.1.3.1 Energetic ZOI Symmetry

The MV SWGR HEAFs have general symmetry over the left and right sides of the enclosure. However, because the flow induced by the HEAF is turbulent, at any instant in time the left and right side flows will not be perfectly symmetric due to the random fluctuations in turbulent flow. Over time, the turbulent fluctuations should average out, resulting in symmetry in the energetic ZOIs on the left and right sides of the enclosure. Figure 6-26 shows the 15 MJ/m<sup>2</sup> target fragility (i.e., thermoplastic (TP) cable or aluminum bus duct) and the 30 MJ/m<sup>2</sup> target fragility (i.e., thermoset (TS) cable or steel bus duct) energetic ZOIs for the left and right sides for the MV SWGR HEAFs. For the largest ZOIs (the longest duration events) the left and right sides are essentially equal. For the smallest ZOIs (the shortest duration events), where there is insufficient time for fluctuations to average out, there is a larger amount of scatter in the left and right side ZOIs. Overall, the high degree of symmetry provides confidence that the simulations remained stable even though extremely high volumetric heat sources are present in the domain as numerically unstable simulations often manifest with large asymmetries.

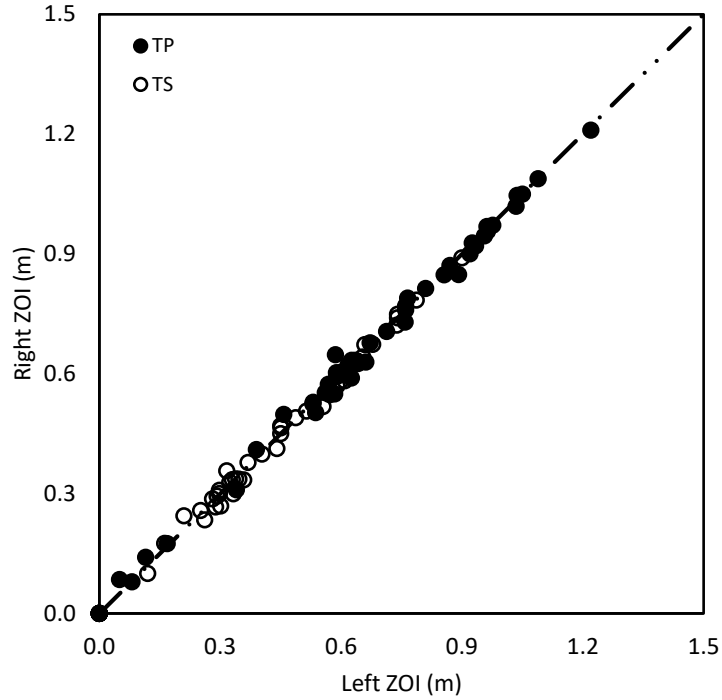


**Figure 6-26**  
**Left versus right energetic ZOIs for all MV SWGR HEAF simulations**

### 6.1.3.2 MV SWGR Energetic ZOI Dependencies

Figure 6-27 shows the energetic ZOIs for the MV SWGR HEAF simulation as a function of the arc energy. The results show an increasing trend in the ZOI distance with respect to the arc energy and that the maximum energetic ZOIs for 15 MJ/m<sup>2</sup> fragility targets are approximately 0.30 m larger than the maximum ZOIs for 30 MJ/m<sup>2</sup> fragility targets. Most of the energetic ZOIs are smaller than the energetic ZOI dimensions recommended in Appendix M of NUREG/CR-6850 Volume 2 [1]. Figure 6-28 through Figure 6-31 show the energetic ZOI results as a function of the arc energy at each arc location evaluated.

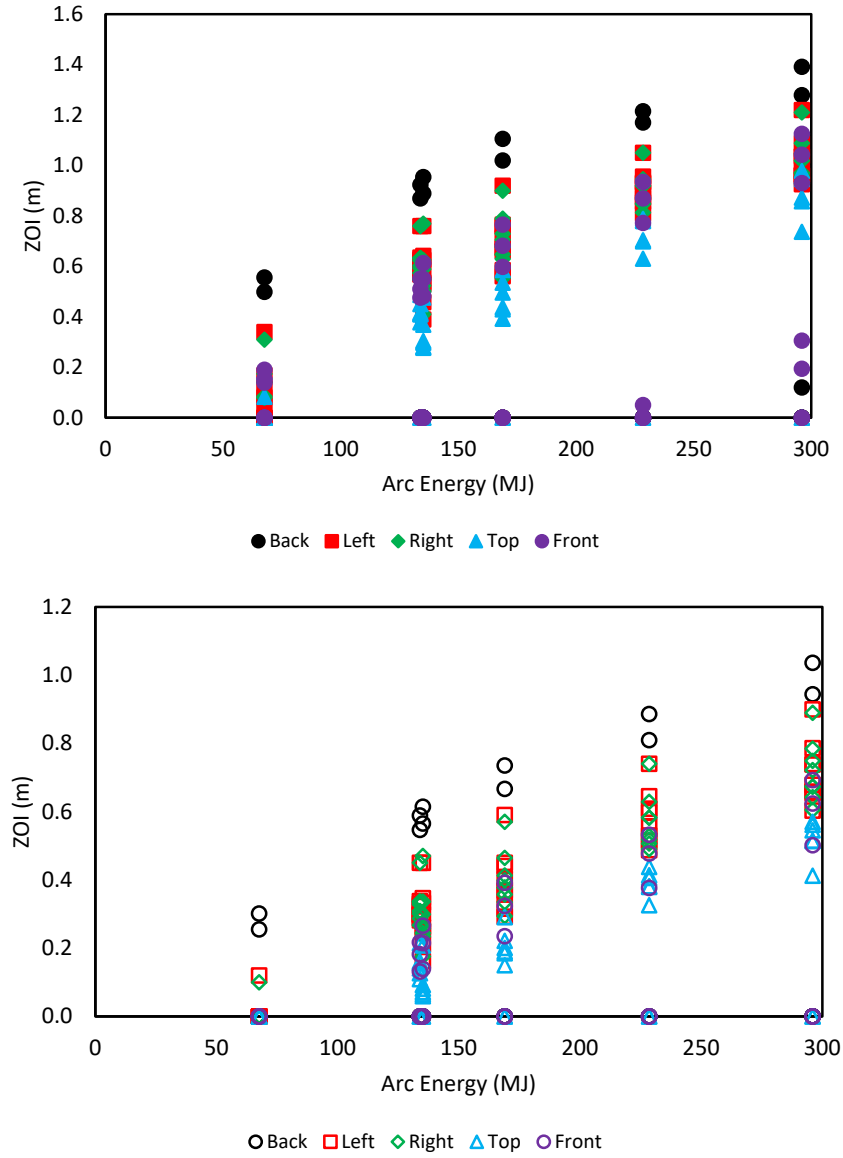


**Figure 6-27**  
**Energetic ZOIs as a function of arc energy for all MV SWGR HEAF simulations. Top (solid symbols) – 15 MJ/m<sup>2</sup> fragility target, bottom (open symbols) – 30 MJ/m<sup>2</sup> fragility target. Symbol shape and color indicates the enclosure face**

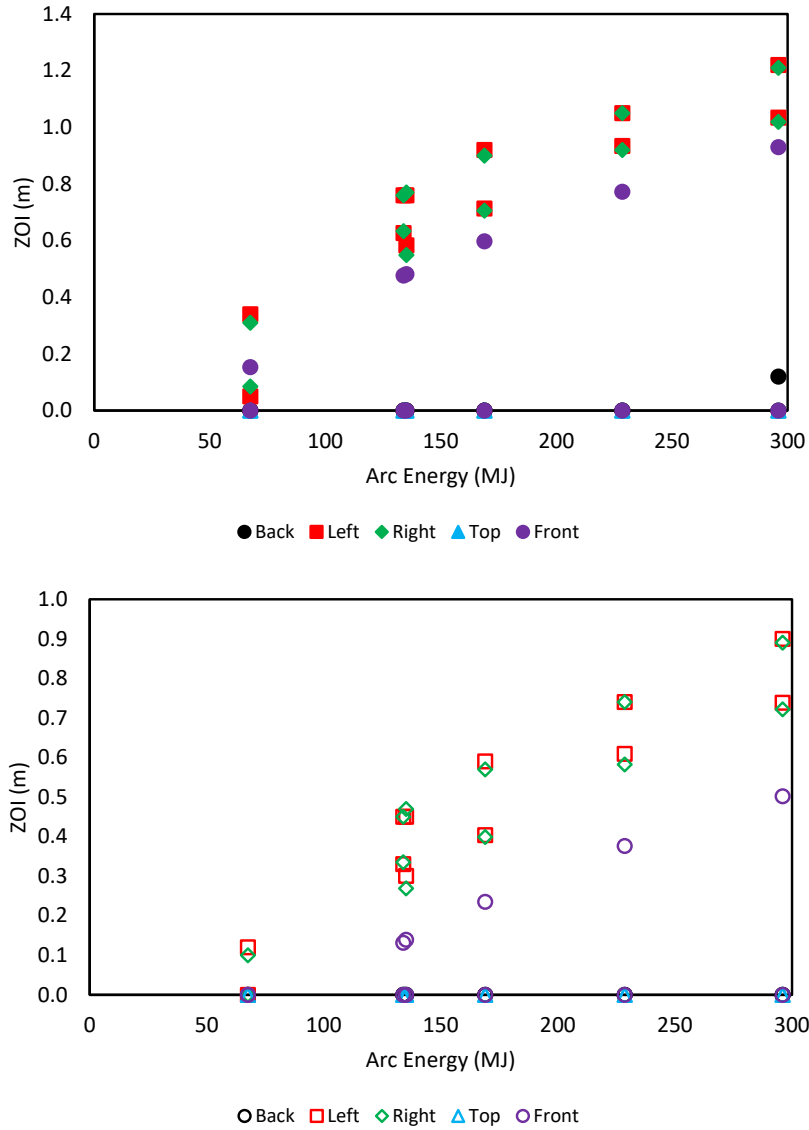


**Figure 6-28**  
**Energetic ZOIs as a function of arc energy for MV SWGR HEAF simulations with the arc initiated at the circuit breaker stabs. Top (solid symbols) – 15 MJ/m<sup>2</sup> fragility target, bottom (open symbols) – 30 MJ/m<sup>2</sup> fragility target. Symbol shape and color indicates the enclosure face**

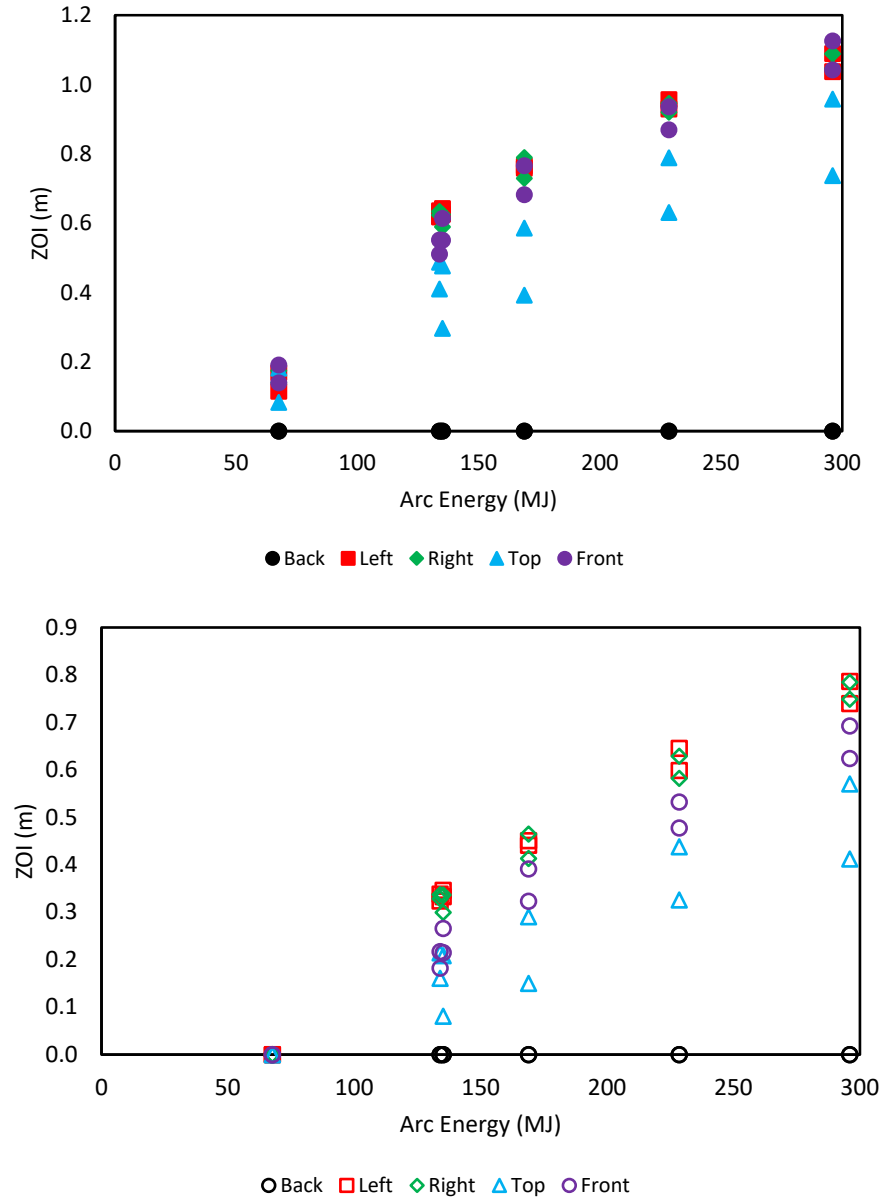


**Figure 6-29**  
**Energetic ZOIs as a function of arc energy for MV SWGR HEAF simulations with the arc initiated at the main bus bars. Top (solid symbols) – 15 MJ/m<sup>2</sup> fragility target, bottom (open symbols) – 30 MJ/m<sup>2</sup> fragility target. Symbol shape and color indicates the enclosure face**

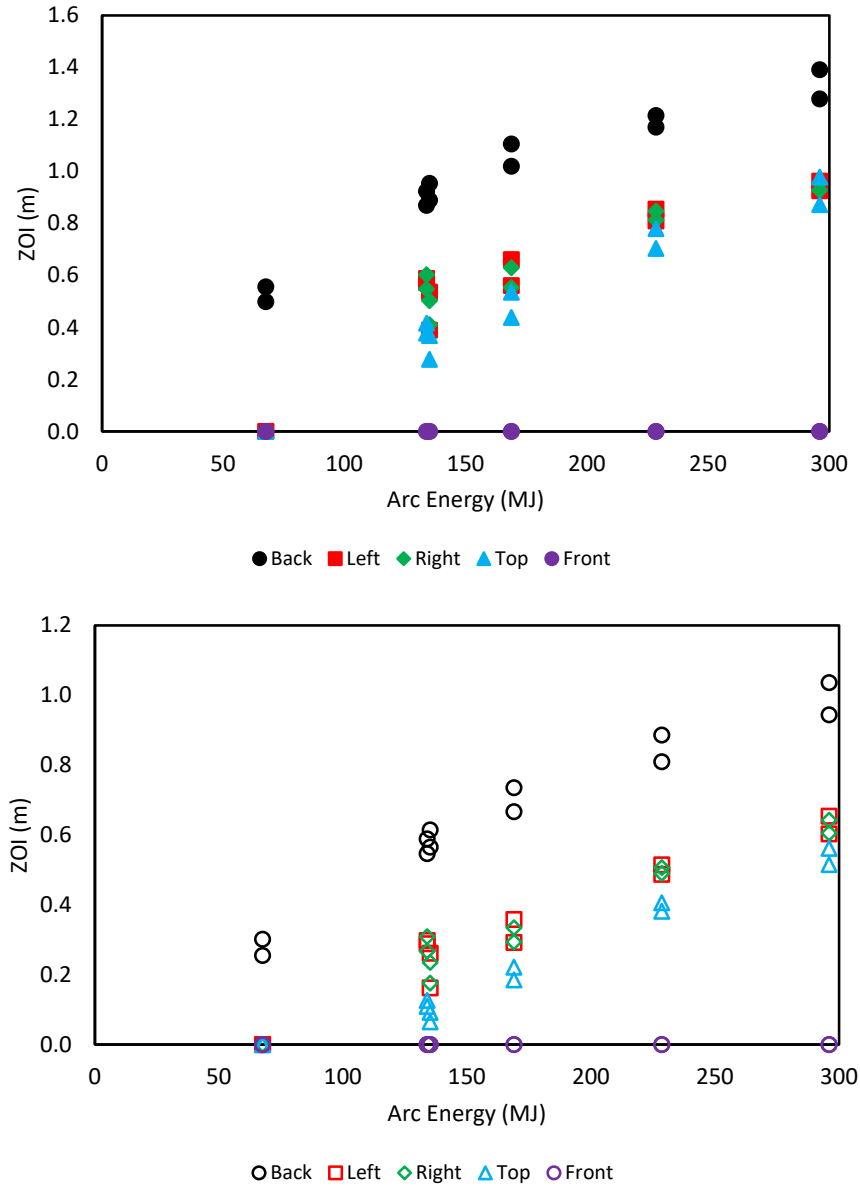


**Figure 6-30**  
**Energetic ZOIs as a function of arc energy for MV SWGR HEAF simulations with arc initiated at the primary cable compartment bus bars (PCCBB) in the load configuration. Top (solid symbols) – 15 MJ/m<sup>2</sup> fragility target, bottom (open symbols) – 30 MJ/m<sup>2</sup> fragility target. Symbol shape and color indicates the enclosure face**

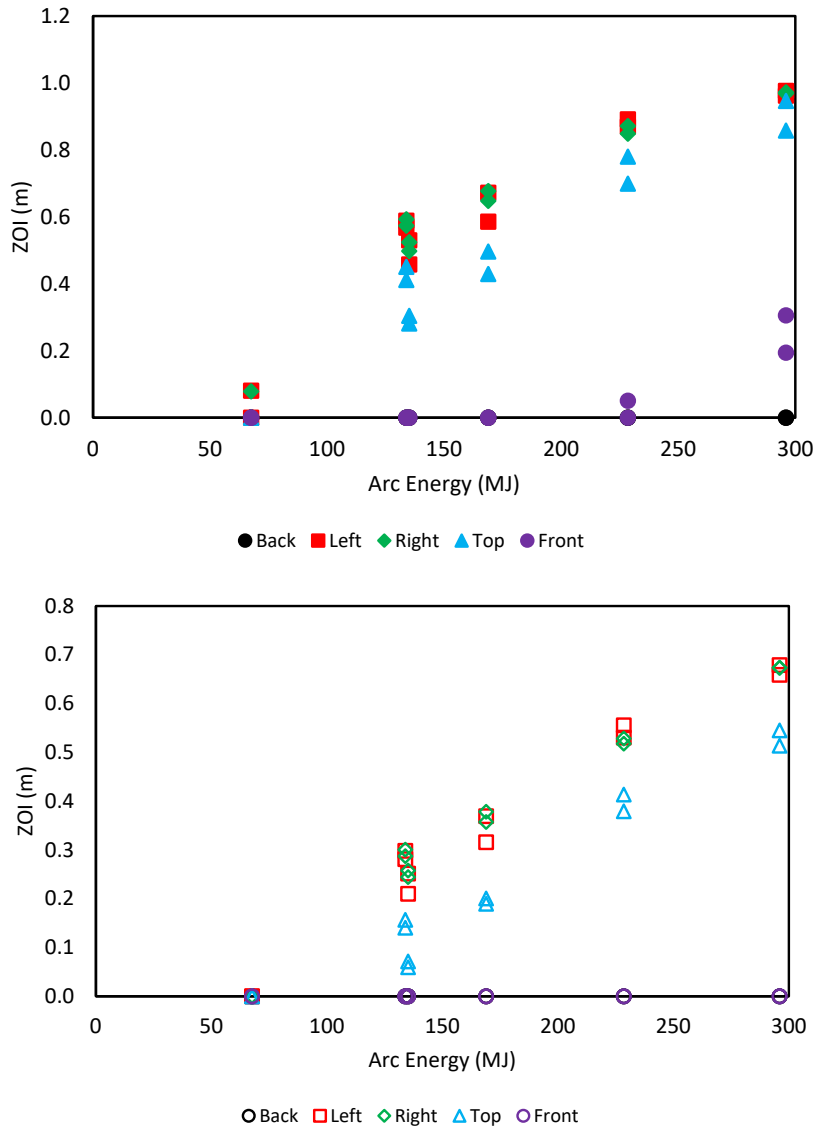


**Figure 6-31**  
**Energetic ZOIs as a function of arc energy for MV SWGR HEAFs with arc initiated at the PCCBB in the supply configuration. Top (solid symbols) – 15 MJ/m<sup>2</sup> fragility target, bottom (open symbols) – 30 MJ/m<sup>2</sup> fragility target. Symbol shape and color indicates the enclosure face**

Figure 6-32 compares the energetic ZOIs for copper and aluminum bus bars for the MV SWGR HEAF simulations except the circuit breaker stab HEAF simulations where only copper electrodes are modeled. The comparison of copper and aluminum bus bar energetic ZOIs in Figure 6-32 identify the line of perfect agreement (the dot-dot-dash line), where copper and aluminum bus bar ZOIs are equal. There is data on each side of the line, indicating the ZOIs are not equal, but the absolute difference in the ZOIs is on the order of 0.1 m or less. As described in Section 4.1.4, there is a known model uncertainty with the FDS exposure predictions, and the 95% confidence intervals are computed for the simulations (see Appendix B). For ZOI differentials of 0.1 m or less, the 95% confidence intervals for the copper bus bar material includes the ZOI for the aluminum bus bar material, and vice versa. There is no significant difference in the aluminum and copper bus bar energetic ZOIs for a given arc power profile,

arc location, and switchgear enclosure face. This is an important conclusion, especially given the treatment of each electrode is different within the FDS model in terms of the energy absorbed by the bus bars, the mass of bus bar consumed during the arc, and the oxidation of the metal particles.

The overall results indicate that while there are differences in the treatment of the copper and aluminum in the FDS model, the resulting differences in the energetic ZOIs are small. In particular, the aluminum bus bar material has a lower melting temperature and a greater oxidation energy, both of which nominally contribute to an increased energy flux at a fixed location. However, the dominant factor in determining the energetic ZOI is the arc energy and the distance from the arc. The differences in the electrode composition are minor in comparison.

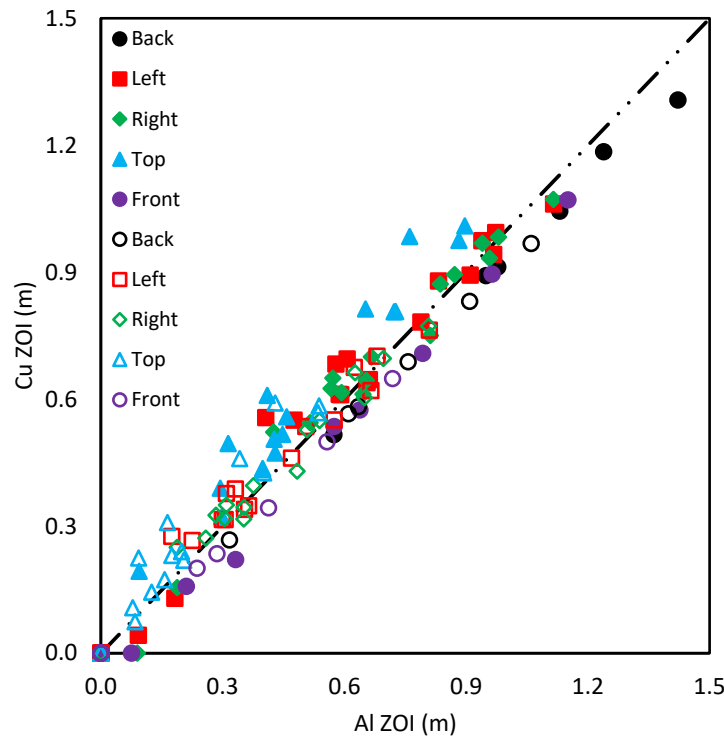


**Figure 6-32**  
**Aluminum versus copper bus bar energetic ZOIs for all MV SWGR HEAF simulations**  
**(except for the circuit breaker stab HEAFs which only used copper)**

### 6.1.3.3 FDS Modeling Insights for MV SWGR

FDS modeling insights for MV SWGR HEAF simulations are as follows:

- There is no significant difference in the energetic ZOI dimensions between copper and aluminum bus bar materials given a common arc power profile, arc location, and switchgear enclosure face. The energetic ZOIs for each material are within the 95<sup>th</sup> percentile of the model uncertainty band as computed from the ZOI predictions for either material.
- The dominant parameter affecting the energetic ZOIs in the MV SWGR is the total arc energy.

- A secondary parameter for the MV SWGR is the circuit breaker orientation (vertical-lift circuit breaker style or horizontal draw-out circuit breaker style).
- The largest factor affecting the energetic ZOIs is the duration and extent of view between the arc volume and the target location. The energetic ZOIs tend to increase within increasing arc energy due to the greater damage to the switchgear boundaries.
- The energetic ZOIs are greater on the switchgear enclosure faces closest to the arc. Switchgear enclosure faces that are near the arc melt sooner, resulting in an opening that increases in size during the arc and shortly after the arc clears. This results in a larger energy flux at the target location and a larger energetic ZOI at these sides.
- The side energetic ZOIs are smaller for vertical-lift circuit breaker style MV SWGR as compared to horizontal draw-out circuit breaker style. The load configuration for vertical-lift circuit breaker style switchgear and the horizontal draw-out circuit breaker style switchgear have comparable top energetic ZOIs.

These insights are consistent with expectations of the HEAF phenomena as modeled in FDS. Since the HEAF is modeled as a high heat release rate per unit volume, the greatest exposure at a fixed location is when the view factor between the arc volume and the location in consideration is maximized.

#### 6.1.3.4 Tabulated MV SWGR Energetic ZOIs

Table 6-1 shows a summary of the energetic ZOIs for the MV SWGR HEAF simulations including the type of enclosure, the bus bar material, the stiff current period for the arc power profile, the decay period for the arc power profile, the arc location, the total energy dissipated by the HEAF, and the ZOIs on each face of the enclosure for both 15 MJ/m<sup>2</sup> and 30 MJ/m<sup>2</sup> fragility targets.

**Table 6-1**  
**Summary of MV SWGR energetic ZOIs**

HEAF simulation summary						Energetic ZOI (m)									
						15 MJ/m <sup>2</sup> target fragility					30 MJ/m <sup>2</sup> target fragility				
HEAF ID <sup>1,2</sup>	Bus bar material	Stiff (s)	Decay (s)	Arc location	Arc energy <sup>3</sup> (MJ)	Back	Left	Right	Top	Front	Back	Left	Right	Top	Front
<b>MV-GE-1</b>	Aluminum	2	0	Main Bus Bar	68	None <sup>4</sup>	0.17	0.17	0.08	0.19	None <sup>4</sup>	None	None	None	None
<b>MV-GE-2</b>	Aluminum	2	0	PCCBB Load	68	0.56	None	None	None	None	0.30	None	None	None	None
<b>MV-GE-3</b>	Aluminum	2	0	PCCBB Supply	68	None	0.08	0.08	None	None	None	None	None	None	None
<b>MV-GE-4</b>	Aluminum	4	0	Main Bus Bar	135	None	0.64	0.63	0.30	0.61	None	0.35	0.34	0.08	0.27
<b>MV-GE-5</b>	Aluminum	4	0	PCCBB Load	135	0.95	0.39	0.41	0.28	None	0.61	0.16	0.18	0.06	None
<b>MV-GE-6</b>	Aluminum	4	0	PCCBB Supply	135	None	0.46	0.50	0.28	None	None	0.21	0.24	0.07	None
<b>MV-GE-7</b>	Aluminum	5	0	Main Bus Bar	169	None	0.77	0.79	0.39	0.77	None	0.45	0.46	0.15	0.39
<b>MV-GE-8</b>	Aluminum	5	0	PCCBB Load	169	1.11	0.56	0.55	0.44	None	0.74	0.29	0.29	0.18	None
<b>MV-GE-9</b>	Aluminum	5	0	PCCBB Supply	169	None	0.59	0.65	0.43	None	None	0.32	0.36	0.19	None
<b>MV-GE-10</b>	Aluminum	0	15	Main Bus Bar	132	None	0.64	0.63	0.41	0.55	None	0.34	0.34	0.16	0.22
<b>MV-GE-11</b>	Aluminum	0	15	PCCBB Load	132	0.92	0.57	0.55	0.38	None	0.59	0.29	0.27	0.11	None
<b>MV-GE-12</b>	Aluminum	0	15	PCCBB Supply	132	None	0.57	0.57	0.41	None	None	0.28	0.29	0.14	None
<b>MV-GE-13</b>	Aluminum	3	15	Main Bus Bar	233	None	0.96	0.95	0.63	0.94	None	0.65	0.63	0.33	0.53
<b>MV-GE-14</b>	Aluminum	3	15	PCCBB Load	233	1.21	0.81	0.81	0.70	None	0.89	0.49	0.49	0.38	None
<b>MV-GE-15</b>	Aluminum	3	15	PCCBB Supply	233	None	0.89	0.85	0.70	0.05	None	0.56	0.52	0.38	None
<b>MV-GE-16</b>	Aluminum	5	15	Main Bus Bar	300	None	1.09	1.09	0.74	1.13	None	0.79	0.78	0.41	0.69
<b>MV-GE-17</b>	Aluminum	5	15	PCCBB Load	300	1.39	0.93	0.93	0.87	None	1.04	0.60	0.61	0.52	None
<b>MV-GE-18</b>	Aluminum	5	15	PCCBB Supply	300	None	0.96	0.97	0.86	0.31	None	0.66	0.70	0.51	None
<b>MV-GE-19</b>	Copper	2	0	Circuit Breaker Stabs	68	None	0.05	0.08	None	0.15	None	None	None	None	None

HEAF simulation summary						Energetic ZOI (m)									
						15 MJ/m <sup>2</sup> target fragility					30 MJ/m <sup>2</sup> target fragility				
HEAF ID <sup>1,2</sup>	Bus bar material	Stiff (s)	Decay (s)	Arc location	Arc energy <sup>3</sup> (MJ)	Back	Left	Right	Top	Front	Back	Left	Right	Top	Front
MV-GE-20	Copper	2	0	Main Bus Bar	68	None	0.11	0.14	0.18	0.14	None	None	None	None	None
MV-GE-21	Copper	2	0	PCCBB Load	68	0.50	None	None	None	None	0.26	None	None	None	None
MV-GE-22	Copper	2	0	PCCBB Supply	68	None	None	None	None	None	None	None	None	None	None
MV-GE-23	Copper	4	0	Circuit Breaker Stabs	135	None	0.58	0.55	None	0.48	None	0.30	0.27	None	0.14
MV-GE-24	Copper	4	0	Main Bus Bar	135	None	0.63	0.59	0.48	0.55	None	0.33	0.30	0.21	0.21
MV-GE-25	Copper	4	0	PCCBB Load	135	0.89	0.54	0.50	0.37	None	0.56	0.23	0.23	0.09	None
MV-GE-26	Copper	4	0	PCCBB Supply	135	None	0.53	0.52	0.30	None	None	0.26	0.26	0.06	None
MV-GE-27	Copper	5	0	Circuit Breaker Stabs	169	None	0.71	0.71	None	0.60	None	0.40	0.40	None	0.24
MV-GE-28	Copper	5	0	Main Bus Bar	169	None	0.76	0.73	0.59	0.68	None	0.41	0.41	0.29	0.32
MV-GE-29	Copper	5	0	PCCBB Load	169	1.02	0.66	0.63	0.54	None	0.67	0.33	0.33	0.22	None
MV-GE-30	Copper	5	0	PCCBB Supply	169	None	0.67	0.68	0.50	None	None	0.38	0.38	0.20	None
MV-GE-31	Copper	0	15	Circuit Breaker Stabs	132	None	0.63	0.63	None	0.48	None	0.34	0.34	None	0.13
MV-GE-32	Copper	0	15	Main Bus Bar	132	None	0.62	0.62	0.49	0.51	None	0.32	0.33	0.21	0.18
MV-GE-33	Copper	0	15	PCCBB Load	132	0.87	0.59	0.60	0.42	None	0.55	0.30	0.31	0.13	None
MV-GE-34	Copper	0	15	PCCBB Supply	132	None	0.59	0.59	0.45	None	None	0.30	0.30	0.16	None
MV-GE-35	Copper	3	15	Circuit Breaker Stabs	233	None	0.93	0.92	None	0.77	None	0.61	0.58	None	0.38
MV-GE-36	Copper	3	15	Main Bus Bar	233	None	0.93	0.92	0.79	0.87	None	0.60	0.58	0.44	0.48
MV-GE-37	Copper	3	15	PCCBB Load	233	1.17	0.86	0.85	0.78	None	0.81	0.51	0.51	0.41	None
MV-GE-38	Copper	3	15	PCCBB Supply	233	None	0.87	0.87	0.78	None	None	0.53	0.53	0.41	None
MV-GE-39	Copper	5	15	Circuit Breaker Stabs	300	None	1.03	1.02	None	0.93	None	0.74	0.72	None	0.50
MV-GE-40	Copper	5	15	Main Bus Bar	300	None	1.04	1.05	0.96	1.04	None	0.74	0.75	0.57	0.62

HEAF simulation summary						Energetic ZOI (m)									
						15 MJ/m <sup>2</sup> target fragility					30 MJ/m <sup>2</sup> target fragility				
HEAF ID <sup>1,2</sup>	Bus bar material	Stiff (s)	Decay (s)	Arc location	Arc energy <sup>3</sup> (MJ)	Back	Left	Right	Top	Front	Back	Left	Right	Top	Front
<b>MV-GE-41</b>	Copper	5	15	PCCBB Load	300	1.28	0.96	0.96	0.98	None	0.94	0.65	0.64	0.56	None
<b>MV-GE-42</b>	Copper	5	15	PCCBB Supply	300	None	0.99	0.97	0.95	0.19	None	0.68	0.67	0.55	None
<b>MV-ABB-1</b>	Copper	2	0	Circuit Breaker Stabs	68	None	0.34	0.31	None	None	None	0.12	0.10	None	None
<b>MV-ABB-2</b>	Copper	4	0	Circuit Breaker Stabs	135	None	0.76	0.77	None	None	None	0.45	0.47	None	None
<b>MV-ABB-3</b>	Copper	5	0	Circuit Breaker Stabs	169	None	0.92	0.90	None	None	None	0.59	0.57	None	None
<b>MV-ABB-4</b>	Copper	0	15	Circuit Breaker Stabs	132	None	0.76	0.76	None	None	None	0.45	0.45	None	None
<b>MV-ABB-5</b>	Copper	3	15	Circuit Breaker Stabs	233	None	1.05	1.05	None	None	None	0.74	0.74	None	None
<b>MV-ABB-6</b>	Copper	5	15	Circuit Breaker Stabs	300	0.12	1.22	1.21	None	None	None	0.90	0.89	None	None

<sup>1</sup>The MV-GE-# designation corresponds to a GE vertical-lift circuit breaker switchgear style and the MV-ABB-# designation corresponds to an ABB horizontal draw-out switchgear style circuit breaker.

<sup>2</sup>The FDS input designator is not the same as the input file name but uniquely corresponds to a single FDS input file. Refer to Appendix B of this report for the corresponding input file nomenclature designator.

<sup>3</sup>The energy input into the FDS model may be different because a) a 0.1 s ramp is used at the beginning and end of the arc profile, b) the generator-fed arc begins at 15 s and 20,000 A rather than at 14.6 s and 20,450 A, and c) a 1 s linear transition is assumed when there is a constant (stiff) period prior to the generator-fed fault (see Appendix A).

<sup>4</sup>None means that there is no external energetic ZOI.

## 6.2 Low Voltage Switchgear HEAF Simulations

This section provides a summary of the FDS results for the LV SWGR simulations. Due to limited HEAF events in LV SWGR, the only well-documented event (FEDB 50935) [12] is used to develop prototypical HEAF simulations in the LV SWGR (including electrical and design characteristics). Graphical results showing the exposure as a function of distance from each face of the enclosure are provided in Appendix B.2 for variations of LV SWGR simulations for baseline and sensitivity cases.

### 6.2.1 Selected Low Voltage Switchgear HEAF Simulations

Two FDS results for the LV SWGR HEAF simulations constructed with Westinghouse Type DS switchgear based on FEDB 50935 are reviewed in detail. Both FDS simulations involved a HEAF at the circuit breaker stabs: one at the middle circuit breaker compartment and the other at a circuit breaker compartment at the top of the switchgear. In both cases, the arc is relocated to the main bus bar compartment after 21 s. The first simulation most closely resembles FEDB 50935. The HEAF energy profile for these simulations is 41 s and is composed of two constant-current stages as depicted in Figure A-8.

Similar to the MV SWGR HEAF simulations, the detailed results include depictions of the switchgear enclosure breach, the particle dispersion, the luminous thermal plume, the heat release rate per unit volume (arc), the enclosure wall temperatures, and the target exposure profiles as a function of distance for each switchgear enclosure surface.

#### 6.2.1.1 Middle-Height Elevation HEAF

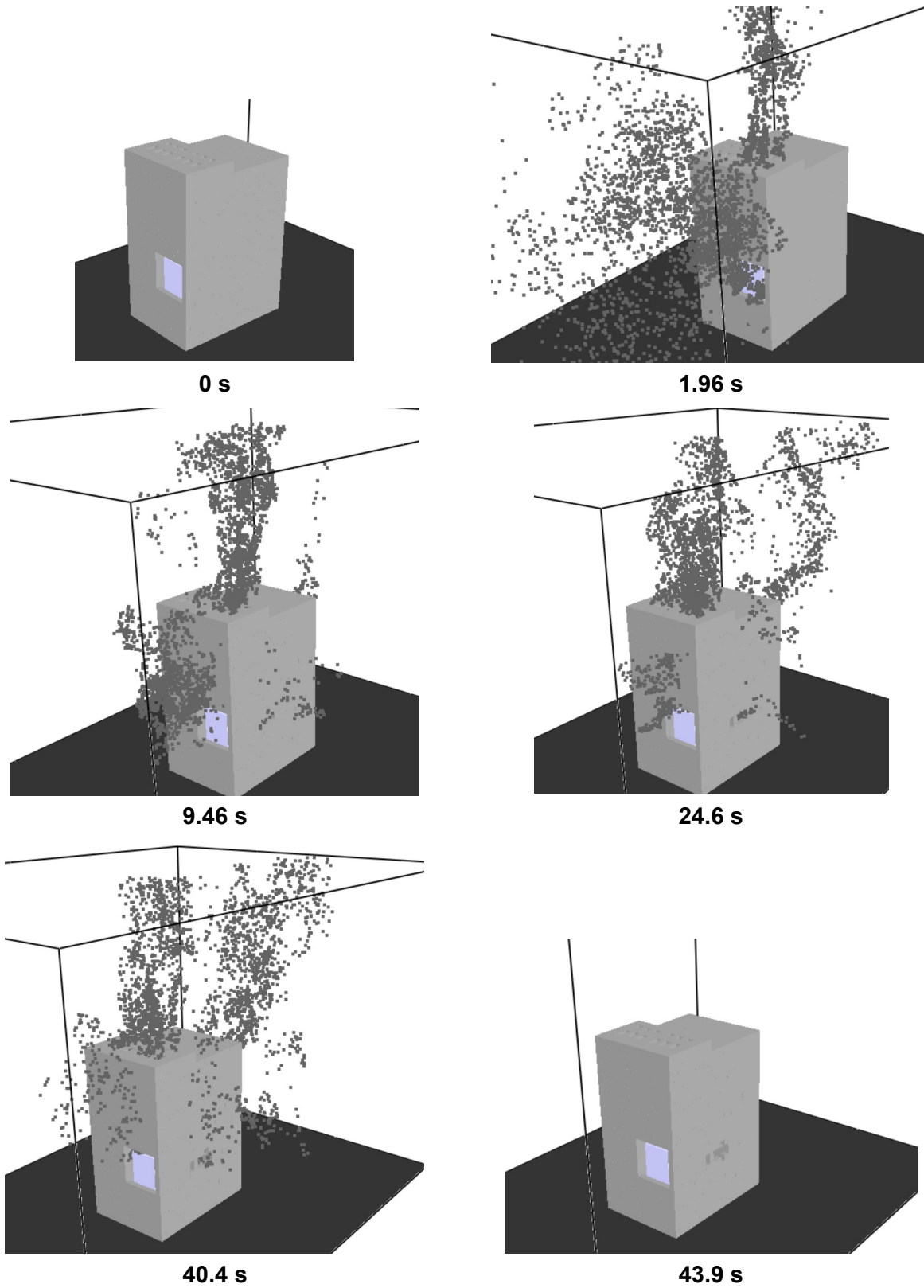
Figure 6-33 depicts the metal particle distribution around the rear, side, and upper portion of the LV SWGR at various times for a HEAF initially located at the circuit breaker stabs at a middle height compartment and migrating to the main bus bar. At 0 s, there are no metal particles and the switchgear enclosure is intact. The openings at 0 s are the front, the top vents, and the rear vents (not shown in Figure 6-33). At 1.96 s, the switchgear enclosure is intact, and particles are ejected through the top and front vents with an increasing number density. At 8 s (not shown in Figure 6-33), a small portion of the switchgear enclosure's right side is breached; however, significant quantities of particles are not ejected from these openings. After 9.46 s, the particles reach a relatively steady density, which persists until 40.4 s. Except for the small openings on the switchgear enclosure face adjacent to the electrode, the switchgear enclosure remains largely intact during the HEAF, and particles are primarily ejected through the existing top and front vents. At 43.9 s, several seconds after the fault is cleared, nearly all particles are dispersed. Internally, the switchgear cubicle containing the HEAF is breached and exposes the adjacent internal switchgear cubicle (see Figure 6-33).

Figure 6-34 depicts the luminous portion of the thermal plume at 1.96 s, 9.46 s, 24.6 s, and 40.4 s, corresponding to the times at which the particle distributions are shown. The luminous thermal plume is relatively constant after 9.46 s and extends minimally beyond the top and front vents.

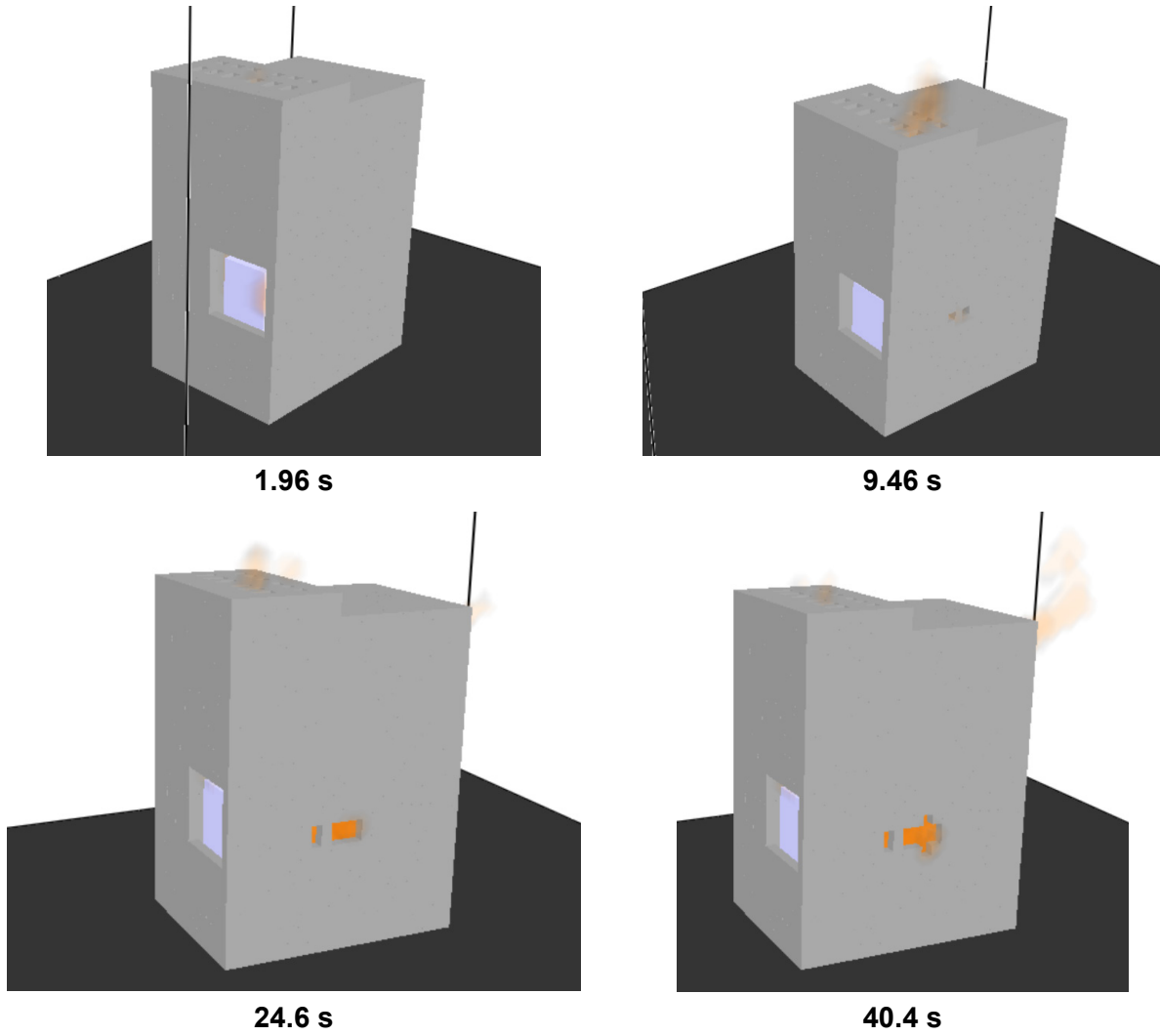
Figure 6-35 depicts the heat release rate per unit volume at 30.2 s from below, which corresponds to the arc energy location in the FDS model. The size of the holes at this time are large enough to view the arc clearly. The intent of this figure is to show the approximate location where holes develop relative to the location where the arc energy is modeled in FDS.

Figure 6-36 depicts the wall temperature at 33.7 s, the time at which the greatest extent of the switchgear enclosure boundary is heated. Although the heated wall temperature contributes to the heat flux at a fixed location, the temperatures are relatively low, suggesting this component is small compared to the energy flux directly from the arc fault and gases.

The total exposure energy as a function of distance is shown in Figure 6-37, which shows the energetic ZOI for this simulation is 0.4 – 0.7 m for the right side and nearly zero from all other surfaces, consistent with the particle distribution and luminous plume location.



**Figure 6-33**  
Particle distribution at various times for a LV SWGR HEAF at the cabinet middle-height elevation with an arc energy profile based on FEDB 50935



**Figure 6-34**  
Luminous portion of the thermal plume at various times for a LV SWGR HEAF at the cabinet middle-height elevation with an arc energy profile based on FEDB 50935

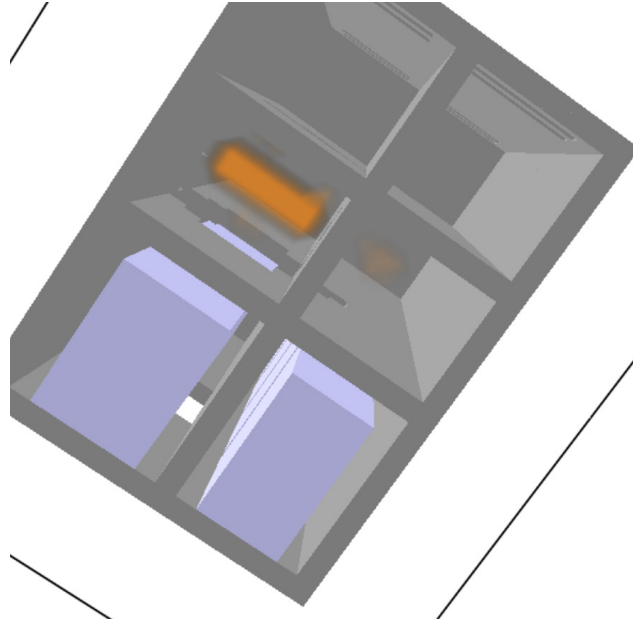


**Figure 6-35**  
Heat release rate per unit volume at 30.2 s for a LV SWGR HEAF at the cabinet middle-height elevation with an arc energy profile based on FEDB 50935 (viewed from below to show the arc)

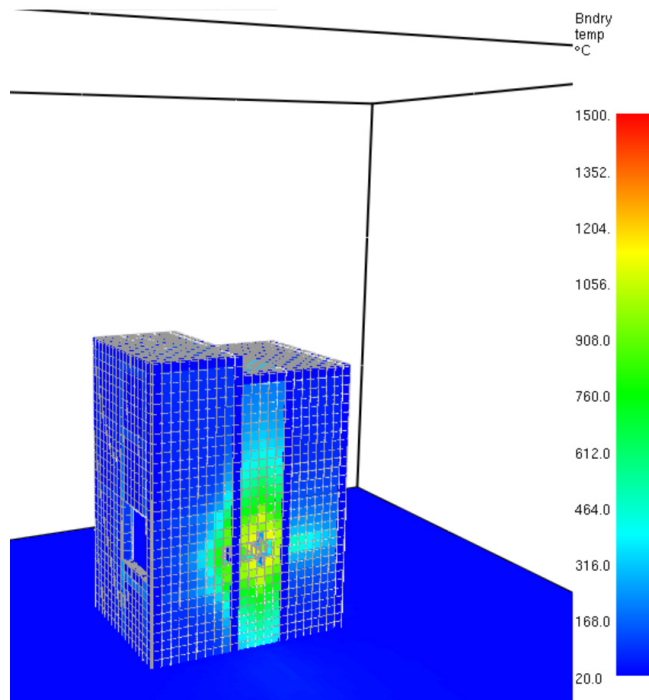


**Figure 6-36**  
Wall temperature at 33.7 s for a LV SWGR HEAF with an arc energy profile based on FEDB 50935

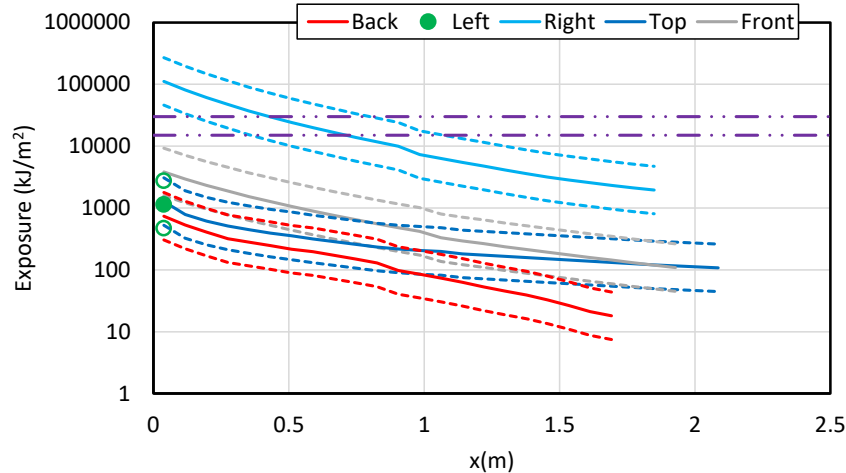


**Figure 6-37**  
**Total energy exposure as a function of distance from each face for a LV SWGR HEAF at the cabinet middle-height elevation with an arc power profile based on FEDB 50935 (HEAF simulation LV-BASE-5). Dashed horizontal lines correspond to the 15 MJ/m<sup>2</sup> and 30 MJ/m<sup>2</sup> target fragility threshold**

### 6.2.1.2 Top Height Elevation HEAF

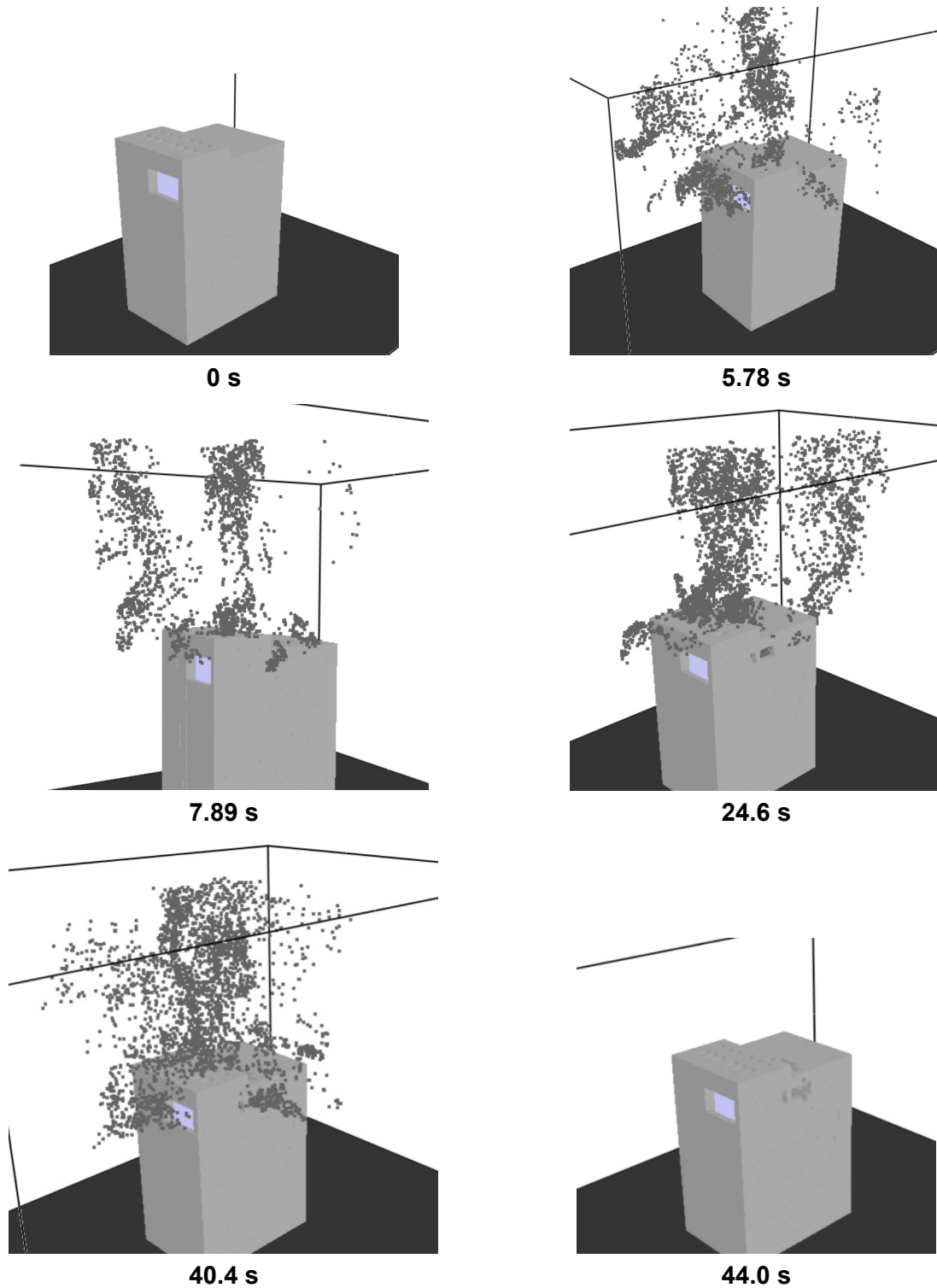
Figure 6-38 depicts the particle distribution around the rear, side, and upper portion of the LV SWGR at various times for a HEAF initially located at the circuit breaker stabs at a top compartment and migrating to a middle-height elevation. At 0 s, there are no metal particles and the switchgear enclosure is intact. The openings at 0 s are the front vent, the top vents, and the rear vents (not shown in Figure 6-38). At 5.78 s, the switchgear enclosure is intact, and particles are ejected through the top and front vents with increasing density. At 7.89 s, a small portion of the switchgear enclosure's right side panel is breached and at 10 s, the top is breached (not shown Figure 6-38). Between 7.89 s and 24.6 s, the breach openings in the top and sides increase in size and greater numbers of particles are ejected through these openings. After 24.6 s, the openings grow more slowly, and the particle density and distribution are relatively steady. At 43.95 s, several seconds after the fault is cleared, nearly all particles are dispersed. Internally, the cubicle with the fault is breached and the internal cubicle is exposed.

Figure 6-39 depicts the luminous portion of the thermal plume at 5.78 s, 7.89 s, 24.6 s, and 40.4 s, corresponding to the times at which the particle distributions are shown.

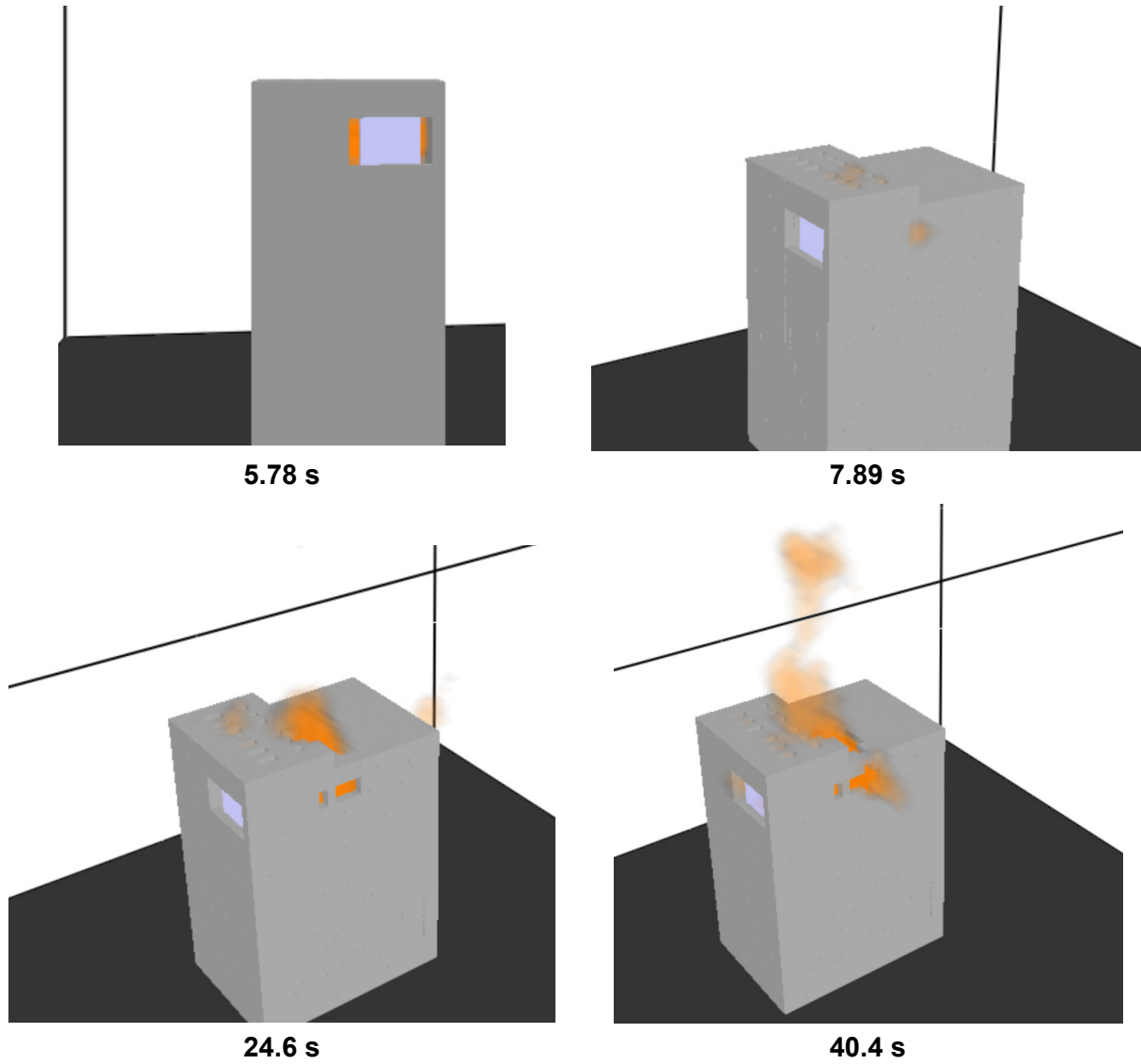
Figure 6-40 depicts the heat release rate per unit volume at 32.4 s from above which corresponds to the arc energy location in the FDS model. The size of the holes at this time are large enough to view the arc clearly. The intent of this figure is to show the approximate location where holes develop relative to the location where the arc energy is modeled in FDS.

Figure 6-41 depicts the wall temperature at 34.3 s, the time at which the greatest extent of the switchgear enclosure boundary is heated. Although the heated wall temperature contributes to the heat flux at a fixed location, the temperatures are relatively low, suggesting this component is small compared to the energy flux directly from the arc fault and gases.

The total exposure energy as a function of distance is shown in Figure 6-42, which shows the energetic ZOI for this simulation is 0.4 – 1.0 m for the right side and top and nearly zero from all other surfaces, consistent with the particle distribution and luminous plume location.



**Figure 6-38**  
Particle distribution at various times for a LV SWGR HEAF at the cabinet top having an arc energy profile based on FEDB 50935



**Figure 6-39**  
Luminous portion of the thermal plume at various times for a LV SWGR HEAF at the cabinet top with an arc energy profile based on FEDB 50935

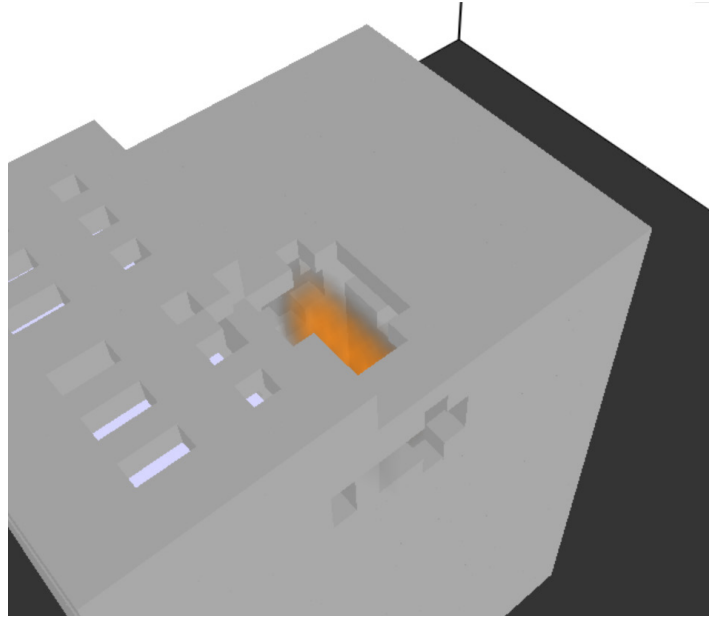


**Figure 6-40**  
Heat release rate per unit volume at 32.4 s for a LV SWGR HEAF at the cabinet top with an arc energy profile based on FEDB 50935 (viewed from top)

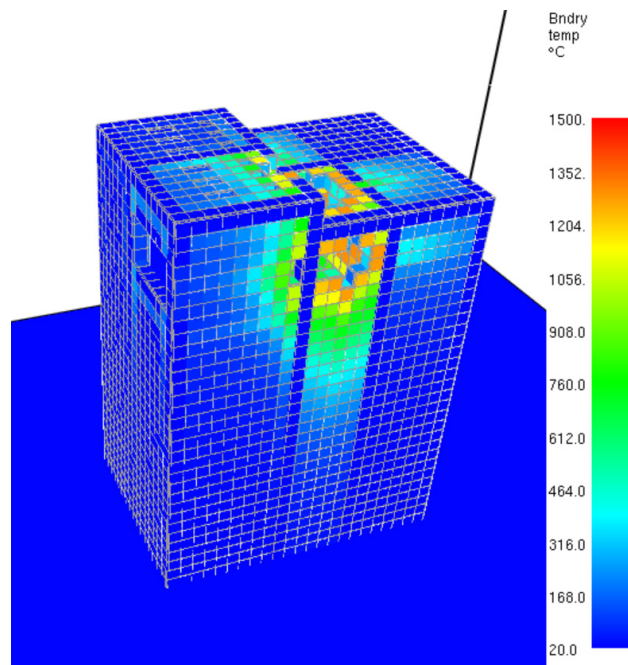


**Figure 6-41**  
Wall temperature at 34.3 s for a LV SWGR HEAF at the cabinet top with an arc power profile based on FEDB 50935

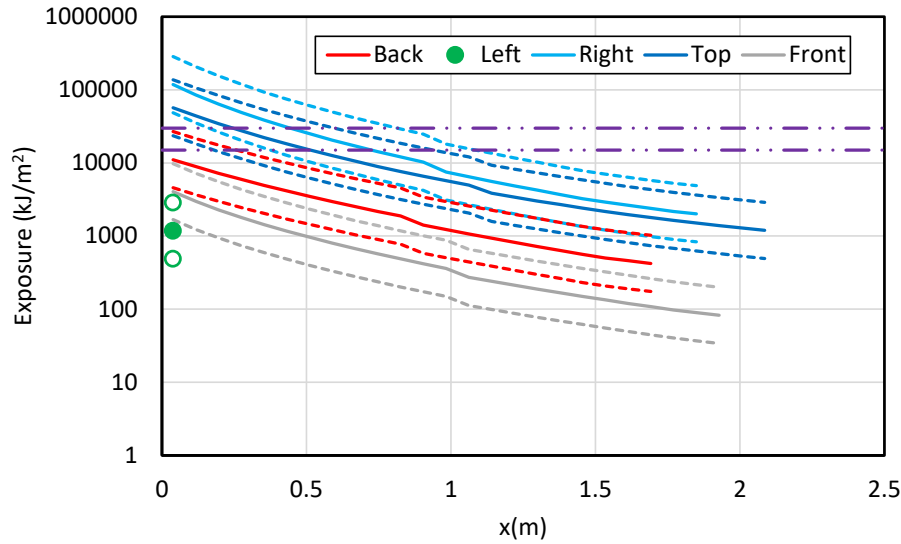


**Figure 6-42**  
**Total energy exposure as a function of distance from each face for a LV SWGR HEAF at the cabinet top with an arc power profile based on FEDB 50935 (HEAF simulation LV-BASE-6). Dashed horizontal lines correspond to the 15 MJ/m<sup>2</sup> and 30 MJ/m<sup>2</sup> target fragility threshold**

### 6.2.1.3 Summary of LV SWGR Results

The exposure profiles as a function of distance for each switchgear enclosure face are generally consistent with the HEAF simulation results as characterized using the particle distributions and luminous plume. The exposure severity is primarily dependent on the location of the HEAF. For example, both HEAFs presented in this section are located in the middle of the switchgear enclosure and are not predicted to have an energetic ZOI on the switchgear enclosure front and back. In addition, the HEAF simulation with the arc inside a middle-height cubicle did not produce an energetic ZOI above the switchgear enclosure due to the presence of an intermediate steel boundary (i.e., the cubicle enclosure) whereas the arc located at a top cubicle did. These results show general consistency between the energetic ZOIs and FDS model predictions as expected.

## 6.2.2 Summary of LV SWGR Results

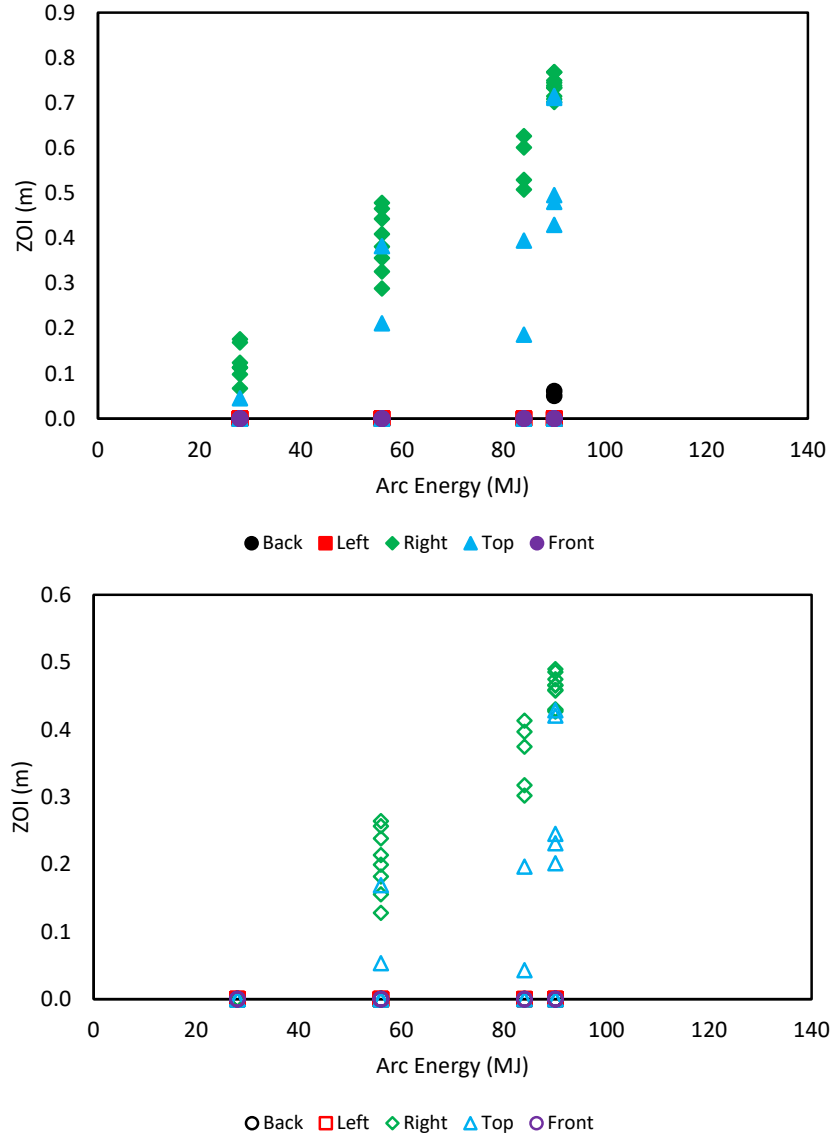
### 6.2.2.1 LV SWGR Energetic ZOI Dependencies

Figure 6-43 shows the energetic ZOIs for each face as a function of the arc energy, 90 MJ (see Appendix A.3), for baseline scenarios. The data at other arc energies correspond to the sensitivity studies. Figure 6-43 shows that the energetic ZOIs for the FEDB 50935 energy profile bound the constant-current power profiles used in the sensitivity studies. This is due to the event having a long duration of exposure after enclosure breach and more of the arc energy is directly visible to targets. A back energetic ZOI is only predicted for the arc located in the bus bar compartment at the top of the enclosure. In this case, the arc breaches the partition to the back compartment allowing high-temperature outflow through the ventilation openings at the back top. Breach of the partition also occurs when the arc is in the bus bar compartment at the mid-height; however, in this case there is not a direct path for the high-temperature outflow, and it

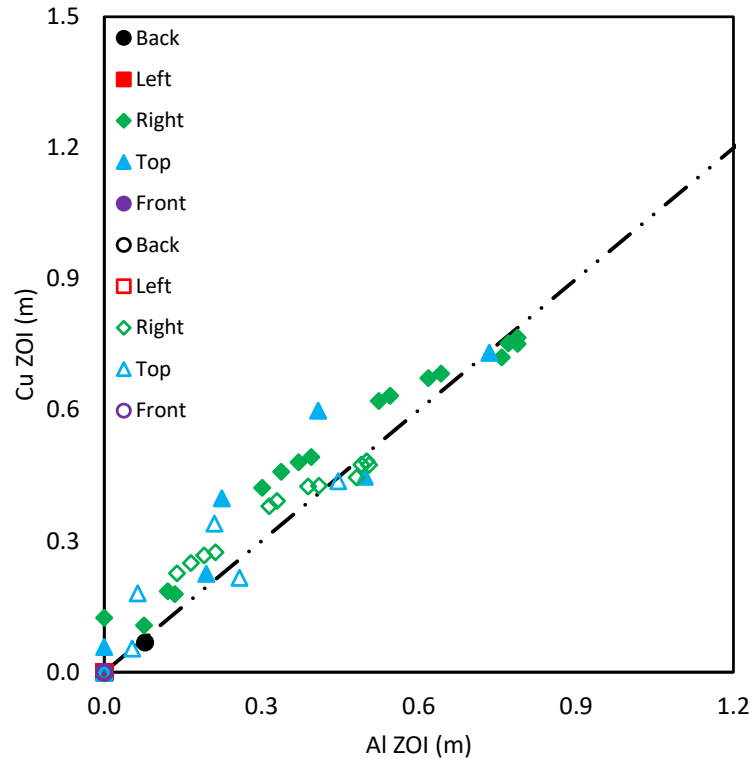
entrains additional air before exiting the top vent reducing the external exposure to the target. Top energetic ZOIs are only predicted when the arc is located at the top of the enclosure. There is no energetic ZOI predicted for the front or the left sides due to the physical separation of the arc from the face. For the front, the body of the circuit breaker blocks the line of sight to the arc. For the left side, there is another column of circuit breaker cubicles, and the arc does not breach the second partition. This result indicates that there is only a side energetic ZOI if the arc has one panel to breach before exposing external targets.

Figure 6-44 shows the aluminum bus bar versus copper bus bar energetic ZOIs for the LV SWGR HEAF simulations. There is a trend for the constant-current cases (sensitivity runs), that copper has larger ZOIs than aluminum; however, the difference is under 0.15 m except for the top face 15 MJ/m<sup>2</sup> target fragility ZOIs for the 4 s and 6 s constant-current arcs in the top of the bus bar compartment. For the FEDB 50935 arc energy profile, the aluminum ZOIs are slightly larger, by less than 5 cm, which is not significant when compared to model uncertainty.

As described in Section 4.1.4, there is a known model uncertainty with the FDS exposure predictions, and 95% confidence intervals are computed for the modeled simulations (see Appendix B). For ZOI differentials of 0.15 m or less, the 95% confidence intervals for the copper bus bar material includes the ZOI for the aluminum bus bar material, and vice versa. There is no significant difference in the aluminum and copper bus bar energetic ZOIs for a given arc energy, arc location, and switchgear enclosure face. Similar to the MV SWGR, this is an important conclusion, especially given the treatment of each electrode is different within the FDS models in terms of the energy absorbed by the bus bars, the bus bar mass consumed during the arc, and the oxidation of the metal particles.



**Figure 6-43**  
Energetic ZOIs as a function of arc energy for the LV SWGR HEAF simulations. Top (solid symbols) – 15 MJ/m<sup>2</sup> fragility target, bottom (open symbols) – 30 MJ/m<sup>2</sup> fragility target. Symbol shape and color indicates the enclosure face



**Figure 6-44**  
**Aluminum versus copper bus bar energetic ZOIs for all LV SWGR HEAF simulations. Solid symbols are 15 MJ/m<sup>2</sup> fragility targets and open symbols are 30 MJ/m<sup>2</sup> fragility targets**

### 6.2.2.2 Modeling Insights

FDS modeling insights for LV SWGR HEAFs are as follows:

- There is no significant difference between the energetic ZOI dimensions between copper and aluminum bus bar materials given an arc energy profile, arc location, and switchgear enclosure face. The energetic ZOIs for each material are within the 95<sup>th</sup> percentile of the model uncertainty band as computed from the ZOI predictions for either material.
- The simulations that reproduce FEDB 50935 involve an arc that begins at the circuit breaker stabs (copper electrode) and migrates to the bus bar compartment (aluminum electrode). Aluminum is used to represent both electrodes in the FDS simulations as a conservative measure; however, given the aluminum and copper results are similar, the conservatism does not affect the energetic ZOI results.
- The largest factor affecting the energetic ZOIs is duration and extent of view between the arc volume and the target location. The energetic ZOIs tend to increase within increasing arc energy due to a larger breach area within the switchgear enclosure.
- The energetic ZOIs are greater on switchgear enclosure faces closest to the arc. Switchgear enclosure faces that are near the arc melt sooner, resulting in an opening that increases in size during and shortly after the arc clears. This results in a larger energy flux at the target location and a larger energetic ZOI at these sides.

These insights are consistent with expectations of the HEAF phenomena as modeled in FDS. Since the HEAF is modeled as a high heat release rate per unit volume, the greatest exposure at a fixed location is when the view factor between the arc volume and the location in consideration is maximized.

### 6.2.2.3 Tabulated LV SWGR Energetic ZOIs

Table 6-2 shows a summary of LV SWGR energetic ZOIs for all of the LV SWGR simulations. A 41 s duration indicates the two-stage arc power profile discussed in Section 3.8.1 and Appendix A. Simulations with a 2 s, 4 s, or 6 s duration are sensitivity cases that use a constant arc current of 21.5 kA.

**Table 6-2**  
**Summary of LV SWGR energetic ZOIs**

HEAF simulation summary						Energetic ZOI (m)									
						15 MJ/m <sup>2</sup> target fragility					30 MJ/m <sup>2</sup> target fragility				
HEAF ID <sup>1,2</sup>	Bus bar material	Arcing fault duration	Arc location	Arc elevation	Arc energy (MJ)	Back	Left	Right	Top	Front	Back	Left	Right	Top	Front
LV-BASE-1	Aluminum	41	Circuit Breaker	Mid-Height	90	None <sup>3</sup>	None	0.74	None	None	None	None	0.47	None	None
LV-BASE-2	Aluminum	41	Circuit Breaker	Top	90	None	None	0.77	0.48	None	None	None	0.49	0.25	None
LV-BASE-3	Aluminum	41	Bus Bar Comp.	Mid-Height	90	None	None	0.77	None	None	None	None	0.49	None	None
LV-BASE-4	Aluminum	41	Bus Bar Comp.	Top	90	0.06	None	0.75	0.72	None	None	None	0.47	0.43	None
LV-BASE-5	Aluminum	41	Circuit Breaker to Bus Bar Comp. <sup>4</sup>	Mid-Height	90	None	None	0.71	None	None	None	None	0.43	None	None
LV-BASE-6	Aluminum	41	Circuit Breaker to Bus Bar Comp. <sup>4</sup>	Top	90	None	None	0.71	0.50	None	None	None	0.43	0.23	None
LV-BASE-7	Copper	41	Circuit Breaker	Mid-Height	90	None	None	0.70	None	None	None	None	0.43	None	None
LV-BASE-8	Copper	41	Circuit Breaker	Top	90	None	None	0.73	0.43	None	None	None	0.46	0.20	None
LV-BASE-9	Copper	41	Bus Bar Comp.	Mid-Height	90	None	None	0.75	None	None	None	None	0.47	None	None
LV-BASE-10	Copper	41	Bus Bar Comp.	Top	90	0.05	None	0.73	0.71	None	None	None	0.46	0.42	None
LV-SENS-1	Aluminum	2	Circuit Breaker	Mid-Height	28	None	None	0.11	None	None	None	None	None	None	None
LV-SENS-2	Aluminum	2	Circuit Breaker	Top	28	None	None	0.12	None	None	None	None	None	None	None
LV-SENS-3	Aluminum	2	Bus Bar Comp.	Mid-Height	28	None	None	None	None	None	None	None	None	None	None
LV-SENS-4	Aluminum	2	Bus Bar Comp.	Top	28	None	None	0.07	None	None	None	None	None	None	None
LV-SENS-5	Copper	2	Circuit Breaker	Mid-Height	28	None	None	0.18	None	None	None	None	None	None	None
LV-SENS-6	Copper	2	Circuit Breaker	Top	28	None	None	0.17	None	None	None	None	None	None	None
LV-SENS-7	Copper	2	Bus Bar Comp.	Mid-Height	28	None	None	0.11	None	None	None	None	None	None	None
LV-SENS-8	Copper	2	Bus Bar Comp.	Top	28	None	None	0.10	0.05	None	None	None	None	None	None
LV-SENS-9	Aluminum	4	Circuit Breaker	Mid-Height	56	None	None	0.38	None	None	None	None	0.20	None	None

HEAF simulation summary						Energetic ZOI (m)									
						15 MJ/m <sup>2</sup> target fragility					30 MJ/m <sup>2</sup> target fragility				
HEAF ID <sup>1,2</sup>	Bus bar material	Arcing fault duration	Arc location	Arc elevation	Arc energy (MJ)	Back	Left	Right	Top	Front	Back	Left	Right	Top	Front
LV-SENS-10	Aluminum	4	Circuit Breaker	Top	56	None	None	0.36	None	None	None	None	0.18	None	None
LV-SENS-11	Aluminum	4	Bus Bar Comp.	Mid-Height	56	None	None	0.29	None	None	None	None	0.13	None	None
LV-SENS-12	Aluminum	4	Bus Bar Comp.	Top	56	None	None	0.33	0.21	None	None	None	0.16	0.05	None
LV-SENS-13	Copper	4	Circuit Breaker	Mid-Height	56	None	None	0.48	None	None	None	None	0.26	None	None
LV-SENS-14	Copper	4	Circuit Breaker	Top	56	None	None	0.47	None	None	None	None	0.26	None	None
LV-SENS-15	Copper	4	Bus Bar Comp.	Mid-Height	56	None	None	0.41	None	None	None	None	0.21	None	None
LV-SENS-16	Copper	4	Bus Bar Comp.	Top	56	None	None	0.44	0.38	None	None	None	0.24	0.17	None
LV-SENS-17	Aluminum	6	Circuit Breaker	Mid-Height	84	None	None	0.63	None	None	None	None	0.40	None	None
LV-SENS-18	Aluminum	6	Circuit Breaker	Top	84	None	None	0.60	0.19	None	None	None	0.37	0.04	None
LV-SENS-19	Aluminum	6	Bus Bar Comp.	Mid-Height	84	None	None	0.51	None	None	None	None	0.30	None	None
LV-SENS-20	Aluminum	6	Bus Bar Comp.	Top	84	None	None	0.53	0.39	None	None	None	0.32	0.20	None
LV-SENS-21	Copper	6	Circuit Breaker	Mid-Height	84	None	None	0.66	None	None	None	None	0.41	None	None
LV-SENS-22	Copper	6	Circuit Breaker	Top	84	None	None	0.66	0.21	None	None	None	0.41	0.04	None
LV-SENS-23	Copper	6	Bus Bar Comp.	Mid-Height	84	None	None	0.60	None	None	None	None	0.36	None	None
LV-SENS-24	Copper	6	Bus Bar Comp.	Top	84	None	None	0.62	0.58	None	None	None	0.38	0.33	None

<sup>1</sup>The LV-BASE-# designation corresponds to FDS simulations using the FEDB 50935 arc energy profile and the LV-SENS-# designation corresponds to FDS sensitivity analysis simulations using other arc power profiles.

<sup>2</sup>The FDS input designator is not the same as the input file name but uniquely corresponds to a single FDS input file. Refer to Appendix B of this report for the corresponding input file nomenclature designator.

<sup>3</sup>None means there is no external energetic ZOI.

<sup>4</sup>Fault begins at the circuit breaker and migrates to the main bus bar compartment after 20 s.

### 6.3 Non-Segregated Bus Duct HEAFs

Forty-eight simulations are run with variations of bus bar material (copper, aluminum), duct housing material (aluminum, steel), duct geometry (straight, tee, or elbow), and duration (2 s stiff, 4 s stiff, 5 s stiff, 0 s stiff 15 s decay, 3 s stiff 15 s decay, 5 s stiff 15 s decay). Six sensitivity simulations are run with a vertical elbow geometry to determine if it was substantially different from the straight or tee duct geometries. An additional four sensitivity simulations are run with a 1 s stiff duration to provide greater resolution into faults with short fault clearing times. In total, 58 bus duct simulations are run and summarized in Table 6-3. One simulation—a straight duct segment with aluminum electrodes, aluminum bus duct housing, 0 s stiff current and 15 s decaying current—failed with a numerical instability and is not reported.

The bus ducts all have nominal duct dimensions of 0.4 m (15.8 inches) tall, 0.56 m (22 inches) wide, and a duct housing thickness of 0.0032 m (0.125 inches), corresponding to 11-gauge steel sheet metal.

The bus duct ZOI orientations vary with the bus duct configuration. Figure 6-45 shows the ZOI orientations for the three bus duct configurations considered in this report.

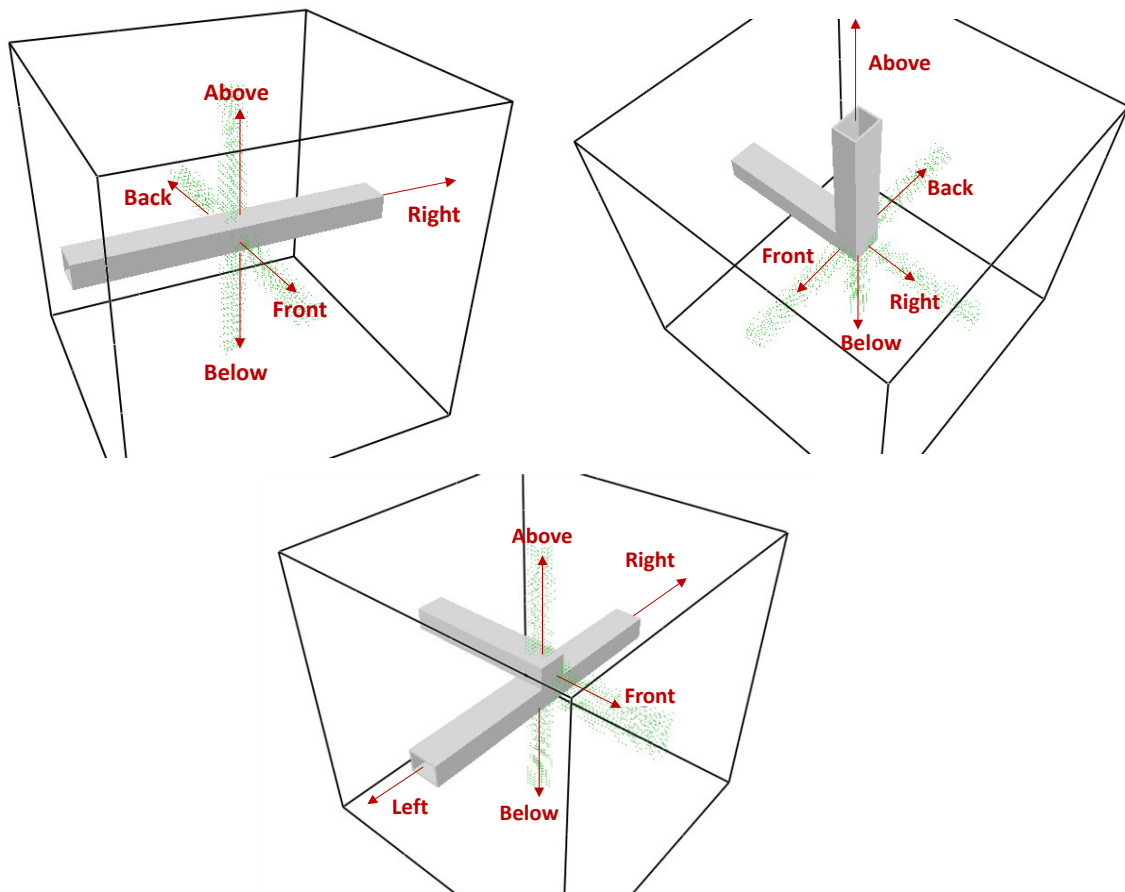


**Figure 6-45**  
Energetic ZOI orientations for the NSBD arc locations. Straight NSBD arc location (top left), elbow arc location (top right), and tee arc location (bottom)

### 6.3.1 Selected Non-Segregated Bus Duct HEAF Simulations

Three NSBD HEAF simulations are reviewed in detail. All three have the same prescribed energy input corresponding to a 3 s stiff fault, followed by a 15 s generator-fed decay, for a total arc energy of 233 MJ. The simulations reviewed are as follows:

1. Straight duct geometry with copper bus bars and steel duct housing
2. Vertical elbow duct geometry with aluminum bus bars and aluminum duct housing
3. Vertical tee duct geometry with aluminum bus bars and steel duct housing

The detailed results include depictions of the duct breach, the particle dispersion, the luminous thermal plume, the heat release rate per unit volume (arc), the duct wall temperatures, and the target exposure profiles as a function of distance.

#### 6.3.1.1 Non-Segregated Bus Duct Straight Section

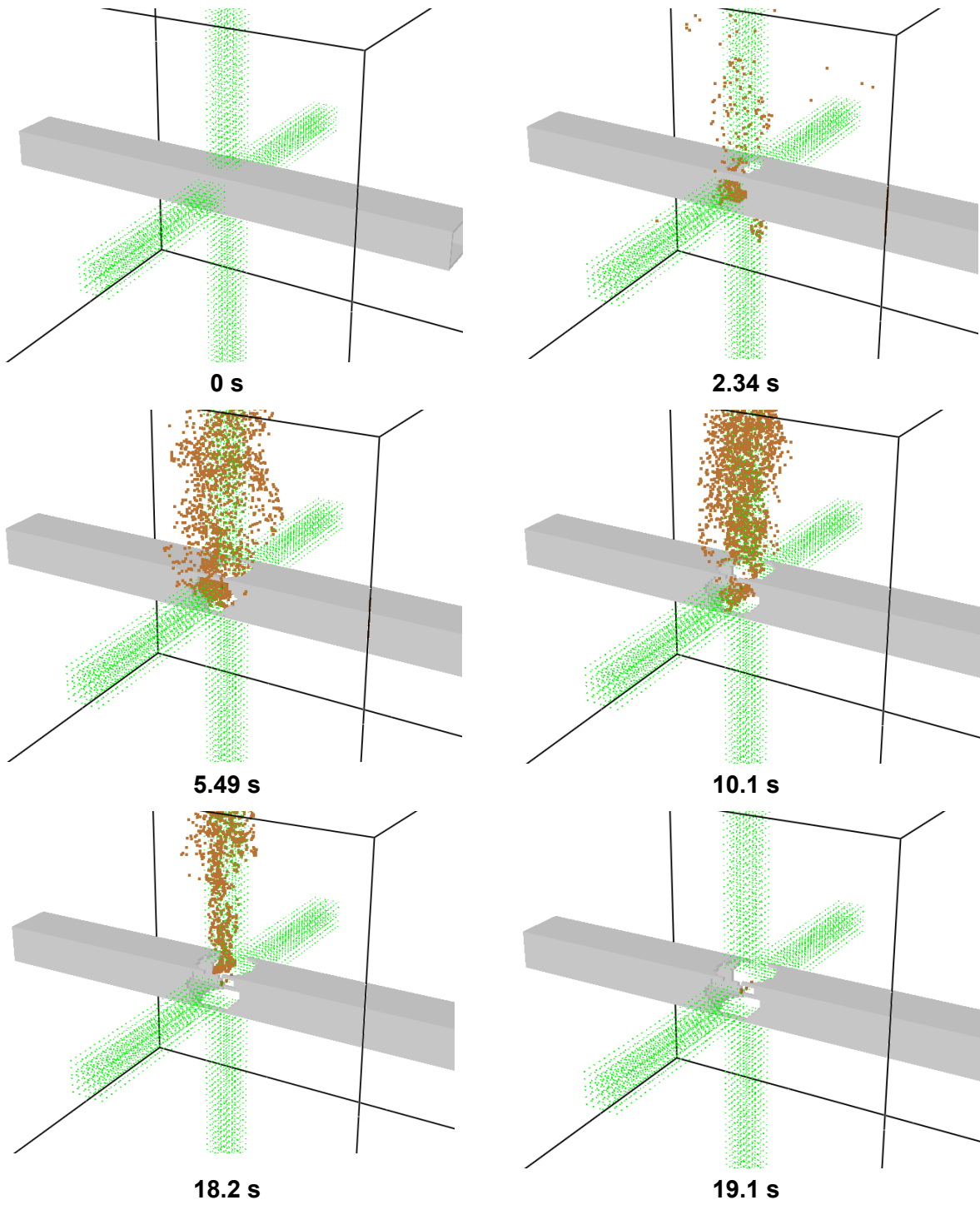
Figure 6-46 depicts the metal particle distribution around the lower, side, and upper portion of the bus duct at various times during the HEAF. At 0 s, there are no metal particles and the duct is intact. At 2.34 s, the duct is breached on all four sides, and particles are ejected in all directions, though buoyancy causes most to exit the duct through the top opening. At 5.49 s, the size of the openings continues to grow, and the particle density has increased and reached steady state. At 10.1 s, the size of the breach reaches its approximate maximum size. Over the next several seconds, the effects of the generator decay become apparent, and there is a visible reduction in the particle density.

Figure 6-47 depicts the luminous portion of the thermal plume at 1.25 s, 1.53 s, 3.09 s, and 8.94 s. From the progression shown, it is evident that early in the HEAF, when the duct is still largely intact, hot gases and particles flow through the duct and out of the computational domain. As the size of the breach grows, the gases and particles leave primarily through the breach.

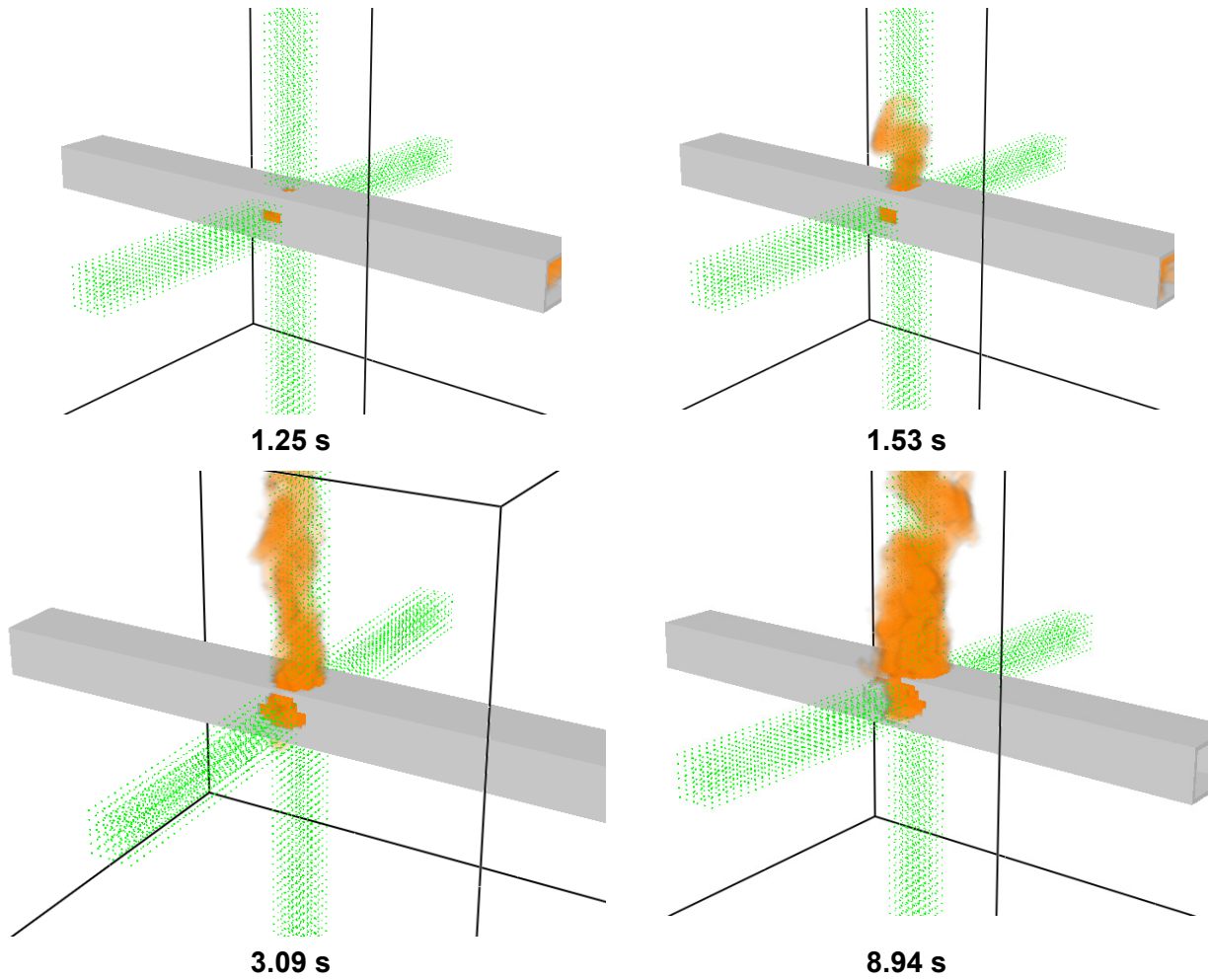
Figure 6-48 depicts the heat release rate per unit volume at 18 s, which corresponds to the arc energy location in the FDS model. The duct damage is about maximized, and the arc is seen clearly at this time. The intent of this figure is to show the approximate location where holes develop relative to the location where the arc energy is modeled in FDS.

Figure 6-49 depicts the wall temperature at 3.9 s, the time at which the greatest extent of the duct surface is heated. Although the arc continues to release heat for some time afterwards, the duct has melted away from the arc, and the heating of the duct surface reaches steady state at this time.

The total exposure energy as a function of distance is shown in Figure 6-50, which shows the energetic ZOI for this simulation is 0.5 – 0.8 m below the duct and 0.7 – 1.1 m from all other surfaces, consistent with the particle distribution and luminous plume location.



**Figure 6-46**  
Copper particle distribution at various times for a 233 MJ NSBD HEAF in a straight duct segment with copper bus bars and steel duct housing



**Figure 6-47**  
Luminous portion of the thermal plume at various times for a 233 MJ NSBD HEAF in a straight duct segment with copper bus bars and steel duct housing

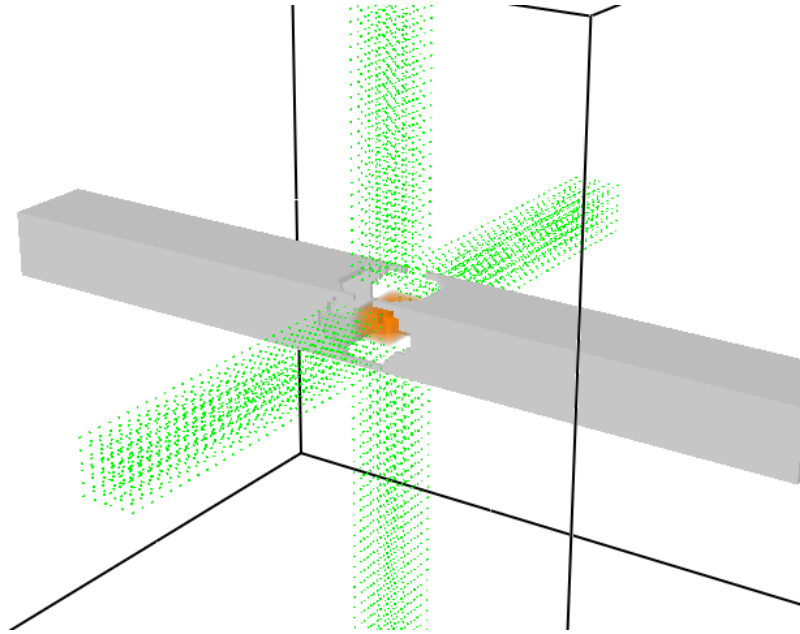


**Figure 6-48**  
Heat release rate per unit volume at 18 s for a 233 MJ NSBD HEAF in a straight duct segment with copper bus bars and steel duct housing

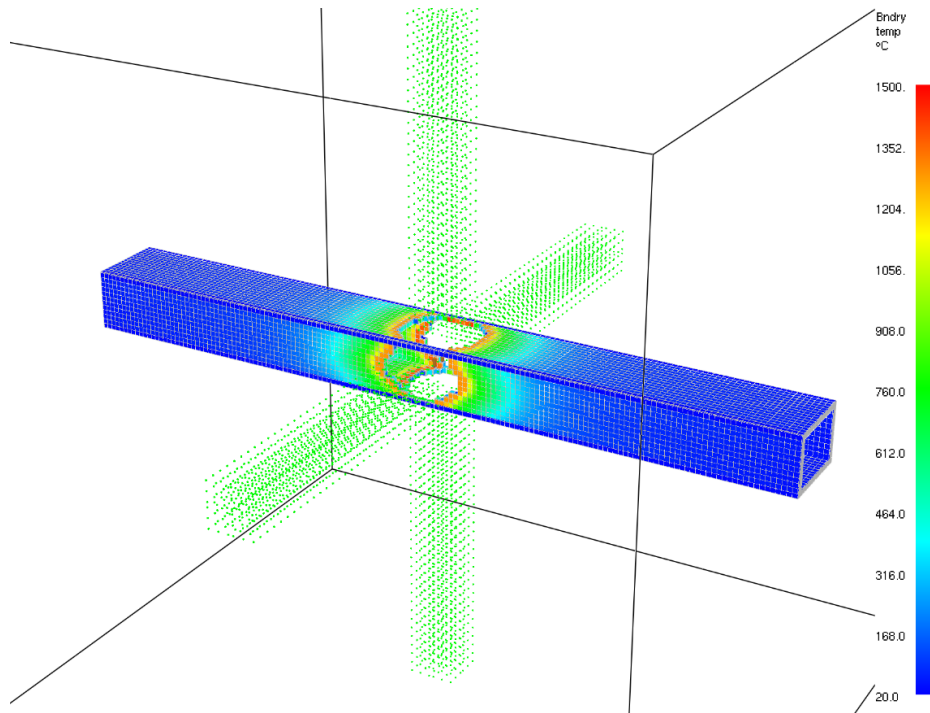


**Figure 6-49**  
Wall temperature of the duct housing at 3.9 s for a 233 MJ NSBD HEAF in a straight duct segment with copper bus bars and steel duct housing

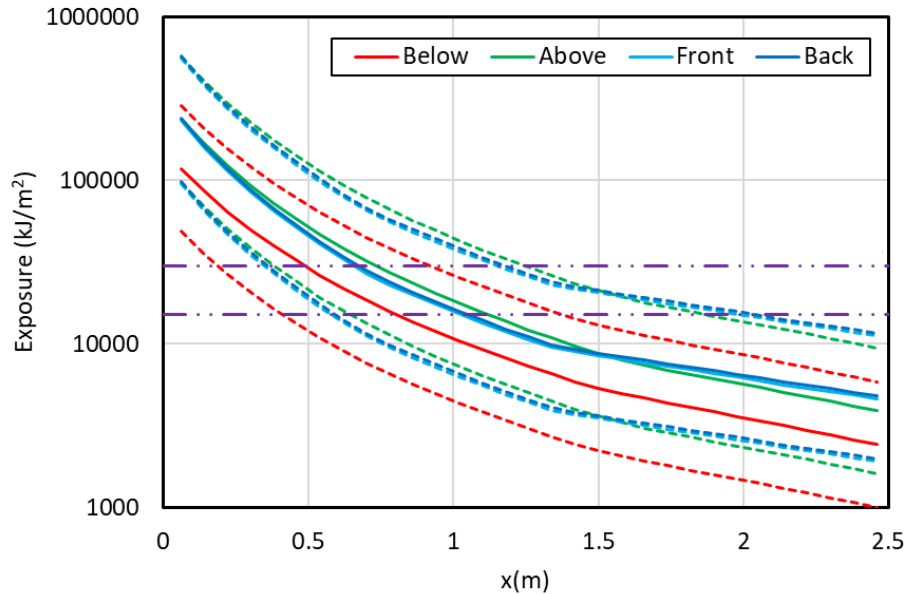


**Figure 6-50**  
**Total energy exposure as a function of distance from each face for a 233 MJ NSBD HEAF in a straight duct segment with copper bus bars and steel duct housing (HEAF simulation NSBD-19). Dashed horizontal lines correspond to the 15 MJ/m<sup>2</sup> and 30 MJ/m<sup>2</sup> target fragility threshold**

### 6.3.1.2 Non-Segregated Bus Duct Elbow

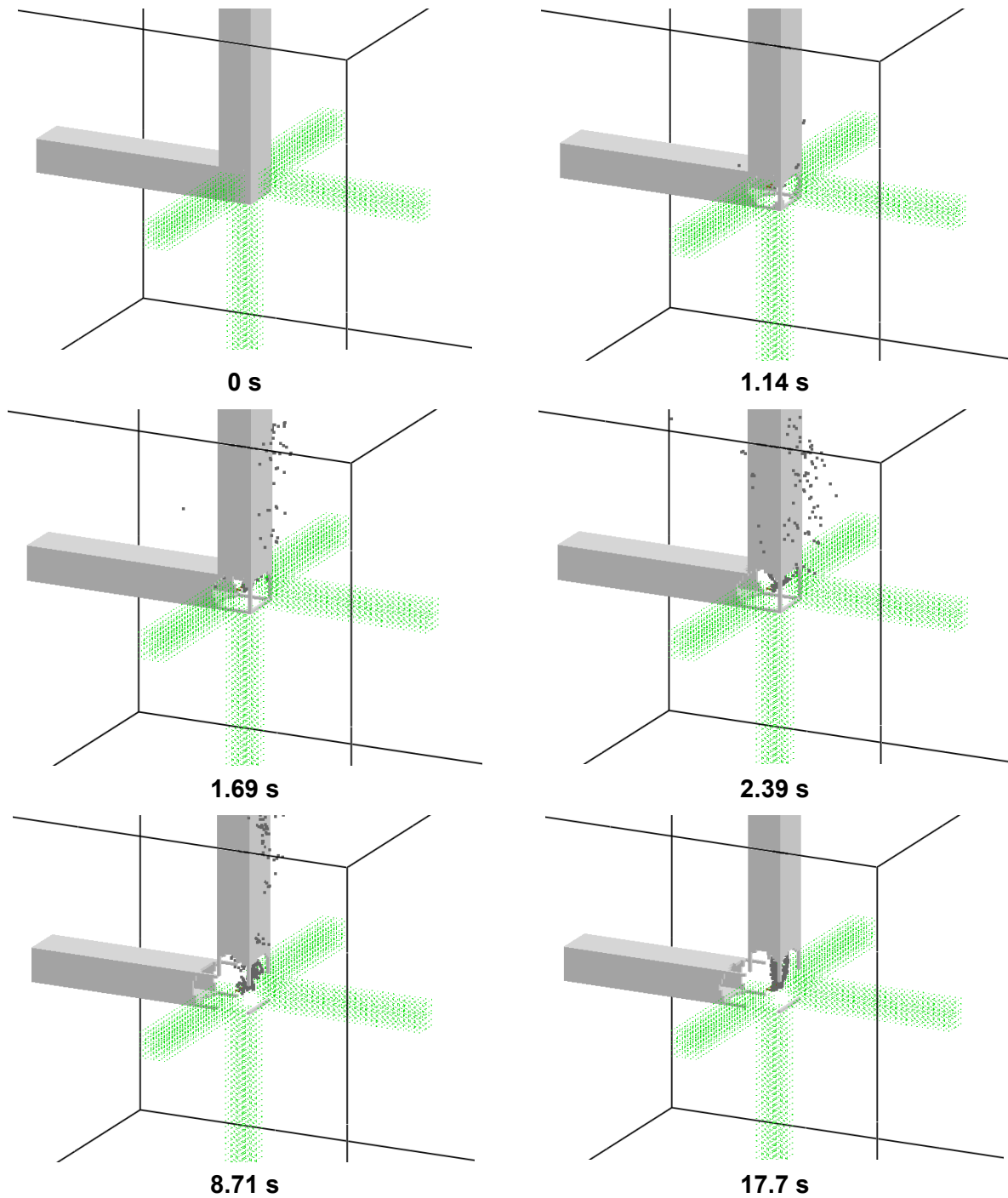
Figure 6-51 depicts the metal particle distribution around the lower, side, and upper portion of the bus duct at various times during the HEAF. At 0 s, there are no metal particles and the duct is intact. 1.14 s, the duct breaches on three sides and particles begin to escape the duct in all directions. The size of the breach grows over the next several seconds, and the particle density continues to increase. Because of the orientation of the vertical elbow, the majority of aluminum particles and hot gases travel upward through the intact duct segment. At 8.71 s, the size of the breach reaches its approximate maximum size, and the particles continue to travel upward through the duct, though there are still enough generated that some escape through the hole on the right side. Over the next several seconds, the effects of the generator decay become apparent, and there is a visible reduction in the particle density.

Figure 6-52 depicts the luminous portion of the thermal plume at 1.04 s, 1.69 s, 2.31 s, and 7.44 s. Because of the orientation of the duct, the plume flow behaves differently than in the straight duct, i.e., early in the simulation, hot gases escape through the holes and later in the simulation, the gases travel through the intact vertical segment.

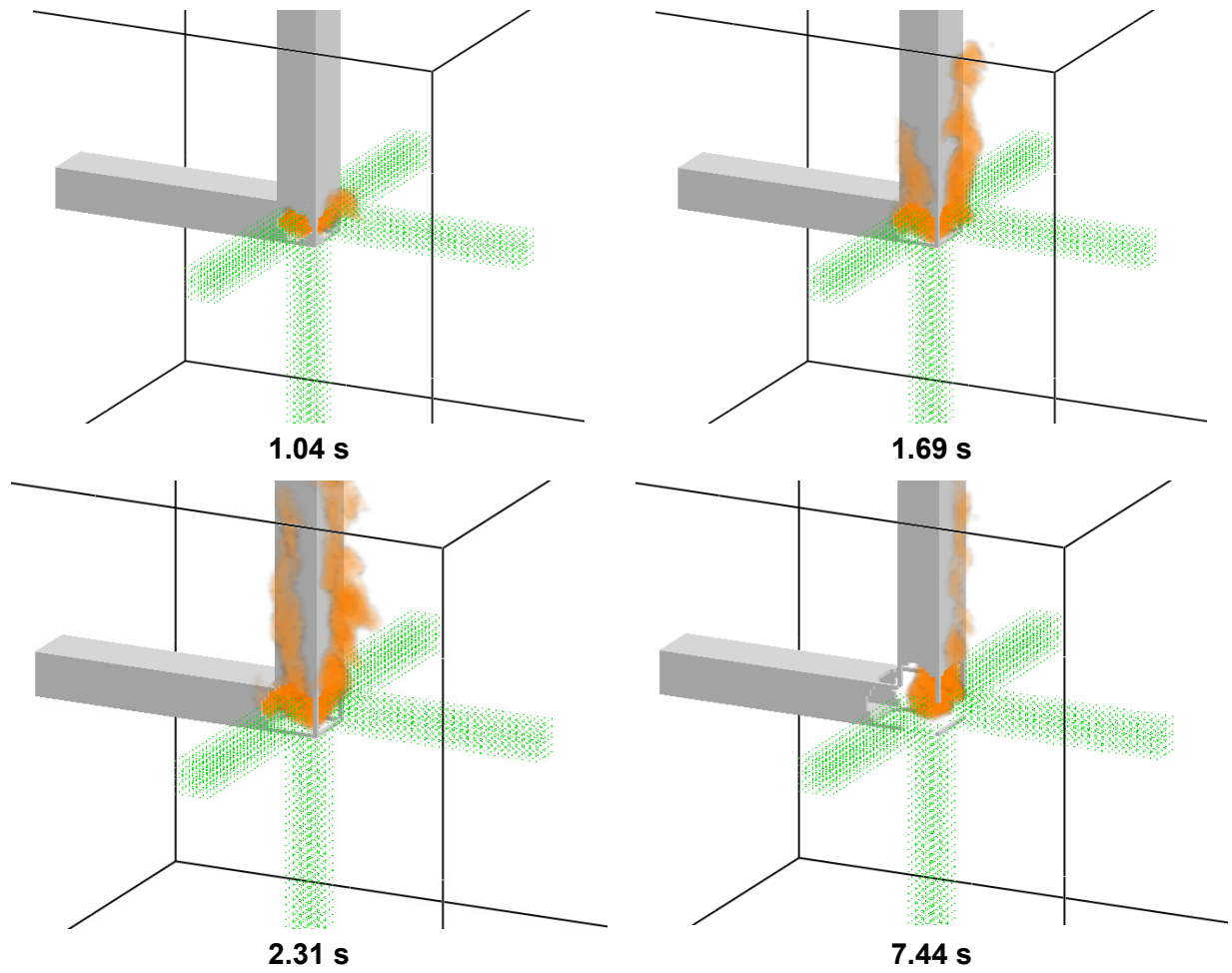
Figure 6-53 depicts the heat release rate per unit volume at 15.5 s, which corresponds to the arc energy location in the FDS model. The duct damage is about maximized, and the arc is seen clearly at this time. The intent of this figure is to show the approximate location where holes develop relative to the location where the arc energy is modeled in FDS.

Figure 6-54 depicts the wall temperature at 5.2 s, the time at which the greatest extent of the duct surface is heated. As with the straight duct, the duct surface melts away from the arc, bringing the duct heating to a steady state; however, it takes longer to reach steady state because significant quantities of gases are still flowing through the vertical segment after the duct melts.

The total exposure energy as a function of distance is shown in Figure 6-55, which shows the energetic ZOI for this simulation is 0.75 – 1.2 for all four sides. The radiant exposure is approximately the same on each side as radiant heating on those sides is fairly consistent, and the bulk of the convective heating is directed upwards, where there is a duct and therefore no energetic ZOI.



**Figure 6-51**  
Aluminum particle distribution at various times for a 233 MJ NSBD HEAF in a vertical elbow duct segment with aluminum bus bars and aluminum duct housing



**Figure 6-52**  
Luminous portion of the thermal plume at various times for a 233 MJ NSBD HEAF in a vertical elbow duct segment with aluminum bus bars and aluminum duct housing

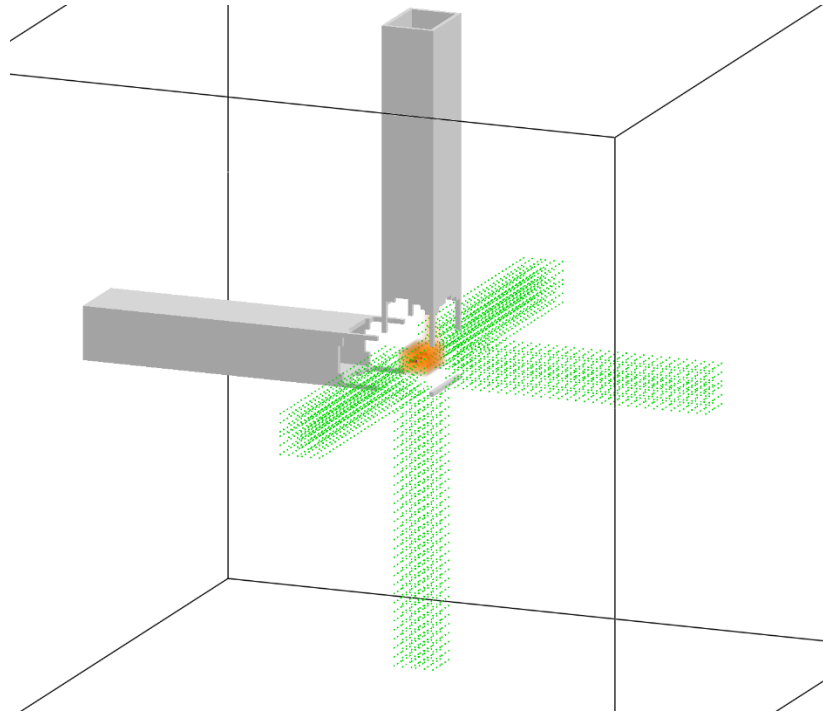


**Figure 6-53**  
Heat release rate per unit volume at 15.5 s for a 233 MJ NSBD HEAF in a vertical elbow duct segment with aluminum bus bars and aluminum duct housing

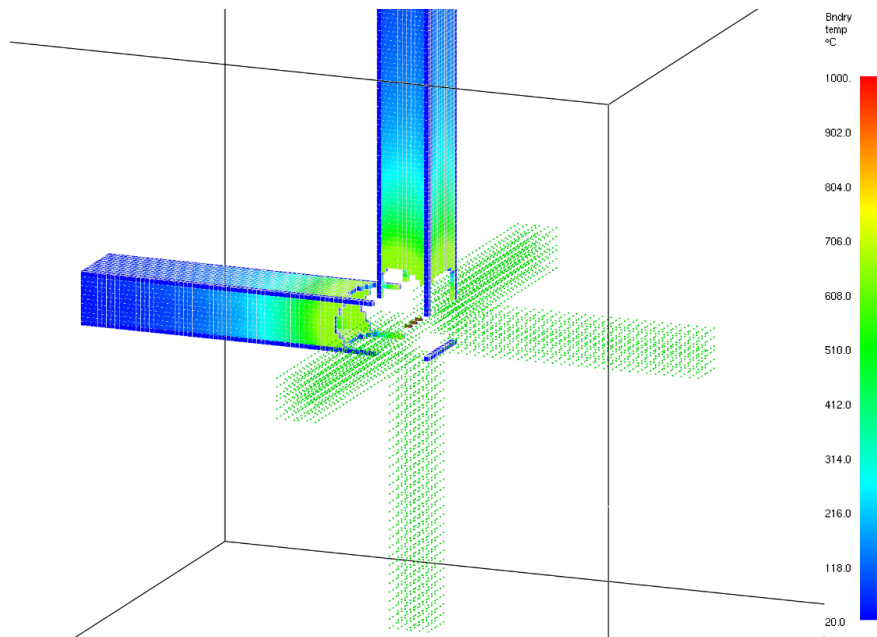


**Figure 6-54**  
Wall temperature of the duct housing at 5.2 s for a 233 MJ NSBD HEAF in a vertical elbow duct segment with aluminum bus bars and aluminum duct housing

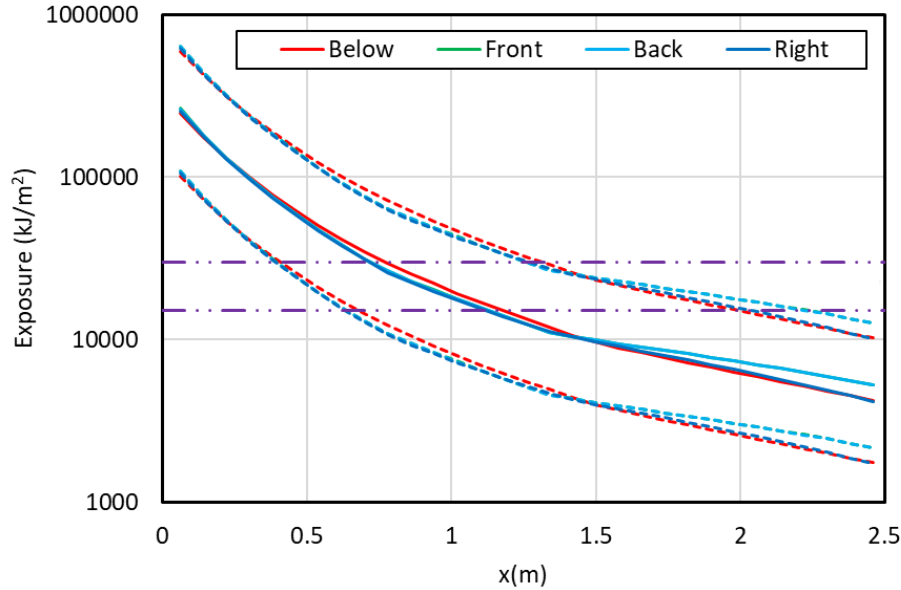


**Figure 6-55**  
**Total energy exposure as a function of distance from each face for a 233 MJ NSBD HEAF in a vertical elbow duct segment with aluminum bus bars and aluminum duct housing (HEAF simulation NSBD-56). Dashed horizontal lines correspond to the 15 MJ/m<sup>2</sup> and 30 MJ/m<sup>2</sup> target fragility threshold**

### 6.3.1.3 Non-Segregated Bus Duct Tee

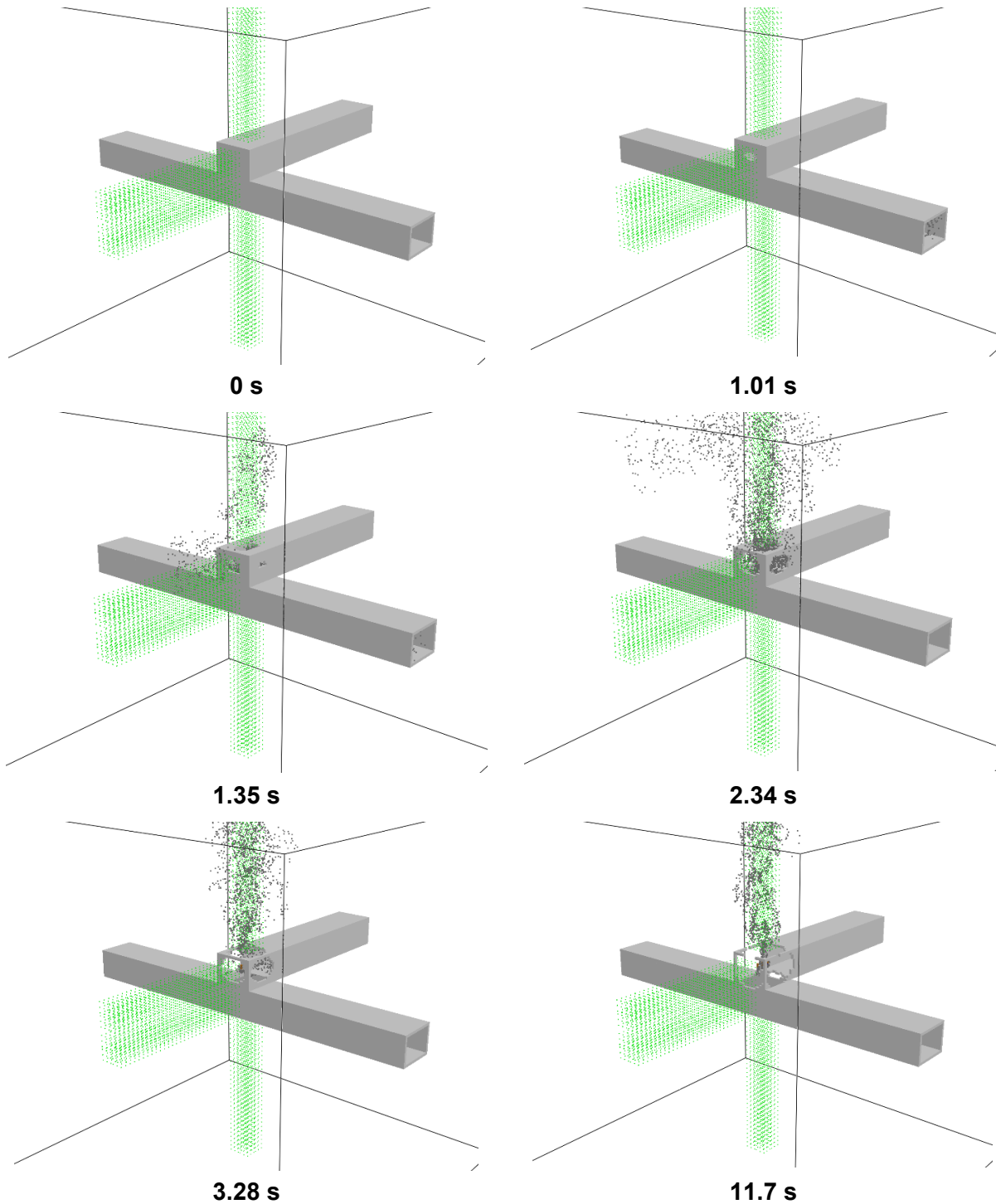
Figure 6-56 depicts the metal particle distribution about the vertical tee intersection of the bus duct segments at various times during the HEAF. At 0 s, there are no metal particles and the duct is intact. At 1.01 s, the upper portion of the duct begins to breach on its front face. At 1.35 s, the front and top of the upper duct breach, and holes in the sides of the upper duct are just beginning to open. Over the next 2 s, the size of the holes continues to grow, the particles trapped in the duct escape through the holes, and the flow of particles from the duct reaches steady state. At about 11.7 s, the damage to the duct is at its maximum, and the particle density is decreasing due to generator decay.

Figure 6-57 depicts the luminous portion of the thermal plume at 1.04 s, 1.69 s, 2.31 s, and 7.44 s. As with the flow of particles, the thermal plume experiences a sudden increase around 2.3 s, as the hot gases trapped in the relatively large duct volume escape through the holes. The lower segment of the duct in this tee acts as an energy store, and the hot gases that are initially pushed into the lower duct flow through the holes in the upper duct when they appear.

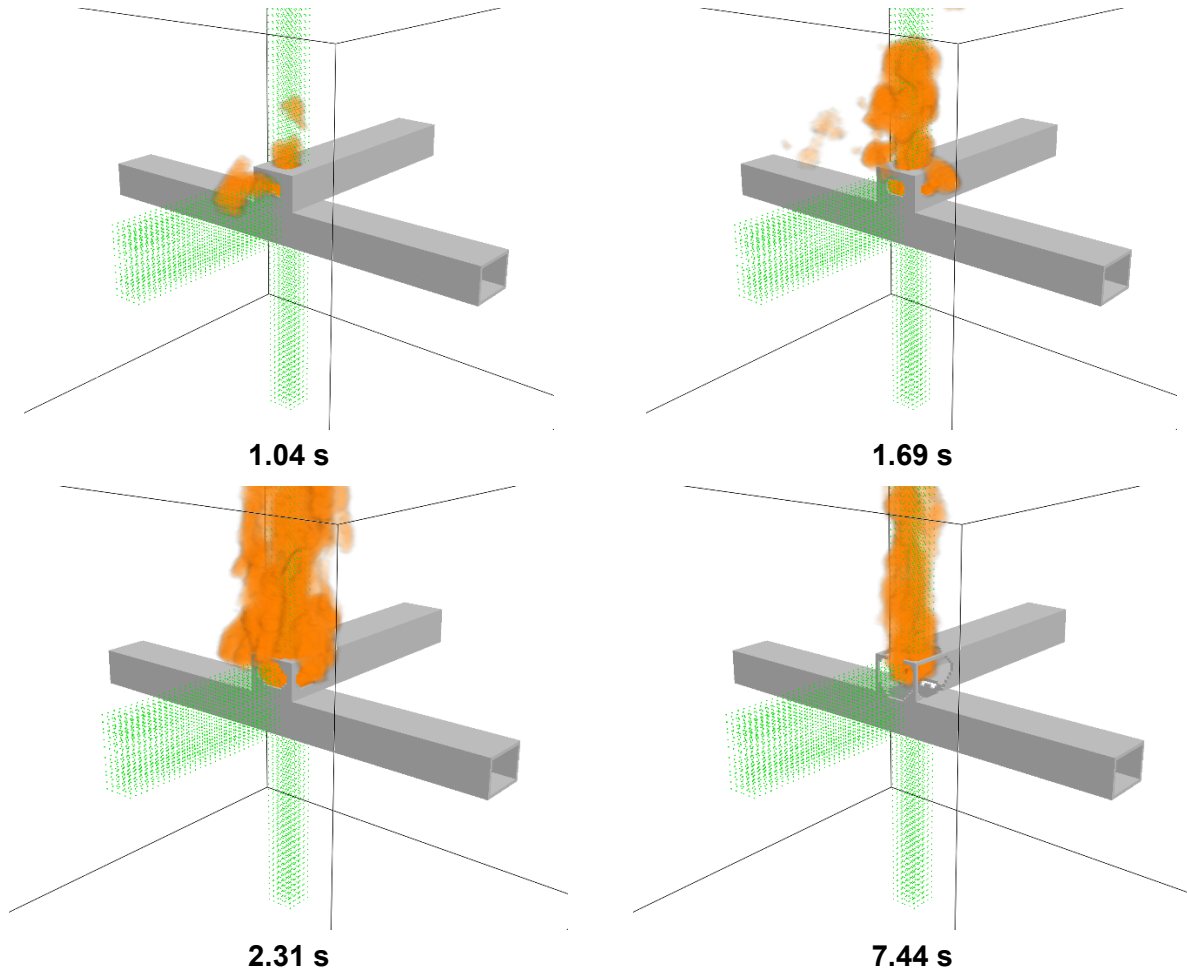
Figure 6-58 depicts the heat release rate per unit volume at 18.1 s, which corresponds to the arc energy location in the FDS model. The duct damage is about maximized, and the arc is seen clearly at this time. The intent of this figure is to show the approximate location where holes develop relative to the location where the arc energy is modeled in FDS.

Figure 6-59 depicts the wall temperature at 7.8 s, the time at which the greatest extent of the duct surface is heated. Although the arc continues to release heat for some time afterwards, the duct has melted away from the arc, and the heating of the duct surface reaches steady state at about this time.

The total exposure energy as a function of distance is shown in Figure 6-60, which shows the energetic ZOI for this simulation is 0.6 – 1 m from the front and above the duct. The incident energy below the duct does not reach the fragility limits due to the distance between the arc and the bottom of the duct, and there is no energetic ZOI in that direction.



**Figure 6-56**  
Aluminum particle distribution at various times for a 233 MJ NSBD HEAF in a vertical tee duct segment with aluminum bus bars and steel duct housing



**Figure 6-57**  
Luminous portion of the thermal plume at various times for a 233 MJ NSBD HEAF in a vertical tee duct segment with aluminum bus bars and steel duct housing

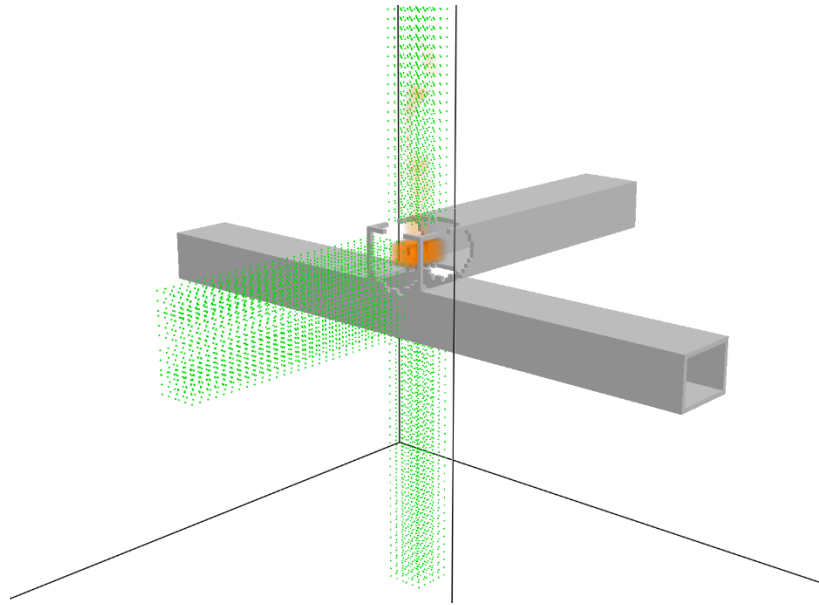


**Figure 6-58**  
Heat release rate per unit volume at 18.1 s for a 233 MJ NSBD HEAF in a vertical tee duct segment with aluminum bus bars and steel duct housing

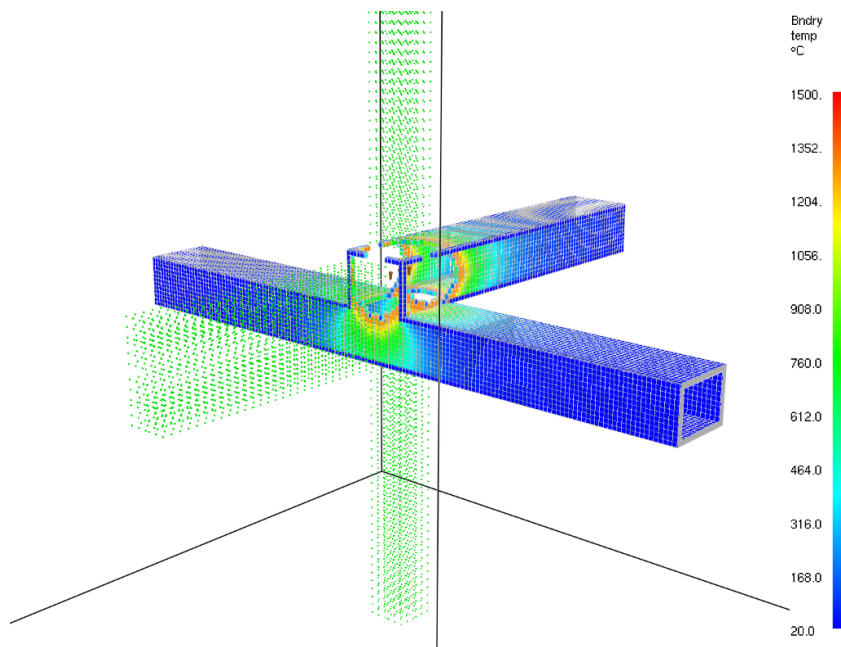


**Figure 6-59**  
Wall temperature of the duct housing at 7.8 s for a 233 MJ NSBD HEAF in a vertical tee duct segment with aluminum bus bars and steel duct housing

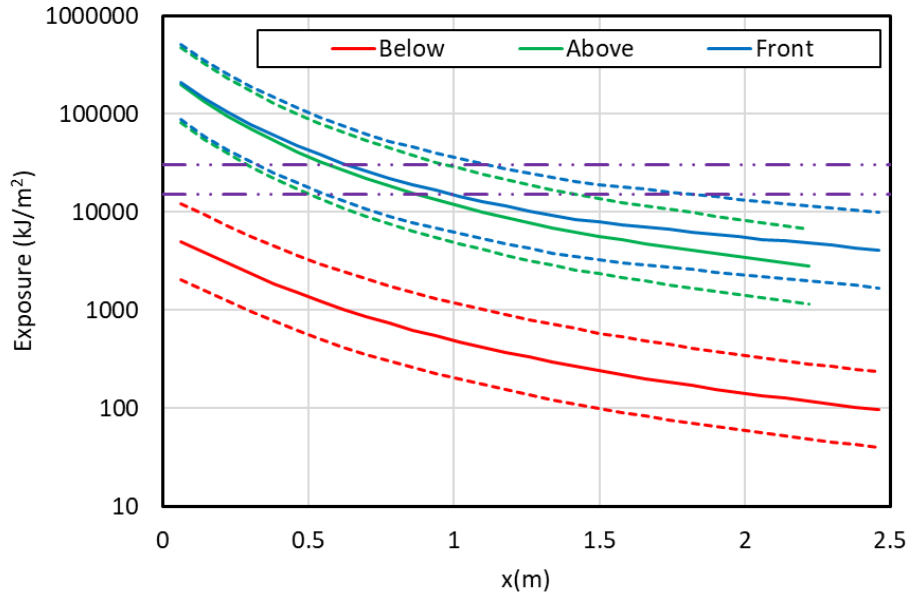
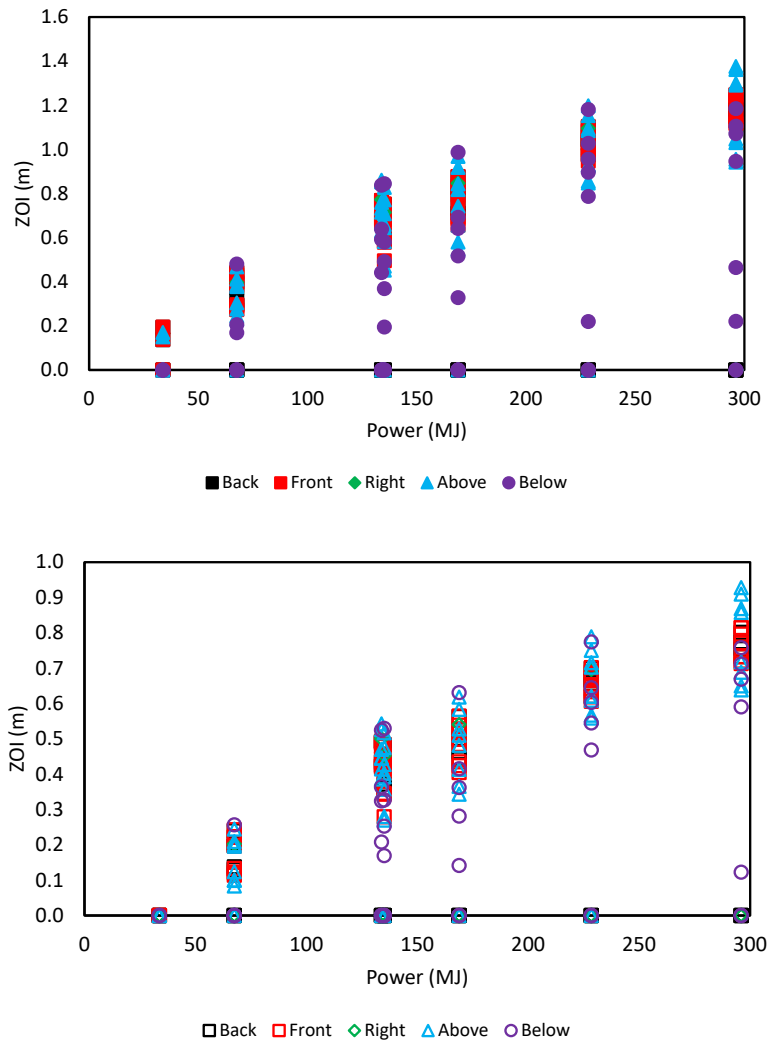


**Figure 6-60**  
**Total energy exposure as a function of distance from each face for a 233 MJ NSBD HEAF in a vertical tee duct segment with aluminum bus bars and steel duct housing (HEAF simulation NSBD-32). Dashed horizontal lines correspond to the 15 MJ/m<sup>2</sup> and 30 MJ/m<sup>2</sup> target fragility threshold. Note there is no bottom exposure for this duct configuration**

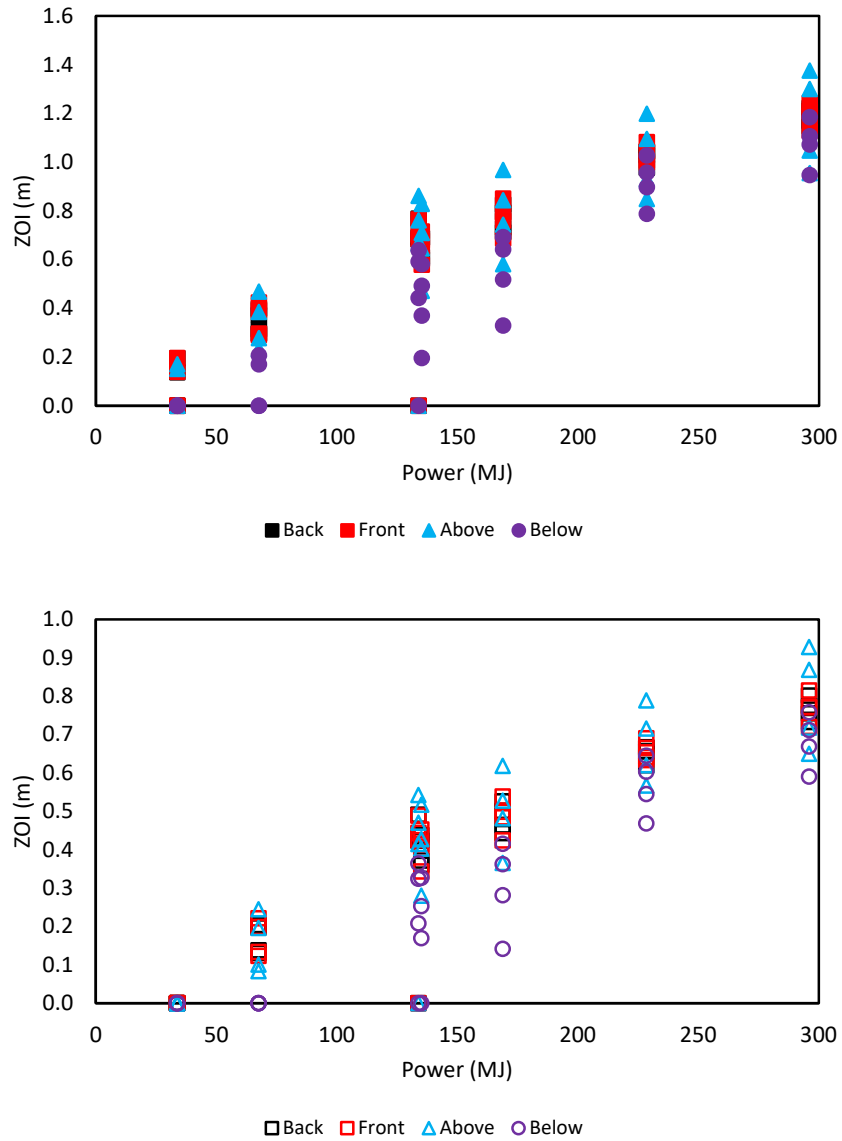
### 6.3.2 Summary of Results

#### 6.3.2.1 Energetic ZOI Dependencies

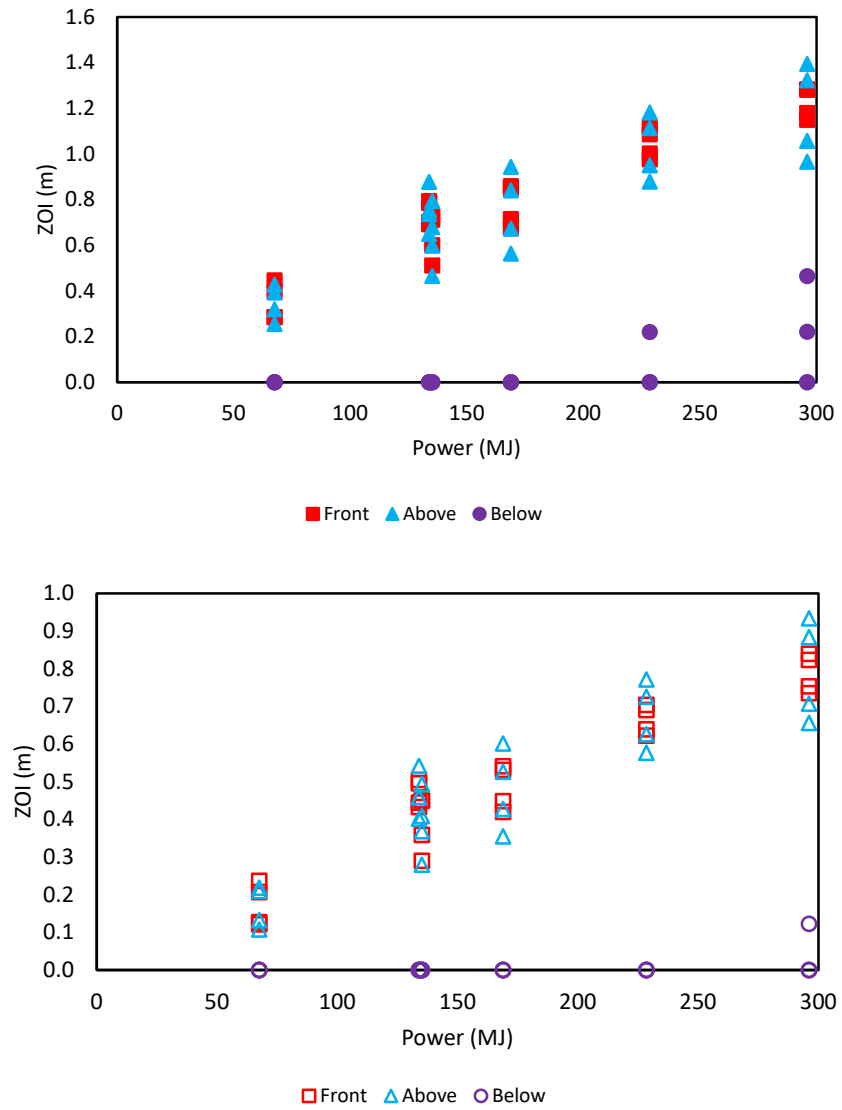
Figure 6-61 shows the energetic ZOIs for the NSBD HEAF simulations. Most energetic ZOIs are predicted to be larger than the bus duct energetic ZOIs recommended in NUREG/CR-6850 Supplement 1 [2]. Figure 6-62 through Figure 6-64 show the energetic ZOIs for the NSBD HEAF simulations for each geometry (straight, tee, and elbow). The elbow geometry shows less data since it was only run with an aluminum bus duct and aluminum bus bars.



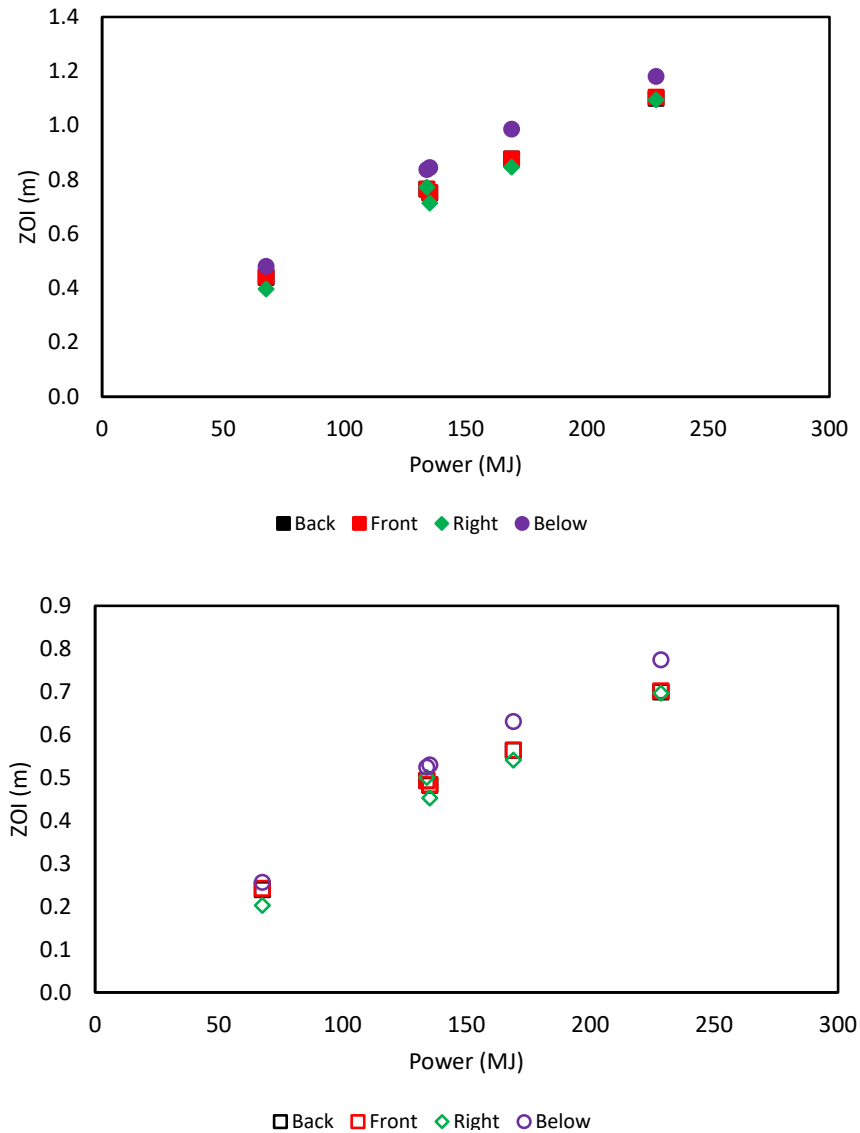
**Figure 6-61**  
**Energetic ZOIs as a function of arc energy for the NSBD HEAF simulations. Top (solid symbols) – 15 MJ/m<sup>2</sup> fragility target, bottom (open symbols) – 30 MJ/m<sup>2</sup> fragility target. Symbol shape and color indicates the enclosure face. Sides without an energetic ZOI component are shown with 0 m ZOI dimensions. Note that there is no left ZOI shown as two geometries (straight and elbow) do not have a left direction and the left direction for the tee is inside the initiating bus duct (see Figure 6-45)**



**Figure 6-62**  
Energetic ZOIs as a function of arc energy for the NSBD straight segment HEAF simulations. Top – 15 MJ/m<sup>2</sup> fragility target, bottom – 30 MJ/m<sup>2</sup> fragility target. Symbol shape and color indicates the enclosure face

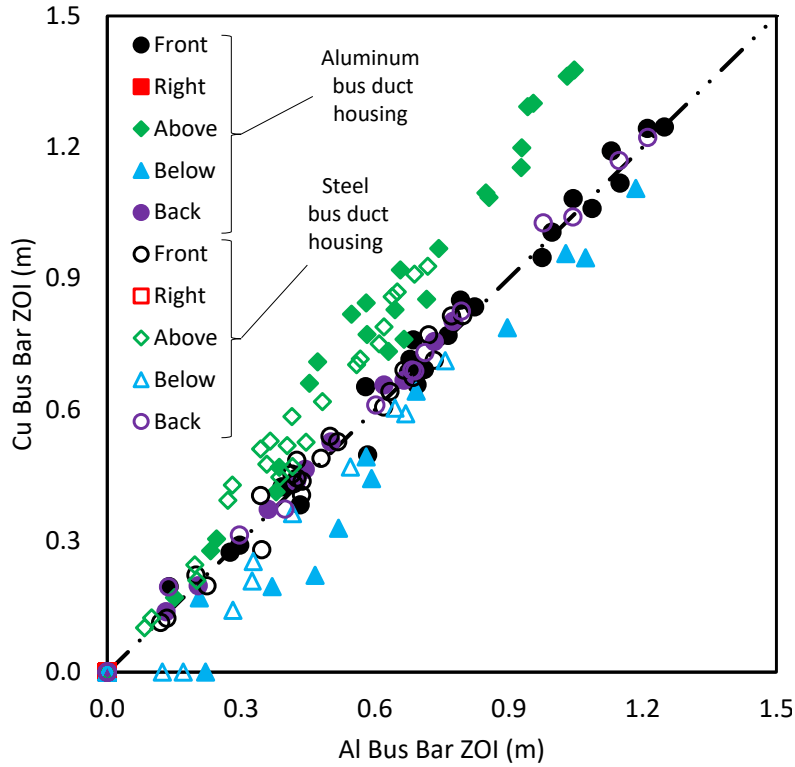


**Figure 6-63**  
**Energetic ZOIs as a function of arc energy for the NSBD tee HEAF simulations. Top – 15 MJ/m<sup>2</sup> fragility target, bottom – 30 MJ/m<sup>2</sup> fragility target. Symbol shape and color indicates the enclosure face**



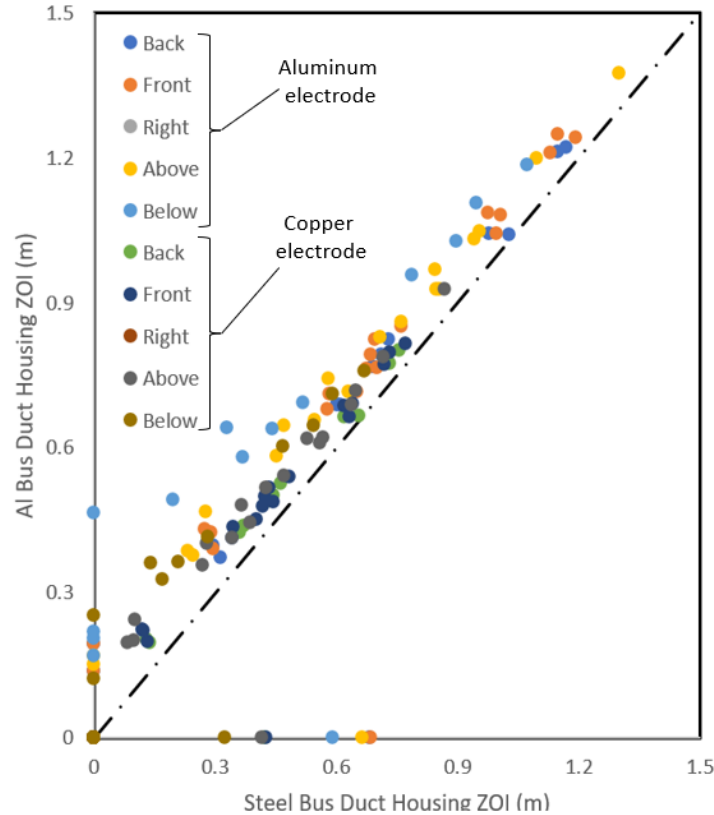
**Figure 6-64**  
**Energetic ZOIs as a function of arc energy for the NSBD elbow HEAF simulations. Top – 15 MJ/m<sup>2</sup> fragility target, bottom – 30 MJ/m<sup>2</sup> fragility target. Symbol shape and color indicates the enclosure face**

Figure 6-65 shows the aluminum versus copper energetic ZOIs for the NSBD HEAF simulations. As observed with the MV SWGR and LV SWGR, the results do not show that one electrode metal is more hazardous than the other. The “above” energetic ZOIs for copper electrodes tend to be larger than the aluminum electrodes (green diamonds in Figure 6-65) and the “below” energetic ZOIs tend to be larger for aluminum electrodes (blue triangles in Figure 6-65). This may be the result of the convective flow patterns that develop within the bus duct after the bus duct is breached. This pattern could be influenced by the melting temperature of the electrode through the generation and subsequent path of the particles generated by the arc and the energy distribution within the bus duct during the arc.



**Figure 6-65**  
**Aluminum versus copper bus bar energetic ZOIs for all NSBD HEAF simulations**

Figure 6-66 shows the aluminum versus steel duct energetic ZOIs for NSBD HEAF simulations. The aluminum duct shows energetic ZOIs approximately 0.15 m larger than the comparable steel duct value. This is due to the shorter breach time for aluminum bus ducts as compared to steel because of aluminum’s lower melting point and specific heat.



**Figure 6-66**  
Steel duct versus aluminum duct energetic ZOIs for all NSBD HEAF simulations

### 6.3.2.2 FDS Model Insights

The NSBD results reveal a number of trends that are unique to bus ducts. Figure 6-61 through Figure 6-64 indicate that, except for the bottom of the duct, all exposures are similar for all faces regardless of the geometric configuration. Whereas switchgear enclosures have partitions, circuit breakers, and vents that influence the direction of the arc energy, the simplistic geometry of bus ducts yields a relatively consistent energy distribution in all directions. Targets located below the bus duct will have lower exposures, as they are not subject to the bulk of the convective heat transfer. This is particularly noticeable for the tee geometries, where the bottom face of the bus duct is at a greater distance from the arc, which is initiated in the top segment of the tee.

The orientation of the duct (straight, elbow, or tee) has little effect on the energetic ZOIs. Although the geometry of the duct may influence the flow of gases early in the event, once the duct is breached, targets are exposed to the same radiant flux resulting in similar energetic ZOIs. The geometric parameter with the largest effect on target incident energy is the distance of the arc to the bus duct wall (i.e., how quickly the bus duct wall will breach) and the difference in this parameter across straight ducts, tees, and elbows is insignificant. This effect is most pronounced when looking at the incident energy at the bottom surface of the tee, as noted above.

Figure 6-65 indicates that, as with the switchgear, there is no significant difference in the energetic ZOIs for bus ducts with aluminum bus bars and bus ducts with copper bus bars. Some configurations have larger energetic ZOIs with aluminum bus bars, others have larger energetic ZOIs for copper bus bars.

Unlike switchgear, which are all assumed to be made of steel, bus duct housings are typically fabricated from steel or aluminum. Figure 6-66 indicates a significant difference between the two materials; HEAFs in bus ducts with aluminum housing have an energetic ZOI that are, on average, 0.15 m larger than those in ducts with steel housing. Differences in specific heat and melting point between the two metals cause the aluminum duct to breach faster than the steel duct, which increases the thermal exposure of external targets.

### 6.3.2.3 Tabulated NSBD Energetic ZOIs

Table 6-3 shows a summary of the NSBD HEAF simulation results. The orientations of the energetic ZOI surfaces relative to each NSBD arc location is depicted in Figure 6-45. The energetic ZOIs in Table 6-3 correspond to the thermal exposure from the arc.

**Table 6-3**  
**Summary of NSBD energetic ZOIs**

HEAF simulation summary							Energetic ZOI (m)									
							15 MJ/m <sup>2</sup> target fragility					30 MJ/m <sup>2</sup> target fragility				
HEAF ID <sup>1</sup>	Duct	Bus bar material	Stiff (s)	Decay (s)	Arc location	Arc energy <sup>2</sup> (MJ)	Back	Front	Right	Above	Below	Back	Front	Right	Above	Below
NSBD-1	Steel	Aluminum	1	0	Straight	34	None	None	N/A <sup>3</sup>	None	None	None	None	N/A	None	None
NSBD-2	Steel	Aluminum	2	0	Straight	68	0.30	0.30	N/A	0.23	None	0.13	0.13	N/A	0.08	None
NSBD-3	Steel	Aluminum	4	0	Straight	135	0.60	0.58	N/A	0.47	0.37	0.36	0.34	N/A	0.28	0.17
NSBD-4	Steel	Aluminum	5	0	Straight	169	0.71	0.69	N/A	0.58	0.52	0.44	0.42	N/A	0.36	0.28
NSBD-5	Steel	Aluminum	0	15	Straight	132	0.68	0.68	N/A	0.66	0.59	0.42	0.42	N/A	0.41	0.32
NSBD-6	Steel	Aluminum	3	15	Straight	233	0.98	1.00	N/A	0.85	0.90	0.62	0.63	N/A	0.57	0.54
NSBD-7	Steel	Aluminum	5	15	Straight	300	1.15	1.13	N/A	0.95	1.07	0.73	0.72	N/A	0.65	0.67
NSBD-8	Aluminum	Aluminum	1	0	Straight	34	0.14	0.14	N/A	0.15	None	None	None	N/A	None	None
NSBD-9	Aluminum	Aluminum	2	0	Straight	68	0.40	0.39	N/A	0.38	0.21	0.20	0.20	N/A	0.19	None
NSBD-10	Aluminum	Aluminum	4	0	Straight	135	0.69	0.68	N/A	0.64	0.58	0.42	0.41	N/A	0.40	0.33
NSBD-11	Aluminum	Aluminum	5	0	Straight	169	0.79	0.79	N/A	0.74	0.69	0.50	0.50	N/A	0.48	0.41
NSBD-12	Aluminum	Aluminum	3	15	Straight	233	1.04	1.04	N/A	0.93	1.03	0.66	0.66	N/A	0.62	0.64
NSBD-13	Aluminum	Aluminum	5	15	Straight	300	1.21	1.21	N/A	1.05	1.18	0.77	0.77	N/A	0.72	0.76
NSBD-14	Steel	Copper	1	0	Straight	34	None	None	N/A	None	None	None	None	N/A	None	None
NSBD-15	Steel	Copper	2	0	Straight	68	0.31	0.29	N/A	0.28	None	0.14	0.12	N/A	0.10	None
NSBD-16	Steel	Copper	4	0	Straight	135	0.61	0.65	N/A	0.71	0.20	0.37	0.40	N/A	0.43	None
NSBD-17	Steel	Copper	5	0	Straight	169	0.73	0.76	N/A	0.84	0.33	0.46	0.48	N/A	0.53	0.14
NSBD-18	Steel	Copper	0	15	Straight	132	0.69	0.70	N/A	0.76	0.44	0.43	0.44	N/A	0.47	0.21
NSBD-19	Steel	Copper	3	15	Straight	233	1.03	1.00	N/A	1.09	0.79	0.66	0.64	N/A	0.71	0.47

HEAF simulation summary							Energetic ZOI (m)									
							15 MJ/m <sup>2</sup> target fragility					30 MJ/m <sup>2</sup> target fragility				
HEAF ID <sup>1</sup>	Duct	Bus bar material	Stiff (s)	Decay (s)	Arc location	Arc energy <sup>2</sup> (MJ)	Back	Front	Right	Above	Below	Back	Front	Right	Above	Below
NSBD-20	Steel	Copper	5	15	Straight	300	1.17	1.19	N/A	1.30	0.95	0.75	0.77	N/A	0.87	0.59
NSBD-21	Aluminum	Copper	1	0	Straight	34	0.19	0.19	N/A	0.17	None	None	0.06	N/A	None	None
NSBD-22	Aluminum	Copper	2	0	Straight	68	0.37	0.42	N/A	0.47	0.17	0.20	0.2	N/A	0.24	None
NSBD-23	Aluminum	Copper	4	0	Straight	135	0.69	0.71	N/A	0.83	0.49	0.44	0.45	N/A	0.52	0.25
NSBD-24	Aluminum	Copper	5	0	Straight	169	0.82	0.85	N/A	0.97	0.64	0.53	0.54	N/A	0.62	0.36
NSBD-25	Aluminum	Copper	0	15	Straight	132	0.77	0.76	N/A	0.86	0.64	0.49	0.49	N/A	0.54	0.36
NSBD-26	Aluminum	Copper	3	15	Straight	233	1.04	1.08	N/A	1.20	0.96	0.67	0.69	N/A	0.79	0.60
NSBD-27	Aluminum	Copper	5	15	Straight	300	1.22	1.24	N/A	1.37	1.10	0.80	0.81	N/A	0.93	0.71
NSBD-28	Steel	Aluminum	2	0	Tee	68	N/A	0.27	N/A	0.24	None	N/A	0.12	N/A	0.10	None
NSBD-29	Steel	Aluminum	4	0	Tee	135	N/A	0.58	N/A	0.45	None	N/A	0.35	N/A	0.27	None
NSBD-30	Steel	Aluminum	5	0	Tee	169	N/A	0.69	N/A	0.55	None	N/A	0.43	N/A	0.34	None
NSBD-31	Steel	Aluminum	0	15	Tee	132	N/A	0.67	N/A	0.63	None	N/A	0.42	N/A	0.39	None
NSBD-32	Steel	Aluminum	3	15	Tee	233	N/A	0.97	N/A	0.85	None	N/A	0.62	N/A	0.56	None
NSBD-33	Steel	Aluminum	5	15	Tee	300	N/A	1.15	N/A	0.94	None	N/A	0.73	N/A	0.64	None
NSBD-34	Aluminum	Aluminum	2	0	Tee	68	N/A	0.43	N/A	0.38	None	N/A	0.22	N/A	0.20	None
NSBD-35	Aluminum	Aluminum	4	0	Tee	135	N/A	0.71	N/A	0.58	None	N/A	0.44	N/A	0.36	None
NSBD-36	Aluminum	Aluminum	5	0	Tee	169	N/A	0.82	N/A	0.66	None	N/A	0.52	N/A	0.41	None
NSBD-37	Aluminum	Aluminum	0	15	Tee	132	N/A	0.76	N/A	0.71	None	N/A	0.48	N/A	0.44	None
NSBD-38	Aluminum	Aluminum	3	15	Tee	233	N/A	1.09	N/A	0.93	0.22	N/A	0.68	N/A	0.61	None
NSBD-39	Aluminum	Aluminum	5	15	Tee	300	N/A	1.25	N/A	1.03	0.47	N/A	0.80	N/A	0.69	0.10
NSBD-40	Steel	Copper	2	0	Tee	68	N/A	0.27	N/A	0.30	None	N/A	0.11	N/A	0.12	None

HEAF simulation summary							Energetic ZOI (m)									
							15 MJ/m <sup>2</sup> target fragility					30 MJ/m <sup>2</sup> target fragility				
HEAF ID <sup>1</sup>	Duct	Bus bar material	Stiff (s)	Decay (s)	Arc location	Arc energy <sup>2</sup> (MJ)	Back	Front	Right	Above	Below	Back	Front	Right	Above	Below
NSBD-41	Steel	Copper	4	0	Tee	135	N/A	0.50	N/A	0.66	None	N/A	0.28	N/A	0.39	None
NSBD-42	Steel	Copper	5	0	Tee	169	N/A	0.66	N/A	0.82	None	N/A	0.40	N/A	0.51	None
NSBD-43	Steel	Copper	0	15	Tee	132	N/A	0.69	N/A	0.73	None	N/A	0.43	N/A	0.44	None
NSBD-44	Steel	Copper	3	15	Tee	233	N/A	0.95	N/A	1.08	None	N/A	0.61	N/A	0.70	None
NSBD-45	Steel	Copper	5	15	Tee	300	N/A	1.12	N/A	1.29	None	N/A	0.71	N/A	0.86	None
NSBD-46	Aluminum	Copper	2	0	Tee	68	N/A	0.38	N/A	0.41	None	N/A	0.20	N/A	0.21	None
NSBD-47	Aluminum	Copper	4	0	Tee	135	N/A	0.69	N/A	0.77	None	N/A	0.44	N/A	0.47	None
NSBD-48	Aluminum	Copper	5	0	Tee	169	N/A	0.83	N/A	0.92	None	N/A	0.53	N/A	0.58	None
NSBD-49	Aluminum	Copper	0	15	Tee	132	N/A	0.77	N/A	0.85	None	N/A	0.49	N/A	0.52	None
NSBD-50	Aluminum	Copper	3	15	Tee	233	N/A	1.06	N/A	1.15	None	N/A	0.67	N/A	0.75	None
NSBD-51	Aluminum	Copper	5	15	Tee	300	N/A	1.24	N/A	1.36	0.20	N/A	0.81	N/A	0.91	None
NSBD-52	Aluminum	Aluminum	2	0	Elbow	68	0.44	0.44	0.40	N/A	0.46	0.24	0.24	0.20	N/A	0.24
NSBD-53	Aluminum	Aluminum	4	0	Elbow	135	0.75	0.75	0.71	N/A	0.82	0.48	0.48	0.45	N/A	0.51
NSBD-54	Aluminum	Aluminum	5	0	Elbow	169	0.88	0.88	0.85	N/A	0.96	0.56	0.56	0.54	N/A	0.61
NSBD-55	Aluminum	Aluminum	0	15	Elbow	132	0.76	0.77	0.77	N/A	0.81	0.49	0.49	0.50	N/A	0.51
NSBD-56	Aluminum	Aluminum	3	15	Elbow	233	1.10	1.10	1.09	N/A	1.15	0.70	0.70	0.70	N/A	0.75
NSBD-57	Aluminum	Aluminum	5	15	Elbow	300	1.28	1.28	1.28	N/A	1.34	0.83	0.83	0.82	N/A	0.89

<sup>1</sup>The FDS input designator is not the same as the input file name but uniquely corresponds to a single FDS input file. Refer to Appendix B of this report for the corresponding input file nomenclature designator.

<sup>2</sup>The energy input into the FDS model may be different because a) a 0.1 s ramp is used at the beginning and end of the arc profile, b) the generator-fed arc begins at 15 s and 20,000 A rather than at 14.6 s and 20,450 A, and c) a 1 s linear transition is assumed when there is a constant (stiff) period prior to the generator-fed fault (see Appendix A).

<sup>3</sup>N/A indicates that there physically is a bus duct in the direction for that HEAF simulation. For example, the straight duct HEAF simulations have the duct running left to right in the FDS model; therefore, the right direction of the arc is inside the initiating component.

# 7

## SUMMARY AND CONCLUSIONS

---

This report documents the FDS-predicted energetic HEAF ZOIs for MV SWGR, LV SWGR, and bus ducts. The effort consists of three parts for developing estimates of the energetic ZOIs:

- The initial trials and development of input files using the CFD model Fire Dynamics Simulator (FDS) to calculate the thermal exposure to targets during the energetic phase of the HEAF.
- The validation and benchmarking of FDS against available data (testing and OE).
- The development of a large matrix of simulations that varied the HEAF duration, location, power, electrode composition, and type of equipment. The results from the simulations are discussed at a high level in Section 6 and the maximum component of the ZOI is reported for each direction at both fragility thresholds in Table 6-1 (MV SWGR), Table 6-2 (LV SWGR), and Table 6-3 (NSBDs).

### 7.1 FDS Input Summary

FDS is utilized to determine the exposure to targets from HEAFs in electrical equipment. Significant aspects of the approach are as described as:

- Simulation time – Based the post-arc results in MV SWGR experiments, the FDS simulations are run for 8 seconds after the termination of the arc fault to capture the effects of gas flows and radiating boundaries on the targets.
- Gas properties – FDS is modified to allow a user-definable upper limit for the temperature arrays. This enabled defining extended specific heat values for nitrogen, carbon dioxide, and oxygen up to 20,000 K. Material property data for copper vapor, aluminum vapor, and  $Al_2O_3$  were taken from NIST-JANAF tables [22] and Cressault et al. [23, 24].
- Thermal radiation – A power law radiant fraction is developed using data from Cressault et al. [26]. The FDS solution resolution is increased from a default 100 solid angles to 500 solid angles for the unit sphere used to solve the radiation transport equations.
- Computational grid – A 0.0762 m grid is used for the MV SWGR and LV SWGR models and a 0.02 m grid is used for the NSBD models. For all geometries, the grid is extended 1.5 to 2 m from the face of the equipment.
- Combustion – Combustion is modeled for the oxidation of metal vapor (see Section 3.7.2 for discussion of vapor addition). The heats of combustion are taken from NIST-JANAF data [22].

- Enclosure breach – The metal switchgear and NSBD boundaries are modeled using a phase change material. This is a material with a single-step reaction that occurs at a threshold temperature (i.e., the melting point). A cell obstruction is removed when the metal temperature reaches the melting point, thereby creating an opening in the enclosure boundary.
- Electrode mass loss – The electrode mass loss rate is determined from empirical correlations of the input current and the electrode material developed by Stanback [28]. These correlations are applied to LV SWGR and NSBD HEAFs. The mass loss rate correlation for MV SWGR is developed from the 2018 MV SWGR test data [6].
- Particle oxidation – Particle oxidation is incorporated into the model for droplet sizes in the 2 - 15  $\mu\text{m}$  range. Smaller diameter particles are shown to represent a negligible electrode mass and larger droplets do not affect the energetic ZOI. The droplets are injected into the FDS model as particles with a specified pyrolysis rate that corresponded to the oxidation fraction observed.
- Arc power – Arc power profiles are developed for MV SWGR and NSBDs with a total energy ranging from 34 – 300 MJ. Arc energies profiles for LV SWGR range from 28 – 90 MJ, with the 90 MJ arc representative of FEDB 50935 [12].
- Input file generation – Input files are generated using a Python script and template to minimize user input errors.

This approach required several modifications to FDS to accommodate the high temperatures involved. These changes were incorporated into several interim FDS versions, with the final simulations performed using FDS, Version 6.7.6. Subsequent FDS versions have retained the modifications required for this effort.

## 7.2 FDS HEAF Validation Summary

The validation of FDS for HEAF is based on the following cases:

- The 2019 MV and LV Open Box tests [4]
- The 2018 MV SWGR tests [6]
- A LV SWGR event (FEDB 50935)
- A full-scale test replicating a NSBD event (FEDB 51764)
- A HEAF event at a NSBD elbow (FEDB 51765)

The 4 s 2018 MV SWGR experiments are considered in the validation effort to develop the overall model relative standard deviation ( $\sigma$ ) and bias ( $\delta$ ) applied to the predicted exposure because the longer post-breach exposure provides a better indication of the model exposure prediction. The resulting relative standard deviation and bias are based on the 4 s switchgear tests given these experiments resulting in a breach of the top and sides of the enclosure, making leakage around the gaps less important to the total exposure. The resulting relative standard deviation and bias as determined from these FDS predictions and experimental results are 0.71 and 0.596, respectively. The bias is used to adjust all FDS outputs to align with the mean and the standard deviation is used to show the 5<sup>th</sup> and 95<sup>th</sup> percent confidence intervals.

### 7.3 FDS Results

The energetic ZOIs predicted by FDS are summarized in Table 6-1 for MV SWGR, Table 6-2 for LV SWGR, and Table 6-3 for NSBDs. Summaries of the ZOI ranges predicted by FDS are provided in Table 7-1 for MV SWGR, Table 7-2 for LV SWGR, and Table 7-3 for NSBDs.

**Table 7-1**  
Summary of MV SWGR energetic ZOI ranges

Switchgear enclosure face	Energetic ZOI (m) for a 15 MJ/m <sup>2</sup> target fragility	Energetic ZOI (m) for a 30 MJ/m <sup>2</sup> target fragility
Back	0 – 1.13	0 – 0.76
Left	0 – 1.24	0 – 0.92
Right	0 – 1.24	0 – 0.92
Top	0 – 1.01	0 – 0.58
Front	0 – 1.31	0 – 0.97

**Table 7-2**  
Summary of LV SWGR energetic ZOI ranges

Switchgear enclosure face	Energetic ZOI (m) for a 15 MJ/m <sup>2</sup> target fragility	Energetic ZOI (m) for a 30 MJ/m <sup>2</sup> target fragility
Back	0 – 0.17	0
Left	0	0
Right	0 – 0.9	0 – 0.59
Top	0 – 0.84	0 – 0.53
Front	0	0

**Table 7-3**  
Summary of NSBD energetic ZOI ranges

NSBD enclosure face	Energetic ZOI (m) for a 15 MJ/m <sup>2</sup> target fragility	Energetic ZOI (m) for a 30 MJ/m <sup>2</sup> target fragility
Back	0 – 1.32	0 – 0.86
Front	0 – 1.32	0 – 0.86
Right	0.41 – 1.31	0.21 – 0.84
Above	0 – 1.39	0 – 0.93
Below	0 – 1.37	0 – 0.92

## 7.4 Significant HEAF Modeling Insights

The significant modeling insights developed during this effort are summarized as:

- There is no significant difference between the energetic ZOIs from HEAFs with aluminum electrode and HEAFs with copper electrodes for all equipment classes. The ZOIs for each material are within the 95<sup>th</sup> percentile of the model uncertainty band as computed from the energetic ZOI predictions for either material.
- The dominant parameter affecting the energetic ZOIs in MV SWGR is the total arc energy.
- A secondary parameter affecting the energetic ZOIs in MV SWGR is the circuit breaker orientation (vertical-lift circuit breaker style or horizontal draw-out circuit breaker style).
  - The side energetic ZOIs are lower for vertical-lift circuit breaker style switchgear as compared to horizontal draw-out circuit breaker style switchgear.
  - For vertical-lift circuit breaker style switchgear in the supply configuration, there is no vertical (top) energetic ZOI component.
  - The load configuration vertical-lift circuit breaker style switchgear and the horizontal draw-out style circuit breaker switchgear have comparable top energetic ZOIs.
- The energetic ZOIs for LV SWGR are smaller than those recommended in Appendix M of NUREG/CR-6850 [1].
- The energetic ZOIs for MV SWGR and bus ducts are smaller than the existing guidance (NUREG/CR-6850 Supplement 1) for some configurations and directions, but larger for others.
- The composition of bus duct housing (steel versus aluminum) has a significant impact on the energetic ZOIs for NSBDs. HEAFs in aluminum bus ducts have energetic ZOIs that are, on average, 0.15 m larger than those in steel bus ducts.
- The energetic ZOIs for LV SWGR and MV SWGR are sensitive to the equipment geometry and circuit breaker orientation. However, the energetic ZOIs for bus ducts, with comparatively simple geometries, are not sensitive.

# 8

## REFERENCES

---

1. *EPRI/NRC-RES Fire PRA Methodology for Nuclear Power Facilities, Volume 2: Detailed Methodology*. Electric Power Research Institute (EPRI), Palo Alto, CA and U.S. Nuclear Regulatory Commission, Washington, DC: September 2005. EPRI 1011989 and NUREG/CR-6850.
2. *EPRI/NRC-RES Fire Probabilistic Risk Assessment Methods Enhancements*. EPRI, Palo Alto, CA and U.S. Nuclear Regulatory Commission, Washington, DC: September 2010. EPRI 1019259 and NUREG/CR-6850 Supplement 1.
3. *Survey and Analysis of U.S. Nuclear Industry Relative to High Energy Arcing Faults in the Presence of Aluminum*. EPRI, Palo Alto, CA: May 2021. EPRI 3002020692.
4. *Report on High Energy Arcing Fault Experiments: Experimental Results from Open Box Enclosures*. U.S. Nuclear Regulatory Commission, Washington DC, National Institute of Standards and Technology, Gaithersburg, MD, and Sandia National Laboratories, Albuquerque, NM. December 2021. Research Information Letter (RIL) 2021-18, NIST TN 2198, and SAND2021-16075 R.
5. *Report on High Energy Arcing Fault Experiments: Experimental Results from Low Voltage Switchgear Enclosures*. U.S. Nuclear Regulatory Commission, Washington DC, and National Institute of Standards and Technology, Gaithersburg, MD. November 2021. RIL 2021-17 and NIST TN 2197.
6. *Report on High Energy Arcing Fault Experiments: Experimental Results from Medium Voltage Electrical Enclosures*. U.S. Nuclear Regulatory Commission, Washington DC, National Institute of Standards and Technology, Gaithersburg, MD, and Sandia National Laboratories, Albuquerque, NM. November 2021. RIL 2021-10, NIST TN 2188, and SAND2021-12049 R.
7. *Report on the Testing Phase (2014-2016) of the High Energy Arcing Fault Events (HEAF) Project: Experimental Results from the International Energy Arcing Fault Research Programme*. Nuclear Energy Agency (NEA). Organisation for Economic Co-operation and Development. Paris, France. May 2017. NEA/CSNI/R(2017)7.
8. *NUREG/IA-0470, Volume 1, International Agreement Report, Nuclear Regulatory Authority Experimental Program to Characterize and Understand High Energy Arcing Fault (HEAF) Phenomena*, Regulatory Standard and Development Department, Secretariat of Nuclear Regulatory Authority (S/NRA/R), Tokyo, Japan, U.S. Nuclear Regulatory Commission, Washington, DC 20555-0001, April 2016.
9. *NUREG/IA-0470, Volume 2, International Agreement Report, Nuclear Regulatory Authority Experimental Program to Characterize and Understand High Energy Arcing Fault (HEAF) Phenomena, Basic Arc Test Experimental Data*, Regulatory Standard and Development Department, Secretariat of Nuclear Regulatory Authority (S/NRA/R), Tokyo, Japan, U.S. Nuclear Regulatory Commission, Washington, DC 20555-0001, October, 2021.

---

References

10. *Target Fragilities for Equipment Vulnerable to High Energy Arcing Faults*. Electric Power Research Institute (EPRI), Palo Alto, CA and U.S. Nuclear Regulatory Commission, Washington, DC: RIL 2022-01 / EPRI 3002023400.
11. *The Updated Fire Events Database: Description of Content and Fire Event Classification Guidance*. EPRI. Palo Alto, CA: 2013. 1025284.
12. *Fire Events Database Update for the Period 2010–2014: Revision 1*. EPRI, Palo Alto, CA: 2016. 3002005302.
13. *Fire Dynamics Simulator User's Guide*, NIST Special Publication 1019 Sixth Edition, DOI: 10.6028/NIST.SP.1019, November 2021.
14. *Fire Dynamics Simulator Technical Reference Guide, Volume 1: Mathematical Model*, NIST Special Publication 1018-1 Sixth Edition, DOI: 10.6028/NIST.SP.1018, November 2021.
15. *Fire Dynamics Simulator Technical Reference Guide, Volume 2: Verification*, NIST Special Publication 1018-1 Sixth Edition, DOI: 10.6028/NIST.SP.1018, November 2021.
16. *Fire Dynamics Simulator Technical Reference Guide, Volume 3: Validation*, NIST Special Publication 1018-1 Sixth Edition, DOI: 10.6028/NIST.SP.1018, November 2021.
17. *Fire Dynamics Simulator Technical Reference Guide, Volume 4: Software Quality Assurance*, NIST Special Publication 1018-1 Sixth Edition, DOI: 10.6028/NIST.SP.1018, November 2021.
18. NRC Information Notice 2018-09: *Electrical Arc Flash Caused by Foreign Material Damages Fire Door*, ADAMS Accession No. ML18150A146, U.S. Nuclear Regulatory Commission, Washington, DC 20555-0001, August 2018.
19. NEA/CSNI/R(2013)6, *OECD Fire Project – Topical Report No. 1 – Analysis of High Energy Arcing Fault (HEAF) Fire Events*, Organisation for Economic Co-operation and Development and Nuclear Energy Agency, 2013.
20. *Verification and Validation of Selected Fire Models for Nuclear Power Plant Applications, Supplement 1*. EPRI, Palo Alto, CA, and U.S. Nuclear Regulatory Commission, Washington, DC, 2016. NUREG-1824 Supplement 1 and EPRI 3002002182.
21. *NASA Glenn Coefficients for Calculating Thermodynamic Properties of Individual Species*, NASA/TP-2002-211556, National Aeronautics and Space Administration, Glenn Research Center, Cleveland, OH, September 2002.
22. *NIST-JANAF Thermochemical Tables*, NIST Standard Reference Database 13, National Institute of Standards and Technology, Gaithersburg, MD, 1998. DOI: 10/18434/T42S31.
23. Cressault, Y., Hannachi, R., et. Al, "Influence of metallic vapors on the properties of air thermal plasmas," *Plasma Sources Sci. Technol.*, 17 (2008), DOI: 10.1088/0963-0252/17/3/035016.
24. Cressault, Y., Gleizes, A., and Riquel, G., "Properties of air-aluminum thermal plasmas," *J. Phys. D: Appl Phys*, 45 (2012), DOI: 10.1088/0022-3727/45/26/265202.
25. W. Grosshandle, *RadCal: A Narrow Band Model for Radiation Calculations in a Combustion Environment*, NIST Technical Note 1402, National Institute of Standards and Technology, Gaithersburg, MD, 1993.
26. Cressault, Y., Bauchire, J., Hong, D., et. Al, "Radiation of long and high power arcs," *J. Phys. D: Appl. Phys.*, 48 (2015), DOI: 10.1088/0022-3727/48/41/415201.

27. Mimura, K., Lim, J., Isshiki, M., Zhu, Y., and Jiang, Q., “Brief Review of Oxidation Kinetics of Copper at 350°C to 1050°C, *Metallurgical and Materials Transactions*, 37, p. 1231-1237 (2006), DOI: 10.1007/s11661-006-1074-y.
28. Stanback, H., “Predicting Damage from 277-V Single Phase to Ground Arcing Faults,” *IEEE Transactions on Industry Applications*, IA-13:4 (1977), DOI:10.1109/TIA.1977.4503412.
29. Siemroth, P., Laux, M., et al., “Diameter and Velocities of Droplets Emitted from the Cu Cathode of a Vacuum Arc,” *IEEE Transactions on Plasma Science*, 47:8 (2019), DOI: 10.1109/TPS.2019.2912518.
30. McGrattan, K. and Toman, B., “Quantifying the Predictive Uncertainty of Complex Numerical Models,” *Metrologia*, 48, p 173-180, doi:10.1088/0026-1394/48/011, 2011.
31. *Verification and Validation of Selected Fire Models for Nuclear Power Plant Applications, Volume 2: Experimental Uncertainty*, EPRI, Palo Alto, CA, and U.S. Nuclear Regulatory Commission, Washington, DC, 2007. NUREG-1824 Volume 1 and EPRI 1011999.
32. *Nuclear Power Plant Fire Modeling Analysis Guidelines (NPP FIRE MAG)*, EPRI, Palo Alto, CA and U.S. Nuclear Regulatory Commission, Washington, DC: December 2012. EPRI 1023259 and NUREG-1934.
33. *High Energy Arcing Fault Operating Experience Panel Discussion*. Public Workshop with NEI, EPRI, and Industry, U. S. NRC, Washington, D.C., October 20, 2021. ML21291A180.
34. *High Energy Arcing Fault (HEAF) Operating Experience (Duke Energy)*. Rishel, R., Public Workshop with NEI, EPRI, and Industry, U. S. NRC, Washington, D.C., October 20, 2021. ML21293A009.
35. *Kerite Analysis in Thermal Environment of FIRE (KATE-Fire): Test Results*. Sandia National Laboratories, Albuquerque, NM and U.S. Nuclear Regulatory Commission, Washington, DC, 2016. NUREG/CR-7102 and SAND2011-6548P.
36. *Tools for the Simulation of the Effects of the Internal Arc in Transmission and Distribution Switchgear*. CIGRE, ISBN: 978-2-85873-303-3, 2014. CIGRE Standard 602.
37. *Predicting High Energy Arcing Fault Zones of Influence for Aluminum Using a Modified Arc Flash Model – Evaluation of a Modified Model Bias, Uncertainty, Parameter Sensitivity, and Zone of Influence Estimation*. Draft for Public Comment, (ADAMS Accession No. ML22095A236) U.S. Nuclear Regulatory Commission, Washington, D.C. 20555-0001, April, 2022.
38. *Nuclear Station Electrical Distribution Systems and High-Energy Arcing Fault Events*. EPRI, Palo Alto, CA, July, 2019. Document 3002015992.
39. *Operating Experience Assessment Energetic Faults in 4.16 to 13.8 kV Switchgear and Bus Ducts That Caused Fires in Nuclear Power Plants 1986-2001*. February, 2002. Adam Package ML021290364.
40. *IEEE Guide for Liquid-Immersed Transformers Through-Fault-Current Duration*. Institute of Electrical and Electronics Engineers (IEEE), 1985. IEEE Standard C57.109-1985.

---

References

41. Madjidian, D. and Wamundson, M., “Technical Services Related to Decrement Curve Testing at High Power Electrical Testing Facility Task 1: Energy Delivery Simulation Modeling,” Power System Analysis, DNV GL, Sweden, April 2, 2020.
42. *IEEE Guide for Performing Arc-Flash Hazard Calculations*. IEEE, 2018. IEEE Standard 1584-2018.
43. Babrauskas, V. and Wichman, I., “Fusing of Wires by Electrical Current,” *Fire and Materials 12<sup>th</sup> International Conference and Exhibition*, p. 769 – 778, 2011.
44. NUREG-2218, *An International Phenomena Identification and Ranking Table (PIRT) Expert Elicitation for High Energy Arcing Faults (HEAFs)*, U.S. Nuclear Regulatory Commission, Washington, DC 20555-0001, January 2018.
45. NRC Inspection Report: *Turkey Point Nuclear Generating Station – NRC Reactive Inspection Report 05000250/2017008 and 05000251/2017008*, U.S. Nuclear Regulatory Commission, Washington, DC 20555-0001, May 2017.
46. Pfeiffer, J., Arc Flash Calculations, An Important Tool in Fire & Electrical Accident Investigations, Fire and Arson Investigator, firearson.com, July 2005.

# A

## ARC POWER AND PROFILE

---

This appendix details the arc power profiles used to model the exposure from HEAFs. The arc power profiles are largely dependent on where the fault occurs in the electrical distribution system and the characteristics of the electrical protection system. The arc power can be determined from the arc voltage and arc current. The arc power profile represents the arc behavior over time as observed in HEAF events.

### A.1 Arc Voltage

The arc voltage is a parameter used to determine the arc energy. The arc voltage is the voltage drop across an arc between the arc roots. The arc voltage depends on several factors, including the electrode configuration, spacing, and other variables. An arc is purely resistive and, as such, it depends on the resistivity and the current, not necessarily the system voltage. The arc voltage is one of the inputs in defining the arc energy for the FDS model.

The arc voltage cannot be obtained directly from HEAF OE [11, 12] and is instead determined through testing or predicted through modeling. The U.S. NRC analyzed existing test data from full-scale tests and evaluated it against predicted values from a model based on CIGRE 602 [28] as described in Appendix A of ML22095A236 [37]. The analysis resulted in an estimated value of 650 V<sub>L-L</sub> for medium-voltage equipment and 375 V<sub>L-L</sub> for low-voltage equipment.

### A.2 Medium Voltage Arc Energy Profiles

The arc energy profiles considered for medium-voltage switchgear and non-segregated bus ducts are derived from HEAF OE [11, 12] and through a review of U.S. NPP electrical distributions systems [38]. The arc energy profile is broken into two types depending on where the HEAF occurs in the electrical distribution system (EDS) and what the ultimate power source is (generator or offsite power). The profiles are as described below.

#### Constant-Current Arcing Fault (stiff-source)

Constant-current arcing faults are ascribed to classical short circuits that are fed by an infinite source and limited by the impedance of the upstream transformer(s). These faults are of constant current until interrupted by the EDS protection scheme (e.g., differential (instantaneous) or time overcurrent relays), which define the duration of constant-current arcing faults.

For conservatism, the fault location in electrical studies is modeled as a zero-impedance fault (commonly referred to as “bolted” fault). However, not all faults are zero impedance and are referred to as an “arcing” fault. For medium-voltage systems, the fault current magnitude is typically 85% of a “bolted” fault. Nonetheless, they are still considered a constant-current arcing fault “stiff” source for the duration of the fault.

Instantaneous protection systems will limit fault duration such that the energy will not rise to the level of a HEAF (typically limited to several cycles). On the other hand, depending on fault clearing time of time overcurrent protection system, the let-through energy can achieve that of a HEAF (typically one or more seconds depending on the equipment).

**Generator-fed Faults (decaying source)**

A generator-fed fault is a type of fault that is not modeled in classical electrical protection and coordination studies and arose out of research and investigation into several medium-voltage HEAF OE events exhibiting similar characteristics. With generator-fed faults, the generator protection system will trip the switchyard circuit breakers, eliminating fault current back-feeding from the switchyard through the generator step-up (GSU) transformer. In addition, the main generator excitation field circuit breaker opens to isolate the voltage regulator/exciter from feeding the generator field (rotor). Nonetheless, some residual energy remains in the rotating generator/rotor pair resulting in an exponential generator voltage and current decay over time. With no other protective device to isolate the fault, this decaying current can feed a fault through the unit auxiliary transformer (UAT) until the rotor field voltage collapses and the arcing fault extinguishes. This is referred to as a “decaying” source or fault.

Table A-1 identifies the medium-voltage HEAF OE events and indicates whether the fault was a generator-fed fault.

**Table A-1  
Medium voltage HEAF events with fault currents**

Event ID	Date	HEAF location	Generator-fed fault	Reported fault current
51764	1/17/2017	NSBD	No	13 kA
50910	3/28/2010	SWGR	No	28 kA
51291	12/9/2013	NSBD	Yes	Unknown
50909	3/7/2010	NSBD	No	Unknown
10584	7/27/2008	NSBD	No	Unknown
732	7/6/1988	SWGR	No	32 kA
162	8/5/2009	NSBD	Yes	Unknown
100	05/15/2000	NSBD	Yes	Unknown
678	3/2/1988	NSBD	Yes	Unknown
922	7/10/1987	NSBD	Yes	Unknown
575	3/19/1987	NSBD	Yes	Unknown
112	8/3/2001	SWGR	Yes	Unknown
106	2/3/2001	SWGR	Yes	Unknown
74	6/10/1995	SWGR	Yes	28 kA
947	1/3/1989	SWGR	Yes	Unknown

### **A.2.1 Medium Voltage Constant-Current Arc Profile**

The energy profile of stiff-source arc faults is simply a constant arc power during the arcing fault. The arc power is the arc current multiplied by the line-to-line arc voltage and  $\sqrt{3}$ . This indicates that both the expected arc current and fault duration are required to identify the range of arc power modeled. The HEAF events in Table A-1 are reviewed to document the arcing fault currents, if available. The review shows that for the HEAF events occurring in medium-voltage equipment (bus ducts and switchgear), the reported arcing faults were generally in the expected range (85% of typical bolted fault currents of medium-voltage). An average value between the highest fault current of 32 kA and the mid-range of 28 kA is selected. 13 kA is excluded as it is significantly lower than that typically associated with medium-voltage available fault current. Therefore, a 30 kA fault current is selected to represent arcing faults in the MV portion of the EDS.

The stiff-source profile maintains the arcing fault current at a constant value for a set duration. This fault emulates a three-phase bolted fault that persists until cleared by an overcurrent protective device. Five events in Table A-1 fit this profile, identified with a “No” in the “Generator-fed fault” column. As these types of HEAF events generally transition rapidly into three-phase bolted faults, it is expected that the available overcurrent protective devices will trip to isolate the fault. Typically, if the overcurrent protective device is an instantaneous differential or overcurrent trip, the event will not rise to the energy level of a HEAF. In order for these types of constant-current arc faults to lead to a HEAF, there must either be a lack of instantaneous protection or a failure of instantaneous overcurrent protection. The lack or failure of the instantaneous protection requires the time overcurrent protection to clear the fault. The primary purpose of time overcurrent relays is to protect the transformer or switchgear from thermal damage due to a sustained through-fault current condition. The backup time overcurrent fault clearing times for faults fed through the UAT and the offsite power transformers (e.g., SAT) for U.S. NPPs were collected in an EPRI survey [3]. These fault clearing times are used for both the SAT (to establish the range of times for the constant-current arc profile) and the UAT (to establish the time at constant-current prior to the generator-fed decay portion of the profile). For both the UAT and SAT, the FCT range was fractions of a second to 5 seconds. The upper FCT of 5 s aligns with IEEE Std C57.109 [39] guidelines in limiting of through-fault current duration to approximately 4 to 5 s for auxiliary power transformers.

To confirm that FCTs up to 5 s are valid for arcing faults that may rely on the time overcurrent settings between supply and feeder circuit breakers and that occur further downstream of the first medium-voltage switchgear, coordination calculations and time current characteristics (TCCs) from a sample set of U.S. NPPs are reviewed. The maximum FCT identified is 4.3 s, with the majority centered around 2 s. Five seconds is determined as the high limit for both medium-voltage switchgear and non-segregated bus ducts for stiff-source faults.

On the lower end of the fault clearing range, the 2018 MV SWGR testing [6] along with review of HEAF events show that for arcing faults under 2 s, the energy is primarily contained in the switchgear. The breaching of the steel switchgear cabinet is observed to take approximately  $\frac{1}{2}$  to 1 s, which limits the external target exposure. Therefore, a minimum threshold of 2 s is utilized for medium-voltage switchgear. For bus ducts, a lower threshold of 1 s is utilized to account for the faster breaching time that bus ducts with aluminum enclosures have as compared to bus ducts with steel enclosures.

In summary, for medium-voltage switchgear, the stiff-source considered is 2 to 5 s. For non-segregated bus ducts, the range is 1 to 5 s.

### A.2.2 Arc Energy Profile of the Generator-fed Fault

There is limited data on how generator-fed fault current decays over the event duration from the HEAF OE. The potential range of durations for the generator to coast down to the point where an arc cannot be sustained was historically estimated as 4 - 8 s [40]. However, a recent generator-fed fault HEAF event (occurred December 2020) lasted approximately 15 s. Fault current data from the HEAF event consisted primarily of the fault current at the UAT secondary side (via the current transformer (CT) currents) that fed the fault, at various times during the arcing fault (see Table A-2). The data from this event is used as the basis for determining the decaying generator-fed fault current over time as, specifically:

- The primary side of the CT fault current is calculated utilizing a CT turns ratio of 400.
- The secondary fault current of the UAT is calculated utilizing the ratio of the 22 kV primary to 6.9 kV secondary.
- The power is then calculated based on an assumed arc voltage of 650 V<sub>L-L</sub> (as discussed Section A.1) multiplied by the secondary fault current and  $\sqrt{3}$ .

**Table A-2**  
**Fault currents at various times for a generator-fed HEAF event (December 2020)**

Time	Primary fault current (CT secondary) (A)	Primary fault current (CT primary) (A)	Secondary fault current (A)	Power ( $\sqrt{3} \cdot I \cdot V_{L-L}$ ) (MW)
0.095	16	6,400	20,348	22.91
5.5	7.1	2,840	9,029	10.17
5.55	6.6	2,640	8,394	9.45
5.6	6.8	2,720	8,648	9.74
5.65	6.63	2,652	8,432	9.49
14.35	1.72	688	2,187	2.46
14.4	1.62	648	2,060	2.32
14.45	1.7	680	2,162	2.43
14.5	1.8	720	2,289	2.58
14.55	1.68	672	2,137	2.41
14.6	1.84	736	2,340	2.63

The arcing fault current and arc power plotted over time and exponential curve fit is shown in Figure A-1 and Figure A-2. Integration of the power curve in Figure A-2 over the arc time interval,  $\int_{0.095}^{14.6} 23.019e^{-0.154t} dt$ , results in a total arc energy of 131.5  $\approx$  132 MJ.

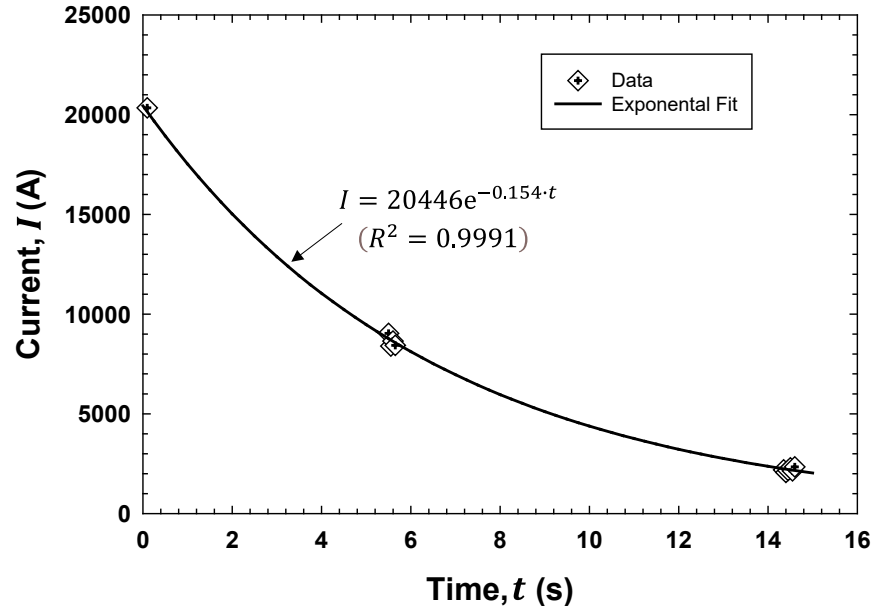


**Figure A-1**  
Plot of the arc current for a generator-fed HEAF event (December 2020)

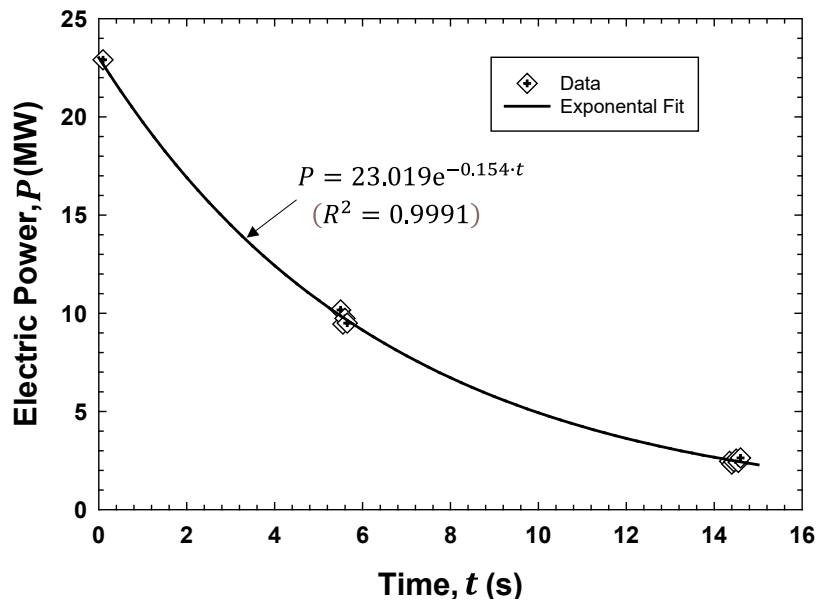


**Figure A-2**  
Plot of the arc power for a generator-fed HEAF event (December 2020)

This exponential profile of the actual current compared favorably to the theoretical profile developed by Madjidian et al. [41] for a typical generator-fed fault. The profile comparison between the actual HEAF event and theoretical curve provided confidence that the actual decaying current can be used to represent all generator-fed faults regardless of the site-specific electrical distribution characteristics. This assumption is necessary due to the complex nature of generator-fed faults. Site-specific prediction of the decaying fault current is extremely complex and would require additional electrical analysis. The decaying current curve and arc energy of 132 MJ is used in FDS to simulate generator-fed HEAFs.

Generator-fed HEAF events may also be preceded by a constant-current “stiff” portion that simulates the delay time until overcurrent protective devices sense the fault and trip the generator for backup transformer protection. The range of the constant-current portion is 0 to 5 s as discussed in Section A.2.1. The profile consists of constant power for the first 0 to 5 s, then transitions to a “decaying” power for the next 15 s. Figure A-3 through Figure A-5 show the power profiles modeled in FDS for generator-fed HEAFs.

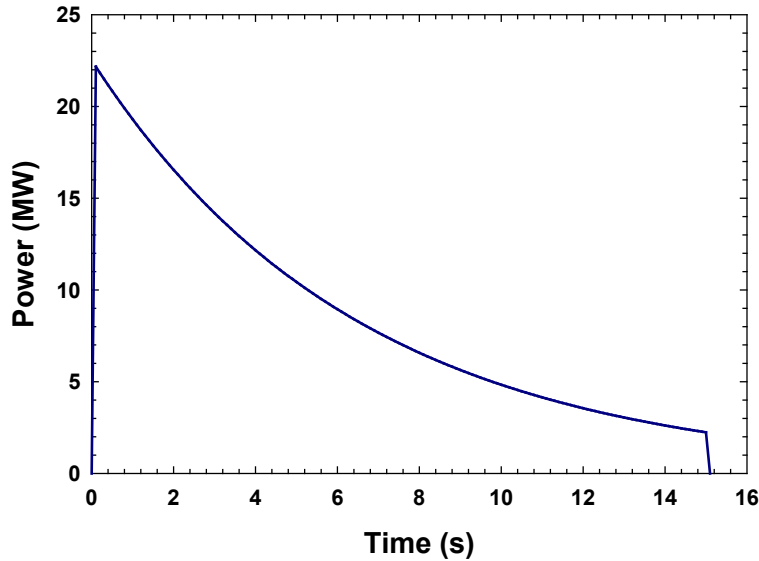


**Figure A-3**  
Power curve for a 0 s stiff and 15 s decay HEAF

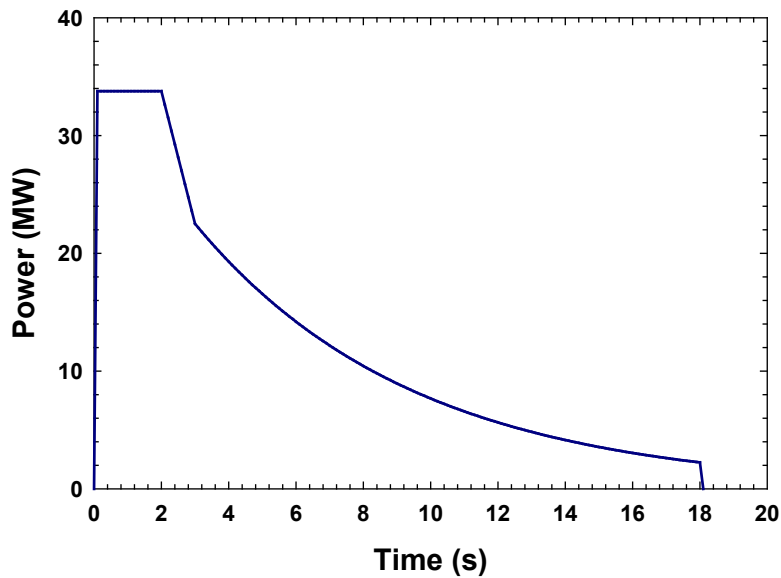


**Figure A-4**  
Power curve for a 3 s stiff and 15 s decay HEAF

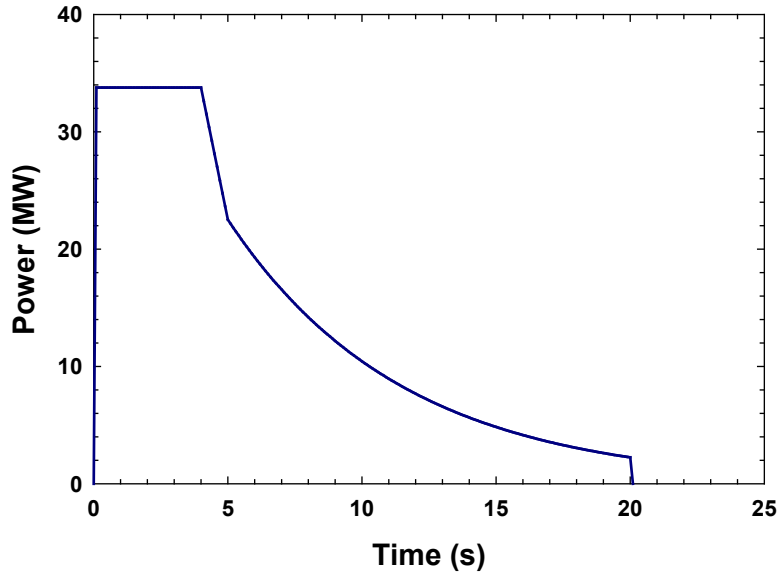


**Figure A-5**  
Power curve for a 5 s stiff and 15 s decay HEAF

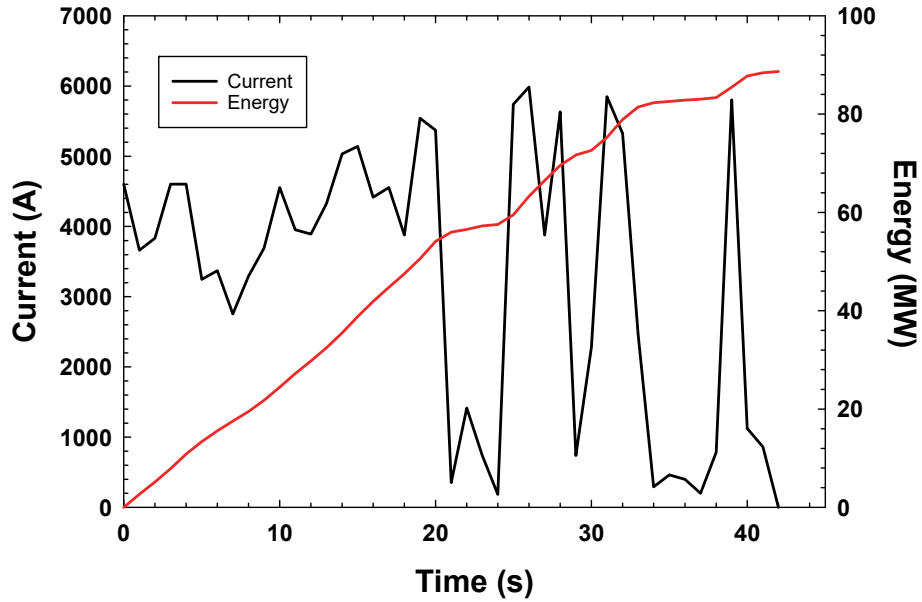
### A.3 Arc Power Profiles for Low Voltage Switchgear

Table A-3 shows the HEAF events in low-voltage equipment (bus ducts and switchgear). Only FEDB 50935 reported the actual arcing fault current, a single-phase arcing fault that lasted for approximately 41 s. This fault current fluctuated significantly over the duration of the event as shown in Figure A-6.

**Table A-3**  
Low voltage HEAF events with fault currents

Event ID	Date	HEAF location	Fault current
434	8/2/1984	SWGR	Unknown
50935	6/7/2011	SWGR	Varied between 200 to 6,000 A
50926	2/12/2011	NSBD	Unknown

Analysis of data from FEDB 50935 resulted in determining the approximate arc power on the secondary side of the transformer feeding the fault as shown in Figure A-6. The current is derived from the power assuming an arc voltage of 375 V<sub>L-L</sub> (as discussed in Section A.1). The event shows two phases of variable current, with the first phase having a higher average overall current, and the second phase current varying from a few hundred amps (almost self-extinguishing) to 6 kA. This resulted in an overall arcing energy of approximately 90 MJ.



**Figure A-6**  
**FEDB 50935 arc power profile**

Figure A-7 shows in red the values used to approximate the current profile in the FDS simulations. This approximation is necessary in order to minimize the complexity of the FDS input. The distinct phases of the event are captured by maintaining an average current observed over the first 20 s (approximately 4.67 kA) and then an average current observed over the next 21 s (about 2.20 kA). This is shown in Figure A-7.

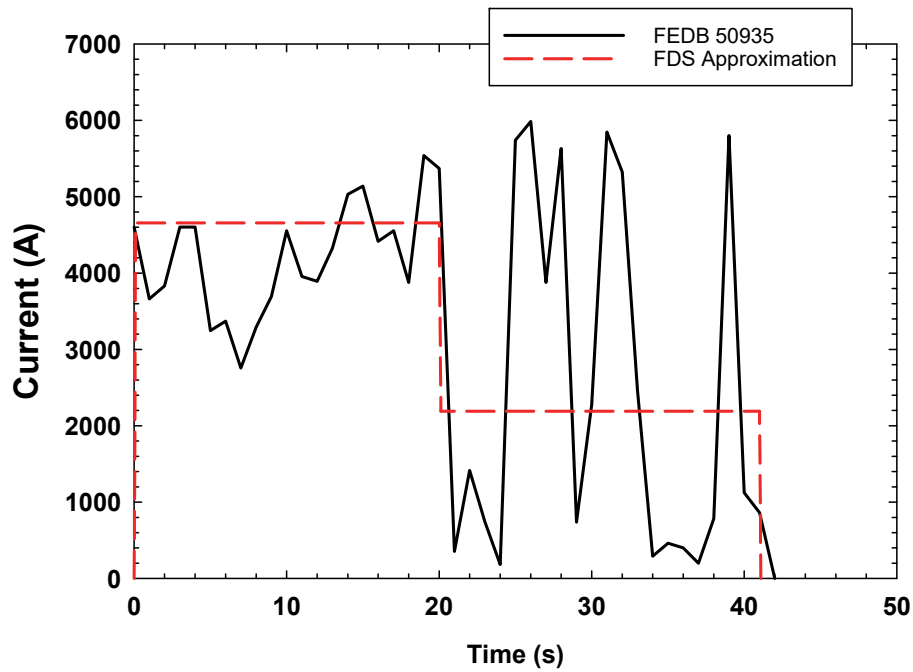


**Figure A-7**  
**Low voltage HEAF current profile**

The profile shown in Figure A-7 represents a long-duration fault at a low fault current. The potential for a higher fault current representing a bolted fault (similar to medium-voltage switchgear HEAF events) is investigated to provide confidence that using the arc energy from FEDB 50935 is appropriate surrogate for all LV SWGR HEAFs.

To determine if 90 MJ total arc energy is appropriate for the higher fault current cases, several protection and coordination calculations for various load center transformer sizes from U.S. nuclear plants are reviewed. The system voltage was 480 V<sub>ac</sub> and in calculating the arcing fault energy, an arc voltage of 375 V<sub>L-L</sub> is assumed. Time current characteristic (TCC) curves from the protection coordination calculations are reviewed to determine the expected fault clearing time of the load center transformer's primary side (MV SWGR) circuit breaker time overcurrent (51) relay to clear a fault on the 480 V<sub>ac</sub> load center assuming the load center bus supply circuit breaker failed (stuck closed). This is performed for both the zero-impedance (bolted fault) and the lower bound arcing fault current. The lower bound arcing fault current is calculated following the methodology of IEEE Standard 1584-2018 [42] for determining the minimum arcing current. Table A-4 documents the expected energy given FCTs at the available arcing fault current and minimum fault current.

**Table A-4**  
**Sampling of low-voltage fault clearing times and fault energies**

Transformer size (kVA)	Available fault current (kA)	FCT at bolted fault (s)	Energy at bolted fault (MJ)	Lower bound arcing fault current (IEEE) (kA)	FCT at lower bound arcing fault (s)	Energy at lower bound arcing fault (MJ)
2,000	50	0.6	18	27	0.9	15
1,500	46	0.5	14	25	0.6	10
2,500	46	0.5	16	25	1.2	20
1,500	46	0.5	16	25	0.9	14
1,000	15	1.6	16	10	2.2	14
300	8	2.4	12	5	4.5	14
1,000	15	1.4	14	10	1.7	11
1,000	15	1.6	16	10	2.0	12
300	8	2.4	12	5	5.0	16
1,000	14	1.4	13	9	1.9	11
1,000	15	1.4	14	10	1.9	12
1,000	15	2.0	20	10	2.6	16
1,000	15	1.3	13	10	2.0	12
1,000	15	1.3	13	10	1.7	11
300	8	2.3	11	5	4.2	13
300	8	2.1	10	5	5.0	15

**Table A-1 (continued)**  
**Sampling of low-voltage fault clearing times and fault energies**

Transformer size (kVA)	Available fault current (kA)	FCT at bolted fault (s)	Energy at bolted fault (MJ)	Lower bound arcing fault current (IEEE) (kA)	FCT at lower bound arcing fault (s)	Energy at lower bound arcing fault (MJ)
1,000	15	1.8	18	10	2.4	15
1,000	15	2.5	24	10	3.6	22
300	8	1.9	10	5	2.5	8
1,250	28	2.5	45	17	5.0	56
1,500	35	1.7	38	21	3.6	49
500	11	1.3	10	7	3.0	13
300	8	0.4	2	5	0.9	3
500	15	0.3	3	9	0.5	3
2,500	52	2.7	91	27	7.5	133
1,500	32	1.9	39	19	3.7	46
1,500	32	0.4	8	19	1.0	13
500	11	0.5	2	7	1.5	7
750	16	0.5	5	10	3.0	19
500	11	0.5	3	7	1.5	7
500	6	0.1	0	4	0.4	1
1,000	15	1.9	19	10	2.6	17
1,500	22	1.6	23	14	2.3	21
1,500	21	1.7	22	13	2.4	20
1,500	21	1.6	22	14	2.6	23
1,500	20	1.7	22	13	3.2	26
1,500	21	1.2	17	14	3.5	31
1,500	21	1.2	17	13	3.5	30
750	13	1.7	14	8	2.4	13

From the results of Table A-4, only one instance of a lower bound fault current is not bounded by 90 MJ. In all other cases, the 90 MJ arc energy provides significant margin and is considered representative for LV SWGR.

In the FDS simulations, 90 MJ is modeled as a fixed power of 3.02 MW over the first 20 s followed by 21 s of 1.42 MW as shown in Figure A-8.

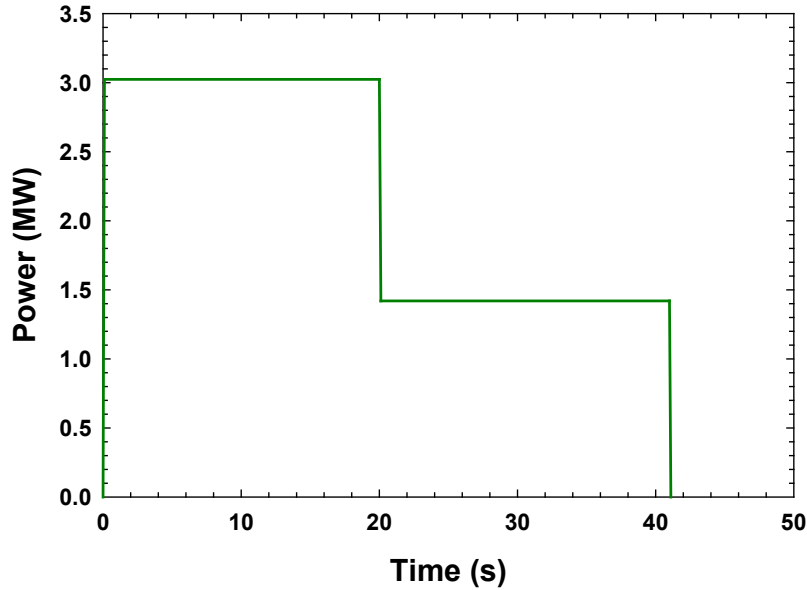


**Figure A-8**  
Low voltage HEAF power profile

#### A.4 Implementation of the Arc Power Profiles in the FDS Model

The arc power profiles are implemented in FDS as a time-dependent volumetric energy source. To avoid rapid transitions in the energy source, the arc power is defined in the FDS model with the following attributes:

- The arc power linearly increases from zero to the peak value over a 0.1 s interval. This applies to all arc power profiles. Similarly, the arc power decreases from a non-zero value to zero over a 0.1 s interval. This is also applied to all arc power profiles.
- The transition from a constant (stiff) current to the decaying generator-fed fault current occurs over a 1 s interval that ends at the transition time. The power linearly decays from a constant (stiff) value to the maximum generator-fed fault value during this interval. This applied only to cases with a non-zero constant current that transitions into a generator-fed fault current.
- The power during the transition between the higher and lower power arc currents occur over a 0.1 s interval for the LV SWGR power profile.
- The generator-fed fault current is evaluated over a 15 s interval rather than a 14.6 s interval. The power profile is calculated using a 20,000 A current rather than a 20,450 A current to compensate for the longer duration.
- The energy required to melt the electrode material is subtracted from the arc power profile as described in Section 3.8.2.

Table A-5 summarizes the total arc power for each arc power profile used.

**Table A-5**  
**Arc power profile total energy**

Fault type	Stiff duration (s)	Generator-fed fault	Ideal energy (MJ) <sup>1</sup>	Ideal modeled energy (MW) <sup>2</sup>	Model volumetric source energy (MW) <sup>3</sup>
NSBD	1	No	34	34	33 (copper electrode) 33 (aluminum electrode)
MV SWGR/ NSBD	2	No	68	68	66 (copper electrode) 66 (aluminum electrode)
MV SWGR/ NSBD	4	No	135	135	132 (copper electrode) 132 (aluminum electrode)
MV SWGR/ NSBD	5	No	169	169	164 (copper electrode) 165 (aluminum electrode)
MV SWGR/ NSBD	0	Yes	132	131	128 (copper electrode) 128 (aluminum electrode)
MV SWGR/ NSBD	3	Yes	233	226	219 (copper electrode) 219 (aluminum electrode)
MV SWGR/ NSBD	5	Yes	300	293	283 (copper electrode) 283 (aluminum electrode)
LV SWGR	Based on FEDB 50935		90	90	90 <sup>4</sup>

<sup>1</sup>Total energy of the idealized arc.

<sup>2</sup>Includes linear transitions.

<sup>3</sup>FDS volumetric source total energy, excludes energy used to melt electrode (see Sections 3.7.1 and 3.8.2).

<sup>4</sup>Electrode melt adjustment is not applied to the low-voltage arc fault power profiles (see Section 3.8.2).

# B

## DETAILED FDS RESULTS

This appendix provides plots of the maximum exposure as a function of distance for each of the simulations in Section 5.1. The distance is measured from the face of the enclosure. The exposure, shown on a log scale, is the total exposure over the duration of the FDS simulations (arcing fault duration plus 8 s (see Section 3.1)). Each plot shows the exposure for the equipment faces noted, with each face in a separate color. The solid line is the bias-adjusted FDS prediction (see Section 4.1.4). The dashed lines are the 95% confidence interval. The two purple dot-dot-dash lines are 15 MJ/m<sup>2</sup> and 30 MJ/m<sup>2</sup> target fragilities [10].

### B.1 Medium Voltage Switchgear

#### B.1.1 Vertical-Lift Circuit Breaker Design

##### B.1.1.1 Main Bus Bar Compartment

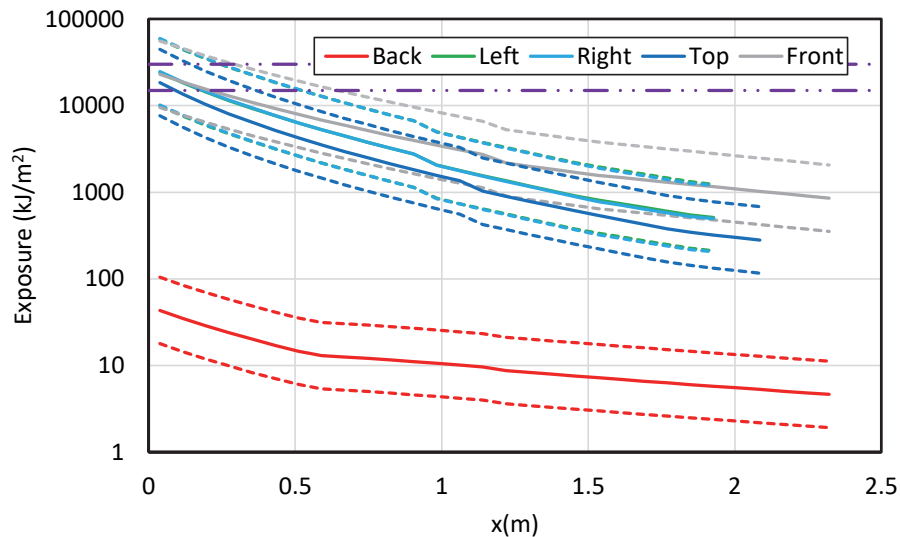


**Figure B-1**  
Results for a vertical-lift circuit breaker MV SWGR with an aluminum bus bar – 68 MJ HEAF located at the main bus bar (FDS simulation MV-GE-1)

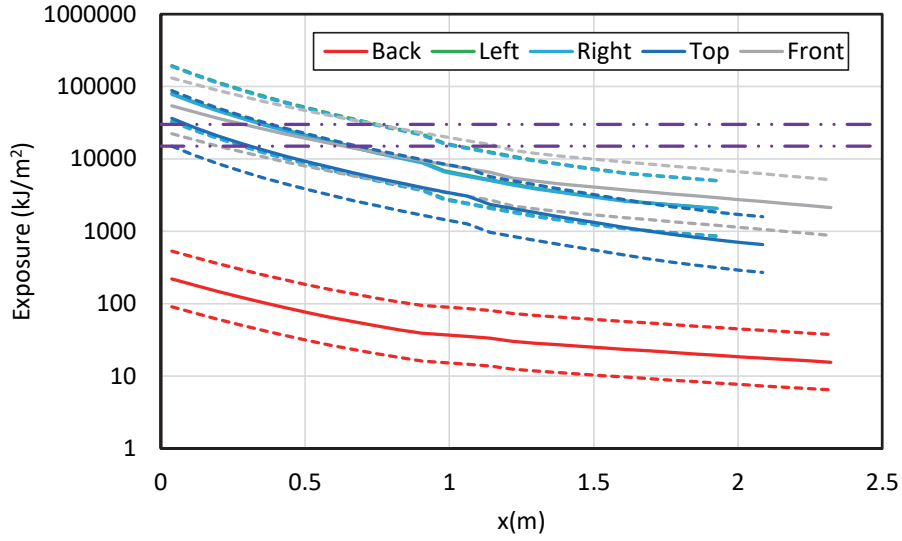


**Figure B-2**  
Results for a vertical-lift circuit breaker MV SWGR with an aluminum bus bar – 135 MJ HEAF located at the main bus bar (FDS simulation MV-GE-4)

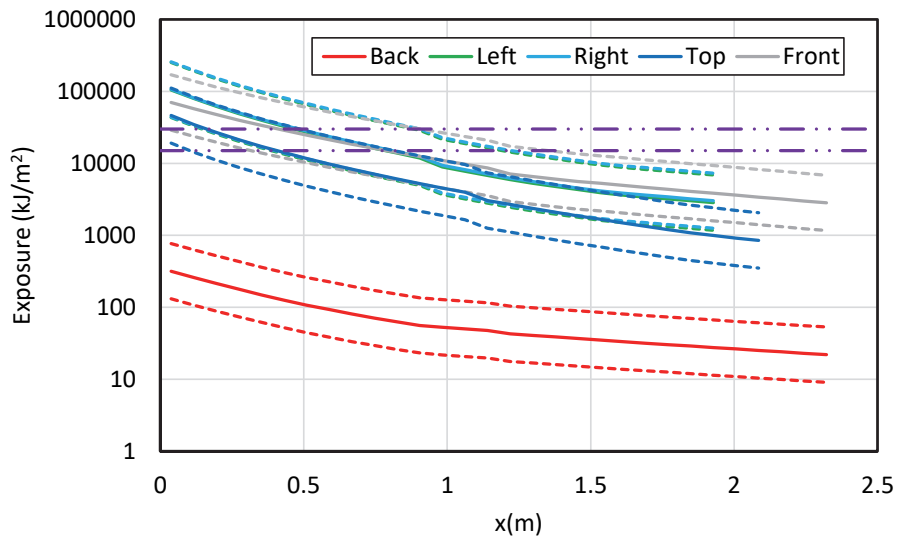


**Figure B-3**  
Results for a vertical-lift circuit breaker MV SWGR with an aluminum bus bar – 169 MJ HEAF located at the main bus bar (FDS simulation MV-GE-7)

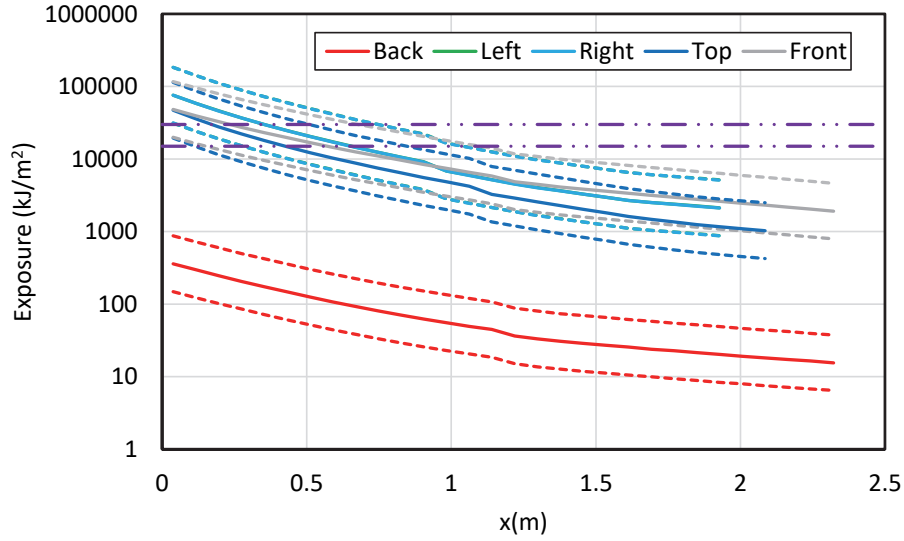


**Figure B-4**  
Results for a vertical-lift circuit breaker MV SWGR with an aluminum bus bar – 132 MJ HEAF located at the main bus bar (FDS simulation MV-GE-10)

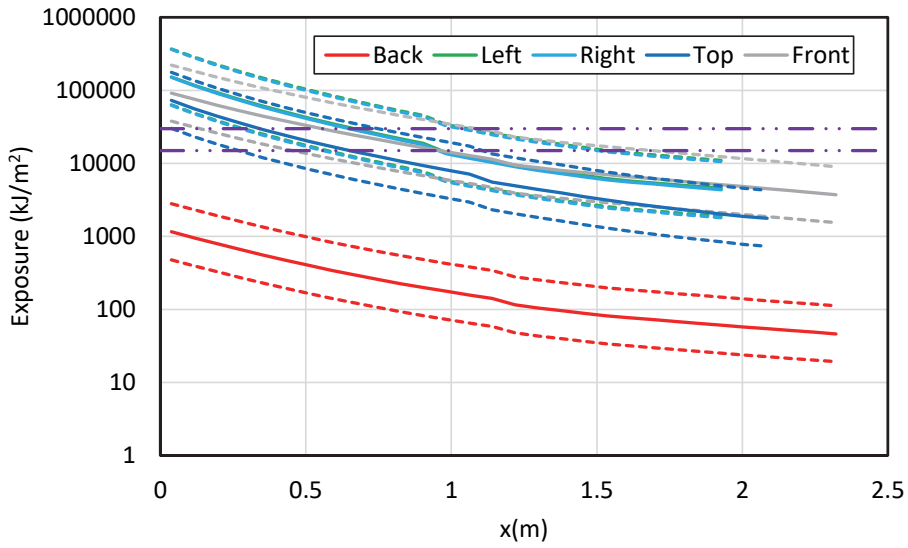


**Figure B-5**  
Results for a vertical-lift circuit breaker MV SWGR with an aluminum bus bar – 233 MJ HEAF located at the main bus bar (FDS simulation MV-GE-13)

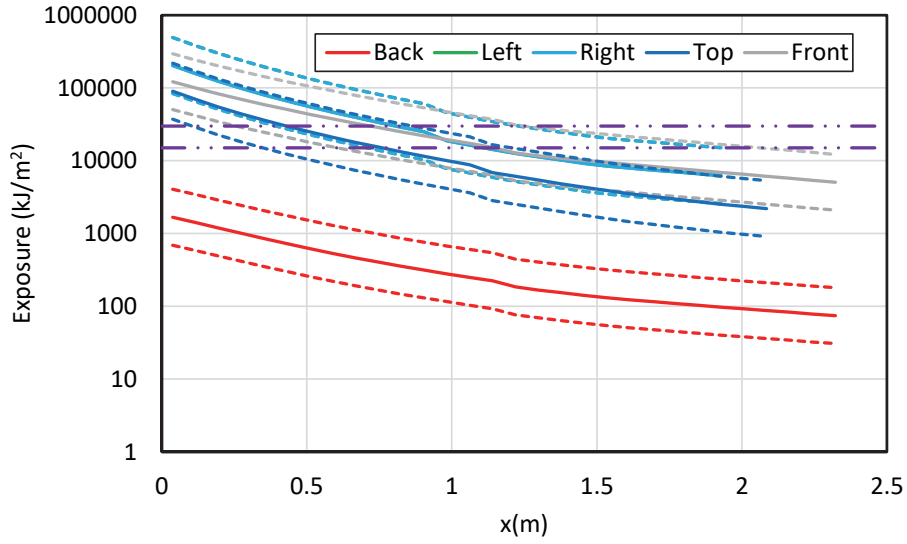


**Figure B-6**  
Results for a vertical-lift circuit breaker MV SWGR with an aluminum bus bar – 300 MJ HEAF located at the main bus bar (FDS simulation MV-GE-16)

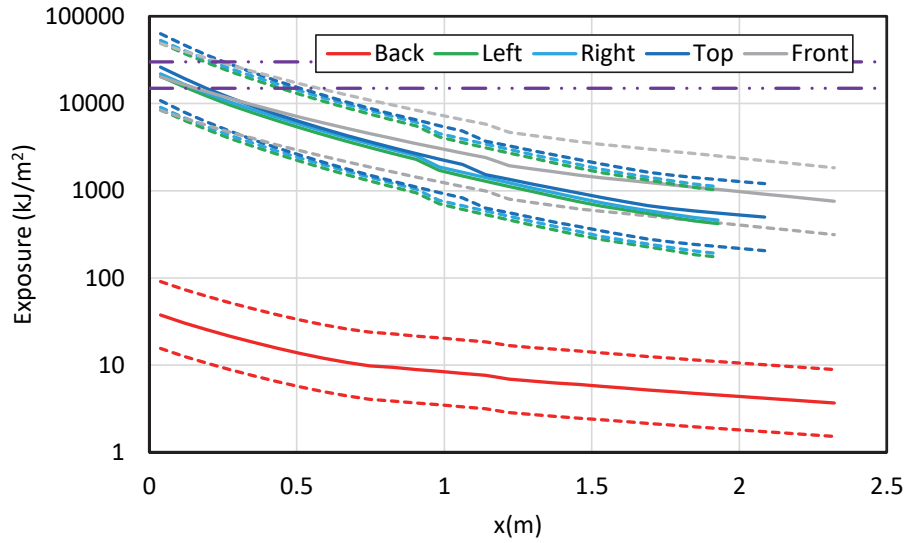


**Figure B-7**  
Results for a vertical-lift circuit breaker MV SWGR with a copper bus bar – 68 MJ HEAF located at the main bus bar (FDS simulation MV-GE-20)

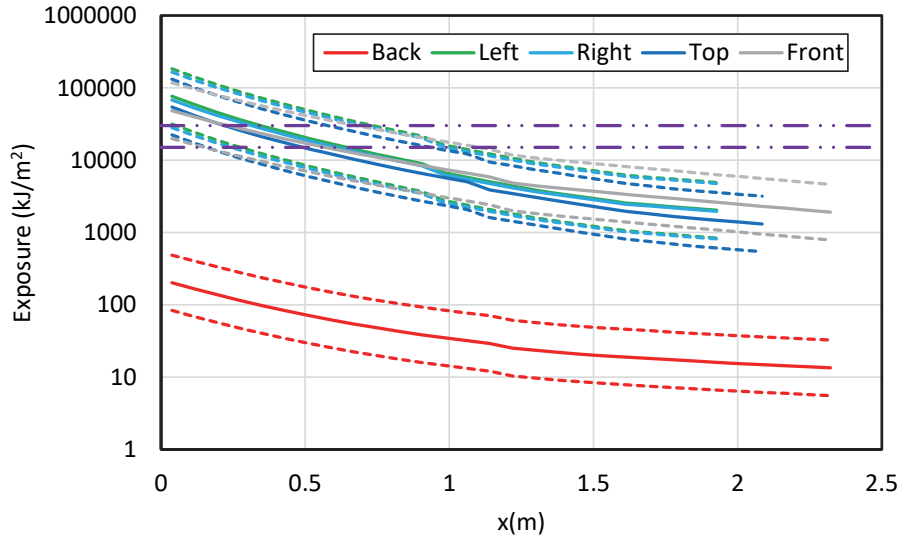


**Figure B-8**  
Results for a vertical-lift circuit breaker MV SWGR with a copper bus bar – 135 MJ HEAF located at the main bus bar (FDS simulation MV-GE-24)

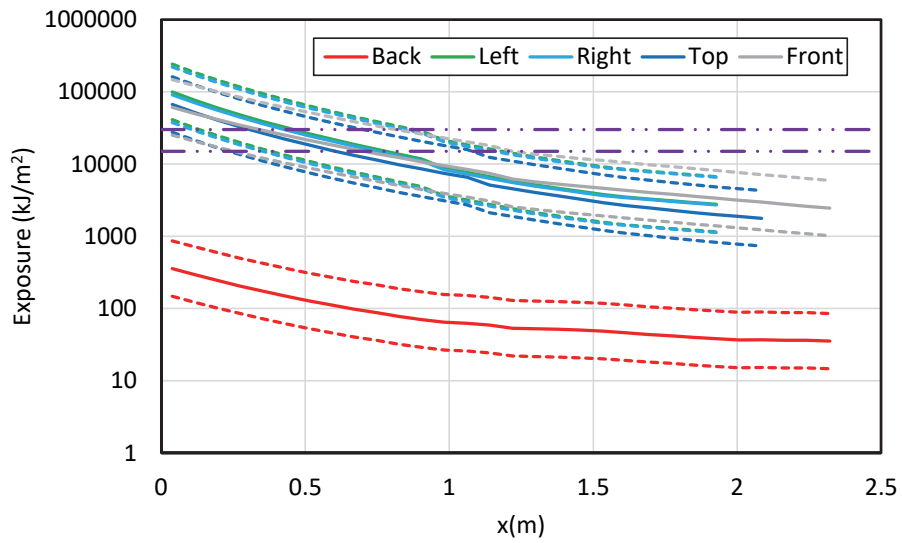


**Figure B-9**  
Results for a vertical-lift circuit breaker MV SWGR with a copper bus bar – 169 MJ HEAF located at the main bus bar (FDS simulation MV-GE-28)

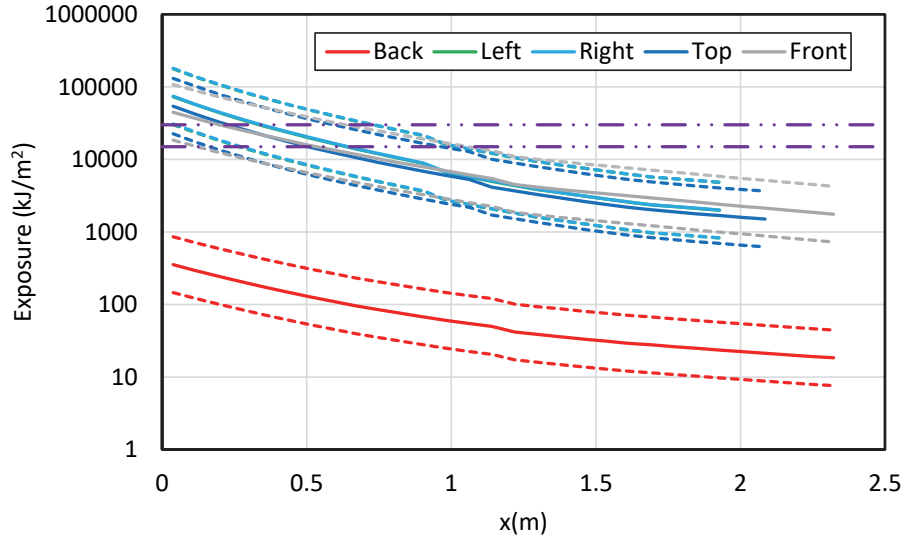


**Figure B-10**  
Results for a vertical-lift circuit breaker MV SWGR with a copper bus bar – 132 MJ HEAF located at the main bus bar (FDS simulation MV-GE-32)

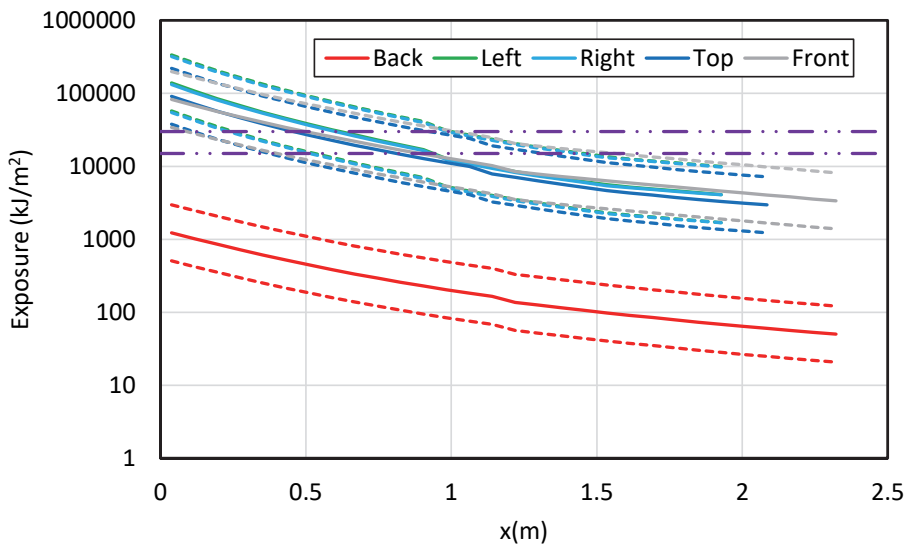


**Figure B-11**  
Results for a vertical-lift circuit breaker MV SWGR with a copper bus bar – 233 MJ HEAF located at the main bus bar (FDS simulation MV-GE-36)

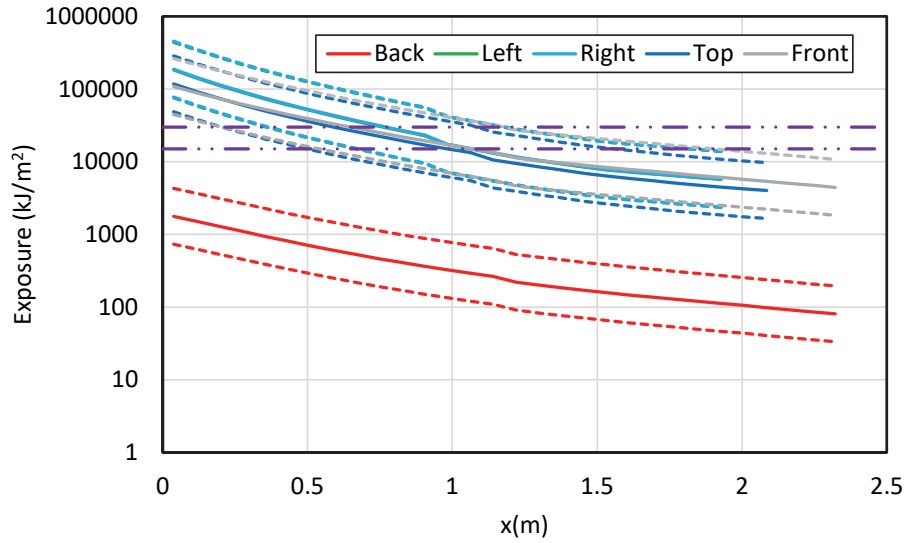


**Figure B-12**  
 Results for a vertical-lift circuit breaker MV SWGR with a copper bus bar – 300 MJ HEAF located at the main bus bar (FDS simulation MV-GE-40)

B.1.1.2 Circuit Breaker Stabs

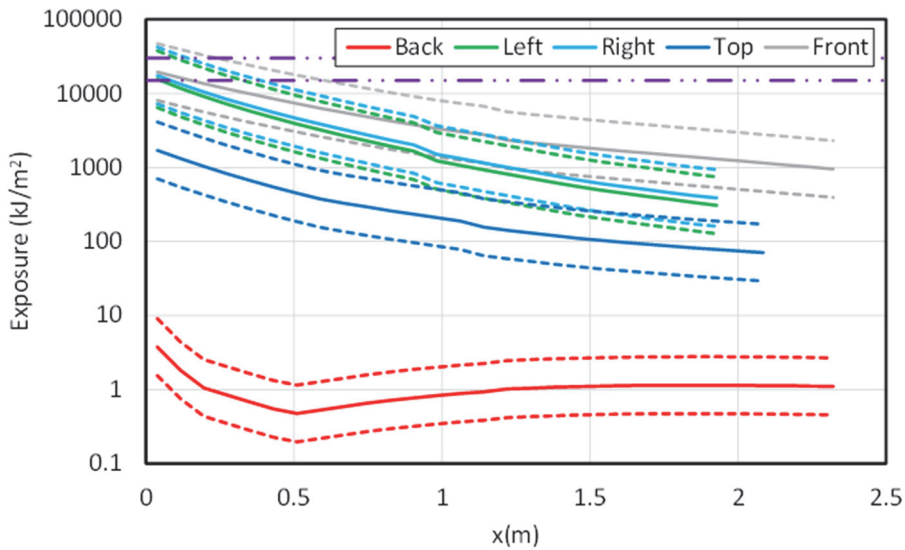


**Figure B-13**  
 Results for a vertical-lift circuit breaker MV SWGR with copper electrodes – 68 MJ HEAF located at the circuit breaker stabs (FDS simulation MV-GE-19)

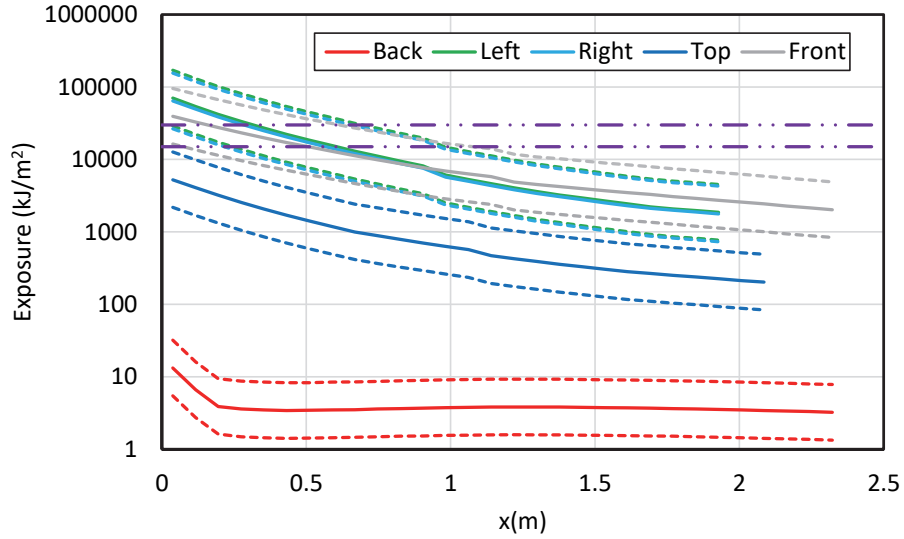


**Figure B-14**  
Results for a vertical-lift circuit breaker MV SWGR with copper electrodes – 135 MJ HEAF located at the circuit breaker stabs (FDS simulation MV-GE-23)

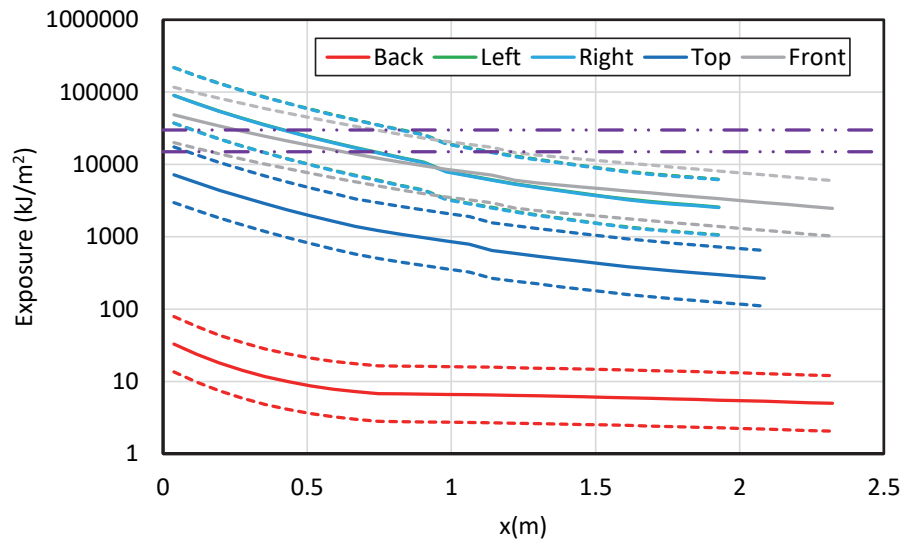


**Figure B-15**  
Results for a vertical-lift circuit breaker MV SWGR with copper electrodes – 169 MJ HEAF located at the circuit breaker stabs (FDS simulation MV-GE-27)

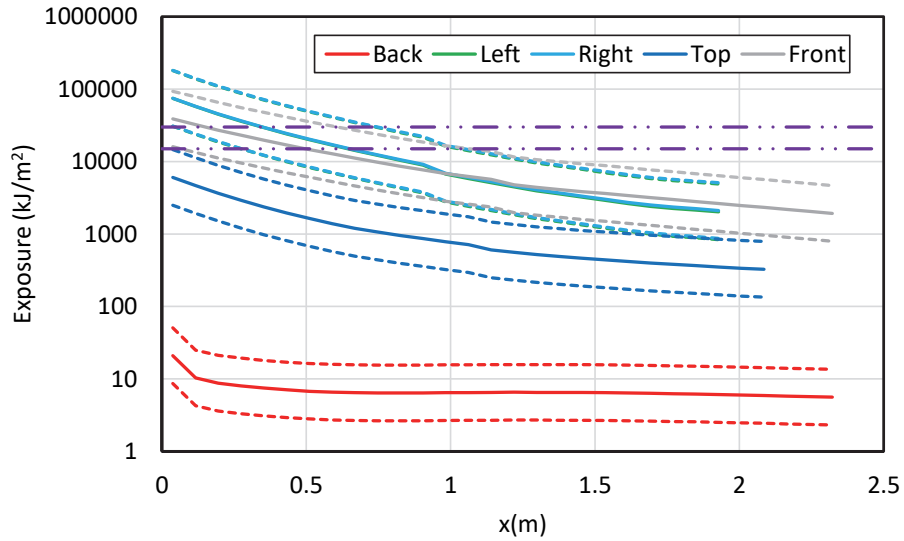


**Figure B-16**  
Results for a vertical-lift circuit breaker MV SWGR with copper electrodes – 132 MJ HEAF located at the circuit breaker stabs (FDS simulation MV-GE-31)

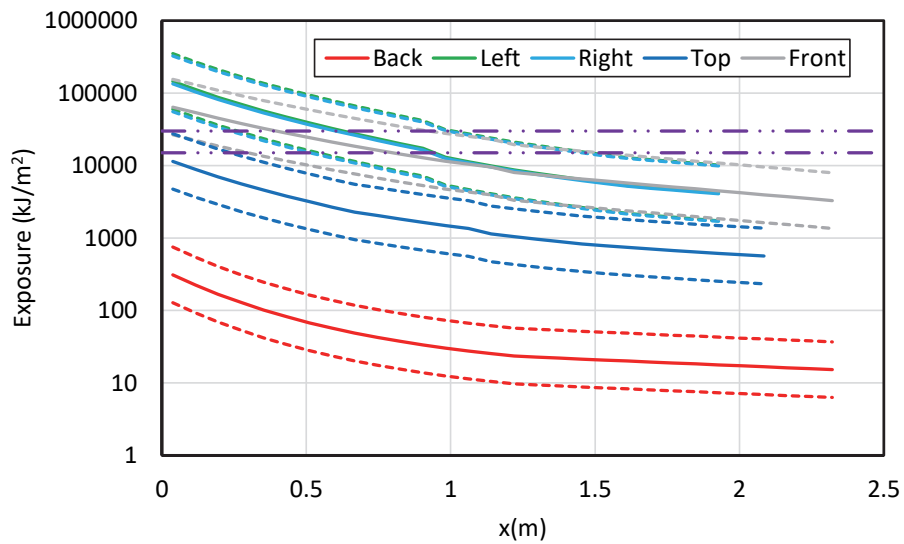


**Figure B-17**  
Results for a vertical-lift circuit breaker MV SWGR with copper electrodes – 233 MJ HEAF located at the circuit breaker stabs (FDS simulation MV-GE-35)

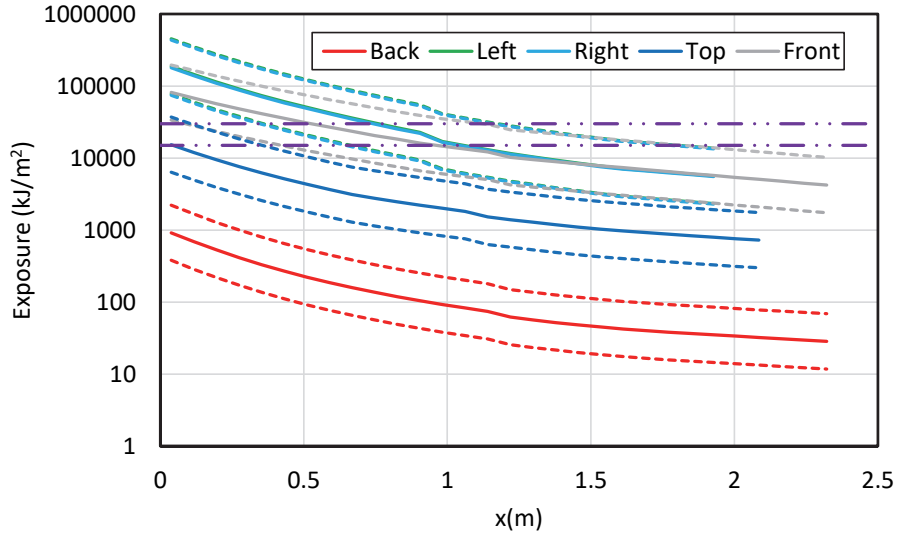


**Figure B-18**  
Results for a vertical-lift circuit breaker MV SWGR with copper electrodes – 300 MJ HEAF located at the circuit breaker stabs (FDS simulation MV-GE-39)

B.1.1.3 Primary Compartment Bus Bar (PCCBB) Load Configuration

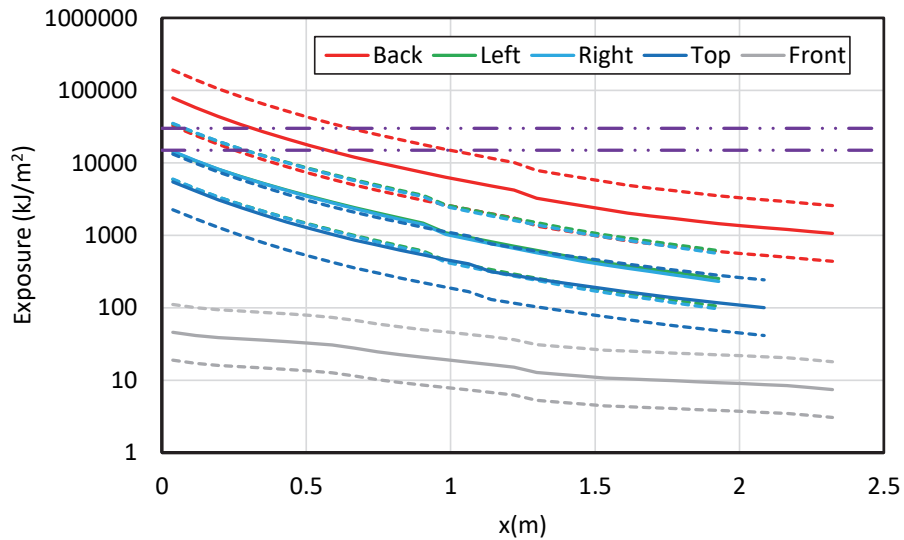


**Figure B-19**  
Results for a vertical-lift circuit breaker MV SWGR with an aluminum bar – 68 MJ HEAF located at the PCCBB (load configuration) (FDS simulation MV-GE-2)

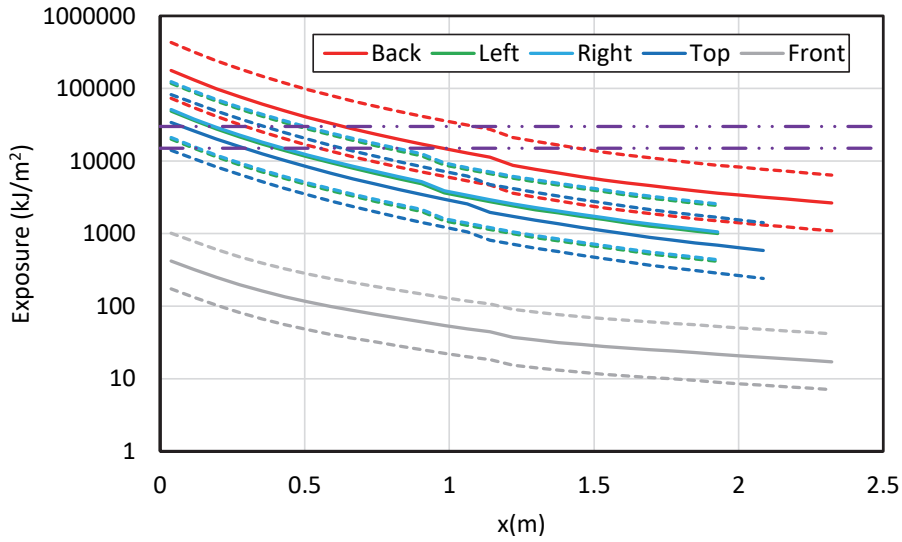


**Figure B-20**  
Results for a vertical-lift circuit breaker MV SWGR with an aluminum bar – 135 MJ HEAF located at the PCCBB (load configuration) (FDS simulation MV-GE-5)

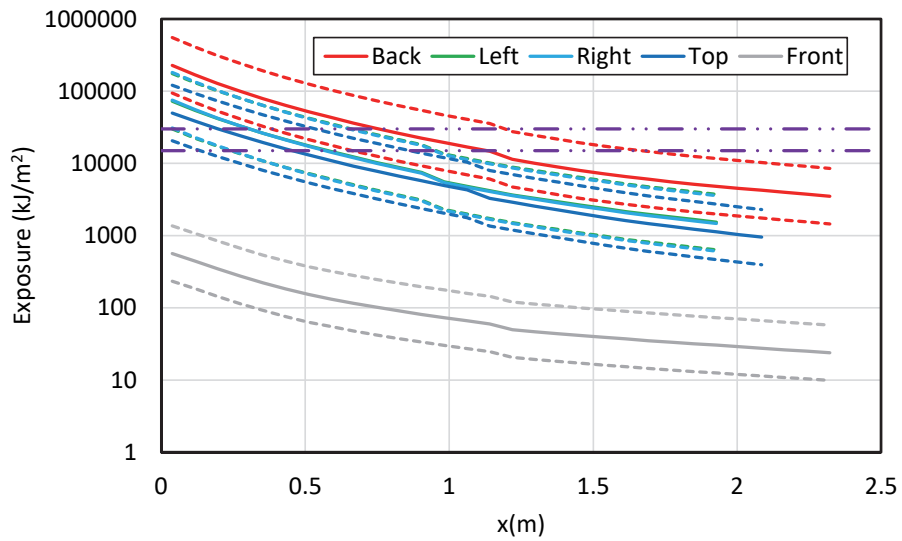


**Figure B-21**  
Results for a vertical-lift circuit breaker MV SWGR with an aluminum bar – 169 MJ HEAF located at the PCCBB (load configuration) (FDS simulation MV-GE-8)

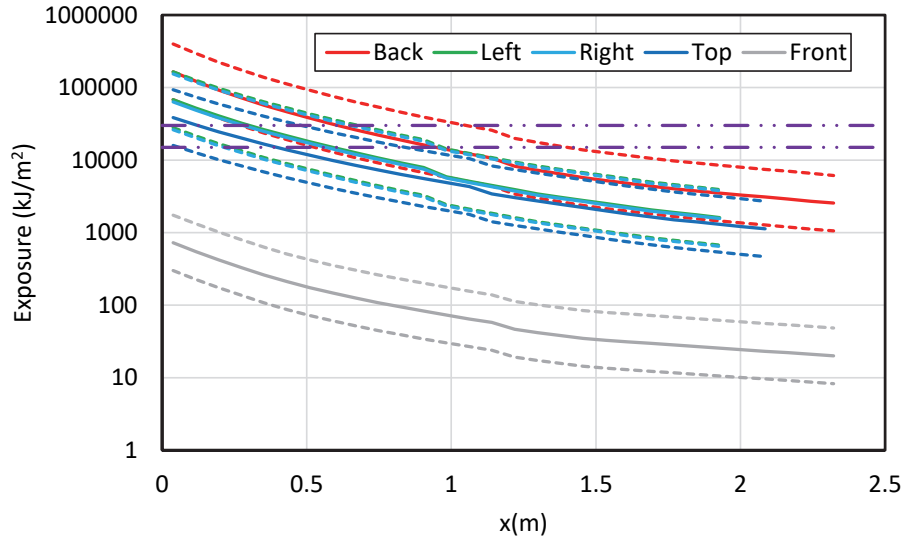


**Figure B-22**  
Results for a vertical-lift circuit breaker MV SWGR with an aluminum bar – 132 MJ HEAF located at the PCCBB (load configuration) (FDS simulation MV-GE-11)

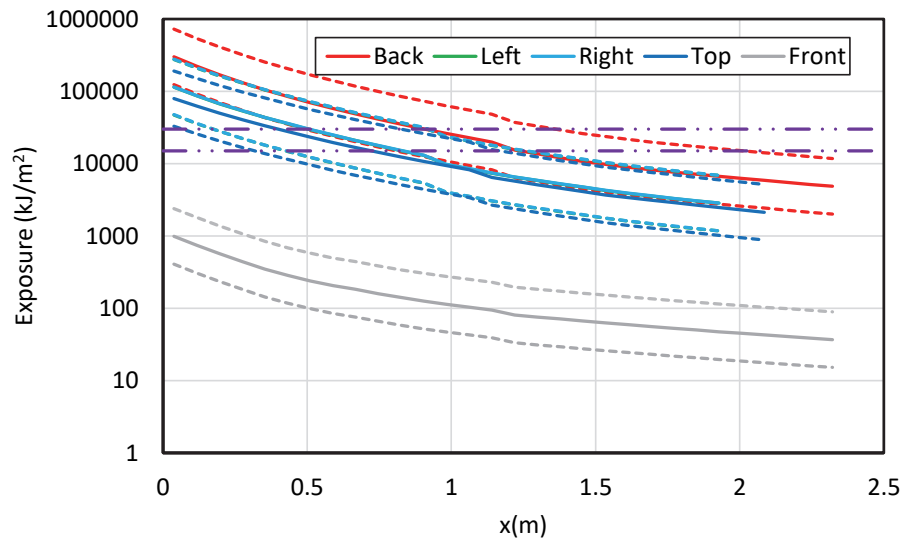


**Figure B-23**  
Results for a vertical-lift circuit breaker MV SWGR with an aluminum bar – 233 MJ HEAF located at the PCCBB (load configuration) (FDS simulation MV-GE-14)

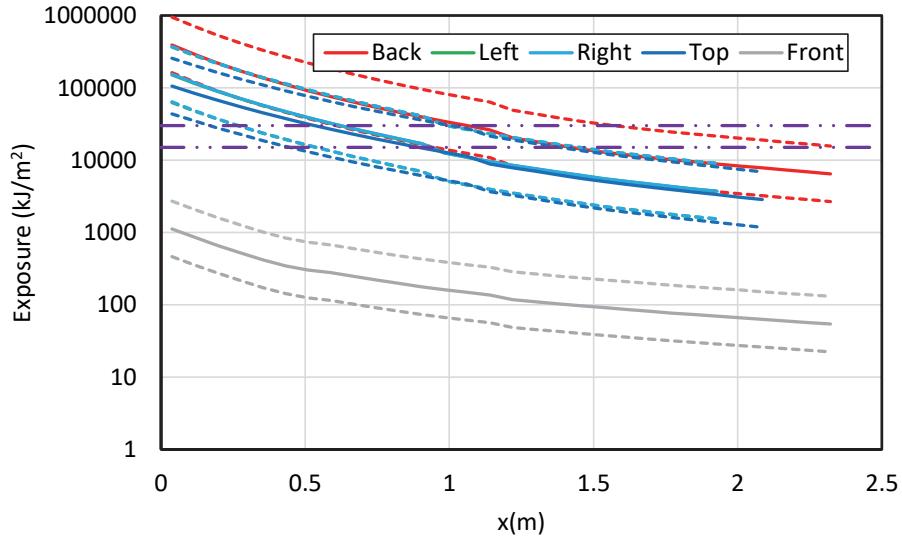


**Figure B-24**  
**Results for a vertical-lift circuit breaker MV SWGR with an aluminum bar – 300 MJ HEAF located at the PCCBB (load configuration) (FDS simulation MV-GE-17)**

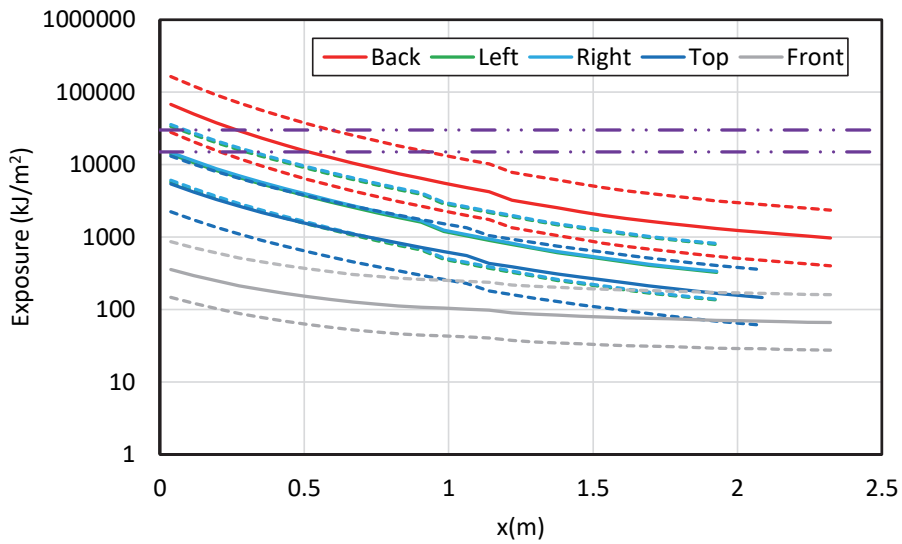


**Figure B-25**  
**Results for a vertical-lift circuit breaker MV SWGR with a copper bar – 68 MJ HEAF located at the PCCBB (load configuration) (FDS simulation MV-GE-21)**

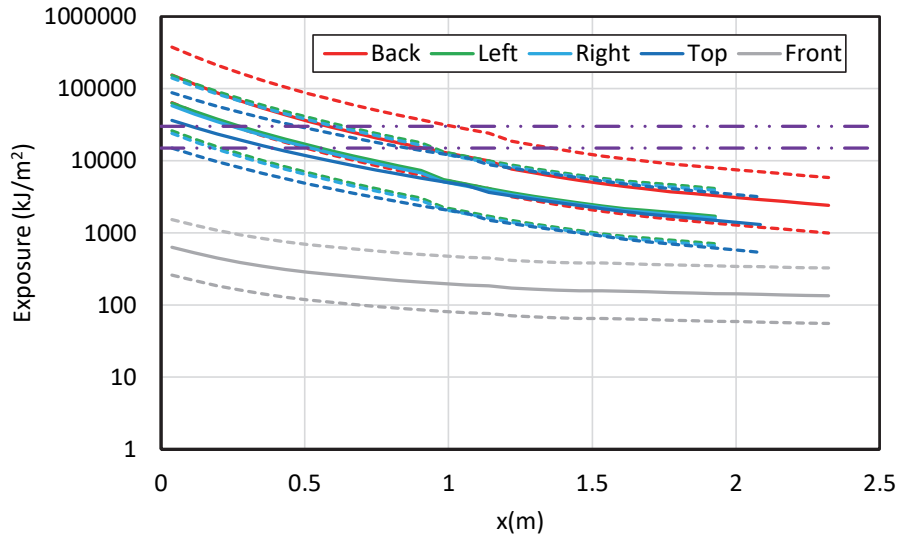


**Figure B-26**  
Results for a vertical-lift circuit breaker MV SWGR with a copper bar – 135 MJ HEAF located at the PCCBB (load configuration) (FDS simulation MV-GE-25)

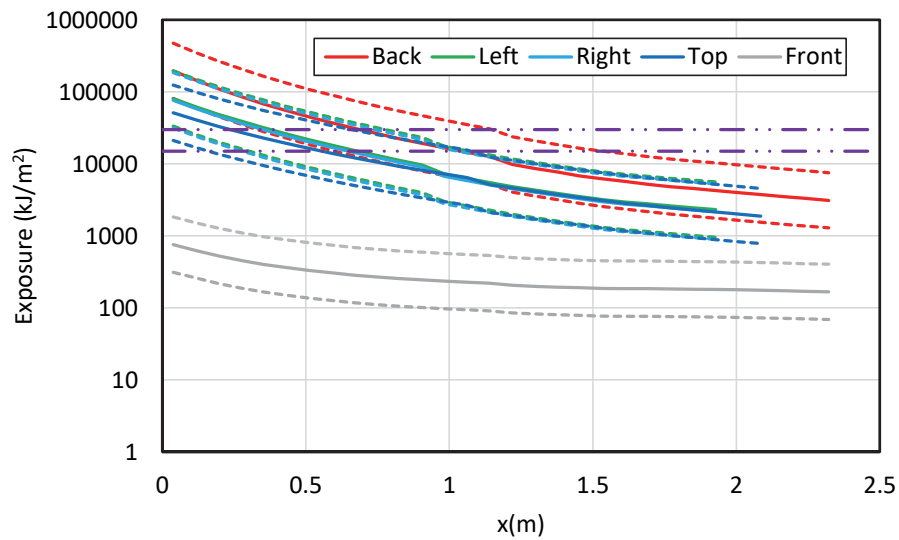


**Figure B-27**  
Results for a vertical-lift circuit breaker MV SWGR with a copper bar – 169 MJ HEAF located at the PCCBB (load configuration) (FDS simulation MV-GE-29)

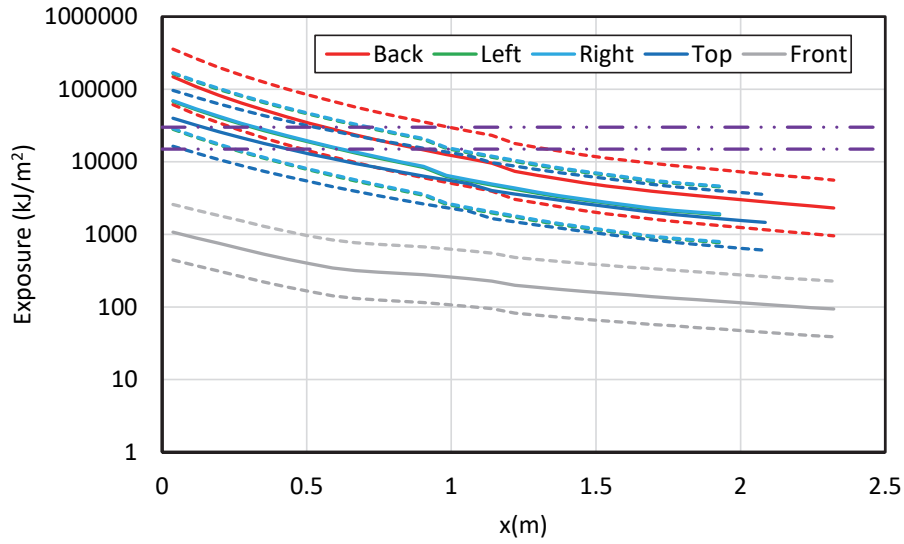


**Figure B-28**  
**Results for a vertical-lift circuit breaker MV SWGR with a copper bar – 132 MJ HEAF**  
**located at the PCCBB (load configuration) (FDS simulation MV-GE-33)**

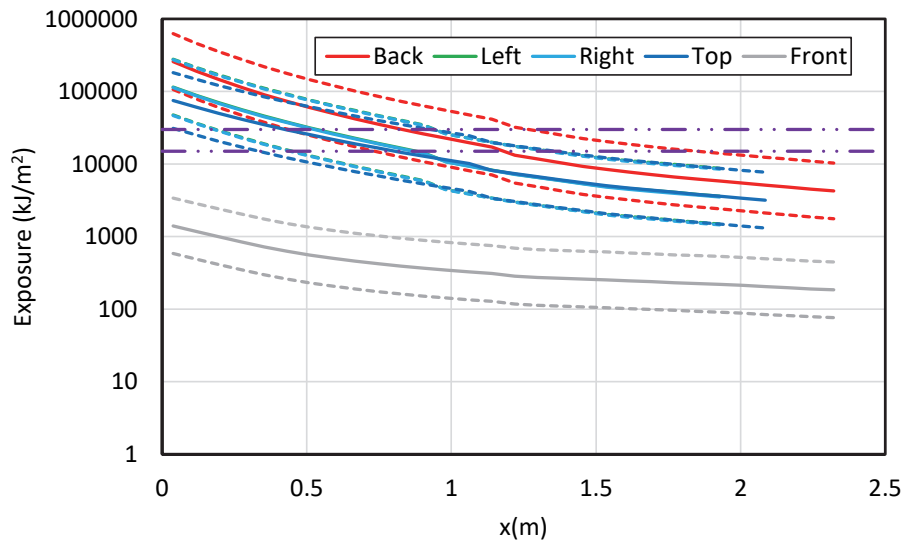


**Figure B-29**  
**Results for a vertical-lift circuit breaker MV SWGR with a copper bar – 233 MJ HEAF**  
**located at the PCCBB (load configuration) (FDS simulation MV-GE-37)**

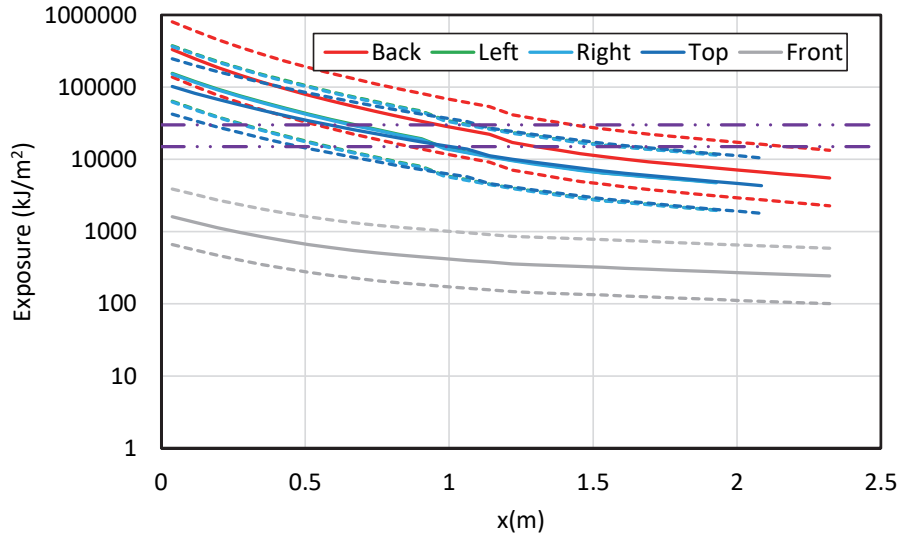


**Figure B-30**  
Results for a vertical-lift circuit breaker MV SWGR with a copper bar – 300 MJ HEAF located at the PCCBB (load configuration) (FDS simulation MV-GE-41)

#### B.1.1.4 Primary Cable Compartment Bus Bar Supply Configuration

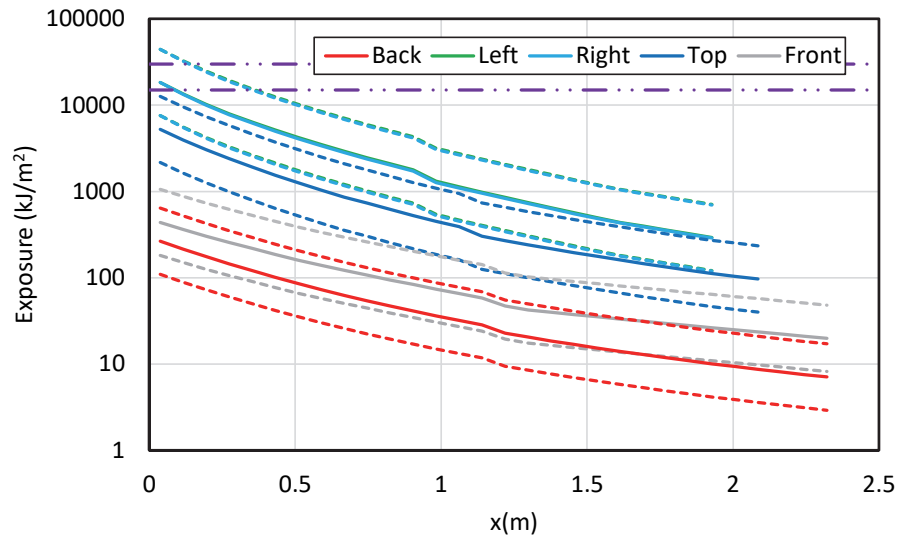


**Figure B-31**  
Results for a vertical-lift circuit breaker MV SWGR with an aluminum bar – 68 MJ HEAF located at the PCCBB (supply configuration) (FDS simulation MV-GE-3)

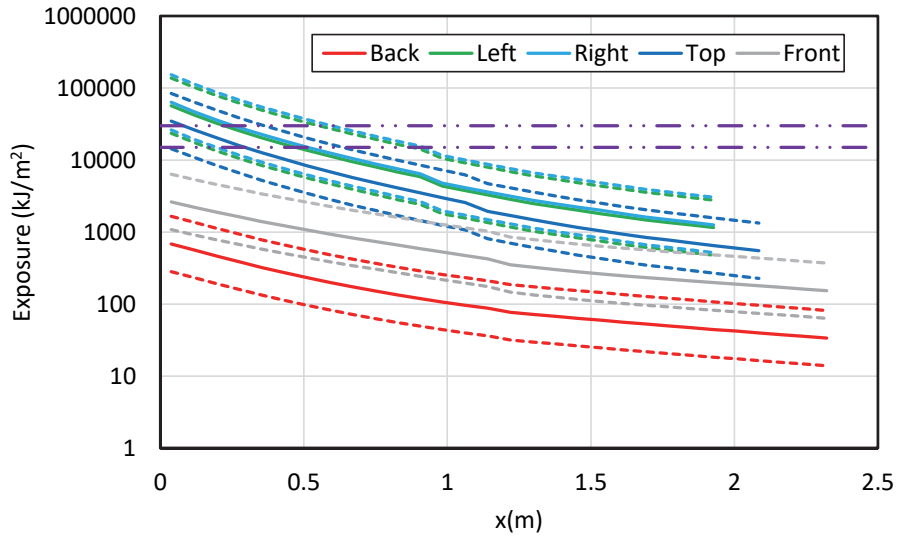


**Figure B-32**  
**Results for a vertical-lift circuit breaker MV SWGR with an aluminum bar – 135 MJ HEAF**  
**located at the PCCBB (supply configuration) (FDS simulation MV-GE-6)**

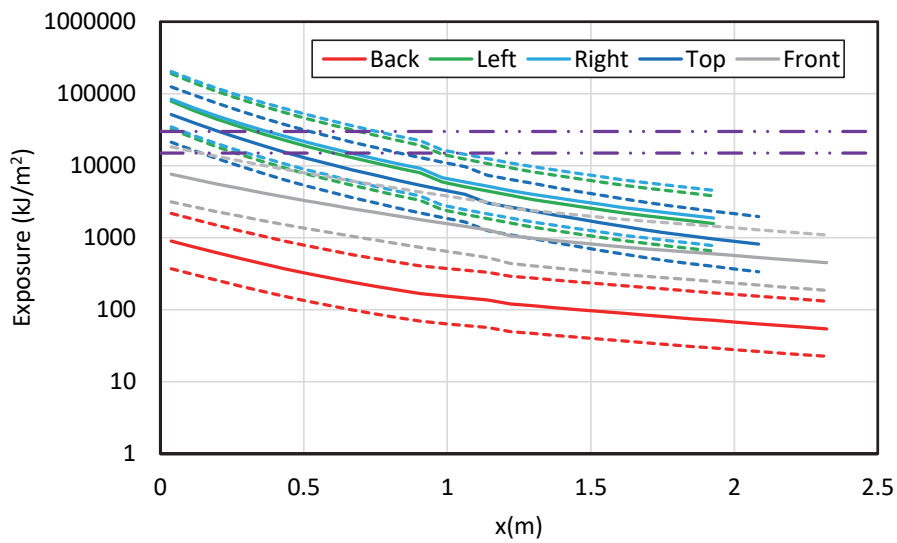


**Figure B-33**  
**Results for a vertical-lift circuit breaker MV SWGR with an aluminum bar – 169 MJ HEAF**  
**located at the PCCBB (supply configuration) (FDS simulation MV-GE-9)**

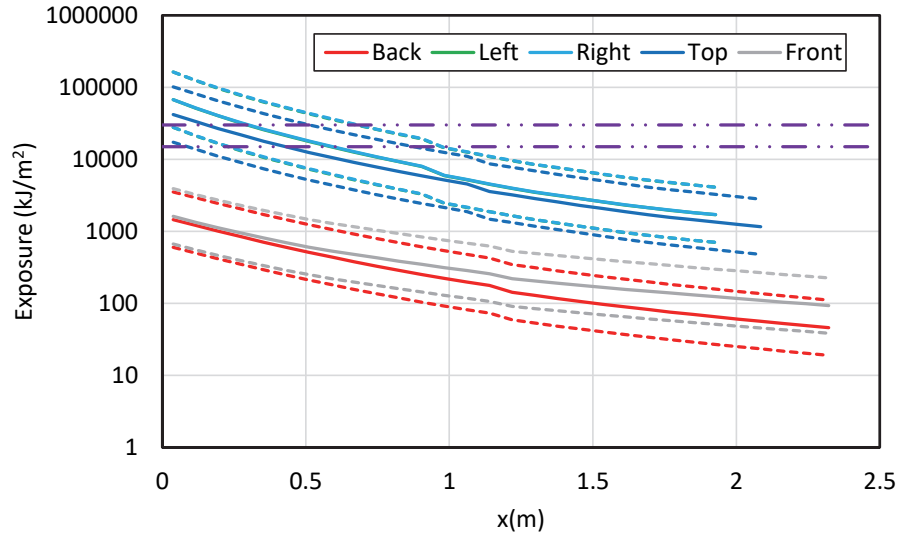


**Figure B-34**  
Results for a vertical-lift circuit breaker MV SWGR with an aluminum bar – 132 MJ HEAF located at the PCCBB (supply configuration) (FDS simulation MV-GE-12)

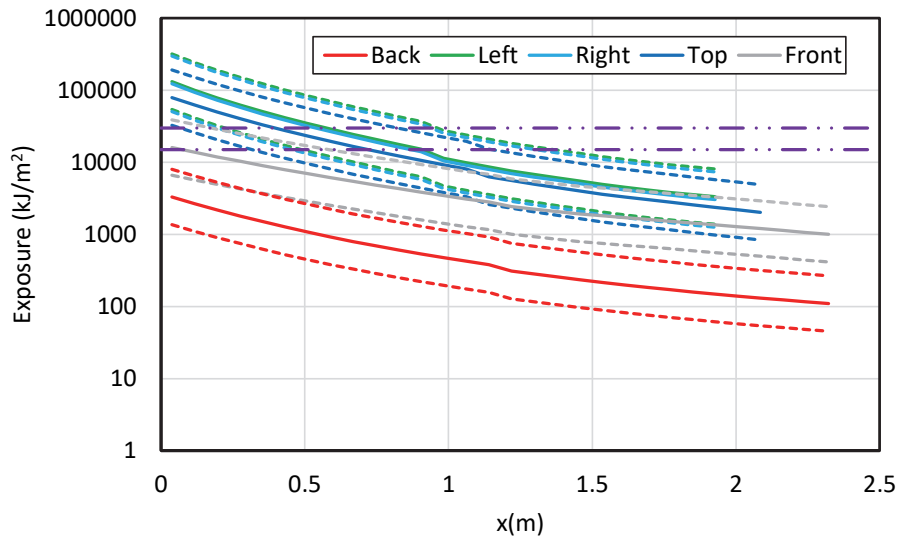


**Figure B-35**  
Results for a vertical-lift circuit breaker MV SWGR with an aluminum bar – 233 MJ HEAF located at the PCCBB (supply configuration) (FDS simulation MV-GE-15)

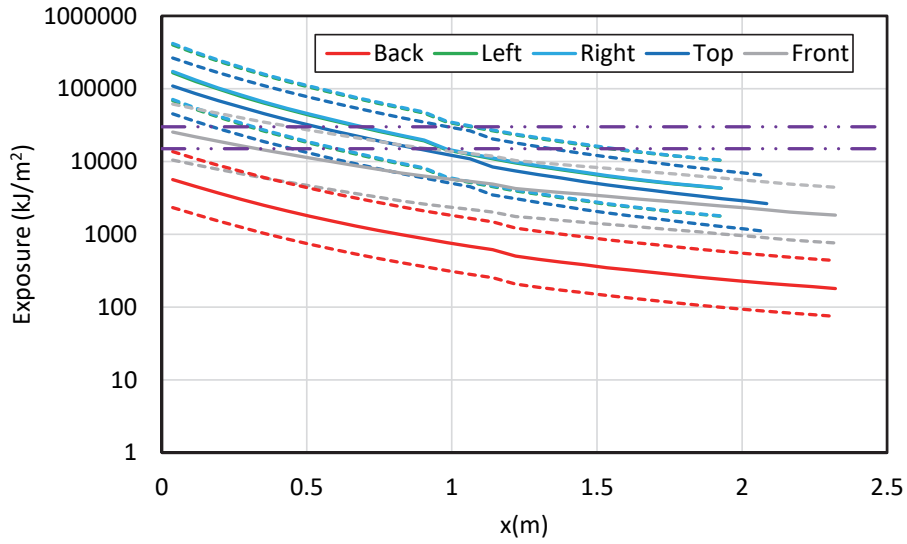


**Figure B-36**  
 Results for a vertical-lift circuit breaker MV SWGR with an aluminum bar – 300 MJ HEAF located at the PCCBB (supply configuration) (FDS simulation MV-GE-18)

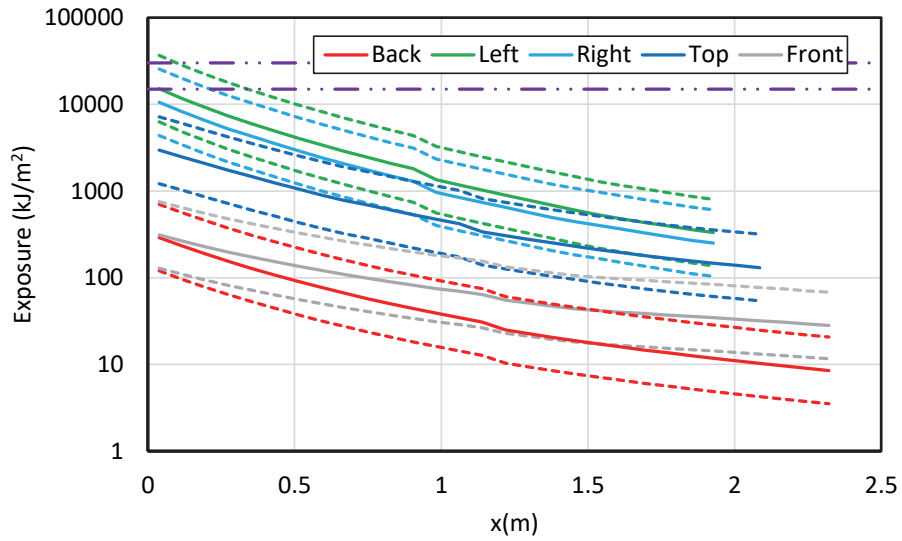


**Figure B-37**  
 Results for a vertical-lift circuit breaker MV SWGR with a copper bar – 68 MJ HEAF located at the PCCBB (supply configuration) (FDS simulation MV-GE-22)

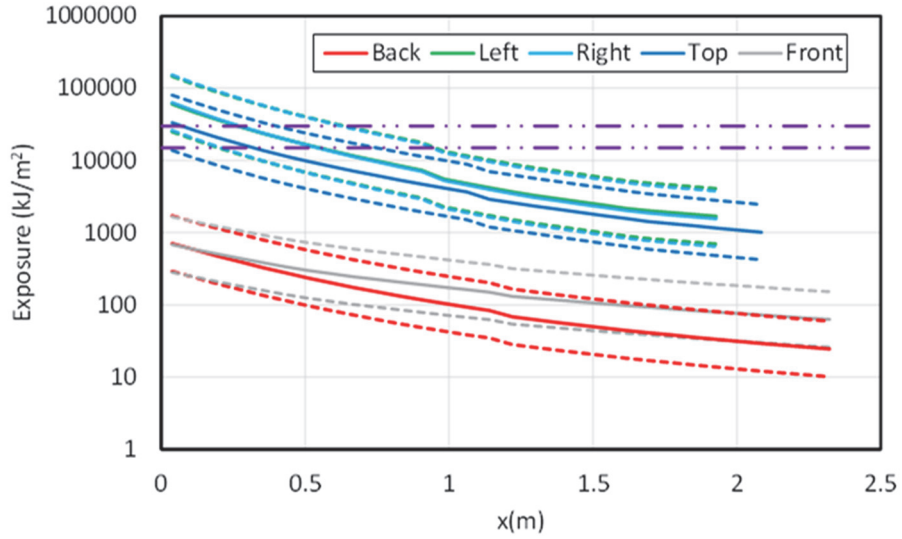


**Figure B-38**  
Results for a vertical-lift circuit breaker MV SWGR with a copper bar – 135 MJ HEAF located at the PCCBB (supply configuration) (FDS simulation MV-GE-26)

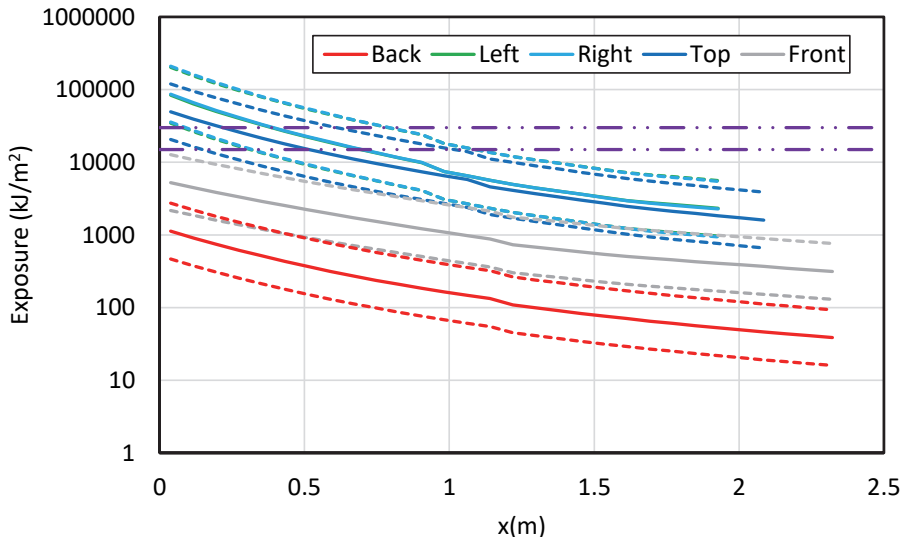


**Figure B-39**  
Results for a vertical-lift circuit breaker MV SWGR with a copper bar – 169 MJ HEAF located at the PCCBB (supply configuration) (FDS simulation MV-GE-30)

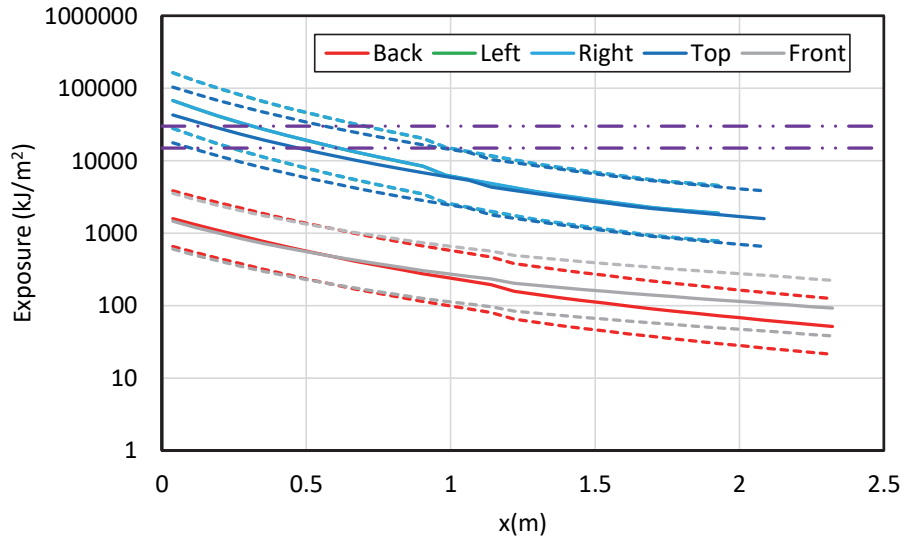


**Figure B-40**  
**Results for a vertical-lift circuit breaker MV SWGR with a copper bar – 132 MJ HEAF**  
**located at the PCCBB (supply configuration) (FDS simulation MV-GE-34)**

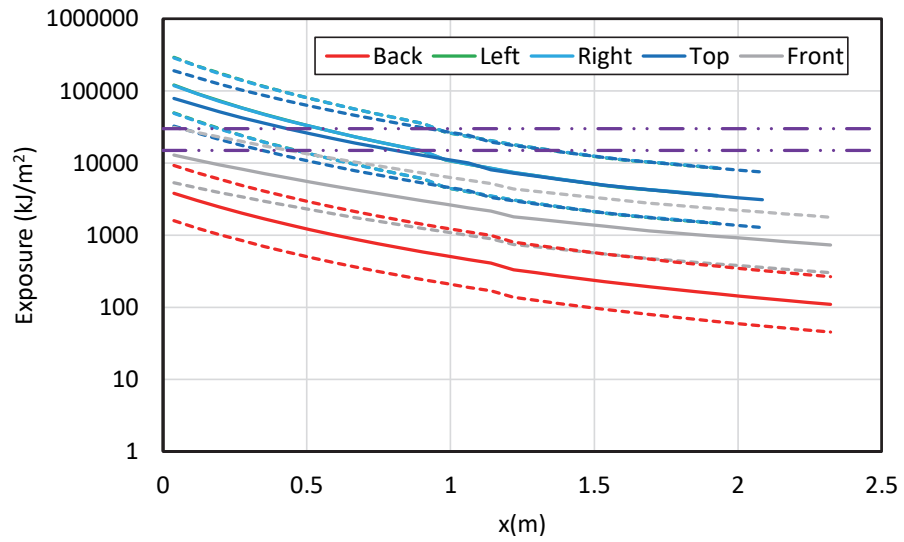


**Figure B-41**  
**Results for a vertical-lift circuit breaker MV SWGR with a copper bar – 233 MJ HEAF**  
**located at the PCCBB (supply configuration) (FDS simulation MV-GE-38)**

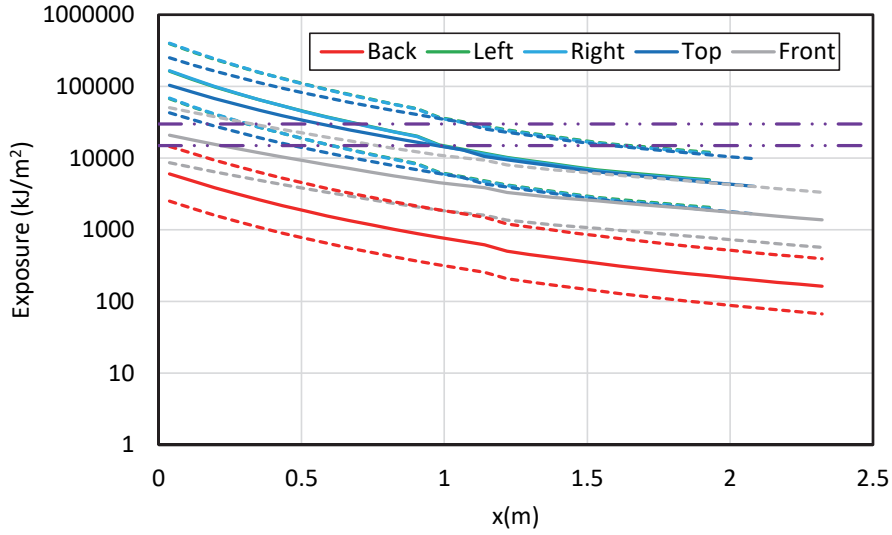


**Figure B-42**  
Results for a vertical-lift circuit breaker MV SWGR with a copper bar – 300 MJ HEAF located at the PCCBB (supply configuration) (FDS simulation MV-GE-42)

### B.1.2 Horizontal Draw-Out Circuit Breaker Stabs

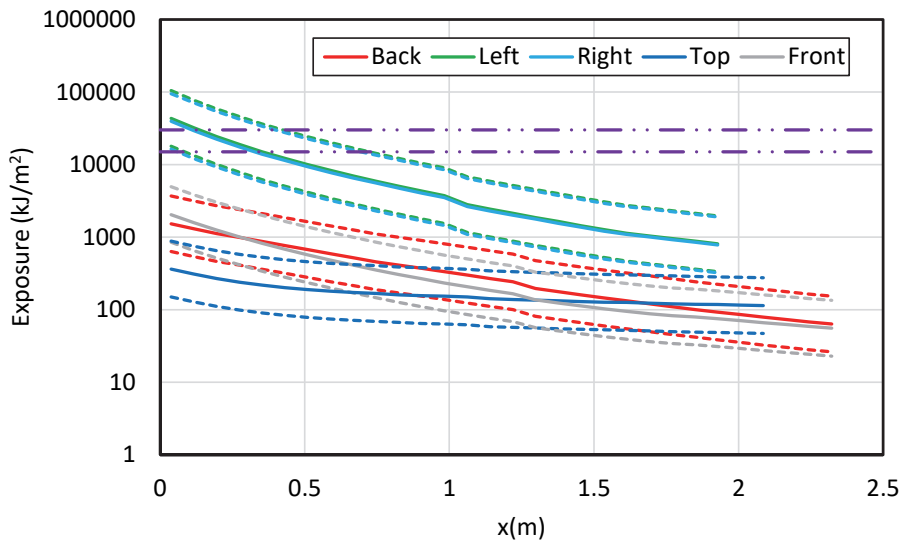


**Figure B-43**  
Results for a horizontal draw-out circuit breaker MV SWGR with copper electrodes – 68 MJ HEAF located at the circuit breaker stabs (FDS simulation MV-ABB-1)

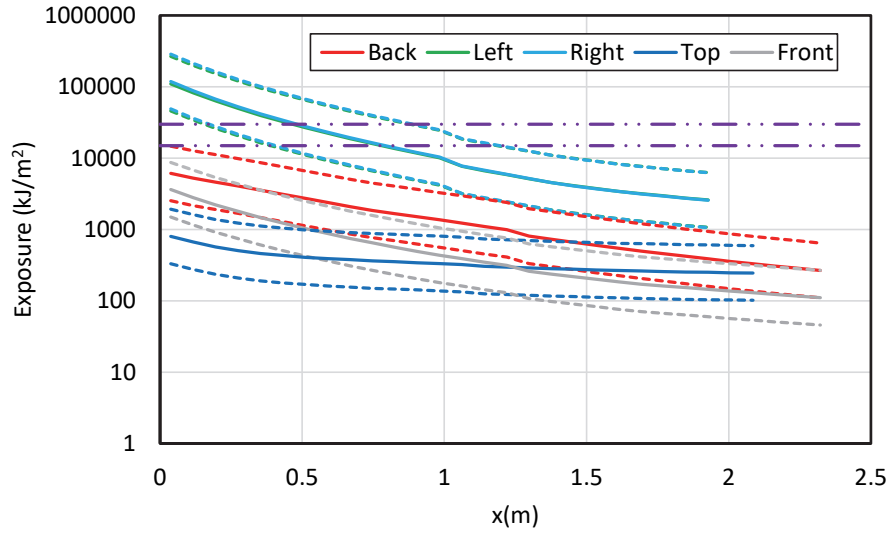


**Figure B-44**  
Results for a horizontal draw-out circuit breaker MV SWGR with copper electrodes – 135 MJ HEAF located at the circuit breaker stabs (FDS simulation MV-ABB-2)

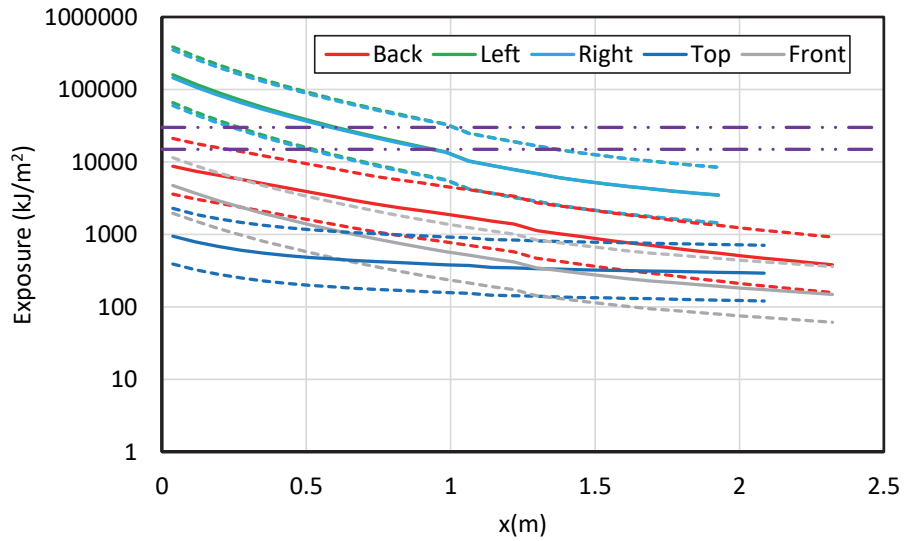


**Figure B-45**  
Results for a horizontal draw-out circuit breaker MV SWGR with copper electrodes – 169 MJ HEAF located at the circuit breaker stabs (FDS simulation MV-ABB-3)

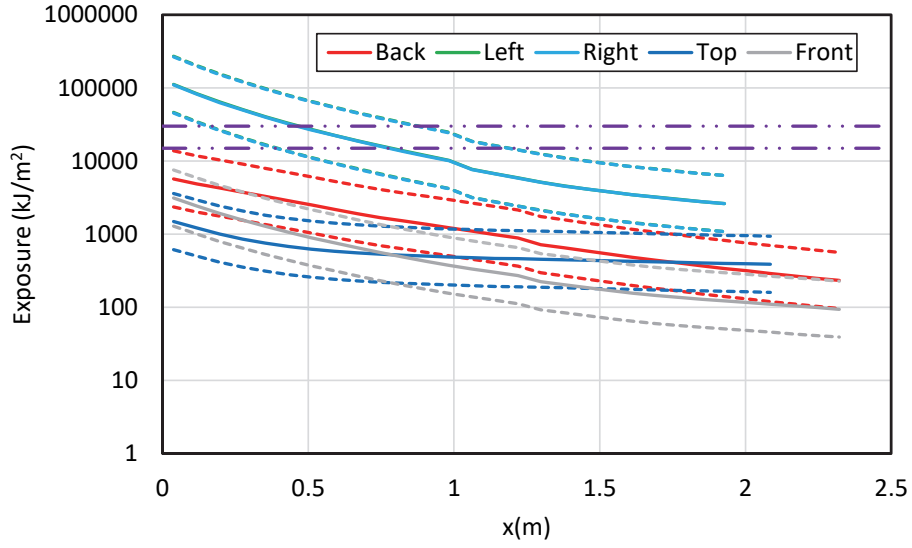


**Figure B-46**  
Results for a horizontal draw-out circuit breaker MV SWGR with copper electrodes – 132 MJ HEAF located at the circuit breaker stabs (FDS simulation MV-ABB-4)

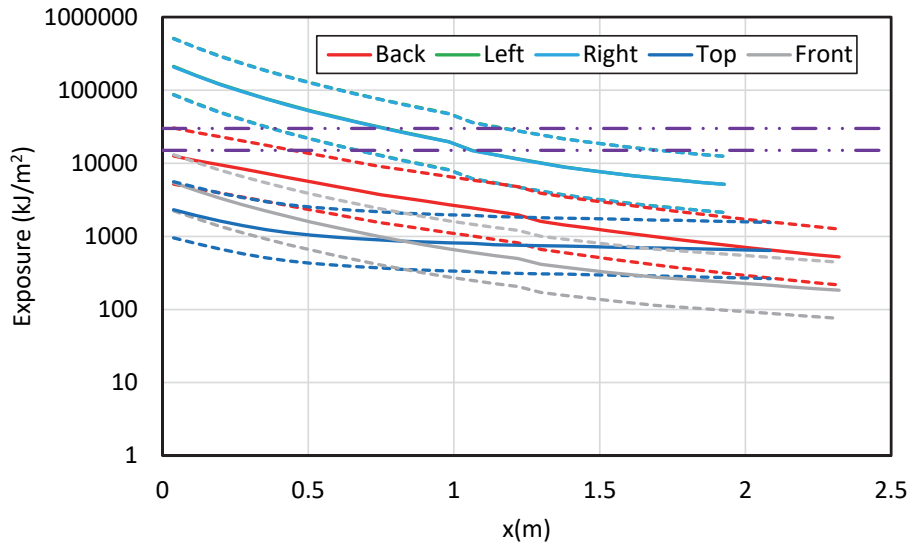


**Figure B-47**  
Results for a horizontal draw-out circuit breaker MV SWGR with copper electrodes – 233 MJ HEAF located at the circuit breaker stabs (FDS simulation MV-ABB-5)

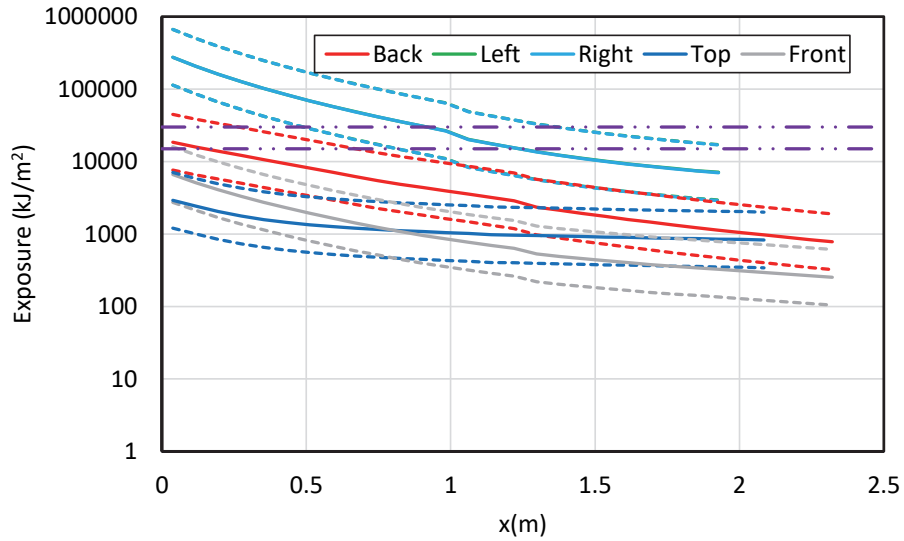


**Figure B-48**  
 Results for a horizontal draw-out circuit breaker MV SWGR with copper electrodes – 300 MJ HEAF located at the circuit breaker stabs (FDS simulation MV-ABB-6)

## B.2 Low Voltage Switchgear

### B.2.1 Circuit Breaker Compartment Middle-Height Elevation

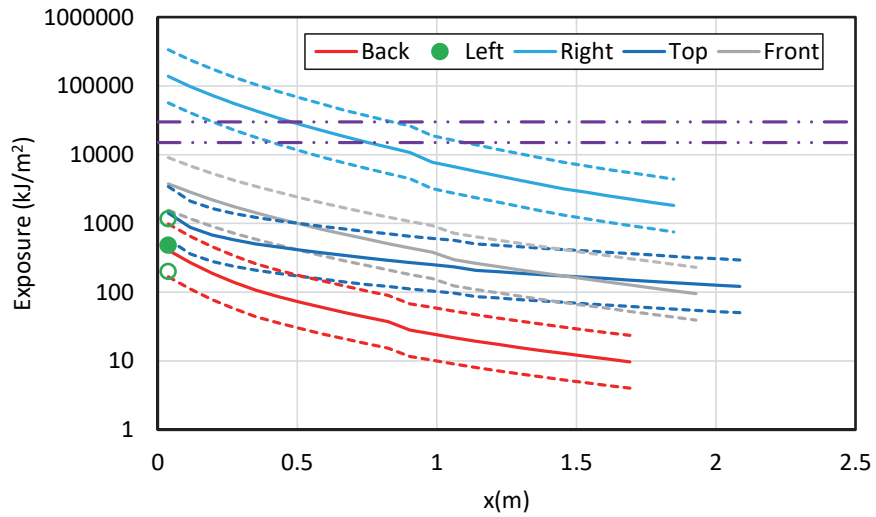


**Figure B-49**  
 Results for a LV SWGR with an aluminum bus bar with a HEAF based on FEDB 50935 – HEAF located in a middle-height circuit breaker compartment (FDS simulation LV-BASE-1)

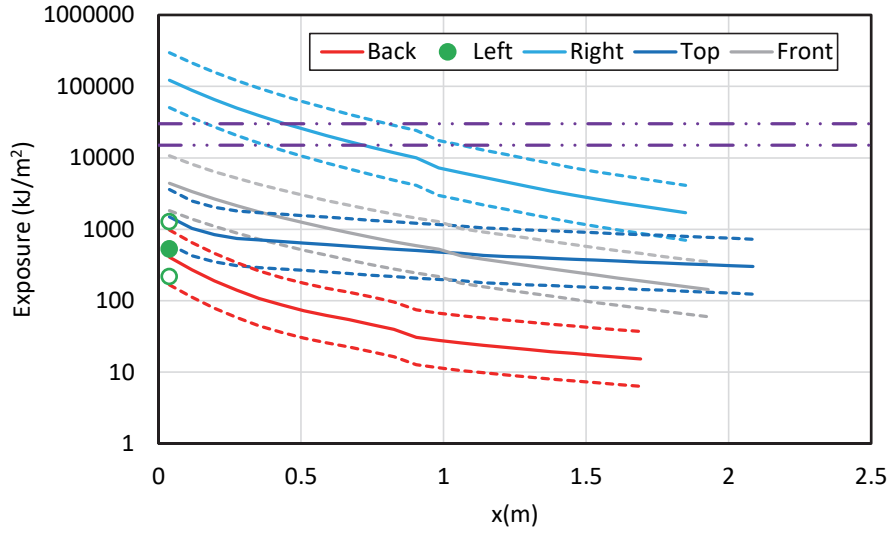


**Figure B-50**  
Results for a LV SWGR with a copper bus bar with a HEAF based on FEDB 50935 – HEAF located in a middle-height circuit breaker compartment (FDS simulation LV-BASE-7)

### B.2.2 Circuit Breaker Compartment Top Elevation

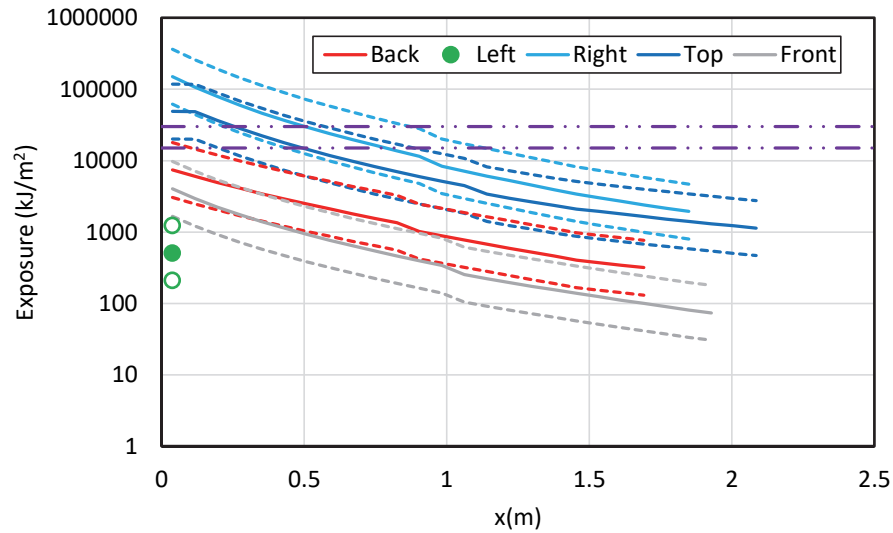


**Figure B-51**  
Results for a LV SWGR with an aluminum bus bar with a HEAF based on FEDB 50935 – HEAF located in a circuit breaker compartment at the top of the switchgear (FDS simulation LV-BASE-2)

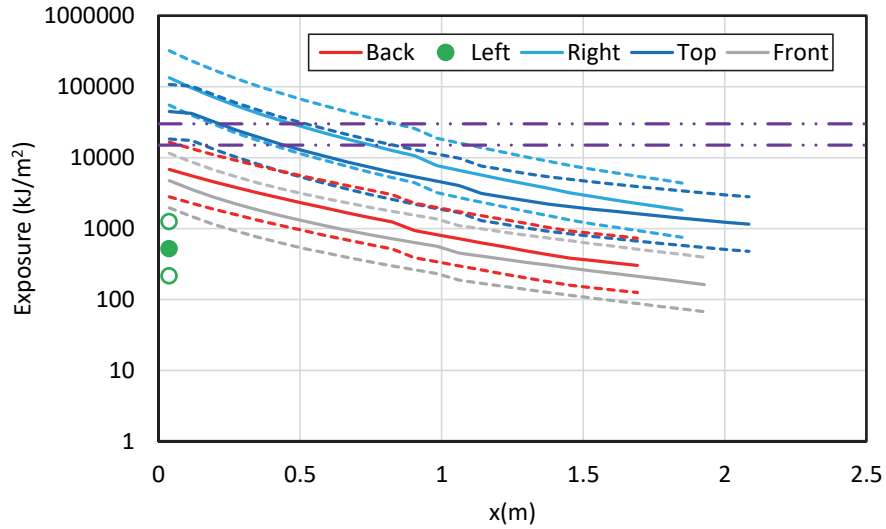


**Figure B-52**  
 Results for a LV SWGR with a copper bus bar with a HEAF based on FEDB 50935 – HEAF located in a circuit breaker compartment at the top of the switchgear (FDS simulation LV-BASE-8)

**B.2.3 Bus Bar Compartment Middle-Height Elevation**

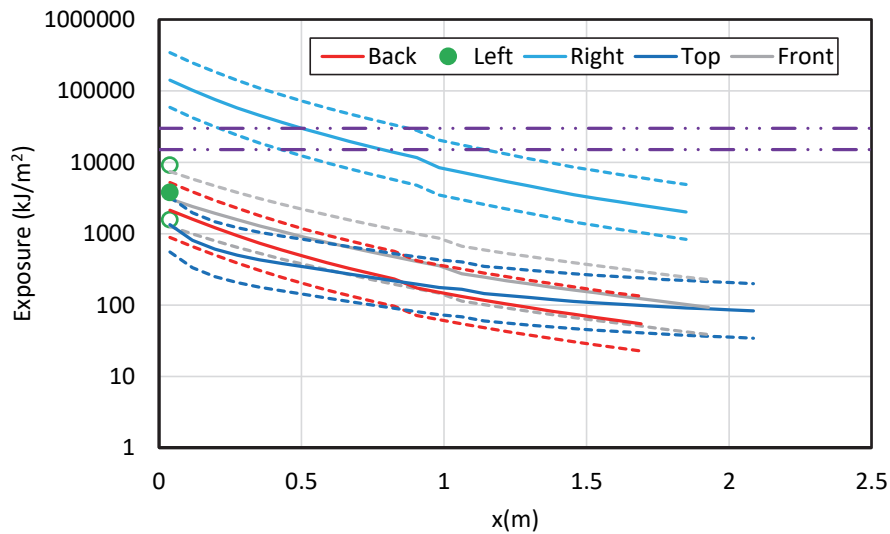


**Figure B-53**  
 Results for a LV SWGR with an aluminum bus bar with a HEAF based on FEDB 50935 – HEAF located in a middle-height bus bar compartment (FDS simulation LV-BASE-3)

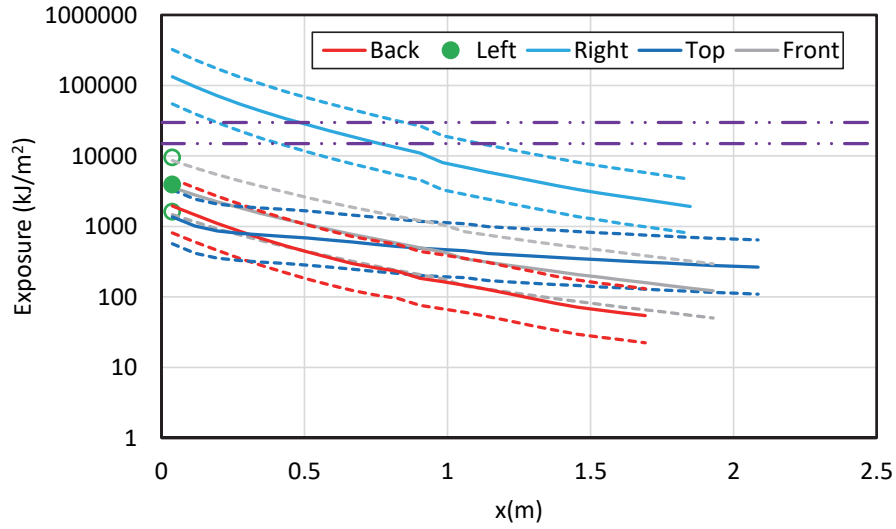


**Figure B-54**  
Results for a LV SWGR with a copper bus bar with a HEAF based on FEDB 50935 – HEAF located in a middle-height bus bar compartment (FDS simulation LV-BASE-9)

### B.2.4 Bus Bar Compartment Top Elevation

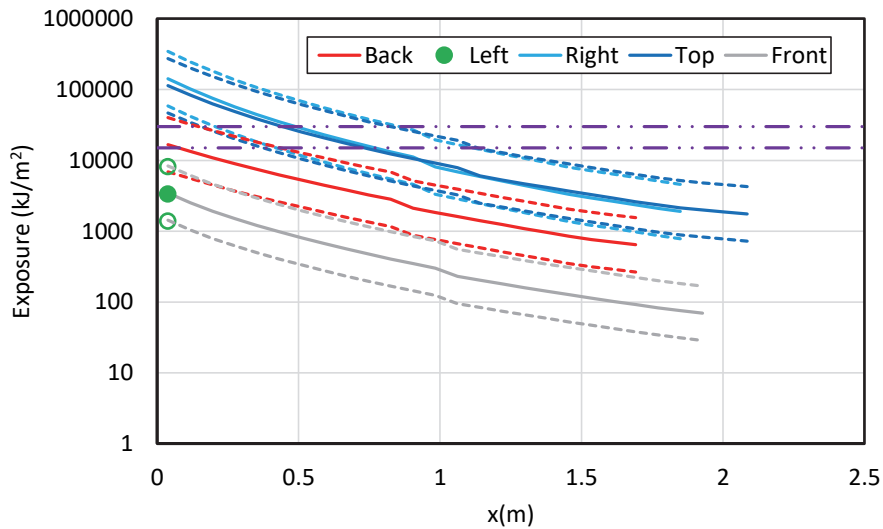


**Figure B-55**  
Results for a LV SWGR with an aluminum bus bar with a HEAF based on FEDB 50935 – HEAF located in a bus bar compartment at the top of the switchgear (FDS simulation LV-BASE-4)

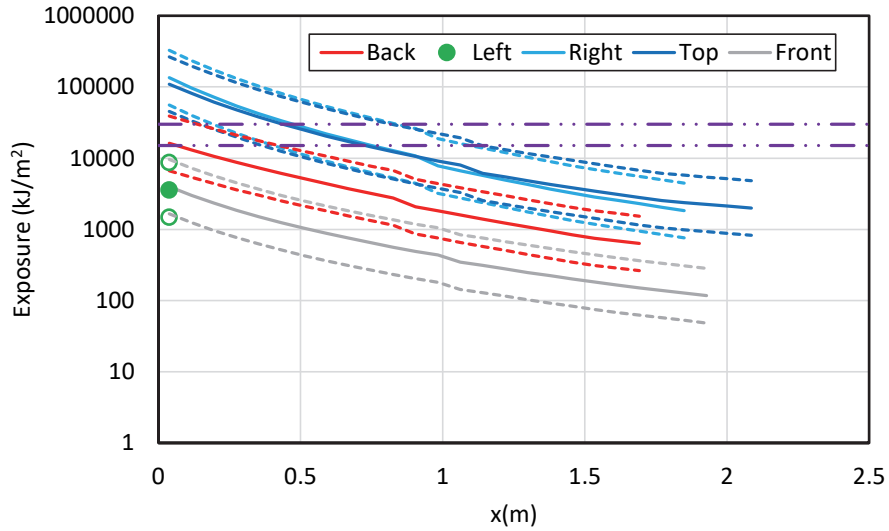


**Figure B-B-56**  
 Results for a LV SWGR with a copper bus bar with a HEAF based on FEDB 50935 – HEAF located in a bus bar compartment at the top of the switchgear (FDS simulation LV-BASE-10)

**B.2.5 Circuit Breaker to Bus Bar Compartment**

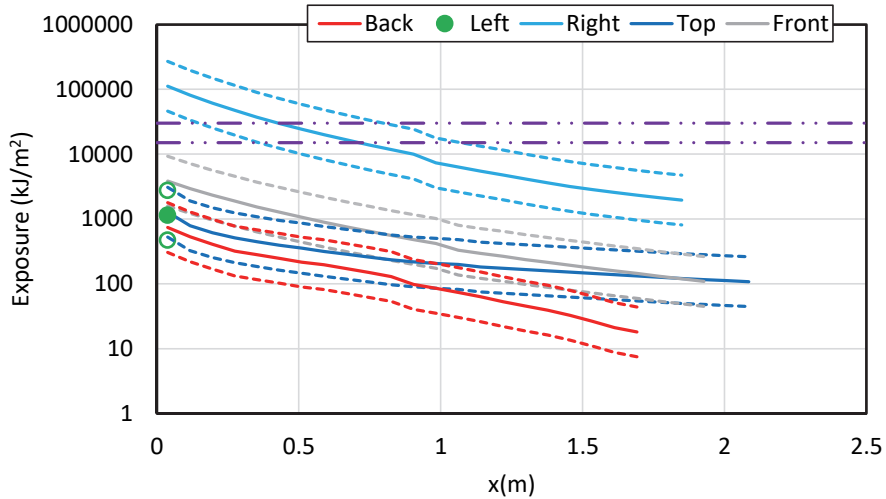


**Figure B-57**  
 Results for a LV SWGR with an aluminum bus bar with a HEAF based on FEDB 50935 – HEAF initially located in a middle-height circuit breaker compartment and moves to the bus bar compartment at the same height (FDS simulation LV-BASE-5)

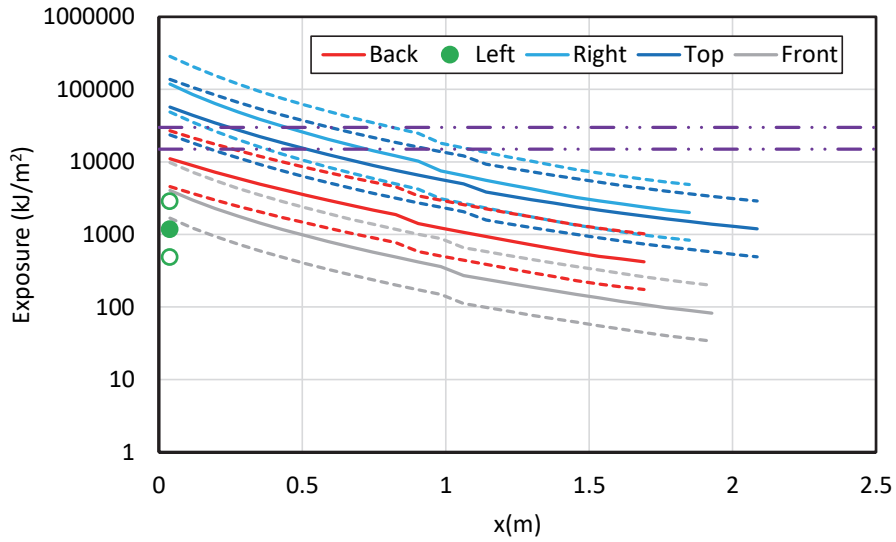


**Figure B-58**  
 Results for a LV SWGR with an aluminum bus bar with a HEAF based on FEDB 50935 – HEAF initially located in a circuit breaker compartment at the top of the switchgear and moves to the bus bar compartment at the same height (FDS simulation LV-BASE-6)

### B.3 Non-Segregated Bus Ducts

#### B.3.1 Bus Duct Straight Segment

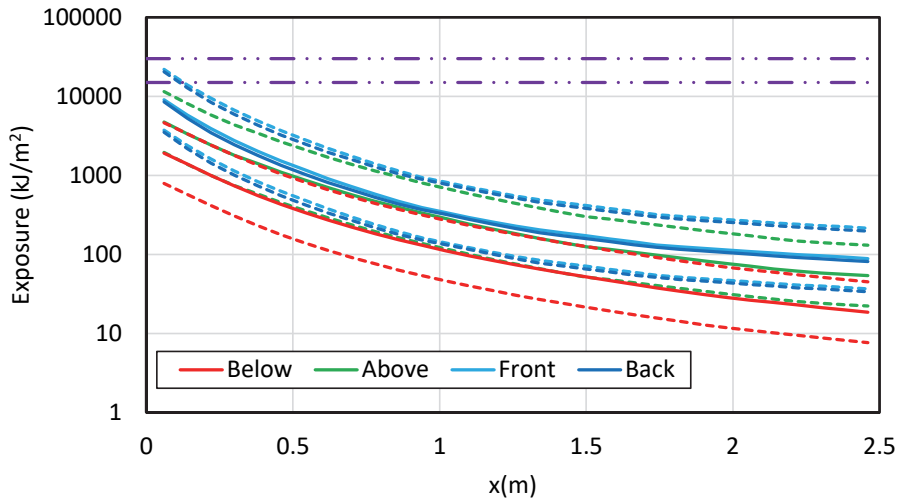


**Figure B-59**  
 Results for a straight run, steel duct NSBD with aluminum bus bars – 34 MJ HEAF (FDS simulation NSBD-1)

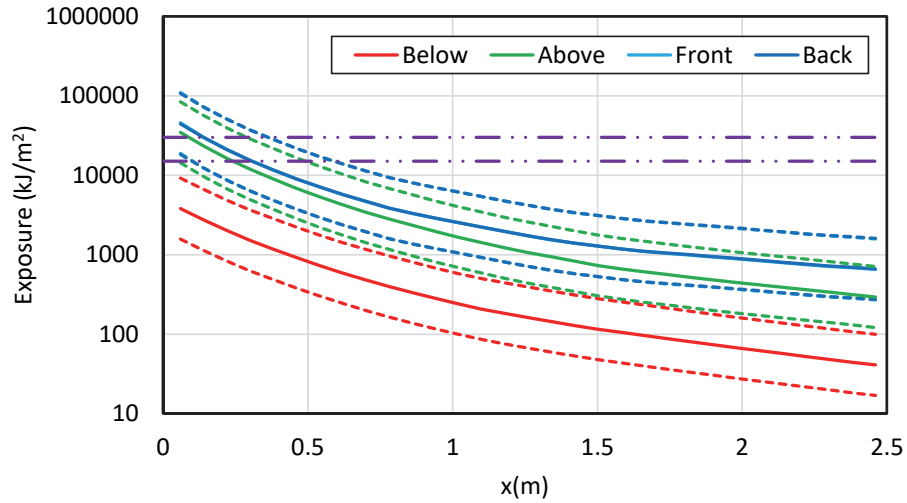


**Figure B-B-60**  
Results for a straight run, steel duct NSBD with aluminum bus bars – 68 MJ HEAF  
(FDS simulation NSBD-2)

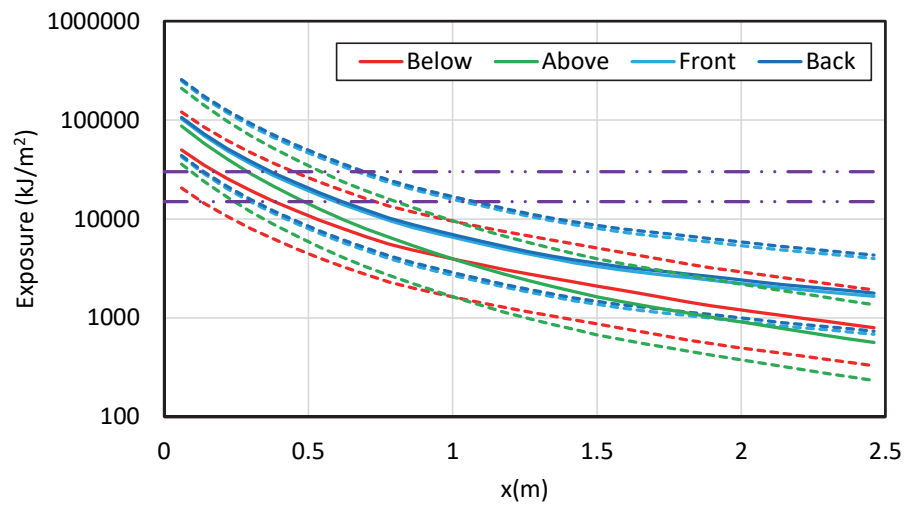


**Figure B-61**  
Results for a straight run, steel duct NSBD with aluminum bus bars – 135 MJ HEAF  
(FDS simulation NSBD-3)

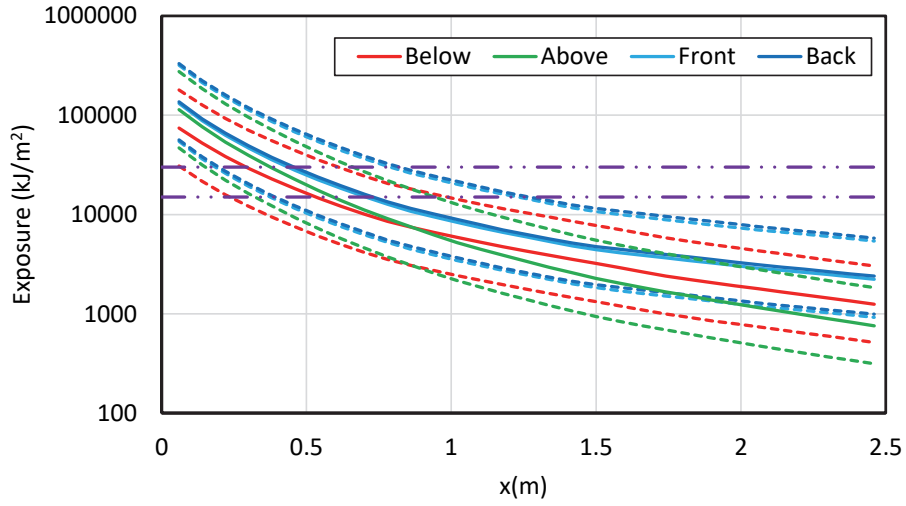


**Figure B-62**  
Results for a straight run, steel duct NSBD with aluminum bus bars – 169 MJ HEAF  
(FDS simulation NSBD-4)

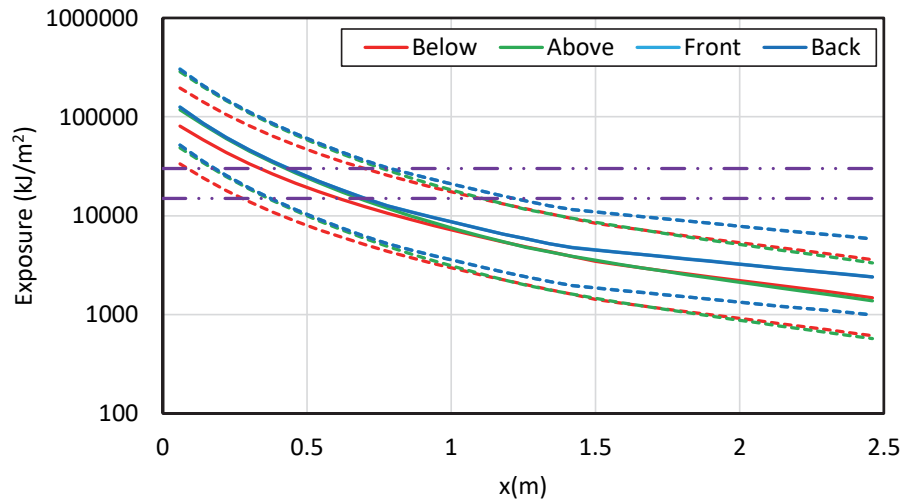


**Figure B-63**  
Results for a straight run, steel duct NSBD with aluminum bus bars – 132 MJ HEAF  
(FDS simulation NSBD-5)

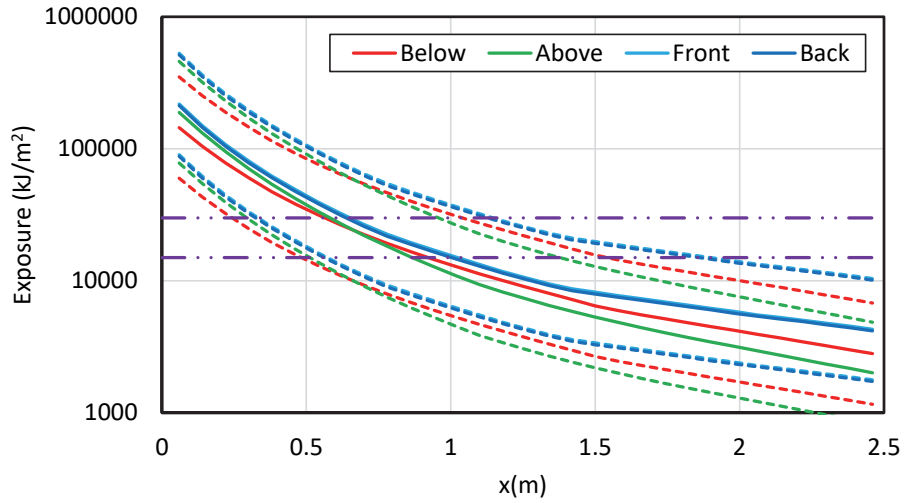


**Figure B-64**  
Results for a straight run, steel duct NSBD with aluminum bus bars – 233 MJ HEAF (FDS simulation NSBD-6)

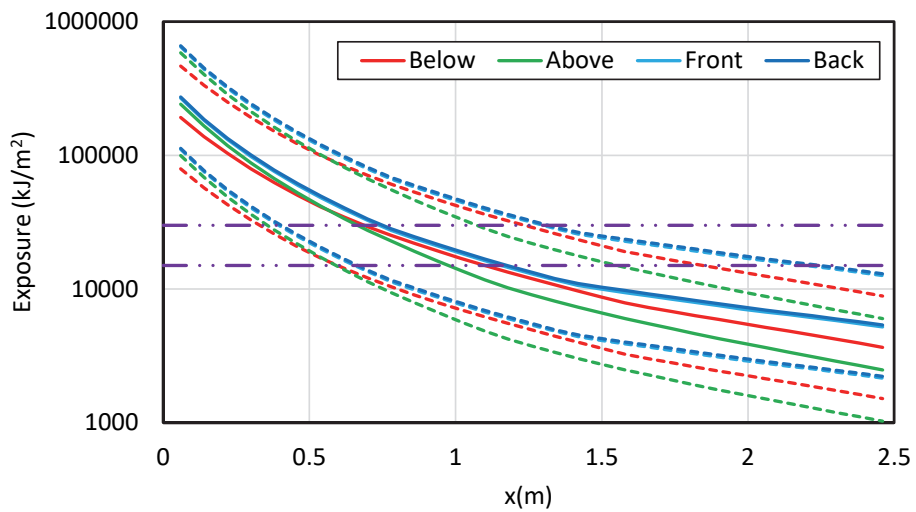


**Figure B-65**  
Results for a straight run, steel duct NSBD with aluminum bus bars – 300 MJ HEAF (FDS simulation NSBD-7)

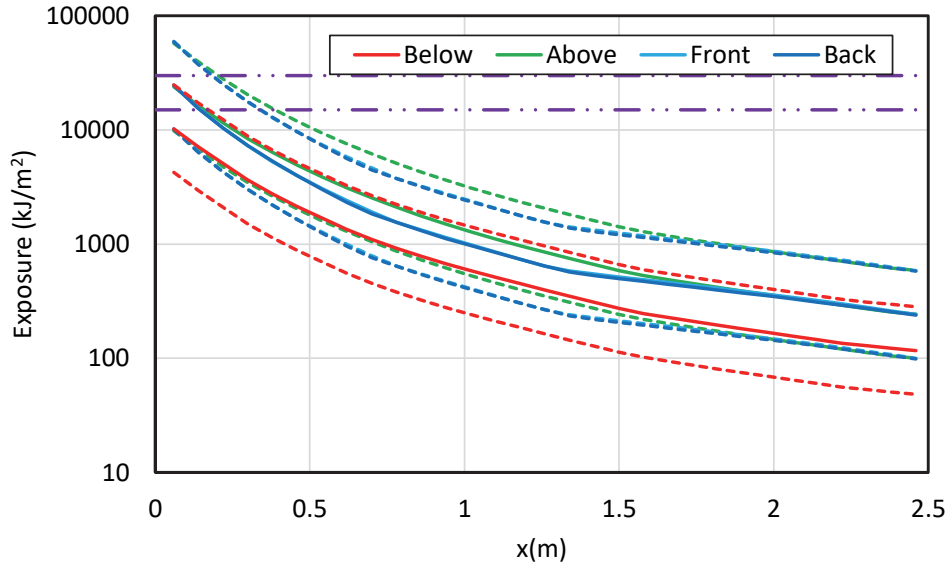


**Figure B-66**  
Results for a straight run, aluminum duct NSBD with aluminum bus bars – 34 MJ HEAF  
(FDS simulation NSBD-8)

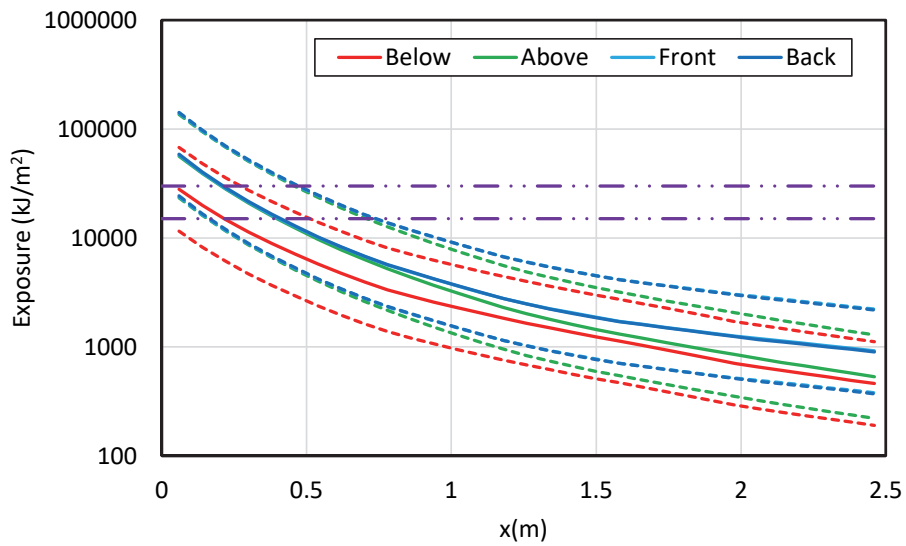


**Figure B-67**  
Results for a straight run, aluminum duct NSBD with aluminum bus bars – 68 MJ HEAF  
(FDS simulation NSBD-9)

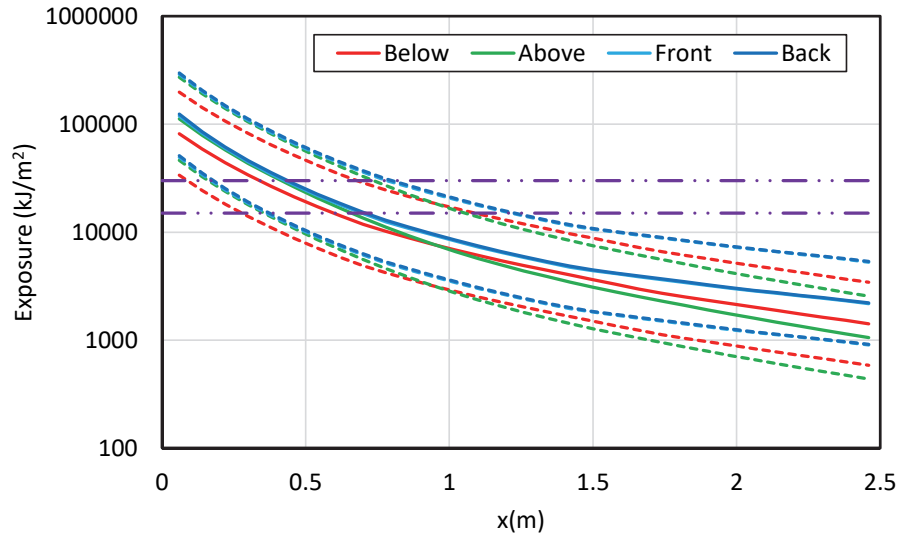


**Figure B-68**  
Results for a straight run, aluminum duct NSBD with aluminum bus bars – 135 MJ HEAF (FDS simulation NSBD-10)

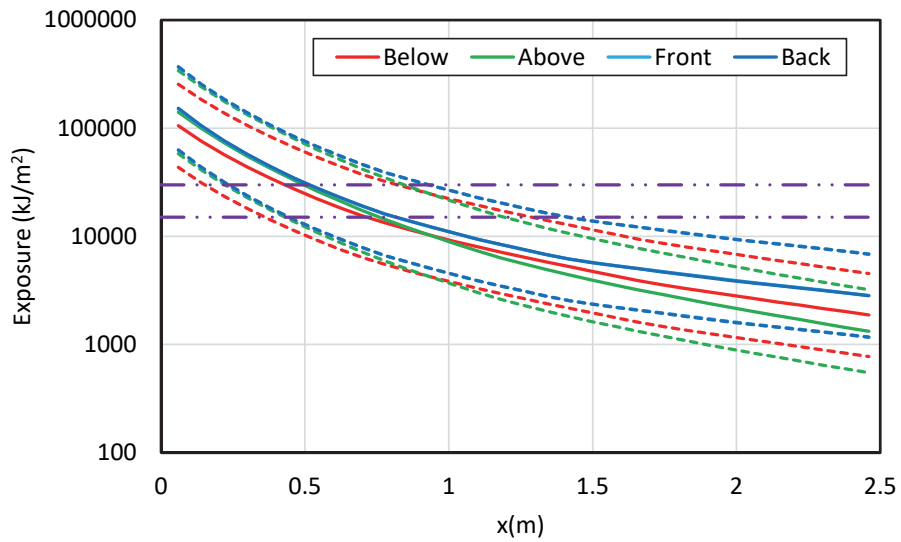


**Figure B-69**  
Results for a straight run, aluminum duct NSBD with aluminum bus bars – 169 MJ HEAF (FDS simulation NSBD-11)

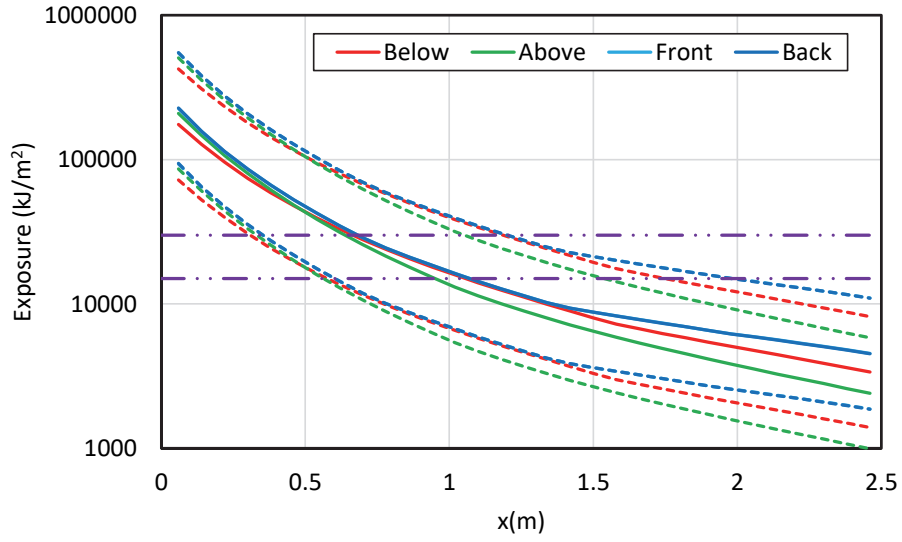


**Figure B-70**  
Results for a straight run, aluminum duct NSBD with aluminum bus bars – 233 MJ HEAF  
(FDS simulation NSBD-12)

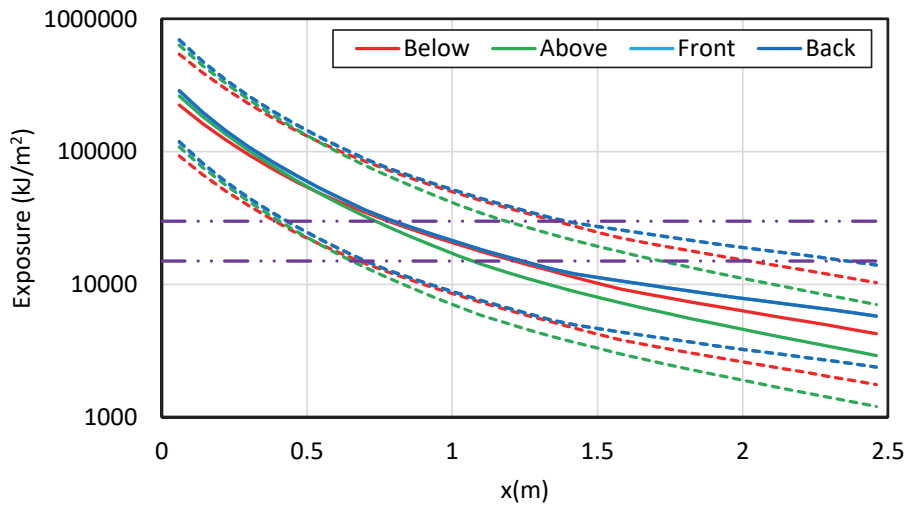


**Figure B-71**  
Results for a straight run, aluminum duct NSBD with aluminum bus bars – 300 MJ HEAF  
(FDS simulation NSBD-13)

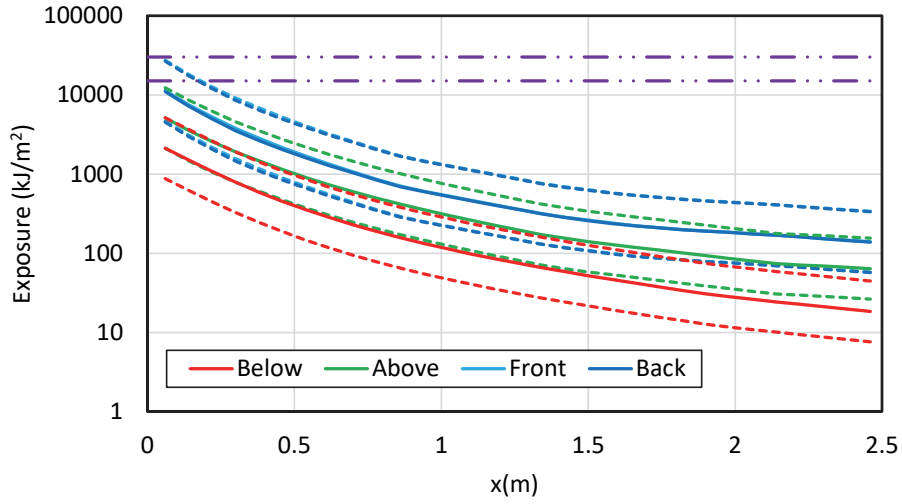


**Figure B-72**  
Results for a straight run, steel duct NSBD with copper bus bars – 34 MJ HEAF (FDS simulation NSBD-14)

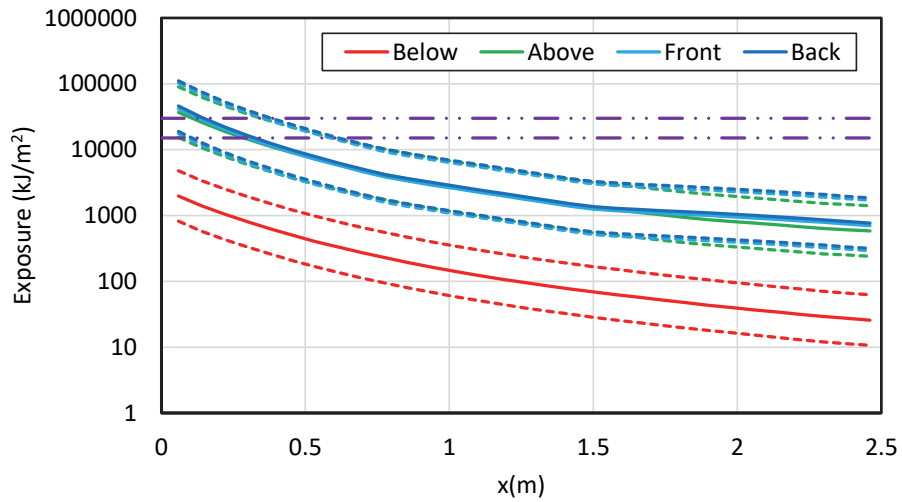


**Figure B-73**  
Results for a straight run, steel duct NSBD with copper bus bars – 68 MJ HEAF (FDS simulation NSBD-15)

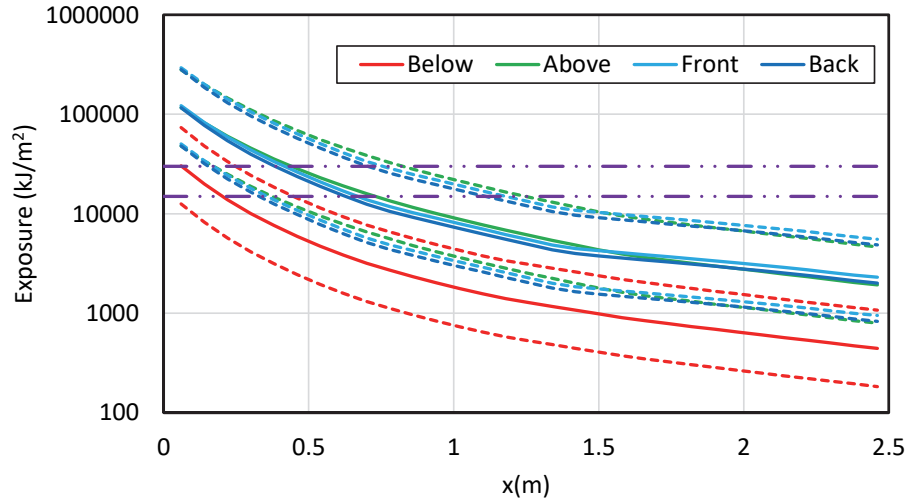


**Figure B-74**  
Results for a straight run, steel duct NSBD with copper bus bars – 135 MJ HEAF (FDS simulation NSBD-16)

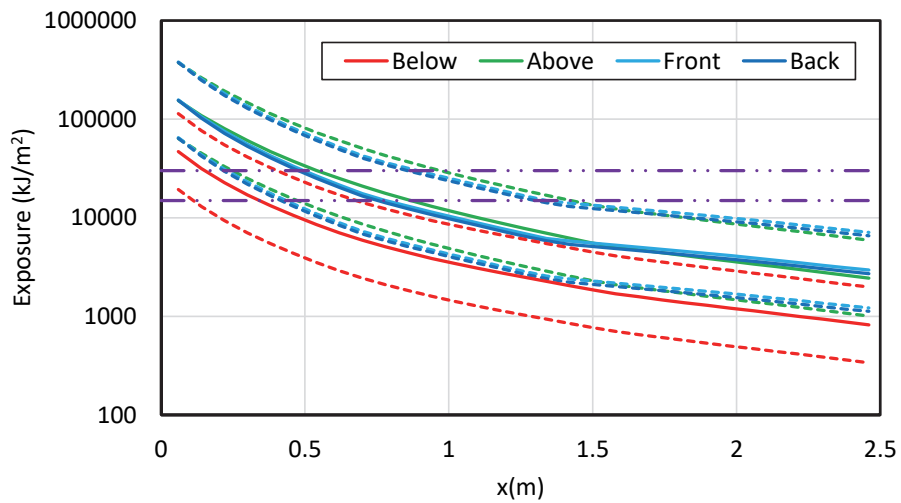


**Figure B-75**  
Results for a straight run, steel duct NSBD with copper bus bars – 169 MJ HEAF (FDS simulation NSBD-17)

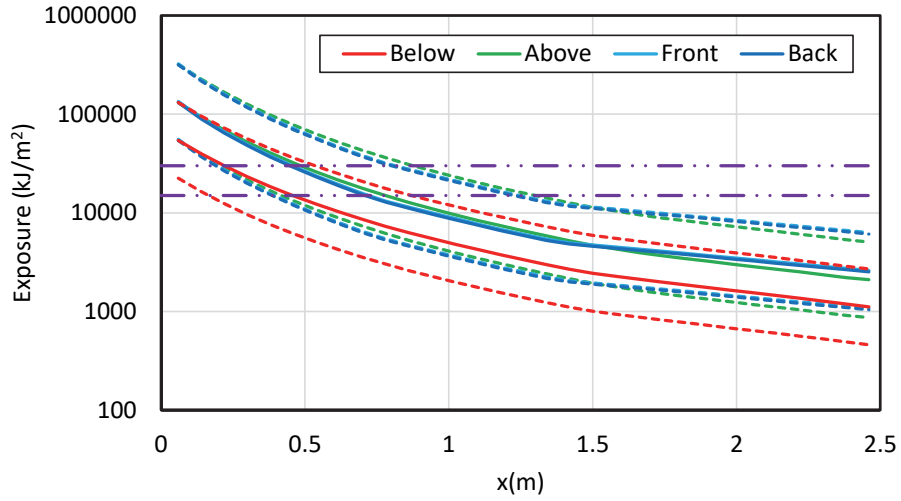


**Figure B-76**  
Results for a straight run, steel duct NSBD with copper bus bars – 132 MJ HEAF  
(FDS simulation NSBD-18)

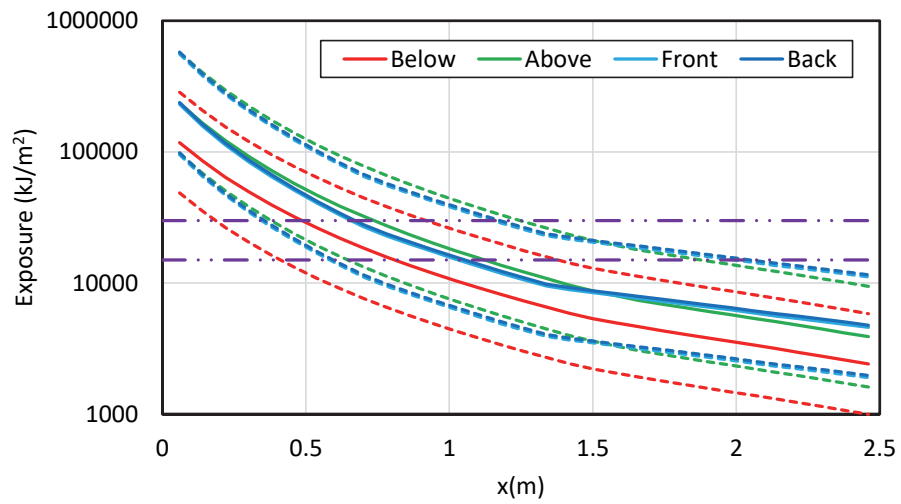


**Figure B-77**  
Results for a straight run, steel duct NSBD with copper bus bars – 233 MJ HEAF  
(FDS simulation NSBD-19)

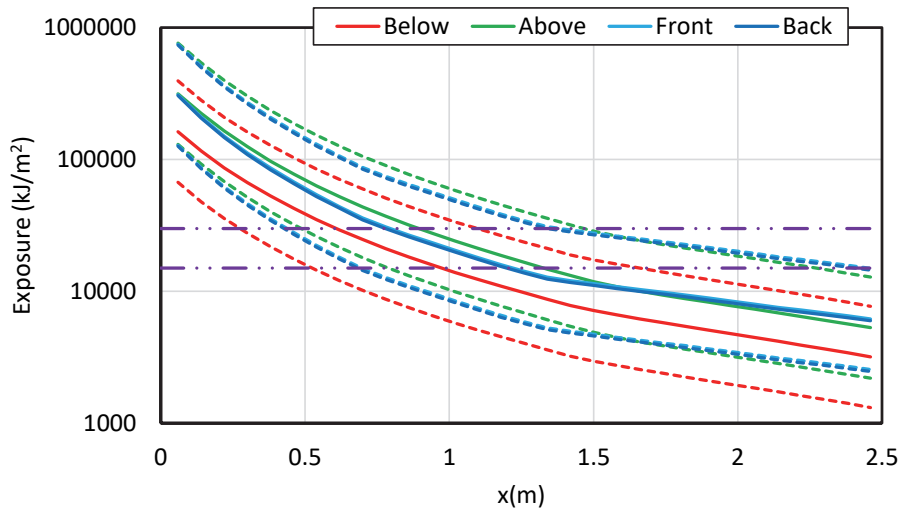


**Figure B-78**  
Results for a straight run, steel duct NSBD with copper bus bars – 300 MJ HEAF  
(FDS simulation NSBD-20)

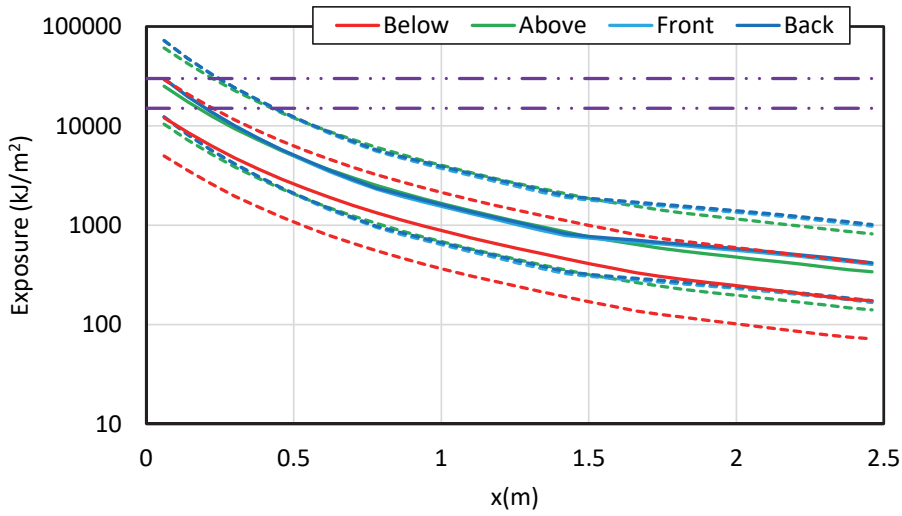


**Figure B-79**  
Results for a straight run, aluminum duct NSBD with copper bus bars – 34 MJ HEAF  
(FDS simulation NSBD-21)

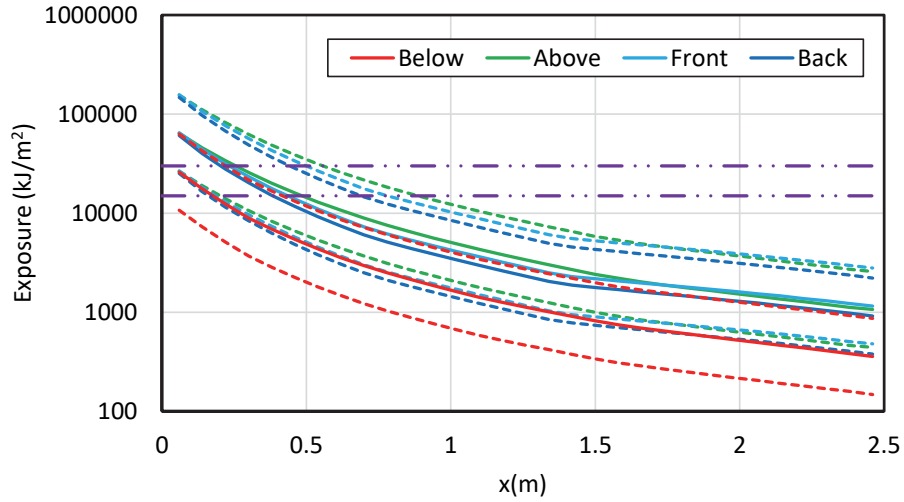


**Figure B-80**  
Results for a straight run, aluminum duct NSBD with copper bus bars – 68 MJ HEAF  
(FDS simulation NSBD-22)

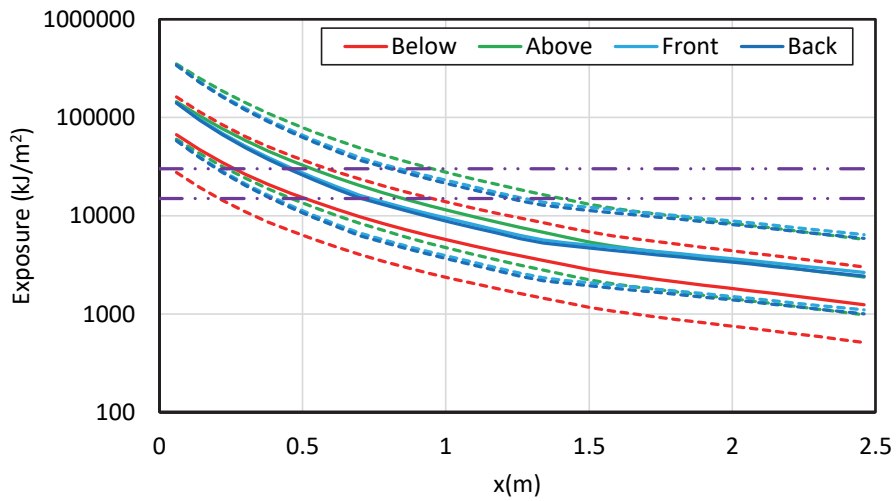


**Figure B-81**  
Results for a straight run, aluminum duct NSBD with copper bus bars – 135 MJ HEAF  
(FDS simulation NSBD-23)

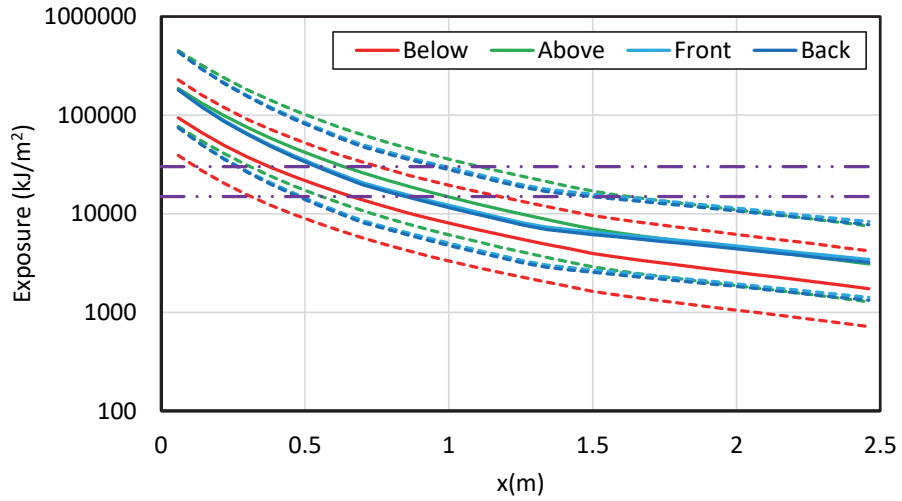


**Figure B-82**  
Results for a straight run, aluminum duct NSBD with copper bus bars – 169 MJ HEAF  
(FDS simulation NSBD-24)

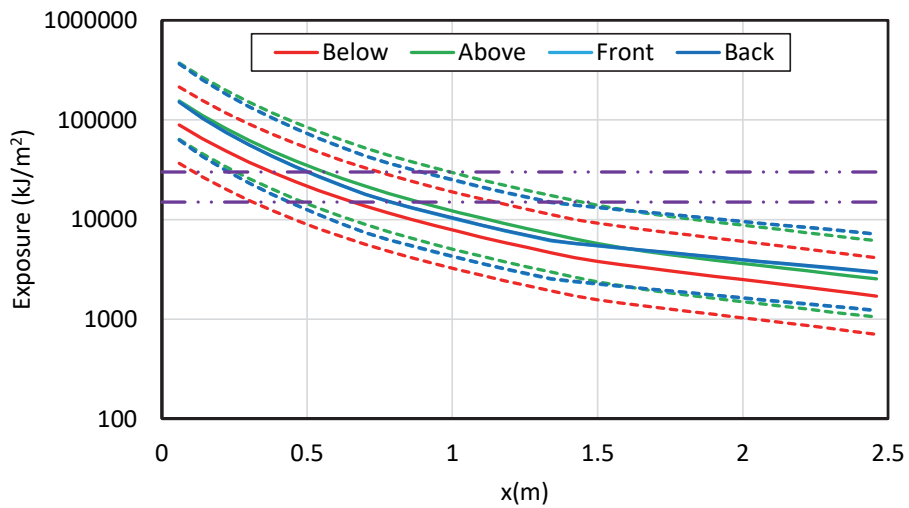


**Figure B-83**  
Results for a straight run, aluminum duct NSBD with copper bus bars – 132 MJ HEAF  
(FDS simulation NSBD-25)

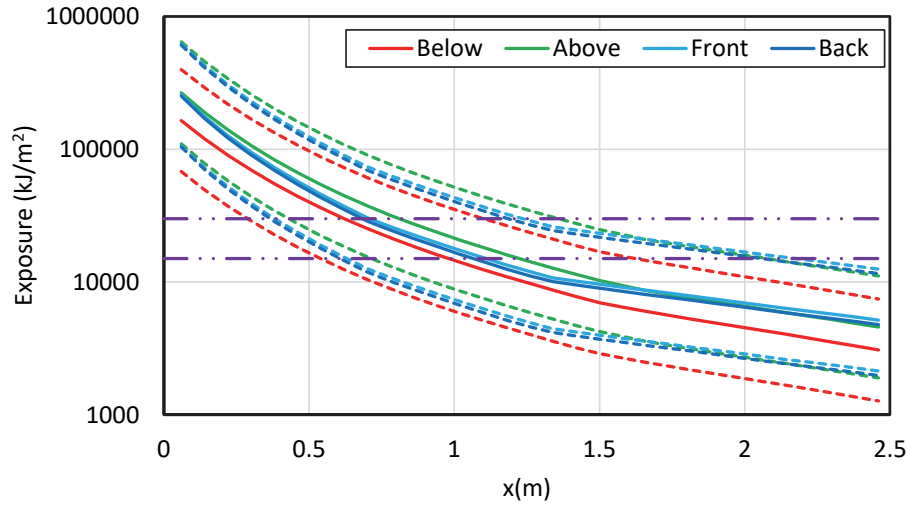


**Figure B-84**  
Results for a straight run, aluminum duct NSBD with copper bus bars – 233 MJ HEAF  
(FDS simulation NSBD-26)

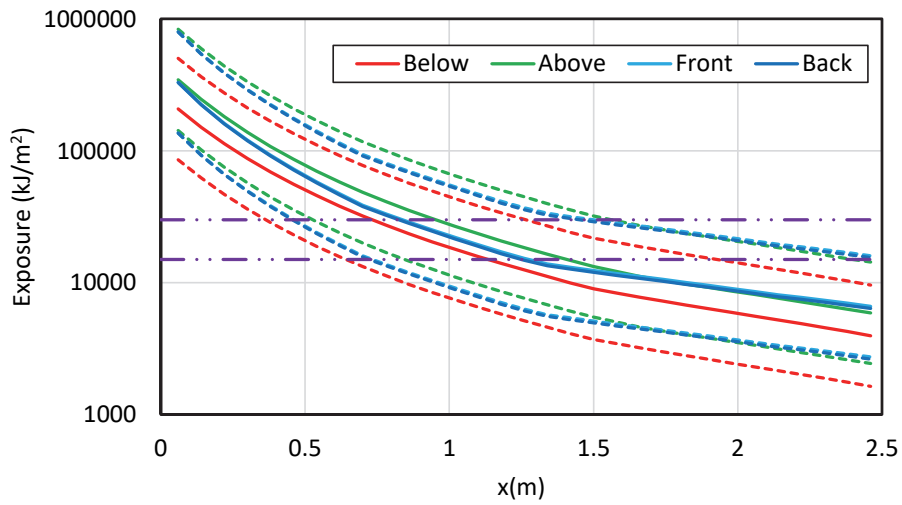


**Figure B-85**  
Results for a straight run, aluminum duct NSBD with copper bus bars – 300 MJ HEAF  
(FDS simulation NSBD-27)

### B.3.2 Bus Duct Elbow

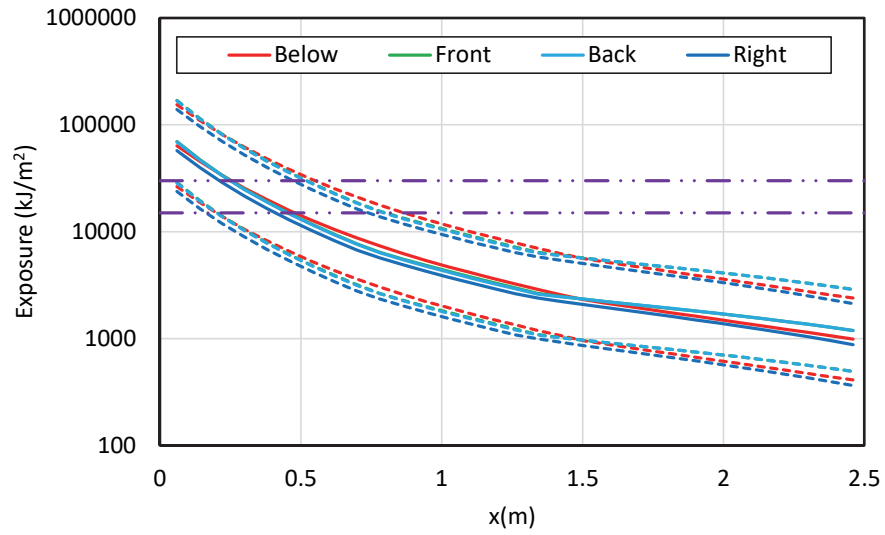


**Figure B-86**  
Results for an aluminum duct NSBD elbow with aluminum bus bars – 68 MJ HEAF  
(FDS simulation NSBD-52)

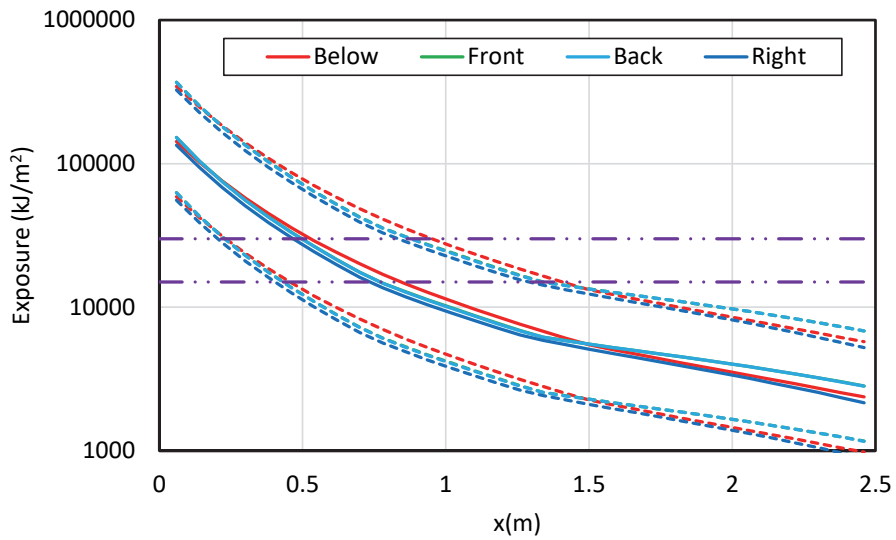


**Figure B-87**  
Results for an aluminum duct NSBD elbow with aluminum bus bars – 135 MJ HEAF  
(FDS simulation NSBD-53)

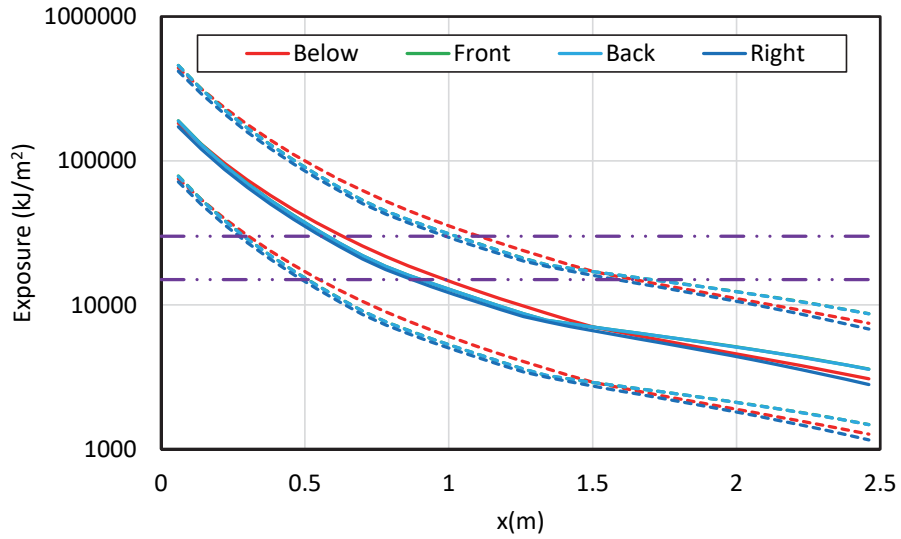


**Figure B-88**  
Results for an aluminum duct NSBD elbow with aluminum bus bars – 169 MJ HEAF (FDS simulation NSBD-54)

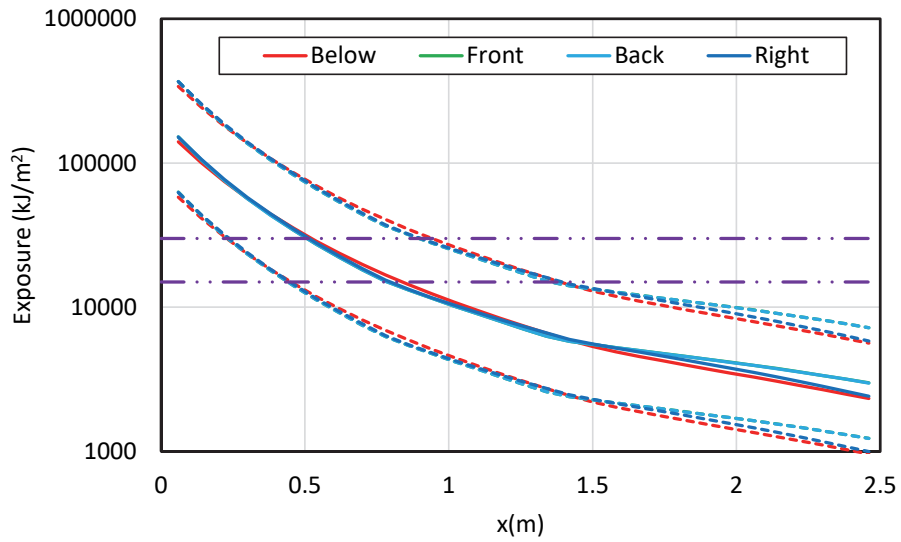


**Figure B-89**  
Results for an aluminum duct NSBD elbow with aluminum bus bars – 132 MJ HEAF (FDS simulation NSBD-55)

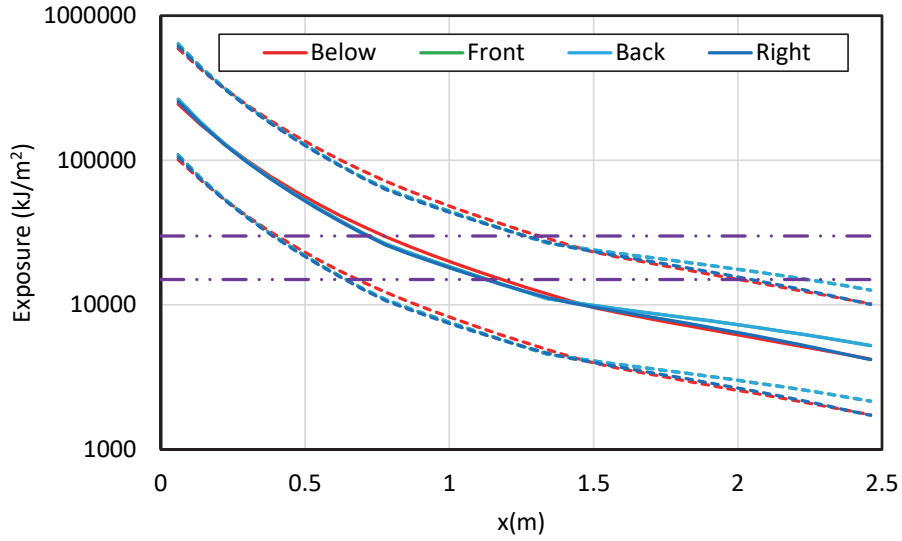


**Figure B-90**  
Results for an aluminum duct NSBD elbow with aluminum bus bars – 233 MJ HEAF (FDS simulation NSBD-56)

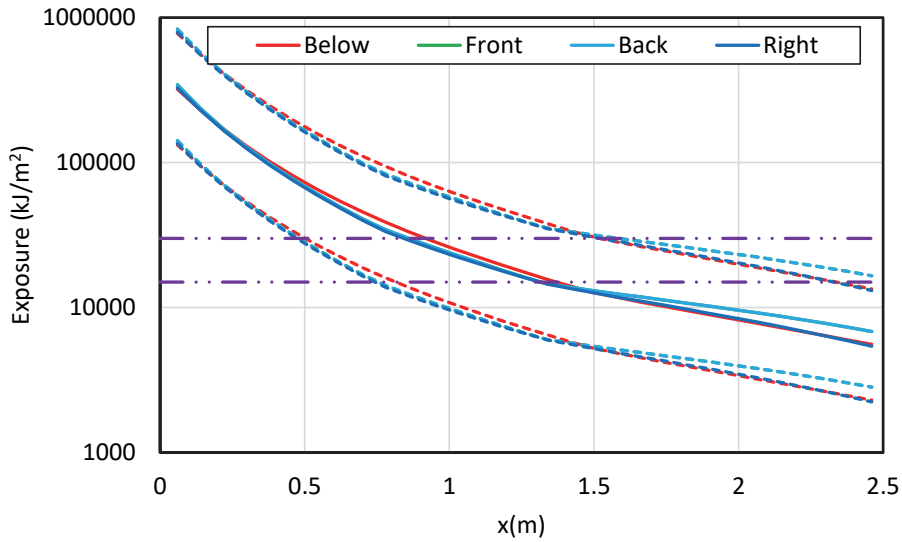


**Figure B-91**  
Results for an aluminum duct NSBD elbow with aluminum bus bars – 300 MJ HEAF (FDS simulation NSBD-57)

### B.3.3 Bus Duct Tee

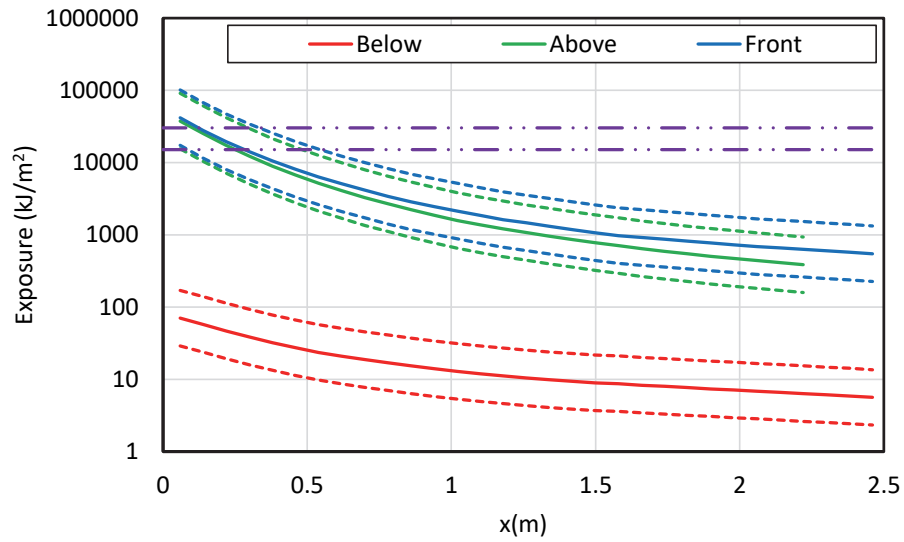


**Figure B-92**  
 Results for a steel duct NSBD tee with aluminum bus bars – 68 MJ HEAF (FDS simulation NSBD-28)

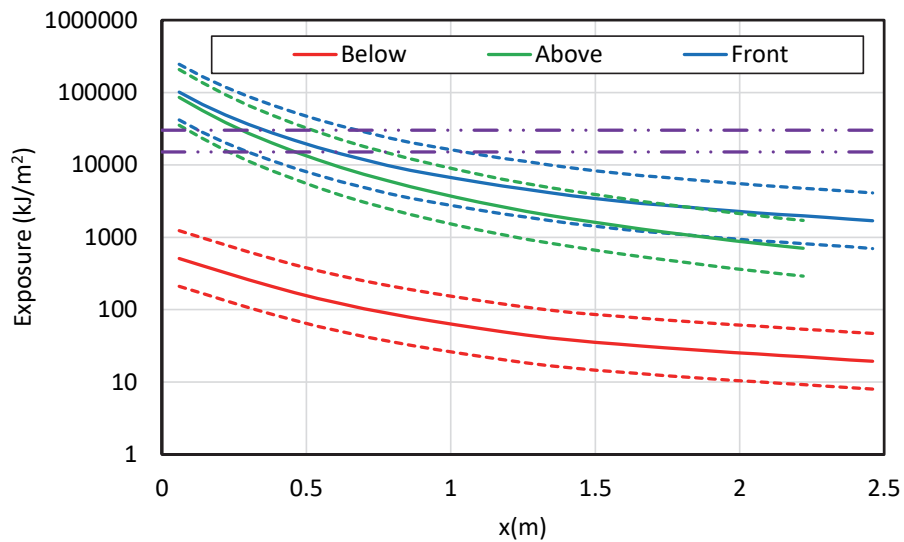


**Figure B-93**  
 Results for a steel duct NSBD tee with aluminum bus bars – 135 MJ HEAF (FDS simulation NSBD-29)

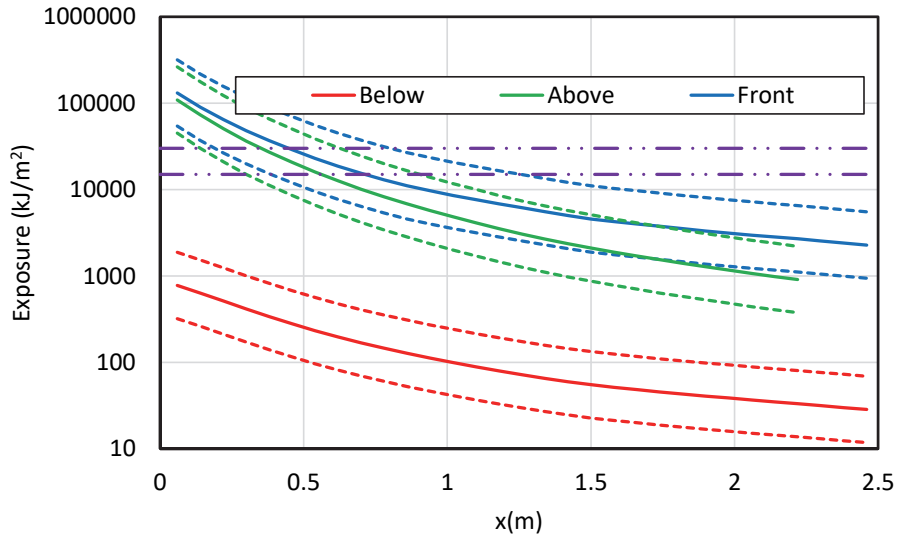


**Figure B-94**  
Results for a steel duct NSBD tee with aluminum bus bars – 169 MJ HEAF (FDS simulation NSBD-30)

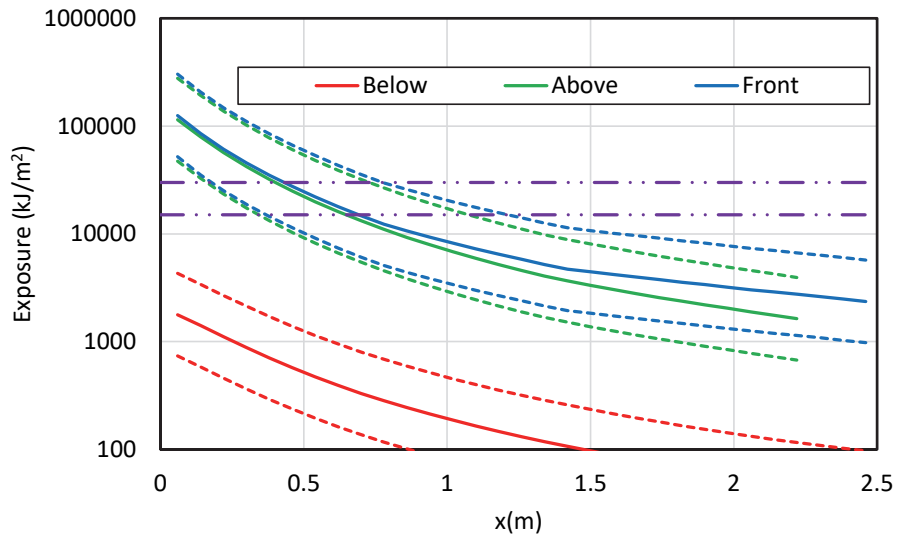


**Figure B-95**  
Results for a steel duct NSBD tee with aluminum bus bars – 132 MJ HEAF (FDS simulation NSBD-31)

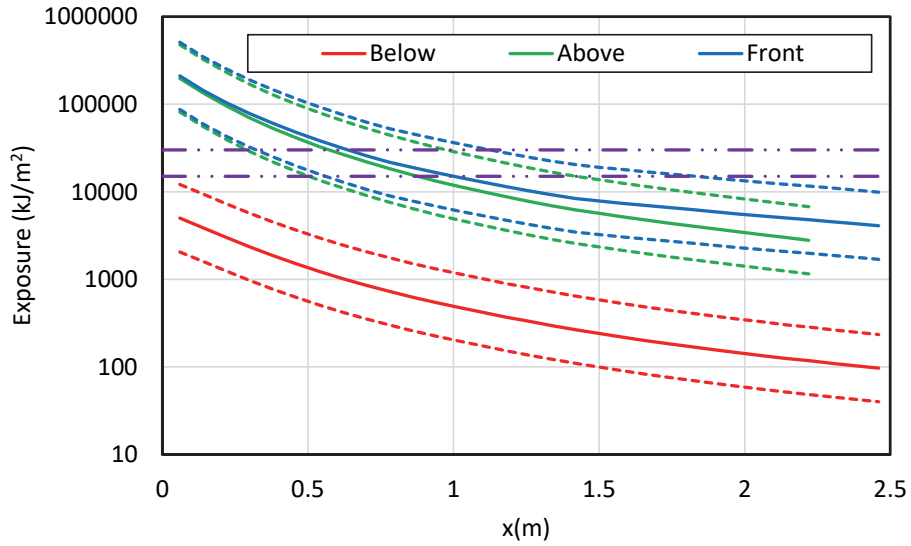


**Figure B-96**  
Results for a steel duct NSBD tee with aluminum bus bars – 233 MJ HEAF (FDS simulation NSBD-32)

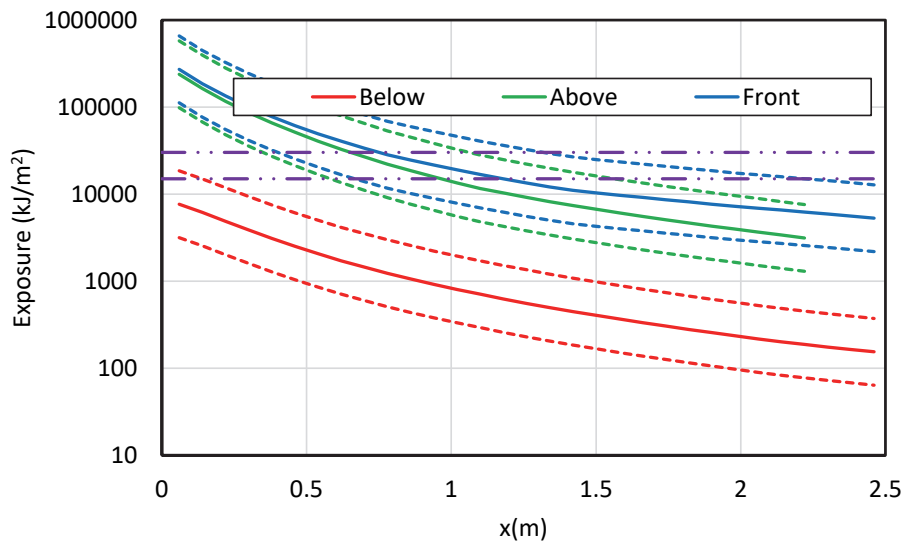


**Figure B-97**  
Results for a steel duct NSBD tee with aluminum bus bars – 300 MJ HEAF (FDS simulation NSBD-33)

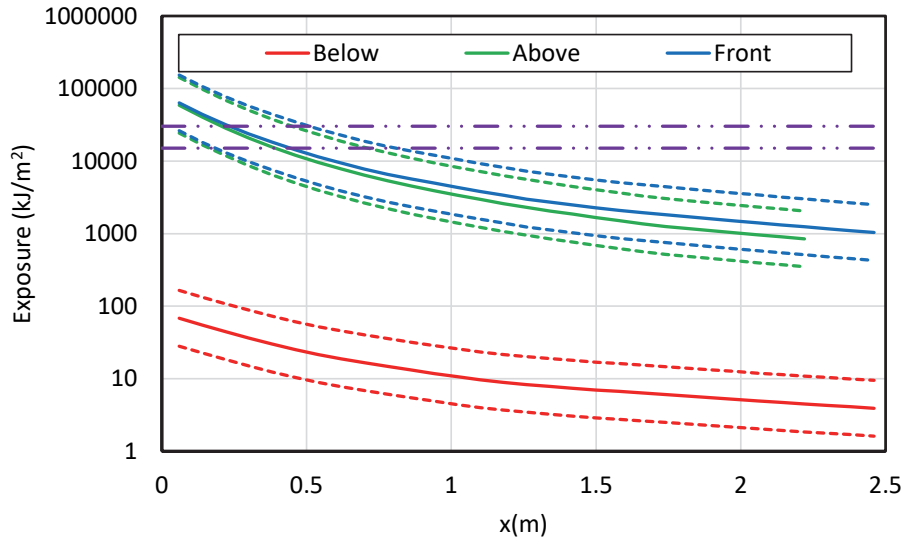


**Figure B-98**  
Results for an aluminum duct NSBD tee with aluminum bus bars – 68 MJ HEAF (FDS simulation NSBD-34)

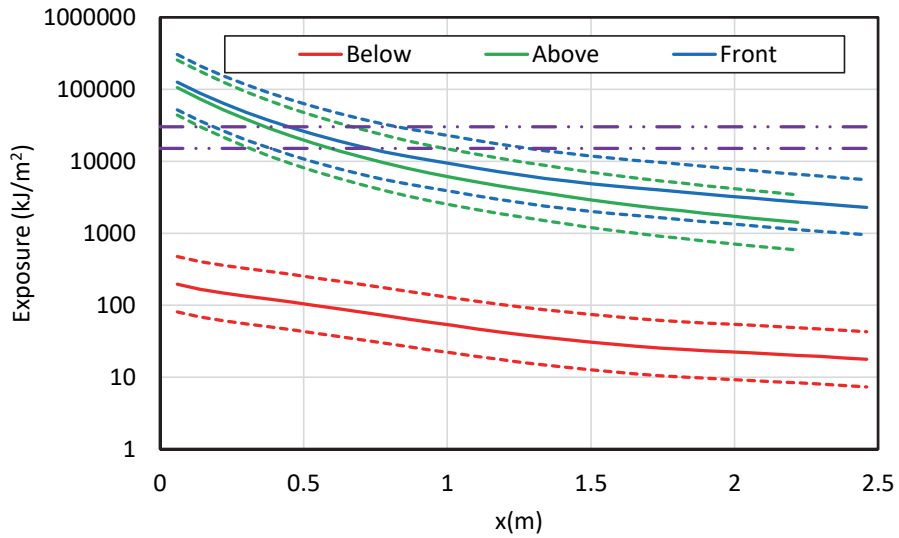


**Figure B-99**  
Results for an aluminum duct NSBD tee with aluminum bus bars – 135 MJ HEAF (FDS simulation NSBD-35)

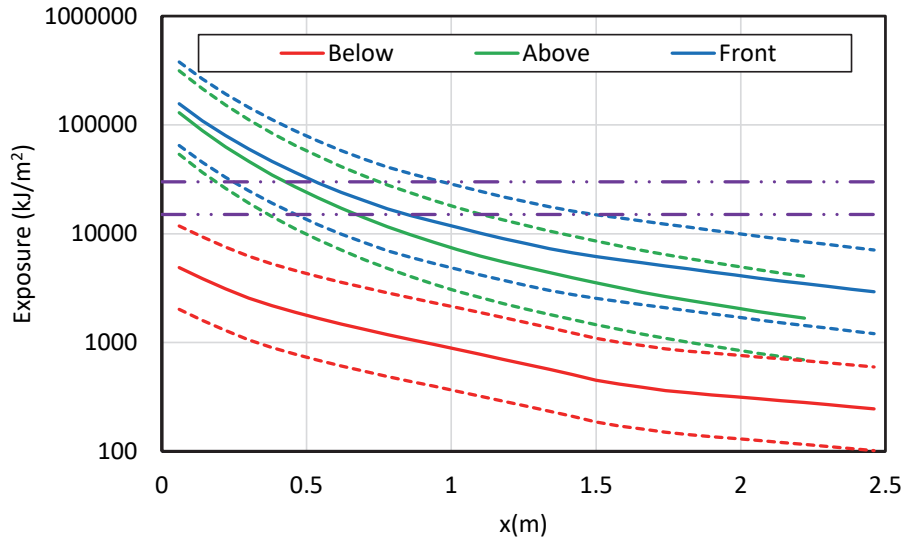


**Figure B-100**  
Results for an aluminum duct NSBD tee with aluminum bus bars – 169 MJ HEAF (FDS simulation NSBD-36)

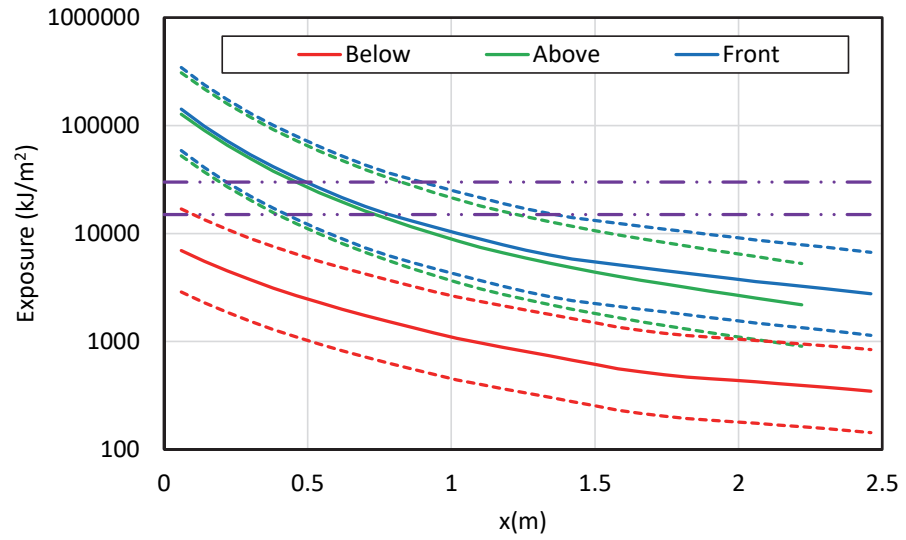


**Figure B-101**  
Results for an aluminum duct NSBD tee with aluminum bus bars – 132 MJ HEAF (FDS simulation NSBD-37)

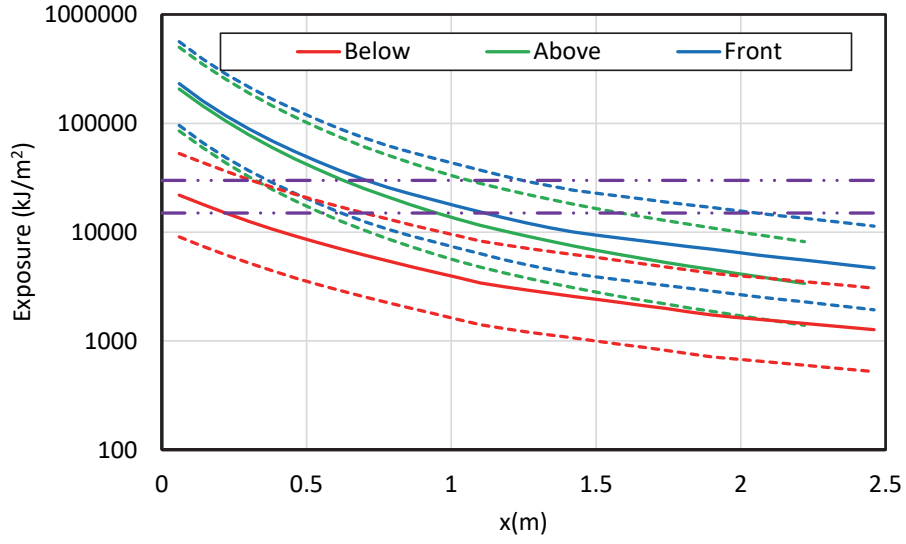


**Figure B-102**  
Results for an aluminum duct NSBD tee with aluminum bus bars – 233 MJ HEAF (FDS simulation NSBD-38)

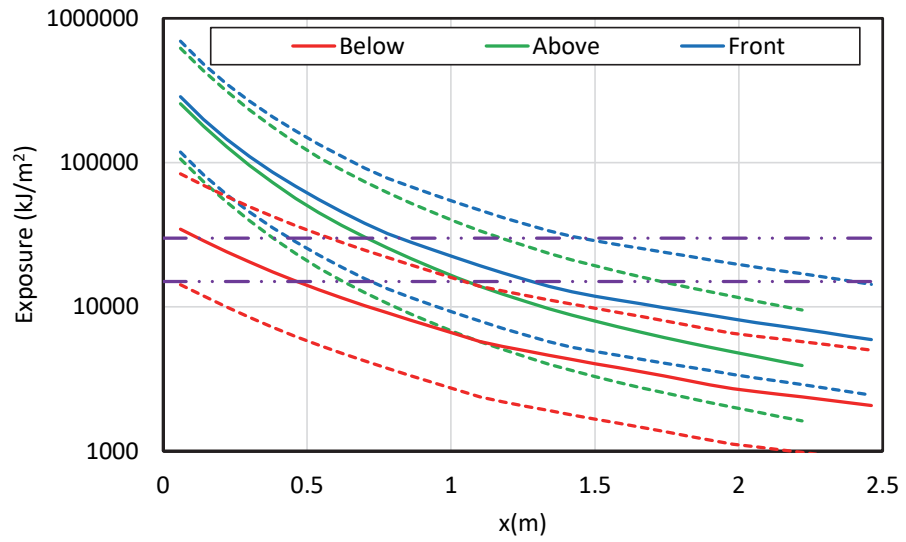


**Figure B-103**  
Results for an aluminum duct NSBD tee with aluminum bus bars – 300 MJ HEAF (FDS simulation NSBD-39)

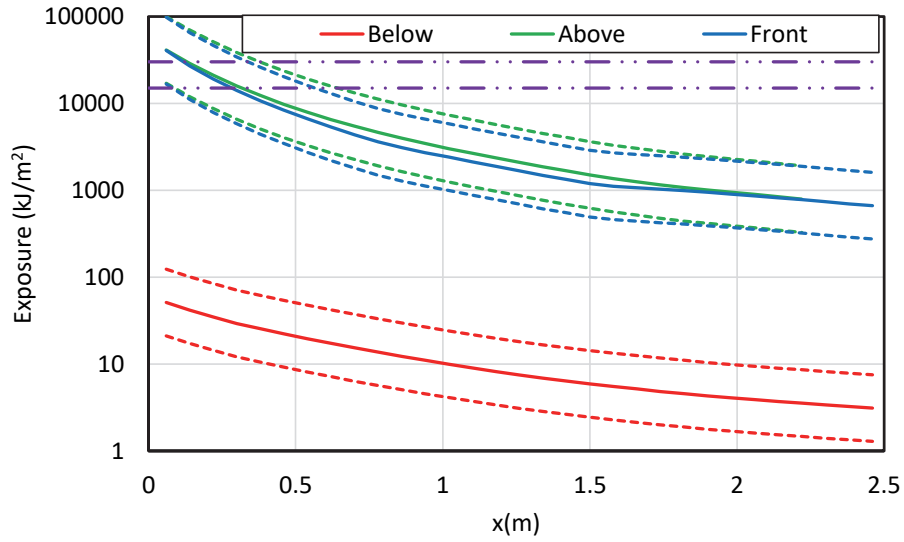


**Figure B-104**  
**Results for a steel duct NSBD tee with copper bus bars – 68 MJ HEAF (FDS simulation NSBD-40)**

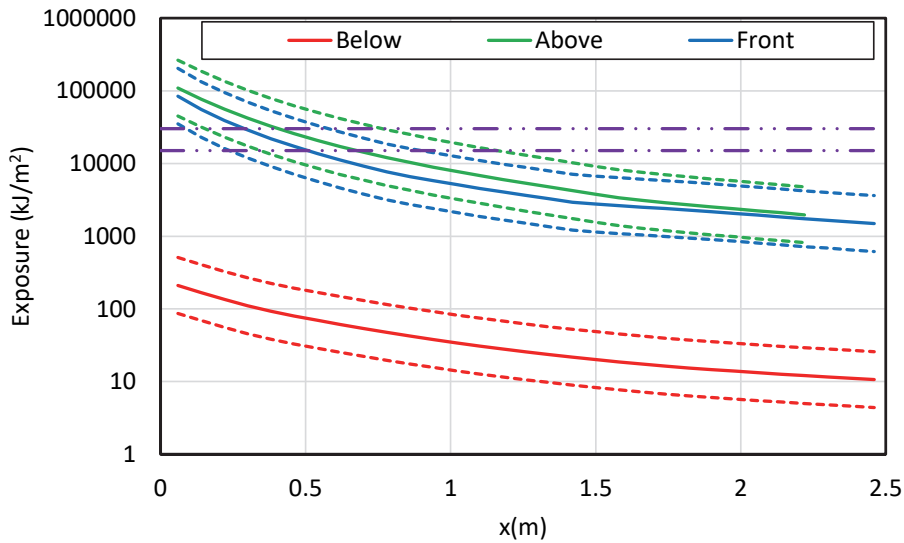


**Figure B-105**  
**Results for a steel duct NSBD tee with copper bus bars – 135 MJ HEAF (FDS simulation NSBD-41)**

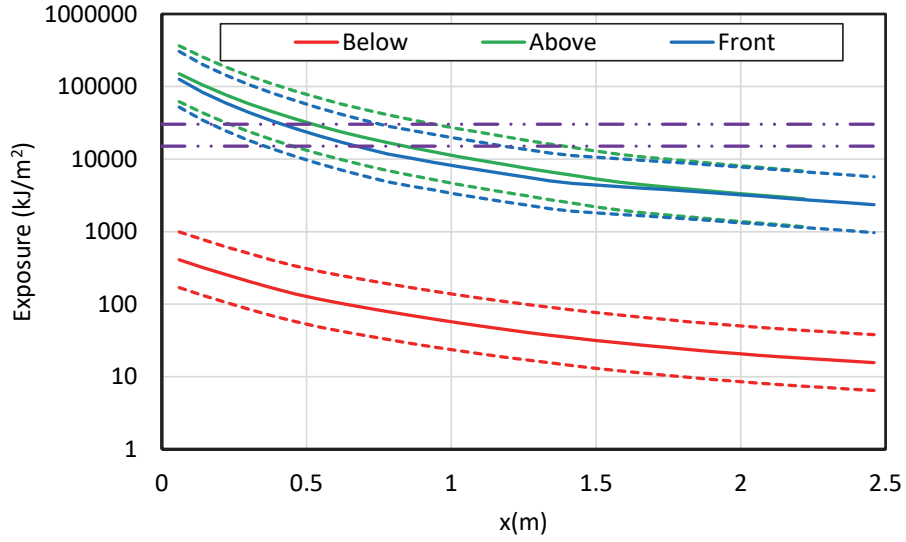


**Figure B-106**  
Results for a steel duct NSBD tee with copper bus bars – 169 MJ HEAF (FDS simulation NSBD-42)

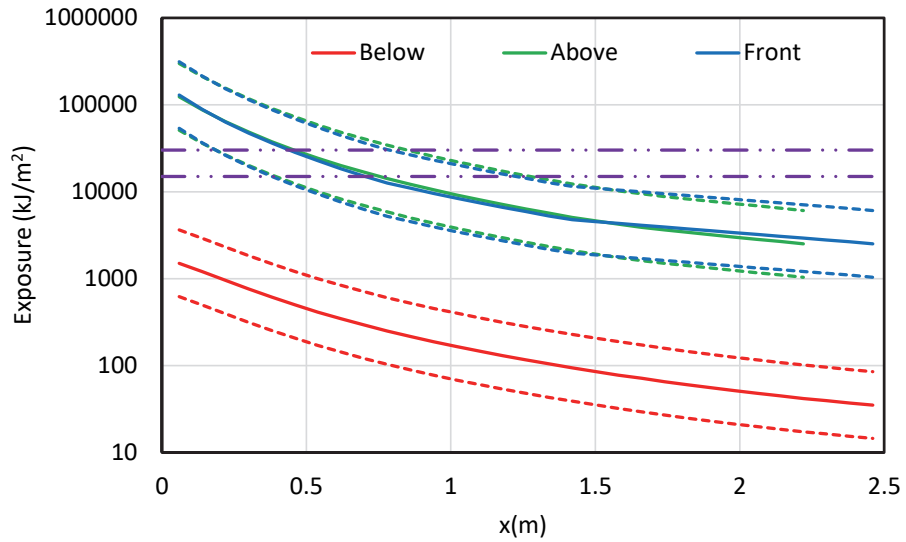


**Figure B-107**  
Results for a steel duct NSBD tee with copper bus bars – 132 MJ HEAF (FDS simulation NSBD-43)

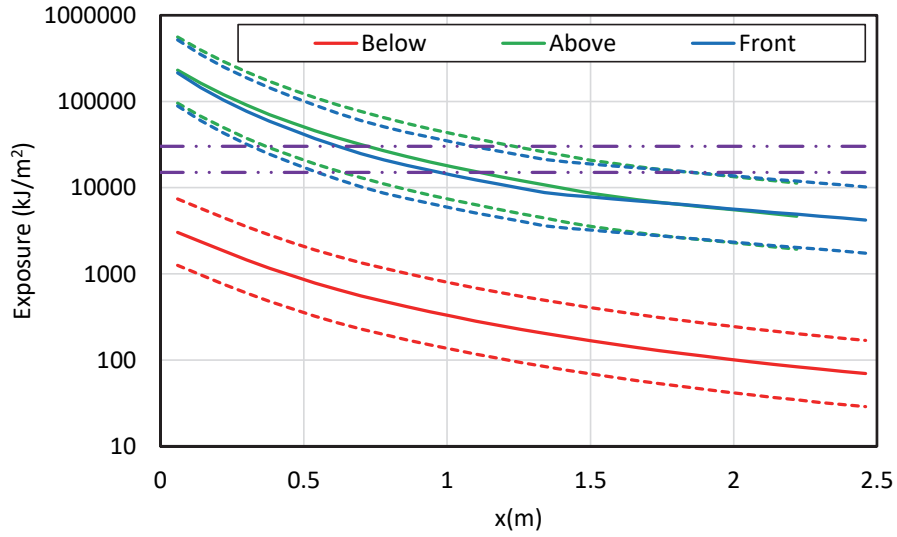


**Figure B-108**  
Results for a steel duct NSBD tee with copper bus bars – 233 MJ HEAF (FDS simulation NSBD-44)

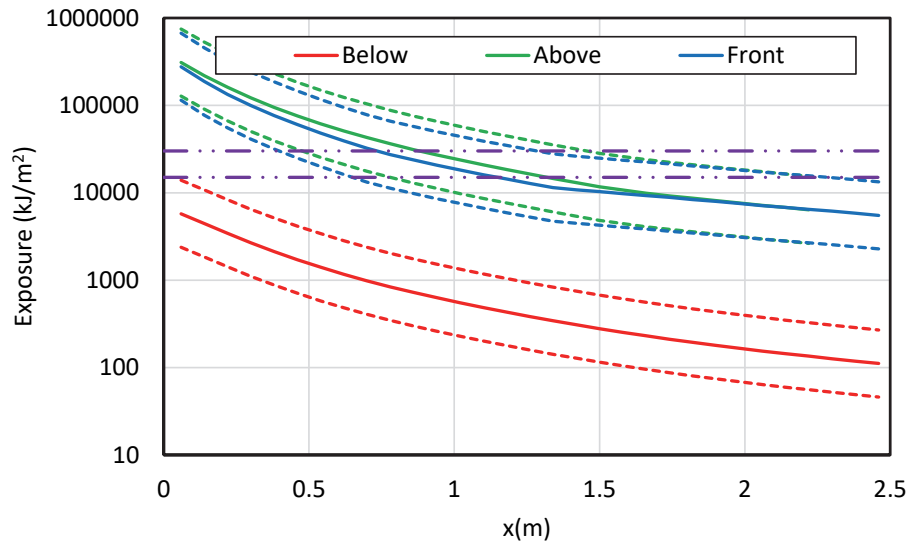


**Figure B-109**  
Results for a steel duct NSBD tee with copper bus bars – 300 MJ HEAF (FDS simulation NSBD-45)

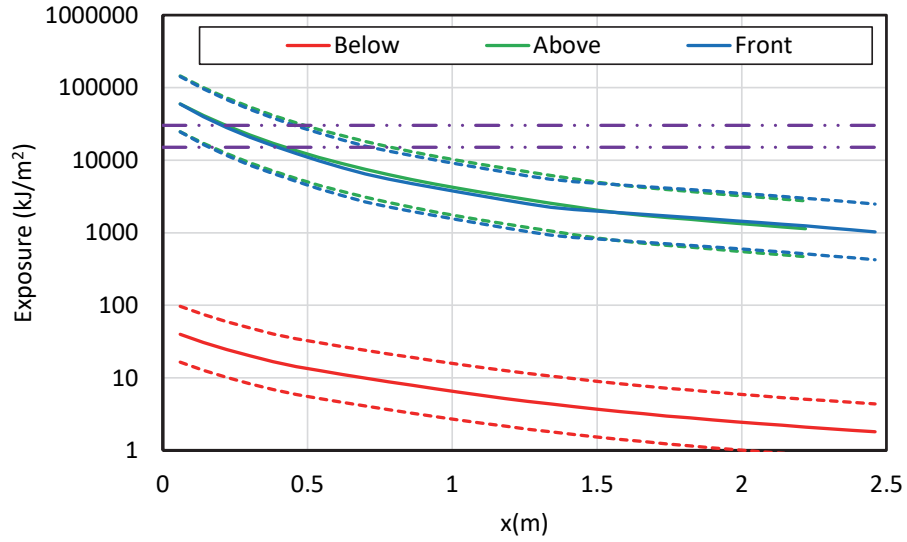


**Figure B-110**  
Results for an aluminum duct NSBD tee with copper bus bars – 68 MJ HEAF (FDS simulation NSBD-46)

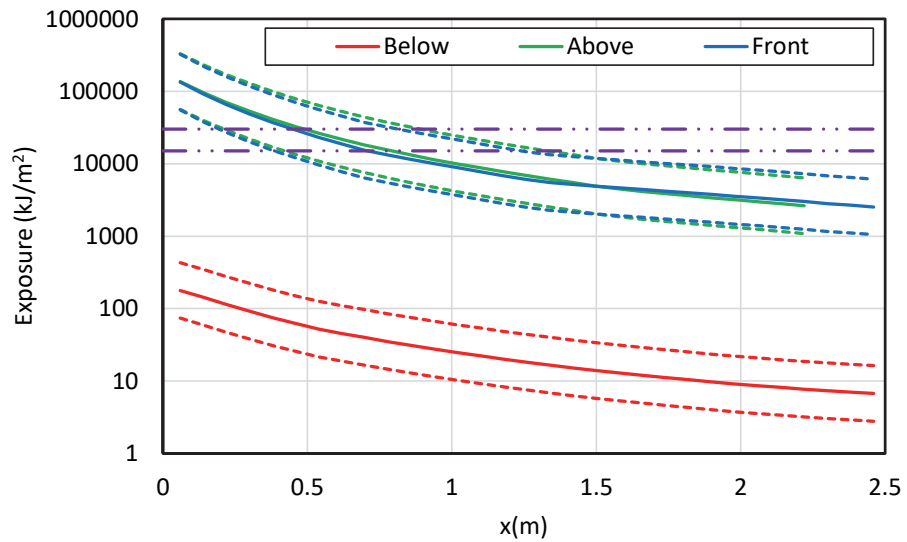


**Figure B-111**  
Results for an aluminum duct NSBD tee with copper bus bars – 135 MJ HEAF (FDS simulation NSBD-47)

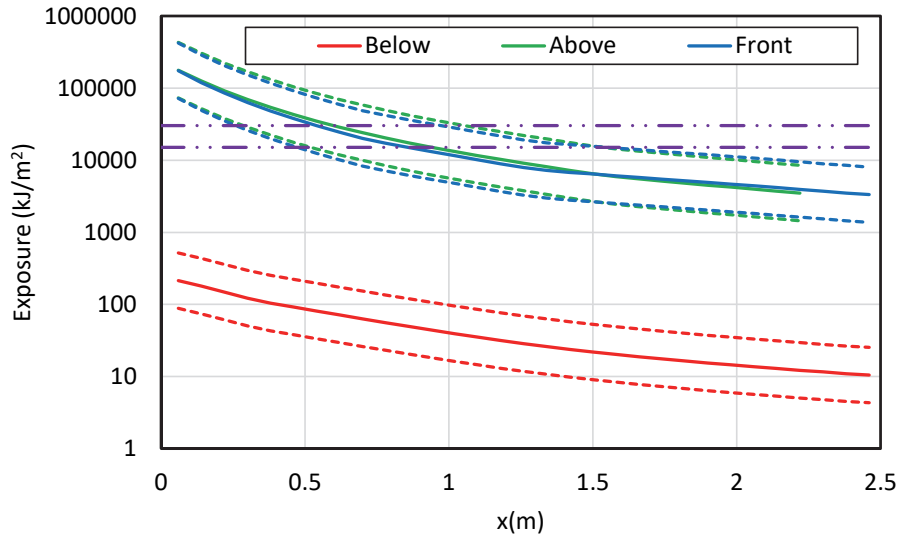


**Figure B-112**  
Results for an aluminum duct NSBD tee with copper bus bars – 169 MJ HEAF (FDS simulation NSBD-48)

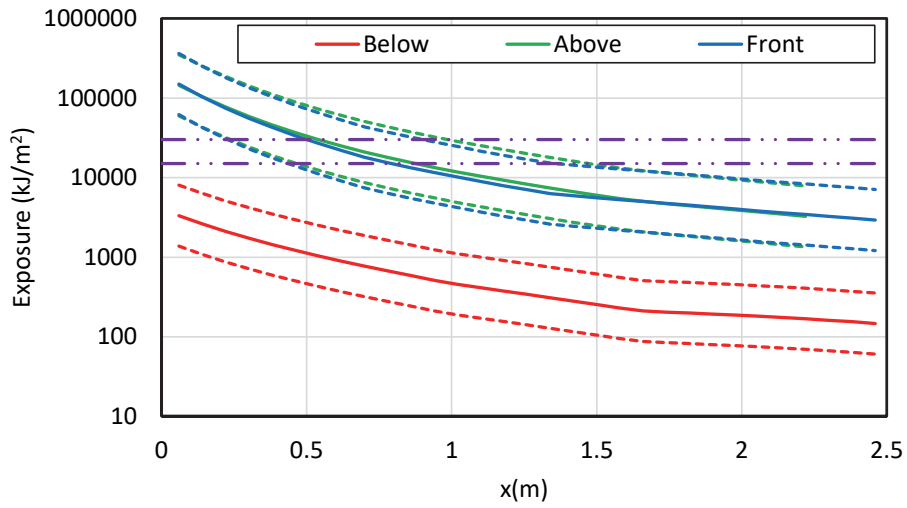


**Figure B-113**  
Results for an aluminum duct NSBD tee with copper bus bars – 132 MJ HEAF (FDS simulation NSBD-49)

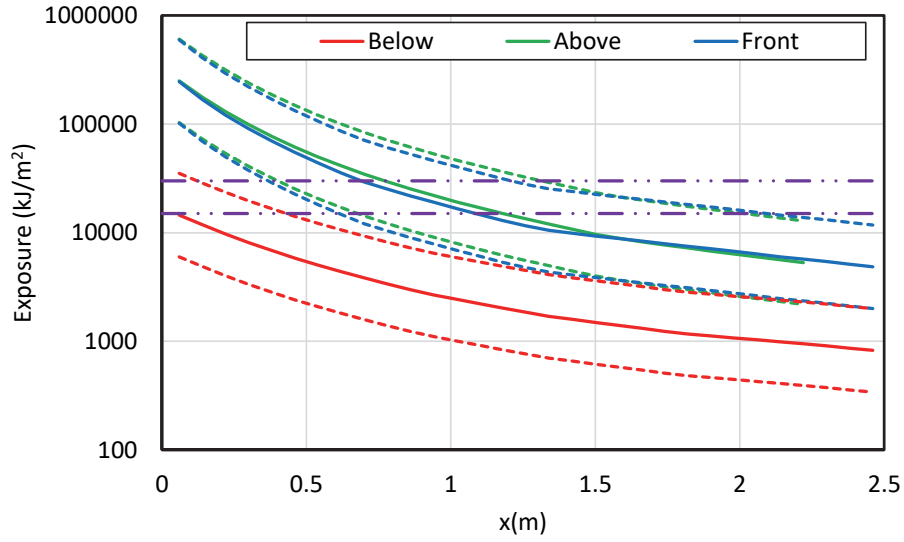


**Figure B-114**  
Results for an aluminum duct NSBD tee with copper bus bars – 233 MJ HEAF (FDS simulation NSBD-50)

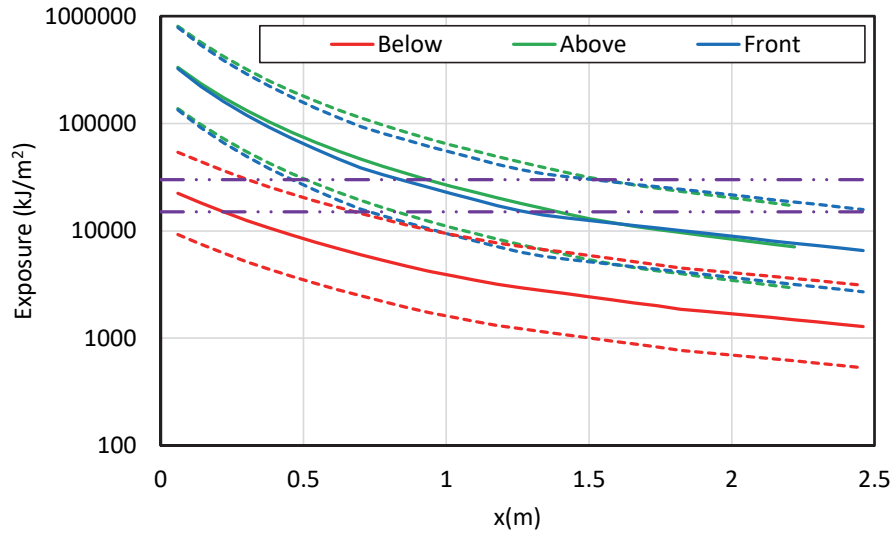


**Figure B-115**  
Results for an aluminum duct NSBD tee with copper bus bars – 300 MJ HEAF (FDS simulation NSBD-51)

# C

## FDS INPUT FILE TEMPLATES

This appendix contains the input file templates for each geometry modeled by FDS and a tabulation of the FDS input files and the specific HEAF simulations presented in Section 6 of this report.

### C.1 FDS Input File Simulation Matrix

Table C-1 provides a summary of the FDS input files associated with each HEAF simulation presented in Section 6.

**Table C-1**  
**FDS input file simulation matrix**

HEAF ID	Results Table	Equipment	FDS Input File
MV-GE-1	6-1	MV SWGR	gemv_eAls2d0p33p81Main.fds
MV-GE-2	6-1	MV SWGR	gemv_eAls2d0p33p81Riser.fds
MV-GE-3	6-1	MV SWGR	gemv_eAls2d0p33p81Riser_Supply.fds
MV-GE-4	6-1	MV SWGR	gemv_eAls4d0p33p81Main.fds
MV-GE-5	6-1	MV SWGR	gemv_eAls4d0p33p81Riser.fds
MV-GE-6	6-1	MV SWGR	gemv_eAls4d0p33p81Riser_Supply.fds
MV-GE-7	6-1	MV SWGR	gemv_eAls5d0p33p81Main.fds
MV-GE-8	6-1	MV SWGR	gemv_eAls5d0p33p81Riser.fds
MV-GE-9	6-1	MV SWGR	gemv_eAls5d0p33p81Riser_Supply.fds
MV-GE-10	6-1	MV SWGR	gemv_eAls0d15p33p81Main.fds
MV-GE-11	6-1	MV SWGR	gemv_eAls0d15p33p81Riser.fds
MV-GE-12	6-1	MV SWGR	gemv_eAls0d15p33p81Riser_Supply.fds
MV-GE-13	6-1	MV SWGR	gemv_eAls3d15p33p81Main.fds
MV-GE-14	6-1	MV SWGR	gemv_eAls3d15p33p81Riser.fds
MV-GE-15	6-1	MV SWGR	gemv_eAls3d15p33p81Riser_Supply.fds
MV-GE-16	6-1	MV SWGR	gemv_eAls5d15p33p81Main.fds
MV-GE-17	6-1	MV SWGR	gemv_eAls5d15p33p81Riser.fds
MV-GE-18	6-1	MV SWGR	gemv_eAls5d15p33p81Riser_Supply.fds
MV-GE-19	6-1	MV SWGR	gemv_eCus2d0p33p81Breaker.fds
MV-GE-20	6-1	MV SWGR	gemv_eCus2d0p33p81Main.fds
MV-GE-21	6-1	MV SWGR	gemv_eCus2d0p33p81Riser.fds

FDS Input File Templates

HEAF ID	Results Table	Equipment	FDS Input File
MV-GE-22	6-1	MV SWGR	gemv_eCus2d0p33p81Riser_Supply.fds
MV-GE-23	6-1	MV SWGR	gemv_eCus4d0p33p81Breaker.fds
MV-GE-24	6-1	MV SWGR	gemv_eCus4d0p33p81Main.fds
MV-GE-25	6-1	MV SWGR	gemv_eCus4d0p33p81Riser.fds
MV-GE-26	6-1	MV SWGR	gemv_eCus4d0p33p81Riser_Supply.fds
MV-GE-27	6-1	MV SWGR	gemv_eCus5d0p33p81Breaker.fds
MV-GE-28	6-1	MV SWGR	gemv_eCus5d0p33p81Main.fds
MV-GE-29	6-1	MV SWGR	gemv_eCus5d0p33p81Riser.fds
MV-GE-30	6-1	MV SWGR	gemv_eCus5d0p33p81Riser_Supply.fds
MV-GE-31	6-1	MV SWGR	gemv_eCus0d15p33p81Breaker.fds
MV-GE-32	6-1	MV SWGR	gemv_eCus0d15p33p81Main.fds
MV-GE-33	6-1	MV SWGR	gemv_eCus0d15p33p81Riser.fds
MV-GE-34	6-1	MV SWGR	gemv_eCus0d15p33p81Riser_Supply.fds
MV-GE-35	6-1	MV SWGR	gemv_eCus3d15p33p81Breaker.fds
MV-GE-36	6-1	MV SWGR	gemv_eCus3d15p33p81Main.fds
MV-GE-37	6-1	MV SWGR	gemv_eCus3d15p33p81Riser.fds
MV-GE-38	6-1	MV SWGR	gemv_eCus3d15p33p81Riser_Supply.fds
MV-GE-39	6-1	MV SWGR	gemv_eCus5d15p33p81Breaker.fds
MV-GE-40	6-1	MV SWGR	gemv_eCus5d15p33p81Main.fds
MV-GE-41	6-1	MV SWGR	gemv_eCus5d15p33p81Riser.fds
MV-GE-42	6-1	MV SWGR	gemv_eCus5d15p33p81Riser_Supply.fds
MV-ABB-1	6-1	MV SWGR	abmv_eCus2d0lBreaker.fds
MV-ABB-2	6-1	MV SWGR	abmv_eCus4d0lBreaker.fds
MV-ABB-3	6-1	MV SWGR	abmv_eCus5d0lBreaker.fds
MV-ABB-4	6-1	MV SWGR	abmv_eCus0d15lBreaker.fds
MV-ABB-5	6-1	MV SWGR	abmv_eCus3d15lBreaker.fds
MV-ABB-6	6-1	MV SWGR	abmv_eCus5d15lBreaker.fds
LV-BASE-1	6-2	LV SWGR	lvswgr_eAlsFC1Br_Mid-RE.fds
LV-BASE-2	6-2	LV SWGR	lvswgr_eAlsFC1Br_Top-RE.fds
LV-BASE-3	6-2	LV SWGR	lvswgr_eAlsFC1Mid_Mid-RE.fds
LV-BASE-4	6-2	LV SWGR	lvswgr_eAlsFC1Mid_Top-RE.fds
LV-BASE-5	6-2	LV SWGR	lvswgr_eAlsFC1BrMid_Mid-RE.fds
LV-BASE-6	6-2	LV SWGR	lvswgr_eAlsFC1BrMid_Top-RE.fds
LV-BASE-7	6-2	LV SWGR	lvswgr_eCusFC1Mid_Mid-RE.fds

HEAF ID	Results Table	Equipment	FDS Input File
LV-BASE-8	6-2	LV SWGR	lvswgr_eCusFC1Mid_Top-RE.fds
LV-BASE-9	6-2	LV SWGR	lvswgr_eCusFC1Br_Mid-RE.fds
LV-BASE-10	6-2	LV SWGR	lvswgr_eCusFC1Br_Top-RE.fds
LV-SENS-1	6-2	LV SWGR	lvswgr_eAls2lBr_Mid.fds
LV-SENS-2	6-2	LV SWGR	lvswgr_eAls2lBr_Top.fds
LV-SENS-3	6-2	LV SWGR	lvswgr_eAls2lMid_Mid.fds
LV-SENS-4	6-2	LV SWGR	lvswgr_eAls2lMid_Top.fds
LV-SENS-5	6-2	LV SWGR	lvswgr_eCus2lBr_Mid.fds
LV-SENS-6	6-2	LV SWGR	lvswgr_eCus2lBr_Top.fds
LV-SENS-7	6-2	LV SWGR	lvswgr_eCus2lMid_Mid.fds
LV-SENS-8	6-2	LV SWGR	lvswgr_eCus2lMid_Top.fds
LV-SENS-9	6-2	LV SWGR	lvswgr_eAls4lBr_Mid.fds
LV-SENS-10	6-2	LV SWGR	lvswgr_eAls4lBr_Top.fds
LV-SENS-11	6-2	LV SWGR	lvswgr_eAls4lMid_Mid.fds
LV-SENS-12	6-2	LV SWGR	lvswgr_eAls4lMid_Top.fds
LV-SENS-13	6-2	LV SWGR	lvswgr_eCus4lBr_Mid.fds
LV-SENS-14	6-2	LV SWGR	lvswgr_eCus4lBr_Top.fds
LV-SENS-15	6-2	LV SWGR	lvswgr_eCus4lMid_Mid.fds
LV-SENS-16	6-2	LV SWGR	lvswgr_eCus4lMid_Top.fds
LV-SENS-17	6-2	LV SWGR	lvswgr_eAls6lBr_Mid.fds
LV-SENS-18	6-2	LV SWGR	lvswgr_eAls6lBr_Top.fds
LV-SENS-19	6-2	LV SWGR	lvswgr_eAls6lMid_Mid.fds
LV-SENS-20	6-2	LV SWGR	lvswgr_eAls6lMid_Top.fds
LV-SENS-21	6-2	LV SWGR	lvswgr_eCus6lBr_Mid.fds
LV-SENS-22	6-2	LV SWGR	lvswgr_eCus6lBr_Top.fds
LV-SENS-23	6-2	LV SWGR	lvswgr_eCus6lMid_Mid.fds
LV-SENS-24	6-2	LV SWGR	lvswgr_eCus6lMid_Top.fds
NSBD-1	6-3	NSBD	bd_eAlhSts1d0cStraight.fds
NSBD-2	6-3	NSBD	bd_eAlhSts2d0cStraight.fds
NSBD-3	6-3	NSBD	bd_eAlhSts4d0cStraight.fds
NSBD-4	6-3	NSBD	bd_eAlhSts5d0cStraight.fds
NSBD-5	6-3	NSBD	bd_eAlhSts0d15cStraight.fds
NSBD-6	6-3	NSBD	bd_eAlhSts3d15cStraight.fds
NSBD-7	6-3	NSBD	bd_eAlhSts5d15cStraight.fds

HEAF ID	Results Table	Equipment	FDS Input File
NSBD-8	6-3	NSBD	bd_eAlhAls1d0cStraight.fds
NSBD-9	6-3	NSBD	bd_eAlhAls2d0cStraight.fds
NSBD-10	6-3	NSBD	bd_eAlhAls4d0cStraight.fds
NSBD-11	6-3	NSBD	bd_eAlhAls5d0cStraight.fds
NSBD-12	6-3	NSBD	bd_eAlhAls3d15cStraight.fds
NSBD-13	6-3	NSBD	bd_eAlhAls5d15cStraight.fds
NSBD-14	6-3	NSBD	bd_eCuhSts1d0cStraight.fds
NSBD-15	6-3	NSBD	bd_eCuhSts2d0cStraight.fds
NSBD-16	6-3	NSBD	bd_eCuhSts4d0cStraight.fds
NSBD-17	6-3	NSBD	bd_eCuhSts5d0cStraight.fds
NSBD-18	6-3	NSBD	bd_eCuhSts0d15cStraight.fds
NSBD-19	6-3	NSBD	bd_eCuhSts3d15cStraight.fds
NSBD-20	6-3	NSBD	bd_eCuhSts5d15cStraight.fds
NSBD-21	6-3	NSBD	bd_eCuhAls1d0cStraight.fds
NSBD-22	6-3	NSBD	bd_eCuhAls2d0cStraight.fds
NSBD-23	6-3	NSBD	bd_eCuhAls4d0cStraight.fds
NSBD-24	6-3	NSBD	bd_eCuhAls5d0cStraight.fds
NSBD-25	6-3	NSBD	bd_eCuhAls0d15cStraight.fds
NSBD-26	6-3	NSBD	bd_eCuhAls3d15cStraight.fds
NSBD-27	6-3	NSBD	bd_eCuhAls5d15cStraight.fds
NSBD-28	6-3	NSBD	bd_eAlhSts2d0cTee.fds
NSBD-29	6-3	NSBD	bd_eAlhSts4d0cTee.fds
NSBD-30	6-3	NSBD	bd_eAlhSts5d0cTee.fds
NSBD-31	6-3	NSBD	bd_eAlhSts0d15cTee.fds
NSBD-32	6-3	NSBD	bd_eAlhSts3d15cTee.fds
NSBD-33	6-3	NSBD	bd_eAlhSts5d15cTee.fds
NSBD-34	6-3	NSBD	bd_eAlhAls2d0cTee.fds
NSBD-35	6-3	NSBD	bd_eAlhAls4d0cTee.fds
NSBD-36	6-3	NSBD	bd_eAlhAls5d0cTee.fds
NSBD-37	6-3	NSBD	bd_eAlhAls0d15cTee.fds
NSBD-38	6-3	NSBD	bd_eAlhAls3d15cTee.fds
NSBD-39	6-3	NSBD	bd_eAlhAls5d15cTee.fds
NSBD-40	6-3	NSBD	bd_eCuhSts2d0cTee.fds
NSBD-41	6-3	NSBD	bd_eCuhSts4d0cTee.fds

HEAF ID	Results Table	Equipment	FDS Input File
NSBD-42	6-3	NSBD	bd_eCuhSts5d0cTee.fds
NSBD-43	6-3	NSBD	bd_eCuhSts0d15cTee.fds
NSBD-44	6-3	NSBD	bd_eCuhSts3d15cTee.fds
NSBD-45	6-3	NSBD	bd_eCuhSts5d15cTee.fds
NSBD-46	6-3	NSBD	bd_eCuhAls2d0cTee.fds
NSBD-47	6-3	NSBD	bd_eCuhAls4d0cTee.fds
NSBD-48	6-3	NSBD	bd_eCuhAls5d0cTee.fds
NSBD-49	6-3	NSBD	bd_eCuhAls0d15cTee.fds
NSBD-50	6-3	NSBD	bd_eCuhAls3d15cTee.fds
NSBD-51	6-3	NSBD	bd_eCuhAls5d15cTee.fds
NSBD-52	6-3	NSBD	bd_eAlhAls2d0cElbow.fds
NSBD-53	6-3	NSBD	bd_eAlhAls4d0cElbow.fds
NSBD-54	6-3	NSBD	bd_eAlhAls5d0cElbow.fds
NSBD-55	6-3	NSBD	bd_eAlhAls0d15cElbow.fds
NSBD-56	6-3	NSBD	bd_eAlhAls3d15cElbow.fds
NSBD-57	6-3	NSBD	bd_eAlhAls5d15cElbow.fds
NSBD-58	6-3	NSBD	bd_eAlhAls0d15cStraight.fds

## C.2 FDS Input File Templates for Medium Voltage Switchgear

### C.2.1 Vertical-Lift Circuit Breaker Style

```
&HEAD CHID='fileid'/
```

```
! 3 in. resolution. Approximately 2 m to each side, 2 m above, and 2.4 m front and back.
```

```
&MESH ID='Cabinet', IJK=23,22,20, XB=-2.4384,-0.6858,-2.5146,-0.8382,0.0000,1.5240, MULT_ID='M1' / 3 in. resolution
```

```
&MULT ID='M1', I_UPPER=3, DX=1.7526, J_UPPER=2, DY=1.6764, K_UPPER=2, DZ=1.5240/
```

```
&VENT MB='ZMAX', SURF_ID='OPEN' /
```

```
&VENT MB='YMAX', SURF_ID='OPEN' /
```

```
&VENT MB='XMAX', SURF_ID='OPEN' /
```

```
&VENT MB='YMIN', SURF_ID='OPEN' /
```

```
&VENT MB='XMIN', SURF_ID='OPEN' /
```

```
! I_MAX_TEMP=35000 ensures property arrays are high enough for the CLIP values.
```

```
! AEROSOL_AL2O3 replaces default SOOT radiative properties with those for AL2O3
```

```
&MISC AEROSOL_AL2O3=T, I_MAX_TEMP=35000 /
```

```
! SMOKE3D_SPEC_ID sets the species used by Smokeview to visualize smoke
```

```
&DUMP SMOKE3D_SPEC_ID='3dsmoke', SUPPRESS_DIAGNOSTICS=F, MASS_FILE=T/
```

---

## FDS Input File Templates

```
! Turns off the extinction model. Default values in the model may not be appropriate
for metal oxidation
&COMB SUPPRESSION=F /

! 0.01 kg/m3 greatly limits clipping of density.
&CLIP MINIMUM_DENSITY=0.01, MAXIMUM_TEMPERATURE=35000.,CLIP_DT_RESTRICTIONS_MAX=0 /

! These cases a very challenging for the pressure solver. The selected values seem to
give enough pressure iterations to
! drop the velocity error down to a plateau value.

&PRES MAX_PRESSURE_ITERATIONS=30, VELOCITY_TOLERANCE=0.001,
SUSPEND_PRESSURE_ITERATIONS=F/

! For ZOI runs suggest T_END = arc time + 8 s

&TIME T_END=tend, DT=0.001,WALL_INCREMENT=1 /

&RADI NUMBER_RADIATION_ANGLES=500 /

! 1 cell thick OBST to help out pressure solver.

&OBST XB=0.0000,0.0762,-0.4572,0.4572,0.4572,2.2860,SURF_ID='CABINET' /
&OBST XB=0.0000,0.0762,-0.4572,0.4572,0.0000,0.1524,SURF_ID='CABINET' /
&OBST XB=0.0000,0.0762,-0.4572,0.4572,0.2286,0.3810,SURF_ID='CABINET' /
&OBST XB=0.0000,0.0762,-0.4572,-0.3048,0.1524,0.2286,SURF_ID='CABINET' /
&OBST XB=0.0000,0.0762,-0.0762,0.0762,0.1524,0.2286,SURF_ID='CABINET' /
&OBST XB=0.0000,0.0762,0.3048,0.4572,0.1524,0.2286,SURF_ID='CABINET' /
&OBST XB=0.0000,0.0762,-0.4572,-0.3048,0.3810,0.4572,SURF_ID='CABINET' /
&OBST XB=0.0000,0.0762,-0.0762,0.0762,0.3810,0.4572,SURF_ID='CABINET' /
&OBST XB=0.0000,0.0762,0.3048,0.4572,0.3810,0.4572,SURF_ID='CABINET' /
&OBST XB=0.0000,1.5240,-0.4572,0.4572,2.2860,2.3622,SURF_ID='CABINET' /
&OBST XB=1.5240,1.7526,-0.1524,-0.0762,2.2860,2.3622,SURF_ID='CABINET' /
&OBST XB=1.5240,1.7526,0.0762,0.1524,2.2860,2.3622,SURF_ID='CABINET' /
&OBST XB=1.7526,2.1336,-0.4572,0.4572,2.2860,2.3622,SURF_ID='CABINET' /
&OBST XB=0.0000,2.1336,-0.5334,-0.4572,0.0000,2.3622,SURF_ID='CABINET' /
&OBST XB=0.0000,2.1336,0.4572,0.5334,0.0000,2.3622,SURF_ID='CABINET' /
&OBST XB=0.5334,1.7526,-0.4572,0.4572,1.3716,1.4478,SURF_ID='CABINET' /
&OBST XB=1.2954,1.3716,-0.4572,0.4572,1.4478,2.2098,SURF_ID='CABINET' /
&OBST XB=1.2954,1.3716,-0.4572,-0.3810,2.2098,2.2860,SURF_ID='CABINET' /
&OBST XB=1.2954,1.3716,0.3810,0.4572,2.2098,2.2860,SURF_ID='CABINET' /
&OBST XB=1.6764,1.7526,-0.4572,0.4572,1.4478,2.2098,SURF_ID='CABINET' /
&OBST XB=1.2954,1.5240,-0.4572,0.4572,2.1336,2.2098,SURF_ID='CABINET' /
&OBST XB=1.6002,1.7526,-0.4572,0.4572,2.1336,2.2098,SURF_ID='CABINET' /
&OBST XB=0.5334,0.6096,-0.4572,0.4572,0.0000,1.3716,SURF_ID='CABINET' /
&OBST XB=0.6858,1.8288,-0.3810,0.3810,0.0762,0.9906,SURF_ID='BREAKER' /
&OBST XB=1.2954,1.8288,-0.3810,0.3810,0.9906,1.0668,SURF_ID='BREAKER' /

! RADCAL_ID='SOOT' makes the SPEC use the SOOT radiation properties which the MISC
line has changed to those for AL2O3
! RAMPS used instead of built in cp data for N2, CO2, and O2 to extend temperature to
20,000 K

&SPEC ID='WET NITROGEN',BACKGROUND=T,SPEC_ID='NITROGEN','CARBON DIOXIDE','WATER
VAPOR',MASS_FRACTION=1,0.000775,0.007792/FDS Default AIR without O2
&SPEC ID='NITROGEN', LUMPED_COMPONENT_ONLY=T,RAMP_CP='N2 C' /
&SPEC ID='CARBON DIOXIDE', LUMPED_COMPONENT_ONLY=T,RAMP_CP='CO2 C' /
&SPEC ID='WATER VAPOR', LUMPED_COMPONENT_ONLY=T /
&SPEC ID='OXYGEN', MASS_FRACTION_0=0.230997,RAMP_CP='O2 C' /
alspec1 ID='ALUMINUM',FORMULA='Al',RAMP_CP='AL
C',SIGMALJ=2.655,EPSILONKLJ=2750.,PR_GAS=1/
alspec2 ID='ALUMINUM
OXIDE',MASS_EXTINCTION_COEFFICIENT=3000,FORMULA='Al2O3',RAMP_CP='AL2O3
C',SIGMALJ=3.186,EPSILONKLJ=557.449,PR_GAS=1,RADCAL_ID='SOOT' /
```

```

cuspec1 ID='COPPER',FORMULA='Cu',RAMP_CP='CU
C',SIGMALJ=5.058,EPSILONKLJ=2983.,PR_GAS=1/
cuspec2 ID='COPPER
OXIDE',MASS_EXTINCTION_COEFFICIENT=3000,FORMULA='Cu2O',SPECIFIC_HEAT=0.7,SIGMALJ=5.403
,PR_GAS=1,RADCAL_ID='SOOT'/C from JANAF, LJ take as CuO

alreac FUEL='ALUMINUM', SPEC_ID_NU='ALUMINUM','OXYGEN','ALUMINUM OXIDE', NU=-2,-1.5,1,
HEAT_OF_COMBUSTION=31100. / Al -> AL2O3
cureac FUEL='COPPER',SPEC_ID_NU='COPPER','OXYGEN','COPPER OXIDE',NU=-2,-
0.5,1,HEAT_OF_COMBUSTION=1340./ Cu->Cu2O

&MATL ID='CONCRETE', DENSITY=2400, CONDUCTIVITY=1.6, SPECIFIC_HEAT=0.75,
EMISSIVITY=0.95 /

! Non-melting steel
&MATL ID='INERT STEEL', DENSITY=7800., SPECIFIC_HEAT_RAMP='STEEL C',
CONDUCTIVITY_RAMP='STEEL K', EMISSIVITY=0.85/

! Melting steel
&MATL ID='STEEL', DENSITY=7800., SPECIFIC_HEAT_RAMP='STEEL C',
CONDUCTIVITY_RAMP='STEEL K', EMISSIVITY=0.85,
THRESHOLD_TEMPERATURE=1300., THRESHOLD_SIGN=1, HEAT_OF_REACTION(1)=250.,
PCR(1)=T, A(1)=0.6, E(1)=0., N_S(1)=0., N_T(1)=1. /

! Eurocode values
&RAMP ID='STEEL C',T=20,F=0.440/
&RAMP ID='STEEL C',T=600,F=0.760/
&RAMP ID='STEEL C',T=700,F=1.008/
&RAMP ID='STEEL C',T=720,F=1.388/
&RAMP ID='STEEL C',T=725,F=1.666/
&RAMP ID='STEEL C',T=730,F=2.291/
&RAMP ID='STEEL C',T=735,F=5.000/
&RAMP ID='STEEL C',T=740,F=2.525/ BCC -> FCC Transition
&RAMP ID='STEEL C',T=745,F=1.818/
&RAMP ID='STEEL C',T=750,F=1.483/
&RAMP ID='STEEL C',T=800,F=0.803/
&RAMP ID='STEEL C',T=900,F=0.650/

&RAMP ID='STEEL K',T=20,F=53.3/
&RAMP ID='STEEL K',T=800,F=27.3/

&SURF ID='BREAKER', MATL_ID='INERT STEEL', THICKNESS=0.02,
RGB=204,204,255,CELL_SIZE_FACTOR=0.05,STRETCH_FACTOR=1 /
&SURF ID='CABINET', MATL_ID='STEEL', THICKNESS=0.002381, COLOR='GRAY 60',
BURN_AWAY=.TRUE.,CELL_SIZE_FACTOR=0.05,STRETCH_FACTOR=1 /
&SURF ID='FLOOR', MATL_ID='CONCRETE', THICKNESS=0.15, RGB=50,50,50, DEFAULT=T /

!The block below defines particles that emit vapor for aluminum.
!The particles are initialized at the melting point.
!The PROP MASS_FLOW_RATE is the maximum liquid production rate divided by the number
of electrodes
!NU_SPEC and NU_MATL are set to get the 75 % oxidation for Al and 25 % for Cu. The
second MOLTEN AL2 and CU2 species have a modified density to preserve diameter.
!A and E are set to give the vapor over 0.3 s.

almatl1 ID='MOLTEN
AL',DENSITY=2375,CONDUCTIVITY=100.,SPECIFIC_HEAT=1.177,EMISSIVITY=0,A=3.333,E=0,
N_REACTIONS=1,HEAT_OF_REACTION=0,HEAT_OF_COMBUSTION=0,MATL_ID(1,1)='MOLTEN
AL2',SPEC_ID(1,1)='ALUMINUM',NU_MATL(1,1)=0.25,NU_SPEC(1,1)=0.75/
almatl2 ID='MOLTEN
AL2',DENSITY=593.75,SPEC_ID='ALUMINUM',NU_SPEC=1,CONDUCTIVITY=100.,SPECIFIC_HEAT=1.177
/

```

---

## FDS Input File Templates

```
alsurf1 ID='AL DROP',MATL_ID='MOLTEN AL',GEOMETRY='SPHERICAL',THICKNESS=5.E-6,HEAT_TRANSFER_COEFFICIENT=0,TMP_INNER=665.3/
alpart1 ID='AL DROPS',SURF_ID='AL
DROP',AGE=2.0,SAMPLING_FACTOR=10,MONODISPERSE=T,RGB=100,100,100/
alprop1 ID='DROPS',PART_ID='AL DROPS',FLOW_RAMP='RAMP
MF',MASS_FLOW_RATE=almfr,PARTICLES_PER_SECOND=20000,PARTICLE_VELOCITY=10,SPRAY_ANGLE=0,60/
```

! The block below is for copper.

```
Cumatl1 ID='MOLTEN
CU',DENSITY=8960,CONDUCTIVITY=340.,SPECIFIC_HEAT=0.517,EMISSIVITY=0,A=3.333,E=0,
N_REACTIONS=1,HEAT_OF_REACTION=0,HEAT_OF_COMBUSTION=0,MATL_ID(1,1)='MOLTEN
CU2',SPEC_ID(1,1)='COPPER',NU_MATL(1,1)=0.75,NU_SPEC(1,1)=0.25/
cumatl2 ID='MOLTEN
CU2',DENSITY=7168,CONDUCTIVITY=340.,SPECIFIC_HEAT=0.517,EMISSIVITY=0/
```

```
cusurf1 ID='CU DROP',MATL_ID='MOLTEN CU',GEOMETRY='SPHERICAL',THICKNESS=5.E-6,HEAT_TRANSFER_COEFFICIENT=0,TMP_INNER=1084.85/
cupart1 ID='CU DROPS',SURF_ID='CU
DROP',AGE=2.0,SAMPLING_FACTOR=10,MONODISPERSE=T,RGB=184,115,51/
cuprop1 ID='DROPS',PART_ID='CU DROPS',FLOW_RAMP='RAMP
MF',MASS_FLOW_RATE=cumfr,PARTICLES_PER_SECOND=20000,PARTICLE_VELOCITY=10,SPRAY_ANGLE=0,60/
```

! First INIT line is the volumetric source term where the RADAITIVE\_FRACTION uses Cressault's data interpolated based on power,. The HRRPUV is ! reduced based on energy needed to degrade the electrodes:  
! Adjusted total energy = (Total arc energy - electrode mass loss \* (vapor fraction \* energy to vaporize + liquid fraction \* energy to melt))

!

! Cressault data:

!

! X<sub>r,Al</sub> = 0.2275\*Max\_Power<sup>0.3292</sup>

! X<sub>r,Al</sub> = 0.1273\*Max\_Power<sup>0.3859</sup>

!

! Phase Energy (kJ/kg)

! Change Al Cu

! Melt 1063.4 695.2

```
&INIT XB=initx1,initx2,inity1,inity2,initz1,initz2,HRRPUV=hrrpuvval,RAMP_Q='RAMP
Q',RADIATIVE_FRACTION=radfrac/
```

! One spray nozzle device per electrode that inject liquid droplets

```
&DEVC
```

```
PROP_ID='DROPS',XYZ=nozx1,nozy1,nozz1,QUANTITY='TIME',SETPOINT=0.0,ORIENTATION=orient1,orient2,orient3/
```

```
&DEVC
```

```
PROP_ID='DROPS',XYZ=nozx2,nozy2,nozz2,QUANTITY='TIME',SETPOINT=0.0,ORIENTATION=orient1,orient2,orient3/
```

```
&DEVC
```

```
PROP_ID='DROPS',XYZ=nozx3,nozy3,nozz3,QUANTITY='TIME',SETPOINT=0.0,ORIENTATION=orient1,orient2,orient3/
```

! An 0.1 s ramp up and down for the arc volumetric source term helps avoid numerical instabilities

```
&RAMP ID='RAMP Q',T=0.0,F=0.0000/
&RAMP ID='RAMP Q',T=0.1,F=rampqf1/
&RAMP ID='RAMP Q',T=0.2,F=rampqf2/
&RAMP ID='RAMP Q',T=0.3,F=rampqf3/
&RAMP ID='RAMP Q',T=0.4,F=rampqf4/
&RAMP ID='RAMP Q',T=0.5,F=rampqf5/
```

```
&RAMP ID=' RAMP Q' ,T=0.6,F=rampqf6/  
&RAMP ID=' RAMP Q' ,T=0.7,F=rampqf7/  
&RAMP ID=' RAMP Q' ,T=0.8,F=rampqf8/  
&RAMP ID=' RAMP Q' ,T=0.9,F=rampqf9/  
&RAMP ID=' RAMP Q' ,T=1.0,F=rampqf10/  
&RAMP ID=' RAMP Q' ,T=1.1,F=rampqf11/  
&RAMP ID=' RAMP Q' ,T=1.2,F=rampqf12/  
&RAMP ID=' RAMP Q' ,T=1.3,F=rampqf13/  
&RAMP ID=' RAMP Q' ,T=1.4,F=rampqf14/  
&RAMP ID=' RAMP Q' ,T=1.5,F=rampqf15/  
&RAMP ID=' RAMP Q' ,T=1.6,F=rampqf16/  
&RAMP ID=' RAMP Q' ,T=1.7,F=rampqf17/  
&RAMP ID=' RAMP Q' ,T=1.8,F=rampqf18/  
&RAMP ID=' RAMP Q' ,T=1.9,F=rampqf19/  
&RAMP ID=' RAMP Q' ,T=2.0,F=rampqf20/  
&RAMP ID=' RAMP Q' ,T=2.1,F=rampqf21/  
&RAMP ID=' RAMP Q' ,T=2.2,F=rampqf22/  
&RAMP ID=' RAMP Q' ,T=2.3,F=rampqf23/  
&RAMP ID=' RAMP Q' ,T=2.4,F=rampqf24/  
&RAMP ID=' RAMP Q' ,T=2.5,F=rampqf25/  
&RAMP ID=' RAMP Q' ,T=2.6,F=rampqf26/  
&RAMP ID=' RAMP Q' ,T=2.7,F=rampqf27/  
&RAMP ID=' RAMP Q' ,T=2.8,F=rampqf28/  
&RAMP ID=' RAMP Q' ,T=2.9,F=rampqf29/  
&RAMP ID=' RAMP Q' ,T=3.0,F=rampqf30/  
&RAMP ID=' RAMP Q' ,T=3.1,F=rampqf31/  
&RAMP ID=' RAMP Q' ,T=3.2,F=rampqf32/  
&RAMP ID=' RAMP Q' ,T=3.3,F=rampqf33/  
&RAMP ID=' RAMP Q' ,T=3.4,F=rampqf34/  
&RAMP ID=' RAMP Q' ,T=3.5,F=rampqf35/  
&RAMP ID=' RAMP Q' ,T=3.6,F=rampqf36/  
&RAMP ID=' RAMP Q' ,T=3.7,F=rampqf37/  
&RAMP ID=' RAMP Q' ,T=3.8,F=rampqf38/  
&RAMP ID=' RAMP Q' ,T=3.9,F=rampqf39/  
&RAMP ID=' RAMP Q' ,T=4.0,F=rampqf40/  
&RAMP ID=' RAMP Q' ,T=4.1,F=rampqf41/  
&RAMP ID=' RAMP Q' ,T=4.2,F=rampqf42/  
&RAMP ID=' RAMP Q' ,T=4.3,F=rampqf43/  
&RAMP ID=' RAMP Q' ,T=4.4,F=rampqf44/  
&RAMP ID=' RAMP Q' ,T=4.5,F=rampqf45/  
&RAMP ID=' RAMP Q' ,T=4.6,F=rampqf46/  
&RAMP ID=' RAMP Q' ,T=4.7,F=rampqf47/  
&RAMP ID=' RAMP Q' ,T=4.8,F=rampqf48/  
&RAMP ID=' RAMP Q' ,T=4.9,F=rampqf49/  
&RAMP ID=' RAMP Q' ,T=5.0,F=rampqf50/  
&RAMP ID=' RAMP Q' ,T=5.1,F=rampqf51/  
&RAMP ID=' RAMP Q' ,T=5.2,F=rampqf52/  
&RAMP ID=' RAMP Q' ,T=5.3,F=rampqf53/  
&RAMP ID=' RAMP Q' ,T=5.4,F=rampqf54/  
&RAMP ID=' RAMP Q' ,T=5.5,F=rampqf55/  
&RAMP ID=' RAMP Q' ,T=5.6,F=rampqf56/  
&RAMP ID=' RAMP Q' ,T=5.7,F=rampqf57/  
&RAMP ID=' RAMP Q' ,T=5.8,F=rampqf58/  
&RAMP ID=' RAMP Q' ,T=5.9,F=rampqf59/  
&RAMP ID=' RAMP Q' ,T=6.0,F=rampqf60/  
&RAMP ID=' RAMP Q' ,T=6.1,F=rampqf61/  
&RAMP ID=' RAMP Q' ,T=6.2,F=rampqf62/  
&RAMP ID=' RAMP Q' ,T=6.3,F=rampqf63/  
&RAMP ID=' RAMP Q' ,T=6.4,F=rampqf64/  
&RAMP ID=' RAMP Q' ,T=6.5,F=rampqf65/  
&RAMP ID=' RAMP Q' ,T=6.6,F=rampqf66/  
&RAMP ID=' RAMP Q' ,T=6.7,F=rampqf67/  
&RAMP ID=' RAMP Q' ,T=6.8,F=rampqf68/  
&RAMP ID=' RAMP Q' ,T=6.9,F=rampqf69/
```

---

## FDS Input File Templates

```
&RAMP ID=' RAMP Q' ,T=7.0,F=rampqf70/  
&RAMP ID=' RAMP Q' ,T=7.1,F=rampqf71/  
&RAMP ID=' RAMP Q' ,T=7.2,F=rampqf72/  
&RAMP ID=' RAMP Q' ,T=7.3,F=rampqf73/  
&RAMP ID=' RAMP Q' ,T=7.4,F=rampqf74/  
&RAMP ID=' RAMP Q' ,T=7.5,F=rampqf75/  
&RAMP ID=' RAMP Q' ,T=7.6,F=rampqf76/  
&RAMP ID=' RAMP Q' ,T=7.7,F=rampqf77/  
&RAMP ID=' RAMP Q' ,T=7.8,F=rampqf78/  
&RAMP ID=' RAMP Q' ,T=7.9,F=rampqf79/  
&RAMP ID=' RAMP Q' ,T=8.0,F=rampqf80/  
&RAMP ID=' RAMP Q' ,T=8.1,F=rampqf81/  
&RAMP ID=' RAMP Q' ,T=8.2,F=rampqf82/  
&RAMP ID=' RAMP Q' ,T=8.3,F=rampqf83/  
&RAMP ID=' RAMP Q' ,T=8.4,F=rampqf84/  
&RAMP ID=' RAMP Q' ,T=8.5,F=rampqf85/  
&RAMP ID=' RAMP Q' ,T=8.6,F=rampqf86/  
&RAMP ID=' RAMP Q' ,T=8.7,F=rampqf87/  
&RAMP ID=' RAMP Q' ,T=8.8,F=rampqf88/  
&RAMP ID=' RAMP Q' ,T=8.9,F=rampqf89/  
&RAMP ID=' RAMP Q' ,T=9.0,F=rampqf90/  
&RAMP ID=' RAMP Q' ,T=9.1,F=rampqf91/  
&RAMP ID=' RAMP Q' ,T=9.2,F=rampqf92/  
&RAMP ID=' RAMP Q' ,T=9.3,F=rampqf93/  
&RAMP ID=' RAMP Q' ,T=9.4,F=rampqf94/  
&RAMP ID=' RAMP Q' ,T=9.5,F=rampqf95/  
&RAMP ID=' RAMP Q' ,T=9.6,F=rampqf96/  
&RAMP ID=' RAMP Q' ,T=9.7,F=rampqf97/  
&RAMP ID=' RAMP Q' ,T=9.8,F=rampqf98/  
&RAMP ID=' RAMP Q' ,T=9.9,F=rampqf99/  
&RAMP ID=' RAMP Q' ,T=10.0,F=rampqf100/  
&RAMP ID=' RAMP Q' ,T=10.1,F=rampqf101/  
&RAMP ID=' RAMP Q' ,T=10.2,F=rampqf102/  
&RAMP ID=' RAMP Q' ,T=10.3,F=rampqf103/  
&RAMP ID=' RAMP Q' ,T=10.4,F=rampqf104/  
&RAMP ID=' RAMP Q' ,T=10.5,F=rampqf105/  
&RAMP ID=' RAMP Q' ,T=10.6,F=rampqf106/  
&RAMP ID=' RAMP Q' ,T=10.7,F=rampqf107/  
&RAMP ID=' RAMP Q' ,T=10.8,F=rampqf108/  
&RAMP ID=' RAMP Q' ,T=10.9,F=rampqf109/  
&RAMP ID=' RAMP Q' ,T=11.0,F=rampqf110/  
&RAMP ID=' RAMP Q' ,T=11.1,F=rampqf111/  
&RAMP ID=' RAMP Q' ,T=11.2,F=rampqf112/  
&RAMP ID=' RAMP Q' ,T=11.3,F=rampqf113/  
&RAMP ID=' RAMP Q' ,T=11.4,F=rampqf114/  
&RAMP ID=' RAMP Q' ,T=11.5,F=rampqf115/  
&RAMP ID=' RAMP Q' ,T=11.6,F=rampqf116/  
&RAMP ID=' RAMP Q' ,T=11.7,F=rampqf117/  
&RAMP ID=' RAMP Q' ,T=11.8,F=rampqf118/  
&RAMP ID=' RAMP Q' ,T=11.9,F=rampqf119/  
&RAMP ID=' RAMP Q' ,T=12.0,F=rampqf120/  
&RAMP ID=' RAMP Q' ,T=12.1,F=rampqf121/  
&RAMP ID=' RAMP Q' ,T=12.2,F=rampqf122/  
&RAMP ID=' RAMP Q' ,T=12.3,F=rampqf123/  
&RAMP ID=' RAMP Q' ,T=12.4,F=rampqf124/  
&RAMP ID=' RAMP Q' ,T=12.5,F=rampqf125/  
&RAMP ID=' RAMP Q' ,T=12.6,F=rampqf126/  
&RAMP ID=' RAMP Q' ,T=12.7,F=rampqf127/  
&RAMP ID=' RAMP Q' ,T=12.8,F=rampqf128/  
&RAMP ID=' RAMP Q' ,T=12.9,F=rampqf129/  
&RAMP ID=' RAMP Q' ,T=13.0,F=rampqf130/  
&RAMP ID=' RAMP Q' ,T=13.1,F=rampqf131/  
&RAMP ID=' RAMP Q' ,T=13.2,F=rampqf132/  
&RAMP ID=' RAMP Q' ,T=13.3,F=rampqf133/
```

```
&RAMP ID=' RAMP Q',T=13.4,F=rampqf134/  
&RAMP ID=' RAMP Q',T=13.5,F=rampqf135/  
&RAMP ID=' RAMP Q',T=13.6,F=rampqf136/  
&RAMP ID=' RAMP Q',T=13.7,F=rampqf137/  
&RAMP ID=' RAMP Q',T=13.8,F=rampqf138/  
&RAMP ID=' RAMP Q',T=13.9,F=rampqf139/  
&RAMP ID=' RAMP Q',T=14.0,F=rampqf140/  
&RAMP ID=' RAMP Q',T=14.1,F=rampqf141/  
&RAMP ID=' RAMP Q',T=14.2,F=rampqf142/  
&RAMP ID=' RAMP Q',T=14.3,F=rampqf143/  
&RAMP ID=' RAMP Q',T=14.4,F=rampqf144/  
&RAMP ID=' RAMP Q',T=14.5,F=rampqf145/  
&RAMP ID=' RAMP Q',T=14.6,F=rampqf146/  
&RAMP ID=' RAMP Q',T=14.7,F=rampqf147/  
&RAMP ID=' RAMP Q',T=14.8,F=rampqf148/  
&RAMP ID=' RAMP Q',T=14.9,F=rampqf149/  
&RAMP ID=' RAMP Q',T=15.0,F=rampqf150/  
&RAMP ID=' RAMP Q',T=15.1,F=rampqf151/  
&RAMP ID=' RAMP Q',T=15.2,F=rampqf152/  
&RAMP ID=' RAMP Q',T=15.3,F=rampqf153/  
&RAMP ID=' RAMP Q',T=15.4,F=rampqf154/  
&RAMP ID=' RAMP Q',T=15.5,F=rampqf155/  
&RAMP ID=' RAMP Q',T=15.6,F=rampqf156/  
&RAMP ID=' RAMP Q',T=15.7,F=rampqf157/  
&RAMP ID=' RAMP Q',T=15.8,F=rampqf158/  
&RAMP ID=' RAMP Q',T=15.9,F=rampqf159/  
&RAMP ID=' RAMP Q',T=16.0,F=rampqf160/  
&RAMP ID=' RAMP Q',T=16.1,F=rampqf161/  
&RAMP ID=' RAMP Q',T=16.2,F=rampqf162/  
&RAMP ID=' RAMP Q',T=16.3,F=rampqf163/  
&RAMP ID=' RAMP Q',T=16.4,F=rampqf164/  
&RAMP ID=' RAMP Q',T=16.5,F=rampqf165/  
&RAMP ID=' RAMP Q',T=16.6,F=rampqf166/  
&RAMP ID=' RAMP Q',T=16.7,F=rampqf167/  
&RAMP ID=' RAMP Q',T=16.8,F=rampqf168/  
&RAMP ID=' RAMP Q',T=16.9,F=rampqf169/  
&RAMP ID=' RAMP Q',T=17.0,F=rampqf170/  
&RAMP ID=' RAMP Q',T=17.1,F=rampqf171/  
&RAMP ID=' RAMP Q',T=17.2,F=rampqf172/  
&RAMP ID=' RAMP Q',T=17.3,F=rampqf173/  
&RAMP ID=' RAMP Q',T=17.4,F=rampqf174/  
&RAMP ID=' RAMP Q',T=17.5,F=rampqf175/  
&RAMP ID=' RAMP Q',T=17.6,F=rampqf176/  
&RAMP ID=' RAMP Q',T=17.7,F=rampqf177/  
&RAMP ID=' RAMP Q',T=17.8,F=rampqf178/  
&RAMP ID=' RAMP Q',T=17.9,F=rampqf179/  
&RAMP ID=' RAMP Q',T=18.0,F=rampqf180/  
&RAMP ID=' RAMP Q',T=18.1,F=rampqf181/  
&RAMP ID=' RAMP Q',T=18.2,F=rampqf182/  
&RAMP ID=' RAMP Q',T=18.3,F=rampqf183/  
&RAMP ID=' RAMP Q',T=18.4,F=rampqf184/  
&RAMP ID=' RAMP Q',T=18.5,F=rampqf185/  
&RAMP ID=' RAMP Q',T=18.6,F=rampqf186/  
&RAMP ID=' RAMP Q',T=18.7,F=rampqf187/  
&RAMP ID=' RAMP Q',T=18.8,F=rampqf188/  
&RAMP ID=' RAMP Q',T=18.9,F=rampqf189/  
&RAMP ID=' RAMP Q',T=19.0,F=rampqf190/  
&RAMP ID=' RAMP Q',T=19.1,F=rampqf191/  
&RAMP ID=' RAMP Q',T=19.2,F=rampqf192/  
&RAMP ID=' RAMP Q',T=19.3,F=rampqf193/  
&RAMP ID=' RAMP Q',T=19.4,F=rampqf194/  
&RAMP ID=' RAMP Q',T=19.5,F=rampqf195/  
&RAMP ID=' RAMP Q',T=19.6,F=rampqf196/  
&RAMP ID=' RAMP Q',T=19.7,F=rampqf197/
```

---

## FDS Input File Templates

```
&RAMP ID=' RAMP Q' ,T=19.8 ,F=rampqf198/  
&RAMP ID=' RAMP Q' ,T=19.9 ,F=rampqf199/  
&RAMP ID=' RAMP Q' ,T=20.0 ,F=rampqf200/  
&RAMP ID=' RAMP Q' ,T=20.1 ,F=0.0000/
```

! RAMP for droplets

```
&RAMP ID=' RAMP MF' ,T=0.00 ,F=0.0000/  
&RAMP ID=' RAMP MF' ,T=0.1 ,F=rampmff1/  
&RAMP ID=' RAMP MF' ,T=0.2 ,F=rampmff2/  
&RAMP ID=' RAMP MF' ,T=0.3 ,F=rampmff3/  
&RAMP ID=' RAMP MF' ,T=0.4 ,F=rampmff4/  
&RAMP ID=' RAMP MF' ,T=0.5 ,F=rampmff5/  
&RAMP ID=' RAMP MF' ,T=0.6 ,F=rampmff6/  
&RAMP ID=' RAMP MF' ,T=0.7 ,F=rampmff7/  
&RAMP ID=' RAMP MF' ,T=0.8 ,F=rampmff8/  
&RAMP ID=' RAMP MF' ,T=0.9 ,F=rampmff9/  
&RAMP ID=' RAMP MF' ,T=1.0 ,F=rampmff10/  
&RAMP ID=' RAMP MF' ,T=1.1 ,F=rampmff11/  
&RAMP ID=' RAMP MF' ,T=1.2 ,F=rampmff12/  
&RAMP ID=' RAMP MF' ,T=1.3 ,F=rampmff13/  
&RAMP ID=' RAMP MF' ,T=1.4 ,F=rampmff14/  
&RAMP ID=' RAMP MF' ,T=1.5 ,F=rampmff15/  
&RAMP ID=' RAMP MF' ,T=1.6 ,F=rampmff16/  
&RAMP ID=' RAMP MF' ,T=1.7 ,F=rampmff17/  
&RAMP ID=' RAMP MF' ,T=1.8 ,F=rampmff18/  
&RAMP ID=' RAMP MF' ,T=1.9 ,F=rampmff19/  
&RAMP ID=' RAMP MF' ,T=2.0 ,F=rampmff20/  
&RAMP ID=' RAMP MF' ,T=2.1 ,F=rampmff21/  
&RAMP ID=' RAMP MF' ,T=2.2 ,F=rampmff22/  
&RAMP ID=' RAMP MF' ,T=2.3 ,F=rampmff23/  
&RAMP ID=' RAMP MF' ,T=2.4 ,F=rampmff24/  
&RAMP ID=' RAMP MF' ,T=2.5 ,F=rampmff25/  
&RAMP ID=' RAMP MF' ,T=2.6 ,F=rampmff26/  
&RAMP ID=' RAMP MF' ,T=2.7 ,F=rampmff27/  
&RAMP ID=' RAMP MF' ,T=2.8 ,F=rampmff28/  
&RAMP ID=' RAMP MF' ,T=2.9 ,F=rampmff29/  
&RAMP ID=' RAMP MF' ,T=3.0 ,F=rampmff30/  
&RAMP ID=' RAMP MF' ,T=3.1 ,F=rampmff31/  
&RAMP ID=' RAMP MF' ,T=3.2 ,F=rampmff32/  
&RAMP ID=' RAMP MF' ,T=3.3 ,F=rampmff33/  
&RAMP ID=' RAMP MF' ,T=3.4 ,F=rampmff34/  
&RAMP ID=' RAMP MF' ,T=3.5 ,F=rampmff35/  
&RAMP ID=' RAMP MF' ,T=3.6 ,F=rampmff36/  
&RAMP ID=' RAMP MF' ,T=3.7 ,F=rampmff37/  
&RAMP ID=' RAMP MF' ,T=3.8 ,F=rampmff38/  
&RAMP ID=' RAMP MF' ,T=3.9 ,F=rampmff39/  
&RAMP ID=' RAMP MF' ,T=4.0 ,F=rampmff40/  
&RAMP ID=' RAMP MF' ,T=4.1 ,F=rampmff41/  
&RAMP ID=' RAMP MF' ,T=4.2 ,F=rampmff42/  
&RAMP ID=' RAMP MF' ,T=4.3 ,F=rampmff43/  
&RAMP ID=' RAMP MF' ,T=4.4 ,F=rampmff44/  
&RAMP ID=' RAMP MF' ,T=4.5 ,F=rampmff45/  
&RAMP ID=' RAMP MF' ,T=4.6 ,F=rampmff46/  
&RAMP ID=' RAMP MF' ,T=4.7 ,F=rampmff47/  
&RAMP ID=' RAMP MF' ,T=4.8 ,F=rampmff48/  
&RAMP ID=' RAMP MF' ,T=4.9 ,F=rampmff49/  
&RAMP ID=' RAMP MF' ,T=5.0 ,F=rampmff50/  
&RAMP ID=' RAMP MF' ,T=5.1 ,F=rampmff51/  
&RAMP ID=' RAMP MF' ,T=5.2 ,F=rampmff52/  
&RAMP ID=' RAMP MF' ,T=5.3 ,F=rampmff53/  
&RAMP ID=' RAMP MF' ,T=5.4 ,F=rampmff54/  
&RAMP ID=' RAMP MF' ,T=5.5 ,F=rampmff55/  
&RAMP ID=' RAMP MF' ,T=5.6 ,F=rampmff56/
```

```
&RAMP ID=' RAMP MF', T=5.7, F=rampmfff57/  
&RAMP ID=' RAMP MF', T=5.8, F=rampmfff58/  
&RAMP ID=' RAMP MF', T=5.9, F=rampmfff59/  
&RAMP ID=' RAMP MF', T=6.0, F=rampmfff60/  
&RAMP ID=' RAMP MF', T=6.1, F=rampmfff61/  
&RAMP ID=' RAMP MF', T=6.2, F=rampmfff62/  
&RAMP ID=' RAMP MF', T=6.3, F=rampmfff63/  
&RAMP ID=' RAMP MF', T=6.4, F=rampmfff64/  
&RAMP ID=' RAMP MF', T=6.5, F=rampmfff65/  
&RAMP ID=' RAMP MF', T=6.6, F=rampmfff66/  
&RAMP ID=' RAMP MF', T=6.7, F=rampmfff67/  
&RAMP ID=' RAMP MF', T=6.8, F=rampmfff68/  
&RAMP ID=' RAMP MF', T=6.9, F=rampmfff69/  
&RAMP ID=' RAMP MF', T=7.0, F=rampmfff70/  
&RAMP ID=' RAMP MF', T=7.1, F=rampmfff71/  
&RAMP ID=' RAMP MF', T=7.2, F=rampmfff72/  
&RAMP ID=' RAMP MF', T=7.3, F=rampmfff73/  
&RAMP ID=' RAMP MF', T=7.4, F=rampmfff74/  
&RAMP ID=' RAMP MF', T=7.5, F=rampmfff75/  
&RAMP ID=' RAMP MF', T=7.6, F=rampmfff76/  
&RAMP ID=' RAMP MF', T=7.7, F=rampmfff77/  
&RAMP ID=' RAMP MF', T=7.8, F=rampmfff78/  
&RAMP ID=' RAMP MF', T=7.9, F=rampmfff79/  
&RAMP ID=' RAMP MF', T=8.0, F=rampmfff80/  
&RAMP ID=' RAMP MF', T=8.1, F=rampmfff81/  
&RAMP ID=' RAMP MF', T=8.2, F=rampmfff82/  
&RAMP ID=' RAMP MF', T=8.3, F=rampmfff83/  
&RAMP ID=' RAMP MF', T=8.4, F=rampmfff84/  
&RAMP ID=' RAMP MF', T=8.5, F=rampmfff85/  
&RAMP ID=' RAMP MF', T=8.6, F=rampmfff86/  
&RAMP ID=' RAMP MF', T=8.7, F=rampmfff87/  
&RAMP ID=' RAMP MF', T=8.8, F=rampmfff88/  
&RAMP ID=' RAMP MF', T=8.9, F=rampmfff89/  
&RAMP ID=' RAMP MF', T=9.0, F=rampmfff90/  
&RAMP ID=' RAMP MF', T=9.1, F=rampmfff91/  
&RAMP ID=' RAMP MF', T=9.2, F=rampmfff92/  
&RAMP ID=' RAMP MF', T=9.3, F=rampmfff93/  
&RAMP ID=' RAMP MF', T=9.4, F=rampmfff94/  
&RAMP ID=' RAMP MF', T=9.5, F=rampmfff95/  
&RAMP ID=' RAMP MF', T=9.6, F=rampmfff96/  
&RAMP ID=' RAMP MF', T=9.7, F=rampmfff97/  
&RAMP ID=' RAMP MF', T=9.8, F=rampmfff98/  
&RAMP ID=' RAMP MF', T=9.9, F=rampmfff99/  
&RAMP ID=' RAMP MF', T=10.0, F=rampmfff100/  
&RAMP ID=' RAMP MF', T=10.1, F=rampmfff101/  
&RAMP ID=' RAMP MF', T=10.2, F=rampmfff102/  
&RAMP ID=' RAMP MF', T=10.3, F=rampmfff103/  
&RAMP ID=' RAMP MF', T=10.4, F=rampmfff104/  
&RAMP ID=' RAMP MF', T=10.5, F=rampmfff105/  
&RAMP ID=' RAMP MF', T=10.6, F=rampmfff106/  
&RAMP ID=' RAMP MF', T=10.7, F=rampmfff107/  
&RAMP ID=' RAMP MF', T=10.8, F=rampmfff108/  
&RAMP ID=' RAMP MF', T=10.9, F=rampmfff109/  
&RAMP ID=' RAMP MF', T=11.0, F=rampmfff110/  
&RAMP ID=' RAMP MF', T=11.1, F=rampmfff111/  
&RAMP ID=' RAMP MF', T=11.2, F=rampmfff112/  
&RAMP ID=' RAMP MF', T=11.3, F=rampmfff113/  
&RAMP ID=' RAMP MF', T=11.4, F=rampmfff114/  
&RAMP ID=' RAMP MF', T=11.5, F=rampmfff115/  
&RAMP ID=' RAMP MF', T=11.6, F=rampmfff116/  
&RAMP ID=' RAMP MF', T=11.7, F=rampmfff117/  
&RAMP ID=' RAMP MF', T=11.8, F=rampmfff118/  
&RAMP ID=' RAMP MF', T=11.9, F=rampmfff119/  
&RAMP ID=' RAMP MF', T=12.0, F=rampmfff120/
```

---

## FDS Input File Templates

```
&RAMP ID=' RAMP MF', T=12.1, F=rampmff121/  
&RAMP ID=' RAMP MF', T=12.2, F=rampmff122/  
&RAMP ID=' RAMP MF', T=12.3, F=rampmff123/  
&RAMP ID=' RAMP MF', T=12.4, F=rampmff124/  
&RAMP ID=' RAMP MF', T=12.5, F=rampmff125/  
&RAMP ID=' RAMP MF', T=12.6, F=rampmff126/  
&RAMP ID=' RAMP MF', T=12.7, F=rampmff127/  
&RAMP ID=' RAMP MF', T=12.8, F=rampmff128/  
&RAMP ID=' RAMP MF', T=12.9, F=rampmff129/  
&RAMP ID=' RAMP MF', T=13.0, F=rampmff130/  
&RAMP ID=' RAMP MF', T=13.1, F=rampmff131/  
&RAMP ID=' RAMP MF', T=13.2, F=rampmff132/  
&RAMP ID=' RAMP MF', T=13.3, F=rampmff133/  
&RAMP ID=' RAMP MF', T=13.4, F=rampmff134/  
&RAMP ID=' RAMP MF', T=13.5, F=rampmff135/  
&RAMP ID=' RAMP MF', T=13.6, F=rampmff136/  
&RAMP ID=' RAMP MF', T=13.7, F=rampmff137/  
&RAMP ID=' RAMP MF', T=13.8, F=rampmff138/  
&RAMP ID=' RAMP MF', T=13.9, F=rampmff139/  
&RAMP ID=' RAMP MF', T=14.0, F=rampmff140/  
&RAMP ID=' RAMP MF', T=14.1, F=rampmff141/  
&RAMP ID=' RAMP MF', T=14.2, F=rampmff142/  
&RAMP ID=' RAMP MF', T=14.3, F=rampmff143/  
&RAMP ID=' RAMP MF', T=14.4, F=rampmff144/  
&RAMP ID=' RAMP MF', T=14.5, F=rampmff145/  
&RAMP ID=' RAMP MF', T=14.6, F=rampmff146/  
&RAMP ID=' RAMP MF', T=14.7, F=rampmff147/  
&RAMP ID=' RAMP MF', T=14.8, F=rampmff148/  
&RAMP ID=' RAMP MF', T=14.9, F=rampmff149/  
&RAMP ID=' RAMP MF', T=15.0, F=rampmff150/  
&RAMP ID=' RAMP MF', T=15.1, F=rampmff151/  
&RAMP ID=' RAMP MF', T=15.2, F=rampmff152/  
&RAMP ID=' RAMP MF', T=15.3, F=rampmff153/  
&RAMP ID=' RAMP MF', T=15.4, F=rampmff154/  
&RAMP ID=' RAMP MF', T=15.5, F=rampmff155/  
&RAMP ID=' RAMP MF', T=15.6, F=rampmff156/  
&RAMP ID=' RAMP MF', T=15.7, F=rampmff157/  
&RAMP ID=' RAMP MF', T=15.8, F=rampmff158/  
&RAMP ID=' RAMP MF', T=15.9, F=rampmff159/  
&RAMP ID=' RAMP MF', T=16.0, F=rampmff160/  
&RAMP ID=' RAMP MF', T=16.1, F=rampmff161/  
&RAMP ID=' RAMP MF', T=16.2, F=rampmff162/  
&RAMP ID=' RAMP MF', T=16.3, F=rampmff163/  
&RAMP ID=' RAMP MF', T=16.4, F=rampmff164/  
&RAMP ID=' RAMP MF', T=16.5, F=rampmff165/  
&RAMP ID=' RAMP MF', T=16.6, F=rampmff166/  
&RAMP ID=' RAMP MF', T=16.7, F=rampmff167/  
&RAMP ID=' RAMP MF', T=16.8, F=rampmff168/  
&RAMP ID=' RAMP MF', T=16.9, F=rampmff169/  
&RAMP ID=' RAMP MF', T=17.0, F=rampmff170/  
&RAMP ID=' RAMP MF', T=17.1, F=rampmff171/  
&RAMP ID=' RAMP MF', T=17.2, F=rampmff172/  
&RAMP ID=' RAMP MF', T=17.3, F=rampmff173/  
&RAMP ID=' RAMP MF', T=17.4, F=rampmff174/  
&RAMP ID=' RAMP MF', T=17.5, F=rampmff175/  
&RAMP ID=' RAMP MF', T=17.6, F=rampmff176/  
&RAMP ID=' RAMP MF', T=17.7, F=rampmff177/  
&RAMP ID=' RAMP MF', T=17.8, F=rampmff178/  
&RAMP ID=' RAMP MF', T=17.9, F=rampmff179/  
&RAMP ID=' RAMP MF', T=18.0, F=rampmff180/  
&RAMP ID=' RAMP MF', T=18.1, F=rampmff181/  
&RAMP ID=' RAMP MF', T=18.2, F=rampmff182/  
&RAMP ID=' RAMP MF', T=18.3, F=rampmff183/  
&RAMP ID=' RAMP MF', T=18.4, F=rampmff184/
```

```

&RAMP ID='RAMP MF',T=18.5,F=rampmff185/
&RAMP ID='RAMP MF',T=18.6,F=rampmff186/
&RAMP ID='RAMP MF',T=18.7,F=rampmff187/
&RAMP ID='RAMP MF',T=18.8,F=rampmff188/
&RAMP ID='RAMP MF',T=18.9,F=rampmff189/
&RAMP ID='RAMP MF',T=19.0,F=rampmff190/
&RAMP ID='RAMP MF',T=19.1,F=rampmff191/
&RAMP ID='RAMP MF',T=19.2,F=rampmff192/
&RAMP ID='RAMP MF',T=19.3,F=rampmff193/
&RAMP ID='RAMP MF',T=19.4,F=rampmff194/
&RAMP ID='RAMP MF',T=19.5,F=rampmff195/
&RAMP ID='RAMP MF',T=19.6,F=rampmff196/
&RAMP ID='RAMP MF',T=19.7,F=rampmff197/
&RAMP ID='RAMP MF',T=19.8,F=rampmff198/
&RAMP ID='RAMP MF',T=19.9,F=rampmff199/
&RAMP ID='RAMP MF',T=20.0,F=rampmff200/
&RAMP ID='RAMP MF',T=20.1,F=0.0000/

```

! Gas phase specific heats. FDS defaults for N2, O2, H2O, and CO2 replaced to extend values to higher temperatures than present in FDS

```

&RAMP ID='AL2O3 C', T=-73, F=0.761/ NASA TP-2002-211556
&RAMP ID='AL2O3 C', T=127, F=0.921/
&RAMP ID='AL2O3 C', T=327, F=0.999/
&RAMP ID='AL2O3 C', T=527, F=1.038/
&RAMP ID='AL2O3 C', T=727, F=1.058/
&RAMP ID='AL2O3 C', T=1727, F=1.090/
&RAMP ID='AL2O3 C', T=2727, F=1.096/
&RAMP ID='AL2O3 C', T=3727, F=1.098/
&RAMP ID='AL2O3 C', T=4727, F=1.099/
&RAMP ID='AL2O3 C', T=5727, F=1.100/

```

```

&RAMP ID='AL C', T=-73, F=0.820/ NASA TP-2002-211556
&RAMP ID='AL C', T=127, F=0.783/
&RAMP ID='AL C', T=327, F=0.776/
&RAMP ID='AL C', T=527, F=0.773/
&RAMP ID='AL C', T=727, F=0.772/
&RAMP ID='AL C', T=1727, F=0.771/
&RAMP ID='AL C', T=2727, F=0.771/
&RAMP ID='AL C', T=3727, F=0.775/
&RAMP ID='AL C', T=4727, F=0.793/
&RAMP ID='AL C', T=5727, F=0.841/
&RAMP ID='AL C', T=6727, F=0.930/
&RAMP ID='AL C', T=7727, F=1.034/
&RAMP ID='AL C', T=8727, F=1.130/
&RAMP ID='AL C', T=9727, F=1.204/
&RAMP ID='AL C', T=10727, F=1.250/
&RAMP ID='AL C', T=11727, F=1.271/
&RAMP ID='AL C', T=12727, F=1.269/
&RAMP ID='AL C', T=13727, F=1.252/
&RAMP ID='AL C', T=14727, F=1.226/
&RAMP ID='AL C', T=15727, F=1.196/
&RAMP ID='AL C', T=16727, F=1.168/
&RAMP ID='AL C', T=17727, F=1.145/
&RAMP ID='AL C', T=18727, F=1.125/
&RAMP ID='AL C', T=19727, F=1.108/

```

```

&RAMP ID='CU C', T=-73, F=0.327/ NASA TP-2002-211556
&RAMP ID='CU C', T=127, F=0.327/
&RAMP ID='CU C', T=327, F=0.327/
&RAMP ID='CU C', T=527, F=0.327/
&RAMP ID='CU C', T=727, F=0.327/
&RAMP ID='CU C', T=1727, F=0.337/
&RAMP ID='CU C', T=2727, F=0.396/

```

---

*FDS Input File Templates*

```
&RAMP ID=' CU C' , T=3727, F=0.471/
&RAMP ID=' CU C' , T=4727, F=0.517/
&RAMP ID=' CU C' , T=5727, F=0.537/
&RAMP ID=' CU C' , T=6727, F=0.551/
&RAMP ID=' CU C' , T=7727, F=0.577/
&RAMP ID=' CU C' , T=8727, F=0.606/
&RAMP ID=' CU C' , T=9727, F=0.633/
&RAMP ID=' CU C' , T=10727, F=0.653/
&RAMP ID=' CU C' , T=11727, F=0.663/
&RAMP ID=' CU C' , T=12727, F=0.664/
&RAMP ID=' CU C' , T=13727, F=0.657/
&RAMP ID=' CU C' , T=14727, F=0.642/
&RAMP ID=' CU C' , T=15727, F=0.622/
&RAMP ID=' CU C' , T=16727, F=0.599/
&RAMP ID=' CU C' , T=17727, F=0.574/
&RAMP ID=' CU C' , T=18727, F=0.550/
&RAMP ID=' CU C' , T=19727, F=0.528/

&RAMP ID=' N2 C' , T=-73, F=1.039/ NASA TP-2002-211556
&RAMP ID=' N2 C' , T=127, F=1.044/
&RAMP ID=' N2 C' , T=327, F=1.075/
&RAMP ID=' N2 C' , T=527, F=1.122/
&RAMP ID=' N2 C' , T=727, F=1.167/
&RAMP ID=' N2 C' , T=1727, F=1.284/
&RAMP ID=' N2 C' , T=2727, F=1.322/
&RAMP ID=' N2 C' , T=3727, F=1.340/
&RAMP ID=' N2 C' , T=4727, F=1.354/
&RAMP ID=' N2 C' , T=5727, F=1.371/
&RAMP ID=' N2 C' , T=6727, F=1.402/
&RAMP ID=' N2 C' , T=7727, F=1.454/
&RAMP ID=' N2 C' , T=8727, F=1.544/
&RAMP ID=' N2 C' , T=9727, F=1.670/
&RAMP ID=' N2 C' , T=10727, F=1.822/
&RAMP ID=' N2 C' , T=11727, F=1.984/
&RAMP ID=' N2 C' , T=12727, F=2.136/
&RAMP ID=' N2 C' , T=13727, F=2.261/
&RAMP ID=' N2 C' , T=14727, F=2.346/
&RAMP ID=' N2 C' , T=15727, F=2.383/
&RAMP ID=' N2 C' , T=16727, F=2.372/
&RAMP ID=' N2 C' , T=17727, F=2.320/
&RAMP ID=' N2 C' , T=18727, F=2.241/
&RAMP ID=' N2 C' , T=19727, F=2.159/

&RAMP ID=' O2 C' , T=-73, F=0.910/ NASA TP-2002-211556
&RAMP ID=' O2 C' , T=127, F=0.941/
&RAMP ID=' O2 C' , T=327, F=1.003/
&RAMP ID=' O2 C' , T=527, F=1.055/
&RAMP ID=' O2 C' , T=727, F=1.090/
&RAMP ID=' O2 C' , T=1727, F=1.181/
&RAMP ID=' O2 C' , T=2727, F=1.249/
&RAMP ID=' O2 C' , T=3727, F=1.303/
&RAMP ID=' O2 C' , T=4727, F=1.344/
&RAMP ID=' O2 C' , T=5727, F=1.373/
&RAMP ID=' O2 C' , T=6727, F=1.386/
&RAMP ID=' O2 C' , T=7727, F=1.376/
&RAMP ID=' O2 C' , T=8727, F=1.344/
&RAMP ID=' O2 C' , T=9727, F=1.296/
&RAMP ID=' O2 C' , T=10727, F=1.241/
&RAMP ID=' O2 C' , T=11727, F=1.184/
&RAMP ID=' O2 C' , T=12727, F=1.128/
&RAMP ID=' O2 C' , T=13727, F=1.077/
&RAMP ID=' O2 C' , T=14727, F=1.030/
&RAMP ID=' O2 C' , T=15727, F=0.989/
&RAMP ID=' O2 C' , T=16727, F=0.953/
```

```

&RAMP ID='O2 C', T=17727, F=0.922/
&RAMP ID='O2 C', T=18727, F=0.894/
&RAMP ID='O2 C', T=19727, F=0.870/

&RAMP ID='CO2 C', T=-73, F=0.735/ NASA TP-2002-211556
&RAMP ID='CO2 C', T=127, F=0.939/
&RAMP ID='CO2 C', T=327, F=1.075/
&RAMP ID='CO2 C', T=527, F=1.169/
&RAMP ID='CO2 C', T=727, F=1.234/
&RAMP ID='CO2 C', T=1727, F=1.371/
&RAMP ID='CO2 C', T=2727, F=1.412/
&RAMP ID='CO2 C', T=3727, F=1.436/
&RAMP ID='CO2 C', T=4727, F=1.466/
&RAMP ID='CO2 C', T=5727, F=1.517/
&RAMP ID='CO2 C', T=6727, F=1.595/
&RAMP ID='CO2 C', T=7727, F=1.694/
&RAMP ID='CO2 C', T=8727, F=1.797/
&RAMP ID='CO2 C', T=9727, F=1.888/
&RAMP ID='CO2 C', T=10727, F=1.957/
&RAMP ID='CO2 C', T=11727, F=2.000/
&RAMP ID='CO2 C', T=12727, F=2.019/
&RAMP ID='CO2 C', T=13727, F=2.020/
&RAMP ID='CO2 C', T=14727, F=2.007/
&RAMP ID='CO2 C', T=15727, F=1.987/
&RAMP ID='CO2 C', T=16727, F=1.965/
&RAMP ID='CO2 C', T=17727, F=1.944/
&RAMP ID='CO2 C', T=18727, F=1.924/
&RAMP ID='CO2 C', T=19727, F=1.905/

```

!Smokeview Outputs. Adjust PBX and PBX for center of arc volume.

```

alslcf1 QUANTITY='MASS FRACTION',SPEC_ID='ALUMINUM',CELL_CENTERED=.TRUE.,PBY=0.0000/
alslcf2 QUANTITY='MASS FRACTION',SPEC_ID='ALUMINUM
OXIDE',CELL_CENTERED=.TRUE.,PBY=0.0000/
cuslcf1 QUANTITY='MASS FRACTION',SPEC_ID='COPPER',CELL_CENTERED=.TRUE.,PBY=0.0000/
cuslcf2 QUANTITY='MASS FRACTION',SPEC_ID='COPPER
OXIDE',CELL_CENTERED=.TRUE.,PBY=0.0000/
&SLCF QUANTITY='MASS FRACTION',SPEC_ID='OXYGEN',CELL_CENTERED=.TRUE.,PBY=0.0000/
&SLCF QUANTITY='HRRPUV',CELL_CENTERED=.TRUE.,PBY=0.0000/
&SLCF QUANTITY='HRRPUV',CELL_CENTERED=.TRUE.,PBX=slcfpbx/
&SLCF QUANTITY='TEMPERATURE',CELL_CENTERED=.TRUE.,PBY=0.0000/
&SLCF QUANTITY='TEMPERATURE',CELL_CENTERED=.TRUE.,PBX=slcfpbx/
&SLCF QUANTITY='INTEGRATED INTENSITY',CELL_CENTERED=.TRUE.,PBY=0.0000/
&SLCF QUANTITY='INTEGRATED INTENSITY',CELL_CENTERED=.TRUE.,PBX=slcfpbx/
&SLCF QUANTITY='VELOCITY',CELL_CENTERED=.TRUE.,PBY=0.0000/
&SLCF QUANTITY='U-VELOCITY',CELL_CENTERED=.TRUE.,PBY=0.0000/
&SLCF QUANTITY='VELOCITY',CELL_CENTERED=.TRUE.,PBX=slcfpbx/
&SLCF QUANTITY='V-VELOCITY',CELL_CENTERED=.TRUE.,PBX=slcfpbx/
&SLCF QUANTITY='PRESSURE',CELL_CENTERED=.TRUE.,PBY=0.0000/

&BNDF QUANTITY='WALL TEMPERATURE',CELL_CENTERED=.TRUE./
&BNDF QUANTITY='GAUGE HEAT FLUX',CELL_CENTERED=.TRUE./
&BNDF QUANTITY='WALL THICKNESS',CELL_CENTERED=.TRUE./
&BNDF QUANTITY='VELOCITY ERROR',CELL_CENTERED=.TRUE./

```

!Example DEVC for ZOI runs. Have planes of devices at a range of distances that look at each face of the enclosure  
!Plane should be large enough to see any permanent venting, plus any area heated by or damaged by the arc, plus any C-17uoyancy impacts  
!Here the DEVC ID my means this is on the (m) minus (y) face at the given x,y,z location  
!The orientation is the unit vector given by Arc Center - DEVC XYZ. Pointing the DEVC at the arc centroid will approximate the worst case view factor  
!for the radiative component.  
!These can easily be generated with Excel using CONCATENATE()

```
!&DEVC XYZ=4.3434,4.8514,2.9210, ORIENTATION=0.131,0.578,-0.805, QUANTITY='GAUGE HEAT  
FLUX GAS', ID='my:x=4.34,y=4.85,z=2.92'/
```

## C.2.2 Horizontal Draw-Out Style Circuit Breaker

```
&HEAD CHID='fileid' /
```

```
! 3 in. resolution. Approximately 2 m to each side, 2 m above, and 2.4 m front and  
back.
```

```
&MESH ID='Cabinet', IJK=24,22,20, XB=-2.4384,-0.6096,-2.5146,-  
0.8382,0.0000,1.5240, MULT_ID='M1' / 3 in. resolution  
&MULT ID='M1', I_UPPER=3, DX=1.8288, J_UPPER=2, DY=1.6764, K_UPPER=2, DZ=1.5240 /
```

```
&VENT MB='ZMAX', SURF_ID='OPEN' /  
&VENT MB='YMAX', SURF_ID='OPEN' /  
&VENT MB='XMAX', SURF_ID='OPEN' /  
&VENT MB='YMIN', SURF_ID='OPEN' /  
&VENT MB='XMIN', SURF_ID='OPEN' /
```

```
! I_MAX_TEMP=35000 ensures property arrays are high enough for the CLIP C-18uoyan.  
! AEROSOL_AL2O3 replaces default SOOT radiative properties with those for AL2O3
```

```
&MISC AEROSOL_AL2O3=T, I_MAX_TEMP=35000 /
```

```
! SMOKE3D_SPEC_ID sets the species used by Smokeview to visualize smoke
```

```
&DUMP SMOKE3D_SPEC_ID='3dsmoke', SUPPRESS_DIAGNOSTICS=F, MASS_FILE=T /
```

```
! Turns off the extinction model. Default values in the model may not be appropriate  
for metal oxidation  
&COMB SUPPRESSION=F /
```

```
! 0.01 kg/m3 greatly limits clipping of density.  
&CLIP MINIMUM_DENSITY=0.01, MAXIMUM_TEMPERATURE=35000., CLIP_DT_RESTRICTIONS_MAX=0 /
```

```
! These cases a very challenging for the pressure solver. The selected values seem to  
give enough pressure iterations to  
! drop the velocity error down to a plateau value.
```

```
&PRES MAX_PRESSURE_ITERATIONS=30, VELOCITY_TOLERANCE=0.001,  
SUSPEND_PRESSURE_ITERATIONS=F /
```

```
! For ZOI runs suggest T_END = arc time + 8 s
```

```
&TIME T_END=tend, DT=0.001, WALL_INCREMENT=1 /
```

```
&RADI NUMBER_RADIATION_ANGLES=500 /
```

```
! 1 cell thick OBST to help out pressure solver.
```

```
&OBST XB=0.0000,0.0762,-0.3810,0.3810,0.3048,2.2860, SURF_ID='CABINET' / rear panel  
&OBST XB=0.0000,0.0762,-0.3810,0.3810,0.0000,0.0762, SURF_ID='CABINET' / thin strip of  
rear panel below vent  
&OBST XB =1.9812,2.0574 , -0.3810,0.3810,1.6002,2.1336, SURF_ID='CABINET' / front top  
panel  
&OBST XB=0.0000,1.2192,-0.3810,0.3810,2.2098,2.2860, SURF_ID='CABINET' / top panel, rear  
section  
&OBST XB=1.3716,2.0574,-0.3810,0.3810,2.2098,2.2860, SURF_ID='CABINET' / top panel,  
front section  
&OBST XB=0.0000,2.0574,-0.4572,-0.3810,0.0000,2.2860, SURF_ID='CABINET' / right panel  
&OBST XB=0.0000,2.0574,0.3810,0.4572,0.0000,2.2860, SURF_ID='CABINET' / left panel
```

```

&OBST XB=1.0668,1.143,-0.3810,0.3810,0.0000,2.2098,SURF_ID='CABINET' / center vertical
internal
&OBST XB=1.2192,1.3716,-0.3048,0.3048,1.9812,2.0574,SURF_ID='CABINET' / hanging piece
below vent
&OBST XB=1.8288,2.0574,-0.3810,0.3810,1.524,1.6002,SURF_ID='CABINET' / horizontal piece
above breaker
&OBST XB=1.524,1.6002,-0.3810,0.3810,1.8288,2.2860,SURF_ID='CABINET' / vertical piece
above breaker
&OBST XB=1.6002,1.6764,-0.3810,0.3810,1.7526,1.8288,SURF_ID='CABINET' / diagonal
&OBST XB=1.6764,1.7526,-0.3810,0.3810,1.6764,1.7526,SURF_ID='CABINET' / diagonal
&OBST XB=1.7526,1.8288,-0.3810,0.3810,1.6002,1.6764,SURF_ID='CABINET' / diagonal
&OBST XB=0.6858,1.0668,-0.3810,0.3810,0.6096,0.6858,SURF_ID='CABINET' / rear partition
shelf
&OBST XB=0.6096,0.7620,-0.3810,0.3810,0.8382,0.9144,SURF_ID='CABINET' / rear partition
shelf
&OBST XB=0.6858,0.7620,-0.3810,0.3810,0.6858,0.8382,SURF_ID='CABINET' / rear partition
shelf
&OBST XB=0.6096,0.6858,-0.3810,0.3810,0.9144,1.524,SURF_ID='CABINET' / rear partition
vertical lower (gap to prevent pressure compt)
&OBST XB=0.6096,0.6858,-0.3810,0.3810,1.6002,2.2098,SURF_ID='CABINET' / rear partition
vertical upper (gap to prevent pressure compt)
&OBST XB=1.524,2.0574,-0.3048,0.3048,0.0000,1.4478,SURF_ID='BREAKER' /

! RADCAL_ID='SOOT' makes the SPEC use the SOOT radiation properties which the MISC
line has changed to those for AL2O3
! RAMPS used instead of built in cp data for N2, CO2, and O2 to extend temperature to
20,000 K

&SPEC ID='WET NITROGEN',BACKGROUND=T,SPEC_ID='NITROGEN','CARBON DIOXIDE','WATER
VAPOR',MASS_FRACTION=1,0.000775,0.007792/FDS Default AIR without O2
&SPEC ID='NITROGEN', LUMPED_COMPONENT_ONLY=T,RAMP_CP='N2 C' /
&SPEC ID='CARBON DIOXIDE', LUMPED_COMPONENT_ONLY=T,RAMP_CP='CO2 C' /
&SPEC ID='WATER VAPOR', LUMPED_COMPONENT_ONLY=T /
&SPEC ID='OXYGEN', MASS_FRACTION_0=0.230997,RAMP_CP='O2 C' /
alspec1 ID='ALUMINUM',FORMULA='Al',RAMP_CP='AL
C',SIGMALJ=2.655,EPSILONKLJ=2750.,PR_GAS=1/
alspec2 ID='ALUMINUM
OXIDE',MASS_EXTINCTION_COEFFICIENT=3000,FORMULA='Al2O3',RAMP_CP='AL2O3
C',SIGMALJ=3.186,EPSILONKLJ=557.449,PR_GAS=1,RADCAL_ID='SOOT' /
cuspec1 ID='COPPER',FORMULA='Cu',RAMP_CP='CU
C',SIGMALJ=5.058,EPSILONKLJ=2983.,PR_GAS=1/
cuspec2 ID='COPPER
OXIDE',MASS_EXTINCTION_COEFFICIENT=3000,FORMULA='Cu2O',SPECIFIC_HEAT=0.7,SIGMALJ=5.403
,PR_GAS=1,RADCAL_ID='SOOT' /C from JANAF, LJ take as CuO

alreac FUEL='ALUMINUM', SPEC_ID_NU='ALUMINUM','OXYGEN','ALUMINUM OXIDE', NU=-2,-1.5,1,
HEAT_OF_COMBUSTION=31100. / Al -> AL2O3
cureac FUEL='COPPER',SPEC_ID_NU='COPPER','OXYGEN','COPPER OXIDE',NU=-2,-
0.5,1,HEAT_OF_COMBUSTION=1340./ Cu->Cu2O

&MATL ID='CONCRETE', DENSITY=2400, CONDUCTIVITY=1.6, SPECIFIC_HEAT=0.75,
EMISSIVITY=0.95 /

! Non-melting steel
&MATL ID='INERT STEEL', DENSITY=7800., SPECIFIC_HEAT_RAMP='STEEL C',
CONDUCTIVITY_RAMP='STEEL K', EMISSIVITY=0.85/

! Melting steel
&MATL ID='STEEL', DENSITY=7800., SPECIFIC_HEAT_RAMP='STEEL C',
CONDUCTIVITY_RAMP='STEEL K', EMISSIVITY=0.85,
THRESHOLD_TEMPERATURE=1300., THRESHOLD_SIGN=1, HEAT_OF_REACTION(1)=250.,
PCR(1)=T, A(1)=0.6, E(1)=0., N_S(1)=0., N_T(1)=1. /

! Eurocode values

```

---

## FDS Input File Templates

```
&RAMP ID='STEEL C',T=20,F=0.440/
&RAMP ID='STEEL C',T=600,F=0.760/
&RAMP ID='STEEL C',T=700,F=1.008/
&RAMP ID='STEEL C',T=720,F=1.388/
&RAMP ID='STEEL C',T=725,F=1.666/
&RAMP ID='STEEL C',T=730,F=2.291/
&RAMP ID='STEEL C',T=735,F=5.000/
&RAMP ID='STEEL C',T=740,F=2.525/ BCC -> FCC Transition
&RAMP ID='STEEL C',T=745,F=1.818/
&RAMP ID='STEEL C',T=750,F=1.483/
&RAMP ID='STEEL C',T=800,F=0.803/
&RAMP ID='STEEL C',T=900,F=0.650/

&RAMP ID='STEEL K',T=20,F=53.3/
&RAMP ID='STEEL K',T=800,F=27.3/

&SURF ID='BREAKER', MATL_ID='INERT STEEL', THICKNESS=0.02,
RGB=204,204,255,CELL_SIZE_FACTOR=0.05,STRETCH_FACTOR=1 /
&SURF ID='CABINET', MATL_ID='STEEL', THICKNESS=0.002381, COLOR='GRAY 60',
BURN_AWAY=.TRUE.,CELL_SIZE_FACTOR=0.05,STRETCH_FACTOR=1 /
&SURF ID='FLOOR', MATL_ID='CONCRETE', THICKNESS=0.15, RGB=50,50,50, DEFAULT=T /

!The block below defines particles that emit vapor for aluminum.
!The particles are initialized at the melting point.
!The PROP MASS_FLOW_RATE is the maximum liquid production rate divided by the number
of electrodes
!NU_SPEC and NU_MATL are set to get the 75 % oxidation for Al and 25 % for Cu. The
second MOLTEN AL2 and CU2 species have a modified density to preserve diameter.
!A and E are set to give the vapor over 0.3 s.

almatl1 ID='MOLTEN
AL',DENSITY=2375,CONDUCTIVITY=100.,SPECIFIC_HEAT=1.177,EMISSIVITY=0,A=3.333,E=0,
N_REACTIONS=1,HEAT_OF_REACTION=0,HEAT_OF_COMBUSTION=0,MATL_ID(1,1)='MOLTEN
AL2',SPEC_ID(1,1)='ALUMINUM',NU_MATL(1,1)=0.25,NU_SPEC(1,1)=0.75/
almatl2 ID='MOLTEN
AL2',DENSITY=593.75,SPEC_ID='ALUMINUM',NU_SPEC=1,CONDUCTIVITY=100.,SPECIFIC_HEAT=1.177
/

alsurf1 ID='AL DROP',MATL_ID='MOLTEN AL',GEOMETRY='SPHERICAL',THICKNESS=5.E-
6,HEAT_TRANSFER_COEFFICIENT=0,TMP_INNER=665.3/
alpart1 ID='AL DROPS',SURF_ID='AL
DROP',AGE=2.0,SAMPLING_FACTOR=10,MONODISPERSE=T,RGB=100,100,100/
alprop1 ID='DROPS',PART_ID='AL DROPS',FLOW_RAMP='RAMP
MF',MASS_FLOW_RATE=almfr,PARTICLES_PER_SECOND=20000,PARTICLE_VELOCITY=10,SPRAY_ANGLE=0
,60/

! The block below is for copper.

Cumatl1 ID='MOLTEN
CU',DENSITY=8960,CONDUCTIVITY=340.,SPECIFIC_HEAT=0.517,EMISSIVITY=0,A=3.333,E=0,
N_REACTIONS=1,HEAT_OF_REACTION=0,HEAT_OF_COMBUSTION=0,MATL_ID(1,1)='MOLTEN
CU2',SPEC_ID(1,1)='COPPER',NU_MATL(1,1)=0.75,NU_SPEC(1,1)=0.25/
cumatl2 ID='MOLTEN
CU2',DENSITY=7168,CONDUCTIVITY=340.,SPECIFIC_HEAT=0.517,EMISSIVITY=0/

cusurf1 ID='CU DROP',MATL_ID='MOLTEN CU',GEOMETRY='SPHERICAL',THICKNESS=5.E-
6,HEAT_TRANSFER_COEFFICIENT=0,TMP_INNER=1084.85/
cupart1 ID='CU DROPS',SURF_ID='CU
DROP',AGE=2.0,SAMPLING_FACTOR=10,MONODISPERSE=T,RGB=184,115,51/
cuprop1 ID='DROPS',PART_ID='CU DROPS',FLOW_RAMP='RAMP
MF',MASS_FLOW_RATE=cumfr,PARTICLES_PER_SECOND=20000,PARTICLE_VELOCITY=10,SPRAY_ANGLE=0
,60/
```

```

! First INIT line is the volumetric source term where the RADAITIVE_FRACTION uses
Cressault's data interpolated based on power,. The HRRPUV is
! reduced based on energy needed to degrade the electrodes:
! Adjusted total energy = (Total arc energy - electrode mass loss * (vapor fraction *
energy to vaporize + liquid fraction * energy to melt))
!
! Cressault data:
!
! X_r,Al = 0.2275*Max_Power^0.3292
! X_r,Al = 0.1273*Max_Power^0.3859
!
! Phase Energy (kJ/kg)
! Change Al Cu
! Melt 1063.4 695.2

&INIT XB=initx1,initx2,inity1,inity2,initz1,initz2,HRRPUV=hrrpuvval,RAMP_Q='RAMP
Q',RADIATIVE_FRACTION=radfrac/

! One spray nozzle device per electrode that inject liquid droplets

&DEVC
PROP_ID='DROPS',XYZ=nozx1,nozy1,nozz1,QUANTITY='TIME',SETPOINT=0.0,ORIENTATION=orient1
,orient2,orient3/
&DEVC
PROP_ID='DROPS',XYZ=nozx2,nozy2,nozz2,QUANTITY='TIME',SETPOINT=0.0,ORIENTATION=orient1
,orient2,orient3/
&DEVC
PROP_ID='DROPS',XYZ=nozx3,nozy3,nozz3,QUANTITY='TIME',SETPOINT=0.0,ORIENTATION=orient1
,orient2,orient3/

! An 0.1 s ramp up and down for the arc volumetric source term helps avoid numerical
instabilities

&RAMP ID='RAMP Q',T=0.0,F=0.0000/
&RAMP ID='RAMP Q',T=0.1,F=rampqf1/
&RAMP ID='RAMP Q',T=0.2,F=rampqf2/
&RAMP ID='RAMP Q',T=0.3,F=rampqf3/
&RAMP ID='RAMP Q',T=0.4,F=rampqf4/
&RAMP ID='RAMP Q',T=0.5,F=rampqf5/
&RAMP ID='RAMP Q',T=0.6,F=rampqf6/
&RAMP ID='RAMP Q',T=0.7,F=rampqf7/
&RAMP ID='RAMP Q',T=0.8,F=rampqf8/
&RAMP ID='RAMP Q',T=0.9,F=rampqf9/
&RAMP ID='RAMP Q',T=1.0,F=rampqf10/
&RAMP ID='RAMP Q',T=1.1,F=rampqf11/
&RAMP ID='RAMP Q',T=1.2,F=rampqf12/
&RAMP ID='RAMP Q',T=1.3,F=rampqf13/
&RAMP ID='RAMP Q',T=1.4,F=rampqf14/
&RAMP ID='RAMP Q',T=1.5,F=rampqf15/
&RAMP ID='RAMP Q',T=1.6,F=rampqf16/
&RAMP ID='RAMP Q',T=1.7,F=rampqf17/
&RAMP ID='RAMP Q',T=1.8,F=rampqf18/
&RAMP ID='RAMP Q',T=1.9,F=rampqf19/
&RAMP ID='RAMP Q',T=2.0,F=rampqf20/
&RAMP ID='RAMP Q',T=2.1,F=rampqf21/
&RAMP ID='RAMP Q',T=2.2,F=rampqf22/
&RAMP ID='RAMP Q',T=2.3,F=rampqf23/
&RAMP ID='RAMP Q',T=2.4,F=rampqf24/
&RAMP ID='RAMP Q',T=2.5,F=rampqf25/
&RAMP ID='RAMP Q',T=2.6,F=rampqf26/
&RAMP ID='RAMP Q',T=2.7,F=rampqf27/
&RAMP ID='RAMP Q',T=2.8,F=rampqf28/
&RAMP ID='RAMP Q',T=2.9,F=rampqf29/
&RAMP ID='RAMP Q',T=3.0,F=rampqf30/

```

---

## FDS Input File Templates

```
&RAMP ID=' RAMP Q' ,T=3.1,F=rampqf31/  
&RAMP ID=' RAMP Q' ,T=3.2,F=rampqf32/  
&RAMP ID=' RAMP Q' ,T=3.3,F=rampqf33/  
&RAMP ID=' RAMP Q' ,T=3.4,F=rampqf34/  
&RAMP ID=' RAMP Q' ,T=3.5,F=rampqf35/  
&RAMP ID=' RAMP Q' ,T=3.6,F=rampqf36/  
&RAMP ID=' RAMP Q' ,T=3.7,F=rampqf37/  
&RAMP ID=' RAMP Q' ,T=3.8,F=rampqf38/  
&RAMP ID=' RAMP Q' ,T=3.9,F=rampqf39/  
&RAMP ID=' RAMP Q' ,T=4.0,F=rampqf40/  
&RAMP ID=' RAMP Q' ,T=4.1,F=rampqf41/  
&RAMP ID=' RAMP Q' ,T=4.2,F=rampqf42/  
&RAMP ID=' RAMP Q' ,T=4.3,F=rampqf43/  
&RAMP ID=' RAMP Q' ,T=4.4,F=rampqf44/  
&RAMP ID=' RAMP Q' ,T=4.5,F=rampqf45/  
&RAMP ID=' RAMP Q' ,T=4.6,F=rampqf46/  
&RAMP ID=' RAMP Q' ,T=4.7,F=rampqf47/  
&RAMP ID=' RAMP Q' ,T=4.8,F=rampqf48/  
&RAMP ID=' RAMP Q' ,T=4.9,F=rampqf49/  
&RAMP ID=' RAMP Q' ,T=5.0,F=rampqf50/  
&RAMP ID=' RAMP Q' ,T=5.1,F=rampqf51/  
&RAMP ID=' RAMP Q' ,T=5.2,F=rampqf52/  
&RAMP ID=' RAMP Q' ,T=5.3,F=rampqf53/  
&RAMP ID=' RAMP Q' ,T=5.4,F=rampqf54/  
&RAMP ID=' RAMP Q' ,T=5.5,F=rampqf55/  
&RAMP ID=' RAMP Q' ,T=5.6,F=rampqf56/  
&RAMP ID=' RAMP Q' ,T=5.7,F=rampqf57/  
&RAMP ID=' RAMP Q' ,T=5.8,F=rampqf58/  
&RAMP ID=' RAMP Q' ,T=5.9,F=rampqf59/  
&RAMP ID=' RAMP Q' ,T=6.0,F=rampqf60/  
&RAMP ID=' RAMP Q' ,T=6.1,F=rampqf61/  
&RAMP ID=' RAMP Q' ,T=6.2,F=rampqf62/  
&RAMP ID=' RAMP Q' ,T=6.3,F=rampqf63/  
&RAMP ID=' RAMP Q' ,T=6.4,F=rampqf64/  
&RAMP ID=' RAMP Q' ,T=6.5,F=rampqf65/  
&RAMP ID=' RAMP Q' ,T=6.6,F=rampqf66/  
&RAMP ID=' RAMP Q' ,T=6.7,F=rampqf67/  
&RAMP ID=' RAMP Q' ,T=6.8,F=rampqf68/  
&RAMP ID=' RAMP Q' ,T=6.9,F=rampqf69/  
&RAMP ID=' RAMP Q' ,T=7.0,F=rampqf70/  
&RAMP ID=' RAMP Q' ,T=7.1,F=rampqf71/  
&RAMP ID=' RAMP Q' ,T=7.2,F=rampqf72/  
&RAMP ID=' RAMP Q' ,T=7.3,F=rampqf73/  
&RAMP ID=' RAMP Q' ,T=7.4,F=rampqf74/  
&RAMP ID=' RAMP Q' ,T=7.5,F=rampqf75/  
&RAMP ID=' RAMP Q' ,T=7.6,F=rampqf76/  
&RAMP ID=' RAMP Q' ,T=7.7,F=rampqf77/  
&RAMP ID=' RAMP Q' ,T=7.8,F=rampqf78/  
&RAMP ID=' RAMP Q' ,T=7.9,F=rampqf79/  
&RAMP ID=' RAMP Q' ,T=8.0,F=rampqf80/  
&RAMP ID=' RAMP Q' ,T=8.1,F=rampqf81/  
&RAMP ID=' RAMP Q' ,T=8.2,F=rampqf82/  
&RAMP ID=' RAMP Q' ,T=8.3,F=rampqf83/  
&RAMP ID=' RAMP Q' ,T=8.4,F=rampqf84/  
&RAMP ID=' RAMP Q' ,T=8.5,F=rampqf85/  
&RAMP ID=' RAMP Q' ,T=8.6,F=rampqf86/  
&RAMP ID=' RAMP Q' ,T=8.7,F=rampqf87/  
&RAMP ID=' RAMP Q' ,T=8.8,F=rampqf88/  
&RAMP ID=' RAMP Q' ,T=8.9,F=rampqf89/  
&RAMP ID=' RAMP Q' ,T=9.0,F=rampqf90/  
&RAMP ID=' RAMP Q' ,T=9.1,F=rampqf91/  
&RAMP ID=' RAMP Q' ,T=9.2,F=rampqf92/  
&RAMP ID=' RAMP Q' ,T=9.3,F=rampqf93/  
&RAMP ID=' RAMP Q' ,T=9.4,F=rampqf94/
```

```
&RAMP ID=' RAMP Q',T=9.5,F=rampqf95/  
&RAMP ID=' RAMP Q',T=9.6,F=rampqf96/  
&RAMP ID=' RAMP Q',T=9.7,F=rampqf97/  
&RAMP ID=' RAMP Q',T=9.8,F=rampqf98/  
&RAMP ID=' RAMP Q',T=9.9,F=rampqf99/  
&RAMP ID=' RAMP Q',T=10.0,F=rampqf100/  
&RAMP ID=' RAMP Q',T=10.1,F=rampqf101/  
&RAMP ID=' RAMP Q',T=10.2,F=rampqf102/  
&RAMP ID=' RAMP Q',T=10.3,F=rampqf103/  
&RAMP ID=' RAMP Q',T=10.4,F=rampqf104/  
&RAMP ID=' RAMP Q',T=10.5,F=rampqf105/  
&RAMP ID=' RAMP Q',T=10.6,F=rampqf106/  
&RAMP ID=' RAMP Q',T=10.7,F=rampqf107/  
&RAMP ID=' RAMP Q',T=10.8,F=rampqf108/  
&RAMP ID=' RAMP Q',T=10.9,F=rampqf109/  
&RAMP ID=' RAMP Q',T=11.0,F=rampqf110/  
&RAMP ID=' RAMP Q',T=11.1,F=rampqf111/  
&RAMP ID=' RAMP Q',T=11.2,F=rampqf112/  
&RAMP ID=' RAMP Q',T=11.3,F=rampqf113/  
&RAMP ID=' RAMP Q',T=11.4,F=rampqf114/  
&RAMP ID=' RAMP Q',T=11.5,F=rampqf115/  
&RAMP ID=' RAMP Q',T=11.6,F=rampqf116/  
&RAMP ID=' RAMP Q',T=11.7,F=rampqf117/  
&RAMP ID=' RAMP Q',T=11.8,F=rampqf118/  
&RAMP ID=' RAMP Q',T=11.9,F=rampqf119/  
&RAMP ID=' RAMP Q',T=12.0,F=rampqf120/  
&RAMP ID=' RAMP Q',T=12.1,F=rampqf121/  
&RAMP ID=' RAMP Q',T=12.2,F=rampqf122/  
&RAMP ID=' RAMP Q',T=12.3,F=rampqf123/  
&RAMP ID=' RAMP Q',T=12.4,F=rampqf124/  
&RAMP ID=' RAMP Q',T=12.5,F=rampqf125/  
&RAMP ID=' RAMP Q',T=12.6,F=rampqf126/  
&RAMP ID=' RAMP Q',T=12.7,F=rampqf127/  
&RAMP ID=' RAMP Q',T=12.8,F=rampqf128/  
&RAMP ID=' RAMP Q',T=12.9,F=rampqf129/  
&RAMP ID=' RAMP Q',T=13.0,F=rampqf130/  
&RAMP ID=' RAMP Q',T=13.1,F=rampqf131/  
&RAMP ID=' RAMP Q',T=13.2,F=rampqf132/  
&RAMP ID=' RAMP Q',T=13.3,F=rampqf133/  
&RAMP ID=' RAMP Q',T=13.4,F=rampqf134/  
&RAMP ID=' RAMP Q',T=13.5,F=rampqf135/  
&RAMP ID=' RAMP Q',T=13.6,F=rampqf136/  
&RAMP ID=' RAMP Q',T=13.7,F=rampqf137/  
&RAMP ID=' RAMP Q',T=13.8,F=rampqf138/  
&RAMP ID=' RAMP Q',T=13.9,F=rampqf139/  
&RAMP ID=' RAMP Q',T=14.0,F=rampqf140/  
&RAMP ID=' RAMP Q',T=14.1,F=rampqf141/  
&RAMP ID=' RAMP Q',T=14.2,F=rampqf142/  
&RAMP ID=' RAMP Q',T=14.3,F=rampqf143/  
&RAMP ID=' RAMP Q',T=14.4,F=rampqf144/  
&RAMP ID=' RAMP Q',T=14.5,F=rampqf145/  
&RAMP ID=' RAMP Q',T=14.6,F=rampqf146/  
&RAMP ID=' RAMP Q',T=14.7,F=rampqf147/  
&RAMP ID=' RAMP Q',T=14.8,F=rampqf148/  
&RAMP ID=' RAMP Q',T=14.9,F=rampqf149/  
&RAMP ID=' RAMP Q',T=15.0,F=rampqf150/  
&RAMP ID=' RAMP Q',T=15.1,F=rampqf151/  
&RAMP ID=' RAMP Q',T=15.2,F=rampqf152/  
&RAMP ID=' RAMP Q',T=15.3,F=rampqf153/  
&RAMP ID=' RAMP Q',T=15.4,F=rampqf154/  
&RAMP ID=' RAMP Q',T=15.5,F=rampqf155/  
&RAMP ID=' RAMP Q',T=15.6,F=rampqf156/  
&RAMP ID=' RAMP Q',T=15.7,F=rampqf157/  
&RAMP ID=' RAMP Q',T=15.8,F=rampqf158/
```

---

## FDS Input File Templates

```
&RAMP ID=' RAMP Q',T=15.9,F=rampqf159/  
&RAMP ID=' RAMP Q',T=16.0,F=rampqf160/  
&RAMP ID=' RAMP Q',T=16.1,F=rampqf161/  
&RAMP ID=' RAMP Q',T=16.2,F=rampqf162/  
&RAMP ID=' RAMP Q',T=16.3,F=rampqf163/  
&RAMP ID=' RAMP Q',T=16.4,F=rampqf164/  
&RAMP ID=' RAMP Q',T=16.5,F=rampqf165/  
&RAMP ID=' RAMP Q',T=16.6,F=rampqf166/  
&RAMP ID=' RAMP Q',T=16.7,F=rampqf167/  
&RAMP ID=' RAMP Q',T=16.8,F=rampqf168/  
&RAMP ID=' RAMP Q',T=16.9,F=rampqf169/  
&RAMP ID=' RAMP Q',T=17.0,F=rampqf170/  
&RAMP ID=' RAMP Q',T=17.1,F=rampqf171/  
&RAMP ID=' RAMP Q',T=17.2,F=rampqf172/  
&RAMP ID=' RAMP Q',T=17.3,F=rampqf173/  
&RAMP ID=' RAMP Q',T=17.4,F=rampqf174/  
&RAMP ID=' RAMP Q',T=17.5,F=rampqf175/  
&RAMP ID=' RAMP Q',T=17.6,F=rampqf176/  
&RAMP ID=' RAMP Q',T=17.7,F=rampqf177/  
&RAMP ID=' RAMP Q',T=17.8,F=rampqf178/  
&RAMP ID=' RAMP Q',T=17.9,F=rampqf179/  
&RAMP ID=' RAMP Q',T=18.0,F=rampqf180/  
&RAMP ID=' RAMP Q',T=18.1,F=rampqf181/  
&RAMP ID=' RAMP Q',T=18.2,F=rampqf182/  
&RAMP ID=' RAMP Q',T=18.3,F=rampqf183/  
&RAMP ID=' RAMP Q',T=18.4,F=rampqf184/  
&RAMP ID=' RAMP Q',T=18.5,F=rampqf185/  
&RAMP ID=' RAMP Q',T=18.6,F=rampqf186/  
&RAMP ID=' RAMP Q',T=18.7,F=rampqf187/  
&RAMP ID=' RAMP Q',T=18.8,F=rampqf188/  
&RAMP ID=' RAMP Q',T=18.9,F=rampqf189/  
&RAMP ID=' RAMP Q',T=19.0,F=rampqf190/  
&RAMP ID=' RAMP Q',T=19.1,F=rampqf191/  
&RAMP ID=' RAMP Q',T=19.2,F=rampqf192/  
&RAMP ID=' RAMP Q',T=19.3,F=rampqf193/  
&RAMP ID=' RAMP Q',T=19.4,F=rampqf194/  
&RAMP ID=' RAMP Q',T=19.5,F=rampqf195/  
&RAMP ID=' RAMP Q',T=19.6,F=rampqf196/  
&RAMP ID=' RAMP Q',T=19.7,F=rampqf197/  
&RAMP ID=' RAMP Q',T=19.8,F=rampqf198/  
&RAMP ID=' RAMP Q',T=19.9,F=rampqf199/  
&RAMP ID=' RAMP Q',T=20.0,F=rampqf200/  
&RAMP ID=' RAMP Q',T=20.1,F=0.0000/
```

! RAMP for droplets

```
&RAMP ID=' RAMP MF',T=0.00,F=0.0000/  
&RAMP ID=' RAMP MF',T=0.1,F=rampmff1/  
&RAMP ID=' RAMP MF',T=0.2,F=rampmff2/  
&RAMP ID=' RAMP MF',T=0.3,F=rampmff3/  
&RAMP ID=' RAMP MF',T=0.4,F=rampmff4/  
&RAMP ID=' RAMP MF',T=0.5,F=rampmff5/  
&RAMP ID=' RAMP MF',T=0.6,F=rampmff6/  
&RAMP ID=' RAMP MF',T=0.7,F=rampmff7/  
&RAMP ID=' RAMP MF',T=0.8,F=rampmff8/  
&RAMP ID=' RAMP MF',T=0.9,F=rampmff9/  
&RAMP ID=' RAMP MF',T=1.0,F=rampmff10/  
&RAMP ID=' RAMP MF',T=1.1,F=rampmff11/  
&RAMP ID=' RAMP MF',T=1.2,F=rampmff12/  
&RAMP ID=' RAMP MF',T=1.3,F=rampmff13/  
&RAMP ID=' RAMP MF',T=1.4,F=rampmff14/  
&RAMP ID=' RAMP MF',T=1.5,F=rampmff15/  
&RAMP ID=' RAMP MF',T=1.6,F=rampmff16/  
&RAMP ID=' RAMP MF',T=1.7,F=rampmff17/
```

```
&RAMP ID=' RAMP MF' ,T=1.8,F=rampmfff18/  
&RAMP ID=' RAMP MF' ,T=1.9,F=rampmfff19/  
&RAMP ID=' RAMP MF' ,T=2.0,F=rampmfff20/  
&RAMP ID=' RAMP MF' ,T=2.1,F=rampmfff21/  
&RAMP ID=' RAMP MF' ,T=2.2,F=rampmfff22/  
&RAMP ID=' RAMP MF' ,T=2.3,F=rampmfff23/  
&RAMP ID=' RAMP MF' ,T=2.4,F=rampmfff24/  
&RAMP ID=' RAMP MF' ,T=2.5,F=rampmfff25/  
&RAMP ID=' RAMP MF' ,T=2.6,F=rampmfff26/  
&RAMP ID=' RAMP MF' ,T=2.7,F=rampmfff27/  
&RAMP ID=' RAMP MF' ,T=2.8,F=rampmfff28/  
&RAMP ID=' RAMP MF' ,T=2.9,F=rampmfff29/  
&RAMP ID=' RAMP MF' ,T=3.0,F=rampmfff30/  
&RAMP ID=' RAMP MF' ,T=3.1,F=rampmfff31/  
&RAMP ID=' RAMP MF' ,T=3.2,F=rampmfff32/  
&RAMP ID=' RAMP MF' ,T=3.3,F=rampmfff33/  
&RAMP ID=' RAMP MF' ,T=3.4,F=rampmfff34/  
&RAMP ID=' RAMP MF' ,T=3.5,F=rampmfff35/  
&RAMP ID=' RAMP MF' ,T=3.6,F=rampmfff36/  
&RAMP ID=' RAMP MF' ,T=3.7,F=rampmfff37/  
&RAMP ID=' RAMP MF' ,T=3.8,F=rampmfff38/  
&RAMP ID=' RAMP MF' ,T=3.9,F=rampmfff39/  
&RAMP ID=' RAMP MF' ,T=4.0,F=rampmfff40/  
&RAMP ID=' RAMP MF' ,T=4.1,F=rampmfff41/  
&RAMP ID=' RAMP MF' ,T=4.2,F=rampmfff42/  
&RAMP ID=' RAMP MF' ,T=4.3,F=rampmfff43/  
&RAMP ID=' RAMP MF' ,T=4.4,F=rampmfff44/  
&RAMP ID=' RAMP MF' ,T=4.5,F=rampmfff45/  
&RAMP ID=' RAMP MF' ,T=4.6,F=rampmfff46/  
&RAMP ID=' RAMP MF' ,T=4.7,F=rampmfff47/  
&RAMP ID=' RAMP MF' ,T=4.8,F=rampmfff48/  
&RAMP ID=' RAMP MF' ,T=4.9,F=rampmfff49/  
&RAMP ID=' RAMP MF' ,T=5.0,F=rampmfff50/  
&RAMP ID=' RAMP MF' ,T=5.1,F=rampmfff51/  
&RAMP ID=' RAMP MF' ,T=5.2,F=rampmfff52/  
&RAMP ID=' RAMP MF' ,T=5.3,F=rampmfff53/  
&RAMP ID=' RAMP MF' ,T=5.4,F=rampmfff54/  
&RAMP ID=' RAMP MF' ,T=5.5,F=rampmfff55/  
&RAMP ID=' RAMP MF' ,T=5.6,F=rampmfff56/  
&RAMP ID=' RAMP MF' ,T=5.7,F=rampmfff57/  
&RAMP ID=' RAMP MF' ,T=5.8,F=rampmfff58/  
&RAMP ID=' RAMP MF' ,T=5.9,F=rampmfff59/  
&RAMP ID=' RAMP MF' ,T=6.0,F=rampmfff60/  
&RAMP ID=' RAMP MF' ,T=6.1,F=rampmfff61/  
&RAMP ID=' RAMP MF' ,T=6.2,F=rampmfff62/  
&RAMP ID=' RAMP MF' ,T=6.3,F=rampmfff63/  
&RAMP ID=' RAMP MF' ,T=6.4,F=rampmfff64/  
&RAMP ID=' RAMP MF' ,T=6.5,F=rampmfff65/  
&RAMP ID=' RAMP MF' ,T=6.6,F=rampmfff66/  
&RAMP ID=' RAMP MF' ,T=6.7,F=rampmfff67/  
&RAMP ID=' RAMP MF' ,T=6.8,F=rampmfff68/  
&RAMP ID=' RAMP MF' ,T=6.9,F=rampmfff69/  
&RAMP ID=' RAMP MF' ,T=7.0,F=rampmfff70/  
&RAMP ID=' RAMP MF' ,T=7.1,F=rampmfff71/  
&RAMP ID=' RAMP MF' ,T=7.2,F=rampmfff72/  
&RAMP ID=' RAMP MF' ,T=7.3,F=rampmfff73/  
&RAMP ID=' RAMP MF' ,T=7.4,F=rampmfff74/  
&RAMP ID=' RAMP MF' ,T=7.5,F=rampmfff75/  
&RAMP ID=' RAMP MF' ,T=7.6,F=rampmfff76/  
&RAMP ID=' RAMP MF' ,T=7.7,F=rampmfff77/  
&RAMP ID=' RAMP MF' ,T=7.8,F=rampmfff78/  
&RAMP ID=' RAMP MF' ,T=7.9,F=rampmfff79/  
&RAMP ID=' RAMP MF' ,T=8.0,F=rampmfff80/  
&RAMP ID=' RAMP MF' ,T=8.1,F=rampmfff81/
```

---

## FDS Input File Templates

```
&RAMP ID=' RAMP MF', T=8.2, F=rampmfff82/  
&RAMP ID=' RAMP MF', T=8.3, F=rampmfff83/  
&RAMP ID=' RAMP MF', T=8.4, F=rampmfff84/  
&RAMP ID=' RAMP MF', T=8.5, F=rampmfff85/  
&RAMP ID=' RAMP MF', T=8.6, F=rampmfff86/  
&RAMP ID=' RAMP MF', T=8.7, F=rampmfff87/  
&RAMP ID=' RAMP MF', T=8.8, F=rampmfff88/  
&RAMP ID=' RAMP MF', T=8.9, F=rampmfff89/  
&RAMP ID=' RAMP MF', T=9.0, F=rampmfff90/  
&RAMP ID=' RAMP MF', T=9.1, F=rampmfff91/  
&RAMP ID=' RAMP MF', T=9.2, F=rampmfff92/  
&RAMP ID=' RAMP MF', T=9.3, F=rampmfff93/  
&RAMP ID=' RAMP MF', T=9.4, F=rampmfff94/  
&RAMP ID=' RAMP MF', T=9.5, F=rampmfff95/  
&RAMP ID=' RAMP MF', T=9.6, F=rampmfff96/  
&RAMP ID=' RAMP MF', T=9.7, F=rampmfff97/  
&RAMP ID=' RAMP MF', T=9.8, F=rampmfff98/  
&RAMP ID=' RAMP MF', T=9.9, F=rampmfff99/  
&RAMP ID=' RAMP MF', T=10.0, F=rampmfff100/  
&RAMP ID=' RAMP MF', T=10.1, F=rampmfff101/  
&RAMP ID=' RAMP MF', T=10.2, F=rampmfff102/  
&RAMP ID=' RAMP MF', T=10.3, F=rampmfff103/  
&RAMP ID=' RAMP MF', T=10.4, F=rampmfff104/  
&RAMP ID=' RAMP MF', T=10.5, F=rampmfff105/  
&RAMP ID=' RAMP MF', T=10.6, F=rampmfff106/  
&RAMP ID=' RAMP MF', T=10.7, F=rampmfff107/  
&RAMP ID=' RAMP MF', T=10.8, F=rampmfff108/  
&RAMP ID=' RAMP MF', T=10.9, F=rampmfff109/  
&RAMP ID=' RAMP MF', T=11.0, F=rampmfff110/  
&RAMP ID=' RAMP MF', T=11.1, F=rampmfff111/  
&RAMP ID=' RAMP MF', T=11.2, F=rampmfff112/  
&RAMP ID=' RAMP MF', T=11.3, F=rampmfff113/  
&RAMP ID=' RAMP MF', T=11.4, F=rampmfff114/  
&RAMP ID=' RAMP MF', T=11.5, F=rampmfff115/  
&RAMP ID=' RAMP MF', T=11.6, F=rampmfff116/  
&RAMP ID=' RAMP MF', T=11.7, F=rampmfff117/  
&RAMP ID=' RAMP MF', T=11.8, F=rampmfff118/  
&RAMP ID=' RAMP MF', T=11.9, F=rampmfff119/  
&RAMP ID=' RAMP MF', T=12.0, F=rampmfff120/  
&RAMP ID=' RAMP MF', T=12.1, F=rampmfff121/  
&RAMP ID=' RAMP MF', T=12.2, F=rampmfff122/  
&RAMP ID=' RAMP MF', T=12.3, F=rampmfff123/  
&RAMP ID=' RAMP MF', T=12.4, F=rampmfff124/  
&RAMP ID=' RAMP MF', T=12.5, F=rampmfff125/  
&RAMP ID=' RAMP MF', T=12.6, F=rampmfff126/  
&RAMP ID=' RAMP MF', T=12.7, F=rampmfff127/  
&RAMP ID=' RAMP MF', T=12.8, F=rampmfff128/  
&RAMP ID=' RAMP MF', T=12.9, F=rampmfff129/  
&RAMP ID=' RAMP MF', T=13.0, F=rampmfff130/  
&RAMP ID=' RAMP MF', T=13.1, F=rampmfff131/  
&RAMP ID=' RAMP MF', T=13.2, F=rampmfff132/  
&RAMP ID=' RAMP MF', T=13.3, F=rampmfff133/  
&RAMP ID=' RAMP MF', T=13.4, F=rampmfff134/  
&RAMP ID=' RAMP MF', T=13.5, F=rampmfff135/  
&RAMP ID=' RAMP MF', T=13.6, F=rampmfff136/  
&RAMP ID=' RAMP MF', T=13.7, F=rampmfff137/  
&RAMP ID=' RAMP MF', T=13.8, F=rampmfff138/  
&RAMP ID=' RAMP MF', T=13.9, F=rampmfff139/  
&RAMP ID=' RAMP MF', T=14.0, F=rampmfff140/  
&RAMP ID=' RAMP MF', T=14.1, F=rampmfff141/  
&RAMP ID=' RAMP MF', T=14.2, F=rampmfff142/  
&RAMP ID=' RAMP MF', T=14.3, F=rampmfff143/  
&RAMP ID=' RAMP MF', T=14.4, F=rampmfff144/  
&RAMP ID=' RAMP MF', T=14.5, F=rampmfff145/
```

```

&RAMP ID=' RAMP MF', T=14.6, F=rampmff146/
&RAMP ID=' RAMP MF', T=14.7, F=rampmff147/
&RAMP ID=' RAMP MF', T=14.8, F=rampmff148/
&RAMP ID=' RAMP MF', T=14.9, F=rampmff149/
&RAMP ID=' RAMP MF', T=15.0, F=rampmff150/
&RAMP ID=' RAMP MF', T=15.1, F=rampmff151/
&RAMP ID=' RAMP MF', T=15.2, F=rampmff152/
&RAMP ID=' RAMP MF', T=15.3, F=rampmff153/
&RAMP ID=' RAMP MF', T=15.4, F=rampmff154/
&RAMP ID=' RAMP MF', T=15.5, F=rampmff155/
&RAMP ID=' RAMP MF', T=15.6, F=rampmff156/
&RAMP ID=' RAMP MF', T=15.7, F=rampmff157/
&RAMP ID=' RAMP MF', T=15.8, F=rampmff158/
&RAMP ID=' RAMP MF', T=15.9, F=rampmff159/
&RAMP ID=' RAMP MF', T=16.0, F=rampmff160/
&RAMP ID=' RAMP MF', T=16.1, F=rampmff161/
&RAMP ID=' RAMP MF', T=16.2, F=rampmff162/
&RAMP ID=' RAMP MF', T=16.3, F=rampmff163/
&RAMP ID=' RAMP MF', T=16.4, F=rampmff164/
&RAMP ID=' RAMP MF', T=16.5, F=rampmff165/
&RAMP ID=' RAMP MF', T=16.6, F=rampmff166/
&RAMP ID=' RAMP MF', T=16.7, F=rampmff167/
&RAMP ID=' RAMP MF', T=16.8, F=rampmff168/
&RAMP ID=' RAMP MF', T=16.9, F=rampmff169/
&RAMP ID=' RAMP MF', T=17.0, F=rampmff170/
&RAMP ID=' RAMP MF', T=17.1, F=rampmff171/
&RAMP ID=' RAMP MF', T=17.2, F=rampmff172/
&RAMP ID=' RAMP MF', T=17.3, F=rampmff173/
&RAMP ID=' RAMP MF', T=17.4, F=rampmff174/
&RAMP ID=' RAMP MF', T=17.5, F=rampmff175/
&RAMP ID=' RAMP MF', T=17.6, F=rampmff176/
&RAMP ID=' RAMP MF', T=17.7, F=rampmff177/
&RAMP ID=' RAMP MF', T=17.8, F=rampmff178/
&RAMP ID=' RAMP MF', T=17.9, F=rampmff179/
&RAMP ID=' RAMP MF', T=18.0, F=rampmff180/
&RAMP ID=' RAMP MF', T=18.1, F=rampmff181/
&RAMP ID=' RAMP MF', T=18.2, F=rampmff182/
&RAMP ID=' RAMP MF', T=18.3, F=rampmff183/
&RAMP ID=' RAMP MF', T=18.4, F=rampmff184/
&RAMP ID=' RAMP MF', T=18.5, F=rampmff185/
&RAMP ID=' RAMP MF', T=18.6, F=rampmff186/
&RAMP ID=' RAMP MF', T=18.7, F=rampmff187/
&RAMP ID=' RAMP MF', T=18.8, F=rampmff188/
&RAMP ID=' RAMP MF', T=18.9, F=rampmff189/
&RAMP ID=' RAMP MF', T=19.0, F=rampmff190/
&RAMP ID=' RAMP MF', T=19.1, F=rampmff191/
&RAMP ID=' RAMP MF', T=19.2, F=rampmff192/
&RAMP ID=' RAMP MF', T=19.3, F=rampmff193/
&RAMP ID=' RAMP MF', T=19.4, F=rampmff194/
&RAMP ID=' RAMP MF', T=19.5, F=rampmff195/
&RAMP ID=' RAMP MF', T=19.6, F=rampmff196/
&RAMP ID=' RAMP MF', T=19.7, F=rampmff197/
&RAMP ID=' RAMP MF', T=19.8, F=rampmff198/
&RAMP ID=' RAMP MF', T=19.9, F=rampmff199/
&RAMP ID=' RAMP MF', T=20.0, F=rampmff200/
&RAMP ID=' RAMP MF', T=20.1, F=0.0000/

```

! Gas phase specific heats. FDS defaults for N2, O2, H2O, and CO2 replaced to extend values to higher temperatures than present in FDS

```

&RAMP ID=' AL2O3 C', T=-73, F=0.761/ NASA TP-2002-211556
&RAMP ID=' AL2O3 C', T=127, F=0.921/
&RAMP ID=' AL2O3 C', T=327, F=0.999/
&RAMP ID=' AL2O3 C', T=527, F=1.038/

```

---

*FDS Input File Templates*

```
&RAMP ID='AL2O3 C', T=727, F=1.058/
&RAMP ID='AL2O3 C', T=1727, F=1.090/
&RAMP ID='AL2O3 C', T=2727, F=1.096/
&RAMP ID='AL2O3 C', T=3727, F=1.098/
&RAMP ID='AL2O3 C', T=4727, F=1.099/
&RAMP ID='AL2O3 C', T=5727, F=1.100/

&RAMP ID='AL C', T=-73, F=0.820/ NASA TP-2002-211556
&RAMP ID='AL C', T=127, F=0.783/
&RAMP ID='AL C', T=327, F=0.776/
&RAMP ID='AL C', T=527, F=0.773/
&RAMP ID='AL C', T=727, F=0.772/
&RAMP ID='AL C', T=1727, F=0.771/
&RAMP ID='AL C', T=2727, F=0.771/
&RAMP ID='AL C', T=3727, F=0.775/
&RAMP ID='AL C', T=4727, F=0.793/
&RAMP ID='AL C', T=5727, F=0.841/
&RAMP ID='AL C', T=6727, F=0.930/
&RAMP ID='AL C', T=7727, F=1.034/
&RAMP ID='AL C', T=8727, F=1.130/
&RAMP ID='AL C', T=9727, F=1.204/
&RAMP ID='AL C', T=10727, F=1.250/
&RAMP ID='AL C', T=11727, F=1.271/
&RAMP ID='AL C', T=12727, F=1.269/
&RAMP ID='AL C', T=13727, F=1.252/
&RAMP ID='AL C', T=14727, F=1.226/
&RAMP ID='AL C', T=15727, F=1.196/
&RAMP ID='AL C', T=16727, F=1.168/
&RAMP ID='AL C', T=17727, F=1.145/
&RAMP ID='AL C', T=18727, F=1.125/
&RAMP ID='AL C', T=19727, F=1.108/

&RAMP ID='CU C', T=-73, F=0.327/ NASA TP-2002-211556
&RAMP ID='CU C', T=127, F=0.327/
&RAMP ID='CU C', T=327, F=0.327/
&RAMP ID='CU C', T=527, F=0.327/
&RAMP ID='CU C', T=727, F=0.327/
&RAMP ID='CU C', T=1727, F=0.337/
&RAMP ID='CU C', T=2727, F=0.396/
&RAMP ID='CU C', T=3727, F=0.471/
&RAMP ID='CU C', T=4727, F=0.517/
&RAMP ID='CU C', T=5727, F=0.537/
&RAMP ID='CU C', T=6727, F=0.551/
&RAMP ID='CU C', T=7727, F=0.577/
&RAMP ID='CU C', T=8727, F=0.606/
&RAMP ID='CU C', T=9727, F=0.633/
&RAMP ID='CU C', T=10727, F=0.653/
&RAMP ID='CU C', T=11727, F=0.663/
&RAMP ID='CU C', T=12727, F=0.664/
&RAMP ID='CU C', T=13727, F=0.657/
&RAMP ID='CU C', T=14727, F=0.642/
&RAMP ID='CU C', T=15727, F=0.622/
&RAMP ID='CU C', T=16727, F=0.599/
&RAMP ID='CU C', T=17727, F=0.574/
&RAMP ID='CU C', T=18727, F=0.550/
&RAMP ID='CU C', T=19727, F=0.528/

&RAMP ID='N2 C', T=-73, F=1.039/ NASA TP-2002-211556
&RAMP ID='N2 C', T=127, F=1.044/
&RAMP ID='N2 C', T=327, F=1.075/
&RAMP ID='N2 C', T=527, F=1.122/
&RAMP ID='N2 C', T=727, F=1.167/
&RAMP ID='N2 C', T=1727, F=1.284/
&RAMP ID='N2 C', T=2727, F=1.322/
```

```
&RAMP ID='N2 C', T=3727, F=1.340/  
&RAMP ID='N2 C', T=4727, F=1.354/  
&RAMP ID='N2 C', T=5727, F=1.371/  
&RAMP ID='N2 C', T=6727, F=1.402/  
&RAMP ID='N2 C', T=7727, F=1.454/  
&RAMP ID='N2 C', T=8727, F=1.544/  
&RAMP ID='N2 C', T=9727, F=1.670/  
&RAMP ID='N2 C', T=10727, F=1.822/  
&RAMP ID='N2 C', T=11727, F=1.984/  
&RAMP ID='N2 C', T=12727, F=2.136/  
&RAMP ID='N2 C', T=13727, F=2.261/  
&RAMP ID='N2 C', T=14727, F=2.346/  
&RAMP ID='N2 C', T=15727, F=2.383/  
&RAMP ID='N2 C', T=16727, F=2.372/  
&RAMP ID='N2 C', T=17727, F=2.320/  
&RAMP ID='N2 C', T=18727, F=2.241/  
&RAMP ID='N2 C', T=19727, F=2.159/  
  
&RAMP ID='O2 C', T=-73, F=0.910/ NASA TP-2002-211556  
&RAMP ID='O2 C', T=127, F=0.941/  
&RAMP ID='O2 C', T=327, F=1.003/  
&RAMP ID='O2 C', T=527, F=1.055/  
&RAMP ID='O2 C', T=727, F=1.090/  
&RAMP ID='O2 C', T=1727, F=1.181/  
&RAMP ID='O2 C', T=2727, F=1.249/  
&RAMP ID='O2 C', T=3727, F=1.303/  
&RAMP ID='O2 C', T=4727, F=1.344/  
&RAMP ID='O2 C', T=5727, F=1.373/  
&RAMP ID='O2 C', T=6727, F=1.386/  
&RAMP ID='O2 C', T=7727, F=1.376/  
&RAMP ID='O2 C', T=8727, F=1.344/  
&RAMP ID='O2 C', T=9727, F=1.296/  
&RAMP ID='O2 C', T=10727, F=1.241/  
&RAMP ID='O2 C', T=11727, F=1.184/  
&RAMP ID='O2 C', T=12727, F=1.128/  
&RAMP ID='O2 C', T=13727, F=1.077/  
&RAMP ID='O2 C', T=14727, F=1.030/  
&RAMP ID='O2 C', T=15727, F=0.989/  
&RAMP ID='O2 C', T=16727, F=0.953/  
&RAMP ID='O2 C', T=17727, F=0.922/  
&RAMP ID='O2 C', T=18727, F=0.894/  
&RAMP ID='O2 C', T=19727, F=0.870/  
  
&RAMP ID='CO2 C', T=-73, F=0.735/ NASA TP-2002-211556  
&RAMP ID='CO2 C', T=127, F=0.939/  
&RAMP ID='CO2 C', T=327, F=1.075/  
&RAMP ID='CO2 C', T=527, F=1.169/  
&RAMP ID='CO2 C', T=727, F=1.234/  
&RAMP ID='CO2 C', T=1727, F=1.371/  
&RAMP ID='CO2 C', T=2727, F=1.412/  
&RAMP ID='CO2 C', T=3727, F=1.436/  
&RAMP ID='CO2 C', T=4727, F=1.466/  
&RAMP ID='CO2 C', T=5727, F=1.517/  
&RAMP ID='CO2 C', T=6727, F=1.595/  
&RAMP ID='CO2 C', T=7727, F=1.694/  
&RAMP ID='CO2 C', T=8727, F=1.797/  
&RAMP ID='CO2 C', T=9727, F=1.888/  
&RAMP ID='CO2 C', T=10727, F=1.957/  
&RAMP ID='CO2 C', T=11727, F=2.000/  
&RAMP ID='CO2 C', T=12727, F=2.019/  
&RAMP ID='CO2 C', T=13727, F=2.020/  
&RAMP ID='CO2 C', T=14727, F=2.007/  
&RAMP ID='CO2 C', T=15727, F=1.987/  
&RAMP ID='CO2 C', T=16727, F=1.965/
```

---

## FDS Input File Templates

```
&RAMP ID='CO2 C', T=17727, F=1.944/  
&RAMP ID='CO2 C', T=18727, F=1.924/  
&RAMP ID='CO2 C', T=19727, F=1.905/
```

!Smokeview Outputs. Adjust PBY and PBX for center of arc volume.

```
Alslcf1 QUANTITY='MASS FRACTION',SPEC_ID='ALUMINUM',CELL_CENTERED=.TRUE.,PBY=0.0000/  
alslcf2 QUANTITY='MASS FRACTION',SPEC_ID='ALUMINUM  
OXIDE',CELL_CENTERED=.TRUE.,PBY=0.0000/  
cuslcf1 QUANTITY='MASS FRACTION',SPEC_ID='COPPER',CELL_CENTERED=.TRUE.,PBY=0.0000/  
cuslcf2 QUANTITY='MASS FRACTION',SPEC_ID='COPPER  
OXIDE',CELL_CENTERED=.TRUE.,PBY=0.0000/  
&SLCF QUANTITY='MASS FRACTION',SPEC_ID='OXYGEN',CELL_CENTERED=.TRUE.,PBY=0.0000/  
&SLCF QUANTITY='HRRPUV',CELL_CENTERED=.TRUE.,PBY=0.0000/  
&SLCF QUANTITY='HRRPUV',CELL_CENTERED=.TRUE.,PBX=slcfpbx/  
&SLCF QUANTITY='TEMPERATURE',CELL_CENTERED=.TRUE.,PBY=0.0000/  
&SLCF QUANTITY='TEMPERATURE',CELL_CENTERED=.TRUE.,PBX=slcfpbx/  
&SLCF QUANTITY='INTEGRATED INTENSITY',CELL_CENTERED=.TRUE.,PBY=0.0000/  
&SLCF QUANTITY='INTEGRATED INTENSITY',CELL_CENTERED=.TRUE.,PBX=slcfpbx/  
&SLCF QUANTITY='VELOCITY',CELL_CENTERED=.TRUE.,PBY=0.0000/  
&SLCF QUANTITY='U-VELOCITY',CELL_CENTERED=.TRUE.,PBY=0.0000/  
&SLCF QUANTITY='VELOCITY',CELL_CENTERED=.TRUE.,PBX=slcfpbx/  
&SLCF QUANTITY='V-VELOCITY',CELL_CENTERED=.TRUE.,PBX=slcfpbx/  
&SLCF QUANTITY='PRESSURE',CELL_CENTERED=.TRUE.,PBY=0.0000/  
  
&BNDF QUANTITY='WALL TEMPERATURE',CELL_CENTERED=.TRUE./  
&BNDF QUANTITY='GAUGE HEAT FLUX',CELL_CENTERED=.TRUE./  
&BNDF QUANTITY='WALL THICKNESS',CELL_CENTERED=.TRUE./  
&BNDF QUANTITY='VELOCITY ERROR',CELL_CENTERED=.TRUE./
```

!Example DEVC for ZOI runs. Have planes of devices at a range of distances that look at each face of the enclosure  
!Plane should be large enough to see any permanent venting, plus any area heated by or damaged by the arc, plus any C-30uoquancy impacts  
!Here the DEVC ID my means this is on the (m)inus (y) face at the given x,y,z location  
!The orientation is the unit vector given by Arc Center - DEVC XYZ. Pointing the DEVC at the arc centroid will approximate the worst case view factor  
!for the radiative component.  
!These can easily be generated with Excel using CONCATENATE()

```
&DEVC XB=-0.0381,-2.4003,-0.1905,-  
0.1905,0.0381,0.0381,POINTS=31,ORIENTATION=1,0,0,ID='BL y:-0.1905  
z:0.0381',QUANTITY='GAUGE HEAT FLUX GAS',STATISTICS_START=0,TEMPORAL_STATISTIC='TIME  
INTEGRAL'/  
&DEVC XB=-0.0381,-2.4003,-0.1905,-  
0.1905,0.1143,0.1143,POINTS=31,ORIENTATION=1,0,0,ID='BL y:-0.1905  
z:0.1143',QUANTITY='GAUGE HEAT FLUX GAS',STATISTICS_START=0,TEMPORAL_STATISTIC='TIME  
INTEGRAL'/  
&DEVC XB=-0.0381,-2.4003,-0.1905,-  
0.1905,0.1905,0.1905,POINTS=31,ORIENTATION=1,0,0,ID='BL y:-0.1905  
z:0.1905',QUANTITY='GAUGE HEAT FLUX GAS',STATISTICS_START=0,TEMPORAL_STATISTIC='TIME  
INTEGRAL'/  
&DEVC XB=-0.0381,-2.4003,-0.1905,-  
0.1905,0.2667,0.2667,POINTS=31,ORIENTATION=1,0,0,ID='BL y:-0.1905  
z:0.2667',QUANTITY='GAUGE HEAT FLUX GAS',STATISTICS_START=0,TEMPORAL_STATISTIC='TIME  
INTEGRAL'/  
&DEVC XB=-0.0381,-2.4003,-0.1905,-  
0.1905,0.3429,0.3429,POINTS=31,ORIENTATION=1,0,0,ID='BL y:-0.1905  
z:0.3429',QUANTITY='GAUGE HEAT FLUX GAS',STATISTICS_START=0,TEMPORAL_STATISTIC='TIME  
INTEGRAL'/  
&DEVC XB=-0.0381,-2.4003,-0.1905,-  
0.1905,0.4191,0.4191,POINTS=31,ORIENTATION=1,0,0,ID='BL y:-0.1905  
z:0.4191',QUANTITY='GAUGE HEAT FLUX GAS',STATISTICS_START=0,TEMPORAL_STATISTIC='TIME  
INTEGRAL'/
```

```

&DEVC XB=-0.0381,-2.4003,-0.1143,-
0.1143,0.0381,0.0381,POINTS=31,ORIENTATION=1,0,0,ID='BL y:-0.1143
z:0.0381',QUANTITY='GAUGE HEAT FLUX GAS',STATISTICS_START=0,TEMPORAL_STATISTIC='TIME
INTEGRAL' /
&DEVC XB=-0.0381,-2.4003,-0.1143,-
0.1143,0.1143,0.1143,POINTS=31,ORIENTATION=1,0,0,ID='BL y:-0.1143
z:0.1143',QUANTITY='GAUGE HEAT FLUX GAS',STATISTICS_START=0,TEMPORAL_STATISTIC='TIME
INTEGRAL' /
&DEVC XB=-0.0381,-2.4003,-0.1143,-
0.1143,0.1905,0.1905,POINTS=31,ORIENTATION=1,0,0,ID='BL y:-0.1143
z:0.1905',QUANTITY='GAUGE HEAT FLUX GAS',STATISTICS_START=0,TEMPORAL_STATISTIC='TIME
INTEGRAL' /
&DEVC XB=-0.0381,-2.4003,-0.1143,-
0.1143,0.2667,0.2667,POINTS=31,ORIENTATION=1,0,0,ID='BL y:-0.1143
z:0.2667',QUANTITY='GAUGE HEAT FLUX GAS',STATISTICS_START=0,TEMPORAL_STATISTIC='TIME
INTEGRAL' /
&DEVC XB=-0.0381,-2.4003,-0.1143,-
0.1143,0.3429,0.3429,POINTS=31,ORIENTATION=1,0,0,ID='BL y:-0.1143
z:0.3429',QUANTITY='GAUGE HEAT FLUX GAS',STATISTICS_START=0,TEMPORAL_STATISTIC='TIME
INTEGRAL' /
&DEVC XB=-0.0381,-2.4003,-0.1143,-
0.1143,0.4191,0.4191,POINTS=31,ORIENTATION=1,0,0,ID='BL y:-0.1143
z:0.4191',QUANTITY='GAUGE HEAT FLUX GAS',STATISTICS_START=0,TEMPORAL_STATISTIC='TIME
INTEGRAL' /
&DEVC XB=-0.0381,-2.4003,-0.0381,-
0.0381,0.0381,0.0381,POINTS=31,ORIENTATION=1,0,0,ID='BL y:-0.0381
z:0.0381',QUANTITY='GAUGE HEAT FLUX GAS',STATISTICS_START=0,TEMPORAL_STATISTIC='TIME
INTEGRAL' /
&DEVC XB=-0.0381,-2.4003,-0.0381,-
0.0381,0.1143,0.1143,POINTS=31,ORIENTATION=1,0,0,ID='BL y:-0.0381
z:0.1143',QUANTITY='GAUGE HEAT FLUX GAS',STATISTICS_START=0,TEMPORAL_STATISTIC='TIME
INTEGRAL' /
&DEVC XB=-0.0381,-2.4003,-0.0381,-
0.0381,0.1905,0.1905,POINTS=31,ORIENTATION=1,0,0,ID='BL y:-0.0381
z:0.1905',QUANTITY='GAUGE HEAT FLUX GAS',STATISTICS_START=0,TEMPORAL_STATISTIC='TIME
INTEGRAL' /
&DEVC XB=-0.0381,-2.4003,-0.0381,-
0.0381,0.2667,0.2667,POINTS=31,ORIENTATION=1,0,0,ID='BL y:-0.0381
z:0.2667',QUANTITY='GAUGE HEAT FLUX GAS',STATISTICS_START=0,TEMPORAL_STATISTIC='TIME
INTEGRAL' /
&DEVC XB=-0.0381,-2.4003,-0.0381,-
0.0381,0.3429,0.3429,POINTS=31,ORIENTATION=1,0,0,ID='BL y:-0.0381
z:0.3429',QUANTITY='GAUGE HEAT FLUX GAS',STATISTICS_START=0,TEMPORAL_STATISTIC='TIME
INTEGRAL' /
&DEVC XB=-0.0381,-2.4003,-0.0381,-
0.0381,0.4191,0.4191,POINTS=31,ORIENTATION=1,0,0,ID='BL y:-0.0381
z:0.4191',QUANTITY='GAUGE HEAT FLUX GAS',STATISTICS_START=0,TEMPORAL_STATISTIC='TIME
INTEGRAL' /
&DEVC XB=-0.0381,-
2.4003,0.0381,0.0381,0.0381,0.0381,POINTS=31,ORIENTATION=1,0,0,ID='BL y:0.0381
z:0.0381',QUANTITY='GAUGE HEAT FLUX GAS',STATISTICS_START=0,TEMPORAL_STATISTIC='TIME
INTEGRAL' /
&DEVC XB=-0.0381,-
2.4003,0.0381,0.0381,0.1143,0.1143,POINTS=31,ORIENTATION=1,0,0,ID='BL y:0.0381
z:0.1143',QUANTITY='GAUGE HEAT FLUX GAS',STATISTICS_START=0,TEMPORAL_STATISTIC='TIME
INTEGRAL' /
&DEVC XB=-0.0381,-
2.4003,0.0381,0.0381,0.1905,0.1905,POINTS=31,ORIENTATION=1,0,0,ID='BL y:0.0381
z:0.1905',QUANTITY='GAUGE HEAT FLUX GAS',STATISTICS_START=0,TEMPORAL_STATISTIC='TIME
INTEGRAL' /
&DEVC XB=-0.0381,-
2.4003,0.0381,0.0381,0.2667,0.2667,POINTS=31,ORIENTATION=1,0,0,ID='BL y:0.0381
z:0.2667',QUANTITY='GAUGE HEAT FLUX GAS',STATISTICS_START=0,TEMPORAL_STATISTIC='TIME
INTEGRAL' /

```

---

*FDS Input File Templates*

```
&DEVC XB=-0.0381,-
2.4003,0.0381,0.0381,0.3429,0.3429,POINTS=31,ORIENTATION=1,0,0,ID='BL y:0.0381
z:0.3429',QUANTITY='GAUGE HEAT FLUX GAS',STATISTICS_START=0,TEMPORAL_STATISTIC='TIME
INTEGRAL'/
&DEVC XB=-0.0381,-
2.4003,0.0381,0.0381,0.4191,0.4191,POINTS=31,ORIENTATION=1,0,0,ID='BL y:0.0381
z:0.4191',QUANTITY='GAUGE HEAT FLUX GAS',STATISTICS_START=0,TEMPORAL_STATISTIC='TIME
INTEGRAL'/
&DEVC XB=-0.0381,-
2.4003,0.1143,0.1143,0.0381,0.0381,POINTS=31,ORIENTATION=1,0,0,ID='BL y:0.1143
z:0.0381',QUANTITY='GAUGE HEAT FLUX GAS',STATISTICS_START=0,TEMPORAL_STATISTIC='TIME
INTEGRAL'/
&DEVC XB=-0.0381,-
2.4003,0.1143,0.1143,0.1143,0.1143,POINTS=31,ORIENTATION=1,0,0,ID='BL y:0.1143
z:0.1143',QUANTITY='GAUGE HEAT FLUX GAS',STATISTICS_START=0,TEMPORAL_STATISTIC='TIME
INTEGRAL'/
&DEVC XB=-0.0381,-
2.4003,0.1143,0.1143,0.1905,0.1905,POINTS=31,ORIENTATION=1,0,0,ID='BL y:0.1143
z:0.1905',QUANTITY='GAUGE HEAT FLUX GAS',STATISTICS_START=0,TEMPORAL_STATISTIC='TIME
INTEGRAL'/
&DEVC XB=-0.0381,-
2.4003,0.1143,0.1143,0.2667,0.2667,POINTS=31,ORIENTATION=1,0,0,ID='BL y:0.1143
z:0.2667',QUANTITY='GAUGE HEAT FLUX GAS',STATISTICS_START=0,TEMPORAL_STATISTIC='TIME
INTEGRAL'/
&DEVC XB=-0.0381,-
2.4003,0.1143,0.1143,0.3429,0.3429,POINTS=31,ORIENTATION=1,0,0,ID='BL y:0.1143
z:0.3429',QUANTITY='GAUGE HEAT FLUX GAS',STATISTICS_START=0,TEMPORAL_STATISTIC='TIME
INTEGRAL'/
&DEVC XB=-0.0381,-
2.4003,0.1143,0.1143,0.4191,0.4191,POINTS=31,ORIENTATION=1,0,0,ID='BL y:0.1143
z:0.4191',QUANTITY='GAUGE HEAT FLUX GAS',STATISTICS_START=0,TEMPORAL_STATISTIC='TIME
INTEGRAL'/
&DEVC XB=-0.0381,-
2.4003,0.1905,0.1905,0.0381,0.0381,POINTS=31,ORIENTATION=1,0,0,ID='BL y:0.1905
z:0.0381',QUANTITY='GAUGE HEAT FLUX GAS',STATISTICS_START=0,TEMPORAL_STATISTIC='TIME
INTEGRAL'/
&DEVC XB=-0.0381,-
2.4003,0.1905,0.1905,0.1143,0.1143,POINTS=31,ORIENTATION=1,0,0,ID='BL y:0.1905
z:0.1143',QUANTITY='GAUGE HEAT FLUX GAS',STATISTICS_START=0,TEMPORAL_STATISTIC='TIME
INTEGRAL'/
&DEVC XB=-0.0381,-
2.4003,0.1905,0.1905,0.1905,0.1905,POINTS=31,ORIENTATION=1,0,0,ID='BL y:0.1905
z:0.1905',QUANTITY='GAUGE HEAT FLUX GAS',STATISTICS_START=0,TEMPORAL_STATISTIC='TIME
INTEGRAL'/
&DEVC XB=-0.0381,-
2.4003,0.1905,0.1905,0.2667,0.2667,POINTS=31,ORIENTATION=1,0,0,ID='BL y:0.1905
z:0.2667',QUANTITY='GAUGE HEAT FLUX GAS',STATISTICS_START=0,TEMPORAL_STATISTIC='TIME
INTEGRAL'/
&DEVC XB=-0.0381,-
2.4003,0.1905,0.1905,0.3429,0.3429,POINTS=31,ORIENTATION=1,0,0,ID='BL y:0.1905
z:0.3429',QUANTITY='GAUGE HEAT FLUX GAS',STATISTICS_START=0,TEMPORAL_STATISTIC='TIME
INTEGRAL'/
&DEVC XB=-0.0381,-
2.4003,0.1905,0.1905,0.4191,0.4191,POINTS=31,ORIENTATION=1,0,0,ID='BL y:0.1905
z:0.4191',QUANTITY='GAUGE HEAT FLUX GAS',STATISTICS_START=0,TEMPORAL_STATISTIC='TIME
INTEGRAL'/

&DEVC XB=1.1811,1.1811,-2.4765,-
0.4953,0.3429,0.3429,POINTS=26,ORIENTATION=0,1,0,ID='SL x:1.1811
z:0.3429',QUANTITY='GAUGE HEAT FLUX GAS',STATISTICS_START=0,TEMPORAL_STATISTIC='TIME
INTEGRAL'/
```

```

&DEVC XB=1.1811,1.1811,-2.4765,-
0.4953,0.4191,0.4191,POINTS=26,ORIENTATION=0,1,0,ID='SL x:1.1811
z:0.4191',QUANTITY='GAUGE HEAT FLUX GAS',STATISTICS_START=0,TEMPORAL_STATISTIC='TIME
INTEGRAL' /
&DEVC XB=1.1811,1.1811,-2.4765,-
0.4953,0.4953,0.4953,POINTS=26,ORIENTATION=0,1,0,ID='SL x:1.1811
z:0.4953',QUANTITY='GAUGE HEAT FLUX GAS',STATISTICS_START=0,TEMPORAL_STATISTIC='TIME
INTEGRAL' /
&DEVC XB=1.1811,1.1811,-2.4765,-
0.4953,0.5715,0.5715,POINTS=26,ORIENTATION=0,1,0,ID='SL x:1.1811
z:0.5715',QUANTITY='GAUGE HEAT FLUX GAS',STATISTICS_START=0,TEMPORAL_STATISTIC='TIME
INTEGRAL' /
&DEVC XB=1.1811,1.1811,-2.4765,-
0.4953,0.6477,0.6477,POINTS=26,ORIENTATION=0,1,0,ID='SL x:1.1811
z:0.6477',QUANTITY='GAUGE HEAT FLUX GAS',STATISTICS_START=0,TEMPORAL_STATISTIC='TIME
INTEGRAL' /
&DEVC XB=1.1811,1.1811,-2.4765,-
0.4953,0.7239,0.7239,POINTS=26,ORIENTATION=0,1,0,ID='SL x:1.1811
z:0.7239',QUANTITY='GAUGE HEAT FLUX GAS',STATISTICS_START=0,TEMPORAL_STATISTIC='TIME
INTEGRAL' /
&DEVC XB=1.2573,1.2573,-2.4765,-
0.4953,0.3429,0.3429,POINTS=26,ORIENTATION=0,1,0,ID='SL x:1.2573
z:0.3429',QUANTITY='GAUGE HEAT FLUX GAS',STATISTICS_START=0,TEMPORAL_STATISTIC='TIME
INTEGRAL' /
&DEVC XB=1.2573,1.2573,-2.4765,-
0.4953,0.4191,0.4191,POINTS=26,ORIENTATION=0,1,0,ID='SL x:1.2573
z:0.4191',QUANTITY='GAUGE HEAT FLUX GAS',STATISTICS_START=0,TEMPORAL_STATISTIC='TIME
INTEGRAL' /
&DEVC XB=1.2573,1.2573,-2.4765,-
0.4953,0.4953,0.4953,POINTS=26,ORIENTATION=0,1,0,ID='SL x:1.2573
z:0.4953',QUANTITY='GAUGE HEAT FLUX GAS',STATISTICS_START=0,TEMPORAL_STATISTIC='TIME
INTEGRAL' /
&DEVC XB=1.2573,1.2573,-2.4765,-
0.4953,0.5715,0.5715,POINTS=26,ORIENTATION=0,1,0,ID='SL x:1.2573
z:0.5715',QUANTITY='GAUGE HEAT FLUX GAS',STATISTICS_START=0,TEMPORAL_STATISTIC='TIME
INTEGRAL' /
&DEVC XB=1.2573,1.2573,-2.4765,-
0.4953,0.6477,0.6477,POINTS=26,ORIENTATION=0,1,0,ID='SL x:1.2573
z:0.6477',QUANTITY='GAUGE HEAT FLUX GAS',STATISTICS_START=0,TEMPORAL_STATISTIC='TIME
INTEGRAL' /
&DEVC XB=1.2573,1.2573,-2.4765,-
0.4953,0.7239,0.7239,POINTS=26,ORIENTATION=0,1,0,ID='SL x:1.2573
z:0.7239',QUANTITY='GAUGE HEAT FLUX GAS',STATISTICS_START=0,TEMPORAL_STATISTIC='TIME
INTEGRAL' /
&DEVC XB=1.3335,1.3335,-2.4765,-
0.4953,0.3429,0.3429,POINTS=26,ORIENTATION=0,1,0,ID='SL x:1.3335
z:0.3429',QUANTITY='GAUGE HEAT FLUX GAS',STATISTICS_START=0,TEMPORAL_STATISTIC='TIME
INTEGRAL' /
&DEVC XB=1.3335,1.3335,-2.4765,-
0.4953,0.4191,0.4191,POINTS=26,ORIENTATION=0,1,0,ID='SL x:1.3335
z:0.4191',QUANTITY='GAUGE HEAT FLUX GAS',STATISTICS_START=0,TEMPORAL_STATISTIC='TIME
INTEGRAL' /
&DEVC XB=1.3335,1.3335,-2.4765,-
0.4953,0.4953,0.4953,POINTS=26,ORIENTATION=0,1,0,ID='SL x:1.3335
z:0.4953',QUANTITY='GAUGE HEAT FLUX GAS',STATISTICS_START=0,TEMPORAL_STATISTIC='TIME
INTEGRAL' /
&DEVC XB=1.3335,1.3335,-2.4765,-
0.4953,0.5715,0.5715,POINTS=26,ORIENTATION=0,1,0,ID='SL x:1.3335
z:0.5715',QUANTITY='GAUGE HEAT FLUX GAS',STATISTICS_START=0,TEMPORAL_STATISTIC='TIME
INTEGRAL' /
&DEVC XB=1.3335,1.3335,-2.4765,-
0.4953,0.6477,0.6477,POINTS=26,ORIENTATION=0,1,0,ID='SL x:1.3335
z:0.6477',QUANTITY='GAUGE HEAT FLUX GAS',STATISTICS_START=0,TEMPORAL_STATISTIC='TIME
INTEGRAL' /

```

---

*FDS Input File Templates*

```
&DEVC XB=1.3335,1.3335,-2.4765,-  
0.4953,0.7239,0.7239,POINTS=26,ORIENTATION=0,1,0,ID='SL x:1.3335  
z:0.7239',QUANTITY='GAUGE HEAT FLUX GAS',STATISTICS_START=0,TEMPORAL_STATISTIC='TIME  
INTEGRAL'/  
&DEVC XB=1.4097,1.4097,-2.4765,-  
0.4953,0.3429,0.3429,POINTS=26,ORIENTATION=0,1,0,ID='SL x:1.4097  
z:0.3429',QUANTITY='GAUGE HEAT FLUX GAS',STATISTICS_START=0,TEMPORAL_STATISTIC='TIME  
INTEGRAL'/  
&DEVC XB=1.4097,1.4097,-2.4765,-  
0.4953,0.4191,0.4191,POINTS=26,ORIENTATION=0,1,0,ID='SL x:1.4097  
z:0.4191',QUANTITY='GAUGE HEAT FLUX GAS',STATISTICS_START=0,TEMPORAL_STATISTIC='TIME  
INTEGRAL'/  
&DEVC XB=1.4097,1.4097,-2.4765,-  
0.4953,0.4953,0.4953,POINTS=26,ORIENTATION=0,1,0,ID='SL x:1.4097  
z:0.4953',QUANTITY='GAUGE HEAT FLUX GAS',STATISTICS_START=0,TEMPORAL_STATISTIC='TIME  
INTEGRAL'/  
&DEVC XB=1.4097,1.4097,-2.4765,-  
0.4953,0.5715,0.5715,POINTS=26,ORIENTATION=0,1,0,ID='SL x:1.4097  
z:0.5715',QUANTITY='GAUGE HEAT FLUX GAS',STATISTICS_START=0,TEMPORAL_STATISTIC='TIME  
INTEGRAL'/  
&DEVC XB=1.4097,1.4097,-2.4765,-  
0.4953,0.6477,0.6477,POINTS=26,ORIENTATION=0,1,0,ID='SL x:1.4097  
z:0.6477',QUANTITY='GAUGE HEAT FLUX GAS',STATISTICS_START=0,TEMPORAL_STATISTIC='TIME  
INTEGRAL'/  
&DEVC XB=1.4097,1.4097,-2.4765,-  
0.4953,0.7239,0.7239,POINTS=26,ORIENTATION=0,1,0,ID='SL x:1.4097  
z:0.7239',QUANTITY='GAUGE HEAT FLUX GAS',STATISTICS_START=0,TEMPORAL_STATISTIC='TIME  
INTEGRAL'/  
&DEVC XB=1.4859,1.4859,-2.4765,-  
0.4953,0.3429,0.3429,POINTS=26,ORIENTATION=0,1,0,ID='SL x:1.4859  
z:0.3429',QUANTITY='GAUGE HEAT FLUX GAS',STATISTICS_START=0,TEMPORAL_STATISTIC='TIME  
INTEGRAL'/  
&DEVC XB=1.4859,1.4859,-2.4765,-  
0.4953,0.4191,0.4191,POINTS=26,ORIENTATION=0,1,0,ID='SL x:1.4859  
z:0.4191',QUANTITY='GAUGE HEAT FLUX GAS',STATISTICS_START=0,TEMPORAL_STATISTIC='TIME  
INTEGRAL'/  
&DEVC XB=1.4859,1.4859,-2.4765,-  
0.4953,0.4953,0.4953,POINTS=26,ORIENTATION=0,1,0,ID='SL x:1.4859  
z:0.4953',QUANTITY='GAUGE HEAT FLUX GAS',STATISTICS_START=0,TEMPORAL_STATISTIC='TIME  
INTEGRAL'/  
&DEVC XB=1.4859,1.4859,-2.4765,-  
0.4953,0.5715,0.5715,POINTS=26,ORIENTATION=0,1,0,ID='SL x:1.4859  
z:0.5715',QUANTITY='GAUGE HEAT FLUX GAS',STATISTICS_START=0,TEMPORAL_STATISTIC='TIME  
INTEGRAL'/  
&DEVC XB=1.4859,1.4859,-2.4765,-  
0.4953,0.6477,0.6477,POINTS=26,ORIENTATION=0,1,0,ID='SL x:1.4859  
z:0.6477',QUANTITY='GAUGE HEAT FLUX GAS',STATISTICS_START=0,TEMPORAL_STATISTIC='TIME  
INTEGRAL'/  
&DEVC XB=1.4859,1.4859,-2.4765,-  
0.4953,0.7239,0.7239,POINTS=26,ORIENTATION=0,1,0,ID='SL x:1.4859  
z:0.7239',QUANTITY='GAUGE HEAT FLUX GAS',STATISTICS_START=0,TEMPORAL_STATISTIC='TIME  
INTEGRAL'/  
&DEVC XB=1.5621,1.5621,-2.4765,-  
0.4953,0.3429,0.3429,POINTS=26,ORIENTATION=0,1,0,ID='SL x:1.5621  
z:0.3429',QUANTITY='GAUGE HEAT FLUX GAS',STATISTICS_START=0,TEMPORAL_STATISTIC='TIME  
INTEGRAL'/  
&DEVC XB=1.5621,1.5621,-2.4765,-  
0.4953,0.4191,0.4191,POINTS=26,ORIENTATION=0,1,0,ID='SL x:1.5621  
z:0.4191',QUANTITY='GAUGE HEAT FLUX GAS',STATISTICS_START=0,TEMPORAL_STATISTIC='TIME  
INTEGRAL'/  
&DEVC XB=1.5621,1.5621,-2.4765,-  
0.4953,0.4953,0.4953,POINTS=26,ORIENTATION=0,1,0,ID='SL x:1.5621  
z:0.4953',QUANTITY='GAUGE HEAT FLUX GAS',STATISTICS_START=0,TEMPORAL_STATISTIC='TIME  
INTEGRAL'/
```

```

&DEVC XB=1.5621,1.5621,-2.4765,-
0.4953,0.5715,0.5715,POINTS=26,ORIENTATION=0,1,0,ID='SL x:1.5621
z:0.5715',QUANTITY='GAUGE HEAT FLUX GAS',STATISTICS_START=0,TEMPORAL_STATISTIC='TIME
INTEGRAL' /
&DEVC XB=1.5621,1.5621,-2.4765,-
0.4953,0.6477,0.6477,POINTS=26,ORIENTATION=0,1,0,ID='SL x:1.5621
z:0.6477',QUANTITY='GAUGE HEAT FLUX GAS',STATISTICS_START=0,TEMPORAL_STATISTIC='TIME
INTEGRAL' /
&DEVC XB=1.5621,1.5621,-2.4765,-
0.4953,0.7239,0.7239,POINTS=26,ORIENTATION=0,1,0,ID='SL x:1.5621
z:0.7239',QUANTITY='GAUGE HEAT FLUX GAS',STATISTICS_START=0,TEMPORAL_STATISTIC='TIME
INTEGRAL' /

&DEVC XB=1.1811,1.1811,0.4953,2.4765,0.3429,0.3429,POINTS=26,ORIENTATION=0,-1,0,ID='SR
x:1.1811 z:0.3429',QUANTITY='GAUGE HEAT FLUX
GAS',STATISTICS_START=0,TEMPORAL_STATISTIC='TIME INTEGRAL' /
&DEVC XB=1.1811,1.1811,0.4953,2.4765,0.4191,0.4191,POINTS=26,ORIENTATION=0,-1,0,ID='SR
x:1.1811 z:0.4191',QUANTITY='GAUGE HEAT FLUX
GAS',STATISTICS_START=0,TEMPORAL_STATISTIC='TIME INTEGRAL' /
&DEVC XB=1.1811,1.1811,0.4953,2.4765,0.4953,0.4953,POINTS=26,ORIENTATION=0,-1,0,ID='SR
x:1.1811 z:0.4953',QUANTITY='GAUGE HEAT FLUX
GAS',STATISTICS_START=0,TEMPORAL_STATISTIC='TIME INTEGRAL' /
&DEVC XB=1.1811,1.1811,0.4953,2.4765,0.5715,0.5715,POINTS=26,ORIENTATION=0,-1,0,ID='SR
x:1.1811 z:0.5715',QUANTITY='GAUGE HEAT FLUX
GAS',STATISTICS_START=0,TEMPORAL_STATISTIC='TIME INTEGRAL' /
&DEVC XB=1.1811,1.1811,0.4953,2.4765,0.6477,0.6477,POINTS=26,ORIENTATION=0,-1,0,ID='SR
x:1.1811 z:0.6477',QUANTITY='GAUGE HEAT FLUX
GAS',STATISTICS_START=0,TEMPORAL_STATISTIC='TIME INTEGRAL' /
&DEVC XB=1.1811,1.1811,0.4953,2.4765,0.7239,0.7239,POINTS=26,ORIENTATION=0,-1,0,ID='SR
x:1.1811 z:0.7239',QUANTITY='GAUGE HEAT FLUX
GAS',STATISTICS_START=0,TEMPORAL_STATISTIC='TIME INTEGRAL' /
&DEVC XB=1.2573,1.2573,0.4953,2.4765,0.3429,0.3429,POINTS=26,ORIENTATION=0,-1,0,ID='SR
x:1.2573 z:0.3429',QUANTITY='GAUGE HEAT FLUX
GAS',STATISTICS_START=0,TEMPORAL_STATISTIC='TIME INTEGRAL' /
&DEVC XB=1.2573,1.2573,0.4953,2.4765,0.4191,0.4191,POINTS=26,ORIENTATION=0,-1,0,ID='SR
x:1.2573 z:0.4191',QUANTITY='GAUGE HEAT FLUX
GAS',STATISTICS_START=0,TEMPORAL_STATISTIC='TIME INTEGRAL' /
&DEVC XB=1.2573,1.2573,0.4953,2.4765,0.4953,0.4953,POINTS=26,ORIENTATION=0,-1,0,ID='SR
x:1.2573 z:0.4953',QUANTITY='GAUGE HEAT FLUX
GAS',STATISTICS_START=0,TEMPORAL_STATISTIC='TIME INTEGRAL' /
&DEVC XB=1.2573,1.2573,0.4953,2.4765,0.5715,0.5715,POINTS=26,ORIENTATION=0,-1,0,ID='SR
x:1.2573 z:0.5715',QUANTITY='GAUGE HEAT FLUX
GAS',STATISTICS_START=0,TEMPORAL_STATISTIC='TIME INTEGRAL' /
&DEVC XB=1.2573,1.2573,0.4953,2.4765,0.6477,0.6477,POINTS=26,ORIENTATION=0,-1,0,ID='SR
x:1.2573 z:0.6477',QUANTITY='GAUGE HEAT FLUX
GAS',STATISTICS_START=0,TEMPORAL_STATISTIC='TIME INTEGRAL' /
&DEVC XB=1.2573,1.2573,0.4953,2.4765,0.7239,0.7239,POINTS=26,ORIENTATION=0,-1,0,ID='SR
x:1.2573 z:0.7239',QUANTITY='GAUGE HEAT FLUX
GAS',STATISTICS_START=0,TEMPORAL_STATISTIC='TIME INTEGRAL' /
&DEVC XB=1.3335,1.3335,0.4953,2.4765,0.3429,0.3429,POINTS=26,ORIENTATION=0,-1,0,ID='SR
x:1.3335 z:0.3429',QUANTITY='GAUGE HEAT FLUX
GAS',STATISTICS_START=0,TEMPORAL_STATISTIC='TIME INTEGRAL' /
&DEVC XB=1.3335,1.3335,0.4953,2.4765,0.4191,0.4191,POINTS=26,ORIENTATION=0,-1,0,ID='SR
x:1.3335 z:0.4191',QUANTITY='GAUGE HEAT FLUX
GAS',STATISTICS_START=0,TEMPORAL_STATISTIC='TIME INTEGRAL' /
&DEVC XB=1.3335,1.3335,0.4953,2.4765,0.4953,0.4953,POINTS=26,ORIENTATION=0,-1,0,ID='SR
x:1.3335 z:0.4953',QUANTITY='GAUGE HEAT FLUX
GAS',STATISTICS_START=0,TEMPORAL_STATISTIC='TIME INTEGRAL' /
&DEVC XB=1.3335,1.3335,0.4953,2.4765,0.5715,0.5715,POINTS=26,ORIENTATION=0,-1,0,ID='SR
x:1.3335 z:0.5715',QUANTITY='GAUGE HEAT FLUX
GAS',STATISTICS_START=0,TEMPORAL_STATISTIC='TIME INTEGRAL' /

```



```

&DEVC XB=1.1811,1.1811,-0.0381,-0.0381,2.3241,4.4577,POINTS=28,ORIENTATION=0,0,-
1,ID='TF x:1.1811 y:-0.0381',QUANTITY='GAUGE HEAT FLUX
GAS',STATISTICS_START=0,TEMPORAL_STATISTIC='TIME INTEGRAL'/
&DEVC XB=1.1811,1.1811,0.0381,0.0381,2.3241,4.4577,POINTS=28,ORIENTATION=0,0,-1,ID='TF
x:1.1811 y:0.0381',QUANTITY='GAUGE HEAT FLUX
GAS',STATISTICS_START=0,TEMPORAL_STATISTIC='TIME INTEGRAL'/
&DEVC XB=1.1811,1.1811,0.1143,0.1143,2.3241,4.4577,POINTS=28,ORIENTATION=0,0,-1,ID='TF
x:1.1811 y:0.1143',QUANTITY='GAUGE HEAT FLUX
GAS',STATISTICS_START=0,TEMPORAL_STATISTIC='TIME INTEGRAL'/
&DEVC XB=1.2573,1.2573,-0.1143,-0.1143,2.3241,4.4577,POINTS=28,ORIENTATION=0,0,-
1,ID='TF x:1.2573 y:-0.1143',QUANTITY='GAUGE HEAT FLUX
GAS',STATISTICS_START=0,TEMPORAL_STATISTIC='TIME INTEGRAL'/
&DEVC XB=1.2573,1.2573,-0.0381,-0.0381,2.3241,4.4577,POINTS=28,ORIENTATION=0,0,-
1,ID='TF x:1.2573 y:-0.0381',QUANTITY='GAUGE HEAT FLUX
GAS',STATISTICS_START=0,TEMPORAL_STATISTIC='TIME INTEGRAL'/
&DEVC XB=1.2573,1.2573,0.0381,0.0381,2.3241,4.4577,POINTS=28,ORIENTATION=0,0,-1,ID='TF
x:1.2573 y:0.0381',QUANTITY='GAUGE HEAT FLUX
GAS',STATISTICS_START=0,TEMPORAL_STATISTIC='TIME INTEGRAL'/
&DEVC XB=1.2573,1.2573,0.1143,0.1143,2.3241,4.4577,POINTS=28,ORIENTATION=0,0,-1,ID='TF
x:1.2573 y:0.1143',QUANTITY='GAUGE HEAT FLUX
GAS',STATISTICS_START=0,TEMPORAL_STATISTIC='TIME INTEGRAL'/
&DEVC XB=1.3335,1.3335,-0.1143,-0.1143,2.3241,4.4577,POINTS=28,ORIENTATION=0,0,-
1,ID='TF x:1.3335 y:-0.1143',QUANTITY='GAUGE HEAT FLUX
GAS',STATISTICS_START=0,TEMPORAL_STATISTIC='TIME INTEGRAL'/
&DEVC XB=1.3335,1.3335,-0.0381,-0.0381,2.3241,4.4577,POINTS=28,ORIENTATION=0,0,-
1,ID='TF x:1.3335 y:-0.0381',QUANTITY='GAUGE HEAT FLUX
GAS',STATISTICS_START=0,TEMPORAL_STATISTIC='TIME INTEGRAL'/
&DEVC XB=1.3335,1.3335,0.0381,0.0381,2.3241,4.4577,POINTS=28,ORIENTATION=0,0,-1,ID='TF
x:1.3335 y:0.0381',QUANTITY='GAUGE HEAT FLUX
GAS',STATISTICS_START=0,TEMPORAL_STATISTIC='TIME INTEGRAL'/
&DEVC XB=1.3335,1.3335,0.1143,0.1143,2.3241,4.4577,POINTS=28,ORIENTATION=0,0,-1,ID='TF
x:1.3335 y:0.1143',QUANTITY='GAUGE HEAT FLUX
GAS',STATISTICS_START=0,TEMPORAL_STATISTIC='TIME INTEGRAL'/
&DEVC XB=1.4097,1.4097,-0.1143,-0.1143,2.3241,4.4577,POINTS=28,ORIENTATION=0,0,-
1,ID='TF x:1.4097 y:-0.1143',QUANTITY='GAUGE HEAT FLUX
GAS',STATISTICS_START=0,TEMPORAL_STATISTIC='TIME INTEGRAL'/
&DEVC XB=1.4097,1.4097,-0.0381,-0.0381,2.3241,4.4577,POINTS=28,ORIENTATION=0,0,-
1,ID='TF x:1.4097 y:-0.0381',QUANTITY='GAUGE HEAT FLUX
GAS',STATISTICS_START=0,TEMPORAL_STATISTIC='TIME INTEGRAL'/
&DEVC XB=1.4097,1.4097,0.0381,0.0381,2.3241,4.4577,POINTS=28,ORIENTATION=0,0,-1,ID='TF
x:1.4097 y:0.0381',QUANTITY='GAUGE HEAT FLUX
GAS',STATISTICS_START=0,TEMPORAL_STATISTIC='TIME INTEGRAL'/
&DEVC XB=1.4097,1.4097,0.1143,0.1143,2.3241,4.4577,POINTS=28,ORIENTATION=0,0,-1,ID='TF
x:1.4097 y:0.1143',QUANTITY='GAUGE HEAT FLUX
GAS',STATISTICS_START=0,TEMPORAL_STATISTIC='TIME INTEGRAL'/

&DEVC XB=2.0955,4.5339,-0.4191,-0.4191,0.0381,0.0381,POINTS=32,ORIENTATION=-
1,0,0,ID='F y:-0.4191 z:0.0381',QUANTITY='GAUGE HEAT FLUX
GAS',STATISTICS_START=0,TEMPORAL_STATISTIC='TIME INTEGRAL'/
&DEVC XB=2.0955,4.5339,-0.3429,-0.3429,0.0381,0.0381,POINTS=32,ORIENTATION=-
1,0,0,ID='F y:-0.3429 z:0.0381',QUANTITY='GAUGE HEAT FLUX
GAS',STATISTICS_START=0,TEMPORAL_STATISTIC='TIME INTEGRAL'/
&DEVC XB=2.0955,4.5339,-0.2667,-0.2667,0.0381,0.0381,POINTS=32,ORIENTATION=-
1,0,0,ID='F y:-0.2667 z:0.0381',QUANTITY='GAUGE HEAT FLUX
GAS',STATISTICS_START=0,TEMPORAL_STATISTIC='TIME INTEGRAL'/
&DEVC XB=2.0955,4.5339,0.4191,0.4191,0.0381,0.0381,POINTS=32,ORIENTATION=-1,0,0,ID='F
y:0.4191 z:0.0381',QUANTITY='GAUGE HEAT FLUX
GAS',STATISTICS_START=0,TEMPORAL_STATISTIC='TIME INTEGRAL'/
&DEVC XB=2.0955,4.5339,0.3429,0.3429,0.0381,0.0381,POINTS=32,ORIENTATION=-1,0,0,ID='F
y:0.3429 z:0.0381',QUANTITY='GAUGE HEAT FLUX
GAS',STATISTICS_START=0,TEMPORAL_STATISTIC='TIME INTEGRAL'/

```







```

&DEVC XB=2.0955,4.5339,-0.2667,-0.2667,0.8763,0.8763,POINTS=32,ORIENTATION=-
1,0,0,ID='F y:-0.2667 z:0.8763',QUANTITY='GAUGE HEAT FLUX
GAS',STATISTICS_START=0,TEMPORAL_STATISTIC='TIME INTEGRAL'/
&DEVC XB=2.0955,4.5339,0.4191,0.4191,0.8763,0.8763,POINTS=32,ORIENTATION=-1,0,0,ID='F
y:0.4191 z:0.8763',QUANTITY='GAUGE HEAT FLUX
GAS',STATISTICS_START=0,TEMPORAL_STATISTIC='TIME INTEGRAL'/
&DEVC XB=2.0955,4.5339,0.3429,0.3429,0.8763,0.8763,POINTS=32,ORIENTATION=-1,0,0,ID='F
y:0.3429 z:0.8763',QUANTITY='GAUGE HEAT FLUX
GAS',STATISTICS_START=0,TEMPORAL_STATISTIC='TIME INTEGRAL'/
&DEVC XB=2.0955,4.5339,0.2667,0.2667,0.8763,0.8763,POINTS=32,ORIENTATION=-1,0,0,ID='F
y:0.2667 z:0.8763',QUANTITY='GAUGE HEAT FLUX
GAS',STATISTICS_START=0,TEMPORAL_STATISTIC='TIME INTEGRAL'/
&DEVC XB=2.0955,4.5339,-0.4191,-0.4191,0.9525,0.9525,POINTS=32,ORIENTATION=-
1,0,0,ID='F y:-0.4191 z:0.9525',QUANTITY='GAUGE HEAT FLUX
GAS',STATISTICS_START=0,TEMPORAL_STATISTIC='TIME INTEGRAL'/
&DEVC XB=2.0955,4.5339,-0.3429,-0.3429,0.9525,0.9525,POINTS=32,ORIENTATION=-
1,0,0,ID='F y:-0.3429 z:0.9525',QUANTITY='GAUGE HEAT FLUX
GAS',STATISTICS_START=0,TEMPORAL_STATISTIC='TIME INTEGRAL'/
&DEVC XB=2.0955,4.5339,-0.2667,-0.2667,0.9525,0.9525,POINTS=32,ORIENTATION=-
1,0,0,ID='F y:-0.2667 z:0.9525',QUANTITY='GAUGE HEAT FLUX
GAS',STATISTICS_START=0,TEMPORAL_STATISTIC='TIME INTEGRAL'/
&DEVC XB=2.0955,4.5339,0.4191,0.4191,0.9525,0.9525,POINTS=32,ORIENTATION=-1,0,0,ID='F
y:0.4191 z:0.9525',QUANTITY='GAUGE HEAT FLUX
GAS',STATISTICS_START=0,TEMPORAL_STATISTIC='TIME INTEGRAL'/
&DEVC XB=2.0955,4.5339,0.3429,0.3429,0.9525,0.9525,POINTS=32,ORIENTATION=-1,0,0,ID='F
y:0.3429 z:0.9525',QUANTITY='GAUGE HEAT FLUX
GAS',STATISTICS_START=0,TEMPORAL_STATISTIC='TIME INTEGRAL'/
&DEVC XB=2.0955,4.5339,0.2667,0.2667,0.9525,0.9525,POINTS=32,ORIENTATION=-1,0,0,ID='F
y:0.2667 z:0.9525',QUANTITY='GAUGE HEAT FLUX
GAS',STATISTICS_START=0,TEMPORAL_STATISTIC='TIME INTEGRAL'/
&DEVC XB=2.0955,4.5339,-0.4191,-0.4191,1.0287,1.0287,POINTS=32,ORIENTATION=-
1,0,0,ID='F y:-0.4191 z:1.0287',QUANTITY='GAUGE HEAT FLUX
GAS',STATISTICS_START=0,TEMPORAL_STATISTIC='TIME INTEGRAL'/
&DEVC XB=2.0955,4.5339,-0.3429,-0.3429,1.0287,1.0287,POINTS=32,ORIENTATION=-
1,0,0,ID='F y:-0.3429 z:1.0287',QUANTITY='GAUGE HEAT FLUX
GAS',STATISTICS_START=0,TEMPORAL_STATISTIC='TIME INTEGRAL'/
&DEVC XB=2.0955,4.5339,-0.2667,-0.2667,1.0287,1.0287,POINTS=32,ORIENTATION=-
1,0,0,ID='F y:-0.2667 z:1.0287',QUANTITY='GAUGE HEAT FLUX
GAS',STATISTICS_START=0,TEMPORAL_STATISTIC='TIME INTEGRAL'/
&DEVC XB=2.0955,4.5339,0.4191,0.4191,1.0287,1.0287,POINTS=32,ORIENTATION=-1,0,0,ID='F
y:0.4191 z:1.0287',QUANTITY='GAUGE HEAT FLUX
GAS',STATISTICS_START=0,TEMPORAL_STATISTIC='TIME INTEGRAL'/
&DEVC XB=2.0955,4.5339,0.3429,0.3429,1.0287,1.0287,POINTS=32,ORIENTATION=-1,0,0,ID='F
y:0.3429 z:1.0287',QUANTITY='GAUGE HEAT FLUX
GAS',STATISTICS_START=0,TEMPORAL_STATISTIC='TIME INTEGRAL'/
&DEVC XB=2.0955,4.5339,0.2667,0.2667,1.0287,1.0287,POINTS=32,ORIENTATION=-1,0,0,ID='F
y:0.2667 z:1.0287',QUANTITY='GAUGE HEAT FLUX
GAS',STATISTICS_START=0,TEMPORAL_STATISTIC='TIME INTEGRAL'/
&DEVC XB=2.0955,4.5339,-0.4191,-0.4191,1.1049,1.1049,POINTS=32,ORIENTATION=-
1,0,0,ID='F y:-0.4191 z:1.1049',QUANTITY='GAUGE HEAT FLUX
GAS',STATISTICS_START=0,TEMPORAL_STATISTIC='TIME INTEGRAL'/
&DEVC XB=2.0955,4.5339,-0.3429,-0.3429,1.1049,1.1049,POINTS=32,ORIENTATION=-
1,0,0,ID='F y:-0.3429 z:1.1049',QUANTITY='GAUGE HEAT FLUX
GAS',STATISTICS_START=0,TEMPORAL_STATISTIC='TIME INTEGRAL'/
&DEVC XB=2.0955,4.5339,-0.2667,-0.2667,1.1049,1.1049,POINTS=32,ORIENTATION=-
1,0,0,ID='F y:-0.2667 z:1.1049',QUANTITY='GAUGE HEAT FLUX
GAS',STATISTICS_START=0,TEMPORAL_STATISTIC='TIME INTEGRAL'/
&DEVC XB=2.0955,4.5339,0.4191,0.4191,1.1049,1.1049,POINTS=32,ORIENTATION=-1,0,0,ID='F
y:0.4191 z:1.1049',QUANTITY='GAUGE HEAT FLUX
GAS',STATISTICS_START=0,TEMPORAL_STATISTIC='TIME INTEGRAL'/
&DEVC XB=2.0955,4.5339,0.3429,0.3429,1.1049,1.1049,POINTS=32,ORIENTATION=-1,0,0,ID='F
y:0.3429 z:1.1049',QUANTITY='GAUGE HEAT FLUX
GAS',STATISTICS_START=0,TEMPORAL_STATISTIC='TIME INTEGRAL'/

```

---

*FDS Input File Templates*

```
&DEVC XB=2.0955,4.5339,0.2667,0.2667,1.1049,1.1049,POINTS=32,ORIENTATION=-1,0,0,ID='F
y:0.2667 z:1.1049',QUANTITY='GAUGE HEAT FLUX
GAS',STATISTICS_START=0,TEMPORAL_STATISTIC='TIME INTEGRAL' /
&DEVC XB=2.0955,4.5339,-0.4191,-0.4191,1.1811,1.1811,POINTS=32,ORIENTATION=-
1,0,0,ID='F y:-0.4191 z:1.1811',QUANTITY='GAUGE HEAT FLUX
GAS',STATISTICS_START=0,TEMPORAL_STATISTIC='TIME INTEGRAL' /
&DEVC XB=2.0955,4.5339,-0.3429,-0.3429,1.1811,1.1811,POINTS=32,ORIENTATION=-
1,0,0,ID='F y:-0.3429 z:1.1811',QUANTITY='GAUGE HEAT FLUX
GAS',STATISTICS_START=0,TEMPORAL_STATISTIC='TIME INTEGRAL' /
&DEVC XB=2.0955,4.5339,-0.2667,-0.2667,1.1811,1.1811,POINTS=32,ORIENTATION=-
1,0,0,ID='F y:-0.2667 z:1.1811',QUANTITY='GAUGE HEAT FLUX
GAS',STATISTICS_START=0,TEMPORAL_STATISTIC='TIME INTEGRAL' /
&DEVC XB=2.0955,4.5339,0.4191,0.4191,1.1811,1.1811,POINTS=32,ORIENTATION=-1,0,0,ID='F
y:0.4191 z:1.1811',QUANTITY='GAUGE HEAT FLUX
GAS',STATISTICS_START=0,TEMPORAL_STATISTIC='TIME INTEGRAL' /
&DEVC XB=2.0955,4.5339,0.3429,0.3429,1.1811,1.1811,POINTS=32,ORIENTATION=-1,0,0,ID='F
y:0.3429 z:1.1811',QUANTITY='GAUGE HEAT FLUX
GAS',STATISTICS_START=0,TEMPORAL_STATISTIC='TIME INTEGRAL' /
&DEVC XB=2.0955,4.5339,0.2667,0.2667,1.1811,1.1811,POINTS=32,ORIENTATION=-1,0,0,ID='F
y:0.2667 z:1.1811',QUANTITY='GAUGE HEAT FLUX
GAS',STATISTICS_START=0,TEMPORAL_STATISTIC='TIME INTEGRAL' /
&DEVC XB=2.0955,4.5339,-0.4191,-0.4191,1.2573,1.2573,POINTS=32,ORIENTATION=-
1,0,0,ID='F y:-0.4191 z:1.2573',QUANTITY='GAUGE HEAT FLUX
GAS',STATISTICS_START=0,TEMPORAL_STATISTIC='TIME INTEGRAL' /
&DEVC XB=2.0955,4.5339,-0.3429,-0.3429,1.2573,1.2573,POINTS=32,ORIENTATION=-
1,0,0,ID='F y:-0.3429 z:1.2573',QUANTITY='GAUGE HEAT FLUX
GAS',STATISTICS_START=0,TEMPORAL_STATISTIC='TIME INTEGRAL' /
&DEVC XB=2.0955,4.5339,-0.2667,-0.2667,1.2573,1.2573,POINTS=32,ORIENTATION=-
1,0,0,ID='F y:-0.2667 z:1.2573',QUANTITY='GAUGE HEAT FLUX
GAS',STATISTICS_START=0,TEMPORAL_STATISTIC='TIME INTEGRAL' /
&DEVC XB=2.0955,4.5339,0.4191,0.4191,1.2573,1.2573,POINTS=32,ORIENTATION=-1,0,0,ID='F
y:0.4191 z:1.2573',QUANTITY='GAUGE HEAT FLUX
GAS',STATISTICS_START=0,TEMPORAL_STATISTIC='TIME INTEGRAL' /
&DEVC XB=2.0955,4.5339,0.3429,0.3429,1.2573,1.2573,POINTS=32,ORIENTATION=-1,0,0,ID='F
y:0.3429 z:1.2573',QUANTITY='GAUGE HEAT FLUX
GAS',STATISTICS_START=0,TEMPORAL_STATISTIC='TIME INTEGRAL' /
&DEVC XB=2.0955,4.5339,0.2667,0.2667,1.2573,1.2573,POINTS=32,ORIENTATION=-1,0,0,ID='F
y:0.2667 z:1.2573',QUANTITY='GAUGE HEAT FLUX
GAS',STATISTICS_START=0,TEMPORAL_STATISTIC='TIME INTEGRAL' /
&DEVC XB=2.0955,4.5339,-0.4191,-0.4191,1.3335,1.3335,POINTS=32,ORIENTATION=-
1,0,0,ID='F y:-0.4191 z:1.3335',QUANTITY='GAUGE HEAT FLUX
GAS',STATISTICS_START=0,TEMPORAL_STATISTIC='TIME INTEGRAL' /
&DEVC XB=2.0955,4.5339,-0.3429,-0.3429,1.3335,1.3335,POINTS=32,ORIENTATION=-
1,0,0,ID='F y:-0.3429 z:1.3335',QUANTITY='GAUGE HEAT FLUX
GAS',STATISTICS_START=0,TEMPORAL_STATISTIC='TIME INTEGRAL' /
&DEVC XB=2.0955,4.5339,-0.2667,-0.2667,1.3335,1.3335,POINTS=32,ORIENTATION=-
1,0,0,ID='F y:-0.2667 z:1.3335',QUANTITY='GAUGE HEAT FLUX
GAS',STATISTICS_START=0,TEMPORAL_STATISTIC='TIME INTEGRAL' /
&DEVC XB=2.0955,4.5339,0.4191,0.4191,1.3335,1.3335,POINTS=32,ORIENTATION=-1,0,0,ID='F
y:0.4191 z:1.3335',QUANTITY='GAUGE HEAT FLUX
GAS',STATISTICS_START=0,TEMPORAL_STATISTIC='TIME INTEGRAL' /
&DEVC XB=2.0955,4.5339,0.3429,0.3429,1.3335,1.3335,POINTS=32,ORIENTATION=-1,0,0,ID='F
y:0.3429 z:1.3335',QUANTITY='GAUGE HEAT FLUX
GAS',STATISTICS_START=0,TEMPORAL_STATISTIC='TIME INTEGRAL' /
&DEVC XB=2.0955,4.5339,0.2667,0.2667,1.3335,1.3335,POINTS=32,ORIENTATION=-1,0,0,ID='F
y:0.2667 z:1.3335',QUANTITY='GAUGE HEAT FLUX
GAS',STATISTICS_START=0,TEMPORAL_STATISTIC='TIME INTEGRAL' /
&DEVC XB=2.0955,4.5339,-0.4191,-0.4191,1.4097,1.4097,POINTS=32,ORIENTATION=-
1,0,0,ID='F y:-0.4191 z:1.4097',QUANTITY='GAUGE HEAT FLUX
GAS',STATISTICS_START=0,TEMPORAL_STATISTIC='TIME INTEGRAL' /
&DEVC XB=2.0955,4.5339,-0.3429,-0.3429,1.4097,1.4097,POINTS=32,ORIENTATION=-
1,0,0,ID='F y:-0.3429 z:1.4097',QUANTITY='GAUGE HEAT FLUX
GAS',STATISTICS_START=0,TEMPORAL_STATISTIC='TIME INTEGRAL' /
```



---

FDS Input File Templates

```
&DEVC XB=2.0955,4.5339,0.2667,0.2667,1.6383,1.6383,POINTS=32,ORIENTATION=-1,0,0,ID='F
y:0.2667 z:1.6383',QUANTITY='GAUGE HEAT FLUX
GAS',STATISTICS_START=0,TEMPORAL_STATISTIC='TIME INTEGRAL'/
&DEVC XB=2.0955,4.5339,-0.4191,-0.4191,1.7145,1.7145,POINTS=32,ORIENTATION=-
1,0,0,ID='F y:-0.4191 z:1.7145',QUANTITY='GAUGE HEAT FLUX
GAS',STATISTICS_START=0,TEMPORAL_STATISTIC='TIME INTEGRAL'/
&DEVC XB=2.0955,4.5339,-0.3429,-0.3429,1.7145,1.7145,POINTS=32,ORIENTATION=-
1,0,0,ID='F y:-0.3429 z:1.7145',QUANTITY='GAUGE HEAT FLUX
GAS',STATISTICS_START=0,TEMPORAL_STATISTIC='TIME INTEGRAL'/
&DEVC XB=2.0955,4.5339,-0.2667,-0.2667,1.7145,1.7145,POINTS=32,ORIENTATION=-
1,0,0,ID='F y:-0.2667 z:1.7145',QUANTITY='GAUGE HEAT FLUX
GAS',STATISTICS_START=0,TEMPORAL_STATISTIC='TIME INTEGRAL'/
&DEVC XB=2.0955,4.5339,0.4191,0.4191,1.7145,1.7145,POINTS=32,ORIENTATION=-1,0,0,ID='F
y:0.4191 z:1.7145',QUANTITY='GAUGE HEAT FLUX
GAS',STATISTICS_START=0,TEMPORAL_STATISTIC='TIME INTEGRAL'/
&DEVC XB=2.0955,4.5339,0.3429,0.3429,1.7145,1.7145,POINTS=32,ORIENTATION=-1,0,0,ID='F
y:0.3429 z:1.7145',QUANTITY='GAUGE HEAT FLUX
GAS',STATISTICS_START=0,TEMPORAL_STATISTIC='TIME INTEGRAL'/
&DEVC XB=2.0955,4.5339,0.2667,0.2667,1.7145,1.7145,POINTS=32,ORIENTATION=-1,0,0,ID='F
y:0.2667 z:1.7145',QUANTITY='GAUGE HEAT FLUX
GAS',STATISTICS_START=0,TEMPORAL_STATISTIC='TIME INTEGRAL'/
&DEVC XB=2.0955,4.5339,-0.4191,-0.4191,1.7907,1.7907,POINTS=32,ORIENTATION=-
1,0,0,ID='F y:-0.4191 z:1.7907',QUANTITY='GAUGE HEAT FLUX
GAS',STATISTICS_START=0,TEMPORAL_STATISTIC='TIME INTEGRAL'/
&DEVC XB=2.0955,4.5339,-0.3429,-0.3429,1.7907,1.7907,POINTS=32,ORIENTATION=-
1,0,0,ID='F y:-0.3429 z:1.7907',QUANTITY='GAUGE HEAT FLUX
GAS',STATISTICS_START=0,TEMPORAL_STATISTIC='TIME INTEGRAL'/
&DEVC XB=2.0955,4.5339,-0.2667,-0.2667,1.7907,1.7907,POINTS=32,ORIENTATION=-
1,0,0,ID='F y:-0.2667 z:1.7907',QUANTITY='GAUGE HEAT FLUX
GAS',STATISTICS_START=0,TEMPORAL_STATISTIC='TIME INTEGRAL'/
&DEVC XB=2.0955,4.5339,0.4191,0.4191,1.7907,1.7907,POINTS=32,ORIENTATION=-1,0,0,ID='F
y:0.4191 z:1.7907',QUANTITY='GAUGE HEAT FLUX
GAS',STATISTICS_START=0,TEMPORAL_STATISTIC='TIME INTEGRAL'/
&DEVC XB=2.0955,4.5339,0.3429,0.3429,1.7907,1.7907,POINTS=32,ORIENTATION=-1,0,0,ID='F
y:0.3429 z:1.7907',QUANTITY='GAUGE HEAT FLUX
GAS',STATISTICS_START=0,TEMPORAL_STATISTIC='TIME INTEGRAL'/
&DEVC XB=2.0955,4.5339,0.2667,0.2667,1.7907,1.7907,POINTS=32,ORIENTATION=-1,0,0,ID='F
y:0.2667 z:1.7907',QUANTITY='GAUGE HEAT FLUX
GAS',STATISTICS_START=0,TEMPORAL_STATISTIC='TIME INTEGRAL'/
&DEVC XB=2.0955,4.5339,-0.1905,-0.1905,1.3335,1.3335,POINTS=32,ORIENTATION=-
1,0,0,ID='F y:-0.1905 z:1.3335',QUANTITY='GAUGE HEAT FLUX
GAS',STATISTICS_START=0,TEMPORAL_STATISTIC='TIME INTEGRAL'/
&DEVC XB=2.0955,4.5339,-0.1143,-0.1143,1.3335,1.3335,POINTS=32,ORIENTATION=-
1,0,0,ID='F y:-0.1143 z:1.3335',QUANTITY='GAUGE HEAT FLUX
GAS',STATISTICS_START=0,TEMPORAL_STATISTIC='TIME INTEGRAL'/
&DEVC XB=2.0955,4.5339,-0.0381,-0.0381,1.3335,1.3335,POINTS=32,ORIENTATION=-
1,0,0,ID='F y:-0.0381 z:1.3335',QUANTITY='GAUGE HEAT FLUX
GAS',STATISTICS_START=0,TEMPORAL_STATISTIC='TIME INTEGRAL'/
&DEVC XB=2.0955,4.5339,0.0381,0.0381,1.3335,1.3335,POINTS=32,ORIENTATION=-1,0,0,ID='F
y:0.0381 z:1.3335',QUANTITY='GAUGE HEAT FLUX
GAS',STATISTICS_START=0,TEMPORAL_STATISTIC='TIME INTEGRAL'/
&DEVC XB=2.0955,4.5339,0.1143,0.1143,1.3335,1.3335,POINTS=32,ORIENTATION=-1,0,0,ID='F
y:0.1143 z:1.3335',QUANTITY='GAUGE HEAT FLUX
GAS',STATISTICS_START=0,TEMPORAL_STATISTIC='TIME INTEGRAL'/
&DEVC XB=2.0955,4.5339,0.1905,0.1905,1.3335,1.3335,POINTS=32,ORIENTATION=-1,0,0,ID='F
y:0.1905 z:1.3335',QUANTITY='GAUGE HEAT FLUX
GAS',STATISTICS_START=0,TEMPORAL_STATISTIC='TIME INTEGRAL'/
&DEVC XB=2.0955,4.5339,-0.1905,-0.1905,1.4097,1.4097,POINTS=32,ORIENTATION=-
1,0,0,ID='F y:-0.1905 z:1.4097',QUANTITY='GAUGE HEAT FLUX
GAS',STATISTICS_START=0,TEMPORAL_STATISTIC='TIME INTEGRAL'/
&DEVC XB=2.0955,4.5339,-0.1143,-0.1143,1.4097,1.4097,POINTS=32,ORIENTATION=-
1,0,0,ID='F y:-0.1143 z:1.4097',QUANTITY='GAUGE HEAT FLUX
GAS',STATISTICS_START=0,TEMPORAL_STATISTIC='TIME INTEGRAL'/
```



```
&DEVC XB=2.0955,4.5339,0.1905,0.1905,1.6383,1.6383,POINTS=32,ORIENTATION=-1,0,0,ID='F
y:0.1905 z:1.6383',QUANTITY='GAUGE HEAT FLUX
GAS',STATISTICS_START=0,TEMPORAL_STATISTIC='TIME INTEGRAL'/
&DEVC XB=2.0955,4.5339,-0.1905,-0.1905,1.7145,1.7145,POINTS=32,ORIENTATION=-
1,0,0,ID='F y:-0.1905 z:1.7145',QUANTITY='GAUGE HEAT FLUX
GAS',STATISTICS_START=0,TEMPORAL_STATISTIC='TIME INTEGRAL'/
&DEVC XB=2.0955,4.5339,-0.1143,-0.1143,1.7145,1.7145,POINTS=32,ORIENTATION=-
1,0,0,ID='F y:-0.1143 z:1.7145',QUANTITY='GAUGE HEAT FLUX
GAS',STATISTICS_START=0,TEMPORAL_STATISTIC='TIME INTEGRAL'/
&DEVC XB=2.0955,4.5339,-0.0381,-0.0381,1.7145,1.7145,POINTS=32,ORIENTATION=-
1,0,0,ID='F y:-0.0381 z:1.7145',QUANTITY='GAUGE HEAT FLUX
GAS',STATISTICS_START=0,TEMPORAL_STATISTIC='TIME INTEGRAL'/
&DEVC XB=2.0955,4.5339,0.0381,0.0381,1.7145,1.7145,POINTS=32,ORIENTATION=-1,0,0,ID='F
y:0.0381 z:1.7145',QUANTITY='GAUGE HEAT FLUX
GAS',STATISTICS_START=0,TEMPORAL_STATISTIC='TIME INTEGRAL'/
&DEVC XB=2.0955,4.5339,0.1143,0.1143,1.7145,1.7145,POINTS=32,ORIENTATION=-1,0,0,ID='F
y:0.1143 z:1.7145',QUANTITY='GAUGE HEAT FLUX
GAS',STATISTICS_START=0,TEMPORAL_STATISTIC='TIME INTEGRAL'/
&DEVC XB=2.0955,4.5339,0.1905,0.1905,1.7145,1.7145,POINTS=32,ORIENTATION=-1,0,0,ID='F
y:0.1905 z:1.7145',QUANTITY='GAUGE HEAT FLUX
GAS',STATISTICS_START=0,TEMPORAL_STATISTIC='TIME INTEGRAL'/

&TAIL/
```

### C.3 FDS Input File Template for Low Voltage Switchgear

Since only a small number of LV SWGR simulations were run, the python tool for generating input files was not used. FDS inputs to define the electrode metal and arc location were edited by hand.

```
&HEAD CHID='LV_FC_Mid_Mid_Al'/

! 3 in. resolution. Approximately 2 m to each side, 2 m above, and 2.4 m front and
back.

&MESH ID='Cabinet',IJK=23,22,20,XB=-2.3622,-0.6096,-2.5146,-
0.8382,0.0000,1.5240,MULT_ID='M1'/ 3 in. resolution
&MULT ID='M1',I_LOWER=-1,I_UPPER=2,DX=1.7526,J_UPPER=2,DY=1.6764,K_UPPER=2,DZ=1.5240/

&VENT MB='ZMAX',SURF_ID='OPEN'/
&VENT PBZ=0,SURF_ID='FLOOR'/
&VENT MB='YMAX',SURF_ID='OPEN'/
&VENT MB='XMAX',SURF_ID='OPEN'/
&VENT MB='YMIN',SURF_ID='OPEN'/
&VENT MB='XMIN',SURF_ID='OPEN'/

&MISC AEROSOL_AL2O3=T,I_MAX_TEMP=35000 /

! SMOKE3D_SPEC_ID sets the species used by Smokeview to visualize smoke

&DUMP SMOKE3D_SPEC_ID='ALUMINUM OXIDE',SUPPRESS_DIAGNOSTICS=F,MASS_FILE=T/

! Turns off the extinction model. Default values in the model may not be appropriate
for metal oxidation
&COMB SUPPRESSION=F /

! 0.01 kg/m3 greatly limits clipping of density.
&CLIP MINIMUM_DENSITY=0.01, MAXIMUM_TEMPERATURE=35000.,CLIP_DT_RESTRICTIONS_MAX=0 /

! These cases a very challenging for the pressure solver. The selected values seem to
give enough pressure iterations to
! drop the velocity error down to a plateau value.
```

```

&PRES MAX_PRESSURE_ITERATIONS=30, VELOCITY_TOLERANCE=0.001,
SUSPEND_PRESSURE_ITERATIONS=F/

! For ZOI runs suggest T_END = arc time + 8 s

&TIME T_END=0., DT=0.001,WALL_INCREMENT=1 /

&RADI NUMBER_RADIATION_ANGLES=500 /

! 1 cell thick OBST to help out pressure solver.

&OBST XB=-0.6858,0.0000,-0.6096,0.6096,2.3622,2.4384,SURF_ID='CABINET' /
&OBST XB=-1.6764,-0.6858,-0.6096,0.6096,2.2098,2.2860,SURF_ID='CABINET' /

&OBST XB=-1.6764,0.0000,-0.6096,-0.5334,0.0000,2.2098,SURF_ID='CABINET' /
&OBST XB=-0.6858,0.0000,-0.6096,-0.5334,2.2098,2.3622,SURF_ID='CABINET' /
&OBST XB=-1.1430,-0.6858,-0.6096,-0.5334,2.2098,2.2860,SURF_ID='CABINET' /
&OBST XB=-1.6764,0.0000,0.5334,0.6096,0.0000,2.2098,SURF_ID='CABINET' /
&OBST XB=-0.6858,0.0000,0.5334,0.6096,2.2098,2.3622,SURF_ID='CABINET' /
&OBST XB=-1.1430,-0.6858,0.5334,0.6096,2.2098,2.2860,SURF_ID='CABINET' /

&OBST XB=-1.7526,-1.6764,-0.6096,0.6096,0.0000,2.2860,SURF_ID='CABINET' /

&OBST XB=-0.0762,0.0000,-0.6096,0.6096,0.0000,2.3622,SURF_ID='CABINET' /

&OBST XB=-0.6858,0.0000,-0.0762,0.0000,0.0000,2.3622,SURF_ID='CABINET' /
&OBST XB=-1.6764,-0.6858,-0.0762,0.0000,0.0000,2.2098,SURF_ID='CABINET' /
&OBST XB=-0.7620,-0.6858,-0.6096,0.6096,0.0000,2.4384,SURF_ID='CABINET' /
&OBST XB=-1.2192,-1.1430,-0.6096,0.6096,0.0000,2.2098,SURF_ID='CABINET' /
&OBST XB=-0.6096,-0.0762,-0.4572,-0.1524,0.0000,0.5334,SURF_ID='BREAKER' /
&OBST XB=-0.6096,-0.0762,0.0762,0.4572,0.0000,0.5334,SURF_ID='BREAKER' /
&OBST XB=-0.6096,-0.0762,-0.4572,-0.1524,0.6096,1.1430,SURF_ID='BREAKER' /
&OBST XB=-0.6096,-0.0762,-0.4572,-0.1524,1.2192,1.7526,SURF_ID='BREAKER' /
&OBST XB=-0.6096,-0.0762,-0.4572,-0.1524,1.8288,2.2860,SURF_ID='BREAKER' /
&OBST XB=-0.6096,-0.0762,0.0762,0.4572,0.6096,1.1430,SURF_ID='BREAKER' /
&OBST XB=-0.6096,-0.0762,0.0762,0.4572,1.2192,1.7526,SURF_ID='BREAKER' /
&OBST XB=-0.6096,-0.0762,0.0762,0.4572,1.8288,2.2860,SURF_ID='BREAKER' /
&OBST XB=-0.0762,0.0000,-0.5334,0.5334,0.6096,0.6858,SURF_ID='CABINET' /
&OBST XB=-0.0762,0.0000,-0.5334,0.5334,1.2192,1.2954,SURF_ID='CABINET' /
&OBST XB=-0.0762,0.0000,-0.5334,0.5334,1.8288,1.9050,SURF_ID='CABINET' /
&HOLE XB=-1.2202,-1.1420,0.2286,0.3048,2.1336,2.2098/
&HOLE XB=-1.2202,-1.1420,-0.3048,-0.2286,2.1336,2.2098/

&HOLE XB=-0.6096,-0.5334,0.3810,0.4572,2.3612,2.4394/
&HOLE XB=-0.3810,-0.2286,0.3810,0.4572,2.3612,2.4394/
&HOLE XB=-0.6096,-0.5334,-0.4572,-0.3810,2.3612,2.4394/
&HOLE XB=-0.3810,-0.2286,-0.4572,-0.3810,2.3612,2.4394/
&HOLE XB=-0.6096,-0.5334,0.2286,0.3048,2.3612,2.4394/
&HOLE XB=-0.3810,-0.2286,0.2286,0.3048,2.3612,2.4394/
&HOLE XB=-0.6096,-0.5334,-0.3048,-0.2286,2.3612,2.4394/
&HOLE XB=-0.3810,-0.2286,-0.3048,-0.2286,2.3612,2.4394/
&HOLE XB=-0.6096,-0.5334,0.0762,0.1524,2.3612,2.4394/
&HOLE XB=-0.3810,-0.2286,0.0762,0.1524,2.3612,2.4394/
&HOLE XB=-0.6096,-0.5334,-0.1524,-0.0762,2.3612,2.4394/
&HOLE XB=-0.3810,-0.2286,-0.1524,-0.0762,2.3612,2.4394/

&HOLE XB=-1.7536,-1.6754,-0.4572,-0.0762,0.0762,0.1524/
&HOLE XB=-1.7536,-1.6754,-0.4572,-0.0762,0.2286,0.3048/
&HOLE XB=-1.7536,-1.6754,-0.4572,-0.0762,1.9050,1.9812/
&HOLE XB=-1.7536,-1.6754,-0.4572,-0.0762,2.0574,2.1336/
&HOLE XB=-1.7536,-1.6754,0.0762,0.4572,0.0762,0.1524/
&HOLE XB=-1.7536,-1.6754,0.0762,0.4572,0.2286,0.3048/
&HOLE XB=-1.7536,-1.6754,0.0762,0.4572,1.9050,1.9812/

```

---

## FDS Input File Templates

```
&HOLE XB=-1.7536,-1.6754,0.0762,0.4572,2.0574,2.1336/

&HOLE XB=-0.0772,0.0010,0.0000,0.5334,0.6858,1.2192/Door
&HOLE XB=-0.7630,-0.6848,0.0000,0.5334,0.7620,0.8382/ ARC

! RADCAL_ID='SOOT' makes the SPEC use the SOOT radiation properties which the MISC
line has changed to those for AL2O3
! RAMPS used instead of built in cp data for N2, CO2, and O2 to extend temperature to
20,000 K

&SPEC ID='WET NITROGEN',BACKGROUND=T,SPEC_ID='NITROGEN','CARBON DIOXIDE','WATER
VAPOR',MASS_FRACTION=1,0.000775,0.007792/FDS Default AIR without O2
&SPEC ID='NITROGEN', LUMPED_COMPONENT_ONLY=T,RAMP_CP='N2 C'/
&SPEC ID='CARBON DIOXIDE', LUMPED_COMPONENT_ONLY=T,RAMP_CP='CO2 C'/
&SPEC ID='WATER VAPOR', LUMPED_COMPONENT_ONLY=T /
&SPEC ID='OXYGEN', MASS_FRACTION_0=0.230997,RAMP_CP='O2 C' /
&SPEC ID='ALUMINUM',FORMULA='Al',RAMP_CP='AL
C',SIGMALJ=2.655,EPSILONKLJ=2750.,PR_GAS=1/
&SPEC ID='ALUMINUM OXIDE',FORMULA='Al2O3',RAMP_CP='AL2O3
C',SIGMALJ=3.186,EPSILONKLJ=557.449,PR_GAS=1,RADCAL_ID='SOOT' /

&REAC FUEL='ALUMINUM', SPEC_ID_NU='ALUMINUM','OXYGEN','ALUMINUM OXIDE', NU=-2,-1.5,1,
HEAT_OF_COMBUSTION=31100. / Al -> AL2O3

&MATL ID='CONCRETE', DENSITY=2400, CONDUCTIVITY=1.6, SPECIFIC_HEAT=0.75,
EMISSIVITY=0.95 /

! Non-melting steel
&MATL ID='INERT STEEL', DENSITY=7800., SPECIFIC_HEAT_RAMP='STEEL C',
CONDUCTIVITY_RAMP='STEEL K', EMISSIVITY=0.85/

! Melting steel
&MATL ID='STEEL', DENSITY=7800., SPECIFIC_HEAT_RAMP='STEEL C',
CONDUCTIVITY_RAMP='STEEL K', EMISSIVITY=0.85,
THRESHOLD_TEMPERATURE=1300., THRESHOLD_SIGN=1, HEAT_OF_REACTION(1)=250.,
PCR(1)=T, A(1)=0.6, E(1)=0., N_S(1)=0., N_T(1)=1. /

! Eurocode values
&RAMP ID='STEEL C',T=20,F=0.440/
&RAMP ID='STEEL C',T=600,F=0.760/
&RAMP ID='STEEL C',T=700,F=1.008/
&RAMP ID='STEEL C',T=720,F=1.388/
&RAMP ID='STEEL C',T=725,F=1.666/
&RAMP ID='STEEL C',T=730,F=2.291/
&RAMP ID='STEEL C',T=735,F=5.000/
&RAMP ID='STEEL C',T=740,F=2.525/ BCC -> FCC Transition
&RAMP ID='STEEL C',T=745,F=1.818/
&RAMP ID='STEEL C',T=750,F=1.483/
&RAMP ID='STEEL C',T=800,F=0.803/
&RAMP ID='STEEL C',T=900,F=0.650/

&RAMP ID='STEEL K',T=20,F=53.3/
&RAMP ID='STEEL K',T=800,F=27.3/

&SURF ID='BREAKER', MATL_ID='INERT STEEL', THICKNESS=0.02,
RGB=204,204,255,CELL_SIZE_FACTOR=0.05,STRETCH_FACTOR=1 /
&SURF ID='CABINET', MATL_ID='STEEL', THICKNESS=0.002381, COLOR='GRAY 60',
BURN_AWAY=.TRUE.,CELL_SIZE_FACTOR=0.05,STRETCH_FACTOR=1 /
&SURF ID='FLOOR', MATL_ID='CONCRETE', THICKNESS=0.15, RGB=50,50,50, DEFAULT=T /

&MATL ID='MOLTEN
AL',DENSITY=2375,CONDUCTIVITY=100.,SPECIFIC_HEAT=1.177,EMISSIVITY=0,A=3.333,E=0,
N_REACTIONS=1,HEAT_OF_REACTION=0,HEAT_OF_COMBUSTION=0,MATL_ID(1,1)='MOLTEN
AL2',SPEC_ID(1,1)='ALUMINUM',NU_MATL(1,1)=0.25,NU_SPEC(1,1)=0.75/
```

```
&MATL ID='MOLTEN
AL2', DENSITY=593.75, SPEC_ID='ALUMINUM', NU_SPEC=1, CONDUCTIVITY=100., SPECIFIC_HEAT=1.177
/
```

```
&SURF ID='AL DROP', MATL_ID='MOLTEN AL', GEOMETRY='SPHERICAL', THICKNESS=5.E-
6, HEAT_TRANSFER_COEFFICIENT=0, TMP_INNER=665.3/
&PART ID='AL DROPS', SURF_ID='AL
DROP', AGE=2.0, SAMPLING_FACTOR=10, MONODISPERSE=T, RGB=100, 100, 100/
&PROP ID='DROPS', PART_ID='AL DROPS', FLOW_RAMP='RAMP
MF', MASS_FLOW_RATE=0.00181, PARTICLES_PER_SECOND=20000, PARTICLE_VELOCITY=10, SPRAY_ANGLE
=0, 60, OFFSET=0.05/
```

```
&INIT XB=-0.9906, -0.9144, 0.0762, 0.4572, 0.7620, 0.8382, HRRPUV=859124, RAMP_Q='RAMP
Q', RADIATIVE_FRACTION=0.316/
```

! One spray nozzle device per electrode that inject liquid droplets

```
&DEVC PROP_ID='DROPS', XYZ=-0.9525,
0.1143, 0.8001, QUANTITY='TIME', SETPOINT=0.0, ORIENTATION=0, 0, 1/
&DEVC PROP_ID='DROPS', XYZ=-0.9525,
0.2667, 0.8001, QUANTITY='TIME', SETPOINT=0.0, ORIENTATION=0, 0, 1/
&DEVC PROP_ID='DROPS', XYZ=-0.9525,
0.4191, 0.8001, QUANTITY='TIME', SETPOINT=0.0, ORIENTATION=0, 0, 1/
```

```
&RAMP ID='RAMP Q', T=0.00, F=0.0000/
&RAMP ID='RAMP Q', T=0.10, F=1.0000/
&RAMP ID='RAMP Q', T=20.0, F=1.0000/
&RAMP ID='RAMP Q', T=20.1, F=0.6058/
&RAMP ID='RAMP Q', T=41.0, F=0.6058/
&RAMP ID='RAMP Q', T=41.1, F=0.0000/
```

```
&RAMP ID='RAMP MF', T= 0.00, F=0.0000/
&RAMP ID='RAMP MF', T=0.10, F=1.0000/
&RAMP ID='RAMP MF', T=20.00, F=1.0000/
&RAMP ID='RAMP MF', T=20.10, F=0.4681/
&RAMP ID='RAMP MF', T=41.00, F=0.4681/
&RAMP ID='RAMP MF', T=41.01, F=0.0000/
```

! Gas phase specific heats. FDS defaults for N2, O2, H2O, and CO2 replaced to extend values to higher temperatures than present in FDS

```
&RAMP ID='AL2O3 C', T=-73, F=0.761/ NASA TP-2002-211556
&RAMP ID='AL2O3 C', T=127, F=0.921/
&RAMP ID='AL2O3 C', T=327, F=0.999/
&RAMP ID='AL2O3 C', T=527, F=1.038/
&RAMP ID='AL2O3 C', T=727, F=1.058/
&RAMP ID='AL2O3 C', T=1727, F=1.090/
&RAMP ID='AL2O3 C', T=2727, F=1.096/
&RAMP ID='AL2O3 C', T=3727, F=1.098/
&RAMP ID='AL2O3 C', T=4727, F=1.099/
&RAMP ID='AL2O3 C', T=5727, F=1.100/
```

```
&RAMP ID='AL C', T=-73, F=0.820/ NASA TP-2002-211556
&RAMP ID='AL C', T=127, F=0.783/
&RAMP ID='AL C', T=327, F=0.776/
&RAMP ID='AL C', T=527, F=0.773/
&RAMP ID='AL C', T=727, F=0.772/
&RAMP ID='AL C', T=1727, F=0.771/
&RAMP ID='AL C', T=2727, F=0.771/
&RAMP ID='AL C', T=3727, F=0.775/
&RAMP ID='AL C', T=4727, F=0.793/
&RAMP ID='AL C', T=5727, F=0.841/
&RAMP ID='AL C', T=6727, F=0.930/
&RAMP ID='AL C', T=7727, F=1.034/
```

---

*FDS Input File Templates*

```
&RAMP ID='AL C', T=8727, F=1.130/  
&RAMP ID='AL C', T=9727, F=1.204/  
&RAMP ID='AL C', T=10727, F=1.250/  
&RAMP ID='AL C', T=11727, F=1.271/  
&RAMP ID='AL C', T=12727, F=1.269/  
&RAMP ID='AL C', T=13727, F=1.252/  
&RAMP ID='AL C', T=14727, F=1.226/  
&RAMP ID='AL C', T=15727, F=1.196/  
&RAMP ID='AL C', T=16727, F=1.168/  
&RAMP ID='AL C', T=17727, F=1.145/  
&RAMP ID='AL C', T=18727, F=1.125/  
&RAMP ID='AL C', T=19727, F=1.108/  
  
&RAMP ID='CU C', T=-73, F=0.327/ NASA TP-2002-211556  
&RAMP ID='CU C', T=127, F=0.327/  
&RAMP ID='CU C', T=327, F=0.327/  
&RAMP ID='CU C', T=527, F=0.327/  
&RAMP ID='CU C', T=727, F=0.327/  
&RAMP ID='CU C', T=1727, F=0.337/  
&RAMP ID='CU C', T=2727, F=0.396/  
&RAMP ID='CU C', T=3727, F=0.471/  
&RAMP ID='CU C', T=4727, F=0.517/  
&RAMP ID='CU C', T=5727, F=0.537/  
&RAMP ID='CU C', T=6727, F=0.551/  
&RAMP ID='CU C', T=7727, F=0.577/  
&RAMP ID='CU C', T=8727, F=0.606/  
&RAMP ID='CU C', T=9727, F=0.633/  
&RAMP ID='CU C', T=10727, F=0.653/  
&RAMP ID='CU C', T=11727, F=0.663/  
&RAMP ID='CU C', T=12727, F=0.664/  
&RAMP ID='CU C', T=13727, F=0.657/  
&RAMP ID='CU C', T=14727, F=0.642/  
&RAMP ID='CU C', T=15727, F=0.622/  
&RAMP ID='CU C', T=16727, F=0.599/  
&RAMP ID='CU C', T=17727, F=0.574/  
&RAMP ID='CU C', T=18727, F=0.550/  
&RAMP ID='CU C', T=19727, F=0.528/  
  
&RAMP ID='N2 C', T=-73, F=1.039/ NASA TP-2002-211556  
&RAMP ID='N2 C', T=127, F=1.044/  
&RAMP ID='N2 C', T=327, F=1.075/  
&RAMP ID='N2 C', T=527, F=1.122/  
&RAMP ID='N2 C', T=727, F=1.167/  
&RAMP ID='N2 C', T=1727, F=1.284/  
&RAMP ID='N2 C', T=2727, F=1.322/  
&RAMP ID='N2 C', T=3727, F=1.340/  
&RAMP ID='N2 C', T=4727, F=1.354/  
&RAMP ID='N2 C', T=5727, F=1.371/  
&RAMP ID='N2 C', T=6727, F=1.402/  
&RAMP ID='N2 C', T=7727, F=1.454/  
&RAMP ID='N2 C', T=8727, F=1.544/  
&RAMP ID='N2 C', T=9727, F=1.670/  
&RAMP ID='N2 C', T=10727, F=1.822/  
&RAMP ID='N2 C', T=11727, F=1.984/  
&RAMP ID='N2 C', T=12727, F=2.136/  
&RAMP ID='N2 C', T=13727, F=2.261/  
&RAMP ID='N2 C', T=14727, F=2.346/  
&RAMP ID='N2 C', T=15727, F=2.383/  
&RAMP ID='N2 C', T=16727, F=2.372/  
&RAMP ID='N2 C', T=17727, F=2.320/  
&RAMP ID='N2 C', T=18727, F=2.241/  
&RAMP ID='N2 C', T=19727, F=2.159/  
  
&RAMP ID='O2 C', T=-73, F=0.910/ NASA TP-2002-211556
```

```

&RAMP ID='O2 C', T=127, F=0.941/
&RAMP ID='O2 C', T=327, F=1.003/
&RAMP ID='O2 C', T=527, F=1.055/
&RAMP ID='O2 C', T=727, F=1.090/
&RAMP ID='O2 C', T=1727, F=1.181/
&RAMP ID='O2 C', T=2727, F=1.249/
&RAMP ID='O2 C', T=3727, F=1.303/
&RAMP ID='O2 C', T=4727, F=1.344/
&RAMP ID='O2 C', T=5727, F=1.373/
&RAMP ID='O2 C', T=6727, F=1.386/
&RAMP ID='O2 C', T=7727, F=1.376/
&RAMP ID='O2 C', T=8727, F=1.344/
&RAMP ID='O2 C', T=9727, F=1.296/
&RAMP ID='O2 C', T=10727, F=1.241/
&RAMP ID='O2 C', T=11727, F=1.184/
&RAMP ID='O2 C', T=12727, F=1.128/
&RAMP ID='O2 C', T=13727, F=1.077/
&RAMP ID='O2 C', T=14727, F=1.030/
&RAMP ID='O2 C', T=15727, F=0.989/
&RAMP ID='O2 C', T=16727, F=0.953/
&RAMP ID='O2 C', T=17727, F=0.922/
&RAMP ID='O2 C', T=18727, F=0.894/
&RAMP ID='O2 C', T=19727, F=0.870/

&RAMP ID='CO2 C', T=-73, F=0.735/ NASA TP-2002-211556
&RAMP ID='CO2 C', T=127, F=0.939/
&RAMP ID='CO2 C', T=327, F=1.075/
&RAMP ID='CO2 C', T=527, F=1.169/
&RAMP ID='CO2 C', T=727, F=1.234/
&RAMP ID='CO2 C', T=1727, F=1.371/
&RAMP ID='CO2 C', T=2727, F=1.412/
&RAMP ID='CO2 C', T=3727, F=1.436/
&RAMP ID='CO2 C', T=4727, F=1.466/
&RAMP ID='CO2 C', T=5727, F=1.517/
&RAMP ID='CO2 C', T=6727, F=1.595/
&RAMP ID='CO2 C', T=7727, F=1.694/
&RAMP ID='CO2 C', T=8727, F=1.797/
&RAMP ID='CO2 C', T=9727, F=1.888/
&RAMP ID='CO2 C', T=10727, F=1.957/
&RAMP ID='CO2 C', T=11727, F=2.000/
&RAMP ID='CO2 C', T=12727, F=2.019/
&RAMP ID='CO2 C', T=13727, F=2.020/
&RAMP ID='CO2 C', T=14727, F=2.007/
&RAMP ID='CO2 C', T=15727, F=1.987/
&RAMP ID='CO2 C', T=16727, F=1.965/
&RAMP ID='CO2 C', T=17727, F=1.944/
&RAMP ID='CO2 C', T=18727, F=1.924/
&RAMP ID='CO2 C', T=19727, F=1.905/

```

!Smokeview Outputs. Adjust PBX and PBX for center of arc volume.

```

&SLCF QUANTITY='MASS FRACTION',SPEC_ID='ALUMINUM',CELL_CENTERED=.TRUE.,PBX=0.2668/
&SLCF QUANTITY='MASS FRACTION',SPEC_ID='ALUMINUM
OXIDE',CELL_CENTERED=.TRUE.,PBX=0.2668/
&SLCF QUANTITY='MASS FRACTION',SPEC_ID='OXYGEN',CELL_CENTERED=.TRUE.,PBX=0.2668/
&SLCF QUANTITY='HRRPUV',CELL_CENTERED=.TRUE.,PBX=0.2668/
&SLCF QUANTITY='HRRPUV',CELL_CENTERED=.TRUE.,PBX=-0.9525/
&SLCF QUANTITY='TEMPERATURE',CELL_CENTERED=.TRUE.,PBX=0.2668/
&SLCF QUANTITY='TEMPERATURE',CELL_CENTERED=.TRUE.,PBX=-0.9525/
&SLCF QUANTITY='INTEGRATED INTENSITY',CELL_CENTERED=.TRUE.,PBX=0.2668/
&SLCF QUANTITY='INTEGRATED INTENSITY',CELL_CENTERED=.TRUE.,PBX=-0.9525/
&SLCF QUANTITY='VELOCITY',CELL_CENTERED=.TRUE.,PBX=0.2668/
&SLCF QUANTITY='U-VELOCITY',CELL_CENTERED=.TRUE.,PBX=0.2668/
&SLCF QUANTITY='VELOCITY',CELL_CENTERED=.TRUE.,PBX=-0.9525/

```

---

## FDS Input File Templates

```
&SLCF QUANTITY='V-VELOCITY',CELL_CENTERED=.TRUE.,PBX=-0.9525/  
&SLCF QUANTITY='PRESSURE',CELL_CENTERED=.TRUE.,PBY=0.2668/  
  
&BNDF QUANTITY='WALL TEMPERATURE',CELL_CENTERED=.TRUE./  
&BNDF QUANTITY='GAUGE HEAT FLUX',CELL_CENTERED=.TRUE./  
&BNDF QUANTITY='WALL THICKNESS',CELL_CENTERED=.TRUE./  
  
&TAIL /
```

### C.4 FDS Input File Template for Non-Segregated Bus Ducts

For the NSBDs, a single template was created that contains all three bus duct geometries. To obtain the elbow, tee, or straight run configuration, the FDS mesh is limited to that specific portion of the overall geometry.

```
&HEAD CHID='fileid', TITLE='Bus Duct fileid' /  
  
&MESH XB=-1.0,1.0,-1.0,1.0,-0.6,0.6, IJK=50,50,30, MULT_ID='mesh' /  
  
!For T, use I_LOWER=-3, I_Upper=-1  
!For straight, use I_LOWER=-1, I_Upper=1  
!For elbow, use I_LOWER=1, I_Upper=3  
&MULT ID='mesh', DX=2.0, DY=2.0, DZ=1.2, I_LOWER=imeshlower, I_UPPER=imeshupper,  
J_LOWER=-1, J_UPPER=1, K_LOWER=-2, K_UPPER=2 /  
  
&VENT MB='XMIN',SURF_ID='OPEN' /  
&VENT MB='XMAX',SURF_ID='OPEN' /  
&VENT MB='YMIN',SURF_ID='OPEN' /  
&VENT MB='YMAX',SURF_ID='OPEN' /  
&VENT MB='ZMIN',SURF_ID='OPEN' /  
&VENT MB='ZMAX',SURF_ID='OPEN' /  
  
! I_MAX_TEMP=35000 ensures property arrays are high enough for the CLIP C-52uoyan.  
! AEROSOL_AL2O3 replaces default SOOT radiative properties with those for AL2O3  
  
&MISC AEROSOL_AL2O3=T,I_MAX_TEMP=35000 /  
  
! SMOKE3D_SPEC_ID sets the species used by Smokeview to visualize smoke  
  
&DUMP SMOKE3D_SPEC_ID='3dsmoke',SUPPRESS_DIAGNOSTICS=F,MASS_FILE=T, DT_RESTART=0.1/  
  
! Turns off the extinction model. Default values in the model may not be appropriate  
for metal oxidation  
&COMB SUPPRESSION=F /  
  
! 0.01 kg/m3 greatly limits clipping of density.  
&CLIP MINIMUM_DENSITY=0.01, MAXIMUM_TEMPERATURE=35000.,CLIP_DT_RESTRICTIONS_MAX=0 /  
  
! These cases a very challenging for the pressure solver. The selected values seem to  
give enough pressure iterations to  
! drop the velocity error down to a plateau value.  
  
&PRES MAX_PRESSURE_ITERATIONS=30, VELOCITY_TOLERANCE=0.001,  
SUSPEND_PRESSURE_ITERATIONS=F/  
  
! For ZOI runs suggest T_END = arc time + 8 s  
  
&TIME T_END=tend, DT=0.001, WALL_INCREMENT=1 /  
  
&RADI NUMBER_RADIATION_ANGLES=500 /  
  
!Geometry for the straight duct
```

```

&OBST XB=-7.00, 4.24,-0.28, 0.28, -0.24, -0.20, SURF_ID='ductsurf' / Straight duct
bottom
&OBST XB=-3.72, 3.76,-0.28, 0.28, 0.20, 0.24, SURF_ID='ductsurf' / Straight duct top
&OBST XB=-7.00, 4.24,-0.32, -0.28, -0.24, 0.24, SURF_ID='ductsurf' / Straight duct
front
&OBST XB=-7.00, 4.24, 0.28, 0.32, -0.24, 0.24, SURF_ID='ductsurf' / Straight duct
back

!Geometry for the Tee
&OBST XB=-3.72, -3.68, -0.28, 3.00, 0.24, 0.72, SURF_ID='ductsurf' / Tee right
&OBST XB=-4.32, -4.28, -0.28, 3.00, 0.24, 0.72, SURF_ID='ductsurf' / Tee left
&OBST XB=-4.28, -3.72, -0.28, 3.00, 0.68, 0.72, SURF_ID='ductsurf' / Tee top
&OBST XB=-4.32, -3.68, 0.28, 3.00, 0.24, 0.28, SURF_ID='ductsurf' / Tee bottom
&OBST XB=-4.32, -3.68, -0.32, -0.28, 0.24, 0.72, SURF_ID='ductsurf' / Tee upper cap
&OBST XB=-7.00, -4.28, -0.28, 0.28, 0.20, 0.24, SURF_ID='ductsurf' / Remaining top
panel

&OBST XB=3.76, 3.80, -0.28, 0.28, 0.24, 3.00, SURF_ID='ductsurf' / Elbow left
&OBST XB=4.20, 4.24, -0.28, 0.28, -0.24, 3.00, SURF_ID='ductsurf' / Elbow right
&OBST XB=3.76, 4.24, -0.32, -0.28, 0.24, 3.00, SURF_ID='ductsurf' / Elbow front
&OBST XB=3.76, 4.24, 0.28, 0.32, 0.24, 3.00, SURF_ID='ductsurf' / Elbow back

&SPEC ID='WET NITROGEN',BACKGROUND=T,SPEC_ID='NITROGEN','CARBON DIOXIDE','WATER
VAPOR',MASS_FRACTION=1,0.000775,0.007792/FDS Default AIR without O2
&SPEC ID='NITROGEN', LUMPED_COMPONENT_ONLY=T,RAMP_CP='N2 C' /
&SPEC ID='CARBON DIOXIDE', LUMPED_COMPONENT_ONLY=T,RAMP_CP='CO2 C' /
&SPEC ID='WATER VAPOR', LUMPED_COMPONENT_ONLY=T /
&SPEC ID='OXYGEN', MASS_FRACTION_0=0.230997,RAMP_CP='O2 C' /
alspec1 ID='ALUMINUM',FORMULA='Al',RAMP_CP='AL
C',SIGMALJ=2.655,EPSILONKLJ=2750.,PR_GAS=1/
alspec2 ID='ALUMINUM
OXIDE',MASS_EXTINCTION_COEFFICIENT=3000,FORMULA='Al2O3',RAMP_CP='AL2O3
C',SIGMALJ=3.186,EPSILONKLJ=557.449,PR_GAS=1,RADCAL_ID='SOOT' /
cuspec1 ID='COPPER',FORMULA='Cu',RAMP_CP='CU
C',SIGMALJ=5.058,EPSILONKLJ=2983.,PR_GAS=1/
cuspec2 ID='COPPER
OXIDE',MASS_EXTINCTION_COEFFICIENT=3000,FORMULA='Cu2O',SPECIFIC_HEAT=0.7,SIGMALJ=5.403
,PR_GAS=1,RADCAL_ID='SOOT'/C from JANAF, LJ take as CuO

alreac FUEL='ALUMINUM', SPEC_ID_NU='ALUMINUM','OXYGEN','ALUMINUM OXIDE', NU=-2,-1.5,1,
HEAT_OF_COMBUSTION=31100. / Al -> AL2O3
cureac FUEL='COPPER',SPEC_ID_NU='COPPER','OXYGEN','COPPER OXIDE',NU=-2,-
0.5,1,HEAT_OF_COMBUSTION=1340./ Cu->Cu2O

&MATL ID='CONCRETE', DENSITY=2400, CONDUCTIVITY=1.6, SPECIFIC_HEAT=0.75,
EMISSIVITY=0.95 /

&MATL ID='STEEL DUCT', DENSITY=7800., SPECIFIC_HEAT_RAMP='STEEL C',
CONDUCTIVITY_RAMP='STEEL K', EMISSIVITY=0.85,
THRESHOLD_TEMPERATURE=1300., THRESHOLD_SIGN=1, HEAT_OF_REACTION(1)=250.,
PCR(1)=T, A(1)=0.6, E(1)=0., N_S(1)=0., N_T(1)=1. /

&MATL ID='ALUMINUM DUCT', DENSITY=2700, CONDUCTIVITY_RAMP='ALUMINUM K',
SPECIFIC_HEAT_RAMP='ALUMINUM C', EMISSIVITY=0.35,
THRESHOLD_TEMPERATURE=650., THRESHOLD_SIGN=1, HEAT_OF_REACTION(1)=320.,
PCR(1)=T, A(1)=1.2, E(1)=0., N_S(1)=0., N_T(1) = 1. /

! Eurocode values
&RAMP ID='STEEL C',T=20,F=0.440/
&RAMP ID='STEEL C',T=600,F=0.760/
&RAMP ID='STEEL C',T=700,F=1.008/
&RAMP ID='STEEL C',T=720,F=1.388/

```

---

## FDS Input File Templates

```
&RAMP ID='STEEL C',T=725,F=1.666/
&RAMP ID='STEEL C',T=730,F=2.291/
&RAMP ID='STEEL C',T=735,F=5.000/
&RAMP ID='STEEL C',T=740,F=2.525/ BCC -> FCC Transition
&RAMP ID='STEEL C',T=745,F=1.818/
&RAMP ID='STEEL C',T=750,F=1.483/
&RAMP ID='STEEL C',T=800,F=0.803/
&RAMP ID='STEEL C',T=900,F=0.650/

&RAMP ID='STEEL K',T=20,F=53.3/
&RAMP ID='STEEL K',T=800,F=27.3/

&RAMP ID='ALUMINUM C',T=27,F=0.898/
&RAMP ID='ALUMINUM C',T=127,F=0.955/
&RAMP ID='ALUMINUM C',T=227,F=0.994/
&RAMP ID='ALUMINUM C',T=327,F=1.033/
&RAMP ID='ALUMINUM C',T=427,F=1.078/
&RAMP ID='ALUMINUM C',T=527,F=1.132/
&RAMP ID='ALUMINUM C',T=627,F=1.197/

&RAMP ID='ALUMINUM K',T=0,F=236/
&RAMP ID='ALUMINUM K',T=127,F=240/
&RAMP ID='ALUMINUM K',T=327,F=232/
&RAMP ID='ALUMINUM K',T=527,F=220/

&SURF ID='ALUMINUM DUCT', MATL_ID='ALUMINUM DUCT', THICKNESS=0.003175, COLOR='GRAY
80', BURN_AWAY=T /
&SURF ID='STEEL DUCT', MATL_ID='STEEL DUCT', THICKNESS=0.003175, COLOR='GRAY 70',
BURN_AWAY=T /
&SURF ID='FLOOR', MATL_ID='CONCRETE', THICKNESS=0.15, RGB=50,50,50, DEFAULT=T /

!The block below defines particles that emit vapor for aluminum.
!The particles are initialized at the melting point.
!The PROP MASS_FLOW_RATE is the maximum liquid production rate divided by the number
of electrodes
!NU_SPEC and NU_MATL are set to get the 75 % oxidation for Al and 25 % for Cu. The
second MOLTEN AL2 and CU2 species have a modified density to preserve diameter.
!A and E are set to give the vapor over 0.3 s.

almatl1 ID='MOLTEN
AL', DENSITY=2375, CONDUCTIVITY=100., SPECIFIC_HEAT=1.177, EMISSIVITY=0, A=3.333, E=0,
N_REACTIONS=1, HEAT_OF_REACTION=0, HEAT_OF_COMBUSTION=0, MATL_ID(1,1)='MOLTEN
AL2', SPEC_ID(1,1)='ALUMINUM', NU_MATL(1,1)=0.25, NU_SPEC(1,1)=0.75/
almatl2 ID='MOLTEN
AL2', DENSITY=593.75, SPEC_ID='ALUMINUM', NU_SPEC=1, CONDUCTIVITY=100., SPECIFIC_HEAT=1.177
/

alsurf1 ID='AL DROP', MATL_ID='MOLTEN AL', GEOMETRY='SPHERICAL', THICKNESS=5.E-
6, HEAT_TRANSFER_COEFFICIENT=0, TMP_INNER=665.3/
alpart1 ID='AL DROPS', SURF_ID='AL
DROP', AGE=2.0, SAMPLING_FACTOR=10, MONODISPERSE=T, RGB=100,100,100/
alprop1 ID='DROPS', PART_ID='AL DROPS', FLOW_RAMP='RAMP
MF', MASS_FLOW_RATE=almfr, PARTICLES_PER_SECOND=20000, PARTICLE_VELOCITY=10, SPRAY_ANGLE=0
,60/

! The block below is for copper.

Cumatl1 ID='MOLTEN
CU', DENSITY=8960, CONDUCTIVITY=340., SPECIFIC_HEAT=0.517, EMISSIVITY=0, A=3.333, E=0,
N_REACTIONS=1, HEAT_OF_REACTION=0, HEAT_OF_COMBUSTION=0, MATL_ID(1,1)='MOLTEN
CU2', SPEC_ID(1,1)='COPPER', NU_MATL(1,1)=0.75, NU_SPEC(1,1)=0.25/
cumatl2 ID='MOLTEN
CU2', DENSITY=7168, CONDUCTIVITY=340., SPECIFIC_HEAT=0.517, EMISSIVITY=0/
```

```

cusurf1 ID='CU DROP',MATL_ID='MOLTEN CU',GEOMETRY='SPHERICAL',THICKNESS=5.E-
6,HEAT_TRANSFER_COEFFICIENT=0,TMP_INNER=1084.85/
cupart1 ID='CU DROPS',SURF_ID='CU
DROP',AGE=2.0,SAMPLING_FACTOR=10,MONODISPERSE=T,RGB=184,115,51/
cuprop1 ID='DROPS',PART_ID='CU DROPS',FLOW_RAMP='RAMP
MF',MASS_FLOW_RATE=cumfr,PARTICLES_PER_SECOND=20000,PARTICLE_VELOCITY=10,SPRAY_ANGLE=0
,60/

```

```

! First INIT line is the volumetric source term where the RADAITIVE_FRACTION uses
Cressault's data interpolated based on power,. The HRRPUV is
! reduced based on energy needed to degrade the electrodes:
! Adjusted total energy = (Total arc energy - electrode mass loss * (vapor fraction *
energy to vaporize + liquid fraction * energy to melt))

```

```

!
! Cressault data:
!
! X_r,Al = 0.2275*Max_Power^0.3292
! X_r,Al = 0.1273*Max_Power^0.3859
!
! Phase Energy (kJ/kg)
! Change Al Cu
! Melt 1063.4 695.2

```

```

&INIT XB=initx1,initx2,inity1,inity2,initz1,initz2,HRRPUV=hrrpuvval,RAMP_Q='RAMP
Q',RADIATIVE_FRACTION=radfrac/

```

```

! One spray nozzle device per electrode that inject liquid droplets

```

```

&DEVC
PROP_ID='DROPS',XYZ=nozx1,nozy1,nozz1,QUANTITY='TIME',SETPOINT=0.0,ORIENTATION=orient1
,orient2,orient3/
&DEVC
PROP_ID='DROPS',XYZ=nozx2,nozy2,nozz2,QUANTITY='TIME',SETPOINT=0.0,ORIENTATION=orient1
,orient2,orient3/
&DEVC
PROP_ID='DROPS',XYZ=nozx3,nozy3,nozz3,QUANTITY='TIME',SETPOINT=0.0,ORIENTATION=orient1
,orient2,orient3/

```

```

! An 0.1 s ramp up and down for the arc volumetric source term helps avoid numerical
instabilities

```

```

&RAMP ID='RAMP Q',T=0.0,F=0.0000/
&RAMP ID='RAMP Q',T=0.1,F=rampqf1/
&RAMP ID='RAMP Q',T=0.2,F=rampqf2/
&RAMP ID='RAMP Q',T=0.3,F=rampqf3/
&RAMP ID='RAMP Q',T=0.4,F=rampqf4/
&RAMP ID='RAMP Q',T=0.5,F=rampqf5/
&RAMP ID='RAMP Q',T=0.6,F=rampqf6/
&RAMP ID='RAMP Q',T=0.7,F=rampqf7/
&RAMP ID='RAMP Q',T=0.8,F=rampqf8/
&RAMP ID='RAMP Q',T=0.9,F=rampqf9/
&RAMP ID='RAMP Q',T=1.0,F=rampqf10/
&RAMP ID='RAMP Q',T=1.1,F=rampqf11/
&RAMP ID='RAMP Q',T=1.2,F=rampqf12/
&RAMP ID='RAMP Q',T=1.3,F=rampqf13/
&RAMP ID='RAMP Q',T=1.4,F=rampqf14/
&RAMP ID='RAMP Q',T=1.5,F=rampqf15/
&RAMP ID='RAMP Q',T=1.6,F=rampqf16/
&RAMP ID='RAMP Q',T=1.7,F=rampqf17/
&RAMP ID='RAMP Q',T=1.8,F=rampqf18/
&RAMP ID='RAMP Q',T=1.9,F=rampqf19/
&RAMP ID='RAMP Q',T=2.0,F=rampqf20/
&RAMP ID='RAMP Q',T=2.1,F=rampqf21/

```

---

## FDS Input File Templates

```
&RAMP ID=' RAMP Q' ,T=2.2,F=rampqf22/  
&RAMP ID=' RAMP Q' ,T=2.3,F=rampqf23/  
&RAMP ID=' RAMP Q' ,T=2.4,F=rampqf24/  
&RAMP ID=' RAMP Q' ,T=2.5,F=rampqf25/  
&RAMP ID=' RAMP Q' ,T=2.6,F=rampqf26/  
&RAMP ID=' RAMP Q' ,T=2.7,F=rampqf27/  
&RAMP ID=' RAMP Q' ,T=2.8,F=rampqf28/  
&RAMP ID=' RAMP Q' ,T=2.9,F=rampqf29/  
&RAMP ID=' RAMP Q' ,T=3.0,F=rampqf30/  
&RAMP ID=' RAMP Q' ,T=3.1,F=rampqf31/  
&RAMP ID=' RAMP Q' ,T=3.2,F=rampqf32/  
&RAMP ID=' RAMP Q' ,T=3.3,F=rampqf33/  
&RAMP ID=' RAMP Q' ,T=3.4,F=rampqf34/  
&RAMP ID=' RAMP Q' ,T=3.5,F=rampqf35/  
&RAMP ID=' RAMP Q' ,T=3.6,F=rampqf36/  
&RAMP ID=' RAMP Q' ,T=3.7,F=rampqf37/  
&RAMP ID=' RAMP Q' ,T=3.8,F=rampqf38/  
&RAMP ID=' RAMP Q' ,T=3.9,F=rampqf39/  
&RAMP ID=' RAMP Q' ,T=4.0,F=rampqf40/  
&RAMP ID=' RAMP Q' ,T=4.1,F=rampqf41/  
&RAMP ID=' RAMP Q' ,T=4.2,F=rampqf42/  
&RAMP ID=' RAMP Q' ,T=4.3,F=rampqf43/  
&RAMP ID=' RAMP Q' ,T=4.4,F=rampqf44/  
&RAMP ID=' RAMP Q' ,T=4.5,F=rampqf45/  
&RAMP ID=' RAMP Q' ,T=4.6,F=rampqf46/  
&RAMP ID=' RAMP Q' ,T=4.7,F=rampqf47/  
&RAMP ID=' RAMP Q' ,T=4.8,F=rampqf48/  
&RAMP ID=' RAMP Q' ,T=4.9,F=rampqf49/  
&RAMP ID=' RAMP Q' ,T=5.0,F=rampqf50/  
&RAMP ID=' RAMP Q' ,T=5.1,F=rampqf51/  
&RAMP ID=' RAMP Q' ,T=5.2,F=rampqf52/  
&RAMP ID=' RAMP Q' ,T=5.3,F=rampqf53/  
&RAMP ID=' RAMP Q' ,T=5.4,F=rampqf54/  
&RAMP ID=' RAMP Q' ,T=5.5,F=rampqf55/  
&RAMP ID=' RAMP Q' ,T=5.6,F=rampqf56/  
&RAMP ID=' RAMP Q' ,T=5.7,F=rampqf57/  
&RAMP ID=' RAMP Q' ,T=5.8,F=rampqf58/  
&RAMP ID=' RAMP Q' ,T=5.9,F=rampqf59/  
&RAMP ID=' RAMP Q' ,T=6.0,F=rampqf60/  
&RAMP ID=' RAMP Q' ,T=6.1,F=rampqf61/  
&RAMP ID=' RAMP Q' ,T=6.2,F=rampqf62/  
&RAMP ID=' RAMP Q' ,T=6.3,F=rampqf63/  
&RAMP ID=' RAMP Q' ,T=6.4,F=rampqf64/  
&RAMP ID=' RAMP Q' ,T=6.5,F=rampqf65/  
&RAMP ID=' RAMP Q' ,T=6.6,F=rampqf66/  
&RAMP ID=' RAMP Q' ,T=6.7,F=rampqf67/  
&RAMP ID=' RAMP Q' ,T=6.8,F=rampqf68/  
&RAMP ID=' RAMP Q' ,T=6.9,F=rampqf69/  
&RAMP ID=' RAMP Q' ,T=7.0,F=rampqf70/  
&RAMP ID=' RAMP Q' ,T=7.1,F=rampqf71/  
&RAMP ID=' RAMP Q' ,T=7.2,F=rampqf72/  
&RAMP ID=' RAMP Q' ,T=7.3,F=rampqf73/  
&RAMP ID=' RAMP Q' ,T=7.4,F=rampqf74/  
&RAMP ID=' RAMP Q' ,T=7.5,F=rampqf75/  
&RAMP ID=' RAMP Q' ,T=7.6,F=rampqf76/  
&RAMP ID=' RAMP Q' ,T=7.7,F=rampqf77/  
&RAMP ID=' RAMP Q' ,T=7.8,F=rampqf78/  
&RAMP ID=' RAMP Q' ,T=7.9,F=rampqf79/  
&RAMP ID=' RAMP Q' ,T=8.0,F=rampqf80/  
&RAMP ID=' RAMP Q' ,T=8.1,F=rampqf81/  
&RAMP ID=' RAMP Q' ,T=8.2,F=rampqf82/  
&RAMP ID=' RAMP Q' ,T=8.3,F=rampqf83/  
&RAMP ID=' RAMP Q' ,T=8.4,F=rampqf84/  
&RAMP ID=' RAMP Q' ,T=8.5,F=rampqf85/
```

```
&RAMP ID=' RAMP Q',T=8.6,F=rampqf86/  
&RAMP ID=' RAMP Q',T=8.7,F=rampqf87/  
&RAMP ID=' RAMP Q',T=8.8,F=rampqf88/  
&RAMP ID=' RAMP Q',T=8.9,F=rampqf89/  
&RAMP ID=' RAMP Q',T=9.0,F=rampqf90/  
&RAMP ID=' RAMP Q',T=9.1,F=rampqf91/  
&RAMP ID=' RAMP Q',T=9.2,F=rampqf92/  
&RAMP ID=' RAMP Q',T=9.3,F=rampqf93/  
&RAMP ID=' RAMP Q',T=9.4,F=rampqf94/  
&RAMP ID=' RAMP Q',T=9.5,F=rampqf95/  
&RAMP ID=' RAMP Q',T=9.6,F=rampqf96/  
&RAMP ID=' RAMP Q',T=9.7,F=rampqf97/  
&RAMP ID=' RAMP Q',T=9.8,F=rampqf98/  
&RAMP ID=' RAMP Q',T=9.9,F=rampqf99/  
&RAMP ID=' RAMP Q',T=10.0,F=rampqf100/  
&RAMP ID=' RAMP Q',T=10.1,F=rampqf101/  
&RAMP ID=' RAMP Q',T=10.2,F=rampqf102/  
&RAMP ID=' RAMP Q',T=10.3,F=rampqf103/  
&RAMP ID=' RAMP Q',T=10.4,F=rampqf104/  
&RAMP ID=' RAMP Q',T=10.5,F=rampqf105/  
&RAMP ID=' RAMP Q',T=10.6,F=rampqf106/  
&RAMP ID=' RAMP Q',T=10.7,F=rampqf107/  
&RAMP ID=' RAMP Q',T=10.8,F=rampqf108/  
&RAMP ID=' RAMP Q',T=10.9,F=rampqf109/  
&RAMP ID=' RAMP Q',T=11.0,F=rampqf110/  
&RAMP ID=' RAMP Q',T=11.1,F=rampqf111/  
&RAMP ID=' RAMP Q',T=11.2,F=rampqf112/  
&RAMP ID=' RAMP Q',T=11.3,F=rampqf113/  
&RAMP ID=' RAMP Q',T=11.4,F=rampqf114/  
&RAMP ID=' RAMP Q',T=11.5,F=rampqf115/  
&RAMP ID=' RAMP Q',T=11.6,F=rampqf116/  
&RAMP ID=' RAMP Q',T=11.7,F=rampqf117/  
&RAMP ID=' RAMP Q',T=11.8,F=rampqf118/  
&RAMP ID=' RAMP Q',T=11.9,F=rampqf119/  
&RAMP ID=' RAMP Q',T=12.0,F=rampqf120/  
&RAMP ID=' RAMP Q',T=12.1,F=rampqf121/  
&RAMP ID=' RAMP Q',T=12.2,F=rampqf122/  
&RAMP ID=' RAMP Q',T=12.3,F=rampqf123/  
&RAMP ID=' RAMP Q',T=12.4,F=rampqf124/  
&RAMP ID=' RAMP Q',T=12.5,F=rampqf125/  
&RAMP ID=' RAMP Q',T=12.6,F=rampqf126/  
&RAMP ID=' RAMP Q',T=12.7,F=rampqf127/  
&RAMP ID=' RAMP Q',T=12.8,F=rampqf128/  
&RAMP ID=' RAMP Q',T=12.9,F=rampqf129/  
&RAMP ID=' RAMP Q',T=13.0,F=rampqf130/  
&RAMP ID=' RAMP Q',T=13.1,F=rampqf131/  
&RAMP ID=' RAMP Q',T=13.2,F=rampqf132/  
&RAMP ID=' RAMP Q',T=13.3,F=rampqf133/  
&RAMP ID=' RAMP Q',T=13.4,F=rampqf134/  
&RAMP ID=' RAMP Q',T=13.5,F=rampqf135/  
&RAMP ID=' RAMP Q',T=13.6,F=rampqf136/  
&RAMP ID=' RAMP Q',T=13.7,F=rampqf137/  
&RAMP ID=' RAMP Q',T=13.8,F=rampqf138/  
&RAMP ID=' RAMP Q',T=13.9,F=rampqf139/  
&RAMP ID=' RAMP Q',T=14.0,F=rampqf140/  
&RAMP ID=' RAMP Q',T=14.1,F=rampqf141/  
&RAMP ID=' RAMP Q',T=14.2,F=rampqf142/  
&RAMP ID=' RAMP Q',T=14.3,F=rampqf143/  
&RAMP ID=' RAMP Q',T=14.4,F=rampqf144/  
&RAMP ID=' RAMP Q',T=14.5,F=rampqf145/  
&RAMP ID=' RAMP Q',T=14.6,F=rampqf146/  
&RAMP ID=' RAMP Q',T=14.7,F=rampqf147/  
&RAMP ID=' RAMP Q',T=14.8,F=rampqf148/  
&RAMP ID=' RAMP Q',T=14.9,F=rampqf149/
```

---

## FDS Input File Templates

```
&RAMP ID=' RAMP Q',T=15.0,F=rampqf150/  
&RAMP ID=' RAMP Q',T=15.1,F=rampqf151/  
&RAMP ID=' RAMP Q',T=15.2,F=rampqf152/  
&RAMP ID=' RAMP Q',T=15.3,F=rampqf153/  
&RAMP ID=' RAMP Q',T=15.4,F=rampqf154/  
&RAMP ID=' RAMP Q',T=15.5,F=rampqf155/  
&RAMP ID=' RAMP Q',T=15.6,F=rampqf156/  
&RAMP ID=' RAMP Q',T=15.7,F=rampqf157/  
&RAMP ID=' RAMP Q',T=15.8,F=rampqf158/  
&RAMP ID=' RAMP Q',T=15.9,F=rampqf159/  
&RAMP ID=' RAMP Q',T=16.0,F=rampqf160/  
&RAMP ID=' RAMP Q',T=16.1,F=rampqf161/  
&RAMP ID=' RAMP Q',T=16.2,F=rampqf162/  
&RAMP ID=' RAMP Q',T=16.3,F=rampqf163/  
&RAMP ID=' RAMP Q',T=16.4,F=rampqf164/  
&RAMP ID=' RAMP Q',T=16.5,F=rampqf165/  
&RAMP ID=' RAMP Q',T=16.6,F=rampqf166/  
&RAMP ID=' RAMP Q',T=16.7,F=rampqf167/  
&RAMP ID=' RAMP Q',T=16.8,F=rampqf168/  
&RAMP ID=' RAMP Q',T=16.9,F=rampqf169/  
&RAMP ID=' RAMP Q',T=17.0,F=rampqf170/  
&RAMP ID=' RAMP Q',T=17.1,F=rampqf171/  
&RAMP ID=' RAMP Q',T=17.2,F=rampqf172/  
&RAMP ID=' RAMP Q',T=17.3,F=rampqf173/  
&RAMP ID=' RAMP Q',T=17.4,F=rampqf174/  
&RAMP ID=' RAMP Q',T=17.5,F=rampqf175/  
&RAMP ID=' RAMP Q',T=17.6,F=rampqf176/  
&RAMP ID=' RAMP Q',T=17.7,F=rampqf177/  
&RAMP ID=' RAMP Q',T=17.8,F=rampqf178/  
&RAMP ID=' RAMP Q',T=17.9,F=rampqf179/  
&RAMP ID=' RAMP Q',T=18.0,F=rampqf180/  
&RAMP ID=' RAMP Q',T=18.1,F=rampqf181/  
&RAMP ID=' RAMP Q',T=18.2,F=rampqf182/  
&RAMP ID=' RAMP Q',T=18.3,F=rampqf183/  
&RAMP ID=' RAMP Q',T=18.4,F=rampqf184/  
&RAMP ID=' RAMP Q',T=18.5,F=rampqf185/  
&RAMP ID=' RAMP Q',T=18.6,F=rampqf186/  
&RAMP ID=' RAMP Q',T=18.7,F=rampqf187/  
&RAMP ID=' RAMP Q',T=18.8,F=rampqf188/  
&RAMP ID=' RAMP Q',T=18.9,F=rampqf189/  
&RAMP ID=' RAMP Q',T=19.0,F=rampqf190/  
&RAMP ID=' RAMP Q',T=19.1,F=rampqf191/  
&RAMP ID=' RAMP Q',T=19.2,F=rampqf192/  
&RAMP ID=' RAMP Q',T=19.3,F=rampqf193/  
&RAMP ID=' RAMP Q',T=19.4,F=rampqf194/  
&RAMP ID=' RAMP Q',T=19.5,F=rampqf195/  
&RAMP ID=' RAMP Q',T=19.6,F=rampqf196/  
&RAMP ID=' RAMP Q',T=19.7,F=rampqf197/  
&RAMP ID=' RAMP Q',T=19.8,F=rampqf198/  
&RAMP ID=' RAMP Q',T=19.9,F=rampqf199/  
&RAMP ID=' RAMP Q',T=20.0,F=rampqf200/  
&RAMP ID=' RAMP Q',T=20.1,F=0.0000/
```

! RAMP for droplets

```
&RAMP ID=' RAMP MF',T=0.00,F=0.0000/  
&RAMP ID=' RAMP MF',T=0.1,F=rampmff1/  
&RAMP ID=' RAMP MF',T=0.2,F=rampmff2/  
&RAMP ID=' RAMP MF',T=0.3,F=rampmff3/  
&RAMP ID=' RAMP MF',T=0.4,F=rampmff4/  
&RAMP ID=' RAMP MF',T=0.5,F=rampmff5/  
&RAMP ID=' RAMP MF',T=0.6,F=rampmff6/  
&RAMP ID=' RAMP MF',T=0.7,F=rampmff7/  
&RAMP ID=' RAMP MF',T=0.8,F=rampmff8/
```

```
&RAMP ID=' RAMP MF', T=0.9, F=rampmfff9/  
&RAMP ID=' RAMP MF', T=1.0, F=rampmfff10/  
&RAMP ID=' RAMP MF', T=1.1, F=rampmfff11/  
&RAMP ID=' RAMP MF', T=1.2, F=rampmfff12/  
&RAMP ID=' RAMP MF', T=1.3, F=rampmfff13/  
&RAMP ID=' RAMP MF', T=1.4, F=rampmfff14/  
&RAMP ID=' RAMP MF', T=1.5, F=rampmfff15/  
&RAMP ID=' RAMP MF', T=1.6, F=rampmfff16/  
&RAMP ID=' RAMP MF', T=1.7, F=rampmfff17/  
&RAMP ID=' RAMP MF', T=1.8, F=rampmfff18/  
&RAMP ID=' RAMP MF', T=1.9, F=rampmfff19/  
&RAMP ID=' RAMP MF', T=2.0, F=rampmfff20/  
&RAMP ID=' RAMP MF', T=2.1, F=rampmfff21/  
&RAMP ID=' RAMP MF', T=2.2, F=rampmfff22/  
&RAMP ID=' RAMP MF', T=2.3, F=rampmfff23/  
&RAMP ID=' RAMP MF', T=2.4, F=rampmfff24/  
&RAMP ID=' RAMP MF', T=2.5, F=rampmfff25/  
&RAMP ID=' RAMP MF', T=2.6, F=rampmfff26/  
&RAMP ID=' RAMP MF', T=2.7, F=rampmfff27/  
&RAMP ID=' RAMP MF', T=2.8, F=rampmfff28/  
&RAMP ID=' RAMP MF', T=2.9, F=rampmfff29/  
&RAMP ID=' RAMP MF', T=3.0, F=rampmfff30/  
&RAMP ID=' RAMP MF', T=3.1, F=rampmfff31/  
&RAMP ID=' RAMP MF', T=3.2, F=rampmfff32/  
&RAMP ID=' RAMP MF', T=3.3, F=rampmfff33/  
&RAMP ID=' RAMP MF', T=3.4, F=rampmfff34/  
&RAMP ID=' RAMP MF', T=3.5, F=rampmfff35/  
&RAMP ID=' RAMP MF', T=3.6, F=rampmfff36/  
&RAMP ID=' RAMP MF', T=3.7, F=rampmfff37/  
&RAMP ID=' RAMP MF', T=3.8, F=rampmfff38/  
&RAMP ID=' RAMP MF', T=3.9, F=rampmfff39/  
&RAMP ID=' RAMP MF', T=4.0, F=rampmfff40/  
&RAMP ID=' RAMP MF', T=4.1, F=rampmfff41/  
&RAMP ID=' RAMP MF', T=4.2, F=rampmfff42/  
&RAMP ID=' RAMP MF', T=4.3, F=rampmfff43/  
&RAMP ID=' RAMP MF', T=4.4, F=rampmfff44/  
&RAMP ID=' RAMP MF', T=4.5, F=rampmfff45/  
&RAMP ID=' RAMP MF', T=4.6, F=rampmfff46/  
&RAMP ID=' RAMP MF', T=4.7, F=rampmfff47/  
&RAMP ID=' RAMP MF', T=4.8, F=rampmfff48/  
&RAMP ID=' RAMP MF', T=4.9, F=rampmfff49/  
&RAMP ID=' RAMP MF', T=5.0, F=rampmfff50/  
&RAMP ID=' RAMP MF', T=5.1, F=rampmfff51/  
&RAMP ID=' RAMP MF', T=5.2, F=rampmfff52/  
&RAMP ID=' RAMP MF', T=5.3, F=rampmfff53/  
&RAMP ID=' RAMP MF', T=5.4, F=rampmfff54/  
&RAMP ID=' RAMP MF', T=5.5, F=rampmfff55/  
&RAMP ID=' RAMP MF', T=5.6, F=rampmfff56/  
&RAMP ID=' RAMP MF', T=5.7, F=rampmfff57/  
&RAMP ID=' RAMP MF', T=5.8, F=rampmfff58/  
&RAMP ID=' RAMP MF', T=5.9, F=rampmfff59/  
&RAMP ID=' RAMP MF', T=6.0, F=rampmfff60/  
&RAMP ID=' RAMP MF', T=6.1, F=rampmfff61/  
&RAMP ID=' RAMP MF', T=6.2, F=rampmfff62/  
&RAMP ID=' RAMP MF', T=6.3, F=rampmfff63/  
&RAMP ID=' RAMP MF', T=6.4, F=rampmfff64/  
&RAMP ID=' RAMP MF', T=6.5, F=rampmfff65/  
&RAMP ID=' RAMP MF', T=6.6, F=rampmfff66/  
&RAMP ID=' RAMP MF', T=6.7, F=rampmfff67/  
&RAMP ID=' RAMP MF', T=6.8, F=rampmfff68/  
&RAMP ID=' RAMP MF', T=6.9, F=rampmfff69/  
&RAMP ID=' RAMP MF', T=7.0, F=rampmfff70/  
&RAMP ID=' RAMP MF', T=7.1, F=rampmfff71/  
&RAMP ID=' RAMP MF', T=7.2, F=rampmfff72/
```

---

## FDS Input File Templates

```
&RAMP ID=' RAMP MF', T=7.3, F=rampmfff73/  
&RAMP ID=' RAMP MF', T=7.4, F=rampmfff74/  
&RAMP ID=' RAMP MF', T=7.5, F=rampmfff75/  
&RAMP ID=' RAMP MF', T=7.6, F=rampmfff76/  
&RAMP ID=' RAMP MF', T=7.7, F=rampmfff77/  
&RAMP ID=' RAMP MF', T=7.8, F=rampmfff78/  
&RAMP ID=' RAMP MF', T=7.9, F=rampmfff79/  
&RAMP ID=' RAMP MF', T=8.0, F=rampmfff80/  
&RAMP ID=' RAMP MF', T=8.1, F=rampmfff81/  
&RAMP ID=' RAMP MF', T=8.2, F=rampmfff82/  
&RAMP ID=' RAMP MF', T=8.3, F=rampmfff83/  
&RAMP ID=' RAMP MF', T=8.4, F=rampmfff84/  
&RAMP ID=' RAMP MF', T=8.5, F=rampmfff85/  
&RAMP ID=' RAMP MF', T=8.6, F=rampmfff86/  
&RAMP ID=' RAMP MF', T=8.7, F=rampmfff87/  
&RAMP ID=' RAMP MF', T=8.8, F=rampmfff88/  
&RAMP ID=' RAMP MF', T=8.9, F=rampmfff89/  
&RAMP ID=' RAMP MF', T=9.0, F=rampmfff90/  
&RAMP ID=' RAMP MF', T=9.1, F=rampmfff91/  
&RAMP ID=' RAMP MF', T=9.2, F=rampmfff92/  
&RAMP ID=' RAMP MF', T=9.3, F=rampmfff93/  
&RAMP ID=' RAMP MF', T=9.4, F=rampmfff94/  
&RAMP ID=' RAMP MF', T=9.5, F=rampmfff95/  
&RAMP ID=' RAMP MF', T=9.6, F=rampmfff96/  
&RAMP ID=' RAMP MF', T=9.7, F=rampmfff97/  
&RAMP ID=' RAMP MF', T=9.8, F=rampmfff98/  
&RAMP ID=' RAMP MF', T=9.9, F=rampmfff99/  
&RAMP ID=' RAMP MF', T=10.0, F=rampmfff100/  
&RAMP ID=' RAMP MF', T=10.1, F=rampmfff101/  
&RAMP ID=' RAMP MF', T=10.2, F=rampmfff102/  
&RAMP ID=' RAMP MF', T=10.3, F=rampmfff103/  
&RAMP ID=' RAMP MF', T=10.4, F=rampmfff104/  
&RAMP ID=' RAMP MF', T=10.5, F=rampmfff105/  
&RAMP ID=' RAMP MF', T=10.6, F=rampmfff106/  
&RAMP ID=' RAMP MF', T=10.7, F=rampmfff107/  
&RAMP ID=' RAMP MF', T=10.8, F=rampmfff108/  
&RAMP ID=' RAMP MF', T=10.9, F=rampmfff109/  
&RAMP ID=' RAMP MF', T=11.0, F=rampmfff110/  
&RAMP ID=' RAMP MF', T=11.1, F=rampmfff111/  
&RAMP ID=' RAMP MF', T=11.2, F=rampmfff112/  
&RAMP ID=' RAMP MF', T=11.3, F=rampmfff113/  
&RAMP ID=' RAMP MF', T=11.4, F=rampmfff114/  
&RAMP ID=' RAMP MF', T=11.5, F=rampmfff115/  
&RAMP ID=' RAMP MF', T=11.6, F=rampmfff116/  
&RAMP ID=' RAMP MF', T=11.7, F=rampmfff117/  
&RAMP ID=' RAMP MF', T=11.8, F=rampmfff118/  
&RAMP ID=' RAMP MF', T=11.9, F=rampmfff119/  
&RAMP ID=' RAMP MF', T=12.0, F=rampmfff120/  
&RAMP ID=' RAMP MF', T=12.1, F=rampmfff121/  
&RAMP ID=' RAMP MF', T=12.2, F=rampmfff122/  
&RAMP ID=' RAMP MF', T=12.3, F=rampmfff123/  
&RAMP ID=' RAMP MF', T=12.4, F=rampmfff124/  
&RAMP ID=' RAMP MF', T=12.5, F=rampmfff125/  
&RAMP ID=' RAMP MF', T=12.6, F=rampmfff126/  
&RAMP ID=' RAMP MF', T=12.7, F=rampmfff127/  
&RAMP ID=' RAMP MF', T=12.8, F=rampmfff128/  
&RAMP ID=' RAMP MF', T=12.9, F=rampmfff129/  
&RAMP ID=' RAMP MF', T=13.0, F=rampmfff130/  
&RAMP ID=' RAMP MF', T=13.1, F=rampmfff131/  
&RAMP ID=' RAMP MF', T=13.2, F=rampmfff132/  
&RAMP ID=' RAMP MF', T=13.3, F=rampmfff133/  
&RAMP ID=' RAMP MF', T=13.4, F=rampmfff134/  
&RAMP ID=' RAMP MF', T=13.5, F=rampmfff135/  
&RAMP ID=' RAMP MF', T=13.6, F=rampmfff136/
```

```
&RAMP ID=' RAMP MF', T=13.7, F=rampmff137/  
&RAMP ID=' RAMP MF', T=13.8, F=rampmff138/  
&RAMP ID=' RAMP MF', T=13.9, F=rampmff139/  
&RAMP ID=' RAMP MF', T=14.0, F=rampmff140/  
&RAMP ID=' RAMP MF', T=14.1, F=rampmff141/  
&RAMP ID=' RAMP MF', T=14.2, F=rampmff142/  
&RAMP ID=' RAMP MF', T=14.3, F=rampmff143/  
&RAMP ID=' RAMP MF', T=14.4, F=rampmff144/  
&RAMP ID=' RAMP MF', T=14.5, F=rampmff145/  
&RAMP ID=' RAMP MF', T=14.6, F=rampmff146/  
&RAMP ID=' RAMP MF', T=14.7, F=rampmff147/  
&RAMP ID=' RAMP MF', T=14.8, F=rampmff148/  
&RAMP ID=' RAMP MF', T=14.9, F=rampmff149/  
&RAMP ID=' RAMP MF', T=15.0, F=rampmff150/  
&RAMP ID=' RAMP MF', T=15.1, F=rampmff151/  
&RAMP ID=' RAMP MF', T=15.2, F=rampmff152/  
&RAMP ID=' RAMP MF', T=15.3, F=rampmff153/  
&RAMP ID=' RAMP MF', T=15.4, F=rampmff154/  
&RAMP ID=' RAMP MF', T=15.5, F=rampmff155/  
&RAMP ID=' RAMP MF', T=15.6, F=rampmff156/  
&RAMP ID=' RAMP MF', T=15.7, F=rampmff157/  
&RAMP ID=' RAMP MF', T=15.8, F=rampmff158/  
&RAMP ID=' RAMP MF', T=15.9, F=rampmff159/  
&RAMP ID=' RAMP MF', T=16.0, F=rampmff160/  
&RAMP ID=' RAMP MF', T=16.1, F=rampmff161/  
&RAMP ID=' RAMP MF', T=16.2, F=rampmff162/  
&RAMP ID=' RAMP MF', T=16.3, F=rampmff163/  
&RAMP ID=' RAMP MF', T=16.4, F=rampmff164/  
&RAMP ID=' RAMP MF', T=16.5, F=rampmff165/  
&RAMP ID=' RAMP MF', T=16.6, F=rampmff166/  
&RAMP ID=' RAMP MF', T=16.7, F=rampmff167/  
&RAMP ID=' RAMP MF', T=16.8, F=rampmff168/  
&RAMP ID=' RAMP MF', T=16.9, F=rampmff169/  
&RAMP ID=' RAMP MF', T=17.0, F=rampmff170/  
&RAMP ID=' RAMP MF', T=17.1, F=rampmff171/  
&RAMP ID=' RAMP MF', T=17.2, F=rampmff172/  
&RAMP ID=' RAMP MF', T=17.3, F=rampmff173/  
&RAMP ID=' RAMP MF', T=17.4, F=rampmff174/  
&RAMP ID=' RAMP MF', T=17.5, F=rampmff175/  
&RAMP ID=' RAMP MF', T=17.6, F=rampmff176/  
&RAMP ID=' RAMP MF', T=17.7, F=rampmff177/  
&RAMP ID=' RAMP MF', T=17.8, F=rampmff178/  
&RAMP ID=' RAMP MF', T=17.9, F=rampmff179/  
&RAMP ID=' RAMP MF', T=18.0, F=rampmff180/  
&RAMP ID=' RAMP MF', T=18.1, F=rampmff181/  
&RAMP ID=' RAMP MF', T=18.2, F=rampmff182/  
&RAMP ID=' RAMP MF', T=18.3, F=rampmff183/  
&RAMP ID=' RAMP MF', T=18.4, F=rampmff184/  
&RAMP ID=' RAMP MF', T=18.5, F=rampmff185/  
&RAMP ID=' RAMP MF', T=18.6, F=rampmff186/  
&RAMP ID=' RAMP MF', T=18.7, F=rampmff187/  
&RAMP ID=' RAMP MF', T=18.8, F=rampmff188/  
&RAMP ID=' RAMP MF', T=18.9, F=rampmff189/  
&RAMP ID=' RAMP MF', T=19.0, F=rampmff190/  
&RAMP ID=' RAMP MF', T=19.1, F=rampmff191/  
&RAMP ID=' RAMP MF', T=19.2, F=rampmff192/  
&RAMP ID=' RAMP MF', T=19.3, F=rampmff193/  
&RAMP ID=' RAMP MF', T=19.4, F=rampmff194/  
&RAMP ID=' RAMP MF', T=19.5, F=rampmff195/  
&RAMP ID=' RAMP MF', T=19.6, F=rampmff196/  
&RAMP ID=' RAMP MF', T=19.7, F=rampmff197/  
&RAMP ID=' RAMP MF', T=19.8, F=rampmff198/  
&RAMP ID=' RAMP MF', T=19.9, F=rampmff199/  
&RAMP ID=' RAMP MF', T=20.0, F=rampmff200/
```

---

## FDS Input File Templates

```
&RAMP ID='RAMP MF',T=20.1,F=0.0000/
```

```
! Gas phase specific heats. FDS defaults for N2, O2, H2O, and CO2 replaced to extend values to higher temperatures than present in FDS
```

```
&RAMP ID='AL2O3 C', T=-73, F=0.761/ NASA TP-2002-211556  
&RAMP ID='AL2O3 C', T=127, F=0.921/  
&RAMP ID='AL2O3 C', T=327, F=0.999/  
&RAMP ID='AL2O3 C', T=527, F=1.038/  
&RAMP ID='AL2O3 C', T=727, F=1.058/  
&RAMP ID='AL2O3 C', T=1727, F=1.090/  
&RAMP ID='AL2O3 C', T=2727, F=1.096/  
&RAMP ID='AL2O3 C', T=3727, F=1.098/  
&RAMP ID='AL2O3 C', T=4727, F=1.099/  
&RAMP ID='AL2O3 C', T=5727, F=1.100/
```

```
&RAMP ID='AL C', T=-73, F=0.820/ NASA TP-2002-211556  
&RAMP ID='AL C', T=127, F=0.783/  
&RAMP ID='AL C', T=327, F=0.776/  
&RAMP ID='AL C', T=527, F=0.773/  
&RAMP ID='AL C', T=727, F=0.772/  
&RAMP ID='AL C', T=1727, F=0.771/  
&RAMP ID='AL C', T=2727, F=0.771/  
&RAMP ID='AL C', T=3727, F=0.775/  
&RAMP ID='AL C', T=4727, F=0.793/  
&RAMP ID='AL C', T=5727, F=0.841/  
&RAMP ID='AL C', T=6727, F=0.930/  
&RAMP ID='AL C', T=7727, F=1.034/  
&RAMP ID='AL C', T=8727, F=1.130/  
&RAMP ID='AL C', T=9727, F=1.204/  
&RAMP ID='AL C', T=10727, F=1.250/  
&RAMP ID='AL C', T=11727, F=1.271/  
&RAMP ID='AL C', T=12727, F=1.269/  
&RAMP ID='AL C', T=13727, F=1.252/  
&RAMP ID='AL C', T=14727, F=1.226/  
&RAMP ID='AL C', T=15727, F=1.196/  
&RAMP ID='AL C', T=16727, F=1.168/  
&RAMP ID='AL C', T=17727, F=1.145/  
&RAMP ID='AL C', T=18727, F=1.125/  
&RAMP ID='AL C', T=19727, F=1.108/
```

```
&RAMP ID='CU C', T=-73, F=0.327/ NASA TP-2002-211556  
&RAMP ID='CU C', T=127, F=0.327/  
&RAMP ID='CU C', T=327, F=0.327/  
&RAMP ID='CU C', T=527, F=0.327/  
&RAMP ID='CU C', T=727, F=0.327/  
&RAMP ID='CU C', T=1727, F=0.337/  
&RAMP ID='CU C', T=2727, F=0.396/  
&RAMP ID='CU C', T=3727, F=0.471/  
&RAMP ID='CU C', T=4727, F=0.517/  
&RAMP ID='CU C', T=5727, F=0.537/  
&RAMP ID='CU C', T=6727, F=0.551/  
&RAMP ID='CU C', T=7727, F=0.577/  
&RAMP ID='CU C', T=8727, F=0.606/  
&RAMP ID='CU C', T=9727, F=0.633/  
&RAMP ID='CU C', T=10727, F=0.653/  
&RAMP ID='CU C', T=11727, F=0.663/  
&RAMP ID='CU C', T=12727, F=0.664/  
&RAMP ID='CU C', T=13727, F=0.657/  
&RAMP ID='CU C', T=14727, F=0.642/  
&RAMP ID='CU C', T=15727, F=0.622/  
&RAMP ID='CU C', T=16727, F=0.599/  
&RAMP ID='CU C', T=17727, F=0.574/  
&RAMP ID='CU C', T=18727, F=0.550/
```

```
&RAMP ID='CU C', T=19727, F=0.528/

&RAMP ID='N2 C', T=-73, F=1.039/ NASA TP-2002-211556
&RAMP ID='N2 C', T=127, F=1.044/
&RAMP ID='N2 C', T=327, F=1.075/
&RAMP ID='N2 C', T=527, F=1.122/
&RAMP ID='N2 C', T=727, F=1.167/
&RAMP ID='N2 C', T=1727, F=1.284/
&RAMP ID='N2 C', T=2727, F=1.322/
&RAMP ID='N2 C', T=3727, F=1.340/
&RAMP ID='N2 C', T=4727, F=1.354/
&RAMP ID='N2 C', T=5727, F=1.371/
&RAMP ID='N2 C', T=6727, F=1.402/
&RAMP ID='N2 C', T=7727, F=1.454/
&RAMP ID='N2 C', T=8727, F=1.544/
&RAMP ID='N2 C', T=9727, F=1.670/
&RAMP ID='N2 C', T=10727, F=1.822/
&RAMP ID='N2 C', T=11727, F=1.984/
&RAMP ID='N2 C', T=12727, F=2.136/
&RAMP ID='N2 C', T=13727, F=2.261/
&RAMP ID='N2 C', T=14727, F=2.346/
&RAMP ID='N2 C', T=15727, F=2.383/
&RAMP ID='N2 C', T=16727, F=2.372/
&RAMP ID='N2 C', T=17727, F=2.320/
&RAMP ID='N2 C', T=18727, F=2.241/
&RAMP ID='N2 C', T=19727, F=2.159/

&RAMP ID='O2 C', T=-73, F=0.910/ NASA TP-2002-211556
&RAMP ID='O2 C', T=127, F=0.941/
&RAMP ID='O2 C', T=327, F=1.003/
&RAMP ID='O2 C', T=527, F=1.055/
&RAMP ID='O2 C', T=727, F=1.090/
&RAMP ID='O2 C', T=1727, F=1.181/
&RAMP ID='O2 C', T=2727, F=1.249/
&RAMP ID='O2 C', T=3727, F=1.303/
&RAMP ID='O2 C', T=4727, F=1.344/
&RAMP ID='O2 C', T=5727, F=1.373/
&RAMP ID='O2 C', T=6727, F=1.386/
&RAMP ID='O2 C', T=7727, F=1.376/
&RAMP ID='O2 C', T=8727, F=1.344/
&RAMP ID='O2 C', T=9727, F=1.296/
&RAMP ID='O2 C', T=10727, F=1.241/
&RAMP ID='O2 C', T=11727, F=1.184/
&RAMP ID='O2 C', T=12727, F=1.128/
&RAMP ID='O2 C', T=13727, F=1.077/
&RAMP ID='O2 C', T=14727, F=1.030/
&RAMP ID='O2 C', T=15727, F=0.989/
&RAMP ID='O2 C', T=16727, F=0.953/
&RAMP ID='O2 C', T=17727, F=0.922/
&RAMP ID='O2 C', T=18727, F=0.894/
&RAMP ID='O2 C', T=19727, F=0.870/

&RAMP ID='CO2 C', T=-73, F=0.735/ NASA TP-2002-211556
&RAMP ID='CO2 C', T=127, F=0.939/
&RAMP ID='CO2 C', T=327, F=1.075/
&RAMP ID='CO2 C', T=527, F=1.169/
&RAMP ID='CO2 C', T=727, F=1.234/
&RAMP ID='CO2 C', T=1727, F=1.371/
&RAMP ID='CO2 C', T=2727, F=1.412/
&RAMP ID='CO2 C', T=3727, F=1.436/
&RAMP ID='CO2 C', T=4727, F=1.466/
&RAMP ID='CO2 C', T=5727, F=1.517/
&RAMP ID='CO2 C', T=6727, F=1.595/
&RAMP ID='CO2 C', T=7727, F=1.694/
```

---

## FDS Input File Templates

```
&RAMP ID='CO2 C', T=8727, F=1.797/  
&RAMP ID='CO2 C', T=9727, F=1.888/  
&RAMP ID='CO2 C', T=10727, F=1.957/  
&RAMP ID='CO2 C', T=11727, F=2.000/  
&RAMP ID='CO2 C', T=12727, F=2.019/  
&RAMP ID='CO2 C', T=13727, F=2.020/  
&RAMP ID='CO2 C', T=14727, F=2.007/  
&RAMP ID='CO2 C', T=15727, F=1.987/  
&RAMP ID='CO2 C', T=16727, F=1.965/  
&RAMP ID='CO2 C', T=17727, F=1.944/  
&RAMP ID='CO2 C', T=18727, F=1.924/  
&RAMP ID='CO2 C', T=19727, F=1.905/
```

!Smokeview Outputs. Adjust PBX and PBX for center of arc volume.

```
alslcf1 QUANTITY='MASS FRACTION',SPEC_ID='ALUMINUM',CELL_CENTERED=.TRUE.,PBX=0.0000/  
alslcf2 QUANTITY='MASS FRACTION',SPEC_ID='ALUMINUM  
OXIDE',CELL_CENTERED=.TRUE.,PBX=0.0000/  
cuslcf1 QUANTITY='MASS FRACTION',SPEC_ID='COPPER',CELL_CENTERED=.TRUE.,PBX=0.0000/  
cuslcf2 QUANTITY='MASS FRACTION',SPEC_ID='COPPER  
OXIDE',CELL_CENTERED=.TRUE.,PBX=0.0000/  
&SLCF QUANTITY='MASS FRACTION',SPEC_ID='OXYGEN',CELL_CENTERED=.TRUE.,PBX=0.0000/  
&SLCF QUANTITY='HRRPUV',CELL_CENTERED=.TRUE.,PBX=0.0000/  
&SLCF QUANTITY='HRRPUV',CELL_CENTERED=.TRUE.,PBX=slcfpbx/  
&SLCF QUANTITY='TEMPERATURE',CELL_CENTERED=.TRUE.,PBX=0.0000/  
&SLCF QUANTITY='TEMPERATURE',CELL_CENTERED=.TRUE.,PBX=slcfpbx/  
&SLCF QUANTITY='INTEGRATED INTENSITY',CELL_CENTERED=.TRUE.,PBX=0.0000/  
&SLCF QUANTITY='INTEGRATED INTENSITY',CELL_CENTERED=.TRUE.,PBX=slcfpbx/  
&SLCF QUANTITY='VELOCITY',CELL_CENTERED=.TRUE.,PBX=0.0000/  
&SLCF QUANTITY='U-VELOCITY',CELL_CENTERED=.TRUE.,PBX=0.0000/  
&SLCF QUANTITY='VELOCITY',CELL_CENTERED=.TRUE.,PBX=slcfpbx/  
&SLCF QUANTITY='V-VELOCITY',CELL_CENTERED=.TRUE.,PBX=slcfpbx/  
&SLCF QUANTITY='PRESSURE',CELL_CENTERED=.TRUE.,PBX=0.0000/  
  
&BNDF QUANTITY='WALL TEMPERATURE',CELL_CENTERED=.TRUE./  
&BNDF QUANTITY='GAUGE HEAT FLUX',CELL_CENTERED=.TRUE./  
&BNDF QUANTITY='WALL THICKNESS',CELL_CENTERED=.TRUE./  
&BNDF QUANTITY='VELOCITY ERROR',CELL_CENTERED=.TRUE./
```

!Example DEVC for ZOI runs. Have planes of devices at a range of distances that look at each face of the enclosure  
!Plane should be large enough to see any permanent venting, plus any area heated by or damaged by the arc, plus any C-64 buoyancy impacts  
!Here the DEVC ID means this is on the (m)inus (y) face at the given x,y,z location  
!The orientation is the unit vector given by Arc Center - DEVC XYZ. Pointing the DEVC at the arc centroid will approximate the worst case view factor  
!for the radiative component.  
!These can easily be generated with Excel using CONCATENATE()

```
&DEVC XB=-4.1800,-4.1800,-0.1800,-0.1800,-2.7000,-  
0.3000,POINTS=31,ORIENTATION=0,0,1,ID='BL x:-4.18 y:-0.18',QUANTITY='GAUGE HEAT FLUX  
GAS',STATISTICS_START=0,TEMPORAL_STATISTIC='TIME INTEGRAL'/  
&DEVC XB=-4.1800,-4.1800,-0.1000,-0.1000,-2.7000,-  
0.3000,POINTS=31,ORIENTATION=0,0,1,ID='BL x:-4.18 y:-0.10',QUANTITY='GAUGE HEAT FLUX  
GAS',STATISTICS_START=0,TEMPORAL_STATISTIC='TIME INTEGRAL'/  
&DEVC XB=-4.1800,-4.1800,-0.0200,-0.0200,-2.7000,-  
0.3000,POINTS=31,ORIENTATION=0,0,1,ID='BL x:-4.18 y:-0.02',QUANTITY='GAUGE HEAT FLUX  
GAS',STATISTICS_START=0,TEMPORAL_STATISTIC='TIME INTEGRAL'/  
&DEVC XB=-4.1800,-4.1800,0.0200,0.0200,-2.7000,-  
0.3000,POINTS=31,ORIENTATION=0,0,1,ID='BL x:-4.18 y:0.02',QUANTITY='GAUGE HEAT FLUX  
GAS',STATISTICS_START=0,TEMPORAL_STATISTIC='TIME INTEGRAL'/
```



---

FDS Input File Templates

```
&DEVC XB=-3.9000,-3.9000,-0.1000,-0.1000,-2.7000,-  
0.3000,POINTS=31,ORIENTATION=0,0,1,ID='BL x:-3.90 y:-0.10',QUANTITY='GAUGE HEAT FLUX  
GAS',STATISTICS_START=0,TEMPORAL_STATISTIC='TIME INTEGRAL'/  
&DEVC XB=-3.9000,-3.9000,-0.0200,-0.0200,-2.7000,-  
0.3000,POINTS=31,ORIENTATION=0,0,1,ID='BL x:-3.90 y:-0.02',QUANTITY='GAUGE HEAT FLUX  
GAS',STATISTICS_START=0,TEMPORAL_STATISTIC='TIME INTEGRAL'/  
&DEVC XB=-3.9000,-3.9000,0.0200,0.0200,-2.7000,-  
0.3000,POINTS=31,ORIENTATION=0,0,1,ID='BL x:-3.90 y:0.02',QUANTITY='GAUGE HEAT FLUX  
GAS',STATISTICS_START=0,TEMPORAL_STATISTIC='TIME INTEGRAL'/  
&DEVC XB=-3.9000,-3.9000,0.1000,0.1000,-2.7000,-  
0.3000,POINTS=31,ORIENTATION=0,0,1,ID='BL x:-3.90 y:0.10',QUANTITY='GAUGE HEAT FLUX  
GAS',STATISTICS_START=0,TEMPORAL_STATISTIC='TIME INTEGRAL'/  
&DEVC XB=-3.9000,-3.9000,0.1800,0.1800,-2.7000,-  
0.3000,POINTS=31,ORIENTATION=0,0,1,ID='BL x:-3.90 y:0.18',QUANTITY='GAUGE HEAT FLUX  
GAS',STATISTICS_START=0,TEMPORAL_STATISTIC='TIME INTEGRAL'/  
&DEVC XB=-3.8200,-3.8200,-0.1800,-0.1800,-2.7000,-  
0.3000,POINTS=31,ORIENTATION=0,0,1,ID='BL x:-3.82 y:-0.18',QUANTITY='GAUGE HEAT FLUX  
GAS',STATISTICS_START=0,TEMPORAL_STATISTIC='TIME INTEGRAL'/  
&DEVC XB=-3.8200,-3.8200,-0.1000,-0.1000,-2.7000,-  
0.3000,POINTS=31,ORIENTATION=0,0,1,ID='BL x:-3.82 y:-0.10',QUANTITY='GAUGE HEAT FLUX  
GAS',STATISTICS_START=0,TEMPORAL_STATISTIC='TIME INTEGRAL'/  
&DEVC XB=-3.8200,-3.8200,-0.0200,-0.0200,-2.7000,-  
0.3000,POINTS=31,ORIENTATION=0,0,1,ID='BL x:-3.82 y:-0.02',QUANTITY='GAUGE HEAT FLUX  
GAS',STATISTICS_START=0,TEMPORAL_STATISTIC='TIME INTEGRAL'/  
&DEVC XB=-3.8200,-3.8200,0.0200,0.0200,-2.7000,-  
0.3000,POINTS=31,ORIENTATION=0,0,1,ID='BL x:-3.82 y:0.02',QUANTITY='GAUGE HEAT FLUX  
GAS',STATISTICS_START=0,TEMPORAL_STATISTIC='TIME INTEGRAL'/  
&DEVC XB=-3.8200,-3.8200,0.1000,0.1000,-2.7000,-  
0.3000,POINTS=31,ORIENTATION=0,0,1,ID='BL x:-3.82 y:0.10',QUANTITY='GAUGE HEAT FLUX  
GAS',STATISTICS_START=0,TEMPORAL_STATISTIC='TIME INTEGRAL'/  
&DEVC XB=-3.8200,-3.8200,0.1800,0.1800,-2.7000,-  
0.3000,POINTS=31,ORIENTATION=0,0,1,ID='BL x:-3.82 y:0.18',QUANTITY='GAUGE HEAT FLUX  
GAS',STATISTICS_START=0,TEMPORAL_STATISTIC='TIME INTEGRAL'/
```

```
&DEVC XB=-4.1800,-4.1800,-0.1800,-0.1800,0.7800,2.9400,POINTS=28,ORIENTATION=0,0,-  
1,ID='AB x:-4.18 y:-0.18',QUANTITY='GAUGE HEAT FLUX  
GAS',STATISTICS_START=0,TEMPORAL_STATISTIC='TIME INTEGRAL'/  
&DEVC XB=-4.1800,-4.1800,-0.1000,-0.1000,0.7800,2.9400,POINTS=28,ORIENTATION=0,0,-  
1,ID='AB x:-4.18 y:-0.10',QUANTITY='GAUGE HEAT FLUX  
GAS',STATISTICS_START=0,TEMPORAL_STATISTIC='TIME INTEGRAL'/  
&DEVC XB=-4.1800,-4.1800,-0.0200,-0.0200,0.7800,2.9400,POINTS=28,ORIENTATION=0,0,-  
1,ID='AB x:-4.18 y:-0.02',QUANTITY='GAUGE HEAT FLUX  
GAS',STATISTICS_START=0,TEMPORAL_STATISTIC='TIME INTEGRAL'/  
&DEVC XB=-4.1800,-4.1800,0.0200,0.0200,0.7800,2.9400,POINTS=28,ORIENTATION=0,0,-  
1,ID='AB x:-4.18 y:0.02',QUANTITY='GAUGE HEAT FLUX  
GAS',STATISTICS_START=0,TEMPORAL_STATISTIC='TIME INTEGRAL'/  
&DEVC XB=-4.1800,-4.1800,0.1000,0.1000,0.7800,2.9400,POINTS=28,ORIENTATION=0,0,-  
1,ID='AB x:-4.18 y:0.10',QUANTITY='GAUGE HEAT FLUX  
GAS',STATISTICS_START=0,TEMPORAL_STATISTIC='TIME INTEGRAL'/  
&DEVC XB=-4.1800,-4.1800,0.1800,0.1800,0.7800,2.9400,POINTS=28,ORIENTATION=0,0,-  
1,ID='AB x:-4.18 y:0.18',QUANTITY='GAUGE HEAT FLUX  
GAS',STATISTICS_START=0,TEMPORAL_STATISTIC='TIME INTEGRAL'/  
&DEVC XB=-4.1000,-4.1000,-0.1800,-0.1800,0.7800,2.9400,POINTS=28,ORIENTATION=0,0,-  
1,ID='AB x:-4.10 y:-0.18',QUANTITY='GAUGE HEAT FLUX  
GAS',STATISTICS_START=0,TEMPORAL_STATISTIC='TIME INTEGRAL'/  
&DEVC XB=-4.1000,-4.1000,-0.1000,-0.1000,0.7800,2.9400,POINTS=28,ORIENTATION=0,0,-  
1,ID='AB x:-4.10 y:-0.10',QUANTITY='GAUGE HEAT FLUX  
GAS',STATISTICS_START=0,TEMPORAL_STATISTIC='TIME INTEGRAL'/  
&DEVC XB=-4.1000,-4.1000,-0.0200,-0.0200,0.7800,2.9400,POINTS=28,ORIENTATION=0,0,-  
1,ID='AB x:-4.10 y:-0.02',QUANTITY='GAUGE HEAT FLUX  
GAS',STATISTICS_START=0,TEMPORAL_STATISTIC='TIME INTEGRAL'/
```



---

## FDS Input File Templates

```
&DEVC XB=-3.8200,-3.8200,-0.1800,-0.1800,0.7800,2.9400,POINTS=28,ORIENTATION=0,0,-
1,ID='AB x:-3.82 y:-0.18',QUANTITY='GAUGE HEAT FLUX
GAS',STATISTICS_START=0,TEMPORAL_STATISTIC='TIME INTEGRAL'/
&DEVC XB=-3.8200,-3.8200,-0.1000,-0.1000,0.7800,2.9400,POINTS=28,ORIENTATION=0,0,-
1,ID='AB x:-3.82 y:-0.10',QUANTITY='GAUGE HEAT FLUX
GAS',STATISTICS_START=0,TEMPORAL_STATISTIC='TIME INTEGRAL'/
&DEVC XB=-3.8200,-3.8200,-0.0200,-0.0200,0.7800,2.9400,POINTS=28,ORIENTATION=0,0,-
1,ID='AB x:-3.82 y:-0.02',QUANTITY='GAUGE HEAT FLUX
GAS',STATISTICS_START=0,TEMPORAL_STATISTIC='TIME INTEGRAL'/
&DEVC XB=-3.8200,-3.8200,0.0200,0.0200,0.7800,2.9400,POINTS=28,ORIENTATION=0,0,-
1,ID='AB x:-3.82 y:0.02',QUANTITY='GAUGE HEAT FLUX
GAS',STATISTICS_START=0,TEMPORAL_STATISTIC='TIME INTEGRAL'/
&DEVC XB=-3.8200,-3.8200,0.1000,0.1000,0.7800,2.9400,POINTS=28,ORIENTATION=0,0,-
1,ID='AB x:-3.82 y:0.10',QUANTITY='GAUGE HEAT FLUX
GAS',STATISTICS_START=0,TEMPORAL_STATISTIC='TIME INTEGRAL'/
&DEVC XB=-3.8200,-3.8200,0.1800,0.1800,0.7800,2.9400,POINTS=28,ORIENTATION=0,0,-
1,ID='AB x:-3.82 y:0.18',QUANTITY='GAUGE HEAT FLUX
GAS',STATISTICS_START=0,TEMPORAL_STATISTIC='TIME INTEGRAL'/

&DEVC XB=-4.1800,-4.1800,-2.7800,-0.3800,-0.1800,-
0.1800,POINTS=31,ORIENTATION=0,1,0,ID='FL x:-4.18 z:-0.18',QUANTITY='GAUGE HEAT FLUX
GAS',STATISTICS_START=0,TEMPORAL_STATISTIC='TIME INTEGRAL'/
&DEVC XB=-4.1800,-4.1800,-2.7800,-0.3800,-0.1000,-
0.1000,POINTS=31,ORIENTATION=0,1,0,ID='FL x:-4.18 z:-0.10',QUANTITY='GAUGE HEAT FLUX
GAS',STATISTICS_START=0,TEMPORAL_STATISTIC='TIME INTEGRAL'/
&DEVC XB=-4.1800,-4.1800,-2.7800,-0.3800,-0.0200,-
0.0200,POINTS=31,ORIENTATION=0,1,0,ID='FL x:-4.18 z:-0.02',QUANTITY='GAUGE HEAT FLUX
GAS',STATISTICS_START=0,TEMPORAL_STATISTIC='TIME INTEGRAL'/
&DEVC XB=-4.1800,-4.1800,-2.7800,-
0.3800,0.0200,0.0200,POINTS=31,ORIENTATION=0,1,0,ID='FL x:-4.18
z:0.02',QUANTITY='GAUGE HEAT FLUX GAS',STATISTICS_START=0,TEMPORAL_STATISTIC='TIME
INTEGRAL'/
&DEVC XB=-4.1800,-4.1800,-2.7800,-
0.3800,0.1000,0.1000,POINTS=31,ORIENTATION=0,1,0,ID='FL x:-4.18
z:0.10',QUANTITY='GAUGE HEAT FLUX GAS',STATISTICS_START=0,TEMPORAL_STATISTIC='TIME
INTEGRAL'/
&DEVC XB=-4.1800,-4.1800,-2.7800,-
0.3800,0.1800,0.1800,POINTS=31,ORIENTATION=0,1,0,ID='FL x:-4.18
z:0.18',QUANTITY='GAUGE HEAT FLUX GAS',STATISTICS_START=0,TEMPORAL_STATISTIC='TIME
INTEGRAL'/
&DEVC XB=-4.1000,-4.1000,-2.7800,-0.3800,-0.1800,-
0.1800,POINTS=31,ORIENTATION=0,1,0,ID='FL x:-4.10 z:-0.18',QUANTITY='GAUGE HEAT FLUX
GAS',STATISTICS_START=0,TEMPORAL_STATISTIC='TIME INTEGRAL'/
&DEVC XB=-4.1000,-4.1000,-2.7800,-0.3800,-0.1000,-
0.1000,POINTS=31,ORIENTATION=0,1,0,ID='FL x:-4.10 z:-0.10',QUANTITY='GAUGE HEAT FLUX
GAS',STATISTICS_START=0,TEMPORAL_STATISTIC='TIME INTEGRAL'/
&DEVC XB=-4.1000,-4.1000,-2.7800,-0.3800,-0.0200,-
0.0200,POINTS=31,ORIENTATION=0,1,0,ID='FL x:-4.10 z:-0.02',QUANTITY='GAUGE HEAT FLUX
GAS',STATISTICS_START=0,TEMPORAL_STATISTIC='TIME INTEGRAL'/
&DEVC XB=-4.1000,-4.1000,-2.7800,-
0.3800,0.0200,0.0200,POINTS=31,ORIENTATION=0,1,0,ID='FL x:-4.10
z:0.02',QUANTITY='GAUGE HEAT FLUX GAS',STATISTICS_START=0,TEMPORAL_STATISTIC='TIME
INTEGRAL'/
&DEVC XB=-4.1000,-4.1000,-2.7800,-
0.3800,0.1000,0.1000,POINTS=31,ORIENTATION=0,1,0,ID='FL x:-4.10
z:0.10',QUANTITY='GAUGE HEAT FLUX GAS',STATISTICS_START=0,TEMPORAL_STATISTIC='TIME
INTEGRAL'/
&DEVC XB=-4.1000,-4.1000,-2.7800,-
0.3800,0.1800,0.1800,POINTS=31,ORIENTATION=0,1,0,ID='FL x:-4.10
z:0.18',QUANTITY='GAUGE HEAT FLUX GAS',STATISTICS_START=0,TEMPORAL_STATISTIC='TIME
INTEGRAL'/
```



---

*FDS Input File Templates*

```
&DEVC XB=-3.8200,-3.8200,-2.7800,-0.3800,-0.1800,-
0.1800,POINTS=31,ORIENTATION=0,1,0,ID='FL x:-3.82 z:-0.18',QUANTITY='GAUGE HEAT FLUX
GAS',STATISTICS_START=0,TEMPORAL_STATISTIC='TIME INTEGRAL'/
&DEVC XB=-3.8200,-3.8200,-2.7800,-0.3800,-0.1000,-
0.1000,POINTS=31,ORIENTATION=0,1,0,ID='FL x:-3.82 z:-0.10',QUANTITY='GAUGE HEAT FLUX
GAS',STATISTICS_START=0,TEMPORAL_STATISTIC='TIME INTEGRAL'/
&DEVC XB=-3.8200,-3.8200,-2.7800,-0.3800,-0.0200,-
0.0200,POINTS=31,ORIENTATION=0,1,0,ID='FL x:-3.82 z:-0.02',QUANTITY='GAUGE HEAT FLUX
GAS',STATISTICS_START=0,TEMPORAL_STATISTIC='TIME INTEGRAL'/
&DEVC XB=-3.8200,-3.8200,-2.7800,-
0.3800,0.0200,0.0200,POINTS=31,ORIENTATION=0,1,0,ID='FL x:-3.82
z:0.02',QUANTITY='GAUGE HEAT FLUX GAS',STATISTICS_START=0,TEMPORAL_STATISTIC='TIME
INTEGRAL'/
&DEVC XB=-3.8200,-3.8200,-2.7800,-
0.3800,0.1000,0.1000,POINTS=31,ORIENTATION=0,1,0,ID='FL x:-3.82
z:0.10',QUANTITY='GAUGE HEAT FLUX GAS',STATISTICS_START=0,TEMPORAL_STATISTIC='TIME
INTEGRAL'/
&DEVC XB=-3.8200,-3.8200,-2.7800,-
0.3800,0.1800,0.1800,POINTS=31,ORIENTATION=0,1,0,ID='FL x:-3.82
z:0.18',QUANTITY='GAUGE HEAT FLUX GAS',STATISTICS_START=0,TEMPORAL_STATISTIC='TIME
INTEGRAL'/

&DEVC XB=-4.1800,-4.1800,-2.7800,-
0.3800,0.3000,0.3000,POINTS=31,ORIENTATION=0,1,0,ID='FU x:-4.18
z:0.30',QUANTITY='GAUGE HEAT FLUX GAS',STATISTICS_START=0,TEMPORAL_STATISTIC='TIME
INTEGRAL'/
&DEVC XB=-4.1800,-4.1800,-2.7800,-
0.3800,0.3800,0.3800,POINTS=31,ORIENTATION=0,1,0,ID='FU x:-4.18
z:0.38',QUANTITY='GAUGE HEAT FLUX GAS',STATISTICS_START=0,TEMPORAL_STATISTIC='TIME
INTEGRAL'/
&DEVC XB=-4.1800,-4.1800,-2.7800,-
0.3800,0.4600,0.4600,POINTS=31,ORIENTATION=0,1,0,ID='FU x:-4.18
z:0.46',QUANTITY='GAUGE HEAT FLUX GAS',STATISTICS_START=0,TEMPORAL_STATISTIC='TIME
INTEGRAL'/
&DEVC XB=-4.1800,-4.1800,-2.7800,-
0.3800,0.5000,0.5000,POINTS=31,ORIENTATION=0,1,0,ID='FU x:-4.18
z:0.50',QUANTITY='GAUGE HEAT FLUX GAS',STATISTICS_START=0,TEMPORAL_STATISTIC='TIME
INTEGRAL'/
&DEVC XB=-4.1800,-4.1800,-2.7800,-
0.3800,0.5800,0.5800,POINTS=31,ORIENTATION=0,1,0,ID='FU x:-4.18
z:0.58',QUANTITY='GAUGE HEAT FLUX GAS',STATISTICS_START=0,TEMPORAL_STATISTIC='TIME
INTEGRAL'/
&DEVC XB=-4.1800,-4.1800,-2.7800,-
0.3800,0.6600,0.6600,POINTS=31,ORIENTATION=0,1,0,ID='FU x:-4.18
z:0.66',QUANTITY='GAUGE HEAT FLUX GAS',STATISTICS_START=0,TEMPORAL_STATISTIC='TIME
INTEGRAL'/
&DEVC XB=-4.1000,-4.1000,-2.7800,-
0.3800,0.3000,0.3000,POINTS=31,ORIENTATION=0,1,0,ID='FU x:-4.10
z:0.30',QUANTITY='GAUGE HEAT FLUX GAS',STATISTICS_START=0,TEMPORAL_STATISTIC='TIME
INTEGRAL'/
&DEVC XB=-4.1000,-4.1000,-2.7800,-
0.3800,0.3800,0.3800,POINTS=31,ORIENTATION=0,1,0,ID='FU x:-4.10
z:0.38',QUANTITY='GAUGE HEAT FLUX GAS',STATISTICS_START=0,TEMPORAL_STATISTIC='TIME
INTEGRAL'/
&DEVC XB=-4.1000,-4.1000,-2.7800,-
0.3800,0.4600,0.4600,POINTS=31,ORIENTATION=0,1,0,ID='FU x:-4.10
z:0.46',QUANTITY='GAUGE HEAT FLUX GAS',STATISTICS_START=0,TEMPORAL_STATISTIC='TIME
INTEGRAL'/
&DEVC XB=-4.1000,-4.1000,-2.7800,-
0.3800,0.5000,0.5000,POINTS=31,ORIENTATION=0,1,0,ID='FU x:-4.10
z:0.50',QUANTITY='GAUGE HEAT FLUX GAS',STATISTICS_START=0,TEMPORAL_STATISTIC='TIME
INTEGRAL'/
```

```
&DEVC XB=-4.1000,-4.1000,-2.7800,-  
0.3800,0.5800,0.5800,POINTS=31,ORIENTATION=0,1,0,ID='FU x:-4.10  
z:0.58',QUANTITY='GAUGE HEAT FLUX GAS',STATISTICS_START=0,TEMPORAL_STATISTIC='TIME  
INTEGRAL'/  
&DEVC XB=-4.1000,-4.1000,-2.7800,-  
0.3800,0.6600,0.6600,POINTS=31,ORIENTATION=0,1,0,ID='FU x:-4.10  
z:0.66',QUANTITY='GAUGE HEAT FLUX GAS',STATISTICS_START=0,TEMPORAL_STATISTIC='TIME  
INTEGRAL'/  
&DEVC XB=-4.0200,-4.0200,-2.7800,-  
0.3800,0.3000,0.3000,POINTS=31,ORIENTATION=0,1,0,ID='FU x:-4.02  
z:0.30',QUANTITY='GAUGE HEAT FLUX GAS',STATISTICS_START=0,TEMPORAL_STATISTIC='TIME  
INTEGRAL'/  
&DEVC XB=-4.0200,-4.0200,-2.7800,-  
0.3800,0.3800,0.3800,POINTS=31,ORIENTATION=0,1,0,ID='FU x:-4.02  
z:0.38',QUANTITY='GAUGE HEAT FLUX GAS',STATISTICS_START=0,TEMPORAL_STATISTIC='TIME  
INTEGRAL'/  
&DEVC XB=-4.0200,-4.0200,-2.7800,-  
0.3800,0.4600,0.4600,POINTS=31,ORIENTATION=0,1,0,ID='FU x:-4.02  
z:0.46',QUANTITY='GAUGE HEAT FLUX GAS',STATISTICS_START=0,TEMPORAL_STATISTIC='TIME  
INTEGRAL'/  
&DEVC XB=-4.0200,-4.0200,-2.7800,-  
0.3800,0.5000,0.5000,POINTS=31,ORIENTATION=0,1,0,ID='FU x:-4.02  
z:0.50',QUANTITY='GAUGE HEAT FLUX GAS',STATISTICS_START=0,TEMPORAL_STATISTIC='TIME  
INTEGRAL'/  
&DEVC XB=-4.0200,-4.0200,-2.7800,-  
0.3800,0.5800,0.5800,POINTS=31,ORIENTATION=0,1,0,ID='FU x:-4.02  
z:0.58',QUANTITY='GAUGE HEAT FLUX GAS',STATISTICS_START=0,TEMPORAL_STATISTIC='TIME  
INTEGRAL'/  
&DEVC XB=-4.0200,-4.0200,-2.7800,-  
0.3800,0.6600,0.6600,POINTS=31,ORIENTATION=0,1,0,ID='FU x:-4.02  
z:0.66',QUANTITY='GAUGE HEAT FLUX GAS',STATISTICS_START=0,TEMPORAL_STATISTIC='TIME  
INTEGRAL'/  
&DEVC XB=-3.9800,-3.9800,-2.7800,-  
0.3800,0.3000,0.3000,POINTS=31,ORIENTATION=0,1,0,ID='FU x:-3.98  
z:0.30',QUANTITY='GAUGE HEAT FLUX GAS',STATISTICS_START=0,TEMPORAL_STATISTIC='TIME  
INTEGRAL'/  
&DEVC XB=-3.9800,-3.9800,-2.7800,-  
0.3800,0.3800,0.3800,POINTS=31,ORIENTATION=0,1,0,ID='FU x:-3.98  
z:0.38',QUANTITY='GAUGE HEAT FLUX GAS',STATISTICS_START=0,TEMPORAL_STATISTIC='TIME  
INTEGRAL'/  
&DEVC XB=-3.9800,-3.9800,-2.7800,-  
0.3800,0.4600,0.4600,POINTS=31,ORIENTATION=0,1,0,ID='FU x:-3.98  
z:0.46',QUANTITY='GAUGE HEAT FLUX GAS',STATISTICS_START=0,TEMPORAL_STATISTIC='TIME  
INTEGRAL'/  
&DEVC XB=-3.9800,-3.9800,-2.7800,-  
0.3800,0.5000,0.5000,POINTS=31,ORIENTATION=0,1,0,ID='FU x:-3.98  
z:0.50',QUANTITY='GAUGE HEAT FLUX GAS',STATISTICS_START=0,TEMPORAL_STATISTIC='TIME  
INTEGRAL'/  
&DEVC XB=-3.9800,-3.9800,-2.7800,-  
0.3800,0.5800,0.5800,POINTS=31,ORIENTATION=0,1,0,ID='FU x:-3.98  
z:0.58',QUANTITY='GAUGE HEAT FLUX GAS',STATISTICS_START=0,TEMPORAL_STATISTIC='TIME  
INTEGRAL'/  
&DEVC XB=-3.9800,-3.9800,-2.7800,-  
0.3800,0.6600,0.6600,POINTS=31,ORIENTATION=0,1,0,ID='FU x:-3.98  
z:0.66',QUANTITY='GAUGE HEAT FLUX GAS',STATISTICS_START=0,TEMPORAL_STATISTIC='TIME  
INTEGRAL'/  
&DEVC XB=-3.9000,-3.9000,-2.7800,-  
0.3800,0.3000,0.3000,POINTS=31,ORIENTATION=0,1,0,ID='FU x:-3.90  
z:0.30',QUANTITY='GAUGE HEAT FLUX GAS',STATISTICS_START=0,TEMPORAL_STATISTIC='TIME  
INTEGRAL'/  
&DEVC XB=-3.9000,-3.9000,-2.7800,-  
0.3800,0.3800,0.3800,POINTS=31,ORIENTATION=0,1,0,ID='FU x:-3.90  
z:0.38',QUANTITY='GAUGE HEAT FLUX GAS',STATISTICS_START=0,TEMPORAL_STATISTIC='TIME  
INTEGRAL'/
```

---

*FDS Input File Templates*

```
&DEVC XB=-3.9000,-3.9000,-2.7800,-  
0.3800,0.4600,0.4600,POINTS=31,ORIENTATION=0,1,0,ID='FU x:-3.90  
z:0.46',QUANTITY='GAUGE HEAT FLUX GAS',STATISTICS_START=0,TEMPORAL_STATISTIC='TIME  
INTEGRAL'/  
&DEVC XB=-3.9000,-3.9000,-2.7800,-  
0.3800,0.5000,0.5000,POINTS=31,ORIENTATION=0,1,0,ID='FU x:-3.90  
z:0.50',QUANTITY='GAUGE HEAT FLUX GAS',STATISTICS_START=0,TEMPORAL_STATISTIC='TIME  
INTEGRAL'/  
&DEVC XB=-3.9000,-3.9000,-2.7800,-  
0.3800,0.5800,0.5800,POINTS=31,ORIENTATION=0,1,0,ID='FU x:-3.90  
z:0.58',QUANTITY='GAUGE HEAT FLUX GAS',STATISTICS_START=0,TEMPORAL_STATISTIC='TIME  
INTEGRAL'/  
&DEVC XB=-3.9000,-3.9000,-2.7800,-  
0.3800,0.6600,0.6600,POINTS=31,ORIENTATION=0,1,0,ID='FU x:-3.90  
z:0.66',QUANTITY='GAUGE HEAT FLUX GAS',STATISTICS_START=0,TEMPORAL_STATISTIC='TIME  
INTEGRAL'/  
&DEVC XB=-3.8200,-3.8200,-2.7800,-  
0.3800,0.3000,0.3000,POINTS=31,ORIENTATION=0,1,0,ID='FU x:-3.82  
z:0.30',QUANTITY='GAUGE HEAT FLUX GAS',STATISTICS_START=0,TEMPORAL_STATISTIC='TIME  
INTEGRAL'/  
&DEVC XB=-3.8200,-3.8200,-2.7800,-  
0.3800,0.3800,0.3800,POINTS=31,ORIENTATION=0,1,0,ID='FU x:-3.82  
z:0.38',QUANTITY='GAUGE HEAT FLUX GAS',STATISTICS_START=0,TEMPORAL_STATISTIC='TIME  
INTEGRAL'/  
&DEVC XB=-3.8200,-3.8200,-2.7800,-  
0.3800,0.4600,0.4600,POINTS=31,ORIENTATION=0,1,0,ID='FU x:-3.82  
z:0.46',QUANTITY='GAUGE HEAT FLUX GAS',STATISTICS_START=0,TEMPORAL_STATISTIC='TIME  
INTEGRAL'/  
&DEVC XB=-3.8200,-3.8200,-2.7800,-  
0.3800,0.5000,0.5000,POINTS=31,ORIENTATION=0,1,0,ID='FU x:-3.82  
z:0.50',QUANTITY='GAUGE HEAT FLUX GAS',STATISTICS_START=0,TEMPORAL_STATISTIC='TIME  
INTEGRAL'/  
&DEVC XB=-3.8200,-3.8200,-2.7800,-  
0.3800,0.5800,0.5800,POINTS=31,ORIENTATION=0,1,0,ID='FU x:-3.82  
z:0.58',QUANTITY='GAUGE HEAT FLUX GAS',STATISTICS_START=0,TEMPORAL_STATISTIC='TIME  
INTEGRAL'/  
&DEVC XB=-3.8200,-3.8200,-2.7800,-  
0.3800,0.6600,0.6600,POINTS=31,ORIENTATION=0,1,0,ID='FU x:-3.82  
z:0.66',QUANTITY='GAUGE HEAT FLUX GAS',STATISTICS_START=0,TEMPORAL_STATISTIC='TIME  
INTEGRAL'/  
  
&DEVC XB=-0.1800,-0.1800,-0.1800,-0.1800,-2.7000,-  
0.3000,POINTS=31,ORIENTATION=0,0,1,ID='BL x:-0.18 y:-0.18',QUANTITY='GAUGE HEAT FLUX  
GAS',STATISTICS_START=0,TEMPORAL_STATISTIC='TIME INTEGRAL'/  
&DEVC XB=-0.1800,-0.1800,-0.1000,-0.1000,-2.7000,-  
0.3000,POINTS=31,ORIENTATION=0,0,1,ID='BL x:-0.18 y:-0.10',QUANTITY='GAUGE HEAT FLUX  
GAS',STATISTICS_START=0,TEMPORAL_STATISTIC='TIME INTEGRAL'/  
&DEVC XB=-0.1800,-0.1800,-0.0200,-0.0200,-2.7000,-  
0.3000,POINTS=31,ORIENTATION=0,0,1,ID='BL x:-0.18 y:-0.02',QUANTITY='GAUGE HEAT FLUX  
GAS',STATISTICS_START=0,TEMPORAL_STATISTIC='TIME INTEGRAL'/  
&DEVC XB=-0.1800,-0.1800,0.0200,0.0200,-2.7000,-  
0.3000,POINTS=31,ORIENTATION=0,0,1,ID='BL x:-0.18 y:0.02',QUANTITY='GAUGE HEAT FLUX  
GAS',STATISTICS_START=0,TEMPORAL_STATISTIC='TIME INTEGRAL'/  
&DEVC XB=-0.1800,-0.1800,0.1000,0.1000,-2.7000,-  
0.3000,POINTS=31,ORIENTATION=0,0,1,ID='BL x:-0.18 y:0.10',QUANTITY='GAUGE HEAT FLUX  
GAS',STATISTICS_START=0,TEMPORAL_STATISTIC='TIME INTEGRAL'/  
&DEVC XB=-0.1800,-0.1800,0.1800,0.1800,-2.7000,-  
0.3000,POINTS=31,ORIENTATION=0,0,1,ID='BL x:-0.18 y:0.18',QUANTITY='GAUGE HEAT FLUX  
GAS',STATISTICS_START=0,TEMPORAL_STATISTIC='TIME INTEGRAL'/  
&DEVC XB=-0.1000,-0.1000,-0.1800,-0.1800,-2.7000,-  
0.3000,POINTS=31,ORIENTATION=0,0,1,ID='BL x:-0.10 y:-0.18',QUANTITY='GAUGE HEAT FLUX  
GAS',STATISTICS_START=0,TEMPORAL_STATISTIC='TIME INTEGRAL'/
```



---

## FDS Input File Templates

```
&DEVC XB=0.1000,0.1000,0.1000,0.1000,-2.7000,-
0.3000,POINTS=31,ORIENTATION=0,0,1,ID='BL x:0.10 y:0.10',QUANTITY='GAUGE HEAT FLUX
GAS',STATISTICS_START=0,TEMPORAL_STATISTIC='TIME INTEGRAL' /
&DEVC XB=0.1000,0.1000,0.1800,0.1800,-2.7000,-
0.3000,POINTS=31,ORIENTATION=0,0,1,ID='BL x:0.10 y:0.18',QUANTITY='GAUGE HEAT FLUX
GAS',STATISTICS_START=0,TEMPORAL_STATISTIC='TIME INTEGRAL' /
&DEVC XB=0.1800,0.1800,-0.1800,-0.1800,-2.7000,-
0.3000,POINTS=31,ORIENTATION=0,0,1,ID='BL x:0.18 y:-0.18',QUANTITY='GAUGE HEAT FLUX
GAS',STATISTICS_START=0,TEMPORAL_STATISTIC='TIME INTEGRAL' /
&DEVC XB=0.1800,0.1800,-0.1000,-0.1000,-2.7000,-
0.3000,POINTS=31,ORIENTATION=0,0,1,ID='BL x:0.18 y:-0.10',QUANTITY='GAUGE HEAT FLUX
GAS',STATISTICS_START=0,TEMPORAL_STATISTIC='TIME INTEGRAL' /
&DEVC XB=0.1800,0.1800,-0.0200,-0.0200,-2.7000,-
0.3000,POINTS=31,ORIENTATION=0,0,1,ID='BL x:0.18 y:-0.02',QUANTITY='GAUGE HEAT FLUX
GAS',STATISTICS_START=0,TEMPORAL_STATISTIC='TIME INTEGRAL' /
&DEVC XB=0.1800,0.1800,0.0200,0.0200,-2.7000,-
0.3000,POINTS=31,ORIENTATION=0,0,1,ID='BL x:0.18 y:0.02',QUANTITY='GAUGE HEAT FLUX
GAS',STATISTICS_START=0,TEMPORAL_STATISTIC='TIME INTEGRAL' /
&DEVC XB=0.1800,0.1800,0.1000,0.1000,-2.7000,-
0.3000,POINTS=31,ORIENTATION=0,0,1,ID='BL x:0.18 y:0.10',QUANTITY='GAUGE HEAT FLUX
GAS',STATISTICS_START=0,TEMPORAL_STATISTIC='TIME INTEGRAL' /
&DEVC XB=0.1800,0.1800,0.1800,0.1800,-2.7000,-
0.3000,POINTS=31,ORIENTATION=0,0,1,ID='BL x:0.18 y:0.18',QUANTITY='GAUGE HEAT FLUX
GAS',STATISTICS_START=0,TEMPORAL_STATISTIC='TIME INTEGRAL' /

&DEVC XB=-0.1800,-0.1800,-0.1800,-0.1800,0.3000,2.7000,POINTS=31,ORIENTATION=0,0,-
1,ID='AB x:-0.18 y:-0.18',QUANTITY='GAUGE HEAT FLUX
GAS',STATISTICS_START=0,TEMPORAL_STATISTIC='TIME INTEGRAL' /
&DEVC XB=-0.1800,-0.1800,-0.1000,-0.1000,0.3000,2.7000,POINTS=31,ORIENTATION=0,0,-
1,ID='AB x:-0.18 y:-0.10',QUANTITY='GAUGE HEAT FLUX
GAS',STATISTICS_START=0,TEMPORAL_STATISTIC='TIME INTEGRAL' /
&DEVC XB=-0.1800,-0.1800,-0.0200,-0.0200,0.3000,2.7000,POINTS=31,ORIENTATION=0,0,-
1,ID='AB x:-0.18 y:-0.02',QUANTITY='GAUGE HEAT FLUX
GAS',STATISTICS_START=0,TEMPORAL_STATISTIC='TIME INTEGRAL' /
&DEVC XB=-0.1800,-0.1800,0.0200,0.0200,0.3000,2.7000,POINTS=31,ORIENTATION=0,0,-
1,ID='AB x:-0.18 y:0.02',QUANTITY='GAUGE HEAT FLUX
GAS',STATISTICS_START=0,TEMPORAL_STATISTIC='TIME INTEGRAL' /
&DEVC XB=-0.1800,-0.1800,0.1000,0.1000,0.3000,2.7000,POINTS=31,ORIENTATION=0,0,-
1,ID='AB x:-0.18 y:0.10',QUANTITY='GAUGE HEAT FLUX
GAS',STATISTICS_START=0,TEMPORAL_STATISTIC='TIME INTEGRAL' /
&DEVC XB=-0.1800,-0.1800,0.1800,0.1800,0.3000,2.7000,POINTS=31,ORIENTATION=0,0,-
1,ID='AB x:-0.18 y:0.18',QUANTITY='GAUGE HEAT FLUX
GAS',STATISTICS_START=0,TEMPORAL_STATISTIC='TIME INTEGRAL' /
&DEVC XB=-0.1000,-0.1000,-0.1800,-0.1800,0.3000,2.7000,POINTS=31,ORIENTATION=0,0,-
1,ID='AB x:-0.10 y:-0.18',QUANTITY='GAUGE HEAT FLUX
GAS',STATISTICS_START=0,TEMPORAL_STATISTIC='TIME INTEGRAL' /
&DEVC XB=-0.1000,-0.1000,-0.1000,-0.1000,0.3000,2.7000,POINTS=31,ORIENTATION=0,0,-
1,ID='AB x:-0.10 y:-0.10',QUANTITY='GAUGE HEAT FLUX
GAS',STATISTICS_START=0,TEMPORAL_STATISTIC='TIME INTEGRAL' /
&DEVC XB=-0.1000,-0.1000,-0.0200,-0.0200,0.3000,2.7000,POINTS=31,ORIENTATION=0,0,-
1,ID='AB x:-0.10 y:-0.02',QUANTITY='GAUGE HEAT FLUX
GAS',STATISTICS_START=0,TEMPORAL_STATISTIC='TIME INTEGRAL' /
&DEVC XB=-0.1000,-0.1000,0.0200,0.0200,0.3000,2.7000,POINTS=31,ORIENTATION=0,0,-
1,ID='AB x:-0.10 y:0.02',QUANTITY='GAUGE HEAT FLUX
GAS',STATISTICS_START=0,TEMPORAL_STATISTIC='TIME INTEGRAL' /
&DEVC XB=-0.1000,-0.1000,0.1000,0.1000,0.3000,2.7000,POINTS=31,ORIENTATION=0,0,-
1,ID='AB x:-0.10 y:0.10',QUANTITY='GAUGE HEAT FLUX
GAS',STATISTICS_START=0,TEMPORAL_STATISTIC='TIME INTEGRAL' /
&DEVC XB=-0.1000,-0.1000,0.1800,0.1800,0.3000,2.7000,POINTS=31,ORIENTATION=0,0,-
1,ID='AB x:-0.10 y:0.18',QUANTITY='GAUGE HEAT FLUX
GAS',STATISTICS_START=0,TEMPORAL_STATISTIC='TIME INTEGRAL' /
```



---

## FDS Input File Templates

```
&DEVC XB=0.1800,0.1800,0.0200,0.0200,0.3000,2.7000,POINTS=31,ORIENTATION=0,0,-1,ID=' AB
x:0.18 y:0.02',QUANTITY='GAUGE HEAT FLUX
GAS',STATISTICS_START=0,TEMPORAL_STATISTIC='TIME INTEGRAL' /
&DEVC XB=0.1800,0.1800,0.1000,0.1000,0.3000,2.7000,POINTS=31,ORIENTATION=0,0,-1,ID=' AB
x:0.18 y:0.10',QUANTITY='GAUGE HEAT FLUX
GAS',STATISTICS_START=0,TEMPORAL_STATISTIC='TIME INTEGRAL' /
&DEVC XB=0.1800,0.1800,0.1800,0.1800,0.3000,2.7000,POINTS=31,ORIENTATION=0,0,-1,ID=' AB
x:0.18 y:0.18',QUANTITY='GAUGE HEAT FLUX
GAS',STATISTICS_START=0,TEMPORAL_STATISTIC='TIME INTEGRAL' /

&DEVC XB=-0.1800,-0.1800,-2.7800,-0.3800,-0.1800,-
0.1800,POINTS=31,ORIENTATION=0,1,0,ID=' FR x:-0.18 z:-0.18',QUANTITY='GAUGE HEAT FLUX
GAS',STATISTICS_START=0,TEMPORAL_STATISTIC='TIME INTEGRAL' /
&DEVC XB=-0.1800,-0.1800,-2.7800,-0.3800,-0.1000,-
0.1000,POINTS=31,ORIENTATION=0,1,0,ID=' FR x:-0.18 z:-0.10',QUANTITY='GAUGE HEAT FLUX
GAS',STATISTICS_START=0,TEMPORAL_STATISTIC='TIME INTEGRAL' /
&DEVC XB=-0.1800,-0.1800,-2.7800,-0.3800,-0.0200,-
0.0200,POINTS=31,ORIENTATION=0,1,0,ID=' FR x:-0.18 z:-0.02',QUANTITY='GAUGE HEAT FLUX
GAS',STATISTICS_START=0,TEMPORAL_STATISTIC='TIME INTEGRAL' /
&DEVC XB=-0.1800,-0.1800,-2.7800,-
0.3800,0.0200,0.0200,POINTS=31,ORIENTATION=0,1,0,ID=' FR x:-0.18
z:0.02',QUANTITY='GAUGE HEAT FLUX GAS',STATISTICS_START=0,TEMPORAL_STATISTIC='TIME
INTEGRAL' /
&DEVC XB=-0.1800,-0.1800,-2.7800,-
0.3800,0.1000,0.1000,POINTS=31,ORIENTATION=0,1,0,ID=' FR x:-0.18
z:0.10',QUANTITY='GAUGE HEAT FLUX GAS',STATISTICS_START=0,TEMPORAL_STATISTIC='TIME
INTEGRAL' /
&DEVC XB=-0.1800,-0.1800,-2.7800,-
0.3800,0.1800,0.1800,POINTS=31,ORIENTATION=0,1,0,ID=' FR x:-0.18
z:0.18',QUANTITY='GAUGE HEAT FLUX GAS',STATISTICS_START=0,TEMPORAL_STATISTIC='TIME
INTEGRAL' /
&DEVC XB=-0.1000,-0.1000,-2.7800,-0.3800,-0.1800,-
0.1800,POINTS=31,ORIENTATION=0,1,0,ID=' FR x:-0.10 z:-0.18',QUANTITY='GAUGE HEAT FLUX
GAS',STATISTICS_START=0,TEMPORAL_STATISTIC='TIME INTEGRAL' /
&DEVC XB=-0.1000,-0.1000,-2.7800,-0.3800,-0.1000,-
0.1000,POINTS=31,ORIENTATION=0,1,0,ID=' FR x:-0.10 z:-0.10',QUANTITY='GAUGE HEAT FLUX
GAS',STATISTICS_START=0,TEMPORAL_STATISTIC='TIME INTEGRAL' /
&DEVC XB=-0.1000,-0.1000,-2.7800,-0.3800,-0.0200,-
0.0200,POINTS=31,ORIENTATION=0,1,0,ID=' FR x:-0.10 z:-0.02',QUANTITY='GAUGE HEAT FLUX
GAS',STATISTICS_START=0,TEMPORAL_STATISTIC='TIME INTEGRAL' /
&DEVC XB=-0.1000,-0.1000,-2.7800,-
0.3800,0.0200,0.0200,POINTS=31,ORIENTATION=0,1,0,ID=' FR x:-0.10
z:0.02',QUANTITY='GAUGE HEAT FLUX GAS',STATISTICS_START=0,TEMPORAL_STATISTIC='TIME
INTEGRAL' /
&DEVC XB=-0.1000,-0.1000,-2.7800,-
0.3800,0.1000,0.1000,POINTS=31,ORIENTATION=0,1,0,ID=' FR x:-0.10
z:0.10',QUANTITY='GAUGE HEAT FLUX GAS',STATISTICS_START=0,TEMPORAL_STATISTIC='TIME
INTEGRAL' /
&DEVC XB=-0.1000,-0.1000,-2.7800,-
0.3800,0.1800,0.1800,POINTS=31,ORIENTATION=0,1,0,ID=' FR x:-0.10
z:0.18',QUANTITY='GAUGE HEAT FLUX GAS',STATISTICS_START=0,TEMPORAL_STATISTIC='TIME
INTEGRAL' /
&DEVC XB=-0.0200,-0.0200,-2.7800,-0.3800,-0.1800,-
0.1800,POINTS=31,ORIENTATION=0,1,0,ID=' FR x:-0.02 z:-0.18',QUANTITY='GAUGE HEAT FLUX
GAS',STATISTICS_START=0,TEMPORAL_STATISTIC='TIME INTEGRAL' /
&DEVC XB=-0.0200,-0.0200,-2.7800,-0.3800,-0.1000,-
0.1000,POINTS=31,ORIENTATION=0,1,0,ID=' FR x:-0.02 z:-0.10',QUANTITY='GAUGE HEAT FLUX
GAS',STATISTICS_START=0,TEMPORAL_STATISTIC='TIME INTEGRAL' /
&DEVC XB=-0.0200,-0.0200,-2.7800,-0.3800,-0.0200,-
0.0200,POINTS=31,ORIENTATION=0,1,0,ID=' FR x:-0.02 z:-0.02',QUANTITY='GAUGE HEAT FLUX
GAS',STATISTICS_START=0,TEMPORAL_STATISTIC='TIME INTEGRAL' /
&DEVC XB=-0.0200,-0.0200,-2.7800,-
0.3800,0.0200,0.0200,POINTS=31,ORIENTATION=0,1,0,ID=' FR x:-0.02
```





```

&DEVC XB=0.0200,0.0200,0.3800,2.7800,-0.0200,-0.0200,POINTS=31,ORIENTATION=0,-
1,0,ID='BK x:0.02 z:-0.02',QUANTITY='GAUGE HEAT FLUX
GAS',STATISTICS_START=0,TEMPORAL_STATISTIC='TIME INTEGRAL'/
&DEVC XB=0.0200,0.0200,0.3800,2.7800,0.0200,0.0200,POINTS=31,ORIENTATION=0,-1,0,ID='BK
x:0.02 z:0.02',QUANTITY='GAUGE HEAT FLUX
GAS',STATISTICS_START=0,TEMPORAL_STATISTIC='TIME INTEGRAL'/
&DEVC XB=0.0200,0.0200,0.3800,2.7800,0.1000,0.1000,POINTS=31,ORIENTATION=0,-1,0,ID='BK
x:0.02 z:0.10',QUANTITY='GAUGE HEAT FLUX
GAS',STATISTICS_START=0,TEMPORAL_STATISTIC='TIME INTEGRAL'/
&DEVC XB=0.0200,0.0200,0.3800,2.7800,0.1800,0.1800,POINTS=31,ORIENTATION=0,-1,0,ID='BK
x:0.02 z:0.18',QUANTITY='GAUGE HEAT FLUX
GAS',STATISTICS_START=0,TEMPORAL_STATISTIC='TIME INTEGRAL'/
&DEVC XB=0.1000,0.1000,0.3800,2.7800,-0.1800,-0.1800,POINTS=31,ORIENTATION=0,-
1,0,ID='BK x:0.10 z:-0.18',QUANTITY='GAUGE HEAT FLUX
GAS',STATISTICS_START=0,TEMPORAL_STATISTIC='TIME INTEGRAL'/
&DEVC XB=0.1000,0.1000,0.3800,2.7800,-0.1000,-0.1000,POINTS=31,ORIENTATION=0,-
1,0,ID='BK x:0.10 z:-0.10',QUANTITY='GAUGE HEAT FLUX
GAS',STATISTICS_START=0,TEMPORAL_STATISTIC='TIME INTEGRAL'/
&DEVC XB=0.1000,0.1000,0.3800,2.7800,-0.0200,-0.0200,POINTS=31,ORIENTATION=0,-
1,0,ID='BK x:0.10 z:-0.02',QUANTITY='GAUGE HEAT FLUX
GAS',STATISTICS_START=0,TEMPORAL_STATISTIC='TIME INTEGRAL'/
&DEVC XB=0.1000,0.1000,0.3800,2.7800,0.0200,0.0200,POINTS=31,ORIENTATION=0,-1,0,ID='BK
x:0.10 z:0.02',QUANTITY='GAUGE HEAT FLUX
GAS',STATISTICS_START=0,TEMPORAL_STATISTIC='TIME INTEGRAL'/
&DEVC XB=0.1000,0.1000,0.3800,2.7800,0.1000,0.1000,POINTS=31,ORIENTATION=0,-1,0,ID='BK
x:0.10 z:0.10',QUANTITY='GAUGE HEAT FLUX
GAS',STATISTICS_START=0,TEMPORAL_STATISTIC='TIME INTEGRAL'/
&DEVC XB=0.1000,0.1000,0.3800,2.7800,0.1800,0.1800,POINTS=31,ORIENTATION=0,-1,0,ID='BK
x:0.10 z:0.18',QUANTITY='GAUGE HEAT FLUX
GAS',STATISTICS_START=0,TEMPORAL_STATISTIC='TIME INTEGRAL'/
&DEVC XB=0.1800,0.1800,0.3800,2.7800,-0.1800,-0.1800,POINTS=31,ORIENTATION=0,-
1,0,ID='BK x:0.18 z:-0.18',QUANTITY='GAUGE HEAT FLUX
GAS',STATISTICS_START=0,TEMPORAL_STATISTIC='TIME INTEGRAL'/
&DEVC XB=0.1800,0.1800,0.3800,2.7800,-0.1000,-0.1000,POINTS=31,ORIENTATION=0,-
1,0,ID='BK x:0.18 z:-0.10',QUANTITY='GAUGE HEAT FLUX
GAS',STATISTICS_START=0,TEMPORAL_STATISTIC='TIME INTEGRAL'/
&DEVC XB=0.1800,0.1800,0.3800,2.7800,-0.0200,-0.0200,POINTS=31,ORIENTATION=0,-
1,0,ID='BK x:0.18 z:-0.02',QUANTITY='GAUGE HEAT FLUX
GAS',STATISTICS_START=0,TEMPORAL_STATISTIC='TIME INTEGRAL'/
&DEVC XB=0.1800,0.1800,0.3800,2.7800,0.0200,0.0200,POINTS=31,ORIENTATION=0,-1,0,ID='BK
x:0.18 z:0.02',QUANTITY='GAUGE HEAT FLUX
GAS',STATISTICS_START=0,TEMPORAL_STATISTIC='TIME INTEGRAL'/
&DEVC XB=0.1800,0.1800,0.3800,2.7800,0.1000,0.1000,POINTS=31,ORIENTATION=0,-1,0,ID='BK
x:0.18 z:0.10',QUANTITY='GAUGE HEAT FLUX
GAS',STATISTICS_START=0,TEMPORAL_STATISTIC='TIME INTEGRAL'/
&DEVC XB=0.1800,0.1800,0.3800,2.7800,0.1800,0.1800,POINTS=31,ORIENTATION=0,-1,0,ID='BK
x:0.18 z:0.18',QUANTITY='GAUGE HEAT FLUX
GAS',STATISTICS_START=0,TEMPORAL_STATISTIC='TIME INTEGRAL'/

&DEVC XB=3.8200,3.8200,-0.1800,-0.1800,-2.7000,-
0.3000,POINTS=31,ORIENTATION=0,0,1,ID='BL x:3.82 y:-0.18',QUANTITY='GAUGE HEAT FLUX
GAS',STATISTICS_START=0,TEMPORAL_STATISTIC='TIME INTEGRAL'/
&DEVC XB=3.8200,3.8200,-0.1000,-0.1000,-2.7000,-
0.3000,POINTS=31,ORIENTATION=0,0,1,ID='BL x:3.82 y:-0.10',QUANTITY='GAUGE HEAT FLUX
GAS',STATISTICS_START=0,TEMPORAL_STATISTIC='TIME INTEGRAL'/
&DEVC XB=3.8200,3.8200,-0.0200,-0.0200,-2.7000,-
0.3000,POINTS=31,ORIENTATION=0,0,1,ID='BL x:3.82 y:-0.02',QUANTITY='GAUGE HEAT FLUX
GAS',STATISTICS_START=0,TEMPORAL_STATISTIC='TIME INTEGRAL'/
&DEVC XB=3.8200,3.8200,0.0200,0.0200,-2.7000,-
0.3000,POINTS=31,ORIENTATION=0,0,1,ID='BL x:3.82 y:0.02',QUANTITY='GAUGE HEAT FLUX
GAS',STATISTICS_START=0,TEMPORAL_STATISTIC='TIME INTEGRAL'/
&DEVC XB=3.8200,3.8200,0.1000,0.1000,-2.7000,-
0.3000,POINTS=31,ORIENTATION=0,0,1,ID='BL x:3.82 y:0.10',QUANTITY='GAUGE HEAT FLUX
GAS',STATISTICS_START=0,TEMPORAL_STATISTIC='TIME INTEGRAL'/

```



```

&DEVC XB=4.1000,4.1000,-0.0200,-0.0200,-2.7000,-
0.3000,POINTS=31,ORIENTATION=0,0,1,ID='BL x:4.10 y:-0.02',QUANTITY='GAUGE HEAT FLUX
GAS',STATISTICS_START=0,TEMPORAL_STATISTIC='TIME INTEGRAL'/
&DEVC XB=4.1000,4.1000,0.0200,0.0200,-2.7000,-
0.3000,POINTS=31,ORIENTATION=0,0,1,ID='BL x:4.10 y:0.02',QUANTITY='GAUGE HEAT FLUX
GAS',STATISTICS_START=0,TEMPORAL_STATISTIC='TIME INTEGRAL'/
&DEVC XB=4.1000,4.1000,0.1000,0.1000,-2.7000,-
0.3000,POINTS=31,ORIENTATION=0,0,1,ID='BL x:4.10 y:0.10',QUANTITY='GAUGE HEAT FLUX
GAS',STATISTICS_START=0,TEMPORAL_STATISTIC='TIME INTEGRAL'/
&DEVC XB=4.1000,4.1000,0.1800,0.1800,-2.7000,-
0.3000,POINTS=31,ORIENTATION=0,0,1,ID='BL x:4.10 y:0.18',QUANTITY='GAUGE HEAT FLUX
GAS',STATISTICS_START=0,TEMPORAL_STATISTIC='TIME INTEGRAL'/
&DEVC XB=4.1800,4.1800,-0.1800,-0.1800,-2.7000,-
0.3000,POINTS=31,ORIENTATION=0,0,1,ID='BL x:4.18 y:-0.18',QUANTITY='GAUGE HEAT FLUX
GAS',STATISTICS_START=0,TEMPORAL_STATISTIC='TIME INTEGRAL'/
&DEVC XB=4.1800,4.1800,-0.1000,-0.1000,-2.7000,-
0.3000,POINTS=31,ORIENTATION=0,0,1,ID='BL x:4.18 y:-0.10',QUANTITY='GAUGE HEAT FLUX
GAS',STATISTICS_START=0,TEMPORAL_STATISTIC='TIME INTEGRAL'/
&DEVC XB=4.1800,4.1800,-0.0200,-0.0200,-2.7000,-
0.3000,POINTS=31,ORIENTATION=0,0,1,ID='BL x:4.18 y:-0.02',QUANTITY='GAUGE HEAT FLUX
GAS',STATISTICS_START=0,TEMPORAL_STATISTIC='TIME INTEGRAL'/
&DEVC XB=4.1800,4.1800,0.0200,0.0200,-2.7000,-
0.3000,POINTS=31,ORIENTATION=0,0,1,ID='BL x:4.18 y:0.02',QUANTITY='GAUGE HEAT FLUX
GAS',STATISTICS_START=0,TEMPORAL_STATISTIC='TIME INTEGRAL'/
&DEVC XB=4.1800,4.1800,0.1000,0.1000,-2.7000,-
0.3000,POINTS=31,ORIENTATION=0,0,1,ID='BL x:4.18 y:0.10',QUANTITY='GAUGE HEAT FLUX
GAS',STATISTICS_START=0,TEMPORAL_STATISTIC='TIME INTEGRAL'/
&DEVC XB=4.1800,4.1800,0.1800,0.1800,-2.7000,-
0.3000,POINTS=31,ORIENTATION=0,0,1,ID='BL x:4.18 y:0.18',QUANTITY='GAUGE HEAT FLUX
GAS',STATISTICS_START=0,TEMPORAL_STATISTIC='TIME INTEGRAL'/

```

```

&DEVC XB=3.8200,3.8200,-2.7800,-0.3800,-0.1800,-
0.1800,POINTS=31,ORIENTATION=0,1,0,ID='FR x:3.82 z:-0.18',QUANTITY='GAUGE HEAT FLUX
GAS',STATISTICS_START=0,TEMPORAL_STATISTIC='TIME INTEGRAL'/
&DEVC XB=3.8200,3.8200,-2.7800,-0.3800,-0.1000,-
0.1000,POINTS=31,ORIENTATION=0,1,0,ID='FR x:3.82 z:-0.10',QUANTITY='GAUGE HEAT FLUX
GAS',STATISTICS_START=0,TEMPORAL_STATISTIC='TIME INTEGRAL'/
&DEVC XB=3.8200,3.8200,-2.7800,-0.3800,-0.0200,-
0.0200,POINTS=31,ORIENTATION=0,1,0,ID='FR x:3.82 z:-0.02',QUANTITY='GAUGE HEAT FLUX
GAS',STATISTICS_START=0,TEMPORAL_STATISTIC='TIME INTEGRAL'/
&DEVC XB=3.8200,3.8200,-2.7800,-
0.3800,0.0200,0.0200,POINTS=31,ORIENTATION=0,1,0,ID='FR x:3.82 z:0.02',QUANTITY='GAUGE
HEAT FLUX GAS',STATISTICS_START=0,TEMPORAL_STATISTIC='TIME INTEGRAL'/
&DEVC XB=3.8200,3.8200,-2.7800,-
0.3800,0.1000,0.1000,POINTS=31,ORIENTATION=0,1,0,ID='FR x:3.82 z:0.10',QUANTITY='GAUGE
HEAT FLUX GAS',STATISTICS_START=0,TEMPORAL_STATISTIC='TIME INTEGRAL'/
&DEVC XB=3.8200,3.8200,-2.7800,-
0.3800,0.1800,0.1800,POINTS=31,ORIENTATION=0,1,0,ID='FR x:3.82 z:0.18',QUANTITY='GAUGE
HEAT FLUX GAS',STATISTICS_START=0,TEMPORAL_STATISTIC='TIME INTEGRAL'/
&DEVC XB=3.9000,3.9000,-2.7800,-0.3800,-0.1800,-
0.1800,POINTS=31,ORIENTATION=0,1,0,ID='FR x:3.90 z:-0.18',QUANTITY='GAUGE HEAT FLUX
GAS',STATISTICS_START=0,TEMPORAL_STATISTIC='TIME INTEGRAL'/
&DEVC XB=3.9000,3.9000,-2.7800,-0.3800,-0.1000,-
0.1000,POINTS=31,ORIENTATION=0,1,0,ID='FR x:3.90 z:-0.10',QUANTITY='GAUGE HEAT FLUX
GAS',STATISTICS_START=0,TEMPORAL_STATISTIC='TIME INTEGRAL'/
&DEVC XB=3.9000,3.9000,-2.7800,-0.3800,-0.0200,-
0.0200,POINTS=31,ORIENTATION=0,1,0,ID='FR x:3.90 z:-0.02',QUANTITY='GAUGE HEAT FLUX
GAS',STATISTICS_START=0,TEMPORAL_STATISTIC='TIME INTEGRAL'/
&DEVC XB=3.9000,3.9000,-2.7800,-
0.3800,0.0200,0.0200,POINTS=31,ORIENTATION=0,1,0,ID='FR x:3.90 z:0.02',QUANTITY='GAUGE
HEAT FLUX GAS',STATISTICS_START=0,TEMPORAL_STATISTIC='TIME INTEGRAL'/

```



```

&DEVC XB=4.1800,4.1800,-2.7800,-0.3800,-0.1000,-
0.1000,POINTS=31,ORIENTATION=0,1,0,ID='FR x:4.18 z:-0.10',QUANTITY='GAUGE HEAT FLUX
GAS',STATISTICS_START=0,TEMPORAL_STATISTIC='TIME INTEGRAL'/
&DEVC XB=4.1800,4.1800,-2.7800,-0.3800,-0.0200,-
0.0200,POINTS=31,ORIENTATION=0,1,0,ID='FR x:4.18 z:-0.02',QUANTITY='GAUGE HEAT FLUX
GAS',STATISTICS_START=0,TEMPORAL_STATISTIC='TIME INTEGRAL'/
&DEVC XB=4.1800,4.1800,-2.7800,-
0.3800,0.0200,0.0200,POINTS=31,ORIENTATION=0,1,0,ID='FR x:4.18 z:0.02',QUANTITY='GAUGE
HEAT FLUX GAS',STATISTICS_START=0,TEMPORAL_STATISTIC='TIME INTEGRAL'/
&DEVC XB=4.1800,4.1800,-2.7800,-
0.3800,0.1000,0.1000,POINTS=31,ORIENTATION=0,1,0,ID='FR x:4.18 z:0.10',QUANTITY='GAUGE
HEAT FLUX GAS',STATISTICS_START=0,TEMPORAL_STATISTIC='TIME INTEGRAL'/
&DEVC XB=4.1800,4.1800,-2.7800,-
0.3800,0.1800,0.1800,POINTS=31,ORIENTATION=0,1,0,ID='FR x:4.18 z:0.18',QUANTITY='GAUGE
HEAT FLUX GAS',STATISTICS_START=0,TEMPORAL_STATISTIC='TIME INTEGRAL'/

&DEVC XB=3.8200,3.8200,0.3800,2.7800,-0.1800,-0.1800,POINTS=31,ORIENTATION=0,-
1,0,ID='BK x:3.82 z:-0.18',QUANTITY='GAUGE HEAT FLUX
GAS',STATISTICS_START=0,TEMPORAL_STATISTIC='TIME INTEGRAL'/
&DEVC XB=3.8200,3.8200,0.3800,2.7800,-0.1000,-0.1000,POINTS=31,ORIENTATION=0,-
1,0,ID='BK x:3.82 z:-0.10',QUANTITY='GAUGE HEAT FLUX
GAS',STATISTICS_START=0,TEMPORAL_STATISTIC='TIME INTEGRAL'/
&DEVC XB=3.8200,3.8200,0.3800,2.7800,-0.0200,-0.0200,POINTS=31,ORIENTATION=0,-
1,0,ID='BK x:3.82 z:-0.02',QUANTITY='GAUGE HEAT FLUX
GAS',STATISTICS_START=0,TEMPORAL_STATISTIC='TIME INTEGRAL'/
&DEVC XB=3.8200,3.8200,0.3800,2.7800,0.0200,0.0200,POINTS=31,ORIENTATION=0,-1,0,ID='BK
x:3.82 z:0.02',QUANTITY='GAUGE HEAT FLUX
GAS',STATISTICS_START=0,TEMPORAL_STATISTIC='TIME INTEGRAL'/
&DEVC XB=3.8200,3.8200,0.3800,2.7800,0.1000,0.1000,POINTS=31,ORIENTATION=0,-1,0,ID='BK
x:3.82 z:0.10',QUANTITY='GAUGE HEAT FLUX
GAS',STATISTICS_START=0,TEMPORAL_STATISTIC='TIME INTEGRAL'/
&DEVC XB=3.8200,3.8200,0.3800,2.7800,0.1800,0.1800,POINTS=31,ORIENTATION=0,-1,0,ID='BK
x:3.82 z:0.18',QUANTITY='GAUGE HEAT FLUX
GAS',STATISTICS_START=0,TEMPORAL_STATISTIC='TIME INTEGRAL'/
&DEVC XB=3.9000,3.9000,0.3800,2.7800,-0.1800,-0.1800,POINTS=31,ORIENTATION=0,-
1,0,ID='BK x:3.90 z:-0.18',QUANTITY='GAUGE HEAT FLUX
GAS',STATISTICS_START=0,TEMPORAL_STATISTIC='TIME INTEGRAL'/
&DEVC XB=3.9000,3.9000,0.3800,2.7800,-0.1000,-0.1000,POINTS=31,ORIENTATION=0,-
1,0,ID='BK x:3.90 z:-0.10',QUANTITY='GAUGE HEAT FLUX
GAS',STATISTICS_START=0,TEMPORAL_STATISTIC='TIME INTEGRAL'/
&DEVC XB=3.9000,3.9000,0.3800,2.7800,-0.0200,-0.0200,POINTS=31,ORIENTATION=0,-
1,0,ID='BK x:3.90 z:-0.02',QUANTITY='GAUGE HEAT FLUX
GAS',STATISTICS_START=0,TEMPORAL_STATISTIC='TIME INTEGRAL'/
&DEVC XB=3.9000,3.9000,0.3800,2.7800,0.0200,0.0200,POINTS=31,ORIENTATION=0,-1,0,ID='BK
x:3.90 z:0.02',QUANTITY='GAUGE HEAT FLUX
GAS',STATISTICS_START=0,TEMPORAL_STATISTIC='TIME INTEGRAL'/
&DEVC XB=3.9000,3.9000,0.3800,2.7800,0.1000,0.1000,POINTS=31,ORIENTATION=0,-1,0,ID='BK
x:3.90 z:0.10',QUANTITY='GAUGE HEAT FLUX
GAS',STATISTICS_START=0,TEMPORAL_STATISTIC='TIME INTEGRAL'/
&DEVC XB=3.9000,3.9000,0.3800,2.7800,0.1800,0.1800,POINTS=31,ORIENTATION=0,-1,0,ID='BK
x:3.90 z:0.18',QUANTITY='GAUGE HEAT FLUX
GAS',STATISTICS_START=0,TEMPORAL_STATISTIC='TIME INTEGRAL'/
&DEVC XB=3.9800,3.9800,0.3800,2.7800,-0.1800,-0.1800,POINTS=31,ORIENTATION=0,-
1,0,ID='BK x:3.98 z:-0.18',QUANTITY='GAUGE HEAT FLUX
GAS',STATISTICS_START=0,TEMPORAL_STATISTIC='TIME INTEGRAL'/
&DEVC XB=3.9800,3.9800,0.3800,2.7800,-0.1000,-0.1000,POINTS=31,ORIENTATION=0,-
1,0,ID='BK x:3.98 z:-0.10',QUANTITY='GAUGE HEAT FLUX
GAS',STATISTICS_START=0,TEMPORAL_STATISTIC='TIME INTEGRAL'/
&DEVC XB=3.9800,3.9800,0.3800,2.7800,-0.0200,-0.0200,POINTS=31,ORIENTATION=0,-
1,0,ID='BK x:3.98 z:-0.02',QUANTITY='GAUGE HEAT FLUX
GAS',STATISTICS_START=0,TEMPORAL_STATISTIC='TIME INTEGRAL'/

```





---

## FDS Input File Templates

```
&DEVC XB=4.3000,6.7000,0.0200,0.0200,0.0200,0.0200,POINTS=31,ORIENTATION=-1,0,0,ID='RT
Y:0.02 Z:0.02',QUANTITY='GAUGE HEAT FLUX
GAS',STATISTICS_START=0,TEMPORAL_STATISTIC='TIME INTEGRAL'/
&DEVC XB=4.3000,6.7000,0.0200,0.0200,0.1000,0.1000,POINTS=31,ORIENTATION=-1,0,0,ID='RT
Y:0.02 Z:0.10',QUANTITY='GAUGE HEAT FLUX
GAS',STATISTICS_START=0,TEMPORAL_STATISTIC='TIME INTEGRAL'/
&DEVC XB=4.3000,6.7000,0.0200,0.0200,0.1800,0.1800,POINTS=31,ORIENTATION=-1,0,0,ID='RT
Y:0.02 Z:0.18',QUANTITY='GAUGE HEAT FLUX
GAS',STATISTICS_START=0,TEMPORAL_STATISTIC='TIME INTEGRAL'/
&DEVC XB=4.3000,6.7000,0.1000,0.1000,-0.1800,-0.1800,POINTS=31,ORIENTATION=-
1,0,0,ID='RT Y:0.10 Z:-0.18',QUANTITY='GAUGE HEAT FLUX
GAS',STATISTICS_START=0,TEMPORAL_STATISTIC='TIME INTEGRAL'/
&DEVC XB=4.3000,6.7000,0.1000,0.1000,-0.1000,-0.1000,POINTS=31,ORIENTATION=-
1,0,0,ID='RT Y:0.10 Z:-0.10',QUANTITY='GAUGE HEAT FLUX
GAS',STATISTICS_START=0,TEMPORAL_STATISTIC='TIME INTEGRAL'/
&DEVC XB=4.3000,6.7000,0.1000,0.1000,-0.0200,-0.0200,POINTS=31,ORIENTATION=-
1,0,0,ID='RT Y:0.10 Z:-0.02',QUANTITY='GAUGE HEAT FLUX
GAS',STATISTICS_START=0,TEMPORAL_STATISTIC='TIME INTEGRAL'/
&DEVC XB=4.3000,6.7000,0.1000,0.1000,0.0200,0.0200,POINTS=31,ORIENTATION=-1,0,0,ID='RT
Y:0.10 Z:0.02',QUANTITY='GAUGE HEAT FLUX
GAS',STATISTICS_START=0,TEMPORAL_STATISTIC='TIME INTEGRAL'/
&DEVC XB=4.3000,6.7000,0.1000,0.1000,0.1000,0.1000,POINTS=31,ORIENTATION=-1,0,0,ID='RT
Y:0.10 Z:0.10',QUANTITY='GAUGE HEAT FLUX
GAS',STATISTICS_START=0,TEMPORAL_STATISTIC='TIME INTEGRAL'/
&DEVC XB=4.3000,6.7000,0.1000,0.1000,0.1800,0.1800,POINTS=31,ORIENTATION=-1,0,0,ID='RT
Y:0.10 Z:0.18',QUANTITY='GAUGE HEAT FLUX
GAS',STATISTICS_START=0,TEMPORAL_STATISTIC='TIME INTEGRAL'/
&DEVC XB=4.3000,6.7000,0.1800,0.1800,-0.1800,-0.1800,POINTS=31,ORIENTATION=-
1,0,0,ID='RT Y:0.18 Z:-0.18',QUANTITY='GAUGE HEAT FLUX
GAS',STATISTICS_START=0,TEMPORAL_STATISTIC='TIME INTEGRAL'/
&DEVC XB=4.3000,6.7000,0.1800,0.1800,-0.1000,-0.1000,POINTS=31,ORIENTATION=-
1,0,0,ID='RT Y:0.18 Z:-0.10',QUANTITY='GAUGE HEAT FLUX
GAS',STATISTICS_START=0,TEMPORAL_STATISTIC='TIME INTEGRAL'/
&DEVC XB=4.3000,6.7000,0.1800,0.1800,-0.0200,-0.0200,POINTS=31,ORIENTATION=-
1,0,0,ID='RT Y:0.18 Z:-0.02',QUANTITY='GAUGE HEAT FLUX
GAS',STATISTICS_START=0,TEMPORAL_STATISTIC='TIME INTEGRAL'/
&DEVC XB=4.3000,6.7000,0.1800,0.1800,0.0200,0.0200,POINTS=31,ORIENTATION=-1,0,0,ID='RT
Y:0.18 Z:0.02',QUANTITY='GAUGE HEAT FLUX
GAS',STATISTICS_START=0,TEMPORAL_STATISTIC='TIME INTEGRAL'/
&DEVC XB=4.3000,6.7000,0.1800,0.1800,0.1000,0.1000,POINTS=31,ORIENTATION=-1,0,0,ID='RT
Y:0.18 Z:0.10',QUANTITY='GAUGE HEAT FLUX
GAS',STATISTICS_START=0,TEMPORAL_STATISTIC='TIME INTEGRAL'/
&DEVC XB=4.3000,6.7000,0.1800,0.1800,0.1800,0.1800,POINTS=31,ORIENTATION=-1,0,0,ID='RT
Y:0.18 Z:0.18',QUANTITY='GAUGE HEAT FLUX
GAS',STATISTICS_START=0,TEMPORAL_STATISTIC='TIME INTEGRAL'/
```

```
&TAIL /
```

# D

## SANDIA PARTICLE TESTING

---

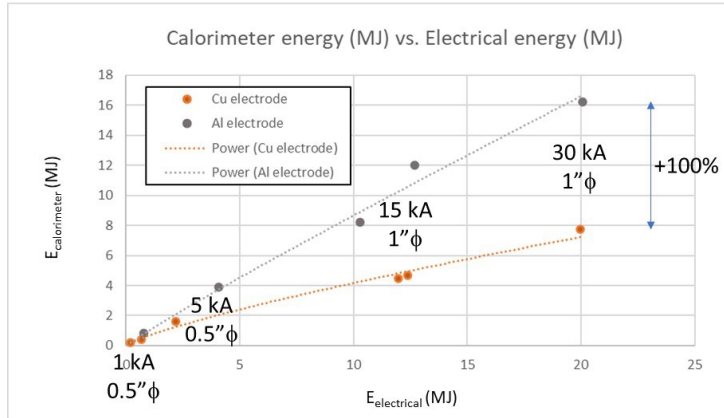
This appendix contains a summary of the scaled aluminum and copper 3-phase alternating current arc testing that was conducted at Sandia National Laboratories (SNL).

### D.1 Summary of Testing Approach and Parameters

#### *D.1.1 Experimental Aims for Scaled Arc Testing and Outputs*

In August 2021, three-phase arc experiments were conducted with the purpose of providing inputs for FDS modeling of aluminum and copper bus bar effects on high energy arcing fault (HEAF) incident energy. The purpose of these tests was to provide input regarding HEAF-evolved metal particle characteristics, including particle size, degree of oxidation, and percentage of bus bar metal melted and vaporized. These tests were designed to be scaled (similar current density) three-phase arcs based on a series of full-scale open-box electrical arc tests performed in August and September of 2019. The purpose of those prior tests was to 1) generate data to support model development and refinement, 2) evaluate existing models' ability to predict material loss and arc voltages and 3) deploy sensors to evaluate the impact of non-thermal hazards. The tests were performed at KEMA Powertest facility located in Chalfont, PA. The tests were supported by a team of testing and measurement experts from the National Institute of Standards and Technology (NIST) and SNL. In the open-box experiments, electrical energy and evolved thermal energy were characterized, but particle capture was not conducted.

In prior open-box HEAF tests, for the same electrical input energy, the evolved thermal energy measured on plate calorimeters appeared to differ between aluminum and copper bus bars of the same dimensions (1.3 – 2.5 cm diameter bus bars). This effect was most notable for higher currents (over 15 kA) and current densities (over 30 A/mm<sup>2</sup>) as shown in Figure D-1.



Current / Area      Current density

$$1 \text{ kA} / 126.6 \text{ mm}^2 = 7.9 \text{ A/mm}^2$$

$$5 \text{ kA} / 126.6 \text{ mm}^2 = 39.5 \text{ A/mm}^2 \leftarrow$$

$$15 \text{ kA} / 506.7 \text{ mm}^2 = 29.6 \text{ A/mm}^2$$

$$30 \text{ kA} / 506.7 \text{ mm}^2 = 59.2 \text{ A/mm}^2 \leftarrow$$

Larger calorimeter energy observed for Al vs. Cu for  $\Delta t = 0.5\text{-}2\text{s}$  & current density  $\geq 30 \text{ A/mm}^2$

**Figure D-1**  
**Summary of open-box calorimeter energy vs. electrical energy for 1-30 kA, 0.5 inch and 1 inch diameter copper and aluminum bus bars**

Since particle capture was not conducted for these tests, the aim of the present scaled HEAF experiments was to provide inputs for FDS arc fault modeling at  $60 \text{ A/mm}^2$  current density for  $1 \text{ mm} \times 1 \text{ mm}$  electrodes.

Particular details requested by modeling experts to guide appropriate FDS modeling, included:

- Particle drop size distribution
- The fraction of bus bars that is initially vapor
- The initial vapor mass fraction, droplet size distribution, and observed droplet oxidation

The scaled experiments were designed to measure differences in behavior between scaled copper and aluminum electrodes of equivalent current density ( $60 \text{ A/mm}^2$ ) to the prior open-box high energy arc fault testing and quantification of:

- Heat rise,  $\Delta T$
- Particle size distribution
- Oxidation degree
- Bus bar mass percent melted, and maximum mass percent vaporized
- Voltage/current/arc resistance

### **D.1.2 Scaled Arc Fault Experimental Approach**

Analysis of three-phase AC arcing was conducted using a Pacific Power Model M2288 AC source, shown in Figure D-2, at a voltage of  $600 \text{ V}_{AC}$ , current of  $60 - 100 \text{ A}$  and conducted for  $0.1 - 2 \text{ s}$  duration, until the bus bar electrodes were fully consumed, or the AC arc extinguished. For these experiments,  $1 \text{ mm} \times 1 \text{ mm} \times 10 \text{ cm}$  length aluminum and copper rods were used to achieve high current densities of  $60 - 100 \text{ A/mm}^2$  for comparison to similar current density ( $29.6 - 59.2 \text{ A/mm}^2$ ) in previous  $5 - 30 \text{ kA}$  open-box HEAF test data using full scale aluminum and copper bus bars.



FINAL CONFIGURATION AND RATINGS			
FINAL MODEL	M2288 Transformer assembly	w/o 5108-1	
MODIFICATIONS	N/A	CONTRACT N/A	
INPUT RATINGS		OUTPUT RATINGS (Tap 1-3) (Tap 1-4) (Tap 1-5)	
VOLTS	0-120/208Vac 4w+G (Tap 1-2)	VOLTS	138/240 242/420 346/600
AMPS	175A	AMPS	150A 85A 60A
POWER	62.5KVA	POWER	62.5KVA
FREQ.	47-63Hz	FREQ.	47-63HZ

**Figure D-2**  
Pacific Power 3-phase continuous AC power source for scaled arc testing

Based on prior open-box testing, three-phase arcs were observed to be sustained at a voltage of 600 V<sub>AC</sub> and above. The aim of this experiment is to strike and sustain stable three-phase arcs within a closed copper cylinder calorimeter volume for 0.1 – 2 s durations and to measure the voltage, current, and temperature rise (to enable calorimetry) of copper and aluminum scaled bus bars of the same dimensions (see Figure D-3, Figure D-4, and Figure D-5).

The mass of the copper cylinder was measured, and the steady-state, post-arc temperature rise of the cylinder was measured using calibrated thermocouples to enable quantification of evolved thermal energy. To quantify the mass of bus bars vaporized, the masses of the bus bars were measured before experiments, and masses of remaining post-arc bus bars and collected macroscopic (0.1 – 3 mm diameter) evolved droplets were measured.

Source: 600 V<sub>AC</sub>: 60-100A  
Equivalent HEAF current 10-100 kA  
Duration: 2 seconds  
Bus bars: 1 mm x 1 mm x 10-20 cm Al or Cu  
Gap: 3 mm, matched Al or Cu bridgewire

Measure: heat rise of copper cylinder, V(t), I(t) at two positions (10cm, 20 cm)  
Evolved particle analysis: SEM EDXA of carbon tape (Al:O and Cu:O ratios)  
Weigh bus bars before/after: quantify mass evaporated & melted

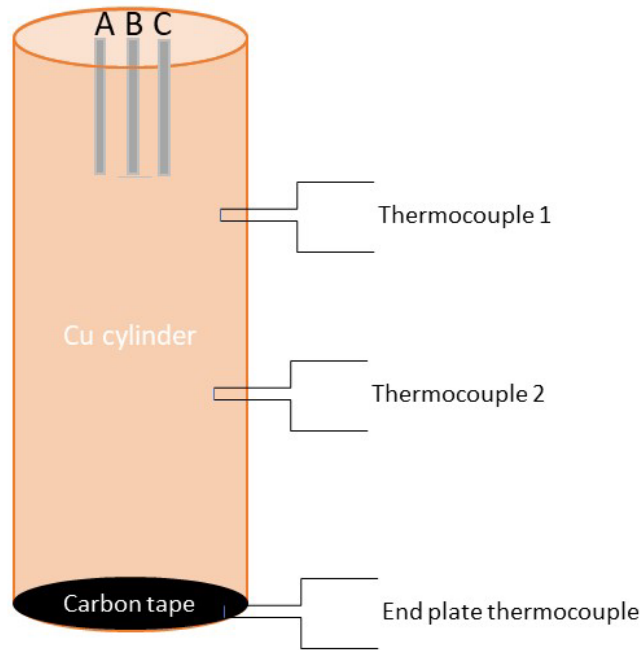


**Figure D-3**  
**Schematic of scaled test method**

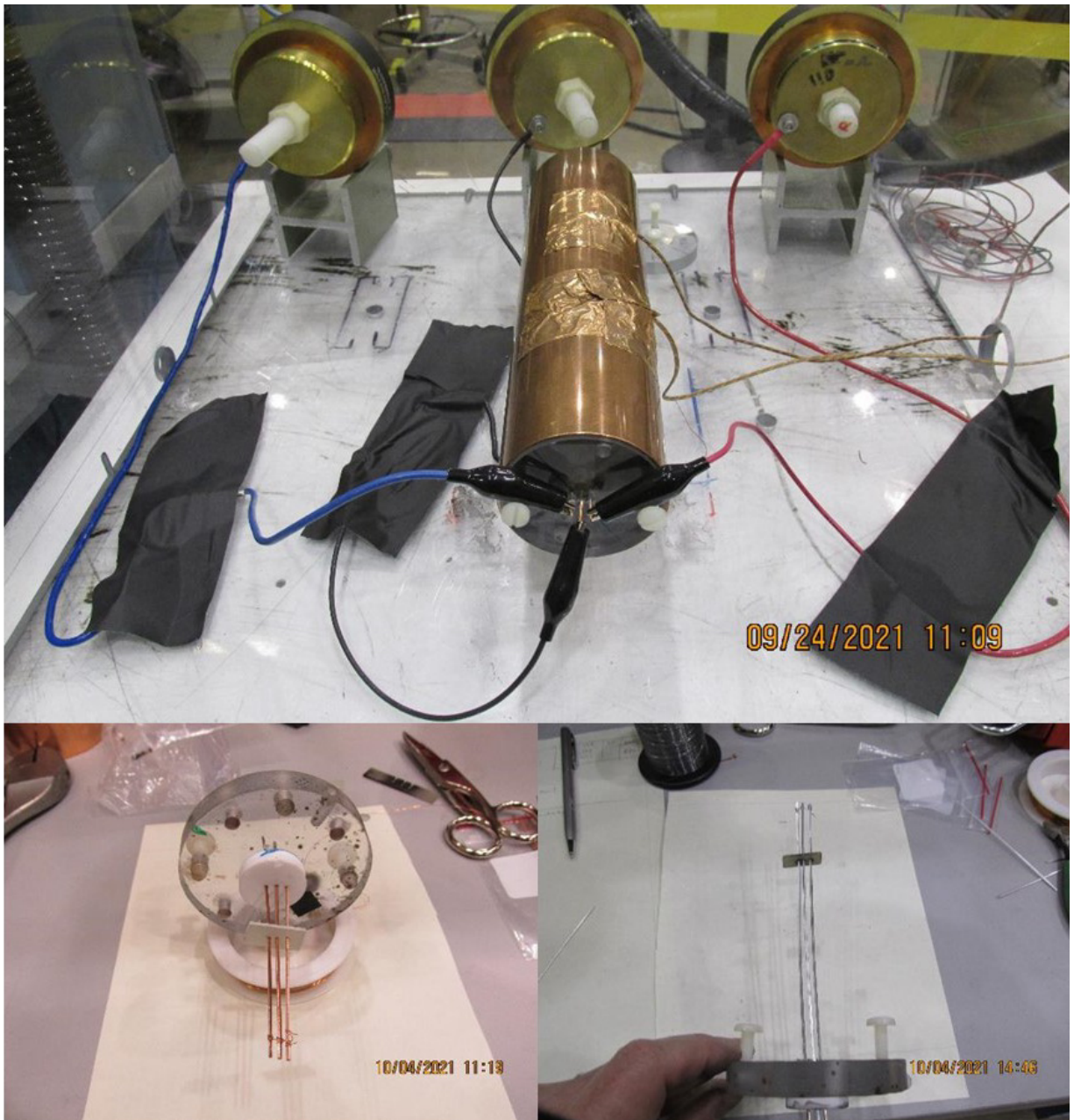


**Figure D-4**  
Images of copper calorimeter enclosure and scaled three-phase bus bars

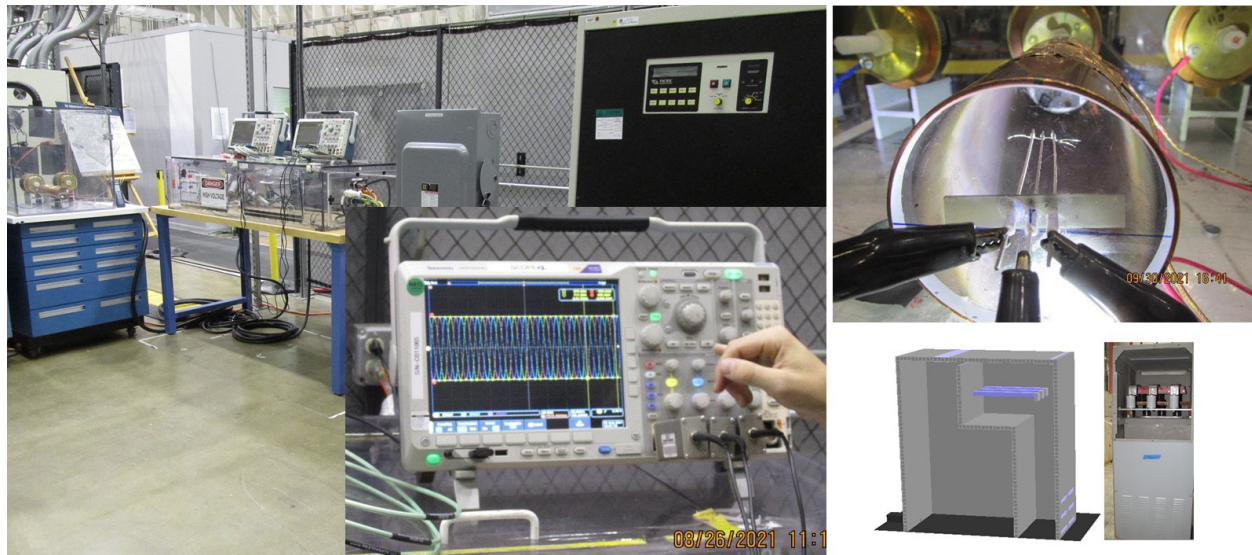


**Figure D-5**  
Oscilloscope collection of three-phase voltage and current (left), internal view of scaled three-phase copper and aluminum bus bars within copper calorimeter (upper right) and schematic of commercial three-phase switchgear bus bar configuration (lower right)

### ***D.1.3 Particle Capture and Analysis Method***

To collect arc-generated particles for analysis of particle size, composition, and state of oxidation, strips of carbon tape attached to scanning electron microscope mounting stubs were mounted on the opposite end of the calorimeter from the scaled bus bars and utilized as particle collectors. The carbon-tape-coated stubs faced the end of the three parallel electrodes. This enabled collection of airborne molten and/or vaporized particles with minimal change in collected particle morphology and strong chemical contrast between the collected particles and the carbon mounting tape.

Evolved airborne particles (all below 0.1 mm) from the three-phase arcs were collected and analyzed using scanning electron microscopy (SEM) for particle size and SEM energy dispersive spectroscopy (SEM EDS) to analyze copper to oxygen ratio and aluminum to oxygen ratio to evaluate the degree of evolved particle oxidation. Hitachi Galileo and FEI Magellan electron microscopes with 2 nm resolution were used to determine particle sizes of evolved particles, analyze surface morphology to determine their origin (melted or vaporized), and analyze the chemical composition via EDS at 5 kV acceleration voltage.

High-magnification analysis using SEM enables the physical and chemical characterization of evolved particle sizes, geometries, and chemical composition. Energy dispersive X-ray analysis enabled the specific identification of the particle composition (e.g., aluminum, copper, or specific alloys) as well as the degree of particle oxidation (the ratio of aluminum to oxygen X-ray fluorescence peak counts, normalized to an  $\text{Al}_2\text{O}_3$  or  $\text{CuO}$  standard). This assisted in the determination of whether the evolved particles were simply resolidified molten droplets of metallic copper or aluminum, or if they had exothermically oxidized, a potential source of added energy during the arc.

## D.2 Scaled Three-Phase Arc Fault Experimental Results

### D.2.1 Aluminum and Copper 1 to 2 s Arcs: 600 V<sub>AC</sub>, 3 Phase, 100 A/mm<sup>2</sup>

During the arc experiments, the three-phase AC voltage and current were measured using calibrated Tektronix P6015 voltage monitors and Pearson 110 current voltage transformers (CVTs). Bus bars were shorted together using a thin, 10 mil diameter wire of the same composition metal (copper or aluminum) as the bus bars, and voltage was applied using the Pacific Power source, as shown in Figure D-6 to initiate three-phase arcs. A sustained arc is indicated by both continuous voltage and current on all three phases. Arc duration was measured as the time during which all three phases conducted current; sustained arc durations ranged from 0.11 s to 1.49 s.

Figure D-6 illustrates a stable, three-phase arc which had a duration of 858 ms before extinguishing. Aluminum bus bars typically extinguished when the full exposed length was consumed; copper bus bars melted roughly three times slower, consistent with the threefold higher density and volumetric heat capacity of copper.

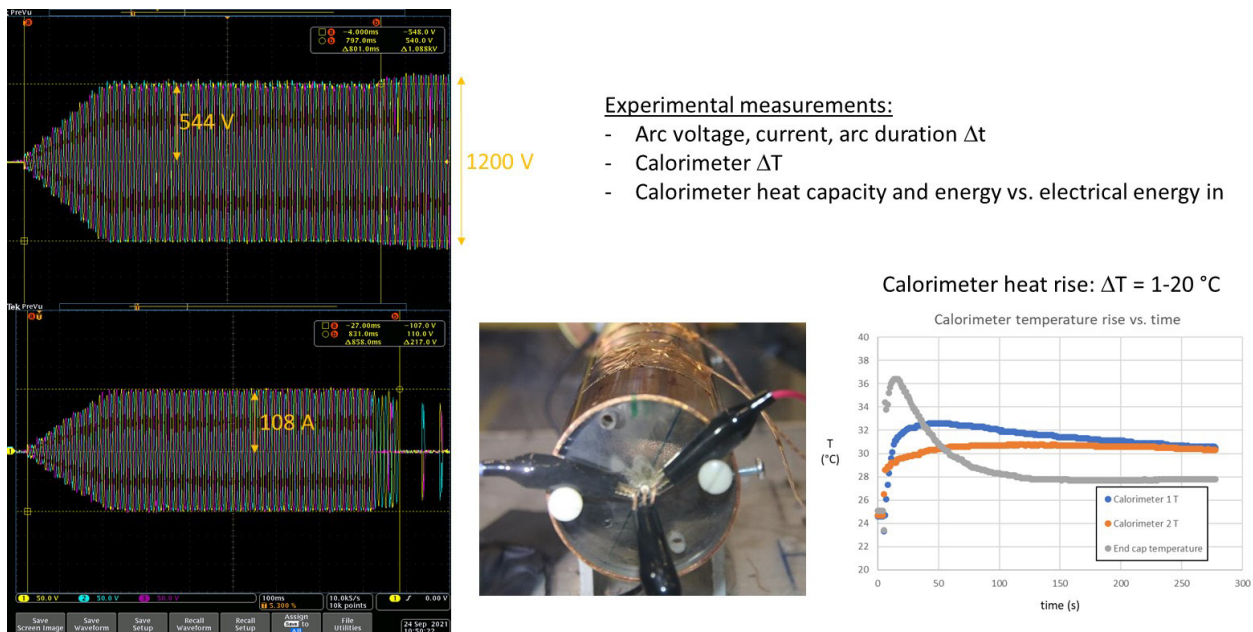
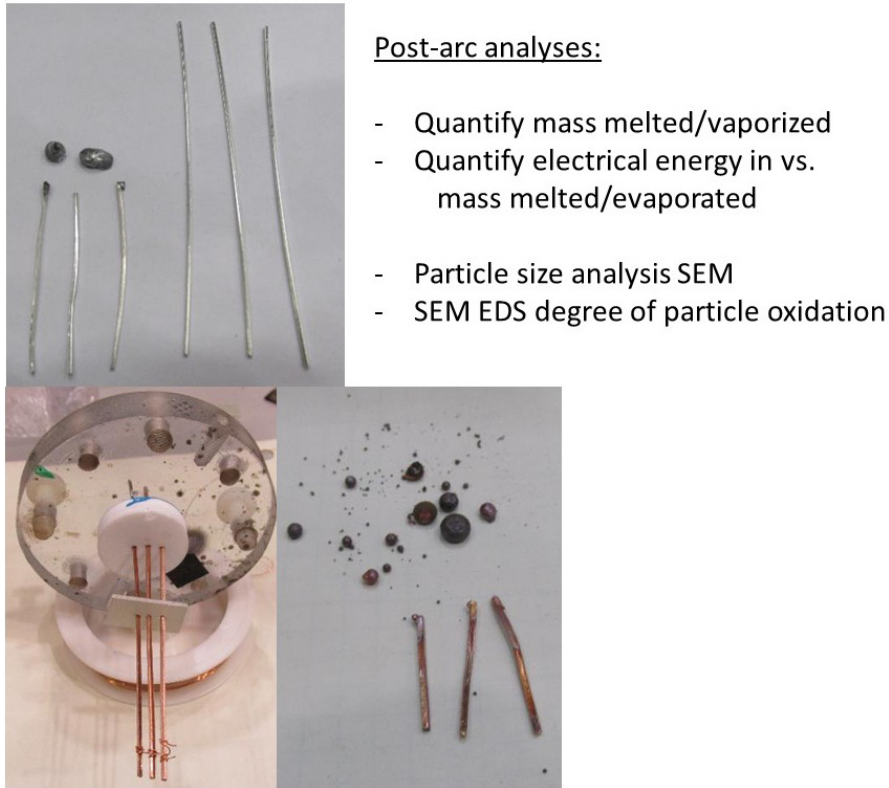


**Figure D-6**

**A three-phase, 544 V<sub>AC</sub>, 858 ms duration arc shown on oscilloscope produced a sustained 108 A arc current on all phases (left), image of three-phase electrical connections (center) and measured heat rise versus time for calorimeter thermocouples (blue and orange traces) and at end cap (gray). The temperature rise  $\Delta T$  is taken as the average of the blue and orange temperatures**

Following testing, post-arc analysis was conducted, including both calorimeter thermal analysis and mass analysis of the bus bar and evolved materials. Characteristics of typical aluminum and copper mass analysis are shown in Figure D-7. Bus bars were measured individually prior to experiments as well as afterward. Additionally, all free evolved particles from within the calorimeter were collected and weighed; these were primarily large millimeter-scale droplets below the original bus bar locations. Remaining “missing” bus bar mass consisted of fine (under 100  $\mu\text{m}$ ) size particles which appeared to have vaporized and condensed on the calorimeter walls and carbon tape collector.



Post-arc analyses:

- Quantify mass melted/vaporized
- Quantify electrical energy in vs. mass melted/evaporated
- Particle size analysis SEM
- SEM EDS degree of particle oxidation

**Figure D-7**

**Images of scaled aluminum bus bar before and after sustained three-phase arc, including collected molten particles (top); copper bus bar samples before (bottom left) and after a sustained arc, including collected droplets (bottom right)**

### ***D.2.2 Heat Rise Versus Arc Duration for Aluminum and Copper***

Two calorimeters were mounted on the copper calorimeter chamber in which the arc experiments were conducted and used to measure the copper temperature rise  $\Delta T$  as well as a measurement of calorimetric energy deposited in the copper as a function of arc duration and electrode type. The calorimeter ends were capped with 1 cm thick plexiglass, containing the heated air inside the chamber, and the calorimeter was supported on thermally insulating fiberglass supports. The temperature rise of the calibrated K-type thermocouples was measured as a function of time by a calibrated Omega measurement unit, with an uncertainty of 0.2°C. The temperature rise ( $\Delta T$ ) was taken as the peak of the average temperature of the two thermocouples, which were located at  $\frac{1}{3}$  and  $\frac{2}{3}$  of the length of the copper cylinder. The thermocouple nearest the arc location initially read higher but equilibrated with the second thermocouple, as shown in Figure D-6; the calorimeter temperature remained within 1 degree of this average for over 5 minutes.

The peak temperature rise values for all experiments were calculated and are plotted in Figure D-8. Among the observations in the experiments were:

1. Heat rise was generally larger for aluminum than copper for the same electrical input and duration.
2. Aluminum electrodes achieved full melting (7.6 – 15 cm) much earlier in time than copper electrodes.

As noted, the volumetric heat capacity of aluminum ( $2.42 \text{ J}/(\text{cm}^3 \cdot \text{K})$ ) is lower than copper ( $3.45 \text{ J}/(\text{cm}^3 \cdot \text{K})$ ), and the resistivity and expected Joule heating effect larger, consistent with a greater linear consumption for the same cross section electrodes.

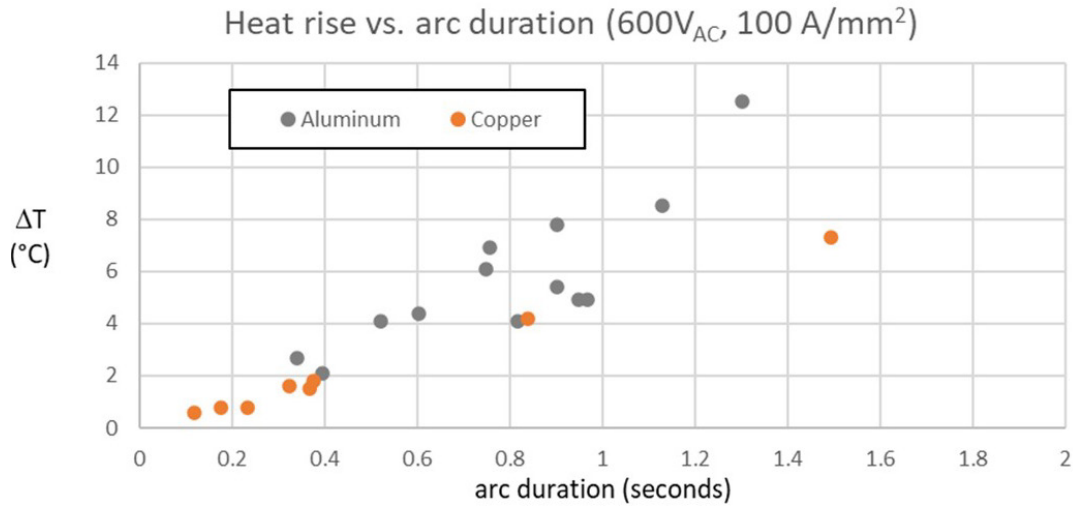


**Figure D-8**  
Summary of measured temperature rise  $\Delta T$  versus arc duration for all aluminum and copper arc experiments

### D.2.3 Heat Rise Versus Arc Duration for Aluminum and Copper

The above copper calorimeter heat rise data was combined with the mass and heat capacity of the copper calorimeter to establish the calorimeter energy increase in Joules. The electrical energy input using the root mean square (RMS) AC voltage and current, and time duration was used to calculate the electrical energy input, and these are plotted in Figure D-9.

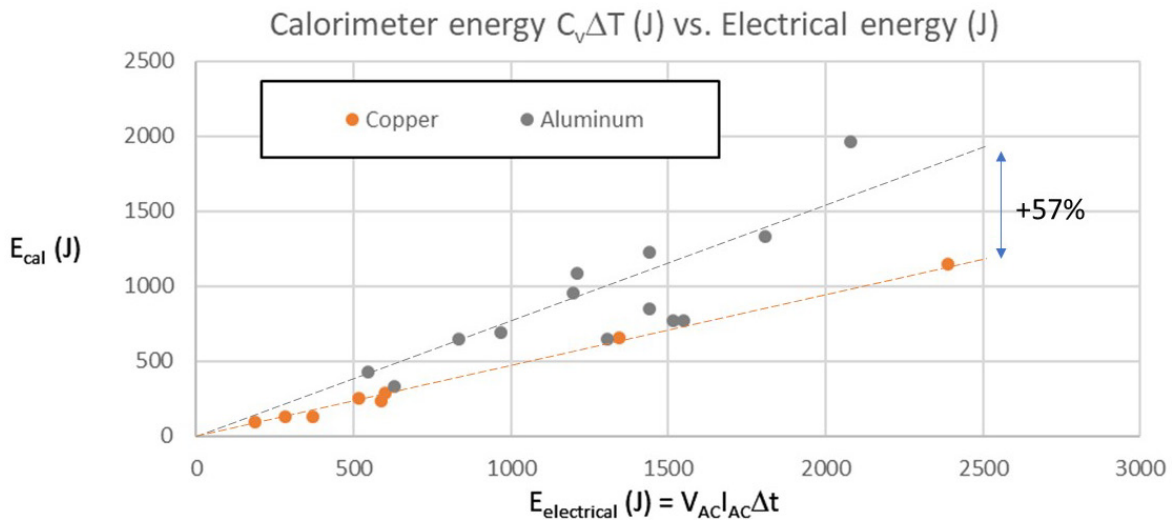


**Figure D-9**  
Calculated calorimeter heat rise plotted vs. electrical energy input

For the collected arc experiments, observations included that the calorimeter energy was generally larger for aluminum than copper for the same electrical input and duration. A linear curve fit to the data suggests an average 57% increase in calorimeter energy increase for the same dimensions and electrical energy input for aluminum electrodes vs. copper electrodes.

#### D.2.4 Analysis of Mass Percent Melted Versus Potential Vaporized

For FDS modeling, key input questions included estimation of the percentage of bus bar that should be treated as melted and vaporized for calculations. Mass analysis of pre- and post-arc samples was used to calculate the percent of mass melted (mass of remaining bus bar and mass of collected macroscopic particles, shown in Figure D-10 center). An estimation of the maximum percent of vaporized material was calculated by subtracting the remaining post-arc bus mass and collected particle mass from the mass of the bus bars and initiating shorting wire prior to each arc experiment. A fine powdered debris condensed with vaporized material collected on the walls of the calorimeter and carbon tape collector and is described in Section D.2.5. The percent melted and maximum percent vaporized are shown in Figure D-10.

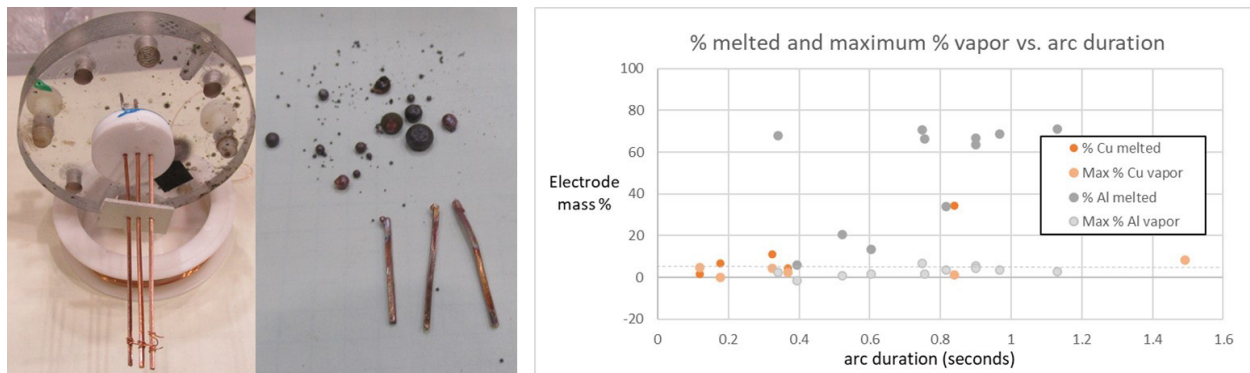


**Figure D-10**  
Image of pre-arc copper bus bar and shorting wire (left), representative collection of post-arc bus bars and collected spherical particles (center) and tabulation of % metal melted and maximum percent vaporized particles (right)

Arcs typically extinguished when reaching the white ceramic insulator sample holder shown at left in Figure D-11, limiting the percent melted to that percent of length beyond the insulator. As shown in Figure D-11, aluminum bus bars often completely consumed the full available length, while copper percent consumed showed a more linear time dependence. Observations from the data include:

- Aluminum electrodes achieve full melting (7.6 to 15 cm) much earlier in time than copper electrodes.
- For longer duration arcs, up to 60 to 80% of electrode length was melted and recovered as large 0.1 mm or larger diameter spheres consistent with melted and resolidified metal.
- In most cases, less than 5% of electrode material was not recovered either as remaining bus bars or large 0.1 to 5 mm solidified molten spheres; this supported setting a bound that 3.5% metal is vaporized (copper: 2.6%, aluminum 3.5%).

### D.2.5 Differences Between Aluminum and Copper Melt Rates

The differences in aluminum and copper melting behavior (Figure D-11) were considered in light of two possible explanations for the much greater percentage of aluminum melted versus time.

1. Aluminum density is three times lower than copper, the aluminum melting point is much lower (660°C versus 1,085°C), and volumetric heat capacity is 42% lower than that of copper; these are consistent with a significantly higher aluminum volume loss than copper for the same arc duration.
2. Using the Preece equation to predict wire fusing currents suggests that fusing current densities for aluminum are lower than copper (Preece equation:  $I_{\text{fusing}} = Ad^{1.5}$ ; where  $A_{\text{Al}} = 59$  and  $A_{\text{Cu}} = 80$  for  $d$  in mm) [43]:
  - Aluminum fusing current density: 75 A/mm<sup>2</sup>
  - Copper fusing current density: 102 A/mm<sup>2</sup>

In certain current density regimes (75 – 102 A/mm<sup>2</sup>), melting of aluminum would be expected when it would not for copper.

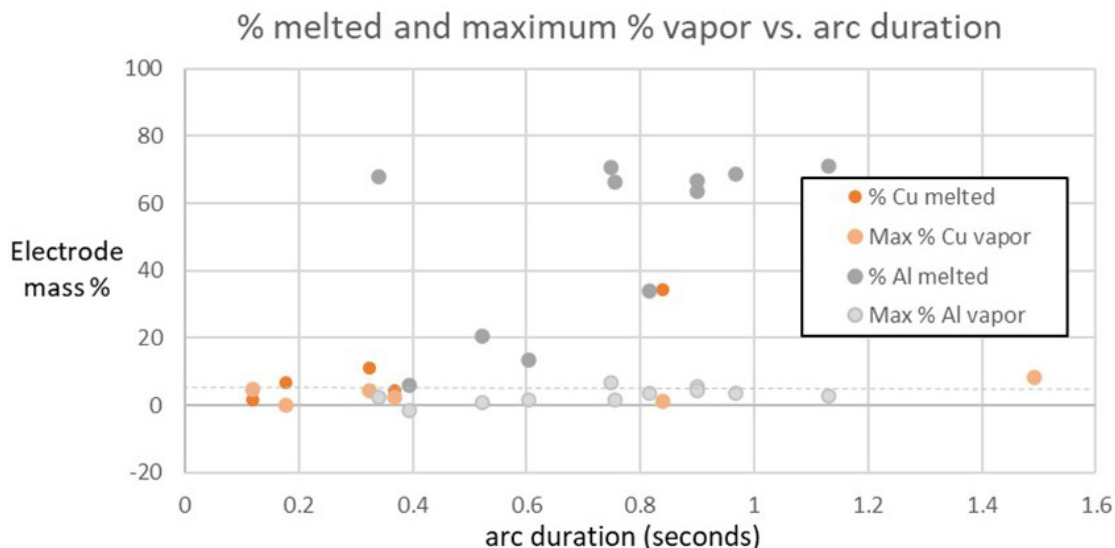


**Figure D-11**  
Plot of percent melted and maximum percent metal vaporized versus arc duration

## D.3 Evolved Particle Oxidation Analysis

### D.3.1 Electron Microscope Analysis of Evolved Aluminum Particles

Particles were collected on carbon tape from the back end of the calorimeter and characterized via scanning electron microscopy and EDS analysis using Hitachi Galileo and FEI Magellan electron microscopes. A fully oxidized standard of aluminum oxide ceramic was utilized for calculation of the degree of oxidation from the oxygen to aluminum EDS peak ratios.

Evolved particles from the Pacific Power three-phase 600 V<sub>AC</sub> testing of aluminum scaled bus bars again demonstrated particle sizes of 2.4 – 28 μm in size. From an SEM analysis of 50 particles, average particle size was 8.96 μm and average particle volume was 880 μm<sup>3</sup>, as shown in Figure D-12 through Figure D-15.

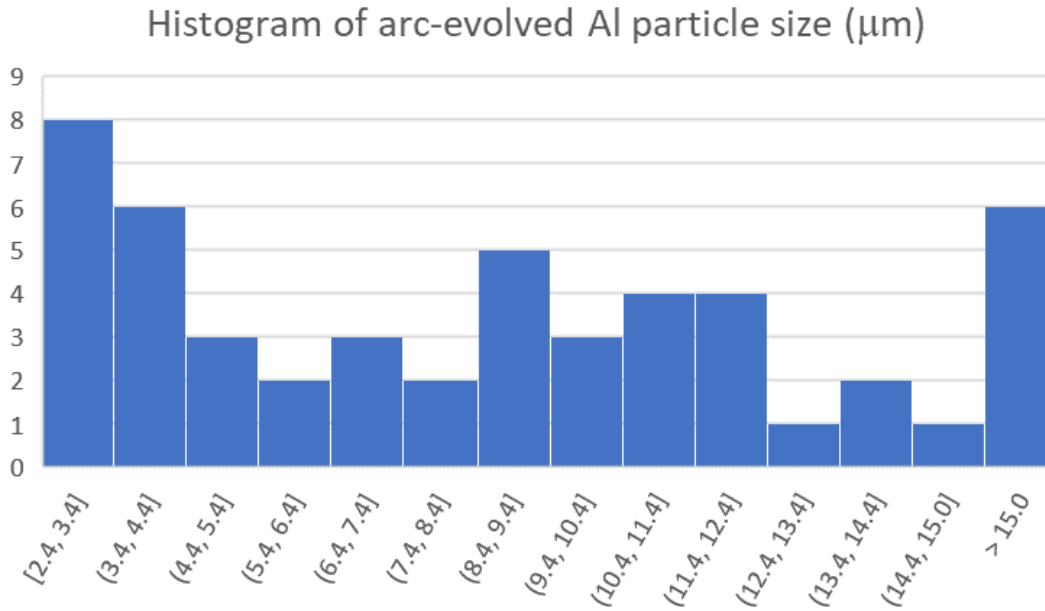


**Figure D-12**  
Histogram of size in μm of 50 aluminum bus bar-evolved particles; the average particle size of these evolved aluminum particles was 8.96 μm

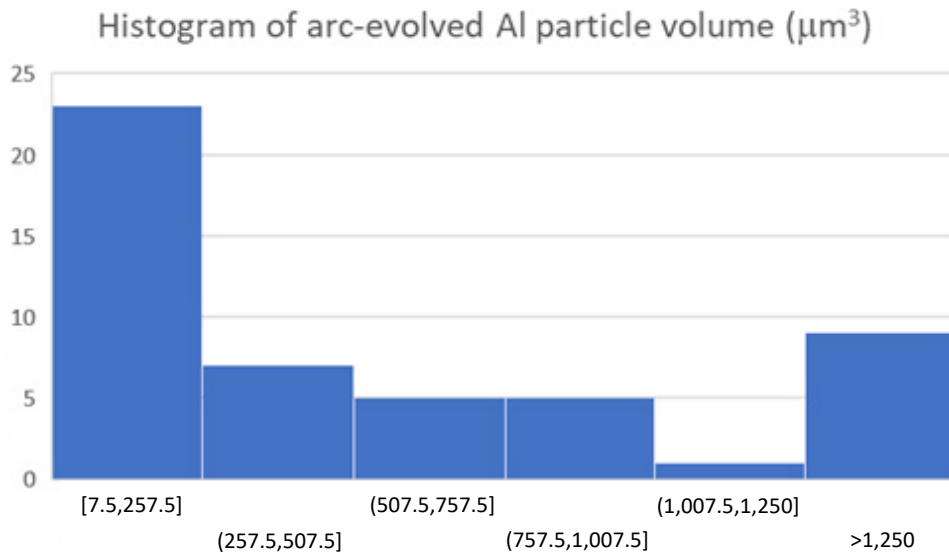


**Figure D-13**  
Histogram of volume in cubic μm of 50 aluminum bus bar-evolved particles; the average particle volume calculated for evolved aluminum particles was 880 cubic μm

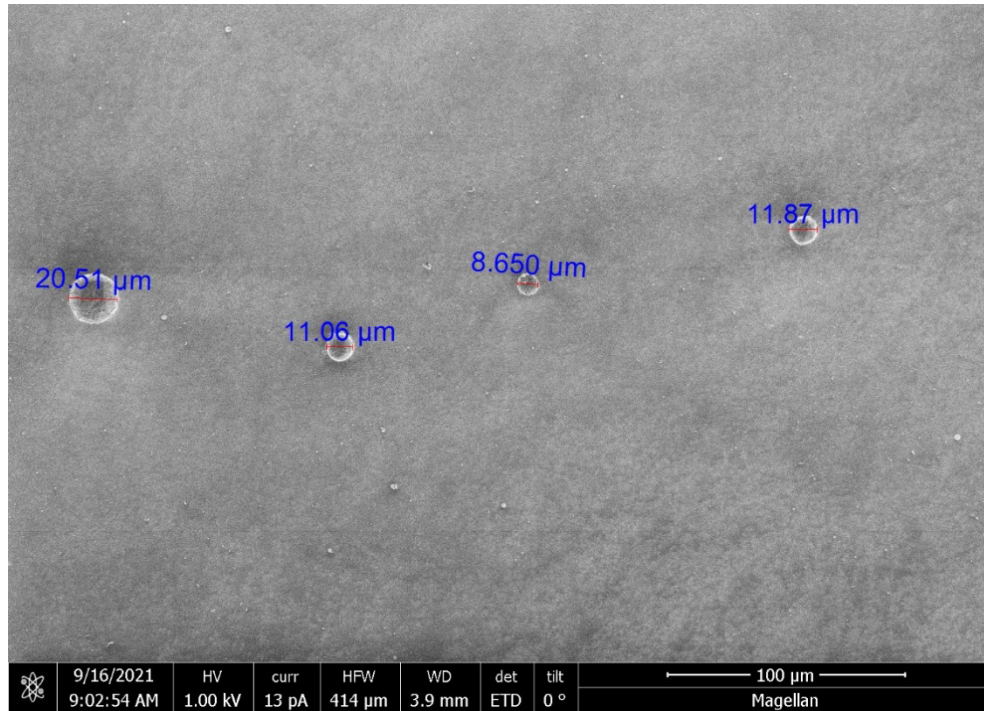


**Figure D-14**  
Representative SEM image and size measurements of aluminum bus bar-evolved particles; the average particle size for these evolved aluminum particles was 8.96  $\mu\text{m}$

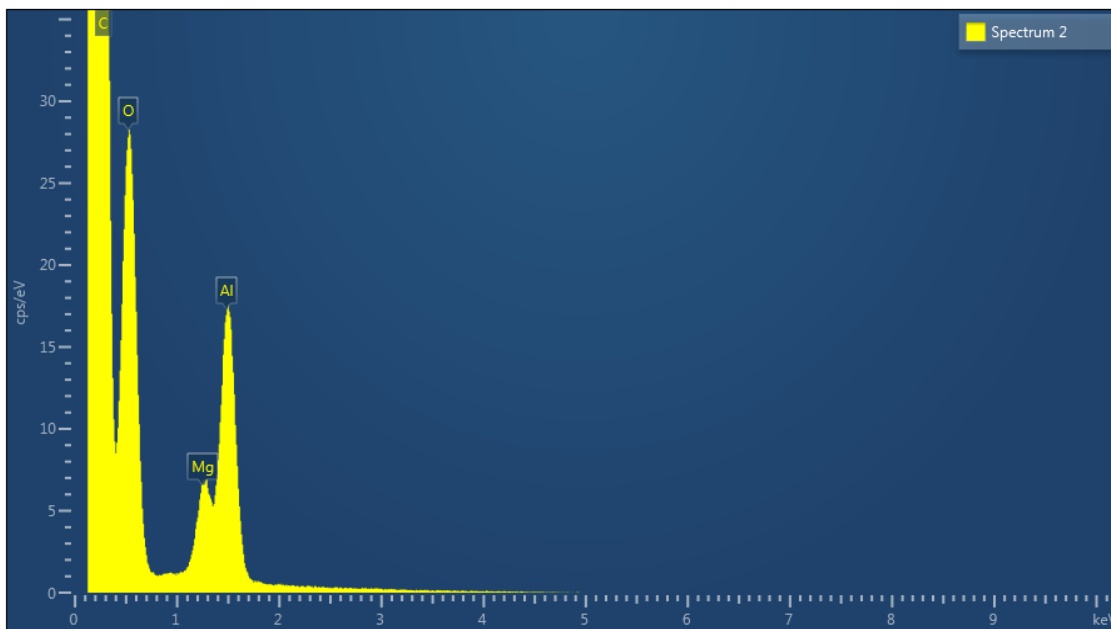


**Figure D-15**  
Representative EDS analysis of a three-phase arc-evolved aluminum particle; from the peak ratios of aluminum, magnesium, and oxygen, an estimated degree of oxidation of 73% was calculated

### D.3.2 Electron Microscope Analysis of Evolved Copper Particles

Analysis of three-phase AC arc-evolved particles was conducted on particles collected from 600 V<sub>AC</sub> arcs of 0.5 s to 2 s duration between 1 mm<sup>2</sup> cross section copper bus bars. Image analysis was conducted on 50 particles to provide a statistical distribution of particle sizes and volumes, and EDS was conducted to quantify oxygen to copper ratio.

Compared to the prior aluminum particle size analysis, the copper particles displayed a broad particle size distribution and were notably finer, with a median particle size of 0.225 μm and median particle volume of 0.056 mm<sup>3</sup> (median volume radius ~0.383 μm, since the volume average is biased toward larger particles). Examples of the particle size distribution and shape are shown in Figure D-16, and a histogram of particle sizes are shown in Figure D-17.

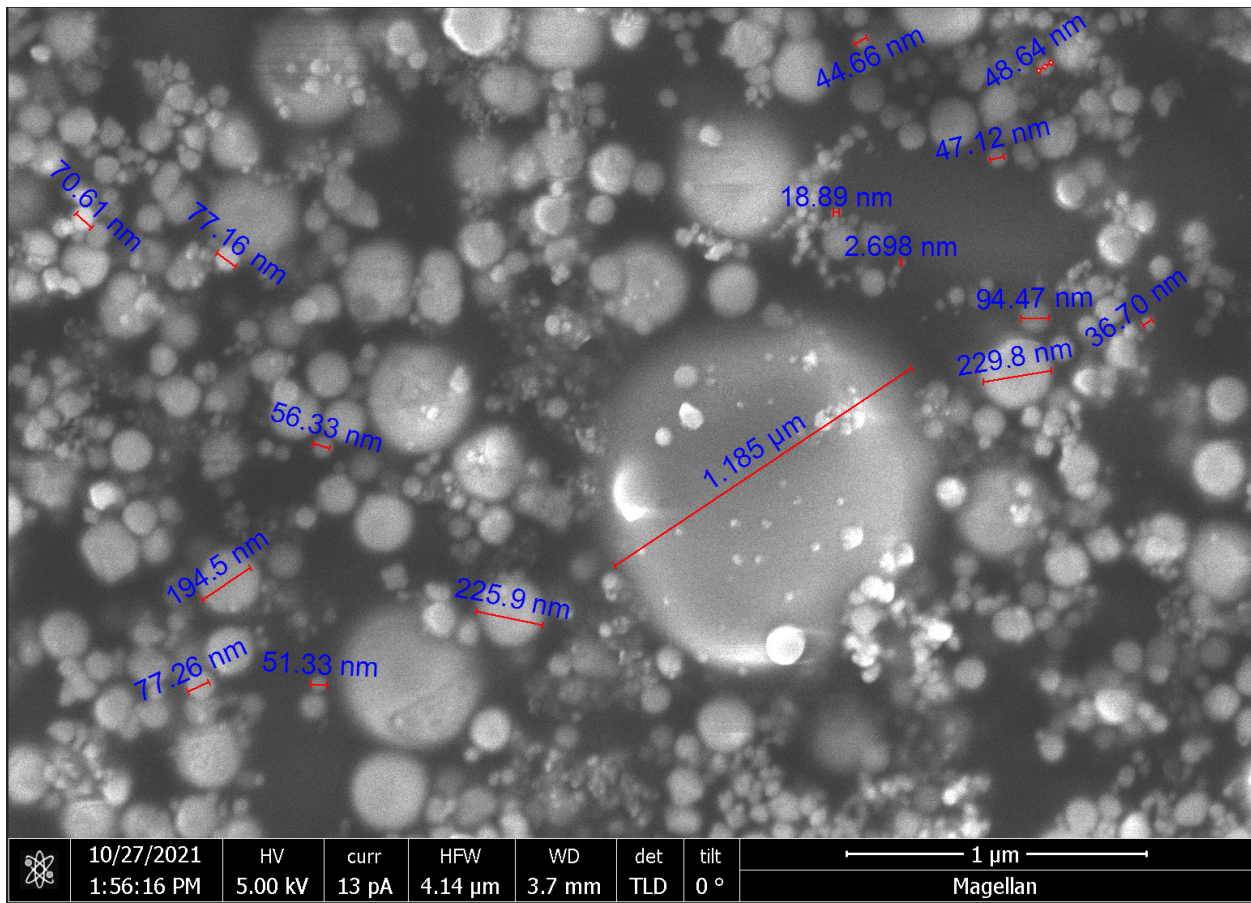


**Figure D-16**  
SEM of 600 V<sub>AC</sub> arc-evolved, 0.02 – 1.2 μm copper particles

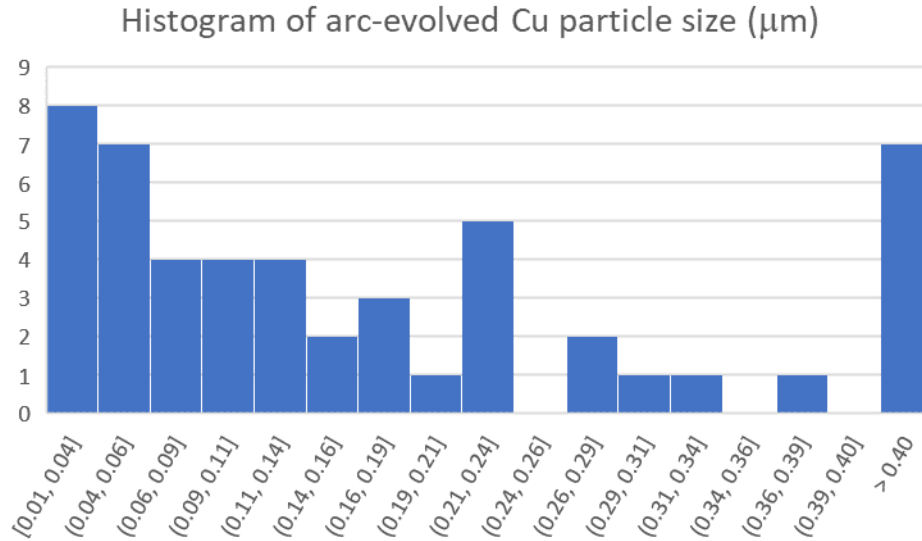


**Figure D-17**  
Histogram of particle sizes of 50 particles evolved from 600 V<sub>AC</sub> arcs, displaying a median particle size of 0.225  $\mu\text{m}$  and median particle volume of 0.056  $\text{mm}^3$

Energy dispersive spectroscopy was conducted on these collected particles. The majority of particles indicated oxygen to copper ratios of 13 – 28%, with one outlier particle with a 51% degree of oxidation, shown in Figure D-18 and Figure D-19.

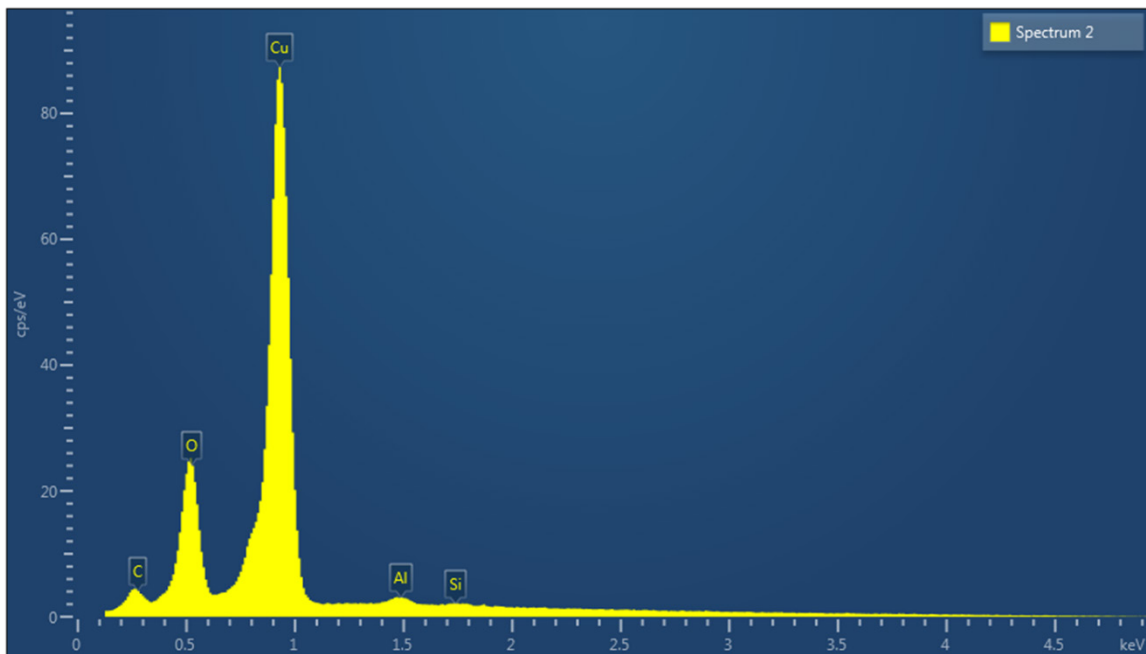


**Figure D-18**  
EDS spectrum of 600 V<sub>AC</sub> arc-evolved, 0.02-2  $\mu\text{m}$  copper particles, displaying oxygen and copper peaks, with an oxygen to copper ratio of 0.28

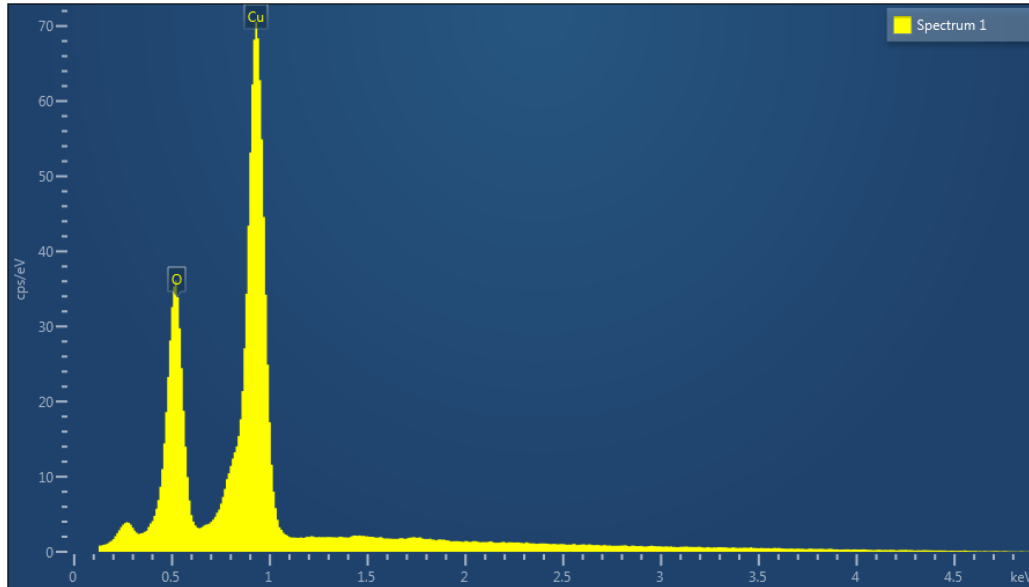


**Figure D-19**  
EDS spectrum of 600 V<sub>AC</sub> arc-evolved, 0.02 – 2 μm copper particles, displaying oxygen and copper peaks, with an oxygen to copper ratio of 0.51

### ***D.3.3 Summary of Particle Collection Data for FDS Modeling Input***

FDS modeling questions posed from the WG considered the following:

- The importance of tracking droplets from the melting enclosure and allow them to combust.
- The drop size distribution that should be applied
- Whether the drop side distribution changes with metal type
- The drop fraction that is initially vapor and the time dependent functional form of this fraction

Overall, the added energy due to metal combustion is based on many unverified assumptions (initial vapor mass fraction 10%, droplet size distribution, droplet initial temperature, arc radiant fraction, and others).

Experimental results as input for FDS modeling include:

- Calorimeter energy output for aluminum appeared larger than for copper. A linear curve fit of the small copper data set shows 57% more energy from vaporized aluminum than vaporized copper.
- Aluminum median droplet size was 9 μm, and median volume 880 μm<sup>3</sup>.
- Copper droplet size displayed a broad range of particle sizes, with a median particle size of 0.225 μm and median particle volume of 0.056 μm<sup>3</sup>.
- Vapor mass fraction was less than 5% (copper: 2.6%, aluminum 3.5%).
- Estimated upper limit of evolved particle droplet oxidation were aluminum 73%, and copper 51%.

# E

## HEAF PRESSURE WAVE EFFECTS

---

This appendix describes HEAF pressure wave effects and a basis for excluding pressure wave impact damage in the HEAF hazard model.

### E.1 Background

When an arc first initiates, there is a pressure wave that results from the sudden release of energy from the arc. In certain events and in some testing, this pressure wave has opened electrical enclosure access doors and panels of the faulted equipment and opened doors to the fire compartment containing the faulting equipment (from OE). During a phenomena identification and ranking table (PIRT) exercise for HEAF [44], a team of experts concluded that pressure effects should be considered for characterizing target damage.

NUREG-2218, *An International Phenomena Identification and Ranking Table (PIRT) Expert Elicitation Exercise for High Energy Arcing Faults (HEAFs)*, [44] identified pressure effects as a level 2 rank of importance. Level 2 is a designation that the PIRT team used to characterize the relative importance of a phenomenon compared to the other phenomena. Level 1 is of higher importance than level 2, which in turn, is of higher importance than level 3. The PIRT ranked HEAF pressure effects as the seventh most important phenomenon out of the thirteen (13). The PIRT report describes the groups evaluation of pressure effects as reproduced below [44]:

Panel discussions on pressure effects were centered on two failure mechanisms: a pressure wave and a projectile. In the former, a wave of pressure disturbance propagates through the medium (air) imparting mechanical energy to targets; in the latter, the pressure wave accelerates a solid object, which subsequently imparts mechanical energy to a target upon impact. The term “shock wave,” which implies supersonic propagation, is not used here. Pressure measurements during phase one experiments were unreliable and noisy, and propagation speed was not measured.

Cabinets in a lineup may be particularly sensitive to a pressure wave depending on their configuration. Where sensitive electronic equipment is present, being in the same bank as a HEAF may be sufficient to cause damage even where no thermal insult is incurred. For the enclosures immediately adjacent to the source cabinet, the construction of the separating walls becomes important. Operating experience and test results clearly document the ability of a HEAF to open or dislodge enclosure doors and bow or deform enclosure walls. The panel theorized that this type of mechanical shock could raise the possibility of a secondary HEAF in an adjacent cabinet.

After thermal effects, the panel ranked pressure effects as the greatest hazard to surrounding systems, structures, and components. The mechanical energy imparted by a pressure wave or projectile has the potential to disable equipment, trip breakers, cause secondary arcs, damage pressure boundaries (fire doors and dampers), and change the ventilation properties of the source enclosure.

## E.2 NUREG/CR-6850 Guidance

NUREG/CR-6850 Volume 2, *EPRI/NRC-RES Fire PRA Methodology for Nuclear Power Facilities, Detailed Methodology* [1] assumes that any vulnerable components or movable/operable structural element located within 0.9 m (3 ft) horizontally of either the front or rear panels/doors, and at or below the top of the faulting cabinet section, will suffer physical damage and functional failure. This includes mobile/operable structural elements like dampers and fire doors.

## E.3 Operating Experience

A review of operating experience did not identify any HEAF events that exhibited pressure damage to fire PRA targets beyond the initiating component or immediately adjacent equipment (e.g., adjacent vertical sections in a switchgear lineup). However, one United States arc blast event pressurized the room and resulted in the failure of a fire door latch mechanism. There was no ensuing fire from this event. Out of the 23 United States HEAF events, no damage to PRA targets due to pressure effects is observed. A second event (GER022-19890909) occurred in a German facility where a double-panel fire door was distorted due to room overpressure from an arc fault. This German operating experience is the only event out of 18 internationally documented<sup>2</sup> HEAF events that resulted in damage to a structure (not fire PRA target) [19].

### E.3.1 Turkey Point (FEDB 51634)

NRC Information Notice 2018-09 identifies an arc flash event caused by foreign material entry into energized equipment and resulted in damage to a room fire door [18]. On March 18, 2017, while installing an electric raceway fire barrier system to protect power cables in support of the licensee's transition to a performance-based fire protection program, an arc flash occurred on a current-limiting reactor coil (inductive device) associated with the unit's 3A 4 kV switchgear bus. The event was caused by carbon dust, carbon fibers, threads, and trimmings from cutting Thermo-Lag 770-1, which became airborne and resulted in a foreign material hazard that initiated the arc flash in the reactor coil. The arc flash created a pressure wave that damaged and opened a fire door. The lock and strike were both broken, and the door suffered a minor z-bend and became bowed at the lock set area. The door separated switchgear room 3A from switchgear room 3B, resulting in the potential for a multi-compartment fire scenario. Upon entry into the room during their response, the fire brigade confirmed there was no fire in the 3A/3B bus rooms. The actual distance from the reactor coil cabinet to the damaged fire door is 4.4 m (14.5 ft) and is outside the HEAF impact assessment area as described in NUREG/CR-6850 [1]. This event is not included in HEAF frequency as there was no ensuing fire [45].

---

<sup>2</sup>HEAFs involving transformers were excluded from this count.

### **E.3.2 GER022-19890909**

On September 9, 1987, arcing occurred in an emergency diesel generator cabinet during a load test. The arc led to a short circuit that lasted approximately 4 s and resulted in the isolation of the emergency bus bar after 0.1 s. The EDG circuit breaker opened 1.5 s later due to low voltage. After another 0.5 s, emergency power was restored automatically to the offsite power bus. The arc caused a sudden pressure increase in the room, resulting in damage to the two-wing (double) fire door. From the event description and post-event photographs, it is unclear if there was an ensuing fire [19].

## **E.4 Test Data**

### **E.4.1 2014-2016 OECD HEAF Testing Program**

Pressure measurements were taken during the 2014-2016 OECD HEAF experimental program performed by the NRC [7]. These experiments measured the pressure within a switchgear enclosure at two locations using one pressure probe at each location. The locations varied based on the equipment design and arc location. The pressure measurements reported appear to be impacted by electromagnetic interference (EMI) at the start and end of each arc. Because of this noise, no conclusions or summary of pressure effects are made in the report.

### **E.4.2 2018 Medium-Voltage Switchgear Experiments**

Similar to the 2014-2016 testing, pressure measurements were taken during the 2018 testing with an improved pressure measurement system [6]. The measurement location within the arcing compartment (primary cable disconnect) displayed a higher peak pressure rise than the other measurement location within the secondary compartment (relay/circuit breaker compartment). The four medium-voltage switchgear experiments were performed at 6.9 kV system voltage, 25-32 kA fault current, and 2 or 4 s arc durations. In all tests, the front door opened due to the pressure increase flexing the door panel and causing the quarter turn latch to slip, but the arc and thermal hazard were located at the opposite end of the switchgear. Thus, there was limited thermal hazard in the region of the door opening. The report concluded that the peak pressure rise within the electrical enclosure was similar among the experiments ranging from 27.6 kPa to 30.3 kPa (4.0 psi to 4.4 psi) above ambient for the switchgear compartment where the arc was initiated and sustained.

### **E.4.3 2019 Low-Voltage Switchgear Experiments**

Similar to the 2018 testing, pressure measurements were taken during the 2019 testing [5]. Measurements were taken within the circuit breaker compartment and the main bus bar compartment. No pressure measurements were made in the rear cable compartment. The experiments on low-voltage switchgear were performed at either 480 V or 600 V system voltage, 10 to 20 kA fault current, and for a 0.4 to 8.3 s arc duration. The internal pressure rise ranged from 0.5 to 1.6 psi above ambient with most tests experiencing approximately 0.5 psi pressure rise. The report concluded that, “pressure increases within the [electrical] enclosure appeared to be minimal and did not cause the [electrical] enclosure panels to deform or doors to open.”

#### **E.4.4 JNRA Box Tests**

The Secretariat of the Nuclear Regulation Authority (Japan) conducted tests to simulate the design and operating conditions of the switchgear HEAF that occurred at the Onagawa nuclear power plant in 2011. In this test series [9], the internal pressure of the switchgear enclosure was measured using a strain-gauge type pneumatic transducer supplied by the testing laboratory. The maximum observed pressure increase above ambient was approximately 5 psi, with most tests experiencing a pressure rise between 0.5 and 4 psi, consistent with subsequent measurements made in the NRC 2018 test series [6].

### **E.5 Analysis**

An uninterrupted electrical arc creates a highly conductive plasma from vaporized source material (e.g., copper, aluminum). The vaporization of the source material results in a volumetric increase of heated air-plasma mixture around the arc path. A conservative estimate for the volumetric increase of the air-metal mixture in the arc path is 40,000 to 1 [46]. When the arc-generated expansion occurs within a confined space (i.e., electrical enclosure or small room) with limited pressure relief, stresses on the electrical enclosure or room structure can occur and potentially cause failure of the structure at a weak point (door or damper).

Examples of the overpressure effect in a room include the two events described in E.3.1 and E.3.2. In both cases, the arc fault occurred in a switchgear within a relatively small room as compared to the typical room size for a nuclear power plant, and the room fire doors (opening outwards) were affected and provided pressure relief. In the U.S. event, there was no fire reported from the arc blast. Given the lack of an ensuing fire, this event is not included in the fire ignition frequency for HEAFs. While the damage to the door locking mechanism defeated a credited fire barrier between the 3A and 3B switchgear rooms, the lack of fire did not create a multi-compartment scenario where both switchgear trains could be impacted. From an application standpoint, fire PRAs include an evaluation of multi-compartment effects through the use of a barrier failure probability. While the barrier failure probabilities currently used do not include a contribution for a HEAF-induced barrier failure, the lack of evidence of HEAFs failing barriers and resulting in an ensuing fire suggest that this phenomenon is not commonly observed and modeling it in a fire PRA is not warranted.

In the international event, it is unclear if a fire existed; post-event photos do not provide definitive evidence of a post-arc fire. The WG noted that from the review of these events as well as non-nuclear events and literature, arc blasts commonly do not exhibit an ensuing fire. Arc blasts are short in duration which results in limited energy release to support development of an ensuing fire.

A pressure wave from an electrical arc refers to the leading peak pressure impulse created by the rapid expansion and compression of the air. The pressure wave rapidly expands away from the arc and dissipates as it migrates through the surrounding air. The pressure wave amplitude is greater closer to the arc and diminishes with distance from the arc. Because of this, the arc pressure wave has a larger impact on the equipment near the arc, such as the enclosure for the initiating equipment and directly adjoining equipment (e.g., adjacent equipment in a switchgear bank).

Evidence of pressure wave impact has been observed in operating experience (for arc blasts) as well as in experiments. In post-event investigation, it is common to observe outward bowing or deflection of cabinet panels due to the pressure wave. In the 2018 testing program, high-speed video showed that the rear panels of the switchgear enclosure deformed in the first 0.01 s of the testing. Beyond the initiating enclosure, there is no evidence of pressure wave effects to equipment or objects within the test cell at the laboratory. Based on this, the WG did not recommend postulating damage to equipment from a HEAF-generated pressure wave.

The projectile concern is related to the pressure effect, and results in the creation of a projectile from equipment component(s) as a result of the failure or yielding of the component experiencing the pressure effect. The projectile momentum (mass and velocity) then has the potential to damage other components that it strikes. From the review of operating experience and testing, there is no evidence that projectiles from HEAF pressure effects pose a threat to fire PRA targets external to the initiating component. In several events, the enclosure door was swung open, or panels were dislodged and fell to the floor. However, in none of these cases did the door or panels impact or damage equipment external to the initiation equipment. Molten particle projectiles are considered a thermal phenomenon and not included in the pressure effect evaluation. Based on this information, the projectile concern does not appear to pose a hazard to fire PRA targets and therefore the WG does not recommend postulating damage from HEAF-generated projectiles.

Review of the test results provides limited evidence of overpressure effects and no evidence of overpressure creating conditions (projectiles) that could damage external PRA targets. In general, the WG did not identify HEAF overpressure as a concern necessitating explicit treatment. Additionally, the lack of evidence of ensuing fires from arc blast events and the evaluation of the multi-room hazard in the fire PRA multi-compartment analysis provides confidence that any potential hazard of HEAF pressure effects are adequately covered by the energetic and ensuing fire ZOIs.

## **E.6 Conclusion**

The WG reviewed and evaluated the available evidence from operating experience and testing to understand the potential hazards from HEAF-induced pressure effects. Beyond the initiating component, there is no evidence that the pressure effects resulted in damage to fire PRA targets. Out of the 23 U.S. HEAF events, no associated pressure effects are significant enough to damage fire PRA targets. In all cases, the HEAF was primarily a thermal event, resulting in thermal damage to the component and in many cases, an ensuing fire. Results from testing did not identify any pressure effects that pose a hazard to external fire PRA targets. Therefore, the WG concluded that the thermal hazard and guidance for the overall ZOI definition adequately bound the pressure effect concern. Therefore, pressure effects do not require independent consideration in the analysis of HEAF hazards.

With regard to fire doors and fire dampers, the available operating experience does not support consideration of HEAF damage. There is no HEAF-related operational experience events that damaged fire doors and/or fire dampers. As such, the WG recommends no additional failures of fire doors and/or dampers post-HEAF.





## **About EPRI**

Founded in 1972, EPRI is the world's preeminent independent, non-profit energy research and development organization, with offices around the world. EPRI's trusted experts collaborate with more than 450 companies in 45 countries, driving innovation to ensure the public has clean, safe, reliable, affordable, and equitable access to electricity across the globe. Together, we are shaping the future of energy.

© 2022 Electric Power Research Institute (EPRI), Inc. All rights reserved. Electric Power Research Institute, EPRI, and TOGETHER...SHAPING THE FUTURE OF ENERGY are registered marks of the Electric Power Research Institute, Inc. in the U.S. and worldwide.

3002025123

## **EPRI**

3420 Hillview Avenue, Palo Alto, California 94304-1338 • PO Box 10412, Palo Alto, California 94303-0813 USA  
800.313.3774 • 650.855.2121 • [askepri@epri.com](mailto:askepri@epri.com) • [www.epri.com](http://www.epri.com)